

**Comprehensive Patient-Specific Prediction Models for Diagnosis and Prognosis of Temporomandibular Joint Osteoarthritis**

by

Najla N. Al Turkestani

A dissertation submitted in partial fulfillment  
of the requirements for the degree of  
Doctor of Philosophy  
(Oral Health Sciences)  
in the University of Michigan  
2023

Doctoral Committee:

Professor Lucia Cevidanes, Chair  
Clinical Professor Erika Benavides  
Professor Margherita Fontana  
Professor Yuji Mishina  
Associate Professor Arvind Rao  
Assistant Professor Fabiana Soki

Najla Neamatallah M. Al Turkestani

alnajla@umich.edu

ORCID iD: 0000-0002-7650-3638

© Najla Al Turkestani 2023

## **Dedication**

To my parents, Neamatallah and Resalah, and my siblings, Nahla, Ahmed, Ibrahim, Razan, and Randa. Thank you for your constant love, support, and encouragement. Without you, my academic journey and success would not have been possible.

## Acknowledgements

I would like to express my gratitude to several people who have made this dissertation possible. First and foremost, I am deeply grateful to my thesis advisor, Lucia Cevidanes, for her exceptional mentorship, encouragement, and tireless dedication to my research. I feel incredibly fortunate to have had the opportunity to work with someone who is not only a brilliant scientist but also a compassionate and kind-hearted person. Thank you, Lucia, for being my rock and for believing in my abilities which has helped me to reach new heights. I am also grateful to my committee members, Dr. Erika Benavides, Dr. Margherita Fontana, Dr. Yuji Mishina, Dr. Arvind Rao, and Dr. Fabiana Soki, for their constructive feedback, insightful comments, and invaluable suggestions that significantly enriched my work.

A very special gratitude goes to Dr. Vesa kaartinen. Thank you for your endless support and sharing your pearls of wisdom whenever I consulted with you.

I would like to express my deep appreciation to Dr. Jacques Nör for his ongoing dedication and commitment to my success that have made such a difference in my life!

I would like to extend my sincere thanks to Dr. Jan Hu, who not only served in my master's thesis work but continued to be my academic advisor in my PhD pre-candidacy years. Thank you for your kind heart and for helping me to grow both personally and professionally.

I would also like to express my heartfelt gratitude to the lab members (Marcela, Felicia, Selene, Martina, Romain, Celia, Maxime, Baptiste, Luc, Nathan, Aron, Juan, and Marilia) who have been more than just colleagues but a family to me. I will cherish the beautiful memories we



created together, from lab meetings to social events, which made this experience not only productive but also enjoyable.

A special thanks to my Michigan family and friends for all their support. Rick Fiedler, Jim Sugai, Veronica Slayton, Keely Russel, Elizabeth Hatfield, Kristine Phillips, Jennifer Crist and residents in the TMD & Orofacial Pain Residency program, thank you for all the support, and the help with patients recruitments.

Kimberly Smith, whom I have had the pleasure of knowing before joining the PhD program. Thank you for being an amazing friend, for your guidance and advice, and for always being there to celebrate the happy moments and offer a listening ear during the challenging ones!

Last, I would like to thank my family at King Abdulaziz University and the Saudi Government for their support and enabling me to pursue my dream at this prestigious institution.

## Table of Contents

Dedication.....	ii
Acknowledgements.....	iii
List of Tables .....	ix
List of Figures.....	xii
Abstract.....	xxi
Chapter 1 Review of Literature.....	1
1.1 Temporomandibular Joint Structure and Development.....	1
1.2 Temporomandibular Disorders .....	4
1.2.1 TMD Terminology Evolution and Prevalence.....	4
1.2.2 Classification of Temporomandibular Disorders.....	5
1.3 Pathogenesis of Temporomandibular Joint Osteoarthritis.....	8
1.4 Treatment Strategies for Temporomandibular Joint Osteoarthritis .....	16
1.5 Diagnosis of Temporomandibular Joint Osteoarthritis.....	23
1.5.1 Crepitus, Pain and Co-morbidities in TMJ OA .....	23
1.5.2 Imaging Signs of TMJ OA, Prevalence, and Modalities .....	28
1.6 DC/TMD Limitations in Diagnosing and Predicting TMJ OA Progression.....	37
1.7 Quantitative Imaging Markers: Pioneering Future Frontiers.....	39
1.7.1 Subchondral Bone Involvement in Early Stages of OA .....	39
1.7.2 Radiomics: Revealing Hidden Insights within Medical Imaging .....	42
1.7.3 Radiomics: Advancing the Diagnosis and Progression Assessment of Osteoarthritis.....	48

1.8 Quantitative Biological Markers in OA: Exploring Disease Development & Progression .....	54
1.9 From Algorithms to Illness: Machine Learning in Medicine .....	81
1.9.1 Machine Learning Categorization & Algorithms .....	82
1.9.2 Development, Evaluation and Explainability of ML models .....	91
1.9.3 Machine Learning in Osteoarthritis: Insights and Considerations.....	103
Chapter 2 Clinical Decision Support Systems in Orthodontics: A Narrative Review of Data Science Approaches .....	106
Abstract .....	106
2.1 Introduction.....	107
2.2 Development of Clinical Decision Support Systems (CDSSs).....	109
2.2.1 Types of CDSSs.....	109
2.2.2 Data Science Approaches for the Development of CDSSs .....	110
2.3 Conclusion .....	124
Chapter 3 A Comprehensive Patient-Specific Prediction Model for Temporomandibular Joint Osteoarthritis Progression.....	125
Abstract.....	125
3.1 Introduction.....	127
3.2 Materials & Methods .....	131
3.3 Results.....	138
3.3.1 Improvement of the Clinical Symptoms in Participants with TMJ OA.....	138
3.3.2 Evidence of Persistence of Radiographic Signs of TMJ OA.....	138
3.3.3 Quantitative Imaging Features Vary Among Control and TMJ OA Participants..	139
3.3.4 Osteoarthritis Alters the Morphology of the Mandibular Condyles .....	140
3.3.5 Individual Features Contribute Differently to the Prediction of TMJ OA Prognosis,.....	141

3.3.6 The EHPN Method Achieves the Highest Accuracy in Predicting TMJ OA Prognosis.....	142
3.3.7 Features' Integration Enhances the EHPN Model's Prediction of TMJ OA Prognosis.....	143
3.3.8 The SHAP Method Determines the Top Contributing Features for TMJ OA Prognosis.....	144
3.4 Discussion.....	145
Chapter 4 Unleashing the Power of Machine Learning: Advancing TMJ Osteoarthritis Diagnosis.....	170
Abstract.....	170
4.1 Introduction.....	172
4.2 Materials & Methods .....	175
4.3 Results.....	180
4.3.1 Clinical Characteristics of the Study Population .....	180
4.3.2 Destructive Bone Changes Detected in TMJ OA Participants .....	180
4.3.3 Quantitative Bone Imaging Features Distinctively Characterize TMJ OA from Controls.....	180
4.3.4 Comparable Expression Levels of Serum and Saliva Protein Biomarkers in Control and TMJ OA Participants .....	181
4.3.5 Features' Integration Amplifies the Robustness of TMJ OA Diagnosis.....	181
4.4 Discussion & Conclusion.....	186
Chapter 5 Osteoarthritis Diagnosis Integrating Whole Joint Radiomics and Clinical Features for Robust Learning Models using Biological Privileged Information .....	210
Abstract.....	210
5.1 Introduction.....	211
5.2 Materials & Methods .....	213
5.3 Results.....	217
5.3.1 LUPI and non-LUPI models .....	217

5.3.2 Feature Integration Comparison .....	218
5.3.3 Feature Occurrence and Importance .....	219
5.4 Discussion .....	221
Bibliography .....	225

## List of Tables

Supplementary Table 3.1: Description for the Trabecular Bone Texture-Based and Morphometry Features.....	139
Supplementary Table 3.2: Descriptive Values for the Imaging Features in the Condyle and the Articular Fossa of the control group (n=40) at Baseline and Follow-up Visits.....	140
Supplementary Table 2.3: Descriptive Values for the Imaging Features in the Condyle and the Articular Fossa of the TMJ OA group (n=34) at Baseline and Follow-up Visit.....	141
Supplementary Table 3.4: Descriptive Values for the Biological Features Evaluated at Baseline.....	142
Supplementary Table 3.5: Performance of the Feature Selection Methods and Machine Learning Approaches on the Validation Dataset .....	143
Supplementary Table 3.6: Performance of the Feature Selection Methods and Machine Learning Approaches on the Test Dataset .....	144
Supplementary Table 3.7: FDR Corrected P Values Between the Top Identified Clinical, Imaging, and Biological Features .....	145
Supplementary Table 4.1: Definitions of Trabecular Bone Texture and Morphometry Features Computed in the Study .....	189
Supplementary Table 4.2: Quantitative Textural Imaging Features of the Condyle and Articular Fossa in Control and TMJ OA Groups .....	190
Supplementary Table 4.3: Descriptive Values of Biological Features in Control and TMJ OA Groups. ....	191
Supplementary Table 4.4: Descriptive Statistics of Log-transformed Biological Features in Control and TMJ OA Groups. Data presented as Mean $\pm$ SD and p-values from independent t-test. ....	193
Supplementary Table 4.5: Performance of the Feature Selection Methods and Machine Learning Approaches on the Validation Dataset Utilizing Clinical, Imaging, and Biological Features.....	194

Supplementary Table 4.5: Performance of the Feature Selection Methods and Machine Learning Approaches on the Validation Dataset Utilizing Clinical, Imaging, and biological Features (Cont.) .....	195
Supplementary Table 4.6: Performance of the Feature Selection Methods and Machine Learning Approaches on the Test Dataset Utilizing Clinical, Imaging, and Biological Features.....	196
Supplementary Table 4.6: Performance of the Feature Selection Methods and Machine Learning Approaches on the Test Dataset Utilizing Clinical, Imaging, and biological Features (Cont.) .....	197
Supplementary Table 4.7: Performance of the Feature Selection Methods and Machine Learning Approaches on the Validation Dataset Utilizing Clinical and Imaging Features.....	198
Supplementary Table 4.7: Performance of the Feature Selection Methods and Machine Learning Approaches on the Validation Dataset Utilizing Clinical and Imaging Features (Cont.) .....	199
Supplementary Table 4.8: Performance of the Feature Selection Methods and Machine Learning Approaches on the Test Dataset Utilizing Clinical and Imaging Features.....	200
Supplementary Table 4.8: Performance of the Feature Selection Methods and Machine Learning Approaches on the Test Dataset Utilizing Clinical and Imaging Features (Cont.) .....	201
Supplementary Table 4.9: Performance of the Feature Selection Methods and Machine Learning Approaches on the Validation Dataset Utilizing Clinical and Biological Features. ....	202
Supplementary Table 4.9: Performance of the Feature Selection Methods and Machine Learning Approaches on the Validation Dataset Utilizing Clinical and Biological Features (Cont.).....	203
Supplementary Table 4.10: Performance of the Feature Selection Methods and Machine Learning Approaches on the Test Dataset Utilizing Clinical and Biological Features. ....	204
Supplementary Table 4.10: Performance of the Feature Selection Methods and Machine Learning Approaches on the Test Dataset Utilizing Clinical and Biological Features (Cont.).....	205
Supplementary Table 4.11: Performance of the Feature Selection Methods and Machine Learning Approaches on the Validation Dataset Utilizing Clinical Features.....	206
Supplementary Table 4.11: Performance of the Feature Selection Methods and Machine Learning Approaches on the Validation Dataset Utilizing Clinical Features (Cont.) .....	207
Supplementary Table 4.12: Performance of the Feature Selection Methods and Machine Learning Approaches on the Test Dataset Utilizing Clinical Features.....	208

Supplementary Table 4.12: Performance of the Feature Selection Methods and Machine Learning Approaches on the Test Dataset Utilizing Clinical Features (Cont.)..... 209

Table 5.1: Comparison of Different Feature Integration Methods (in Percentage %) .....219



## List of Figures

- Figure 1.1: Gross anatomy of the Temporomandibular joint. The TMJ’s skeletal components, surrounded by the synovial capsule (SC), includes: the articular eminence (AE) and the glenoid fossa (GF) of the temporal bone (TB), the mandibular condyle (MC), and the intervening articular disc (AD). Adapted from “TMJ disorders: Future innovations in diagnostics and therapeutics,” by S. Wadhwa and S. Kapila, 2008, *Journal of Dental Education*, 72(8), pp. 930-947..... 2
- Figure 1.2: Representation of rat TMJ, showing the position of the condylar head of the mandible (CHM) with respect to the TMJ disc and eminence–glenoid fossa of the temporal bone (GFTB). Box on the right showing fiber organization and cellular composition of these condylar articular fibrocartilage. FZ: fibrous zone, HZ: hypertrophic zone, and PZ: proliferative zone. Adapted from “Biomechanical properties of the mandibular condylar cartilage and their relevance to the TMJ disc” by Singh, M. and Detamore, M.S., 2009, *Journal of Biomechanics*, 42(4), pp. 405–417..... 3
- Figure 1.3: Illustration of mechanisms involved in temporomandibular joint osteoarthritis development. Adapted from “Current understanding of pathogenesis and treatment of TMJ osteoarthritis” by Wang, X.D. et al., 2015, *Journal of Dental Research*, 94(5), pp. 666–673..... 9
- Figure 1.4: Utilization of Michigan splint for treatment of TMD. Adapted from “Occlusal splints-types and effectiveness in temporomandibular disorder management” by Albageieh et al. 2023, *Saudi Dent J.* 2023 Jan; 35(1): 70–79..... 18
- Figure 1.5: Schematic representation of TMJ arthrocentesis procedure with two needles insertion into the joint space. Adapted from “What is TMJ arthrocentesis?” Available at: <https://dentagama.com/news/what-is-tmj-arthrocentesis> (Accessed: 12 July 2023)..... 20
- Figure 1.6: The relationship between head posture and lower back pain in patients with temporomandibular disorders. Adapted from “Connection between TMJ and body posture” Available at: <https://www.tonguetieindia.com/connection-between-tmj-and-body-posture.html> (Accessed: 12 July 2023)..... 26
- Figure 1.7: Representations of a healthy TMJ and degenerative bone changes in sagittal (1) and coronal (2) CBCT orientations. Each letter corresponds to an image of the same individual. (A) A healthy TMJ with smooth, rounded, and well-defined condylar cortical margins. (B,C) Flattening and localized subcortical sclerosis of the condylar head, respectively, suggestive of joint remodeling. (G-I) Degenerative bone changes in TMJ OA (G1) An osteophyte on the anterior aspect of the condyle. (G2) Flattening of the superior and lateral slopes of the condyle. (H) The presence of osteophytes and multiple subchondral cysts. (I) The presence of osteophytes and

multiple areas of erosion. Adapted from “Temporomandibular joint disorders and orofacial pain” by Ahmad, M. and Schiffman, E.L, 2016, *Dental Clinics of North America*, 60(1), pp. 105–124..... 29

Figure 1.8: The ability of CBCT machines to customize the collimation of the X-ray beam (select the FOV), minimizing patient exposure, reducing scattered radiation that can affect image quality, and accommodating specific clinical requirements. Adapted from “Cone beam computed tomography: basics and applications in dentistry” by Venkatesh et al., 2017, *J Istanbul Univ Fac Dent*, 51(3 Suppl 1):S102-S121..... 36

Figure 1.9: Normal human joint articular cartilage and subchondral bone structure. NCC, non-calcified cartilage; CC, calcified cartilage; SBP, subchondral bone plate; STB, subchondral trabecular bone. Adapted from “Subchondral bone in osteoarthritis: insight into risk factors and microstructural changes” by Li G et al., 2013, *Arthritis Res Ther*. 15(6):223. doi: 10.1186/ar4405. PMID: 24321104; PMCID: PMC4061721..... 39

Figure 1.10: A model for OA pathogenesis: (A) In healthy individuals, subchondral bone has an optimized microstructure with a balanced distribution of trabecular rods and plates, providing even support for cartilage. (B-D) During early OA stages, cartilage mostly remains intact, but abnormal bone resorption, triggered by trauma or abnormal mechanical stress (overloading), begins to target trabecular rods. Rods are more vulnerable due to their higher surface-to-volume ratio and relative thinness compared to plates. This leads to fewer load-supporting trabeculae, resulting in increased mechanical demand on the remaining trabeculae and short-term thickening. (E) Ultimately, these microstructural changes disrupt the normal support for cartilage, causing an uneven distribution of rod-and-plate microstructure and localized subchondral bone stiffening. These events can severely impact the overlying cartilage, with unfavorable mechanical conditions and local stress concentrations contributing to advanced OA-related degradation. Adapted from “Subchondral trabecular rod loss and plate thickening in the development of osteoarthritis” by Chen, Y. et al., 2017, *Journal of Bone and Mineral Research*, 33(2), pp. 316–327. doi:10.1002/jbmr.3313..... 41

Figure 1.11: Workflow of Radiomics. Adapted from “Radiomics in medical imaging—“how-to” guide and critical reflection” by Timmeren et al., 2020, *Insights Imaging* 11, 91. <https://doi.org/10.1186/s13244-020-00887-2>..... 43

Figure 1.12: Comparison of first- and second-order statistics features. Two different images exhibit identical histograms, representing the same number of black, light gray, gray, and dark gray pixels (first-order statistics). However, when considering second-order statistics that account for pixel interactions, distinct matrices are obtained. This demonstrates that second-order statistics reveal valuable insights into the relationships between pixels, making them better suited for demonstrating intra-lesion heterogeneity. Adapted from “Radiomics in bone pathology of the jaws” by Santos et al., 2022, *Dentomaxillofacial Radiology* Vol. 52,1. <https://doi-org.proxy.lib.umich.edu/10.1259/dmfr.20220225>..... 44

Figure 1.13: Schematic illustration of the extraction of textural features from a 3x3 pixel image with three distinct grayscale levels. Adapted from “Radiomics and Deep Learning: Hepatic Applications”, by Park et al., 2020, *Korean J Radiol.* 21(4): 387–401, doi: 10.3348/kjr.2019.0752..... 46

Figure 1.14: Schematic illustration of a) The condyle bony sample, b) the obtained hr-CBCT and  $\mu$ CT images, and c) Histology analysis depicting osteoclasts’ presence adjacent to areas of trabecular bone loss. Adapted from “Detection of Bone Loss via Subchondral Bone Analysis”, by Vimort et al., 2018, *Proc SPIE Int Soc Opt Eng.* 2018 Feb;10578:105780Q. doi: 10.1117/12.2293654. Epub 2018 Mar 12. PMID: 29769754; PMCID: PMC5950720..... 52

Figure 1.15: Outcome of Shape Analysis MANCOVA for Proteins in the synovial fluid and serum, showing statistically significant Pearson correlations between biomarker levels and condylar morphology. Adapted from “3D osteoarthritic changes in TMJ condylar morphology correlates with specific systemic and local biomarkers of disease” by Cevidanes et al., 2014, *Osteoarthritis Cartilage*;22(10):1657-67. doi: 10.1016/j.joca.2014.06.014..... 57

Figure 1.16: The involvement of MMP-3 in osteoarthritis progression. MMP-3 facilitates osteoarthritis progression in the preclinical and clinical stages. It promotes inflammatory cell accumulation, vascular invasion, cartilage matrix degradation, osteoclast differentiation, while inhibiting the differentiation of mesenchymal stem cells. Adapted from “Matrix metalloproteinase 3: a promoting and destabilizing factor in the pathogenesis of disease and cell differentiation” by Wan et al., 2021, *Front. Physiol*;12. <https://doi.org/10.3389/fphys.2021.663978>..... 59

Figure 1.17: Metalloproteinases facilitate interactions among bone cells. (A) At normal levels, the shedding of RANKL from stromal cells or osteoblasts reduces the active RANKL quantity, leading to diminished osteoclastogenesis. (B) In disease conditions, heightened RANKL shedding produces a localized concentration of soluble RANKL, which stimulates osteoclast precursors and enhances osteoclastogenesis. Adapted from “Unraveling metalloproteinase function in skeletal biology and disease using genetically altered mice” by Aiken A., and Khokha, R, 2010, *Biochimica et Biophysica Acta (BBA) - Molecular Cell Research*;1803(1):P121-132. <https://doi.org/10.1016/j.bbamcr.2009.07.002>..... 61

Figure 1.18: 3D Reconstructions of Subchondral Bone Microstructures Using Synchrotron Radiation  $\mu$ CT: (A) CA+ Regions and (B) CA- Regions. Subchondral bone beneath extensively de-

graded cartilage shows a marked increase in bone volume and trabecular number, with reduced trabecular spacing. Adapted from “Elevated levels of active Transforming Growth Factor  $\beta$ 1 in the subchondral bone relate spatially to cartilage loss and impaired bone quality in human knee osteoarthritis” by Muratovic et al., 2022, *Osteoarthritis and Cartilage*; 30 (6): 896-907. <https://doi.org/10.1016/j.joca.2022.03.004>..... 67

Figure 1.19: 3D Reconstructions of Subchondral Bone (light grey) and Vascular Canals (red) Using Synchrotron Radiation  $\mu$ CT in (A)CA+ and (B) CA- Regions. (C) Quantitative findings highlight a notable increase in the density of vascular canals within the bone matrix. Adapted from “Elevated levels of active Transforming Growth Factor  $\beta$ 1 in the subchondral bone relate spatially to cartilage loss and impaired bone quality in human knee osteoarthritis” by Muratovic et al., 2022, *Osteoarthritis and Cartilage*; 30 (6): 896-907. <https://doi.org/10.1016/j.joca.2022.03.004>..... 67

Figure 1.20: Primary Categories of Machine Learning. Adapted from What is reinforcement learning?- MATLAB & Simulink. Available at: <https://www.mathworks.com/discovery/reinforcement-learning.html> (Accessed: 23 August 2023)..... 82

Figure 1.21: Schematic Representation of Supervised and Unsupervised Learning Methods. Adapted from “Data Annotation for Machine Learning: A to Z guide: Lotusqa2021, Lotus QA - Leading IT Outsourcing Company in Vietnam. Available at: <https://www.lotusqa.com/blog/data-annotation-guide/> (Accessed: 23 August 2023)..... 84

Figure 1.22: A Graphic Demonstration of the Support Vector Machine's Process. The SVM discerns a hyperplane that optimally differentiates the 'star' and 'circle' categories. Adapted from “Comparing different supervised machine learning algorithms for disease prediction” by Uddin et al, 2019, *BMC Medical Informatics and Decision Making* ,19:281. <https://doi.org/10.1186/s12911-019-1004-8> ..... 86

Figure 1.23: A Graphical Representation of a Decision Tree. Circles denote each variable (C1, C2, and C3), while the resultant decisions (Class A and Class B) are displayed using rectangles. To accurately assign a sample to a specific class, each branch is marked as 'True' or 'False', depending on the result derived from its preceding node's test. Adapted from “Comparing different supervised machine learning algorithms for disease prediction” by Uddin et al, 2019, *BMC Medical Informatics and Decision Making* ,19:281..... 87

Figure 1.24: A Visual Depiction of a Random Forest Model. Every decision tree within it was trained on a distinct random segment of the training dataset. Adapted from “Comparing different supervised machine learning algorithms for disease prediction” by Uddin et al, 2019, *BMC Medical Informatics and Decision Making* ,19:281. <https://doi.org/10.1186/s12911-019-1004-8> ..... 88

Figure 1.25: An Illustration of the Naïve Bayes Method. The 'white' circle represents a new data point that needs to be categorized as either the 'red' or 'green' class. Adapted from “Comparing different supervised machine learning algorithms for disease prediction” by Uddin et al, 2019,

BMC Medical Informatics and Decision Making ,19:281. <https://doi.org/10.1186/s12911-019-1004-8> ..... 90

Figure 1.26: A basic depiction of the K-nearest neighbor method. With  $K=3$ , the data point (represented by a 'star') is identified as 'black' due to receiving a majority of 'votes' from the 'black' category. Conversely, when  $K=5$ , it's labeled as 'red' because it garners more 'votes' from the 'red' category. Adapted from “Comparing different supervised machine learning algorithms for disease prediction” by Uddin et al, 2019, BMC Medical Informatics and Decision Making ,19:281. <https://doi.org/10.1186/s12911-019-1004-8> ..... 91

Figure 1.27: A Visual Representation Of An Artificial Neural Network With Two Hidden Layers. The arrows indicate the flow from the output nodes of one layer to the input nodes of the subsequent layer. Adapted from “Comparing different supervised machine learning algorithms for disease prediction” by Uddin et al, 2019, BMC Medical Informatics and Decision Making ,19:281. <https://doi.org/10.1186/s12911-019-1004-8> ..... 92

Figure 1.28: The Probability Density Curves of a Hypothetical Diagnostic Test. The density of the diagnostic test is graphed for two populations: the nondiseased population (Non-D) and the sick population (D). These populations are assumed to conform to the binormal model, with a mixture of  $N(0,1)$  and  $N(1.87,1.52)$  distributions, respectively. The representation of the diagnostic test's specificity is denoted by the shaded region beneath the distribution of individuals without the disease (A), when considering the arbitrary threshold of  $t=1$ . The measure of sensitivity is quantified by the region of shading that is beneath the distribution of the diseased population (B) when subjected to a common threshold value of 1. As an illustration, when the threshold value  $t$  is set to 1, the corresponding values for sensitivity and specificity are 0.72 and 0.84, respectively. When the test is dichotomized by considering a positive result if the test value exceeds a certain threshold, both the sensitivity and specificity exhibit changes in response. As the threshold increases, the sensitivity decreases while the specificity increases. Adapted from <https://www.ahajournals.org/doi/10.1161/circulationaha.105.594929> ..... 97

Figure 1.29: An illustration of the ROC curve . Adapted from “Comparing different supervised machine learning algorithms for disease prediction” by Uddin et al, 2019, BMC Med Inform Decis Mak 19, 281. <https://doi.org/10.1186/s12911-019-1004-8>..... 98

Figure 1.30: SHAP Summary Plot. The metabolic features are organized in a decreasing order according to their relative significance within the plot. Each data point in the summary plot represents a sample that has been plotted according to its influence on the model's output. The relative quantity of metabolites is visually represented by the hue of each sample, with lower abundance shown by blue and higher abundance indicated by red (A). Figure 4B exhibits the predominant metabolite inside the panel, namely testosterone glucuronide. Metabolites with high feature values generally exhibit positive SHAP values, leading the model to make predictions favoring males. Conversely, metabolites with low feature values, such as testosterone glucuronide, tend to have negative SHAP values, influencing the model to forecast the female sex. P-anisic acid displays a contrasting trend (B). Adapted from “Interpretable machine learning with tree-based shapley additive explanations: Application to metabolomics datasets for binary classification” by

Bifarin et al, 2023, Application to metabolomics datasets for binary classification. PLOS ONE 18(5): e0284315. .... 103

Figure 2.1: Gaps of knowledge in (A) TMJ and (B) Dental diagnosis and prognosis assessment tools..... 107

Figure 2.2: Overview of steps involved in developing clinical decision support systems (CDSSs). A, General spectrum of data science approaches in the CDSSs. B, Implementation of robust data management, Dental Storage for Computation and Integration, in the CDSSs..... 109

Figure 2.3: Data Science Approaches in the TMJ Clinical Decision Support System..... 121

Figure 2.4: Sequence of Data Science Approaches in the Dental Decision Support System.....123

Figure 3.1: Descriptive Values of the Participants' Clinical Characteristics and the Radiographic Determinants of Temporomandibular Joint Osteoarthritis. A) The box plots depict gender distribution and mean age ( $\pm$ SD) of the participants at follow-up visit. B) The mean ( $\bar{x}$ ), median, interquartile range, and the range of TMJ pain related characteristics (0-10 scale:0= no pain and 10= the worst possible pain) are shown in the TMJ OA group. The control subjects did not present TMJ pain at baseline (an inclusion criteria) and follow-up visits. C,D) Values of the clinical co-morbidities rated using Likert scale that ranged from 0-4: 0=not at all and 4= extremely. As clinical variables were not statistically significant within each group, only group comparisons were reported. P-values were computed using AChi-square test, AIndependent samples t test, CWilcoxon signed rank test, and DMann-Whitney U tests, values<0.05 were considered statistically significant. E) Examples of the degenerative bone changes observed in the mandibular condyles of the study participants are indicated by arrowheads pointing towards the affected areas of the bone. B) The frequency of osteoarthritic condylar bone changes identified in the high resolution-CBCT scans of the TMJ OA subjects at baseline and follow-up visits. .... 151

Figure 3.2: Measurement of Trabecular Bone Textural and Structural Parameters, and the the Three-dimensional Superior TMJ Space. A) A workflow for the pre-processing steps of the hr-CBCT scans prior to quantification of the imaging markers in mandibular condyles and articular fossae. B) The median values for the radiomics and bone morphometry features that significantly varied between control and TMJ OA subjects at baseline visits. C) Lef panel shows the placement of two landmarks in the sagittal view of the oriented CBCT scans in ITK-SNAP. After the volumetric reconstruction of the identified landmarks, linear measurements of the superior joint space were obtained in millimeters (mm), using the Quantification of 3D Components tool in 3D Slicer. The box plots demonstrate the median, interquartile, and the range of the SJS in the control and the TMJ OA participants at baseline and follow-up visits. P<0.05 were considered statistically significant ..... 152

Figure 3.3: The Three-Dimensional Analyses of Condyles' Morphology. A) The average group morphology of condyles at baseline (BL) and follow-up (FU) visits. B) The semi-transparent overlays, in the top panel, are depicting morphological differences of the composite condyles within/between the control and TMJ OA groups- the orange and blue arrow heads are pointing,

successively, at the resorptive and appositional changes along the condyles' surfaces. The color distance maps are showing the quantitative bone changes across the condyles' surface meshes- negative values denote areas of bone resorption (blue) and positive values indicate sites of bone proliferation (red). The vectors, in the lower panel, are representing the magnitude and direction of bone changes across the condyles- vectors are pointing inward and outward, successively, indicative of bone resorption and proliferation..... 153

Figure 3.4: Quantitative Assessment of Bone Remodeling in the Composite Condyles of the Control and the TMJ OA Groups. A) The workflow for the steps of measuring regional bone changes in the average group condyles. B) The mean (x), median, interquartile, and range of appositional and resorptive bone changes observed in the anterior and lateral surfaces of the condyles, compared to baseline levels.  $P < 0.05$  were considered statistically significant. n.s., non-significant. C) The frequency of bone resorption and formation among the study participants..... 154

Figure 3.5: Schematic Representation for the Steps of the TMJ OA Prognosis Prediction Model's Development. A) Clinical, imaging and biological data were collected from the study subjects, at baseline, and utilized to create the OA Prognosis Prediction model. B) Clinical and imaging data were collected, at follow-up visits, to label the training dataset with the changes of the participants' health status following a 2-3 years of conservative management..... 155

Figure 3.6: Comparison of the Models' Performances in Predicting the TMJ OA Prognosis. A) The performance of the top feature selection and machine learning approaches on the validation and test datasets. B) Schematic representation of the EHPN method that combines 18 models with optimal predictive performance on the validation dataset. Our data was split into 10 folds: a test set and the remaining were subdivided into training and test sets, ten-fold cross validation was applied in both loops. We carried out the model ensemble on the validation dataset and evaluated its performance using the test dataset. C) The performance of the EHPN method on the validation and test datasets using different feature sets..... 156

Figure 3.7: The Top Contributing Features in Predicting TMJ OA Prognosis. A) SHAP values for the features' impact on the EHPN model's prediction. The ranking numbers in the first column are the SHAP importance by averaging the absolute Shapley values per feature across the data. Each feature contribution is calculated by the SHAP importance of each feature/the sum of all SHAP importance. The SHAP value for each dot indicates the change of log-odds (increased probability) of no recovery for a specific subject if you exclude the specific feature. The location of the purple and yellow dots indicates the SHAP value for each subject. For example, if the purple dot for headache was on the left, it means higher occurrence of headache may negatively contribute to recovery from TMJ OA. B) Correlation matrix between the top contributing clinical, imaging and biological features in TMJ OA prognosis. The color-coding scale denotes the degree of positive and negative Pearson correlation between the features. \*Raw  $p < 0.05$ , \*\* raw  $p < 0.01$ , and \*\*\* raw  $p < 0.001$ ..... 157

Supplementary Figure 3.1: Logistic Regression Analysis for the Association between the Individual Features and the Presence of TMJ OA. The AUC values, the  $-\text{Log}_{10}$  [P-values], and –

Log10 [FDR adjusted p-values] are shown, successively, in the outer, middle and inner circles. Af, Articular fossa; C, Condyle; Sal, Saliva; JS, Joint Space; Ser, Serum..... 165

Supplemental Figure 3.2: Assessment of the Participants' Health Status at Follow-up. (A) An example of a case that was labeled as worsened based on the overall changes of the clinical signs and symptoms, as well as the three-dimensional semi-transparent overlays that displayed significant bone degenerative changes at follow-up visit. (B) An example of a case that was labeled as stayed the same. Note that cases had to demonstrate pain levels less than 5 and a mouth opening equals to 40 to be considered as improved..... 159

Supplementary Figure 3.3: The Top Performing Methods in Predicting TMJ OA Prognosis. A summary plot of the SHAP values for the methods' global impact on the EHPN model's prediction..... 167

Supplementary Figure 3.4: Graphical Display of the Top Contributing Features in TMJ OA Prognosis. The box plots display the median, interquartile, and range of the top contributing features' values in the model prediction for the asymptomatic/improved (0) and remained the same/worsened (1) TMJ OA groups..... 168

Figure 4.1: Framework for the Development of TMJ OA Diagnosis Prediction Models. A) Data Synthesis and Machine Learning Testing: Comprehensive integration of clinical, imaging, and biological data from study participants, followed by features' selection and exploration of the efficiency of ensemble learning and privileged information in model crafting. B) Insightful Interpretation: Application of shapley additive explanations (SHAP) analysis to discern the key features contributing to the models' predictions for TMJ OA cases. DC/TMD, diagnostic criteria for temporomandibular disorders; AI, artificial intelligence..... 179

Figure 4.2: Participants' Clinical Characteristics and Radiographic Determinants of Temporomandibular Joint Osteoarthritis. A) Box plots illustrate the mean (x), median, and interquartile range for TMJ pain-related characteristics on a 0-10 scale, where 0 signifies no pain and 10 corresponds to the highest level of pain; control subjects reported no TMJ pain. B, C) Measurements of unassisted vertical mouth opening (mm) and the rates of clinical co-morbidities, evaluated using a Likert scale ranging from 0-4; 0 implies "not at all," and 4 signifies "extremely." A p-value below 0.05 was deemed statistically significant. D) Grading of radiographic signs of TMJ OA following the diagnostic criteria for temporomandibular disorder (DC/TMD). E) Examples of degenerative bone changes in the mandibular condyles of the TMJ OA participants, with arrowheads pointing to the affected areas. F) Percentage of osteoarthritic alterations in the condylar bone, identified in the high-resolution CBCT scans of the TMJ OA participants..... 183

Figure 4.3: Evaluation of Trabecular Bone Texture, Structural Parameters, and the three-dimensional Superior TMJ Space. A) Workflow for pre-processing hr-CBCT scans before quantifying the imaging markers in mandibular condyles and articular fossae. B) Comparative Analysis of Mean Values for Radiomics and Bone Morphometry Features Significantly Distinguishing Control and TMJ OA Subjects. C) Box plots demonstrating the mean, interquartile range, and



variability of superior TMJ space in control and TMJ OA participants. Statistical significance was defined at  $P < 0.05$ ..... 184

Figure 4.4: Comparison of Models' Performances in Predicting the TMJ OA Diagnosis. A) Schematic representation of the steps for developing the TMJOA model. Our dataset was divided into 10 folds, with one serving as a test set, while the rest were subdivided into training and validation sets. We applied ten-fold cross-validation in both loops and assessed model performance by averaging results across the 10-fold cross-validation on the test dataset. Additionally, we utilized Shapley values to identify contributing factors to the model's predictions. B) Performance evaluations of top feature selection and machine learning methods across various feature sets emphasize the key role of feature integration in optimizing TMJ OA diagnostic prediction models. Lightgbm, Light gradient boosting machine; SVM, Support vector machine; ; AUC, Area under the curve; NNET, Neural network. C) SHAP values interpret machine learning predictions for TMJ OA cases. On the y-axis, features are ranked based on their global importance, which is determined by averaging all SHAP values for a specific feature. Each dot on the plot represents the SHAP value of an individual prediction, corresponding to a specific subject from the testing dataset. The color of the dot reflects the value of the respective feature, while its position along the x-axis indicates its influence on the model's prediction. For instance, if a purple dot representing 'headache' is positioned to the left, it suggests that a higher occurrence of headaches decreases the probability of the individual not having TMJ OA..... 185

Supplementary Figure 4.1: Analysis of Biological Features in Control and TMJ OA Groups. A) Summary report displaying protein levels in serum and saliva. B) Standard curves from microarray analysis for individual proteins. LOD, Limit of detection..... 192

Figure 5.1: Diagram of Training and Testing Process ..... 215

Figure 5.2: The Architecture of KRVFL+ Network. Solid lines are output weights and dash lines stand for random weights and biases. .... 217

Figure 5.3: Comparison of LUPI and non-LUPI Models. The non-LUPI models only trained with normal features and RVFL model. The LUPI model trained with KRVFL+ and biological data as privilege information ..... 218

Figure 5.4: A. Feature occurrence in 50 trained models using NMIFS method. B. Feature importance measured as the mean absolute Shapley values in 50 models. C. Distribution of Shapley values in each query point in the 50 models. The order of the features shown in the x-axis is based on the feature occurrence. D. Shapley summary plot for one model. The boxplots represent the distribution of TMJOA and control groups (each TMJOA patient is shown as a circle and control as a diamond). The Heatmap color bar shows the value of the feature itself from high to low (yellow to blue). Low number of Shapley value of features reduce the predicted TMJOA diseased probability, a large number of Shapley value increase the probability ..... 220

## Abstract

Osteoarthritis is the most common degenerative joint disease, affecting 15% of the global population. Osteoarthritis in temporomandibular joint (TMJ OA) can cause chronic pain, facial deformity, joint dysfunction, impacting the quality of life. Unlike weight-bearing joints, TMJ OA primarily affects individuals between the ages of 20 and 40 and can also appear in adolescents.

Current standards for diagnosing TMJ OA rely on clinical and imaging criteria. However, these criteria have limited efficacy in detecting early-stage TMJ OA, posing challenges to timely intervention and mitigation of irreversible tissue damage. Hence, it becomes imperative to identify additional objective diagnostic criteria. In addition, determining which patients are at increased risk of disease progression is critical for making informed clinical decisions and designing more effective and individualized treatments.

Radiomics is a newly established field propelled by advancements in computational power. It extracts quantitative imaging features from radiological images, aiming to identify subtle tissue variations and reduce subjectivity in image interpretation. Beyond radiomics, metabolic abnormalities in joint tissues serve as early indicators of osteoarthritis. Although there has been progress in studying osteoarthritis biomarkers, they have not yet been clinically established. Evaluating multiple markers may reveal their intricate interrelations and fully harness their potential.

With the advent of powerful machine learning (ML) methods, analysis of complex multisource data became feasible. Nevertheless, applying feature selection methods is crucial to eliminate

redundant and irrelevant data, improving the output accuracy. Unlike knee osteoarthritis, which has been extensively studied using ML models, TMJ OA remains an underexplored area. Therefore, we aimed to 1) Develop a reliable prediction tool for TMJ OA progression and identify the contributing factors during a 2–3-year follow-up period, 2) Develop a comprehensive prediction tool tailored for TMJ OA diagnosis and use explainable methods to identify key factors driving diagnosis, and 3) Investigate the feasibility of privileged learning in addressing missing data when diagnosing TMJ OA.

We successfully developed an open-source tool which combined 18 feature selection and ML methods. This allowed for the prediction of disease progression with an accuracy=0.87, area under the ROC curve (AUC)=0.72, and an F1 score=0.82. Using the interpretable SHAP analysis method, we identified the strongest predictors for TMJ OA progression. These included: clinical (headache, lower back pain, restless sleep), quantitative imaging (condyle high-grey-level-run-emphasis (HGLRE), articular fossa GL-non-uniformity, and long-run-low-GLRE, joint space), and biological markers in saliva (Osteoprotegerin, Angiogenin, VEGF, and MMP-7) and serum samples (ENA-78).

Utilizing clinical, CBCT imaging, and biological data from 162 prospectively recruited subjects, we evaluated 77 ML methods. Random forest demonstrated the best diagnostic performance, achieving AUC=0.90, accuracy=0.79, precision=0.80, and F1=0.80. The integration of clinical, imaging, and biological markers enhanced TMJ OA diagnosis. The top contributing features were clinical (headache, restless sleep, mouth opening, muscle soreness), objective quantitative imaging (condyle Cluster-Prominence, HGLRE, SRHGLRE, Trabecular Thickness), and biological markers in saliva (TGFB-1, TRANCE, TIMP-1, PAI-1, VECadherin, CXCL-16) and serum (Angiogenin, PAI-1, VEGF, TRANCE, TIMP-1, BDNF, VECadherin). Lastly, we developed the

KRVFL+ diagnostic tool, which can be used when only clinical and imaging data are available.

It achieved an AUC, specificity, and precision of 0.81, 0.79, and 0.77, respectively.

Collectively, these efforts emphasize the immense potential of multi-source data and ML applications in presenting solutions for predicting TMJ OA progression and diagnosis, with potential implications for timely interventions and a transformative impact on TMJ OA healthcare delivery.

## **Chapter 1 Review of Literature**

### **1.1 Temporomandibular Joint Structure and Development**

The temporomandibular joint (TMJ) is a synovial joint that is characterized by the presence of a joint cavity, synovial membrane, synovial fluid, and articular cartilage. It is also classified as a ginglymoarthrodial joint, as it can perform both hinge (ginglymus) and gliding (arthrodial) movements. Its complex anatomical structure consists of the temporal bone of the skull, the condyle of the mandible, and a fibrocartilaginous articular disc (Bender et al., 2018).

The condyle of the mandible articulates with the temporal bone in the glenoid fossa, which is bounded posteriorly by the articular ridge and anteriorly by the articular eminence (Bender et al., 2018). Separating the condyle and glenoid bones is an articular disc, which divides the joint into two compartments. The inferior compartment allows for rotation of the condylar head around an instantaneous axis of rotation, corresponding to the first 20 millimeter (mm) of mouth opening. Beyond this extent, the superior compartment of the TMJ becomes active, allowing for the translatory movement of the entire apparatus, condylar head and articular disc (Figure 1.1). The fibrocartilaginous articular disc plays a crucial role in shock absorption, distribution of joint loads, and providing resilience against high-pressure occlusal forces. It also allows for the range of motion necessary for jaw movements involved in speech, mastication, respiration, and swallowing (Bender et al., 2018; Yildirim et al., 2011).

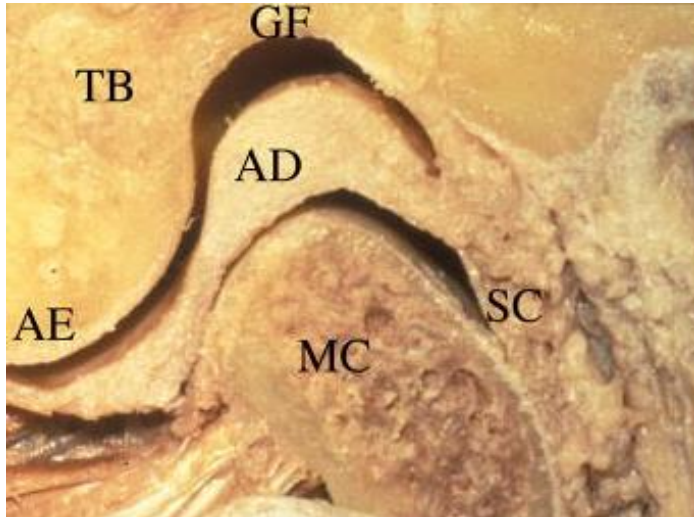


Figure 1.1: Gross anatomy of the Temporomandibular joint. The TMJ's skeletal components, surrounded by the synovial capsule (SC), includes: the articular eminence (AE) and the glenoid fossa (GF) of the temporal bone (TB), the mandibular condyle (MC), and the intervening articular disc (AD). Adapted from "TMJ Disorders: Future Innovations in Diagnostics and Therapeutics," by S. Wadhwa and S. Kapila, 2008, *Journal of Dental Education*, 72(8), pp. 930-947.

The unique nature of TMJ development is intriguing, especially when compared to other similar joints, even though it shares some common characteristics among mammals. This process proceeds through three distinct phases: the blastemic, cavitation, and maturation stages. In contrast to the formation of long bone joints via a single skeletal condensation, TMJ originates from two separate mesenchymal condensations—glenoid fossa and condylar blastema. While the former undergoes membranous ossification as it emerges from the otic capsule, the latter forms bone via endochondral ossification from the mandible's secondary condyle cartilage. During the cavitation stage, the dense mesenchyme between the blastemas differentiates into fibrous tissue layers, leading to the development of the upper and lower joint spaces of the future disc. The maturation stage, extending from the 12th week of gestation to birth, involves the development of the glenoid fossa and the condyle. The influence of mechanical forces from the vasculature and surrounding muscles shapes the anatomy of the glenoid fossa and condyle. At birth, the TMJ is not yet fully developed. In newborns, the glenoid fossa shows less density, and cartilage development is yet to occur; only fibrous connective tissue is found. During the age span of five to ten years, the condyles undergo growth in posterior, lateral, and upward directions. The form of the

joint is further molded by the mechanical forces exerted by the teeth and masticatory muscles (Bender et al., 2018; Bordoni & Varacallo, 2023; Liang et al., 2016).

Contrary to other synovial joints that are coated by hyaline cartilage, the TMJ has a thin fibrous tissue layer populated with mesenchymal cells that differentiate into chondrocyte, earning its classification as fibrocartilage (Artuzi et al., 2020; Purcell et al., 2009). This cartilage, which primarily consists of type I and II Collagens, gives the TMJ the ability to withstand significant occlusal load and shear forces directed at the joint. Additionally, it has densely packed fibers which increases its capacity for self-repair (Figure 1.2). Nevertheless, several factors can impact the fibrocartilage in the TMJ, rendering it vulnerable to degenerative alterations (Wadhwa & Kapila, 2008).

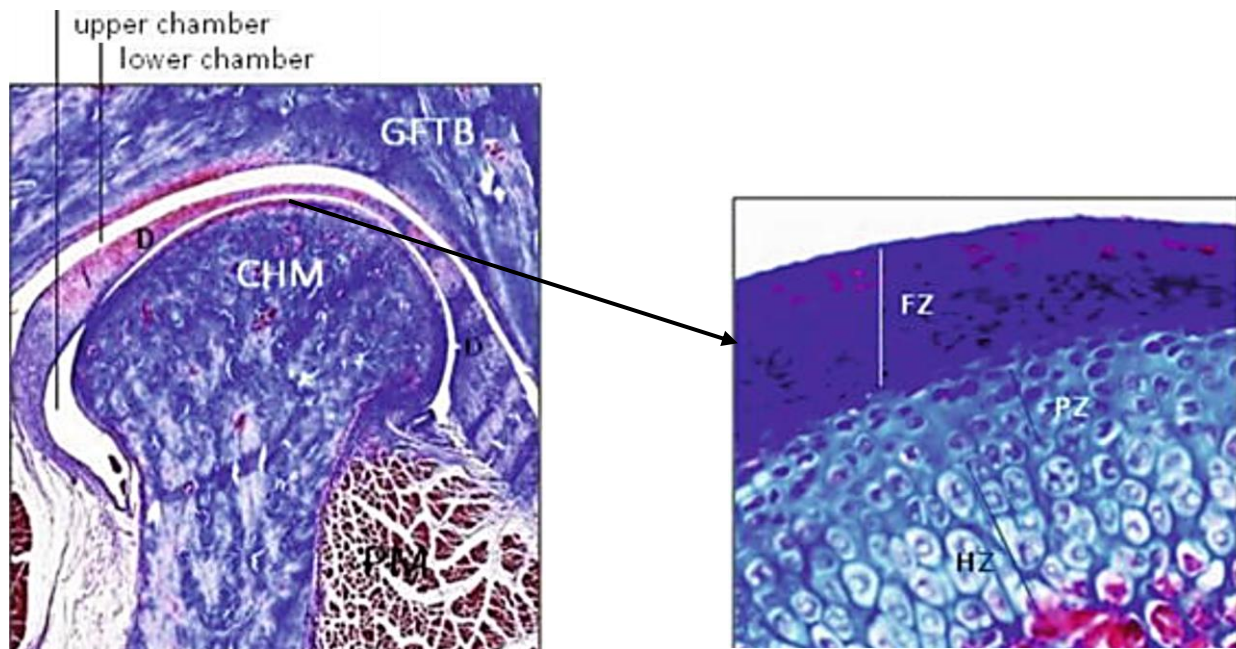


Figure 1.2: Representation of rat TMJ, showing the position of the condylar head of the mandible (CHM) with respect to the TMJ disc and eminence–glenoid fossa of the temporal bone (GFTB). Box on the right showing fiber organization and cellular composition of these condylar articular fibrocartilage. FZ: fibrous zone, HZ: hypertrophic zone, and PZ: proliferative zone. Adapted from “Biomechanical properties of the mandibular condylar cartilage and their relevance to the TMJ disc” by Singh, M. and Detamore, M.S., 2009, *Journal of Biomechanics*, 42(4), pp. 405–417.

## **1.2 Temporomandibular Disorders (TMD)**

### ***1.2.1 TMD Terminology Evolution and Prevalence***

Temporomandibular disorders serve as an umbrella term for more than 30 health disorders musculoskeletal conditions characterized by pain and/or dysfunction in the masticatory muscles, temporomandibular joints, and associated structures (Kapos et al. 2020; Yost et al. 2020). The evolution of this term traces back to 1887, when a British surgeon published the first report on the surgical management of disc displacements in the temporomandibular joint. James Costen further contributed by identifying a constellation of symptoms concentrated around the ear and TMJ, giving rise to the term 'Costen's syndrome' (Costen, 1934). The timeline progressed to 1947, when Nogaard applied arthrographic techniques to visualize anterior displacement of the articular disc in a clicking temporomandibular joint (Riesner, 1947). In the 1950s, the term 'temporomandibular joint pain dysfunction syndrome' was introduced, followed by 'functional temporomandibular joint disturbances'. Later, Bell suggested the term 'temporomandibular disorders,' which was widely accepted and has been officially adopted by the American Dental Association (List & Jensen, 2017; Sharma et al., 2011).

Temporomandibular disorders constitute the most common non-dental pain complaint in the maxillofacial region and rank as the second most common musculoskeletal disorder, surpassed only by chronic low-back pain (Kapos et al., 2020; Khan et al., 2019; List & Jensen, 2017). According to the OPPERA study, a comprehensive multisite prospective cohort study conducted in the United States, around 4% of previously TMD-free adults aged 18 to 44 experience their first clinically confirmed TMD each year. Interestingly, the study also observed that the annual incidence rate increases with age: 2.5% for ages 18–25, 3.7% for ages 25–34, and 4.5% for ages 35–



44 (Kapos et al., 2020). Generally, it is estimated that TMD affects 5 to 15% of the adult population. However, it's noteworthy that signs associated with TMD have been detected in up to 50% of adults. In fact, recent data points towards a rising trend in TMD prevalence (Li and Leung 2021). Echoing this observation, a comprehensive systematic review and meta-analysis reported that TMD symptoms were present in 31% of adults and 11% of children and adolescents (Valesan et al., 2021).

### ***1.2.2 Classification of Temporomandibular Disorders***

Clinical researchers frequently used the term TMD as a descriptor for most encountered conditions in practice. Nonetheless, it's imperative to also differentiate other disorders that may initially present symptoms similar to typical TMDs but require distinct management strategies. As a result, there has been an ongoing efforts to classify TMD under different categories (Li and Leung 2021).

The categorization of temporomandibular disorders was initially divided into two types: arthrogeous and myogenous. This bifurcation served as a beneficial tool, guiding clinicians towards the suitable treatment course during the early management stages. However, as these classes did not always offer clear distinction and substantial overlap or progression could occur from one syndrome to another, a demand for more specific classification emerge (Li & Leung, 2021; Marjaana Kuttilla et al., 1998). In 1990, the American Academy of Orofacial Pain introduced the diagnostic classification for TMD. This system subdivided the myogenous category, mainly distinguishing between muscular hyperactivity due to stress, and muscular abnormalities related to parafunctional oral habits. Simultaneously, the arthrogeous category was further differentiated based on specific structural abnormalities, such as internal derangement of the temporomandibular joint or degenerative disease (Klasser et al., 2018). In 1992, Truelove and his team developed

the clinical diagnostic criteria for temporomandibular disorders. This classification presented explicit diagnostic criteria for each clinical category for the first time. This system also accommodated multiple diagnoses and identified three main categories: muscle alterations (such as myalgia and myofascial pain), internal joint changes (including disc displacement with or without reduction, capsulitis/synovitis, and disc perforation), and degenerative disorders (Truelove et al., 1992). Building on this classification, Dworkin and LeResche established a pivotal milestone in TMD classification, known as the research diagnostic criteria for temporomandibular disorders (RDC/TMD). This groundbreaking system, that is based on the biopsychosocial model of pain, introduced a dual-diagnosis approach acknowledging both physical conditions and psychosocial factors. The physical conditions, referred to as Axis I, encompassed muscle disorders, disc displacements, and other joint conditions that contribute to the pain disorder. In addition, Axis II addressed psychosocial factors, encompassing elements that contribute to suffering and disability. The objective behind this classification was to maximize reliability and minimize variability of examination methods and clinical judgment (Li and Leung 2021; Schiffman, Ohrbach, et al. 2014; Schiffman et al. 2010). The RDC/TMD also improved the understanding of TMD epidemiology. Earlier, the reported prevalence of TMD was remarkably inconsistent, with estimates suggesting that between 1% and 75% of the general population exhibited at least one objective sign of TMD. However, the application of the RDC/TMD brought a considerable improvement in these estimates. A systematic review of peer-reviewed literature on the prevalence of various RDC/TMD Axis I diagnoses showed that muscle disorders were the most common diagnosis in patient populations. Nearly half of the patients (45.3%) met the criteria for myofascial pain, with or without limited mouth opening. Group II disorders diagnosis was allocated to 41.1% of patients, the vast majority of which were identified as having disc displacement with reduction

(41.5%). Degenerative disorders, categorized as Group III, were diagnosed in roughly a third of the patients (30.1%) (Manfredini et al., 2011).

Although the RDC/TMD provided significant advantages and made substantial contributions to the field, numerous publications have proposed potential improvements. These suggestions aimed to enhance the accuracy and comprehensiveness of TMD diagnosis, improve differentiation between TMD cases and control groups, and refine the distinction between various diagnostic subgroups (Manfredini et al. 2011; Schmitter et al. 2008; Limchaichana et al. 2007; Emshoff et al. 2002; Ohlmann et al. 2006; Huddleston Slater, Lobbezoo, and Naeije 2002; Shaefer et al. 2001). Responding to this need, the national institutes of health/ national institute of dental and craniofacial research (NIH/NIDCR) has sponsored a series of multisite studies to comprehensively assess the reliability and validity of the RDC/TMD classification (Schiffman and Ohrbach 2016; Schiffman, Ohrbach, et al. 2014; Anderson et al. 2010; Manfredini et al. 2011; Look et al. 2010; Schiffman et al. 2010; Ahmad et al. 2009; Truelove et al. 1992).

These series of studies, referred to as the validation project, were conducted over a span of four years. The population participating in these studies was comparable to those involved in previous research using the RDC/TMD. Notably, the NIDCR took an active role in conducting these studies by establishing an advisory panel to oversee the project. This panel consisted of twelve experts and represented all relevant clinical and basic science areas. As a result of their collective efforts, the panel revised the criteria and developed the diagnostic criteria/temporomandibular disorders (DC/TMD). These revised criteria demonstrated an improvement in various areas, including the reliability, validity, sensitivity, and specificity of the examination algorithms, compared to the original research diagnostic criteria for temporomandibular disorders. It is also deemed appropriate for use in clinical and research settings. These advancements in understand-

ing TMDs have established a foundation for in-depth exploration of specific conditions within this category. Among these, one of the most debilitating is temporomandibular joint osteoarthritis (Al-Ghurabi & Al-Hawa, 2023; Schiffman et al., 2014).

### **1.3. Pathogenesis of Temporomandibular Joint Osteoarthritis**

Osteoarthritis is the most common degenerative joint disease, affecting around 15 % of the population globally (Feng et al., 2022; Kalladka et al., 2014). Temporomandibular joint osteoarthritis (TMJ OA) is a chronic degenerative disease characterized by synovitis, cartilage destruction, deterioration of articular tissues and subchondral bone remodeling. These changes can lead to pain, facial deformity, joint dysfunction and progressive disability (Mélou et al. 2023; Manfredini et al. 2016; Wang et al. 2015). Distinct from weight-bearing joints, TMJ OA predominantly affects individuals aged between 20 and 40 years. Furthermore, its prevalence has seen a drastic increase among adolescents and young adults, particularly peaking between the ages of 15 and 19. Since the TMJ is still developing during these years, osteoarthritic changes can disrupt normal condylar formation, resulting in complications such as hyperdivergent facial profile, mandibular deviation, and mandibular retrusion (Mélou et al., 2023; Donovan et al., 2018). Furthermore, TMJ OA shows a higher prevalence in females, with a female-to-male ratio exceeding 2:1. This disparity could be attributed to an interplay of various factors, including differences in sex hormone levels, stress management, pain sensitivity, and healthcare seeking habits (Mélou et al., 2023; Kalladka et al., 2014; Reneker et al., 2011).

The etiology of most TMJ OA cases is multifaceted and complex, or even unknown. While osteoarthritis has been thoroughly investigated in larger joints, such as those in the hip and knee, research specifically pertaining to TMJ OA remains relatively scarce. Nonetheless, the existing literature identifies several factors that may influence the development and progression of TMJ

OA, including inflammation, mechanical overload, estrogen, cartilage destruction, and irregular subchondral bone remodeling (Figure 1.3) (Delpachitra and Dimitroulis 2022; Wang et al. 2015). Temporomandibular joint osteoarthritis is typically classified as a "low-inflammatory arthritic condition" and is not considered a systemic inflammatory condition. However, evidence indicates the significant involvement of various pro-inflammatory cytokines in its pathology, affecting both the articular cartilage and subchondral bone. These cytokines create an inflammatory environment within the synovial fluid, marked by increased secretion of molecules such as interleukin-1beta (IL-1 $\beta$ ), tumor necrosis factor alpha (TNF- $\alpha$ ), and interferon (IFN)- $\gamma$  (Deng et al., 2022; Lu et al., 2021; Goldring & Otero, 2011; Vernal et al., 2008). They also manipulate osteoclast production and bone resorption by amplifying the secretion of the receptor activator of nuclear factor (NF)- $\kappa$ B ligand (RANKL) in osteoblasts and synovial membrane fibroblasts (Lu et al., 2022).

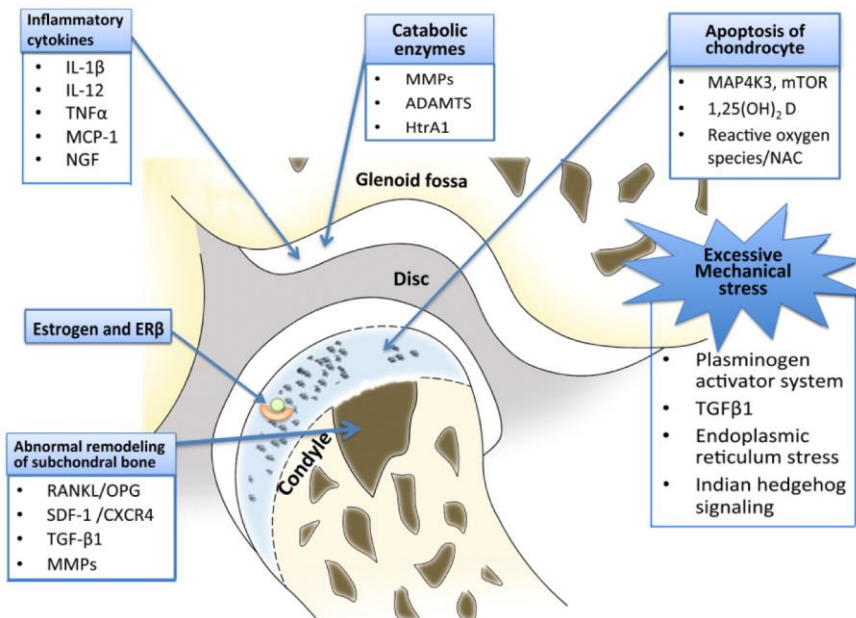


Figure 1.3: Illustration of mechanisms involved in temporomandibular joint osteoarthritis development. Adapted from "Current understanding of pathogenesis and treatment of TMJ osteoarthritis" by Wang, X.D. et al., 2015, Journal of Dental Research, 94(5), pp. 666–673.

Studies on rodent models indicate that chronic inflammation impacts the biomechanical properties of the TMJ disc, compromising its adaptive capacity and initiating degenerative changes (Cardoneanu et al., 2022; Wang et al., 2015). IL-1 $\beta$  also stimulates the TMJ synoviocytes and augments their production of monocyte chemoattractant protein-1 (MCP-1). Recent studies suggest that MCP-1 may initiate and sustain inflammation, even in the absence of IL-1 $\beta$ . In conjunction with this, the secretion of these cytokines appears to be inversely related to the synthesis of the articular cartilage matrix, suggesting a regulatory role in cartilage health (Ibi et al. 2018; Ogura et al. 2010; Wang et al. 2015). Moreover, inflammation significantly influences joint pain development, a common symptom among these patients. Specifically, pro-inflammatory cytokines like TNF- $\alpha$  or IL-1 $\beta$  can directly stimulate nociceptive receptors, increasing sensory neuron excitability. Other molecules, such as growth factors, proteoglycans, or proteases, are also implicated in arthritic pain development. In particular, matrix metalloproteinases-1, 3, and 9 (MMP-1, MMP-3, MMP-9) are identified as indicators of TMJ pain (Cardoneanu et al. 2022; Ita et al. 2022; Shrivastava, Battaglino, and Ye 2021; Schaible 2014). Interestingly, persistent mouth opening in mice lead to the development of chronic temporomandibular disorder and orofacial mechanical allodynia. This was accompanied by an increase in macrophages, which are indicators of inflammation, and activation of microglia in the trigeminal subnucleus caudalis, an essential component of the pain processing pathway. The utilization of a colony-stimulating factor-1 receptor inhibitor led to the deactivation of microglia and a decrease in pain sensitivity. These findings emphasize the involvement of inflammation in the emergence of temporomandibular disorder and indicate potential hazards associated with prolonged mouth opening during clinical procedures (Wang et al. 2018).

Along with the inflammation, mechanical overload also contributes to the development of TMJ OA. The distribution of mechanical loading on the joint's surface is pivotal for maintaining its integrity and functionality (Frost, 2001). The avascular TMJ cartilage relies on mechanical loading to facilitate the diffusion of synovial fluid within the cartilage matrix and deliver essential nutrients. Moreover, it enhances the diffusion of molecules such as growth factors, hormones, enzymes, and cytokines, while aiding in the removal of waste materials like lactate and carbon dioxide. Mechanical loading is also essential for mandibular growth and the maintenance of joint homeostasis (Betti et al., 2018; Kaul et al., 2016). As a biological system, the TMJ possesses the ability to adapt to changes in functional demands. For instance, when there is an increase in the load exerted on the TMJ, it triggers adaptive responses aimed at developing tissue structures capable of withstanding the imposed load. This adaptive process manifests as bone deposition or thickening of the articular cartilage, known as progressive remodeling. However, if the TMJ is consistently subjected to excessive loading, it can exceed its adaptive capacity, leading to regressive remodeling and the initiation of degenerative changes within the joint (Tran et al., 2023).

The anatomical and positional changes in the fibrocartilaginous disc between the condyles and the joint fossa may also contribute to TMJ OA (Cardoneanu et al. 2022; Wang et al. 2015). Studies have shown that approximately 60% of adolescents and young adults diagnosed with internal derangement of the joints, specifically disc displacement without reduction, also presented signs of condylar osteoarthritis. In these cases, there was a notable loss of continuity in the articular surfaces. This occurrence can be attributed to the interference caused by the displaced disc, which affected condylar mobility and subsequently increased the load on the articular surface. (Lei et al., 2017; Dias et al., 2016). Moreover, mechanical overloading of the TMJ has been associated with a decrease in the concentration of lubricin in the synovial fluid. This decrease

compromises the lubrication between articulating surfaces, alters the frictional properties of the condylar cartilage, and triggers the release of proinflammatory and matrix degradation mediators. Consequently, it results in a degeneration that resembles TMJ osteoarthritis (Asakawa-Tanne et al., 2015; Hill et al., 2014). Furthermore, in an experimental model of TMJ osteoarthritis induced by mechanical overload, Hif-1 $\alpha$  activation in mature chondrocytes has been observed. This activation leads to the repression of osteoprotegerin (OPG) expression, which, in turn, promotes osteoclastogenesis (Shirakura et al., 2010).

Interestingly, studies indicate that during the developmental stages in rats, a soft diet also detrimentally affects the quality and quantity of collagen and chondrocytes in the cartilage of the TMJ, as well as the density of the mandibular condyle's subchondral bone (Uekita et al., 2015; Chen et al., 2009). In cases of TMJ OA, the reduction of mechanical loading achieved through a soft diet results in a significant increase in the frequency of irregularities on articular surfaces, compared to a group maintained on a normal diet. Furthermore, rats with TMJ OA on a normal diet exhibited a greater increase in their bone volume fraction compared to those on a soft diet at a later stage. Based on these findings, it is crucial to transition TMJ OA patients back to a normal diet after implementing a soft diet during the acute stage of the disease (Tran et al., 2023).

The higher prevalence of TMJ OA among females, particularly during their reproductive years, has led researchers to investigate the potential contribution of estrogen to the degenerative changes observed in bone and cartilage in cases of TMJ OA (Sannajust et al. 2019; Lee et al. 2012). Estrogen exerts its regulatory influence on TMJ OA through estrogen-related receptors. Since these receptors have been identified in human articular chondrocytes, it is plausible that the combination of estrogen and estrogen receptors plays a role in estrogen's regulation of target organs (Zhao et al. 2019; Ahmad et al. 2009). Ovariectomized female rats, the standard animal



model for determining the effects of estrogen on tissues, were used in a recent in vivo study. One of the study groups was injected with  $17\beta$ -estradiol estrogen daily until the end of the experiment, which resulted in elevated estrogen plasma concentrations. This increase was associated with significant degradation of the mandibular condyle's cartilage in TMJ OA cases, which had been induced by a unilateral anterior cross bite. The degradation was characterized by a further decrease in cartilage thickness, an increased loss of extracellular matrix components such as collagen II and proteoglycan, and a heightened expression of pro-inflammatory (TNF- $\alpha$ ), catabolic (MMP-13 and VEGF), and hypertrophic (Collagen X) factors. Conversely, a lack of estrogen significantly mitigated these effects (Ye et al., 2020). Notably, DNA samples from 42 patients with degenerative joint disease had a higher prevalence of  $ERR\alpha$  genotypes compared to 36 control samples. This finding suggests that the presence of polymorphism could potentially influence  $ERR\alpha$  activity in bone, thereby contributing to the degenerative changes in the TMJ (Stemig et al., 2015).

Despite some studies showing the negative effects of estrogen, there are other reports indicating its protective influence on TMJ health. For instance, estrogen deficiency in ovariectomized mice resulted in decreased cartilage thickness, increased expression of pro-inflammatory cytokines, heightened osteoclastic activity, and TMJ degeneration (Wu et al., 2019). Given the inconclusive nature of the effects of estrogen on TMJ, researchers are still investigating the specific mechanisms behind these effects (Tian et al., 2022; Wu et al., 2019).

The female predominance of TMJ OA has also been linked to variations in TMJ anatomy and structure. On average, male condyles are larger and elliptical in shape, whereas female condyles tend to be smaller and more rounded. These differences may lead to altered biomechanics, rendering the female joint more prone to mechanical fatigue induced by joint loading (Coogan et

al., 2018). Comprehensive mechanical analyses of fibrocartilage-subchondral bone units in samples from human mandibular condyles have shown gender differences in energy dissipation and tissue loading. The articular fibrocartilage played an important role in dissipating energy and protecting the underlying subchondral bone against damage caused by high-energy occlusal loading. When the cartilage layer was removed to mimic osteoarthritis, the subchondral bone significantly contributed to energy dissipation in males. Conversely, the mechanical behavior of the cartilage-subchondral bone construct in females did not correlate with the properties of the subchondral bone. These findings suggest that the female mandibular condyle might have a mechanically disadvantageous structure when subjected to static occlusal and dynamic masticatory loading at the macro-level, increasing their risk to develop temporomandibular disorders (Kim et al., 2017). Assessments of joint-specific contact mechanics, employing, dynamic stereometry, have also shown a gender difference in the energy densities of TMJs. Specifically, women demonstrated significantly higher average energy densities compared to men. This discrepancy might accelerate the rate of mechanical fatigue on the articulating surfaces in females, contributing to their higher incidence of TMJ degenerative diseases (Robinson et al. 2020; Iwasaki et al. 2017).

Numerous studies have been conducted to investigate the involvement of cartilage in the pathology of TMJ osteoarthritis (Wang et al. 2015). The initial deterioration of cartilage can be driven by either metabolic or mechanical factors and involves a series of biomechanical changes in the joint's hard and soft tissues. This subsequently stimulates the immune response, culminating in the release of inflammatory substances like cytokines and chemokines. Alongside this, there is activation of the complement system and production of molecules that degrade cartilage, leading to the eventual wearing of joint cartilage and changes in the underlying bone (Cardoneanu et al.,

2022). Furthermore, disruptions in chondrocyte-matrix interactions, impairments in chondrocyte function and viability, and an imbalance in the formation and degradation of the cartilage matrix can contribute to TMJ OA pathology (Wang et al. 2015).

Over the past few years, a significant amount of research has focused on examining the impact of subchondral bone on the development of TMJ osteoarthritis (Ma et al. 2022; Zhang et al. 2022; Li et al. 2021; Embree et al. 2011). Irregular subchondral bone remodeling is suggested to be a key pathogenic process in TMJ OA. Specifically, an initial reduction in bone mass occurs, which acts as a catalyst for TMJ OA development and contributes to articular cartilage degradation. As the disease progresses, a gradual bone repair ensues, increasing bone density and resulting in higher stiffness at the condylar osteochondral interface (Hong & Kang, 2021; Chang et al., 2018).

At the cellular level, irregular bone remodeling in TMJ OA is associated with a decrease in the quantity and activity of osteoblasts (Cui et al., 2020). This shift in cellular dynamics includes an increase in metabolic processes favoring angiogenesis and osteoclastogenesis (Cardoneanu et al., 2022). The nuanced role of osteoblasts extends to the progression of subchondral sclerosis. These cells exhibit a distinct phenotype, producing higher levels of IL-6, IL-8, prostaglandin E2, VEGF and MMP-9, in comparison to osteoblasts from non-sclerotic areas (Sanchez et al., 2018; Jiao et al., 2014). Although sclerotic bone shows an increase in bone density and volume, it encounters a deficit in mineralization. The major molecular mechanism underlying this impaired matrix mineralization is the excessive production of type I collagen, the primary organic component of the bone matrix. This abnormal collagen synthesis is primarily attributed to altered signaling pathways, such as transforming growth factor- $\beta$  (TGF- $\beta$ ) and WNT/ $\beta$ -catenin (Bianco et al. 2018; Zuo et al. 2016; Li et al. 2013). In addition to the observed hypomineralization in the

sclerotic subchondral bone, there is an elevated intra-fibrillar mineral density, which reduces the ductility of the fibrils and exposes them to higher compressive stresses. Moreover, the sclerotic bone contains a larger number of chemically stable crystals, resulting in heightened bone stiffness and lower rates of bone turnover (Zuo et al., 2016).

Changes in osteoclasts activity were also observed in mouse models of TMJ OA. A TMJ differential gene analysis showed an increase in the expression of genes involved in osteoclast activity. There was also an increase in the migration and differentiation of osteoclast precursors, the number of TRAP-positive cells, and the ratio of RANKL to OPG within the TMJ subchondral bone. These results suggest an increase in osteoclast activity, which may have contributed to the initial increase in subchondral bone turnover (Wang et al. 2015; Yang et al. 2015; Embree et al. 2011). Adding to the intricate cellular dynamics involved in TMJ OA, osteocytes, the most abundant type of bone cell, also play an essential role in its pathogenesis. Their sensitivity to mechanical joint loading and production of RANKL contribute to osteoclastogenesis. Furthermore, osteocytes respond to various mechanical forces by resorbing the bone matrix, resulting in periacular/canalicular remodeling. The impairment of osteocyte-mediated bone remodeling can hasten the development of OA, eventually leading to subchondral bone sclerosis (Cardoneanu et al., 2022; Mazur et al., 2019).

#### **1.4. Treatment Strategies for Temporomandibular Joint Osteoarthritis**

The primary objectives in treating TMJ OA are pain relief, restoration of normal mandibular movements, and improvement in patients' quality of life (Al-Moraissi et al., 2020). In recent years, stem cell-based therapy has garnered considerable interest as a potential method for tissue repair and regeneration. Mesenchymal stem cells (MSCs) have the capacity for multilineage differentiation, including chondrogenic and osteogenic differentiation. When combined with suita-

ble scaffolds, MSCs can form cartilaginous or even osseous compartments to repair damaged tissue and restore TMJ function (Minervini et al., 2022). In a rabbit model of TMJ OA, intra-articular injection of MSCs was found to alleviate cartilage degeneration, disruption of the osteochondral junction, and loss of condylar bony surfaces in the subchondral bone compared to the untreated group (Kim, Yang, et al. 2019). Despite the promising preclinical evidence of stem cells' potential, the evaluation of this approach as a therapeutic measure for treating joint diseases in humans is limited due to FDA restrictions, particularly regarding drug-device combinations or biologic-device combinations, which require laboratory manipulation. Furthermore, for future studies, the standardization of animal models and quantitative outcome evaluations, including biomechanical, biochemical, histomorphometric, and radiographic assessments, would enable more reliable comparisons of the efficacy and safety of these approaches. Ultimately, this would increase the validity of the results, providing a solid foundation for clinical application (Matheus, Özdemir, and Guastaldi 2022; Almarza et al. 2018; Helgeland et al. 2018).

Currently, treatment strategies for TMJ OA fall into three categories. Firstly, conservative approaches encompass patient education and counseling, occlusal splints, physiotherapy (including manual therapy and home muscle exercises), and medications. Secondly, minimally invasive options involve intraarticular injections of pharmacological agents such as hyaluronic acid, corticosteroid, and growth factors found in platelet-rich plasma, as well as arthrocentesis. Lastly, surgical interventions ranging from arthroscopic procedures to open joint surgeries such as disc plication, discectomy, and arthroplasty (Murakami 2022; Derwich, Mitus-Kenig, and Pawlowska 2020; Schiffman, Velly, et al. 2014).

Patient education and counseling are essential aspects of managing TMD, involving the provision of information on the underlying causes, treatment options, and prognosis of the condition,

along with recommendations for behavioral changes. Patient education has been shown to influence patients' behaviors related to TMD, such as habits of "putting pressure on the jaw", "chewing food on one side" "pressing, touching, or holding teeth together at times other than eating", "eating between meals", and "yawning". However, it is important to note that education should be conducted at different intervals to ensure the continuity of desired behavioral changes. (Xu et al., 2021).

Occlusal splint is an important element in non-surgical therapy (Figure 1.4). It prevents patients from achieving maximum intercuspation and promotes proper jaw positioning with equal intensity stops on all teeth. Occlusal splint also facilitates positioning



the condyles in centric relation, leading to the development of new muscle and articular balance (Albageieh et al., 2023; Yadav & Karani, 2011). Consequently, the detrimental effects of traumatizing factors and overloading on the joint are reduced, resulting in decreased inflammation and pain (Al-Ani, 2021; Machon et al., 2011). The duration of wearing occlusal splints varies according to the type of therapy and rate of recovery. Notably, a splint that does not cover all teeth or achieve balanced occlusion with the opposing teeth should not be worn continuously to prevent irreversible occlusion changes (Albageieh et al., 2023). In follow-up trials ranging from one month to a year, the use of occlusal splints has consistently demonstrated positive treatment out-

Figure 1.4: Utilization of Michigan splint for treatment of TMD. Adapted from "Occlusal splints-types and effectiveness in temporomandibular disorder management" by Albageieh et al. 2023, Saudi Dent J. 2023 Jan; 35(1): 70–79.

comes, including reduced TMJ pain and improved mouth opening capacity (Albagieh et al., 2023; Fouda, 2020).

Physiotherapy is another therapeutic option for TMJ OA. It improves strength, mobility, and coordination, along with reducing joint and muscle discomfort (Rashid et al., 2013). A recent meta-analysis showed that occlusal splint therapy and exercise therapy had comparable effectiveness in alleviating pain and enhancing mandibular movement during the treatment (Zhang, Xu, et al. 2021).

Nonsteroidal anti-inflammatory drugs (NSAIDs) are advantageous in the treatment of TMJ OA as they can reduce pain and inflammation simultaneously. To maximize their anti-inflammatory effect, it is important to take NSAIDs not only when necessary but also on a regular basis (Al-Ani, 2021). The average duration of NSAID use is two to four weeks. To reduce the risk of gastrointestinal and cardiovascular complications associated with their use, it is critical to use the lowest effective dose for the shortest possible duration. Combining splint therapy with NSAIDs administration has shown to provide earlier pain relief, especially for patients experiencing severe pain in the TMJ area in the course of TMJ (Derwich, Mitus-Kenig, and Pawlowska 2021).

In symptomatic patients unresponsive to conservative treatment, intra-articular injections of hyaluronic acid (HA), corticosteroid (CS), and growth factors found in platelet-rich plasma (PRP) can be utilized either independently or as a post-operative measure following procedures such as arthrocentesis or arthroscopy (Bergstrand et al., 2019; Bouloux et al., 2017; Hegab et al., 2015; Fernández Sanromán et al., 2016). HA is a polysaccharide produced by chondrocytes and synovocytes in the joints. The introduction of HA into the TMJ may be beneficial due to its lubricating and anti-inflammatory properties. Additionally, HA possesses analgesic properties due to its ability to reduce ion channel sensitivity in mechanoreceptors and nociceptors (Bouloux et al.,

2017). Corticosteroids are frequently used for their potent anti-inflammatory effect, which aids in relieving joint pain and improving functionality (Al-Ani, 2021). PRP is an autologous solution of platelets containing multiple growth factors, with concentrations 3 to 8 times higher than that of whole blood. It can stimulate chondrocytes to produce cartilage matrix and increase the production of hyaluronic acid by synoviocytes (Zotti et al., 2019). In the treatment of TMJ OA, intra-articular injections of HA have been found to be more effective at reducing pain compared to injections of CS or physiological saline solution (Derwich, Mitus-Kenig, and Pawlowska 2021). Interestingly, in long-term follow-up studies extending up to one year, PRP intra-articular injections have consistently shown superior results to HA in terms of pain reduction and increasing interincisal distance (Zotti et al., 2019; Hegab et al., 2015).

Another minimally invasive procedure, recommended for patients experiencing pain unresponsive to conservative treatment, is arthrocentesis.

This technique involves the insertion of a cannula into the joint space to flush the TMJ using sterile needles and irrigation solutions (Figure 1.5). The procedure does not require direct visualization of the joint space. Its principal advantage is the direct removal of inflammatory substances, degradation products, and adhesions from within the joint. This process effectively alleviates pain and enhances jaw mobility, ultimately leading to an increase in maximal interincisal opening (Al-Ani,

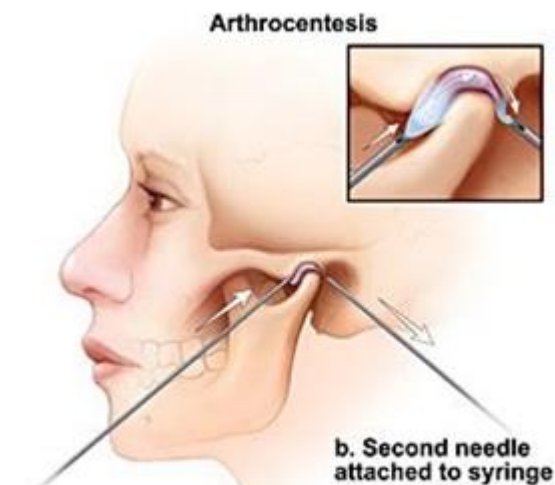


Figure 1.5: Schematic representation of TMJ arthrocentesis procedure with two needles insertion into the joint space. Adapted from “What is TMJ arthrocentesis?” Available at: <https://dentagama.com/news/what-is-tmj-arthrocentesis> (Accessed: 12 July 2023).

2021; Bergstrand et al., 2019; Soni, 2019; Leibur et al., 2015). Compared to arthrocentesis alone,



the combination of arthrocentesis with hyaluronic acid injection results in a significant improvement in mouth opening, as well as lateral and protrusive movements (Gurung et al., 2017).

Arthroscopy is a surgical technique that lies on the spectrum between arthrocentesis, a less invasive procedure, and open surgery, a more invasive approach (Fernández Sanromán et al., 2016). This procedure involves the insertion of an arthroscope into the joint space, providing a visual examination of internal joint structures, including articular disc perforations, synovitis, and adhesions (Fernández Sanromán et al., 2016). It also allows removal of osteophytes, expansion of the joint space through the inflation of balloon stents, joint lavage, and the precise delivery of therapeutic agents to specific areas within the joint, minimizing the impact on unaffected regions (Al-Ani, 2021). Patients with TMJ OA who undergo arthroscopic surgery experience statistically significant reductions in pain and enhancements in maximum interincisal opening distance. However, candidates who received earlier intervention have better outcomes than those who received intervention later, suggesting that early arthroscopic surgery intervention is beneficial (Israel et al., 2010).

Open TMJ surgery is typically advised when minimally invasive procedures are unable to effectively treat the condition or in cases of advanced disease accompanied by severe joint degeneration, functional impairment, and/or dentofacial deformity. Arthroplasty is often the prevailing surgical technique for patients with TMJ OA. It entails reshaping the bone through a range of procedures, starting with a high condylar shave and extending to a condylectomy (Renapurkar, 2018). A total joint replacement becomes the treatment of choice when all other modalities, including conservative measures, minimally invasive procedures, and surgical interventions, have failed to restore normal mouth function and alleviate pain (Balon et al., 2019).

The literature that compares various invasive, minimally invasive, and non-invasive treatments for temporomandibular joint osteoarthritis presents diverse, and at times, conflicting views. As such, providing definitive therapeutic guidelines has been a significant challenge. Interestingly, a recent network meta-analysis has demonstrated that minimally invasive procedures significantly outperform non-invasive procedures in both short-term (up to 5 months) and intermediate-term (6 months–4 years) durations, particularly in alleviating pain and enhancing maximum mouth opening in TMJ OA patients. Intriguingly, intra-articular injections with hyaluronic acid appear to be the most effective among minimally invasive procedures for short-term pain relief. For intermediate-term pain reduction, however, there was no discernible difference among intra-articular HA injections, arthrocentesis, and arthroscopy. When it comes to improving mouth opening, arthroscopy—whether used with or without drug instillations—clearly dominates, as it is significantly more effective than intra-articular injections and arthrocentesis, including those utilizing drug instillations. Both arthroscopy and arthrocentesis benefit greatly from the addition of pharmacological instillations, such as platelet-rich plasma and hyaluronic acid. Contrary to traditional beliefs that advocate for the full exploration of conservative treatments before resorting to minimally invasive procedures, these findings propose that techniques such as intra-articular injections and arthrocentesis should be initiated earlier, particularly when patients do not show noticeable benefits from the initial conservative treatments (Al-Moraissi et al., 2020). Notably, prolonged delays not only contribute to increased time and expenses but may also exacerbate the ongoing TMJ pathophysiology and potentially compromise the patient's capacity to manage symptoms, thereby diminishing the prospects for optimal outcomes that are typically associated with earlier treatment initiation (Murakami, 2022; Vos et al., 2014).

Given the rising prevalence of temporomandibular joint osteoarthritis and the multifaceted nature of its causes, as well as the limited efficacy of current therapeutic approaches in arresting or reversing cartilage and subchondral bone deterioration, and the challenge in determining when to switch to other treatment measures, the scientific importance of predicting the disease response to conservative interventions and early diagnosis becomes paramount (Murakami 2022; Yuan et al. 2022; Lee, Park, et al. 2020).

## **1.5. Diagnosis of Temporomandibular Joint Osteoarthritis**

### ***1.5.1 Crepitus, Pain and Co-morbidities in TMJ OA***

According to the DC/TMD, the physical diagnosis of TMJ OA (axis I) is considered positive when either the patient reports any TMJ noise in the last 30 days (during mastication or any jaw movement) or the clinician detects any noise with jaw movements during the clinical examination. TMJ OA diagnosis also requires the detection of crepitus (eg, crunching, grinding, or grating noises) during the examination (Schiffman and Ohrbach 2016; Schiffman, Ohrbach, et al. 2014).

Crepitus can arise from the heightened friction between the articulating surfaces in the joint, as well as from direct bony contacts in cases of TMJ OA cases that are associated with disc displacement or perforation of the posterior disc attachments (Cardoneanu et al. 2022; Mehndiratta et al. 2019; Vrbanović and Alajbeg 2017).

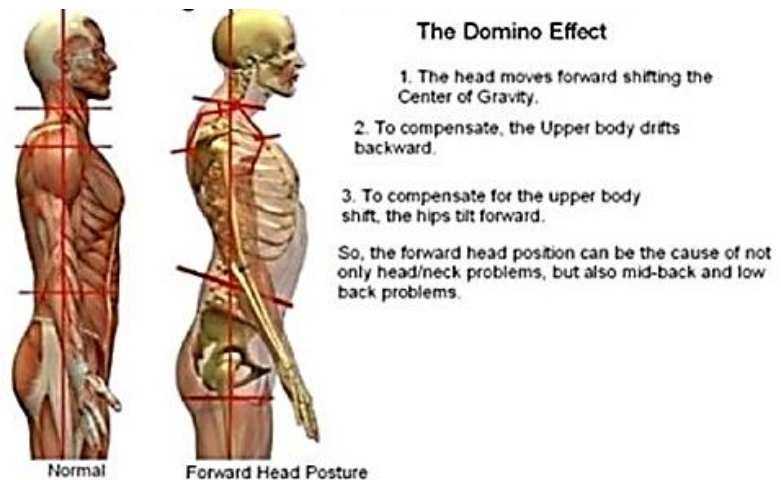
In conjunction with validated clinical examination criteria for diagnosing TMJ OA, the DC/TMD provides a questionnaire to assess the patient's pain history and evaluate the psychosocial and behavioral factors (axis II) that might influence their response to treatment (Schiffman and Ohrbach 2016).

Patients with TMJ OA frequently experience debilitating joint pain, with females being more prone to chronic and persistent pain than males (Sannajust et al. 2019). The primary source of pain in OA is commonly attributed to the activation of an inflammatory process which affects different components of the joint, such as the bone, periosteum, synovium, capsule, and peri-articular structures (Al-Ani 2021). In fact, individuals with higher levels of inflammatory mediators exhibit higher levels of pain intensity during maximum mouth opening and increased discomfort with mandibular movements compared to those with lower inflammatory activity (Chung et al. 2023). Importantly, elevated levels of pain may indicate presence of a clinically significant disease as well as the patient's experience of symptom amplification due to emotional distress or central sensitization (Ferrillo et al. 2022). Individuals with TMJ OA also show increased mechanical hyperalgesia when blunt pressure is applied to the skin overlying the affected joint, compared to patients with TMJ pain without degeneration (arthralgia). This heightened pain sensitivity can result from sensitization in the central and peripheral nervous systems, where pain processing by nociceptive pathways is altered, as well as changes in membrane channels and neurotransmitters. These alterations ultimately lead to a decrease in neuronal threshold activation, an increase in firing rate, expansion of receptor fields, and a change in the sensory response to normal input (Ferrillo et al. 2022; La Touche et al. 2018; Kothari et al. 2016). In cases of widespread pain, it is crucial to assess the patient's systemic condition as it might have a clinically significant impact on localized joint pain (Shim et al. 2020). Furthermore, parafunctional behaviors should be thoroughly examined as they may place undue strain on masticatory structures, triggering or exacerbating the patients' pain (Abouelhuda et al. 2017; Schiffman and Ohrbach 2016; Cairns 2010).

Interestingly, individuals with painful temporomandibular disorders (TMD) exhibit a high prevalence of comorbidities, including headaches, lower back pain, and sleeping disorders (Shrivastava, Battaglino, and Ye 2021; Bair et al. 2016; Slade et al. 2016). Subjects with TMD pain are approximately twice as likely to report headaches compared to subjects without TMD pain. Furthermore, the presence of headaches has been linked to an increased risk of developing TMD (Yakkaphan et al. 2022; Nixdorf, Velly, and Alonso 2008). The association between headaches and TMD can be attributed to genetic, anatomical and neurological connections (Byun et al. 2020). Certain genes, such as ESR1 and COMT, have been identified as potential factors predisposing individuals to the concurrent development of TMD and headaches (Cruz et al. 2022). Both conditions are also intricately connected to the nociceptive system. The initial neurons involved in headaches are connected to the first branch of the trigeminal nerve, while in cases of TMD, they are associated with the third branches of the trigeminal nerve (Mello et al. 2012; Pedullà et al. 2009). This nociceptive information converges at the caudal nucleus of the trigeminal nerve, where headaches and TMD share specific ascending pain pathways, thus playing a role in pain modulation (Yakkaphan et al. 2022). Aside from their shared neurophysiological connections, headaches and TMD may share a hormonal basis as both conditions are more common in females. Sex hormones may also influence trigeminal nerve sensitization by modulating nociceptive mediators like calcitonin gene-related peptide. Additionally, they affect the synthesis of serotonin neurotransmitters in the brain, which is known to participate in pain signaling and modulation within the central nervous system (Byun et al. 2020; Plesh et al. 2012; Gupta et al. 2011). Importantly, the presence of headaches intensifies joint pain, which can influence the efficacy of the disease management (Byun et al., 2020; Di Paolo et al., 2017; Proporatti et al., 2015; Christidis et al., 2014).

Chronic low-back pain (LBP) is the most common musculoskeletal disorder in adults, with chronic TMD pain being the second most common (Wieckiewicz, Shiau, and Boening 2018). A longitudinal study conducted on a nationwide-matched cohort population showed a 1.5-fold increased risk of first onset TMD in patients with LBP. This was particularly noticeable when the duration of LBP exceeded six years, during which TMD symptoms became more pronounced (Lee, Wu, et al. 2020). Interestingly, individuals with TMD are 5.5 times more likely to endure pain in other joints, with the lower back being one of the most frequently affected areas (Wiesinger et al. 2007). The high prevalence of back pain in TMD patients may be linked to the broader impact of TMD on overall body posture. Factors such as the center of foot pressure, body sway, and spinal

curvature are all likely to be influenced by TMD (Kim, Ko, et al. 2019). In patients with TMD, the position of the head is often depressed due to alterations in the masticatory muscles that influence the position of the jaw. Hence, changes in proprioceptive afferents related to mandibular



position may occur, potentially affecting gait stability and the center of pressure on the foot

Figure 1.6: The relationship between head posture and lower back pain in patients with temporomandibular disorders. Adapted from “Connection between TMJ and body posture” Available at: <https://www.tonguetieindia.com/connection-between-tmj-and-body-posture.html> (Accessed: 12 July 2023).

(Minervini et al. 2023; Kang 2020; Chung et al. 2016). Changes in foot function, as measured by center of pressure, have been linked to low back pain in women (Menz et al. 2013). Therefore,

alterations in the masticatory muscles and mandibular position in TMD patients may ultimately lead to low back pain (Figure 1.6) (Garstka et al. 2022).

To maintain balance, the axial muscles of the human body, including the head and vertebral column, contract simultaneously. The contraction of each muscle is often interconnected with the contraction of other muscles. Continuous muscle contraction can restrict blood flow and trigger the activation of pain receptors. As a result, when the muscles in the face are consistently contracted, motor centers in the face and spinal cord may be activated, resulting in muscle contractions in these areas. This process can reduce blood supply over time, resulting in muscle spasms and pain. This lends credence to the clinical link between lower back pain and TMD (Agha-Hosseini et al. 2023). Furthermore, those with LBP experience greater difficulty in recruiting neck muscles to assist with jaw-related tasks. Consequently, increased stress is placed on the masticatory system and jaw muscles, promoting the development of TMD over time (Lee, Wu, et al. 2020). An additional factor that may influence this complex interplay is the presence of a common central dysregulation in the modulatory pathways of pain processing in both TMD and lower back pain (Minervini et al. 2023; Kim, Ko, et al. 2019; Prim et al. 2019; Monaco et al. 2017).

Sleep disturbances are frequently observed in individuals with painful temporomandibular joint disorder, with 82% of TMJ OA patients experiencing them when compared to healthy controls. Despite the reduction in pain symptoms, approximately 71% of the TMJ OA group continues to experience poor sleep quality during the follow-up period. This suggests that there may be other contributing factors to their sleep problems, such as chronic lower back pain (Rener-Sitar et al. 2016). Interestingly, the quality of sleep among individuals with painful TMD can vary depending on the origin of the pain. Specifically, those experiencing mixed pain tend to have signifi-

cantly higher Pittsburgh Sleep Quality Index scores, indicating poorer quality of sleep, compared to individuals with arthralgia only. Furthermore, the mixed pain group often reports experiencing headaches along with the sleep problems (Lee and Auh 2022; Roithmann et al. 2021). Importantly, research has shown that sleep disturbances are not merely a consequence of TMD pain, but they can also be a predictor of TMD onset. Individuals with primary sleeping disorders are at a 44% higher risk of developing TMD compared to those without such disorders. The interrelationship between sleep problems and TMD may involve several pathological processes. However, the exact mechanism underlying this interplay has yet to be elucidated (Kim et al. 2021). Sleep disturbances are linked to increased levels of circulating cytokines, which may contribute to the development of TMD. These cytokines can cause pain either directly by activating specific receptors on nociceptive sensory neurons or indirectly through other mediators such as prostanooids and amines (Park and Chung 2016). Sleep disturbances can worsen people's psychological conditions, which contribute to the exacerbation of TMD symptoms (Roithmann et al. 2021). During normal sleep in healthy individuals, nociceptive transmission is partially attenuated to preserve sleep continuity, resulting in a higher threshold or lower response rate to noxious stimuli (Lavigne and Sessle 2016). On the other hand, individuals with temporomandibular disorder experience heightened pain sensitivity and central sensitization, which may influence nociceptive transmission, disrupt their sleep, and significantly increase their pain reactivity (Reid et al. 2022; Krause et al. 2019).

### ***1.5.2 Imaging Signs of TMJ OA, Prevalence, and Modalities***

Considering the suboptimal sensitivity and specificity of TMJ OA clinical criteria (55% and 61%, respectively), imaging emerges as the gold standard for its diagnosis (Hilgenberg-Sydney et al. 2018; Schiffman and Ohrbach 2016; Schiffman, Ohrbach, et al. 2014). The significance of



integrating imaging techniques with history and clinical examination in assisting physicians' clinical decision-making is further emphasized, as it has been shown to alter 58% of the primary diagnosis and planned management in patients with temporomandibular disorders. This is particularly noteworthy for individuals experiencing restricted mandibular movement, functional limitations, and joint pain upon palpation (Talmaceanu et al., 2018; de Boer et al., 2014). The RDC/TMD criteria briefly described the tomography-based image analysis criteria for TMJ OA (Dworkin and LeResche 1992). However, as the utilization of orthopantomogram, magnetic resonance imaging, and computed tomography increased, the RDC/TMD validation initiative recognized the need for comprehensive criteria that would accommodate these advanced imaging techniques (Ahmad et al. 2009). Consequently, radiologists and TMD clinicians collaborated to develop diagnostic criteria for image analysis by leveraging a thorough review of existing literature, recommendations from an external advisory panel appointed by the NIDCR, and input from the TMD and radiology communities. Osteophytes, surface erosions, subchondral cysts, and generalized sclerosis were identified as the cardinal diagnostic imaging features for TMJ OA (Figure 1.7) (Schiffman and Ohrbach 2016; Schiffman, Ohrbach, et al. 2014; Ahmad et al. 2009).

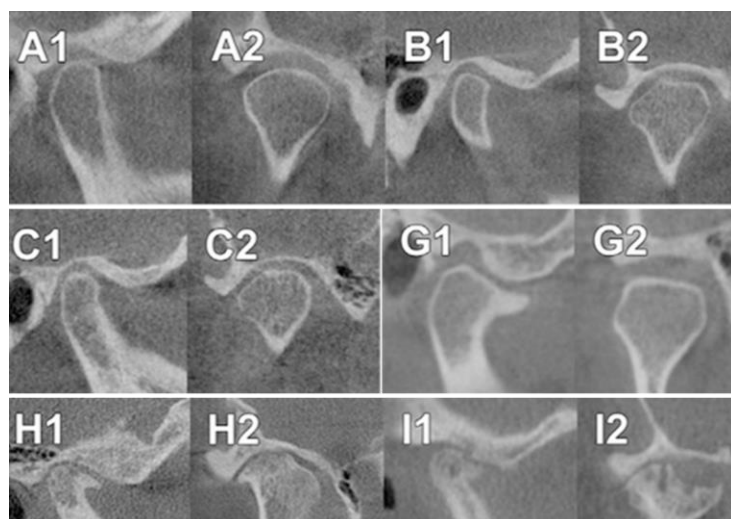


Figure 1.7: Representations of a healthy TMJ and degenerative bone changes in sagittal (1) and coronal (2) CBCT orientations. Each letter corresponds to an image of the same individual. (A) A healthy TMJ with smooth, rounded, and well-defined condylar cortical margins. (B,C) Flattening and localized subcortical sclerosis of the condylar head, respectively, suggestive of joint remodeling. (G-I) Degenerative bone changes in TMJ OA (G1) An osteophyte on the anterior aspect of the condyle. (G2) Flattening of the superior and lateral slopes of the condyle. (H) The presence of osteophytes and multiple subchondral cysts. (I) The presence of osteophytes and multiple areas of erosion. Adapted

from “Temporomandibular joint disorders and orofacial pain” by Ahmad, M. and Schiffman, E.L, 2016, *Dental Clinics of North America*, 60(1), pp. 105–124.

Osteophytes refer to the development of angular osseous tissues with sclerotic borders projecting from the surface (Ahmad and Schiffman 2016; Sadaksharam and Khobre 2016; Ahmad et al. 2009). They can emerge from distinct locations within the joints including periarticular sites adjacent to hyperplastic synovial membrane and the articulating surfaces, with skeletal progenitor cells of distinct origins involved in the initiation of these skeletal defects (Bechtold et al. 2016). Instability of the joint serves as a biomechanical trigger for the formation of osteophytes. This occurs when mechanical stresses exceed the body's capacity for adaptation, resulting in the formation of osteophytes. The purpose of these growths is to increase the joint's surface area in order to improve its resistance to loaded forces (Lan et al. 2022; Sadaksharam and Khobre 2016). However, the presence of osteophytes on the condylar surface can also contribute to irregularities, leading to a more damaging distribution of forces within the joint. This effect is particularly prominent in specific regions where the contact area is diminished. When concentrated force vectors develop on a particular area of the condylar surface, the disparity in force generation between the superior and inferior joint compartments becomes significant. This imbalance in loading forces and torque ultimately results in an advanced disease state (Kirk and Kirk 2006). Osteophytes can also lead to pain, reduced jaw mobility, and limited joint function (Sadaksharam & Khobre, 2016; Kraan & Berg, 2007).

Surface erosions refer to discontinuities in the articular cortex of the condyle or the fossa. While the presence of osteophytes suggests that the condyle has adapted to degenerative changes, the radiographic evidence of erosions indicates a potentially active destructive process (Bae et al. 2017). Several mechanical factors can contribute to erosion formation, including disc displace-

ment, overloading, increased friction during mandibular movement, and trauma (Emshoff et al. 2021; Ahmad et al. 2009). The presence of erosions increases the risk of osteoarthritis development by a factor of 1.6 to 27.4 (Al-Ghurabi and Al-Hawa 2023). Their frequency is also directly proportional to pain intensity in patients with degenerative joint diseases (Chung et al. 2023; Bae et al. 2017; Emshoff et al. 2016).

Subchondral cysts are commonly observed in individuals with temporomandibular joint osteoarthritis. They are characterized as cavities that deviate from the normal marrow pattern and are typically located adjacent to the joint surface where the initial load bearing takes place during activities (Jeon et al. 2022; Ahmad and Schiffman 2016; Ferrazzo, Osório, and Ferrazzo 2013; Ahmad et al. 2009). Based on the histological characteristics of subchondral cysts, it could be argued that the term 'cyst' is not wholly accurate, as these cavities are not lined by epithelial cells and do not contain evenly distributed liquid components (Kaspiris et al. 2023). The subchondral cysts are usually spherical or ellipsoidal in shape, occur in multiple numbers, vary in size, and emerge as the result of the bone's attempt to adapt to increased loads (Crema et al. 2010; Bancroft, Peterson, and Kransdorf 2004). Currently, there are two hypotheses that could explain the origin of subchondral cysts in OA: the bone contusion theory and the synovial fluid invasion theory. According to the bone contusion theory, subchondral bone cysts develop as a result of traumatic impact or repetitive microtrauma, which cause localized damage and disruption of the trabecular bone architecture. Following the contusion, the affected area undergoes a reparative process involving the recruitment of osteoclasts and osteoblasts. However, an increase in bone resorption and inadequate bone formation occur, resulting in the formation of a cavity that gradually enlarges into a cyst (Jeon et al. 2022; Pouders et al. 2008). On the other hand, the synovial fluid invasion theory proposes that subchondral bone cysts develop when synovial fluid infil-

trates the subchondral bone. Under normal circumstances, a thin layer of cartilage separates the subchondral bone from the synovial fluid. However, in certain conditions such as joint trauma, repetitive joint loading, or increased friction between the opposing surfaces, the integrity of the articular cartilage may be compromised. This can lead to the formation of fissures, clefts, or defects that allow the synovial fluid to invade the subchondral bone. The synovial fluid contains enzymes and inflammatory mediators, eventually resulting in a net loss of bone and the formation of a subchondral bone cyst (Jeon et al. 2022; Bessa et al. 2020; Chiba et al. 2014; Li et al. 2013). Notably, the frequency of subchondral cysts could increase with the severity of the disease. The heightened expression of MMP-1 in the osteoblast-like cells lining the subchondral cyst may account for the degradation of non-mineralized collagen type I, leading to the exposure of binding sites on the bone surface and the subsequent stimulation of osteoclasts, ultimately contributing to the progression of the disease (Kaspiris et al. 2013).

Additional radiographic findings that can be observed in TMJ OA are the flattening of the articular surface and the presence of subcortical sclerosis. Articular surface flattening refers to the loss of the normal rounded shape of either the condyle or the articular eminence surface. However, if there is no evidence of osteophyte, sclerosis, subchondral cyst, or erosion, and if the thickness of the cortical plate appears relatively even, then surface flattening alone is not a reliable indicator of OA. In such cases, it should be interpreted as a remodeled or deformed joint, particularly in young patients who often have joint deformities resulting from previous traumas (Larheim et al. 2015; Ahmad et al. 2009). Subcortical sclerosis is characterized by an increased thickness of the cortical plate in areas subjected to load bearing, compared to adjacent non-load-bearing areas. When this thickening is localized, it is considered indeterminate for osteoarthritis and is believed to be a result of elevated or normal loading when the disc in the TMJ is displaced. However,

when the orientation of trabecular bone and the differentiation between the cortical layer and trabecular bone on the condylar head become unclear, which is known as generalized sclerosis, it is considered a feature of the late stage of temporomandibular joint osteoarthritis (Larheim et al. 2015; Li et al. 2013; Ahmad and Schiffman 2016; Ahmad et al. 2009).

Although imaging features such as osteophytes, erosions, cysts, and generalized sclerosis are commonly observed in temporomandibular joint osteoarthritis, their distribution varies among different studies (Bae et al. 2017). According to the Otterson group (2019), the most prevalent imaging signs of TMJ OA include articular surface flattening (79%), osteophytes (72%), and subcortical sclerosis (70%), followed by surface erosion (40%) and subcortical cysts (15%) (Ottersen et al. 2019). Conversely, Dumbuya and colleagues (2020) reported that subchondral cysts (63.3%) and osteophytes (60%) were the most frequently observed degenerative bone changes in the condyles. In a study by Maleki et al. (2018), the most common bony changes in the temporomandibular joint were found to be flattening (82.5%), erosion (41.25%), sclerosis (28.12%), and osteophytes (25.62%), in descending order.

The inconsistencies in the findings may stem from varying sample sizes, differences in study population, and diverse study design. For instance, retrospective studies often suffer from incomplete and heterogeneous data, as well as data collection performed by different clinicians using different protocols (Arayasantiparb et al. 2020; Ottersen et al. 2019).

Interestingly, disparities in imaging techniques and interpretation appear to have an impact on the identification of bone changes associated with osteoarthritis (Bae et al. 2017). In fact, a study investigating the reliability of radiologists in diagnosing the status of osseous tissue for osteoarthritis using orthopantomogram (OPG) reported poor inter-examiner reliability, with a kappa ( $\kappa$ ) value of only 0.16. However, when magnetic resonance imaging (MRI) was used, the reliability

improved to a fair level ( $\kappa = 0.47$ ). The highest reliability was observed when diagnosing hard tissue status using computed tomography (CT) images, reaching good levels ( $\kappa = 0.71$ ), almost reaching the threshold for excellent reliability ( $\kappa > 0.75$ ). The agreement rate among the examiners for diagnosing OA using panoramic radiography images was found to be 19%. However, when MRI was employed, the agreement rate increased to 59%. Furthermore, the highest agreement rate was achieved when CT images were used, reaching 84%. Using CT as the reference standard, panoramic radiography had low sensitivity in detecting osteoarthritis, yet the specificity was high. Conversely, MRI had marginal sensitivity, while the specificity remained high. When osteoarthritis was detected on CT, 26% of panoramic radiographs and 59% of MRI scans displayed positive findings. When osteoarthritis was not detected on CT, 99% of panoramic radiographs and 98% of MRI scans were also negative for osteoarthritis. These findings indicate that panoramic radiography and MRI have their respective strengths and limitations in terms of sensitivity and specificity in detecting temporomandibular joint osteoarthritis. Hence, the DC/TMD recommends utilizing CT to confirm the diagnosis of TMJ OA (Hilgenberg-Sydney et al. 2018; Schiffman and Ohrbach 2016; Larheim et al. 2015; Schiffman, Ohrbach, et al. 2014; Ahmad et al. 2009).

The low sensitivity of OPG in detecting signs of TMJ OA may be attributed to the ability to assess only the lateral portion of the condyle. This limitation hampers the detection of osteophytes that are frequently present on the anterior surface of the condyle. Furthermore, the erosion of the condyle's articular margin remains concealed due to overlapping with the zygomatic arch and the base of the skull (Kaimal et al., 2018; Talmaceanu et al., 2018; Ferrazzo et al., 2013; Ahmad et al., 2009). MRI offers several benefits, including the absence of ionizing radiation exposure, enhanced visualization of soft tissue details, bone marrow alterations, and assessment of disc posi-

tion, shape, and integrity. However, the moderate sensitivity of MRI in detecting bone changes is likely attributed to challenges in detecting minor osteophytes or erosive changes in the cortical plate (Kaimal et al. 2018; Ahmad et al. 2009). Although CT demonstrated superiority over panoramic radiography and MRI in displaying TMJ OA features, cone-beam CT (CBCT) is recommended for evaluating TMJ OA due to its superior cost-benefit ratio and lower radiation dose (Arayasantiparb et al. 2020; Dumbuya et al. 2020; Abrahamsson et al. 2017). The effective radiation exposure of CBCT scanners can vary between 7.3 and 288.9  $\mu\text{Sv}$ , whereas conventional CT scans typically range from 1320 to 1400  $\mu\text{Sv}$ , depending on the utilized protocol (Larheim et al. 2015; Hussain et al. 2008). CBCT also has the capability to capture all essential images in a single rotation, resulting in a scanning time ranging from 10 to 70 seconds (Larheim et al. 2015; Krishnamoorthy, Mamatha, and Kumar 2013). Moreover, the diagnostic accuracy of CBCT in detecting condylar osseous abnormalities (0.9) is comparable to that of CT (0.86) (Figure 1.7) (de Boer et al. 2014). This can be attributed to the isotropic voxel resolution in CBCT as well as its spatial resolution that ranges from 0.4 mm to 0.09 mm, achieving sub-millimeter accuracy (Venkatesh and Elluru 2017). In terms of sensitivity, CBCT exhibits a value of 0.8 in detecting degenerative bone changes in TMJ, while CT has a value of 0.7. Therefore, the diagnostic qualities of CBCT are comparable to or even superior to those of the current imaging modalities (Larheim et al. 2015; de Boer et al. 2014; Spin-Neto, Gotfredsen, and Wenzel 2013). Interestingly, as the extent of bone defects reduces, the sensitivity of CBCT in detecting decreases. Specifically, when employing CBCT images with a voxel size of 0.4 mm, one-third of the simulated bone defects with a diameter and depth less than 2 mm can be missed during diagnosis. However, by employing a greater scan resolution (0.2-mm voxel size), all defects can be detected, regardless of their size, with an accuracy exceeding 80% (A. Patel et al. 2014).

The diagnostic accuracy of CBCT scans for condyle defects is also influenced by the size of the field of view (FOV), with smaller FOV achieving higher accuracy (Salemi et al. 2016). Therefore, it is essential for the clinician to adjust the parameters appropriately during CBCT imaging in order to achieve optimal images tailored to the specific diagnostic requirements. For instance, when utilizing a limited CBCT unit, the FOV can be reduced to 4 cm x 4 cm x 4 cm, and images can be captured with a voxel size as low as 78  $\mu\text{m}$ . Such limited FOV scans facilitate adequate assessment of the anatomical structures within a single temporomandibular joint, including the condylar head, glenoid fossa, and articular eminence (Figure 1.8) (Venkatesh and Elluru 2017; Barghan, Tetradis, and Mallya 2012).

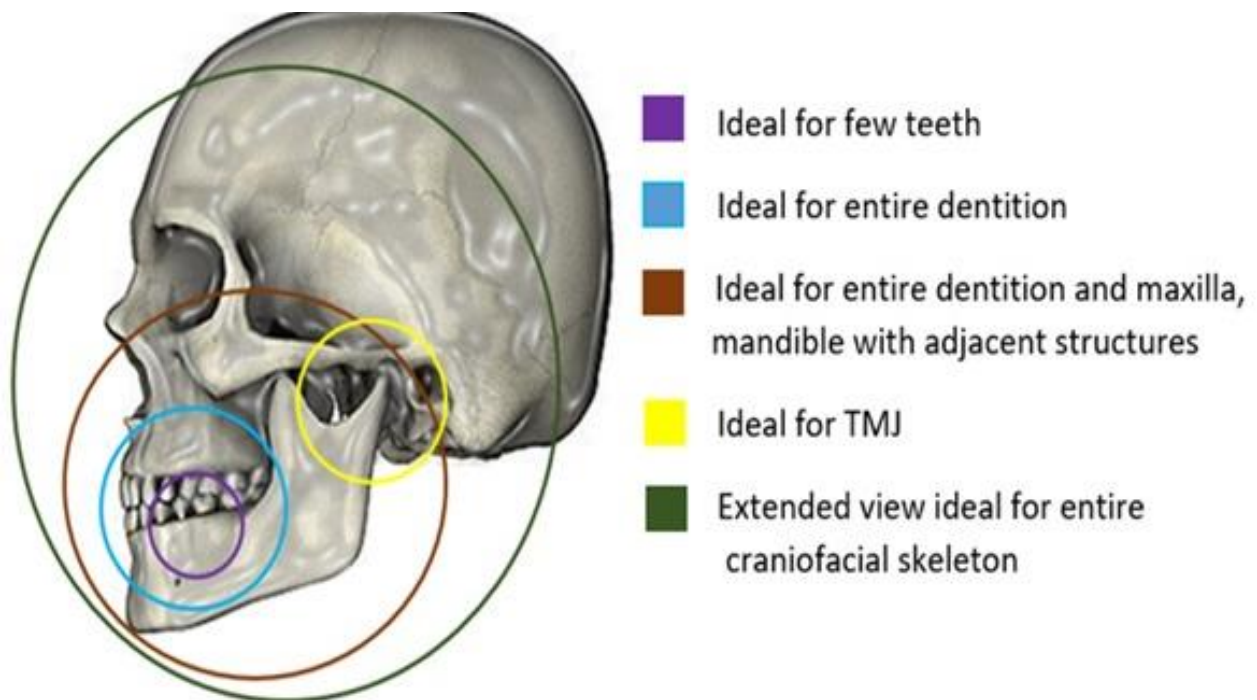


Figure 1.8: The ability of CBCT machines to customize the collimation of the X-ray beam (select the FOV), minimizing patient exposure, reducing scattered radiation that can affect image quality, and accommodating specific clinical requirements. Adapted from “Cone beam computed tomography: basics and applications in dentistry” by Venkatesh et al., 2017, J Istanb Univ Fac Dent, 51(3 Suppl 1):S102-S121.



## **1.6 DC/TMD Limitations in Diagnosing and Predicting TMJ OA Progression**

The current standards for diagnosing TMJ OA rely on both clinical and imaging criteria due to the suboptimal sensitivity and specificity demonstrated by clinical features alone in detecting diseased cases (Hilgenberg-Sydney et al., 2018; Schiffman & Ohrbach, 2016; Schiffman et al., 2014). By incorporating imaging criteria, the sensitivity and specificity of TMJOA diagnosis are enhanced, and insights into various disease stages can be obtained. For example, erosive lesions may suggest acute or active changes, while sclerosis, flattening, and osteophytes may indicate advanced stages of the disease (Zhao et al. 2011). However, the efficacy of these criteria in detecting early-stage TMJ OA is limited, creating challenges in timely intervention, prevention of chronicity, and mitigation of irreversible bone damage associated with the disease (Almășan et al. 2023). Hence, it becomes imperative to identify additional objective criteria that can assist in achieving accurate diagnosis. Such criteria may also enable earlier detection of the disease, thus advancing the preventive strategies for osteoarthritis (Derwich et al. 2023; Hawker and Lohmander 2021). These new criteria should be evaluated in conjunction with the present clinical criteria in the diagnosis process, as the latter include pain and limited mouth opening, which are the key motivations for seeking medical attention and determining the efficacy of treatment measures (Derwich et al. 2023; Suenaga et al. 2016).

In addition to early disease identification, determining which TMJ OA patients are at a higher risk of disease progression is critical for making informed clinical decisions and designing more effective and tailored therapeutic strategies (Delpachitra and Dimitroulis 2022). This is particularly important given the absence of disease-modifying drugs that can effectively delay or reverse the degenerative changes associated with osteoarthritis (Liu et al. 2022; Thomas et al. 2019). The use of DC/TMD to predict disease prognosis is hampered by the fact that clinical

symptoms observed in patients do not always correspond with the imaging features of the disease (Chung et al. 2023; Bakke et al. 2014; Lamot, Strojan, and Šurlan Popovič 2013; Larheim 2005). For instance, severe condylar alteration, characterized by condylar defects accompanied by erosion, has been associated with a higher prevalence of TMJ pain (Takahara et al. 2017). However, no correlation has been found between the overall severity of radiographic changes of the condyles and the symptoms in patients with TMJ OA (Arayasantiparb et al. 2020; Kim, Wojczyńska, and Lee 2016; Lee et al. 2012). Predicting disease progression using the DC/TMD criteria is further complicated by the difficulty of quantifying degenerative bone changes and the variability of their response to treatment. Several studies, for instance, have reported an increase in flattening and sclerosis and gradual resolution of erosions with conservative treatment (Jung, Lee, and Suh 2022; Lee et al. 2012). While others mentioned that bone degenerative changes remained mostly unchanged following conservative treatments (Song et al. 2020; Zhao et al. 2011). Therefore, relying solely on the current imaging criteria to predict disease response to conservative treatments is unreliable, and alternative markers are required. Nonetheless, identifying factors that contribute to joint degeneration and pain remains essential as they can serve as markers of disease onset and progression, facilitating timely diagnosis and treatment (Toshima and Ogura 2020).

## **1.7 Quantitative Imaging Markers: Pioneering Future Frontiers**

### ***1.7.1 Subchondral Bone Involvement in Early Stages of OA***

TMJ OA is characterized by progressive degeneration of the articular cartilage and alterations of the subchondral bone (Yang et al. 2020). The subchondral bone is composed of two anatomical components: the subchondral plate and the subchondral trabecular bone. The subchondral bone plate (SBP) is a thin cortical lamella directly beneath the calcified cartilage. It contains channels

that connect the articular cartilage to the subchondral trabecular bone, hence, microenvironmental changes in subchondral bone may influence the overlaying cartilage (Figure 1.9) (Hu, Chen, Dou, et al. 2021).

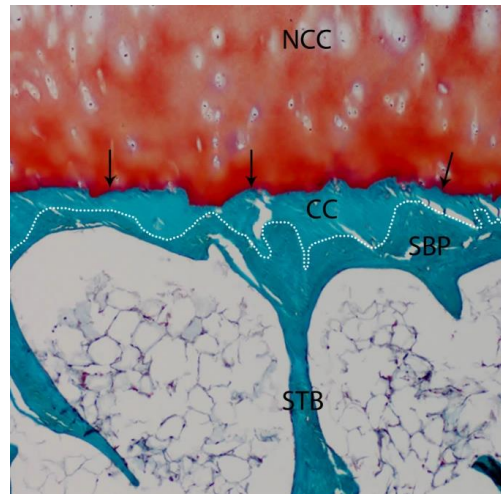


Figure 1.9: Normal human joint articular cartilage and subchondral bone structure. NCC, non-calcified cartilage; CC, calcified cartilage; SBP, subchondral bone plate; STB, subchondral trabecular bone. Adapted from “Subchondral bone in osteoarthritis: insight into risk factors and microstructural changes” by Li G et al., 2013, *Arthritis Res Ther.* 15(6):223. doi: 10.1186/ar4405. PMID: 24321104; PMCID: PMC4061721.

The subchondral trabecular bone lies beneath the SBP and exhibits increased porosity and metabolic activity. Moreover, it responds to different stressors by adjusting its bone remodeling, trabecular orientation, and scale parameters (Zhu et al. 2021; Finnilä et al. 2017; Li et al. 2013). Importantly, a notable increase in remodeling of the subchondral bone in the mandibular condyle is often evident during the early stages of TMJ OA (Jiao et al. 2014; Embree et al. 2011; Jiao et al. 2011). A study used the CED mouse, an osteoblast-specific mutant TGF-1 transgenic mouse in which excessive quantities of active TGF-1 appear in bone marrow, resulting in aberrant bone remodeling. In 1- and 4-month CED mouse groups, notable microstructural alterations such as changes in bone volume/bone surface (BV/BS), trabecular number, and separation were found using micro-computed tomography ( $\mu$ CT). Surprisingly, cartilage deterioration was seen in 4-

month CED mice but not in 1-month CED mice. This shows that aberrant remodeling within the mandibular condyle's subchondral bone precedes and may potentially induce increasing cartilage degradation during TMJ OA (Jiao et al., 2014). Comparable results have been observed in various animal models, such as guinea pigs, rats, and mice (Chen et al., 2018). Consequently, there has been a growing interest in investigating the subchondral bone involvement in the initiation and advancement of osteoarthritis (Hirvasniemi et al. 2021). Importantly, the subchondral bone trabecular volume fraction (BV/TV), trabecular number (Tb.N), and trabecular thickness (Tb.Th) were all found to be positively connected with the severity of osteoarthritis, which was based on imaging as well as histological score of the defects (Zhang et al., 2023). Furthermore, the segmentation of individual trabeculae in  $\mu$ CT images of human knees with osteoarthritis revealed a significant decrease in rod-like trabeculae and an increase in plate-like trabeculae, both beneath severely damaged and still intact cartilage (Figure 1.10). This suggests that microstructural alterations in the subchondral trabecular bone might contribute to the development of OA in humans. Accordingly, there is a need for advanced microstructural analysis techniques to accurately detect these early yet subtle changes. Such changes could potentially serve as markers for clinical diagnosis or for evaluating the progression of OA (Chen et al., 2018).

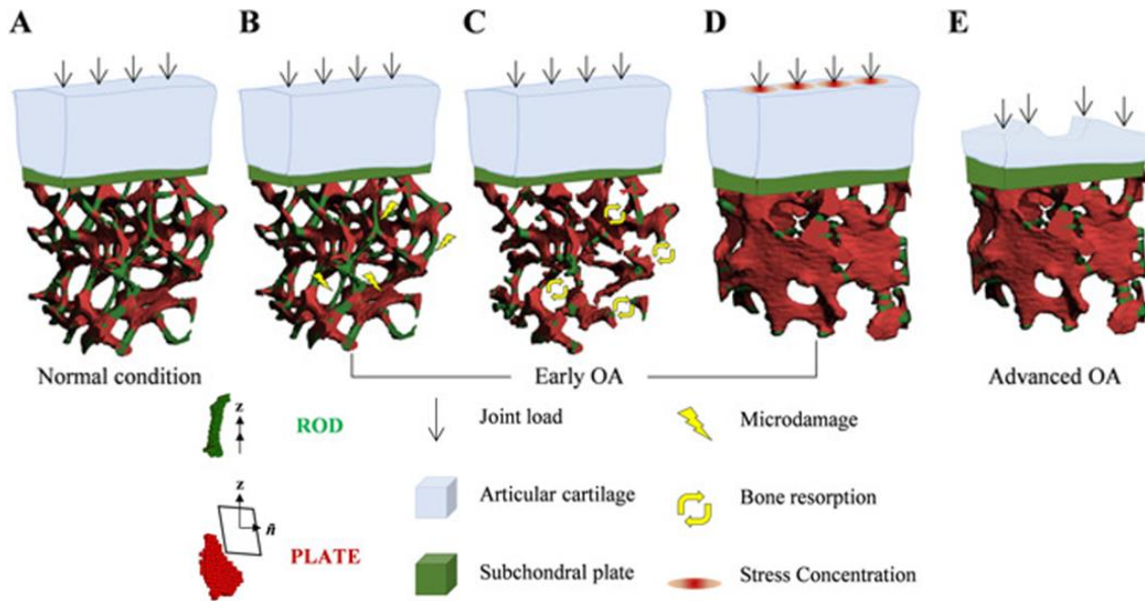


Figure 1.10: A model for OA pathogenesis: (A) In healthy individuals, subchondral bone has an optimized microstructure with a balanced distribution of trabecular rods and plates, providing even support for cartilage. (B-D) During early OA stages, cartilage mostly remains intact, but abnormal bone resorption, triggered by trauma or abnormal mechanical stress (overloading), begins to target trabecular rods. Rods are more vulnerable due to their higher surface-to-volume ratio and relative thinness compared to plates. This leads to fewer load-supporting trabeculae, resulting in increased mechanical demand on the remaining trabeculae and short-term thickening. (E) Ultimately, these microstructural changes disrupt the normal support for cartilage, causing an uneven distribution of rod-and-plate microstructure and localized subchondral bone stiffening. These events can severely impact the overlying cartilage, with unfavorable mechanical conditions and local stress concentrations contributing to advanced OA-related degradation. Adapted from “Subchondral trabecular rod loss and plate thickening in the development of osteoarthritis” by Chen, Y. et al., 2017, *Journal of Bone and Mineral Research*, 33(2), pp. 316–327. doi:10.1002/jbmr.3313.

### ***1.7.2 Radiomics: Revealing Hidden Insights within Medical Imaging***

Recent advances in computing power have spawned a new research discipline known as radiomics. This field entails retrieving quantitative imaging features from radiological images in a high-throughput manner with the goal of analyzing tissue pathology and improving the existing data available to clinicians through sophisticated mathematical analysis (Avery et al. 2022; Bera, Velcheti, and Madabhushi 2018). Radiomics is based on the premise that biomedical images contain concealed information about disease-specific processes that are undetectable to the eyes of humans and therefore inaccessible via conventional visual inspection of the generated images. This hidden data can be extracted and quantified utilizing advanced texture and shape analysis, providing greater insight into subtle changes in tissues and overcoming the subjectivity inherent in image interpretation (Avanzo et al. 2020; Neisius et al. 2019; Bera, Velcheti, and Madabhushi 2018).

The application of radiomics in clinical settings follows a structured framework (Figure 1.11), which involves several phases. Initially, radiographic images are obtained. Subsequently, regions of interests (ROIs) are determined in two-dimensional (2D) approaches or the volume of interests (VOIs) in three-dimensional (3D) approaches. Accurate delineation of these ROIs/VOIs is crucial as it dictates the locations where radiomic characteristics will be computed (van Timmeren et al. 2020; Mayerhoefer et al. 2020). The identification and segmentation of the target tissue's ROI/VOI can be achieved manually, semi-automatically (using standard image segmentation algorithms like region-growing or thresholding), or automatically (Avery et al. 2022; Zhang et al. 2013). Various software, both open-source and commercial, such as 3D Slicer (Fedorov et al. 2012), Free Surfer (Fischl 2012), ITK-SNAP (Yushkevich, Yang Gao, and Gerig 2016), and ImageJ (Girish and Vijayalakshmi 2004), can be utilized for these tasks.

Image processing is a significant step that occurs between image segmentation and the extraction of radiomics features. Its primary objective is to standardize the images from which radiomic characteristics will be extracted. This standardization addresses a variety of factors, including pixel spacing, grey-level intensities, and grey-level histogram divisions. The consistency and reliability of extracted radiomic features are highly dependent on the image processing parameters. For research to be reproducible, it is important to meticulously document the steps of the image processing process (Elmahdy and Sebro 2023; Wichtmann et al. 2023; Zhao 2021; van Timmeren et al. 2020; Zwanenburg et al. 2019).

The third stage revolves around extracting radiomic features from the identified ROIs/VOIs

where feature descriptors are used to quantify characteristics of the grey levels within the ROI/VOI. This step involves performing texture, filtering, and morphological analyses, leading

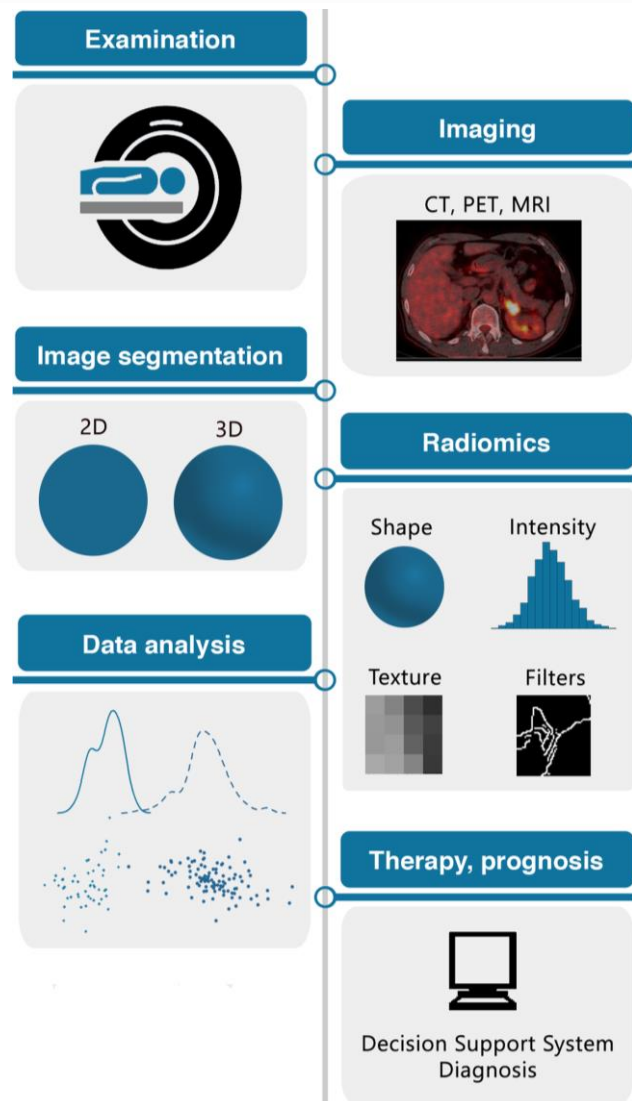


Figure 1.11: Workflow of Radiomics. Adapted from “Radiomics in medical imaging—“how-to” guide and critical reflection” by Timmeren et al., 2020, *Insights Imaging* 11, 91. <https://doi.org/10.1186/s13244-020-00887-2>.

to the generation of a large number of radiomic features (Scapicchio et al. 2021; Parekh and Jacobs 2016).

Image texture analysis plays a crucial role in radiomics. In material science, texture is defined as a measurement of surface variation, where a rough-textured material exhibits a greater rate of change in the high and low points of its surface compared to a smooth-textured material. Similarly, in medical imaging, texture refers to the variations in grayscale that represent a specific region (van Timmeren et al. 2020; Varghese et al. 2019; Castellano et al. 2004).

In an effort to comprehend the information contained in image texture, image texture features have evolved into a vast class of metrics capable of quantifying complex image attributes and textural patterns. Currently, two statistical methods commonly employed to describe the spatial distribution of gray levels within an image: first and second order statistics (Figure 1.12) (Santos et al. 2023; Nisbett, Kavuri, and Das 2020).

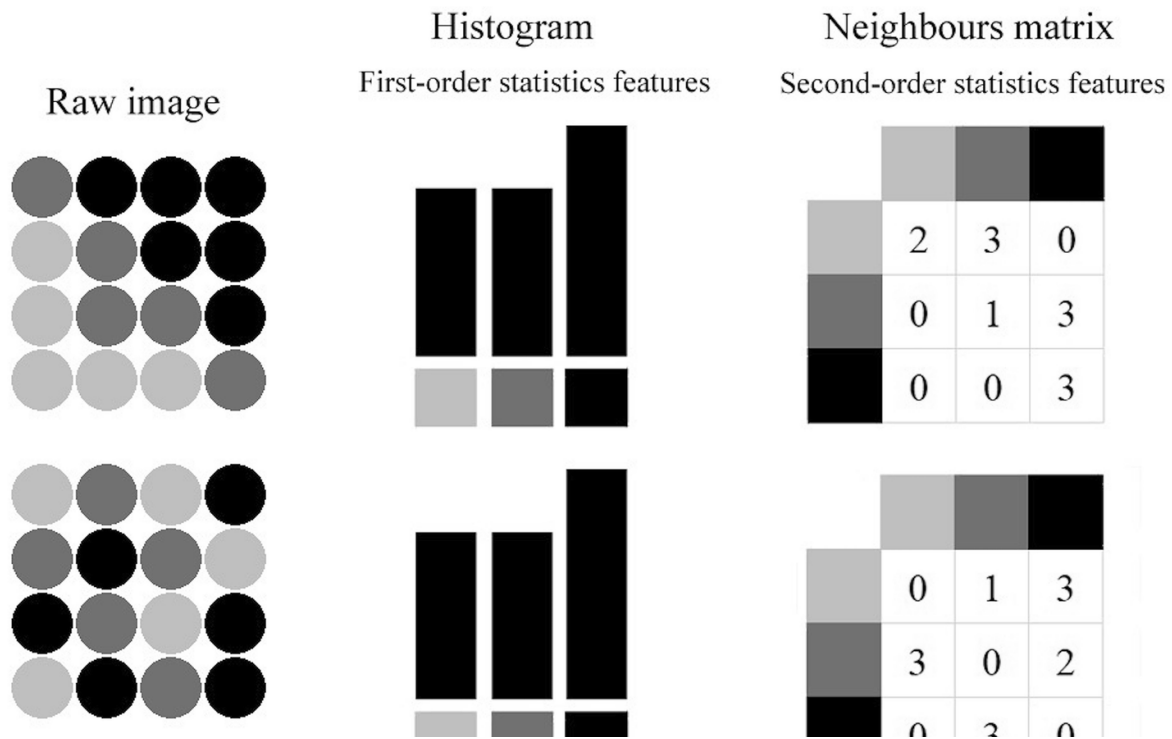


Figure 1.12: Comparison of first- and second-order statistics features. Two different images exhibit identical histograms, representing the same number of black, light gray, gray, and dark gray pixels (first-order statistics). However, when considering second-order statistics that account for pixel interactions, distinct matrices are obtained. This demonstrates that second-order statistics reveal valuable insights into the relationships between pixels, making them better suited for demonstrating intra-lesion heterogeneity. Adapted from “Radiomics in bone pathology of the jaws” by Santos et al., 2022, Dentomaxillofacial Radiology Vol. 52,1. <https://doi-org.proxy.lib.umich.edu/10.1259/dmfr.20220225>.



First-order texture statistics are derived from the image's pixel/voxel intensity distribution, represented by its histogram. Several features can be derived from a histogram, which provide information about the magnitude (mean), spread (standard deviation), asymmetry (skewness), peakedness or flatness (kurtosis), randomness (entropy), uniformity (energy and uniformity), and the variation relative to the magnitude (coefficient of variation) of gray-level pixel values. These histogram features describe how gray-level pixel/voxel values are distributed within a ROI/VOI as a whole. However, they do not account for the spatial arrangement of the textural pattern (Scapicchio et al. 2021; Park, Park, and Lee 2020; van Timmeren et al. 2020; Parekh and Jacobs 2016). In contrast, the inter-pixel/voxel relationships in an image can be measured using second-order statistics, such as the gray-level co-occurrence matrix (GLCM) and gray-level run length matrix (GLRLM) (Santos et al. 2023; Parekh and Jacobs 2016).

The GLCM contains statistical information regarding the frequency of two neighboring pixels/voxels in an image with specific gray level values at a defined distance and a fixed direction (horizontal, diagonal, or vertical for a 2D analysis or 13 directions for a 3D analysis). The GLCM count relies on identifying pixel pairs that share a similar distribution of gray-level values. On the other hand, the GLRLM assesses the length of consecutive pixels/voxels with particular grey level values in a predetermined direction in the image. The GLRLM Counts are made for specific gray-level runs in a chosen direction. For instance, if three consecutive pixels have the same gray-level value along the horizontal direction, it is considered a run of length three. Short runs are indicative of fine textures, while longer runs are characteristic of coarse textures. Since the GLCM and GLRLM depend on direction, enhancing directional invariance is recommended by computing textural features from various directional matrices (Figure 1.13) (Santos et

al. 2023; Scapicchio et al. 2021; Mayerhoefer et al. 2020; Park, Park, and Lee 2020; Larroza et al. 2016).

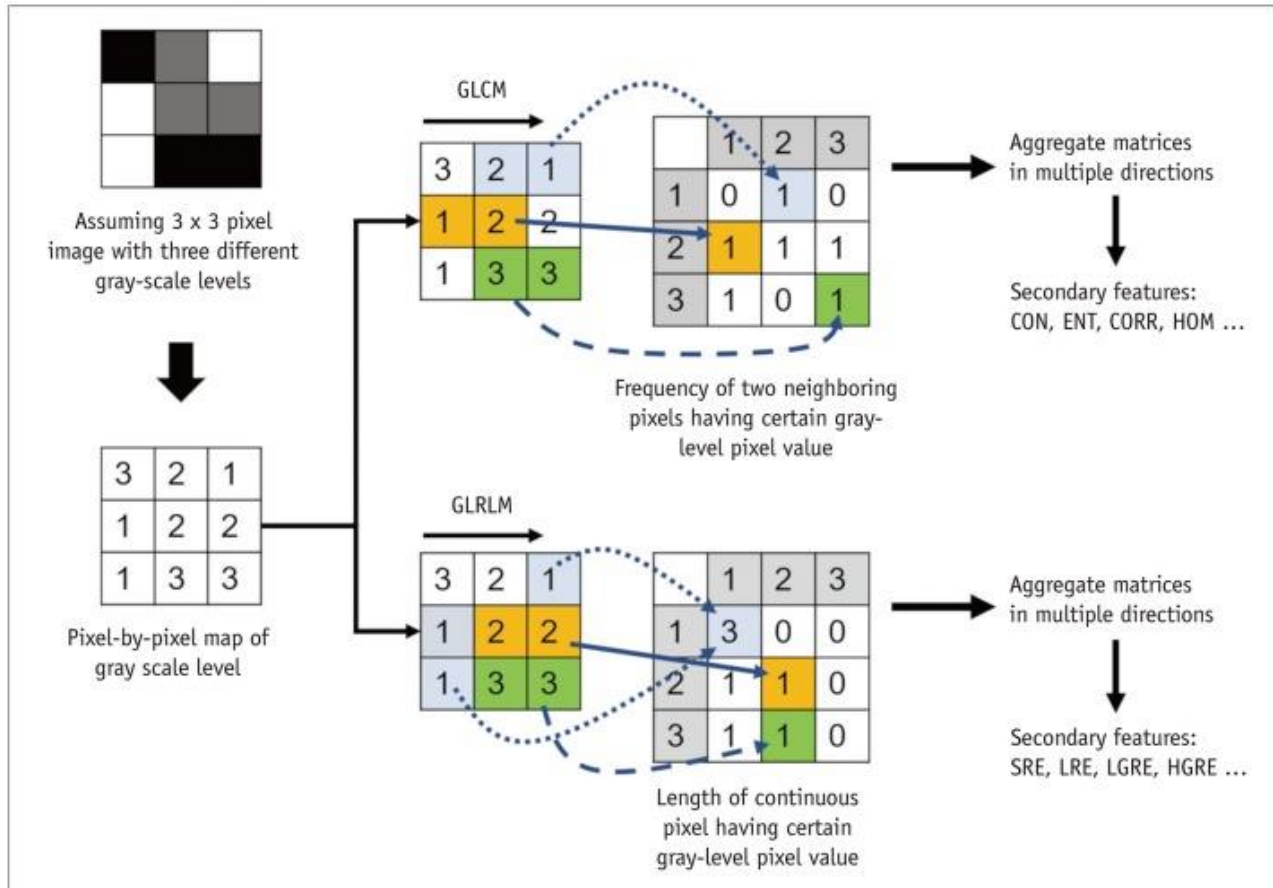


Figure 1.13: Schematic illustration of the extraction of textural features from a 3x3 pixel image with three distinct grayscale levels. Adapted from “Radiomics and Deep Learning: Hepatic Applications”, by Park et al., 2020, Korean J Radiol. 21(4): 387–401,doi: [10.3348/kjr.2019.0752](https://doi.org/10.3348/kjr.2019.0752).

Following radiomics’ extraction, the features are subjected to a selection process based on user-defined criteria. This selection aims to exclude non-reproducible, redundant, and non-relevant features from the dataset and retain the most informative features for the respective task. These "highly" informative features are then chosen for further analysis and processing. The final stage involves the classification of the user-defined features. This classification can be employed for

various purposes, such as distinguishing between malignant and benign tumors or predicting survival outcomes, providing valuable insights into the decision-making in clinical applications (Park, Park, and Lee 2020; van Timmeren et al. 2020).

Interestingly, GLCM and GLRLM features were first developed in the 1970s (Nisbett et al., 2020). Haralick was the first to recognize the GLCM features' capability to identify the texture of image blocks. These images were created using high-resolution photomicrographs of five distinct types of sandstones, aerial photographs of eight different land-use categories, and low-resolution satellite imagery of seven various land-use categories. The results indicated that GLCM's quantitative textural analysis could be useful for a wide range of picture classification applications (Haralick, Shanmugam, and Dinstein 1973). Galloway reported similar findings, where the GLRLM characteristics were shown to be capable of classifying 54 photos belonging to 9 categories, including those studied by Haralick, based on their textures. The findings suggested that more research with diverse data sets should be conducted (Galloway, 1975). Consequently, more research was conducted utilizing these quantitative texture analyses. However, it was not until 2012 that Lambin et al. coined the term "radiomics. Moreover, texture features have only been integrated into other sectors, including medical imaging, recently, in line with advancements in machine learning and computational power (Alderson and Summers 2020; Nisbett, Kavuri, and Das 2020).

The majority of radiomics research is primarily involved in the oncology field. This can be attributed to the abundance of available imaging and non-imaging data, extensive clinical trials, and the influence of social and economic factors that drive oncology research (Scapicchio et al. 2021; Neri et al. 2018). Examples of radiomics application in oncological research include distinguishing between different neoplasms, differentiating malignant and benign lesions, predicting

tumor stage, evaluating treatment response, foreseeing survival rates, discerning treatment-related changes from post-radiotherapy metastases, and predicting the origin of metastases (Lohmann et al. 2020; Kocher et al. 2020; Park, Kim, et al. 2020). Aside from its applications in oncology, radiomics has demonstrated considerable promise in neuroimaging, enabling the identification of disease features related to neurodegenerative disorders or mental illnesses (Zhao et al. 2020; Park, Choi, et al. 2020). Texture quantitative analysis is also anticipated to enhance the significance of musculoskeletal imaging by enabling the development of diagnostic and prognostic predictive models (Cuadra, Favre, and Omoumi 2020).

### ***1.7.3 Radiomics: Advancing the Diagnosis and Progression Assessment of Osteoarthritis***

Recent studies have been investigating the application of radiomics for the detection of knee osteoarthritis and estimation of disease progression (Teoh et al. 2022). In a study conducted by Harrar et al., GLCM quantitative textural analysis was performed on regions of interest extracted from the subchondral bone of 200 knee radiographs. The study's results demonstrated the effectiveness of radiomics in distinguishing between knee X-ray images without osteoarthritis and those with mild osteoarthritis, achieving an accuracy of 77% (Harrar, Messaoudene, and Ammar 2018). Similar findings were reported by the Hirvasti group, who extracted radiomic features, including texture analysis (e.g., GLCM and GLRLM), from 655 knee images. A model employing these radiomics distinguished between knees with and without osteoarthritis, obtaining a receiver operating characteristic area under the curve (ROC AUC) score of 0.80. In contrast, a model that incorporated covariates such as age and body mass index, in addition to the qualitative imaging indicators of the disease, yielded a lower AUC of 0.68. These findings indicate the potential use of radiomic features as effective imaging biomarkers for the diagnosis of subchondral osteoarthritis (Hirvasniemi et al. 2021). Importantly, when extracting textural features from

X-rays of 25 patients with distinct degrees of knee osteoarthritis (grades I-III) and 25 healthy individuals, the OA cases were recognized with an AUC value of 0.77, including grades that radiologists consider challenging to identify. This demonstrates that textural features are useful indicators for the early detection of knee osteoarthritis. Increasing the sample size may reduce the inherent heterogeneity among individuals and further improve the detection rate (Madrid et al. 2022). Indeed, combinations of various textural feature sets in a dataset comprising 620 radiographs (310 images of healthy subjects and 310 images from patients with mild knee osteoarthritis) yielded the highest detection rate for knee osteoarthritis, achieving an accuracy of 91% (Messaoudene and Harrar 2022).

Notably, a model based on radiomics, which assesses quantitative textural features in subchondral bone, demonstrated superior performance compared to a traditional structural model that evaluates microstructural properties in bone when differentiating between healthy and osteoarthritic knees. Additionally, strong associations were found between the radiomics features and trabecular bone parameters, as indicated by Pearson's correlation coefficients ( $r > 0.60$ ,  $P < 0.05$ ). This suggests that multidimensional radiomics features may reflect changes in the microstructure of subchondral bone. Furthermore, cases with advanced OA exhibited higher bone volume-to-total volume (BV/TV) and trabecular bone thickness, and lower trabecular separation (Tb.Sp) compared to normal cases. Similarly, an increase in certain texture features was strongly correlated with an increase in BV/TV and Tb.Th, as well as a decrease in Tb.Sp. This indicates that changes in texture may also mirror structural alterations in trabecular tissue, and thus, can potentially provide insights into the progression of OA (Xue et al. 2022).

Several longitudinal studies have been conducted to trace knee OA disease progression over time (Collins, Neogi, and Losina 2021). In one such study, trabecular bone texture features were uti-

lized to predict the advancement of knee osteoarthritis over six years in 683 patients with early knee OA (Kellgren and Lawrence grades II and III). The results demonstrated its superior performance compared to KL-based models, achieving an AUC of 0.81 (Almhdie-Imjabbar et al. 2022). Moreover, the application of trabecular bone texture analysis in different locations of the knee joints, using 1124 radiographs, exhibited the capability of these features to predict OA progression over 48 months (Janvier et al. 2017). An analysis was conducted on data from 122 patient records. Out of these, 61 patients were classified as progressors based on a decrease in the minimum joint space width of at least 0.7 mm over the three years following their initial baseline measurements. Non-progressors were matched by age and gender to individuals who did not meet the radiographic progression criterion. The texture analysis of the subchondral bone succeeded in predicting disease progression over three years, achieving a sensitivity of 86% and a specificity of 64% (Kaggie et al. 2018). Another retrospective study examined the potential of the initial state or changes in subchondral bone texture within the first 12 to 18 months to predict the progression of knee osteoarthritis over a 36-month period. Individuals with knee osteoarthritis who showed progression at the 36-month mark, and controls with comparable age, gender, body mass index, and initial joint space width were included. The analysis of texture features and their association with radiographic progression revealed that the initial subchondral bone texture and the changes observed between 12 and 18 months were linked to radiographic progression at the 36-month follow-up. This suggests that texture analysis could serve as a valuable biomarker for monitoring subchondral bone alterations throughout the progression of knee osteoarthritis (MacKay et al. 2018).

In contrast to osteoarthritis of the knee, the role of radiomics in TMJ OA is still evolving (Bianchi, de Oliveira Ruellas, et al. 2020). A retrospective study evaluated TMJ-MRI radiographs

from 107 patients with temporomandibular disorders. The TMJs were classified as either normal (showing no osseous changes) or with osseous changes, such as flattening, erosions, anterior osteophytes, and/or subchondral cysts. A radiomics platform was employed to extract imaging features including GLCM and GLRLM. Among various learning models tested, the k-nearest neighbors and random forest classifiers were demonstrated the most optimal performance for predicting TMJ pathologies, achieving an AUC of 0.77 (Orhan et al. 2021). Promising results have been reported for the application of local binary patterns and histogram-oriented gradients of CBCT images as a diagnostic tool for assessing temporomandibular disorders. A collection of CBCT images for the head of the mandibular condyle from 66 TMD patients and 66 normal cases was evaluated. The K-nearest neighbor model showed high accuracy (0.92), sensitivity (0.95), and specificity (0.90) in detecting patients with TMD based on texture changes (Haghnegahdar et al. 2018). These studies have shown the potential of texture analysis in detecting subchondral trabecular bone changes. However, the application of radiomics in diagnosing TMJ OA and assessing the disease progression is still largely unexplored. To address this gap, our group aimed to develop and validate a tool for the extraction of quantitative bone markers, including GLCM, GLRLM, as well as bone morphometry features such as BV/TV, BS/BV, Tb.Th, Tb.Sp, and trabecular number (Bianchi et al. 2021; 2019; Vimort et al. 2018).

Several open-source programs, such as Ibex and BoneJ, are frequently used to compute bone texture features in medical imaging. However, these software applications have complex user interfaces and are not tailored specifically to CBCT images, limiting their user-friendliness and suitability for this purpose (Bianchi et al. 2019; Zhang et al. 2015; Doube et al. 2010). Hence, our group developed a new software in 3D-Slicer called BoneTexture. The tool was validated by comparing it with  $\mu$ CT imaging of ex vivo bone samples. Briefly, 16 condylar bone specimens

were obtained from patients diagnosed with TMJ OA and underwent surgical resection. A total of 35 images were acquired using CBCT and  $\mu$ CT, with a focus on areas of subchondral trabecular bone that remained unaffected, as well as areas that experienced bone loss. The presence of osteoclastic lacunae in histological sections stained with hematoxylin and eosin confirmed the identification of bone defect regions (Figure 1.14). In both  $\mu$ CT and CBCT images, the computed texture and bone morphometry features demonstrated a very high separability value (AUC=0.85) between unaffected and affected trabeculae, suggesting their sensitivity to subtle bone changes (Vimort et al. 2018). Interestingly, the GLRLM and GLCM features computed from CBCT images did not demonstrate a strong correlation with the number of osteoclasts in the histological analysis of corresponding bone samples. This suggests that these biomarkers may be associated predominantly with other bone characteristics, such as 3D morphology and grayscale organization (Ebrahim et al. 2017).

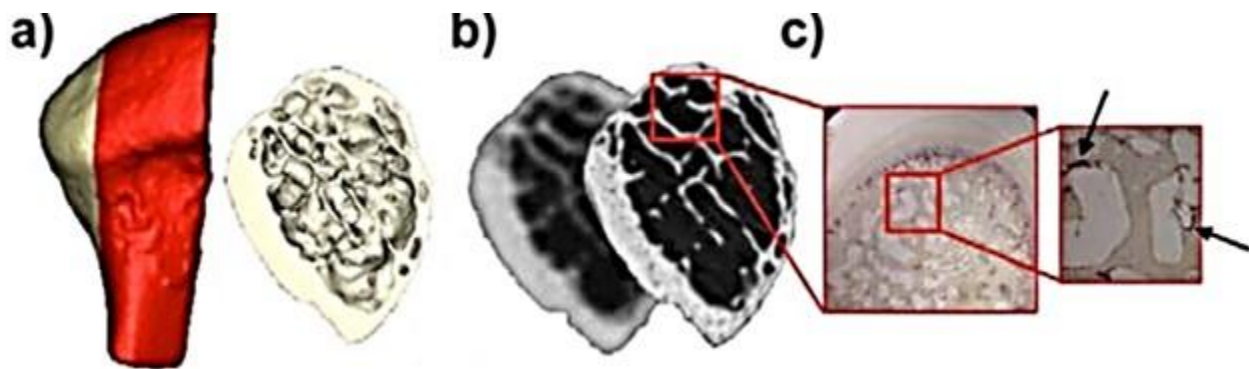


Figure 1.14: Schematic illustration of a) The condyle bony sample, b) the obtained hr-CBCT and  $\mu$ CT images, and c) Histology analysis depicting osteoclasts' presence adjacent to areas of trabecular bone loss. Adapted from "Detection of Bone Loss via Subchondral Bone Analysis", by Vimort et al., 2018, Proc SPIE Int Soc Opt Eng. 2018 Feb;10578:105780Q. doi: 10.1117/12.2293654. Epub 2018 Mar 12. PMID: 29769754; PMCID: PMC5950720.

In order to assess the compatibility between the Bone texture tool with Ibex and BoneJ software for computing bone textural features, a dataset comprising 66 high-resolution cone-beam com-



puted tomography (hr-CBCT) images of mandibular condyles was employed. These images, obtained from both healthy individuals and those with temporomandibular joint osteoarthritis, had an isotropic voxel size of 0.08 mm<sup>3</sup>. The results indicated a strong Spearman correlation (ranging from 0.7 to 1) among the software applications, with statistical significance observed for all variables, except for Grey Level Non-Uniformity ( $p = 0.627$ ) and Short Run Emphasis ( $p = 0.06$ ). The Bland–Altman plots displayed favorable agreement between the software applications along the vertical axis, while the horizontal axis demonstrated a narrow average distribution for Correlation, Long Run Emphasis, and Long Run High Grey Level Emphasis. Overall, the data indicated consistency among the three applications for analyzing bone radiomics in hr-CBCT. Nevertheless, further studies are warranted to assess the suitability of these variables as novel bone imaging biomarkers for diagnosing TMJ-related bone diseases (Bianchi et al. 2019).

Despite the promising potential of quantitative imaging markers in detecting subtle tissue changes, the complex and multifaceted nature of osteoarthritis disease, coupled with the limited understanding of the interactions between joint structures and factors involved in OA, necessitates the integration of imaging with patient-derived clinical features as well as other sensitive markers of the disease (Xuan et al. 2023; Teoh et al. 2022; Cuadra, Favre, and Omoumi 2020).

In the initial phases of osteoarthritis, changes in the metabolism of joint tissues occur before any evident structural alterations. By examining specific biological markers released into bodily fluids as a result of this tissue turnover, valuable data could be obtained for diagnosing the condition, predicting its progression, and developing innovative treatment approaches (Liem et al. 2022; Rousseau, Chapurlat, and Garnero 2021).

## **1.8 Quantitative Biological Markers in OA: Exploring Disease Development & Progression**

A biomarker is a trait that can be objectively evaluated and used as an indication of regular biological processes, disease-causing actions, or responses to treatments (Puntmann 2009). An optimal biomarker should be present in all individuals diagnosed with a particular condition, be specific to that disease, and be detectable before apparent clinical symptoms arise. Additionally, it should be reversible with proper treatment and allow for a cut-off value that minimizes overlap between normal health and the disease state (Zwiri et al. 2020; Califf 2018).

A working group funded by the NIH introduced a goal-oriented classification system symbolized by the acronym BIPED, denoting the five categories of markers: burden of disease, investigative, prognostic, efficacy of intervention, and diagnostic. This classification scheme aimed to promote the development of a shared language and structure, allowing for clearer communication of knowledge and progress concerning OA biomarkers within both clinical and research contexts (Henrotin 2022; Rousseau, Chapurlat, and Garnero 2021).

To date, no direct disease markers panel for temporomandibular disorders is used in routine clinical practice. However, there has been significant progress in exploring biological markers, reflecting ongoing efforts to conduct an in-depth evaluation of this field, and paving the way for future research directions based on the accumulated evidence previously discussed (Zwiri et al. 2020).

Many studies on temporomandibular disorders have mainly focused on the local effects of inflammatory cytokine concentrations, and their role in communication between various temporomandibular tissues during both health and disease. This is particularly pertinent because synovial fluid surrounds the entire joint and can provide a direct indication of tissue turnover or disease-

related changes (Kalogera et al. 2023; Ali et al. 2022; Kellesarian et al. 2016). However, serum biomarkers, which offer a nonlocalized assessment of the joint biochemical changes, are often more practical and less invasive in a clinical setting compared to acquiring intra-articular synovial fluid samples. Moreover, despite their systemic nature, serum markers frequently align with local joint changes (Burland, Hunt, and Lattermann 2023; Keemu et al. 2021). Similarly, saliva offers a noninvasive, convenient, and cost-effective method for collecting biomarkers compared to synovial fluid. Due to the proximity of the salivary glands to blood vessels, many proteins found in human serum can also be detected in saliva. Moreover, disease-discriminating biomarkers can be found solely in saliva (Aoun et al. 2023; Dawes and Wong 2019; Jasim et al. 2018). As a result, researchers have been motivated to investigate the association between serum and saliva biomarkers and disease processes, as well as their potential for early detection and prediction of disease progression (Doshi et al. 2020; Ishibashi et al. 2020; Jasim et al. 2020; Dawes and Wong 2019).

Persuasive evidence indicates that systemic processes may have a significant impact on TMD. Indeed, the levels of pro-inflammatory proteins circulating throughout the body have been recognized as contributing factors to the underlying mechanisms of TMJ disorders (Watanabe et al. 2023; Ali et al. 2022; Kellesarian et al. 2016; Kristensen et al. 2014).

One of the pioneering studies that revealed a connection between localized and systemic changes in painful temporomandibular disorders was conducted by Slade et al. In this research, blood was drawn from 344 participants, and the plasma samples were processed using a standard multiplex platform, allowing the simultaneous measurement of 22 specific cytokines. These cytokines encompassed monocyte chemoattractant protein-1 (MCP-1), macrophage inflammatory protein-1 $\alpha$ ,  $\beta$ , epithelial-derived neutrophil-activating peptide-78 (ENA-78), fibroblast growth factor basic

(FGF basic), granulocyte colony-stimulating factor (G-CSF), granulocyte-macrophage colony-stimulating factor (GM-CSF), thrombopoietin (Tpo), IFN- $\gamma$ , IL-1 $\alpha$ , IL-1 $\beta$ , IL-1 receptor antagonist (IL-1ra), IL-2, IL-4, IL-5, IL-6, IL-8, IL-10, IL-17, TNF- $\alpha$ , , and VEGF. The analytical outcomes revealed statistically significant variations in the cytokine profiles between different TMD subgroups compared to the controls. This suggested that serum levels of cytokines could be employed as valuable diagnostic indicators to differentiate between various etiologically-distinct forms of TMD (Slade et al. 2011). Building on these findings, another study investigated for the first time the correlation between local and systemic biomarker profiles and 3D condylar morphology changes in TMJ OA patients compared to healthy controls. A total of 24 participants, including 12 with TMJ OA and 12 healthy individuals, underwent TMJ arthrocentesis and venipuncture. Biomarker expression was assessed locally (in synovial fluid) and systemically (in serum samples) using a custom quantibody protein microarray. Out of the 50 evaluated biomarkers associated with arthritis onset and progression, 32 biomarkers consistently fell within the standard curve of detection in either blood or synovial fluid. These biomarkers showed statistical correlation with variations in the condylar surfaces at specific anatomical regions ( $p < 0.05$ ) using Pearson correlation color maps in the MANCOVA shape analysis tool (Figure 1.15). Furthermore, synovial fluid levels of angiogenin (ANG), growth differentiation factor 15 (GDF15), tissue inhibitor of metalloproteinase-1 (TIMP-1), Chemokine (C-X-C motif) ligand 16 (CXCL-16), MMP-3, and MMP-7 were significantly correlated with bone apposition of the condylar anterior surface. On the other hand, serum levels of ENA-78, MMP-3, Plasminogen activator inhibitor-1 (PAI-1), vascular endothelial (VE)-Cadherin, VEGF, GM-CSF, TGF- $\beta$ 1, IFN- $\gamma$  , TNF- $\alpha$ , IL-1,

and IL-6 were significantly correlated with flattening of the lateral pole (Cevidane et al. 2014).

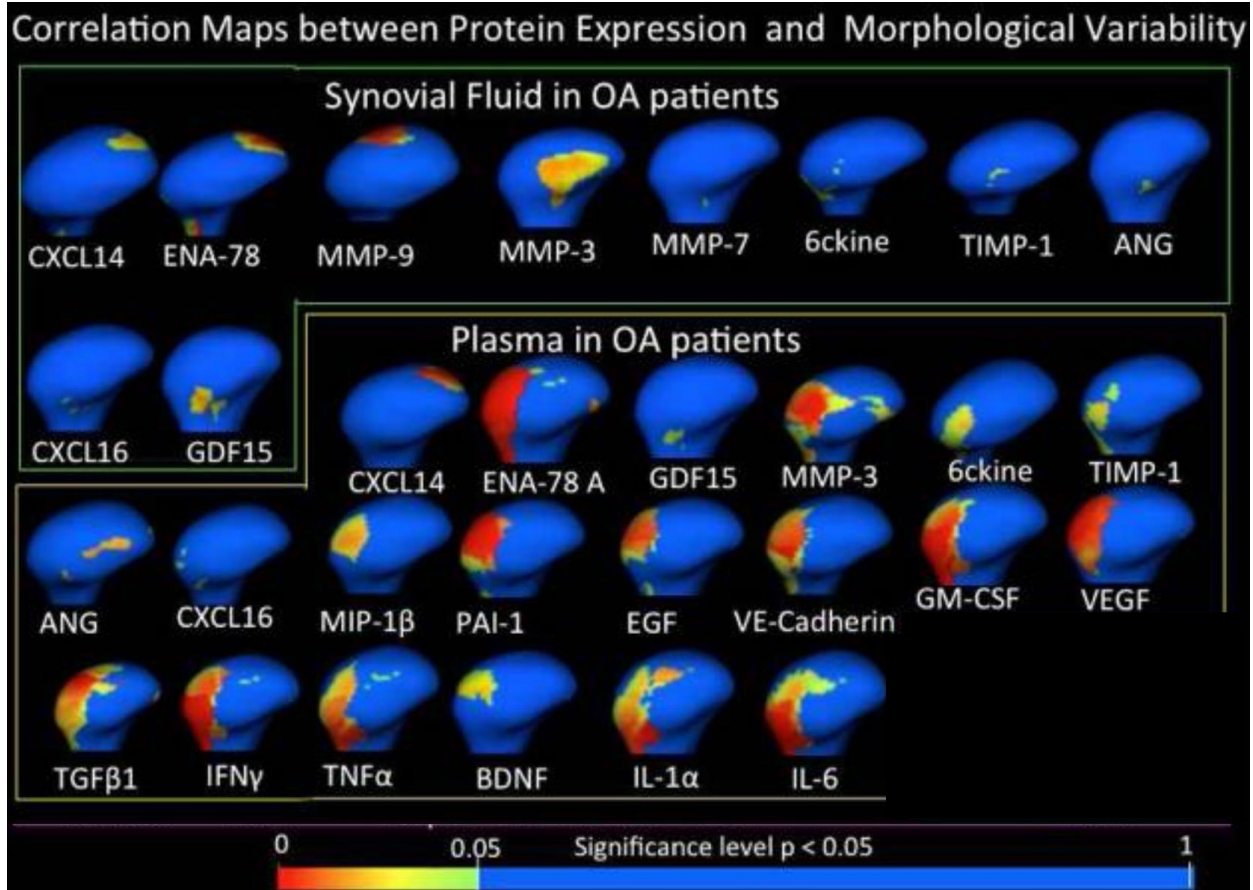


Figure 1.15: Outcome of Shape Analysis MANCOVA for Proteins in the synovial fluid and serum, showing statistically significant Pearson correlations between biomarker levels and condylar morphology. Adapted from “3D osteoarthritic changes in TMJ condylar morphology correlates with specific systemic and local biomarkers of disease” by Cevidane et al., 2014, *Osteoarthritis Cartilage*;22(10):1657-67. doi: 10.1016/j.joca.2014.06.014.

Markers associated with alterations in the surface morphology of the mandibular condyle in TMJ OA patients are briefly described below. The existing literature presents a growing body of evidence demonstrating the significance of these markers, but primarily based on studies conducted in the context of knee osteoarthritis.

Matrix metalloproteinases (MMPs) are a family of zinc-dependent endopeptidases that contribute to the degradation and remodeling of extracellular matrix (ECM) proteins. They are involved in several physiological and biological activities, such as blood vessel formation, structural devel-

opment, and repair of tissue (Cabral-Pacheco et al. 2020; Tokuhara et al. 2019; Cui, Hu, and Khalil 2017). Metalloproteinases are also essential regulators of physiological and pathological osteoclastogenesis, as their capacity to shed RANKL grants stromal cells and osteoblasts with another level of control over osteoclast maturation and activation (Aiken and Khokha 2010).

Matrix Metalloproteinase-3 (MMP-3) is a member of the MMPs family. It is produced by fibroblasts, chondrocytes, synoviocytes, and macrophages (Jarecki et al. 2022; Guo et al. 2017). Immunohistochemical analysis of 90 patients with different stages of OA showed MMP-3 protein presence in the synovial tissue of all knees, even in the early stages of the disease. The OA group exhibited significantly higher MMP-3 protein expression compared to the normal synovium ( $P < 0.05$ ). Additionally, there was a direct correlation between MMP-3 protein expression and OA severity ( $P < 0.05$ ) (Chen, Huang, et al. 2014). Likewise, in a study of 56 patients with primary knee OA, the serum levels of MMP-3 were noticeably higher than those in 31 healthy individuals (Georgiev et al. 2018). ELISA analysis of synovial fluid and peripheral blood samples from 39 females with knee osteoarthritis disclosed significantly higher MMP-3 levels in both serum ( $p = 0.006$ ) and synovial fluid ( $p = 0.03$ ) in patients with more advanced disease stage (Jarecki et al. 2022). A notable connection was observed between four polymorphisms (rs639752, rs520540, rs602128, and rs679620) in the MMP-3 gene and a heightened risk of OA, implying that single nucleotide polymorphisms might play a role in the onset of OA (Guo et al. 2017). MMP-3 knockout (MMP-3 KO) in mice negated the negative effects of ovariectomy on bone mineral density. This protective effect was correlated with a decreased DPD/creatinine ratio in MMP-3 KO mice relative to wild-type mice, implying a reduction in osteoclast activity (Jehan et al. 2022). Furthermore, MMP-3 plays a pivotal role in the onset and progression of osteoarthritis, influencing nearly every phase of OA's advancement. (Figure 1.16) (Wan et al. 2021).

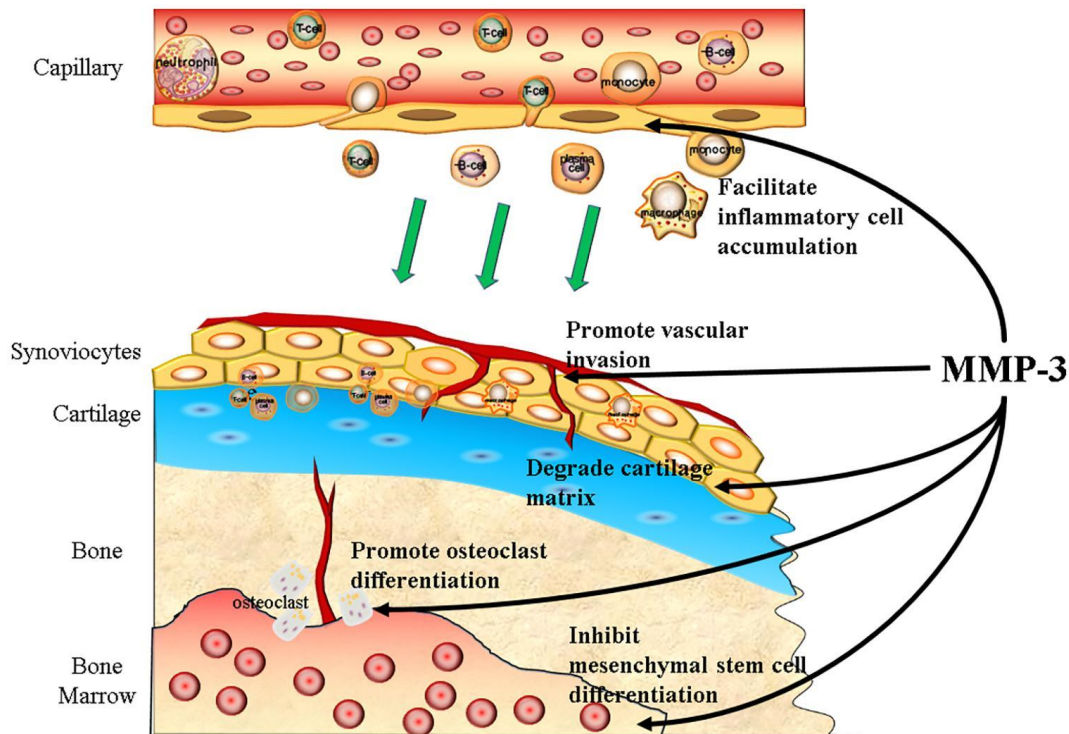


Figure 1.16: The involvement of MMP-3 in osteoarthritis progression. MMP-3 facilitates osteoarthritis progression in the preclinical and clinical stages. It promotes inflammatory cell accumulation, vascular invasion, cartilage matrix degradation, osteoclast differentiation, while inhibiting the differentiation of mesenchymal stem cells. Adapted from “Matrix metalloproteinase 3: a promoting and destabilizing factor in the pathogenesis of disease and cell differentiation” by Wan et al., 2021, *Front. Physiol*;12. <https://doi.org/10.3389/fphys.2021.663978>.

MMP-7, also known as matrilysin, is the smallest member of the MMP family, consisting solely of the common catalytic domain and the zinc-binding region. MMP-7 can degrade both non-ECM substrates and ECM molecules (Liu, Tan, and Liu 2020; Tao et al. 2015). The onset of knee and/or hand osteoarthritis was investigated by evaluating serum proteins several years prior to radiographic evidence of the disease. Using microarray platforms, 169 proteins were assessed in a case-control study. The cohort consisted of 22 incident OA cases and 66 age-and-sex-matched controls. Serum samples were analyzed at the time of radiographic classification of participants into diseased and control cases, as well as 10 years prior, during which all participants lacked radiographic signs of OA. Proteins exhibiting mean signal intensities fourfold greater than

the background were compared statistically. Notably, MMP-7 and PAI-1 presented differential levels prior and at the time of radiographic diagnosis of OA. These results suggest that alterations in serum proteins, particularly those involved in matrix degradation, cellular activation, inflammation, and bone collagen degradation may be indicative of early OA pathogenesis (Ling et al. 2009). Other studies also highlighted the potential involvement of MMP-7 in osteoarthritis. In a rat model of knee OA, MMP-7 levels were significantly elevated in OA synoviocytes compared to controls. This elevation suggests a link between MMP-7 and the pathogenic mechanisms underlying OA (Pérez-García et al. 2019). Furthermore, a study involving 60 participants, which included 30 individuals with knee OA and 30 healthy counterparts, found that MMP-7 protein expression in the articular cartilage and serum was substantially higher in the OA cohort. This further indicates that MMP-7 might play a role in the development of OA (Tao et al. 2015). Effective bone remodeling is achieved through a balance between bone resorption and bone formation. RANKL is a protein that binds to its receptor, RANK, on the surface of osteoclast precursors and mature osteoclasts. This binding promotes the differentiation, activation, and survival of osteoclasts. Hence, RANKL ensures normal breakdown of bone tissue. RANKL operates in conjunction with osteoprotegerin, which acts as a decoy receptor for RANKL. OPG prevents RANKL from binding to RANK, thus regulating bone resorption. The equilibrium between RANKL and OPG is crucial for bone homeostasis (Kitaura et al. 2020; Kohli and Kohli 2011). In pathological settings, the activity of soluble RANKL and the MMP responsible for its shedding changes. While normal shedding of RANKL inhibits osteoclast activation, increased levels of soluble RANKL can activate osteoclasts. Within a mouse model of bone metastasis, the release of RANKL by MMP-7 led to osteoclast activation and osteolysis (Figure 1.17) (Aiken and Khokha 2010; Thiollay et al. 2009).



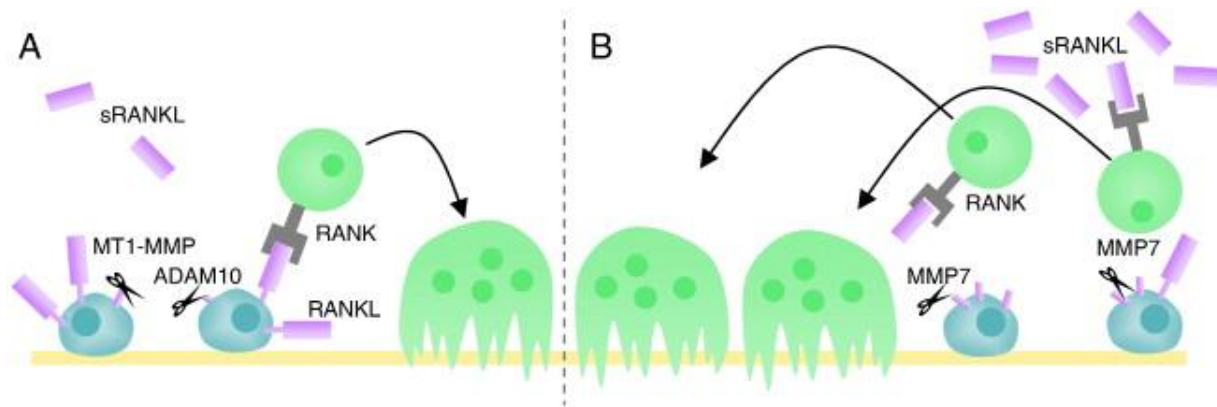


Figure 1.17: Metalloproteinases facilitate interactions among bone cells. (A) At normal levels, the shedding of RANKL from stromal cells or osteoblasts reduces the active RANKL quantity, leading to diminished osteoclastogenesis. (B) In disease conditions, heightened RANKL shedding produces a localized concentration of soluble RANKL, which stimulates osteoclast precursors and enhances osteoclastogenesis. Adapted from “Unraveling metalloproteinase function in skeletal biology and disease using genetically altered mice” by Aiken A., and Khokha, R, 2010, *Biochimica et Biophysica Acta (BBA) - Molecular Cell Research*;1803(1):P121-132. <https://doi.org/10.1016/j.bbamcr.2009.07.002>.

The activity and expression of MMPs are controlled at various phases, from gene transcription and the production and secretion of proenzymes to their activation and inactivation. This regulation is influenced by factors such as cytokines, growth factors, integrins, and ECM proteins. Examples of MMPs activators include TNF- $\alpha$ , TGF- $\beta$ , as well as certain interleukins, whereas TIMPs, brief for tissue inhibitors of MMPs, are the primary MMP inhibitors (Liang et al. 2016). IL-1, IL-6, and TNF- $\alpha$  are key inflammatory mediators driving OA's pathogenesis. These cytokines trigger a self-perpetuating cycle culminating in damage to cartilage and intra-articular structures that arises primarily from the activation of catabolic enzymes such as MMPs (Molnar et al. 2021).

Chondrocytes, synoviocytes, osteoblasts, osteoclasts, and macrophages in knee joints express a receptor called type I IL-1 receptor I (IL-1RI) to which IL-1 $\beta$  binds (Fields, Günther, and Sundberg 2019). IL-1 $\beta$  induces catabolic events that result in cartilage degradation via mitogen-

activated protein kinase (MAPK) signaling. IL-1 $\beta$  also stimulates the secretion of IL-6, which both amplifies IL-1 $\beta$ 's catabolic effects and functions as a catabolic mediator in its own right. IL-1 $\beta$  induces other inflammatory mediators via the extracellular signal-regulated kinase (ERK) pathway, contributing to synovial inflammation, which further enhances the secretion of IL-1 $\beta$  and other cytokines and accelerates the progression of OA (Chow and Chin 2020; Jenei-Lanzl, Meurer, and Zaucke 2019). As a potential therapeutic strategy for treating OA and halting its progression, the inhibition of IL-1 $\beta$  action has been investigated. IL-1 $\beta$  inhibition did not produce the desired effects of preventing OA progression, demonstrating that OA pathogenesis is not dependent on a single cytokine; rather, the same signaling pathways can be activated through various cytokines, and the interaction of multiple factors is essential for the onset and progression of the disease (Molnar et al. 2021; Theeuwes et al. 2021; Chevalier and Eymard 2019; Chevalier, Eymard, and Richette 2013).

IL-6 belongs to the IL-6 family of cytokines that utilize the common signal-transducing protein gp130, signaling through pathways like Janus kinase/signal transducers and activators of transcription (JAK/STAT), MAPK, and phosphoinositide 3-kinases (PI3K) (Baran et al. 2018; Rose-John 2018). Various cells, such as chondrocytes, osteoblasts, and synoviocytes, produce IL-6 (Wiegertjes et al. 2019).

When IL-6 binds to soluble IL-6 receptor (sIL-6R), it activates trans-signaling, leading to its pro-inflammatory actions. In contrast, IL-6's binding to membrane-bound IL-6 receptor (mbIL-6R) triggers classic-signaling, which has anti-inflammatory and regenerative effects (Scheller et al. 2011). The dominance between trans- and classic signaling is often determined by the sIL-6R concentration (Reeh et al. 2019). The primary source of sIL-6R in OA is the proteolytic cleavage

of mbIL-6R, a process amplified by proteases such as metalloproteinases (Akeson and Malemud 2017).

IL-6 treatment of chondrocytes and cartilage explants results in reduced proteoglycan content and an increased production of matrix metalloproteinase such as MMP-3. Systemic anti-IL-6 treatment alleviated cartilage damage, osteophyte development, and synovitis in experimental knee mouse models (Latourte et al. 2017). When compared to healthy controls, the concentration of IL-6 in synovial fluid is substantially higher in patients with end-stage OA (Li et al. 2020; Beekhuizen et al. 2013). In addition, IL-6 appears to have a predictive value in OA. In a prospective cohort study involving 163 participants with knee OA, a higher baseline concentration of IL-6 and TNF- $\alpha$  was associated with a greater cartilage volume loss after 3 years (Stannus et al. 2010).

TNF- $\alpha$  is a member of the tumor necrosis factor superfamily, which includes soluble and membrane-bound type II transmembrane proteins. The membrane-bound variant is biologically more active than its soluble counterpart (Z. Su, Dhusia, and Wu 2022). TNF- $\alpha$  interacts with two types of membrane receptors present on almost all cell types, each of which initiates a distinct signaling pathway (Jang et al. 2021). Complex 2 induces apoptosis and cell death, whereas Complex 1 promotes cell survival and upregulates pro-inflammatory genes. Important transcriptional pathways include NF- $\kappa$ B, AP-1, and MAPK (Wojdasiewicz, Poniatowski, and Szukiewicz 2014; Zelová and Hošek 2013). TNF- $\alpha$  plays a significant role in bone remodeling. It directly influences the levels of osteoclast precursors in the bone marrow by increasing the expression of c-fms. Additionally, it stimulates osteoclast activation by enhancing the signaling pathways of the receptor activator of NF- $\kappa$ B (Atzeni and Sarzi-Puttini 2013). Furthermore, TNF- $\alpha$  hinders the formation of proteoglycan components in chondrocytes and contributes to the degradation of the

ECM by prompting the release of collagenases and aggrecanases, such as MMP-3, mirroring the impacts of IL-1 $\beta$  (Molnar et al. 2021). Considering its potent pro-inflammatory actions, the neutralization of TNF- $\alpha$  might be a potential therapeutic strategy for OA. However, in a network meta-analysis that compared the efficacy and safety of biologics neutralizing TNF- $\alpha$  in knee OA patients, it was found that while pain relief was achieved, no significant differences were observed between biologics and placebo in terms of physical function and stiffness (Li, Mai, et al. 2022).

TGF- $\beta$  constitutes a large family of growth factors that play an essential role in early embryonic development, postnatal growth, regulation of cell proliferation, differentiation, apoptosis, migration in various tissues. In mammals, TGF- $\beta$  is synthesized and secreted with a latency-associated peptide domain. Activation of TGF- $\beta$  necessitates the cleavage of this latency-associated peptide domain, which subsequently leads to the release of the mature functional domain (van der Kraan 2022; Shen, Li, and Chen 2014; Pm et al. 2009; Gordon and Blobel 2008).

TGF- $\beta$  has been shown to activate both canonical (SMAD-dependent) and non-canonical (MAPK, PI3K, Rho-like GTPases, and Janus kinases (JAK)-signal transducer and activator of transcription proteins (STAT) signaling pathways (Thielen et al. 2021; Matsuzaki 2013). Macrophages, fibroblasts, and osteoblast cells are capable of producing and activating TGF- $\beta$  within joints (Thielen et al. 2021; Zheng et al. 2018). Activation of TGF- $\beta$  inhibits chondrocyte hypertrophy and stimulates the expression of Prg4, the gene that encodes lubricin, an essential molecule that reduces joint friction (Miyatake et al. 2016). In addition, TGF- $\beta$  inhibits inflammatory pathways, including IL-6 signaling (Wiegertjes et al. 2019).

While the absence of TGF- $\beta$  signaling is detrimental to healthy joints, inhibiting TGF- $\beta$  limits osteoarthritis progression in experimental animal models (van der Kraan 2022). The analysis of subchondral bone in a mouse model of knee osteoarthritis, induced by changes in mechanical loading, revealed disruptions in the subchondral bone microstructure. Additionally, there was an increase in the number of osteoclasts, evidenced by a rise in tartrate-resistant acid phosphatase (TRAP)-positive staining. These changes resembled patterns seen in a mouse model of Camurati-Engelmann disease (CED) that is characterized by TGF- $\beta$  activation in the subchondral bone. Administering the T $\beta$ RI inhibitor SB-505124 (1 mg/kg) to knee-OA mice prevented osteoarthritis changes in both the subchondral bone and articular cartilage. However, high concentrations of the T $\beta$ RI inhibitor (2.5 and 5 mg/kg) resulted in the loss of proteoglycan in the articular cartilage, suggesting that TGF- $\beta$  has distinct roles in the subchondral bone and articular cartilage. Consequently, inhibiting TGF- $\beta$  activity in the subchondral bone could potentially prevent articular cartilage degeneration during osteoarthritis development (Zhen et al. 2013). Similar findings, as observed in knee osteoarthritis, were also reported in a recent study investigating the role of TGF- $\beta$  signaling in the cartilage and subchondral bone of the TMJ in TMD rat model induced by occlusal changes. When compared to controls, the TMJ's subchondral bone in the TMD rat models was notably altered, as shown by  $\mu$ CT analysis. The TMD group exhibited a significant decrease in BV/TV and a marked increase in Tb.Sp. Additionally, TMD rats presented a considerable rise in the number of TRAP-positive cells in the subchondral bone compared to controls. When using CED mouse models that possess mutations to release active TGF- $\beta$ 1 by osteoblasts, it was also evident that an increase in TGF- $\beta$ 1 triggers OA in the TMJ. This was confirmed through histological changes in the articular cartilage and  $\mu$ CT images of the subchondral bone. Importantly, inhibiting the TGF- $\beta$  receptor I mitigated the progression of TMJ OA in the TMD

models, implying that the activation of TGF- $\beta$  signaling might be instrumental in TMJ OA development (Zheng et al. 2018).

While the impact of inhibiting TGF- $\beta$  activity in clinical studies remains unreported, an association between TGF- $\beta$  concentrations and the severity of Knee OA has been observed (van der Kraan 2022). In one study involving 160 patients with knee OA and 80 healthy controls, TGF- $\beta$ 1 serum levels were found to be significantly higher in the knee OA group ( $p=0.01$ ). Moreover, the average TGF- $\beta$ 1 serum levels directly correlated with the Kellgren-Lawrence (KL) knee OA severity grading system. Serum levels of TGF- $\beta$ 1 were significantly lower in KL grade 1 compared to those in KL grades 2, 3, and 4 ( $p=0.002$ ). Logistic regression analysis showed a positive correlation between TGF- $\beta$ 1 levels and the onset of knee OA (He et al. 2017). Another study investigated the subchondral bone regions beneath cartilage that was visibly present (CA+) and cartilage that was denuded (CA-) in 35 OA arthroplasty patients, consisting of 15 men and 20 women. The researchers measured the concentration of active TGF- $\beta$ 1 using ELISA and evaluated its correlation with bone quality (via synchrotron micro-CT), cellularity, and vascularization (using histology). Bone samples from CA- regions exhibited significantly higher concentrations of active TGF- $\beta$ 1 protein than those from CA+ regions. Furthermore, trabecular bone in CA- areas had increased bone volume, greater trabecular number, and reduced trabecular separation compared to CA+ regions (Figure 1.18). Additionally, CA- bone areas revealed a higher osteocyte density with larger, less spherical osteocyte lacunae and enhanced bone matrix vascularity compared to CA+ regions (Figure 1.19). A statistically significant relationship was found between an increase in levels of active TGF- $\beta$ 1 and an increase in bone volume. Additionally, more severe OA was associated with a decrease in osteoclast density and lacunar volume. Overall, the results of this study indicate that an augmented concentration of active TGF- $\beta$ 1 in the subchondral bone

of human knee OA is spatially linked to compromised bone quality and heightened disease severity. Furthermore, it suggests TGF- $\beta$ 1's potential as a therapeutic target in curbing or mitigating the progression of human OA (Muratovic et al. 2022).

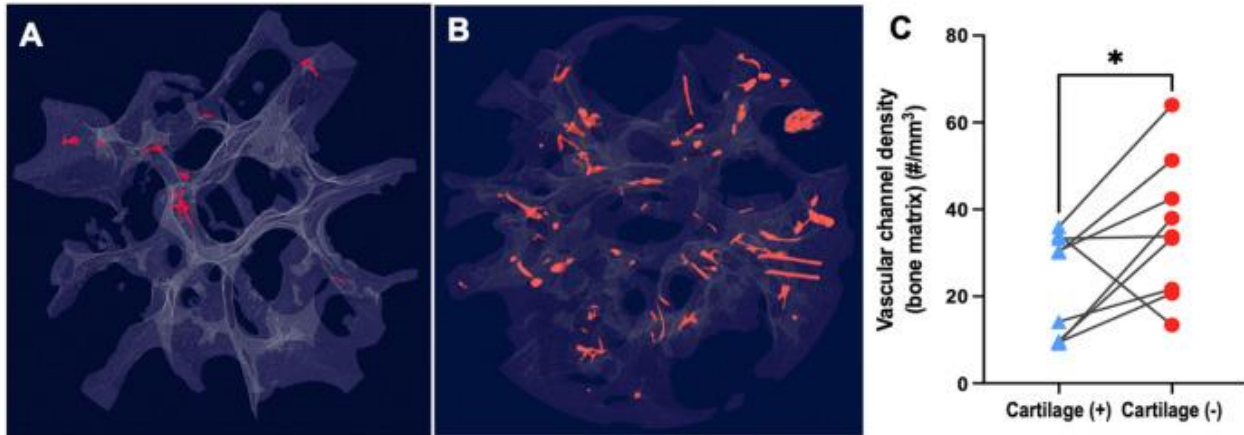


Figure 1.18: 3D Reconstructions of Subchondral Bone Microstructures Using Synchrotron Radiation  $\mu$ CT: (A) CA+ Regions and (B) CA- Regions. Subchondral bone beneath extensively degraded cartilage shows a marked increase in bone volume and trabecular number, with reduced trabecular spacing. Adapted from “Elevated levels of active Transforming Growth Factor  $\beta$ 1 in the subchondral bone relate spatially to cartilage loss and impaired bone quality in human knee osteoarthritis” by Muratovic et al., 2022, *Osteoarthritis and Cartilage*; 30 (6): 896-907. <https://doi.org/10.1016/j.joca.2022.03.004>

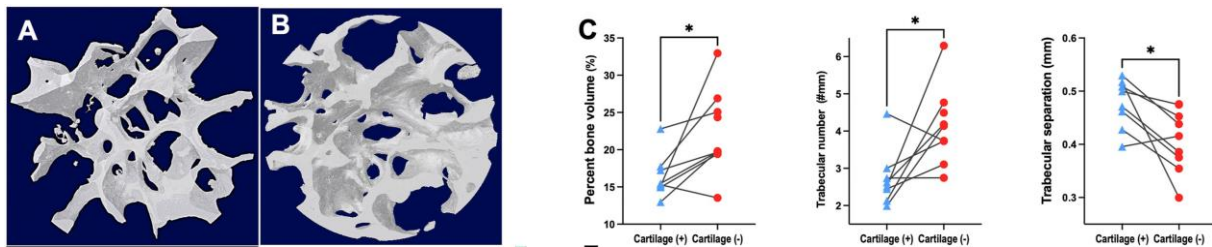


Figure 1.19: 3D Reconstructions of Subchondral Bone (light grey) and Vascular Canals (red) Using Synchrotron Radiation  $\mu$ CT in (A)CA+ and (B) CA- Regions. (C) Quantitative findings highlight a notable increase in the density of vascular canals within the bone matrix. Adapted from “Elevated levels of active Transforming Growth Factor  $\beta$ 1 in the subchondral bone relate spatially to cartilage loss and impaired bone quality in human knee osteoarthritis” by Muratovic et al., 2022, *Osteoarthritis and Cartilage*; 30 (6): 896-907. <https://doi.org/10.1016/j.joca.2022.03.004>.

Tissue inhibitors of metalloproteinases (TIMPs) represent intrinsic proteins that control MMP activity. Variations in the levels of TIMPs or MMPs can induce changes to the MMP/TIMP ratio, consequently impacting MMP function. Apart from their MMP inhibitory role, TIMPs regulate extracellular matrix turnover, tissue remodeling, and cellular conduct. In vitro studies have demonstrated the presence of TIMP-1 in chondrocytes, osteoblasts, osteocytes, and osteoclasts, suggesting its potential influence on bone maintenance and remodeling (Cabral-Pacheco et al. 2020; Xi et al. 2020; Cui, Hu, and Khalil 2017; Brew and Nagase 2010; Haeusler et al. 2005). Overexpression of TIMP-1 in osteoblasts led to an increase in trabecular bone volume and a reduction in trabecular separation in female mice. Furthermore, an assessment of the bone's dynamic histomorphometric parameters indicated declines in both the mineralizing surfaces and the bone formation rate (Geoffroy et al. 2004). Interestingly, although higher concentrations of TIMP-1 result in decreased bone resorption, physiological concentrations of TIMP-1 enhance the bone-resorbing activity of osteoclasts in vitro, a function that appears distinct from its MMP inhibiting activity (Liang et al. 2016; Sobue et al. 2001).

In a prospective clinical study, a cohort of 29 patients was recruited to investigate the association between TIMP-1 serum levels and the rapid progression of hip osteoarthritis, which was defined by the rate of joint space narrowing. Among these 29 individuals, ten displayed joint space narrowing exceeding 0.6 mm per year, a categorization referred to as accelerated progression. Within this subgroup of patients, both the initial TIMP-1 concentration and the delta value representing the change in TIMP-1 serum levels (measured as the difference between the initial and final TIMP-1 concentrations) exhibited correlations with the progression of joint space narrowing. The reduction in TIMP-1 serum levels could potentially be ascribed to a decrease in localized



production (and/or an increase in consumption), thus contributing to degradation of the cartilage's extracellular matrix (Chevalier et al. 2001). Employing a multiplex immunoassay technique, an in-depth analysis was conducted on synovial fluid collected from 25 patients diagnosed with knee osteoarthritis. The relationship between knee osteoarthritis symptoms and radiographic severity and 47 cytokines, chemokines, and growth factors was investigated using multivariate regression analysis with adjustments for false discovery rate. The severity of radiographic knee osteoarthritis was determined by parameters like Kellgren-Lawrence grade, joint space narrowing, and osteophyte scores. TIMP-1 and VEGF were found to be significantly correlated to radiographic osteoarthritis severity. Additionally, VEGF, MMP-3, TIMP-1, and MCP-1 were associated with knee osteoarthritis symptoms. These findings suggest that these specific biomarkers might hold promise as potential therapeutic targets, particularly for individuals at elevated risk of progressive knee osteoarthritis (Haraden et al. 2019).

In a recent study, synovial fluid samples were collected from the knees of 65 patients diagnosed with osteoarthritis, comprising 46 individuals in the early knee OA category (KL grade  $\leq 2$ ) and 19 individuals in the advanced knee OA category (KL grade  $\geq 3$ ). An assessment of interleukin levels, matrix metalloproteinase concentrations, and tissue inhibitor of metalloproteinase levels was conducted using a multiplex ELISA-based method. The results revealed significantly lower concentrations of MMP-3 and TIMP-1 in the early OA patient group compared to the end-stage OA patient group ( $P < 0.01$ ). These findings imply the potential utility of these markers in providing comprehensive insights into the pathological progression of OA (Plsikova Matejova et al. 2021).

Plasminogen activator inhibitor-1 (PAI-1) belongs to the family of serine protease inhibitors (Serpin). It mainly inhibits tissue-type and urokinase-type plasminogen activators, preventing

fibrinolysis. Recent studies have shed light on expanding function of serine proteinases in cartilage degradation such as activation of inactive matrix metalloproteinases, interaction with cell-surface receptors, cytokine regulation, and the direct breakdown of the extracellular matrix. Additionally, research has demonstrated that the levels of their inhibitors influence the progression of osteoarthritis (Wilkinson 2021; Ajekigbe et al. 2019; Moritake et al. 2017; Kaji 2016; Czekay et al. 2011). One study involved isolating human articular chondrocytes from osteochondral specimens taken from ten patients with advanced knee osteoarthritis undergoing arthroplasty. There was a marked decline in PAI-1 expression in chondrocytes located in lesioned areas compared to non-lesioned areas. Moreover, the chondrocytes from both lesional and non-lesional areas of human cartilage showed varied reactions to shear stress in terms of PAI-1 gene expression. Under moderate shear stress, chondrocytes from non-lesional areas displayed an increase in PAI-1 expression. Whereas chondrocytes from lesioned areas not only had significantly reduced PAI-1 expression at rest but also lacked the capacity to enhance PAI-1 expression in response to moderate shear stresses. This atypical chondrocyte response to excessive loading might disrupt the balance between catabolic and anabolic activities during cartilage ECM remodeling, leading to an increase in MMPs and potentially accelerating the progression of OA (Yeh et al. 2009). Another study examined the roles of PAI-1 in the subchondral bone of OA knees utilizing PAI-1-knock out (KO) and wild type (WT) mice. The researchers' findings indicated that OA led to a reduction in trabecular bone mineral density of the subchondral bone in PAI-1 KO mice, as determined by quantitative computed tomography. Moreover, the deficiency of PAI-1 appeared to exacerbate subchondral osteopenia after OA's induction in mice. This compounded effect seemed to further deteriorate cartilage, although the observed statistical differences were not significant. In addition, the absence of PAI-1 was associated with an elevated RANKL expression, triggered

by IL-1 $\beta$ , in mouse osteoblasts. There was also an increased osteoclast formation from mouse bone marrow cells in the presence of RANKL and M-CSF. Remarkably, the lack of PAI-1 significantly enhanced the RANKL expression and the RANKL/OPG mRNA ratio in mouse primary osteoblasts. Based on these observations, the researchers suggested that PAI-1 could offer protection against bone resorption in the subchondral bone associated with osteoarthritis (Moritake et al. 2017).

Interferons (IFNs) were first identified as agents that inhibit viral replication. They are divided into type I, type II, and type III, based on receptor specificity and sequence homology. IFN- $\gamma$  is a type II interferon produced by CD4<sup>+</sup> T helper cell type 1 (Th1) lymphocytes, CD8<sup>+</sup> cytotoxic lymphocytes, natural killer (NK) cells, and professional antigen-presenting cells (APCs). The role of IFN- $\gamma$  varies depending on its cellular source: production by APCs is essential for their self-activation and for activating adjacent cells; when secreted by NK cells, it plays a crucial role in early host defense against infections, and T lymphocytes become the primary source of IFN- $\gamma$  during the adaptive immune response (Shan et al. 2017; Lin and Young 2014; Schroder et al. 2004).

While osteoarthritis has traditionally been categorized as a non-inflammatory condition when compared to rheumatoid arthritis (RA), recent research suggests that for specific patient subsets, OA exhibits characteristics of inflammation. In such cases, patients frequently display instances of inflammatory infiltration in their synovial membranes (Hügler and Geurts 2017; Withrow et al. 2016; Ponchel et al. 2015; de Lange-Brokaar et al. 2012; Sakkas and Platsoucas 2007). Investigations have indicated that the number of inflammatory cells within synovial tissue tends to be lower in OA patients compared to those with RA, but still higher than healthy individuals (Li et

al. 2017; Pessler et al. 2008; Rollín et al. 2008; Ishii et al. 2002). Among the inflammatory cells identified within the synovial membranes of OA patients, T cells were notably abundant. A study involving 25 OA patients and 13 healthy controls revealed that circulating Th1 cells (IFN- $\gamma$ +CD4+CD8- T cells) and serum IFN- $\gamma$  levels were notably higher in OA patients compared to healthy controls (Qi et al. 2016; Pessler et al. 2008). Despite early experiments suggesting that IFN- $\gamma$  concentrations in OA patients' synovial fluid fell below the limit of detection through ELISA analysis, reverse transcription polymerase chain reaction (RT-PCR) analysis demonstrated IFN- $\gamma$  expression in cells from OA patients' synovial fluid when stimulated with PHA and ionomycin (Li et al. 2017; Haynes, Hume, and Smith 2002). Using knee OA mouse models, the expression of IFN- $\gamma$  was observed to increase at the onset of OA (30 days after induction) and subsequently decrease in later stages (90 days after induction) (Shen et al. 2011). Meanwhile, a study analyzing the synovial fluid from 34 OA patients undergoing knee arthroplasty found a significant correlation between OA severity and knee pain levels with IFN- $\gamma$  concentrations, suggesting that IFN- $\gamma$  might be involved in osteoarthritis progression (Nees et al., 2019). In chondrocytes isolated from undamaged femoral head cartilage of patients with hip osteoarthritis, the capacity of IFN- $\gamma$  to suppress IL-1-induced MMP expression was reduced. This reduction was attributed to decreased levels, activity, and signal transduction of IFN- $\gamma$ R1. Thus, the modulation of IFN- $\gamma$ R1 and the diminished response to endogenous IFN- $\gamma$  may be key mechanisms in the pathogenesis of osteoarthritis and cartilage degradation (Ahmad, El Mabrouk, et al. 2009).

Chemokines constitute a family of small cytokines (8–14 kDa) that hold a pivotal role in orchestrating the movement of inflammatory cells from the vascular system to tissues at the site of inflammation. Specifically, they exhibit the ability to induce chemotaxis in neutrophils, macrophages, and T lymphocytes. This, in turn, triggers the production of inflammatory cytokines, fur-

ther prompting the upregulation of matrix-degrading enzymes, leading to degradation of the extracellular matrix. Additionally, the inflammatory cytokines possess the capacity to stimulate both synovium and other tissues to generate additional chemokines (Qiao et al. 2023; Tipton, Christian, and Blumer 2016; Raman, Sobolik-Delmaire, and Richmond 2011).

CXCL-16 represents a membrane-bound protein chemokine characterized by a glycosylated mucin-like stalk and a cytoplasmic domain. Following cleavage, soluble CXCL-16 functions as a chemoattractant for cells that express the CXCR6 receptor, including CD8 T cells, NK T cells, and Th-1 polarized T cells. The interaction between CXCL-16 and CXCR6 initiates the activation of various pathways such as calcium mobilization, Akt/mTOR, and ERK/MAPK, along with their downstream effectors like NF- $\kappa$ B which potentially underlies the heightened secretion of cytokines such as TNF- $\alpha$  and IFN- $\gamma$  (Li, Pan, et al. 2022; Nakase et al. 2012).

Significant expression of CXCL-16 has been observed in the serum of knee osteoarthritis patients (n=32) compared to healthy subjects (n=40), as determined through ELISA assay (Alimoradi et al. 2023; Li et al. 2016). Interestingly, investigation into osteoclast-derived factors, such as TGF- $\beta$ 1, as contributors to bone remodeling, has revealed that TGF- $\beta$ 1 enhances the expression of CXCL-16 in osteoclasts. This enhancement subsequently facilitates the migration of osteoblasts, potentially serving to restore lost bone during the resorptive phase of bone turnover (Ibáñez et al. 2022; Ota et al. 2013). Moreover, the 3D chemotaxis assay demonstrated that CXCL-16 at a concentration of 50 ng/mL, unlike at 10 ng/mL, triggers chemotaxis in C3H10T1/2 cells. These cells share functional similarities with mesenchymal stem cells, suggesting a potential role in aiding the recovery of damaged bones (Redding et al. 2020).

CC represents another subfamily within the chemokines. The interplay between chemokine ligands (CCLs) and receptors (CCRs) is crucial, as it facilitates the recruitment of various immune cells and activates several signaling pathways, both of which are implicated in the onset and progression of osteoarthritis. Moreover, CCLs can augment the expression of matrix metalloproteinases, leading to cartilage degradation (Mehana, Khafaga, and El-Blehi 2019; Miller et al. 2016; Xu et al. 2015; Vergunst et al. 2005). A study sought to identify molecules that may play roles in communication among different structures within the knee joint, potentially contributing to osteoarthritis development. In this study, synovium and meniscus samples were collected from both early and end-stage OA patients; each group included five individuals. Researchers assessed genes and proteins of several cytokines, chemokines, metalloproteases, and their inhibitors. Intriguingly, the gene expression of CCL21/6ckine was detected in both individually cultured synovial biopsies and those in coculture settings. The 6ckine protein was more abundant in meniscus cultures, both on their own and in combination, compared to the synovium-only cultures. Most notably, the protein levels of CCL21 were higher in cultures derived from end-stage OA samples. Specifically, cocultures showed significantly elevated levels when compared to individual cultures ( $p = 0.0264$ ). These findings indicate that 6ckine might play a role in triggering inflammatory changes in early OA and exacerbate the loss of extracellular matrix during the progressive and late stages of OA pathology (Favero et al. 2019).

In addition to the aforementioned roles, CC chemokines are known to influence the differentiation of osteoblasts and osteoclasts within OA joints and can also trigger pain responses (Brylka and Schinke 2019; Glyn-Jones et al. 2015). Interestingly, the CCR7/Rho signaling axis enhances the migration and resorption activities of osteoclasts in response to CCL21. This, in turn, modifies the remodeling of the subchondral bone. Furthermore, CCL21 stimulates the migration and

differentiation of osteoclast precursor cells. This observation points to the potential therapeutic benefits of selectively inhibiting CCL21 to address the disturbed subchondral bone remodeling associated with OA (Zhang, Liu, et al. 2023; Lee et al. 2017).

Brain-derived neurotrophic factor (BDNF) belongs to the neurotrophin family of growth factors and plays an essential role in neuronal growth, survival, and the modulation of pain sensitivity in the central nervous system (Miranda et al. 2019; Bathina and Das 2015). Changes in its levels have been observed in certain chronic pain conditions and during inflammation (Chen, Walwyn, et al. 2014; Simão et al. 2014; Sarchielli et al. 2007). Multiple studies have highlighted the significance of neurotrophins, including BDNF, in arthritis (Zhang et al. 2022; Orhurhu et al. 2020; Forsgren 2009; Asami et al. 2006). Elevated BDNF staining has been noted in fibroblasts and macrophages of osteoarthritic synovial tissue compared to healthy counterparts, with increased BDNF mRNA levels also identified in OA synovial fluid cells (Bratus-Neuenschwander et al. 2018; Blaschke et al. 2003). In a study involving 27 knee OA patients and 19 healthy participants, knee OA patients demonstrated significantly higher mean plasma BDNF levels compared to the healthy group ( $p < 0.05$ ). Further, a significant correlation emerged between plasma BDNF levels and self-reported pain. These results imply that BDNF levels might be linked to the joint pain mechanism during the early inflammatory phase of knee OA (Gowler et al. 2020). Utilizing clinical knee synovial samples from OA patients and animal models with induced knee OA were analyzed to investigate the impact of BDNF/TrkB signaling on chronic OA pain. Both BDNF and TrkB mRNA and proteins were detected in the knee synovia of OA patients. In experiments involving rats with induced knee OA, the effects of peripheral BDNF injections and the neutralization of endogenous BDNF using the TrkB-Fc chimera on established pain behaviors were as-

sessed. Direct administration of BDNF into the joint intensified OA pain behavior in rats, whereas the injection of the TrkB-Fc chimera mitigated these behaviors. These findings indicate a possible role of peripheral knee joint BDNF/TrkB signaling in chronic OA joint pain and suggest a potential therapeutic approach for addressing OA pain (Sorkpor et al., 2021).

While many studies primarily explore the relationship between BDNF and pain, it's important to highlight that BDNF can also influence bone health. Research demonstrates that neurotrophins are prevalent in skeletal tissues and play roles in chondrogenesis, osteoblastogenesis, and osteoclastogenesis (Raheem1 et al. 2020; Skaper 2008; Mogi et al. 2000). Specifically, BDNF promotes the differentiation of osteoblast-lineage cells in vitro and enhances the formation of new bone in vivo. The expression of TrkB by osteoblasts and osteocytes on the bone surface of mouse mandibles up to 28 days post-osteotomy indicates that bone cells continue to receive exogenous BDNF signals. This interaction subsequently results in persistent active bone remodeling, which correlates with the narrowing of the bone marrow space and bone lacunae. These findings suggest that BDNF, produced due to peripheral nerve damage, may contribute to sclerotic changes in the surrounding alveolar bone (Ida-Yonemochi et al. 2017).

Epithelial Neutrophil-Activating Peptide 78 (ENA-78), also known as CXC Chemokine Ligand 5 (CXCL5), is a potent chemotactic agent that directs neutrophils to sites of infection or inflammation. Furthermore, its angiogenic properties, attributed to the presence of the ELR motif, also contribute to inflammation and disease progression (Cheng et al. 2019; Yoshida et al. 2014; Szekekanecz et al. 2010; Koch et al. 2001). Using Spearman correlation analysis, it was found that the concentrations of ENA-78/CXCL5 in the synovial fluid samples from 41 patients with knee OA were positively associated with increased T1rho relaxation times, which suggest decreased proteoglycan content in the cartilage and potential cartilage matrix loss. This correlation suggests



that ENA-78/CXCL5 might be involved in the development of knee osteoarthritis. Among various cytokines, it was demonstrated that the ENA-78 protein played a role in the onset of adjuvant induced arthritis in rats (Szekanecz et al. 2000). Interestingly, when anti-human ENA-78 was administered prior to the onset of arthritis, it impacted the disease's severity. However, administering it after the clinical manifestation had no discernible effect on the disease's progression (Haringman, Ludikhuizen, and Tak 2004).

Vascular endothelial growth factor (VEGF) is a potent angiogenic factor and an essential regulator of angiogenesis during bone development and remodeling. During osteogenesis, VEGF secretion not only plays a crucial role in stimulating endothelial cells to proliferate, migrate, differentiate, and form tubes but also promotes bone formation and healing by directly influencing osteoblast survival, chemotactic migration, and activity (Hamilton et al. 2016; Yuan et al. 2014; Neve et al. 2013). In OA, VEGF expression increases in the articular cartilage, synovium, synovial fluid, subchondral bone, and serum (Sohn et al. 2012; Fransès et al. 2010; Walsh et al. 2010; Ray, Shakya, and Ray 2007; Giatromanolaki et al. 2003; Smith et al. 2003; Pfander et al. 2001). Local intra-articular injections of VEGF into the knee joints of mice led to OA-like changes, characterized by proteoglycan loss, calcification of the articular cartilage, cartilage degradation, subchondral bone sclerosis, osteophyte formation, and synovial hyperplasia. Notably, changes in the subchondral bone appeared before cartilage degeneration, and the severity of these changes intensified with the number of VEGF injections. Meanwhile, the control group that received saline injections displayed no signs of OA-like alterations (Ludin et al. 2013). Interestingly, in a meta-analysis evaluating genes associated with osteoarthritis, 199 genes were initially identified using the Human Genome Epidemiology Navigator. An ensuing analysis of 9 genome-wide as-

sociation studies, encompassing thousands of patients with knee OA, hip OA, and control subjects, revealed that VEGF was significantly associated with OA (Rodriguez-Fontenla et al. 2014). A concurrent meta-analysis of 11 case-control studies, involving 302 osteoarthritis patients and 195 healthy individuals, demonstrated that VEGF expression levels were significantly elevated in osteoarthritis patients compared to healthy controls (Yuan et al. 2014). Notably, the analysis of 20 patients with knee osteoarthritis further demonstrated that synovial VEGF levels had a significant correlation not only with the radiographic severity of the disease but also with the intensity of OA pain (Gaballah et al. 2016). In a study with Sprague-Dawley mice, the impact of weekly intraarticular injections of VEGF on the temporomandibular joint was assessed. The mice exhibited significant cartilage degradation, accompanied by elevated levels of RANKL and an increase in VEGFR2-positive chondrocytes. Micro-CT scans revealed subchondral bone loss, and histological analyses highlighted an upsurge in TRAP<sup>+</sup> osteoclasts within this bone. Additionally, *in vitro* evaluations demonstrated VEGF's capacity to amplify osteoclast differentiation. These findings suggest that VEGF may induce TMJ OA by detrimentally affecting both the cartilage and subchondral bone (Shen et al. 2015).

Vascular Endothelial (VE)-cadherin is a specific adhesion protein found in the adherens junction of the vascular endothelium (Grimsley-Myers et al. 2020; Sauteur et al. 2014; Lenard et al. 2013). Utilizing a microarray platform, VE-cadherin emerged as one of the proteins with markedly different expression levels in the serum of patients with knee OA, exhibiting an increase of 20–35% compared to control individuals (Ling et al. 2009). VE-cadherin serves an important role in endothelial barrier maintenance and is pivotal in the maturation, extension, and remodeling of blood vessels, which are defining features of angiogenesis. VE-cadherin is composed of extracellular cadherin motifs, a transmembrane domain and an intracellular domain that mediates

interactions with  $\beta$ -catenin, p120-catenin, and  $\gamma$ -catenin.  $\beta$ -catenin and  $\gamma$ -catenin in turn connect to actin-binding  $\alpha$ -catenin and other proteins. The intracellular complex of VE-cadherin and catenins is essential for junctional stability. Several soluble factors, such as VEGF and TNF- $\alpha$ , elicit tyrosine phosphorylation of VE-cadherin, which corresponds with an increase in vascular permeability and impacts the stability of endothelial cell-cell junctions (Claesson-Welsh, Dejana, and McDonald 2021; Aragon-Sanabria et al. 2017; Barry, Wang, and Leckband 2015; Niessen, Leckband, and Yap 2011; Harris and Nelson 2010). VE-cadherin has also been found to enhance the TGF- $\beta$  response in endothelial cells, suggesting its role in effectively activating this signaling pathway (Rudini et al., 2008). A recent study has demonstrated that the CDH5 gene, responsible for encoding VE-cadherin, is prominently related with the dysregulation of TGF- $\beta$  signaling. This finding suggests that CDH5 may play a significant role in the pathogenesis and advancement of osteoarthritis. (Wang, Jiang, and Zhang 2019).

Angiogenin (ANG) is a ribonuclease known for its growth-stimulating properties. Specifically, it stimulates the growth and proliferation of endothelial cells and promotes neovascularization. Moreover, ANG plays pivotal roles in various physiological and pathological processes, governing cell proliferation, viability, migration, infiltration, and differentiation. It achieves these effects by activating specific signaling transduction pathways in different target cells (Liu et al. 2021; Sheng and Xu 2016; Kishimoto et al. 2005). Within the metaphyseal region, ANG+ cells are predominantly expressed in RANK+TRAP+ osteoclasts located just below the growth plate. This suggests that ANG produced by these osteoclasts is crucial for sustaining the adjacent blood vessels in developing long bones (Liu et al. 2021). An analysis of synovial fluid showed significantly heightened concentrations of angiogenin in patients with acute and chronic synovitis. The angiogenin protein was found to be secreted by synovial fibroblasts cultured from patients with

OA. Such findings suggest the potential role of angiogenin in mediating local inflammation in arthritis, possibly through its influence on angiogenesis and leucocyte activity (Liote et al., 2003). Moreover, proteomic analysis of articular cartilage samples from patients with knee OA showed that ANG expression levels were significantly higher in cases of early-stage cartilage destruction than in more advanced stages (Chae et al. 2021).

Over the past three decades, the diverse nature of osteoarthritis has been described as a "mixed bag of disorders." While there has been significant interest in using emerging and traditional OA-related molecules as biomarkers for disease assessment, their integration into clinical diagnosis remains limited due to the low sensitivity of existing markers and pronounced phenotypic heterogeneity among patients. Given this complexity, there is a prevailing argument that osteoarthritis may be more accurately described as a syndrome rather than a singular disease. To harness the full potential of these biomarkers in optimizing patient care, and to advance more precise diagnostic and disease progression prediction and methodologies, there is a need to assess a set of biological markers in tandem with comprehensive, longitudinal multicenter studies. Such in-depth investigations are pivotal to validate existing biomarkers, decipher their intricate interrelationships, and ascertain their distribution across different biofluids (Sandhu et al. 2023; Bernotiene et al. 2020; Deveza and Loeser 2018; Arden et al. 2015; Henrotin, Pessesse, and Lambert 2014; Blagojevic et al. 2010; Felson 1993; Bjelle 1983).

### **1.9 From Algorithms to Illness: Machine Learning in Medicine**

Worldwide, a significant gap in the effective diagnosis of diverse diseases exists. The intricate nature of disease pathways and the inherent symptomatology in patient cohorts pose profound obstacles in the creation of tools for early detection and efficacious treatment (Ahsan, Luna, and

Siddique 2022a). Progressions in artificial intelligence methodologies, however, have ushered in pivotal transformations within the healthcare sector. Utilizing advanced algorithms allows for the efficient analysis of extensive datasets, yielding precision-targeted information for medical practitioners. This enhances their capacity for evidence-based diagnostic and therapeutic decisions, which can lead to optimized patient outcomes, decreased healthcare expenditure, and heightened patient satisfaction (Sanchez-Martinez et al., 2022).

The Merriam–Webster lexicon defines artificial intelligence “AI” as ‘the capacity of a machine to replicate cognitive human actions.’ At its core, AI represents the emulation of human cognitive functions via computational frameworks. Typically, AI architectures are honed through extensive data sets, discerning patterns therein, which subsequently facilitate prediction for novel data instances (Ozsari et al. 2023; Jha, Lee, and Kim 2022).

Machine learning (ML) represents a fundamental technique for developing AI systems. In 1959, Arthur Samuel, for the first time, introduced the concept of ML by employing it in games and pattern recognition algorithms to assimilate knowledge through experience (Esteva et al. 2017; Awad and Khanna 2015a). Despite this groundbreaking advancement, ML, akin to AI, underwent extended phases characterized by diminished interest and funding, commonly termed as “AI winters”. However, the landscape of ML has undergone a significant transformation in the current era. This change is primarily driven by a combination of recent technological advancements and the introduction of innovative ML frameworks. For instance, the advent of cost-effective parallel computing now enables us to implement sophisticated deep learning models, such as recurrent neural networks. At the same time, algorithms like support vector machines and random forests, when enhanced with techniques like kernelization, bagging, and boosting, allow for ML applications even on smaller datasets. Furthermore, the widespread availability of open-

source tools has made machine learning more popular and accessible. Alongside these changes, the integration of computational tools in healthcare, particularly through electronic health record systems and structured administrative datasets, has enhanced the accessibility of vast health databases for scientific research (Kokol, Kokol, and Zagoranski 2022; Gogas and Papadimitriou 2021; Uddin et al. 2019).

### 1.9.1 Machine Learning Categorization & Algorithms

Machine learning is typically categorized into three main types: supervised learning, unsupervised learning, and reinforcement learning (Figure 1.20).

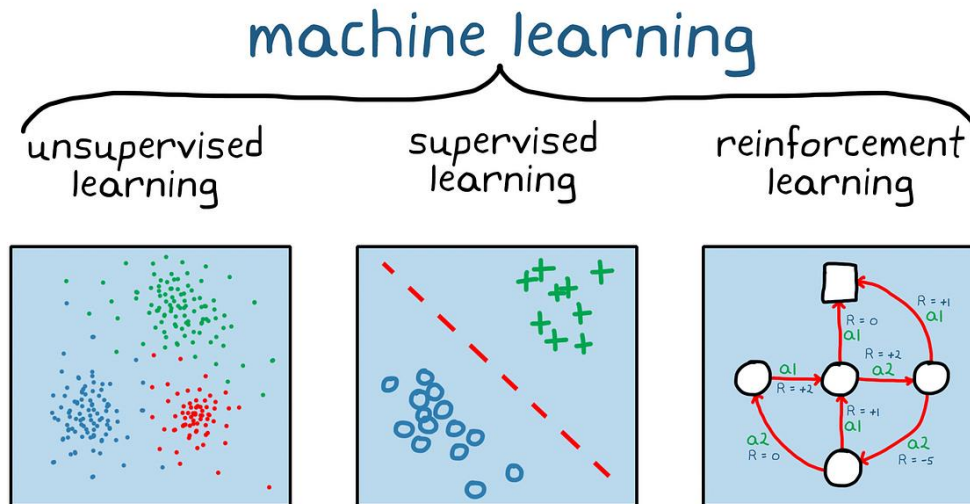


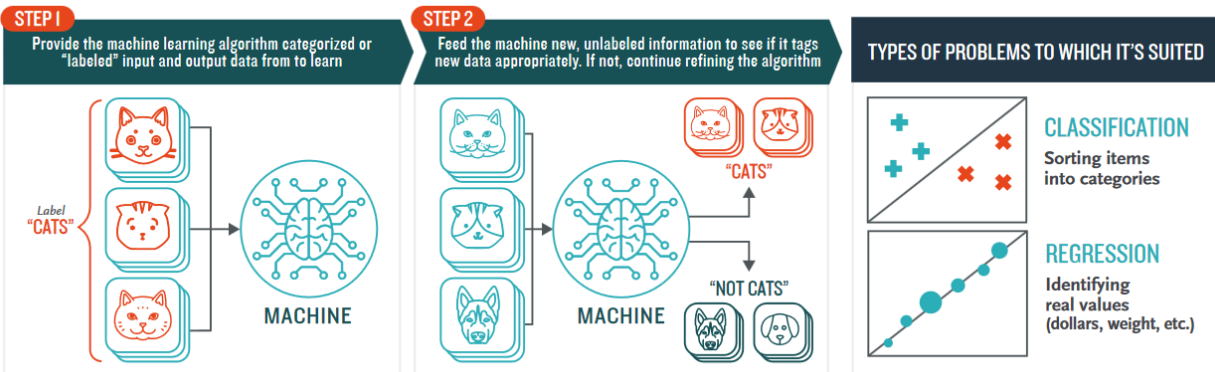
Figure 1.20: Primary Categories of Machine Learning. Adapted from What is reinforcement learning?- MATLAB & Simulink. Available at: <https://www.mathworks.com/discovery/reinforcement-learning.html> (Accessed: 23 August 2023).

Supervised learning algorithms analyze labeled training data sets, where each input is paired with its respective output. Consequently, the inferred ML model can predict the outputs of new data. Common tasks of supervised learning algorithms include classification and regression. The classification task aims to detect a function (discrete value) that aids in splitting the data set into classes based on various parameters. In the regression task, the correlation between dependent

and independent variables is detected during the machine training, and the developed model can predict continuous variables. In unsupervised learning, algorithms detect hidden patterns within an unlabeled data set. That means all variables within the training data set are utilized as inputs, and the machine will automatically discover structures/patterns within that data set without receiving instructions about the desired outcomes. Based on the problem at hand, unsupervised learning algorithms will split the data set into groups (clustering) or find rules representing the relationship between variables within a data set (association) (Figure 1.21). Reinforcement learning, on the other hand, directs an agent to interact with its environment and learn by receiving feedback in the form of rewards or penalties. It is a commonly used for training AI systems in complex domains like robotics, autonomous driving, and logistics (Ghaffar Nia, Kaplanoglu, and Nasab 2023; Ozsari et al. 2023; Ahsan, Luna, and Siddique 2022b; Sarker 2021; Alloghani et al. 2020; Stafford et al. 2020).

Some of the popular ML algorithms include logistic regression, Linear discriminant analysis, support vector machines, decision tree, random forest, naïve Bayes, K-nearest neighbour, and artificial neural network (Ghaffar Nia, Kaplanoglu, and Nasab 2023; Ozsari et al. 2023; Ahsan, Luna, and Siddique 2022b; Sarker 2021).

## How Supervised Machine Learning Works



## How Unsupervised Machine Learning Works

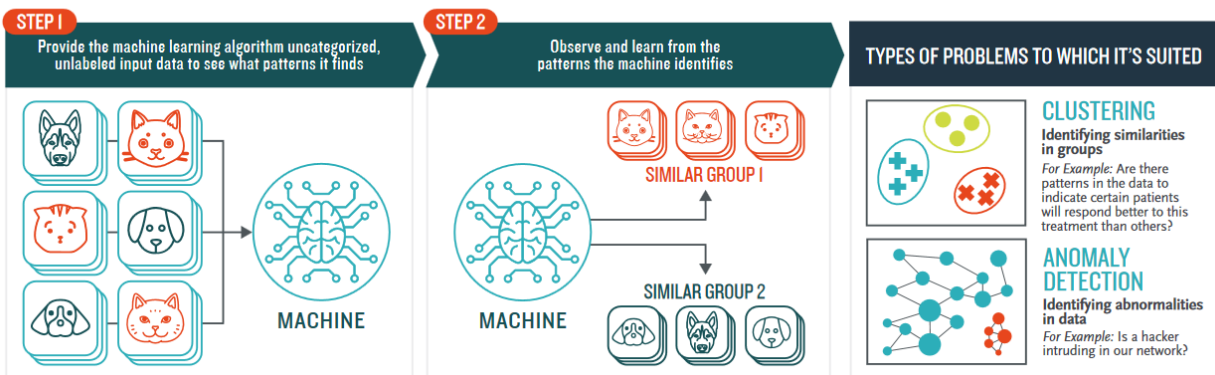


Figure 1.21: Schematic Representation of Supervised and Unsupervised Learning Methods. Adapted from "Data Annotation for Machine Learning: A to Z guide: Lotusqa2021, Lotus QA - Leading IT Outsourcing Company In Vietnam. Available at: <https://www.lotusqa.com/blog/data-annotation-guide/> (Accessed: 23 August 2023).

Logistic regression (LR) is a potent method in supervised classification. Viewed as an advanced form of standard regression, it's tailored to predict binary outcomes, commonly denoting the event's presence or absence. Through LR, one can reduce the likelihood of a data point belonging to a specific category, with outcomes varying between 0 and 1. To use LR effectively for binary categorization, a defining threshold is required. For instance, if the probability of an input exceeds 0.50, it can be categorized under 'class A', otherwise it falls into 'class B'. Furthermore, LR can be adapted to predict variables with multiple categories, a variant called multinomial logistic regression. The applications of logistic regression (LR) in the field of machine learning encom-



pass a wide range of tasks, including but not limited to the identification of spam emails, the detection of fraudulent online transactions, and the identification of malignant tumors (Ahsan, Luna, and Siddique 2022a; Uddin et al. 2019; Ranganathan, Pramesh, and Aggarwal 2017).

Linear discriminant analysis (LDA) is a method that establishes a linear decision boundary by modeling class conditional densities and implementing Bayes' rule. It can also be viewed as an extension of Fisher's linear discriminant, aiming to project data into a space with fewer dimensions, thus simplifying the model and decreasing computational demands. Typically, LDA assumes each class is fit with a Gaussian density and that all classes have a common covariance matrix. LDA is akin to ANOVA and regression analysis, both of which try to represent a dependent variable through a linear mix of other variables or metrics (Sarker 2021; Pedregosa et al. 2011).

The Support vector machine (SVM) is a widely recognized machine learning technique. That was introduced by Vapnik in the latter part of the 20th century. It is versatile and capable of classifying both linear and non-linear data sets. In its workings, SVM initially projects every data piece into an  $n$ -dimensional feature realm, where ' $n$ ' represents the count of features. The primary objective is to pinpoint a hyperplane that distinguishes data into two classes. This is done by optimizing the margin distance for each class while simultaneously reducing classification inaccuracies. The margin for a given class is defined as the distance from the decision-making hyperplane to the closest data point of that particular class. To put it more technically, each data piece is represented as a dot in  $n$ -dimensional space (with ' $n$ ' being the feature count) and each feature value signifies a distinct coordinate's value. The classification task is achieved by determining a

hyperplane that best divides the two classes with the greatest possible margin (Figure 1.22). In addition to medical diagnosis, SVMs have found utility in a myriad of fields such as facial expression analysis, protein folding predictions, and several others (Alkinani, Al-Hameedi, and Dunn-Norman 2020; Uddin et al. 2019; Gholami and Fakhari 2017; Awad and Khanna 2015b).

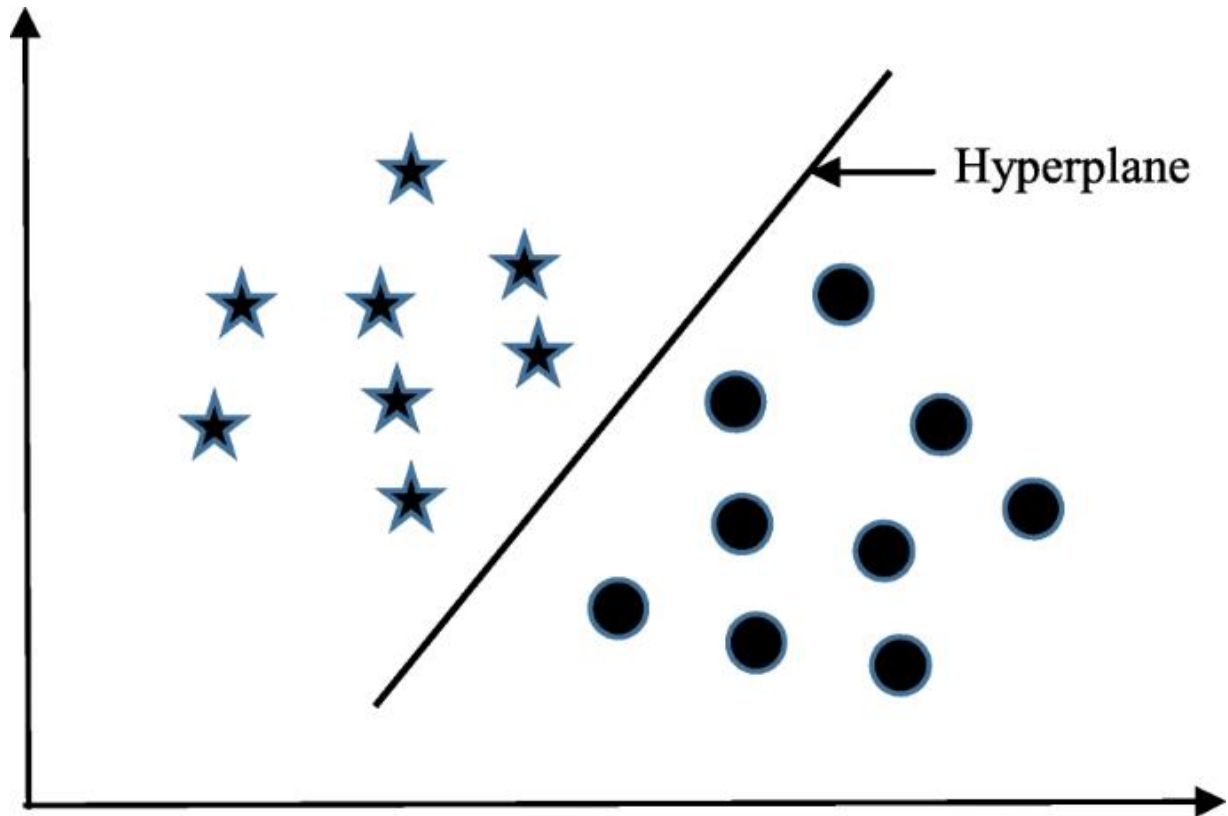


Figure 1.22: A Graphic Demonstration of the Support Vector Machine's Process. The SVM discerns a hyperplane that optimally differentiates the 'star' and 'circle' categories. Adapted from “Comparing different supervised machine learning algorithms for disease prediction” by Uddin et al, 2019, BMC Medical Informatics and Decision Making ,19:281. <https://doi.org/10.1186/s12911-019-1004-8>

A decision tree (DT) serves as one of the earliest and most distinguished machine learning algorithms. It models decision-making logic by mapping tests and their corresponding outcomes in a tree-like framework. In a DT, there are several layers of nodes, with the topmost being the root node. Internal nodes, which have at least one child, symbolize tests on input attributes or varia-

bles. Based on the result of these tests, the classification mechanism moves to the appropriate child node. This testing and branching continue until a leaf node is reached, which represents the final decision outcome (Figure 1.23). Decision trees are valued for their ease of interpretation and fast learning capability. They are frequently integrated into many medical diagnostic procedures. When classifying a sample by navigating through the tree, the cumulative results from tests at every node offer ample information to predict its class. Decision tree algorithms are versatile, serving as the foundation for models like random forest, light gradient boosting machine (LightGBM), and the extreme gradient boosting (XGBoost) (Lai et al. 2023; Sarker 2021; Banerjee et al. 2019; Uddin et al. 2019; Podgorelec and Zorman 2014).

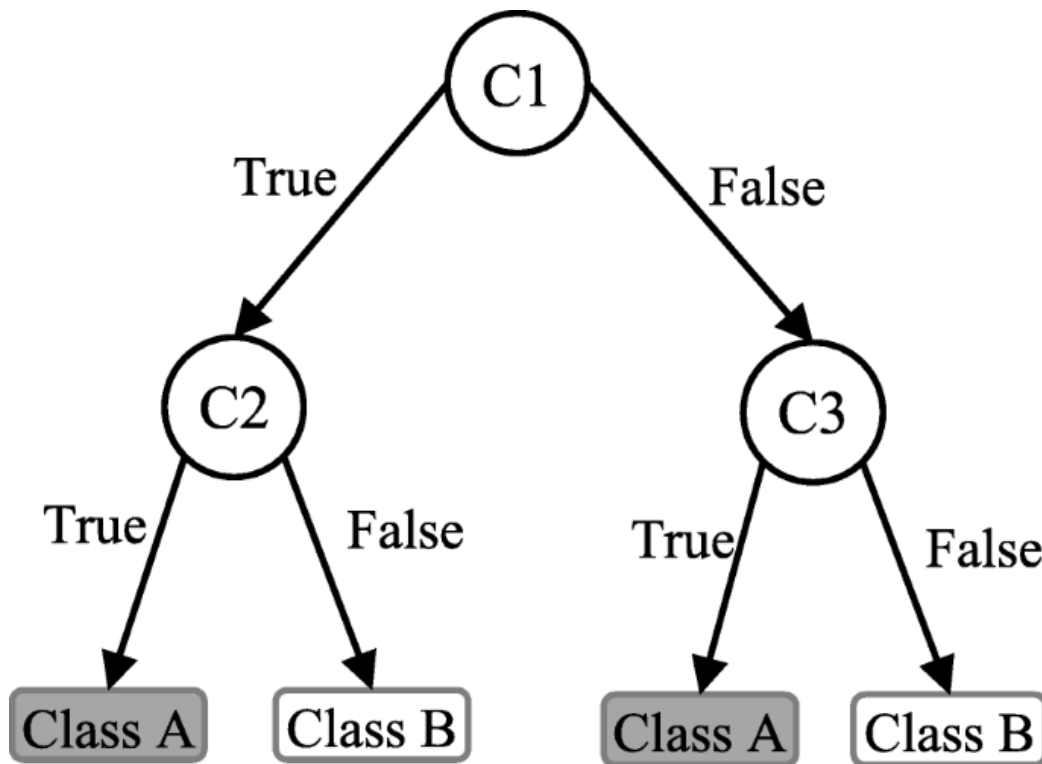


Figure 1.23: A Graphical Representation of a Decision Tree. Circles denote each variable (C1, C2, and C3), while the resultant decisions (Class A and Class B) are displayed using rectangles. To accurately assign a sample to a specific class, each branch is marked as 'True' or 'False', depending on the result derived from its preceding node's test. Adapted from “Comparing different supervised machine learning algorithms for disease prediction” by Uddin et al, 2019, BMC Medical Informatics and Decision Making ,19:281.

A random forest (RF) is an ensemble classifier composed of numerous decision trees (DTs), much like a forest consists of multiple trees. When DTs grow too deep, they tend to overfit the training data, leading to significant classification variations from minor changes in input. These trees can be highly sensitive to their training data, which makes them susceptible to errors on test datasets. In an RF, different DTs are trained on various portions of the training dataset. To classify a new sample, its input vector is passed through each DT in the forest. Each tree examines a distinct segment of the input vector and produces a classification. The forest then selects the classification with the most 'votes' (for discrete outcomes) or averages the results from all trees (for numeric outcomes) (Figure 1.24). Since the RF approach aggregates results from multiple DTs, it mitigates the variance that could arise from using just one DT on the same dataset (Jalloul, Chethan, and Alkhatib 2023; Ali and Ahmed 2022; Sairam Mishra et al. 2021; Uddin et al. 2019).

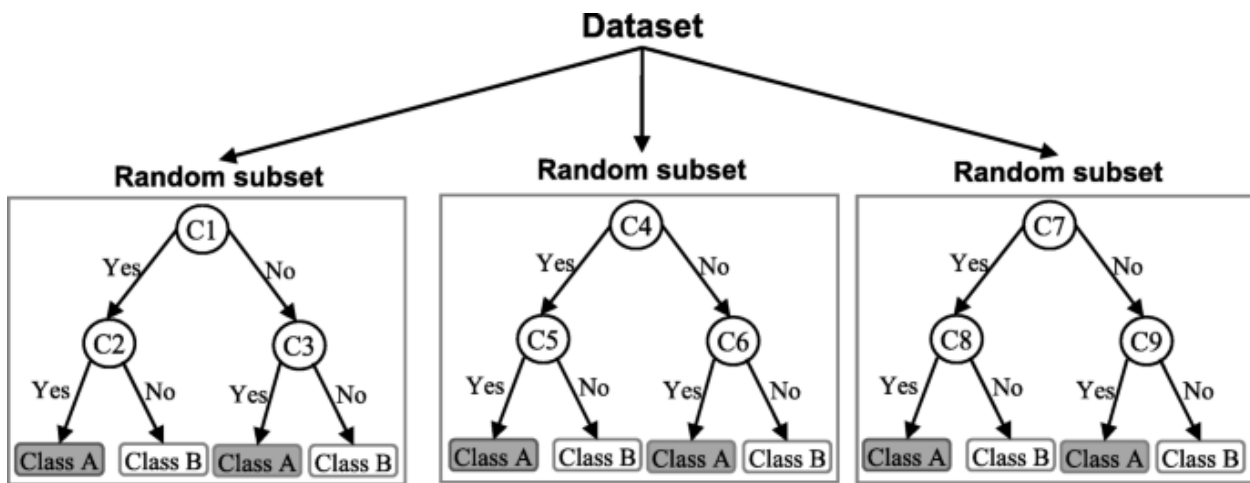


Figure 1.24: A Visual Depiction of a Random Forest Model. Every decision tree within it was trained on a distinct random segment of the training dataset. Adapted from “Comparing different supervised machine learning algorithms for disease prediction” by Uddin et al, 2019, BMC Medical Informatics and Decision Making ,19:281. <https://doi.org/10.1186/s12911-019-1004-8>

Gradient boosted trees (GBT), sometimes referred to as Gradient Descent, is a method that leverages the synergies of multiple models to predict or determine a response. In the boosting approach, models are sequentially constructed. This means that with each new model, weights get refined based on insights from the preceding one. The essence of GBT lies in its step-by-step error reduction; if one model makes mistakes, the subsequent one aims to correct them. This process of combining multiple simple trees significantly improves detection accuracy compared to relying on a single tree, leading to quicker and more efficient performance. Within the GBT framework, every model tree addresses all data points to minimize errors. One key distinction between random forest and gradient boosted trees is the manner of their construction: RF models are developed concurrently, whereas GBTs are formed one after the other (Ali and Ahmed 2022; Wassan et al. 2022; Shailendra Mishra 2022).

Naïve Bayes is a classification method based on Bayes' theorem, which calculates the probability of an event using prior knowledge associated with that event. This method operates on the assumption that a specific attribute within a category is independent of any other attribute, even if they belong to the same category and might be interdependent. Figure 1.25 provides a visual representation of this method. When classifying a new object, represented as a white circle, into the 'green' or 'red' category, an example indicates a higher number of 'green' objects than 'red'. This observation establishes the prior probability regarding the likely categorization of the new object. To classify the 'white' object, a circle encompasses it, capturing various points irrespective of their labels. In the given example, multiple 'red' and a single 'green' point are included. Based on these points, there are specific probabilities associated with the 'white' object being 'green' or 'red'. While the prior probability might suggest a 'green' classification for the 'white' object, the current evidence indicates a 'red' category. The Bayesian approach combines both the prior prob-

ability and the likelihood. Through a multiplication function, the 'posterior' probability is derived. Using both these probabilities, the Naïve Bayes method determines that the 'white' object belongs to the 'red' category (Gohari et al. 2023; de Souza et al. 2022; Uddin et al. 2019)

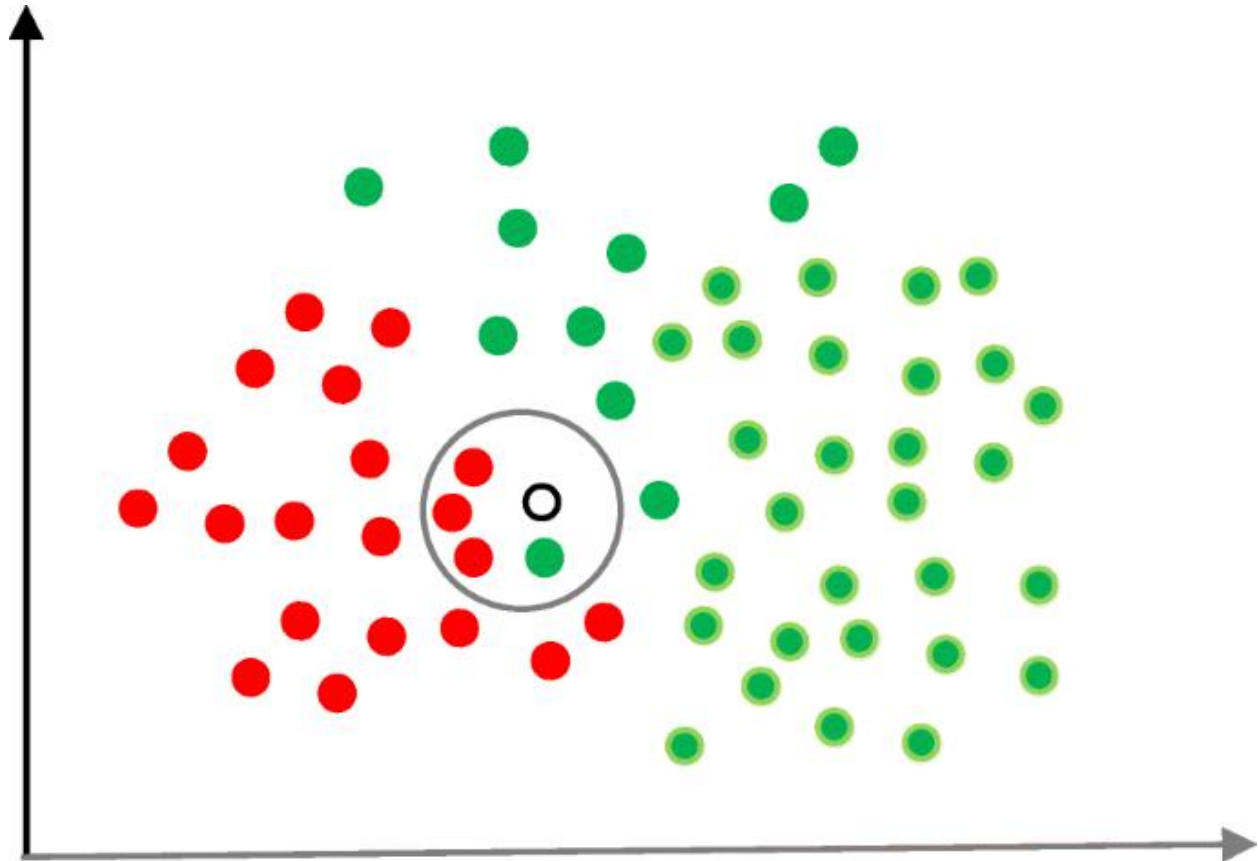


Figure 1.25: An Illustration of the Naïve Bayes Method. The 'white' circle represents a new data point that needs to be categorized as either the 'red' or 'green' class. Adapted from “Comparing different supervised machine learning algorithms for disease prediction” by Uddin et al, 2019, BMC Medical Informatics and Decision Making ,19:281. <https://doi.org/10.1186/s12911-019-1004-8>

The K-Nearest Neighbor (KNN) algorithm, developed in 1951 by Evelyn Fix and Joseph Hodges, is among the most straightforward and earliest classification techniques. It is not only apt for classification but also for regression analysis. KNN can be viewed as a simplified version of the Naïve Bayes classifier. However, unlike NB, KNN doesn't rely on probability values. In KNN, the 'K' denotes the number of nearest neighbors that are consulted for their 'votes' during classifi-

cation. Adjusting the value of 'K' can yield different classification outcomes for the same data point. Figure 1.26 demonstrates how KNN operates: with  $K=3$ , the new data point (represented as a star) is classified as 'black', but with  $K=5$ , it's classified as 'red'. The KNN classification result indicates class membership, and the algorithm employs a voting mechanism for this purpose (Abu Alfeilat et al. 2019; Uddin et al. 2022; 2019)

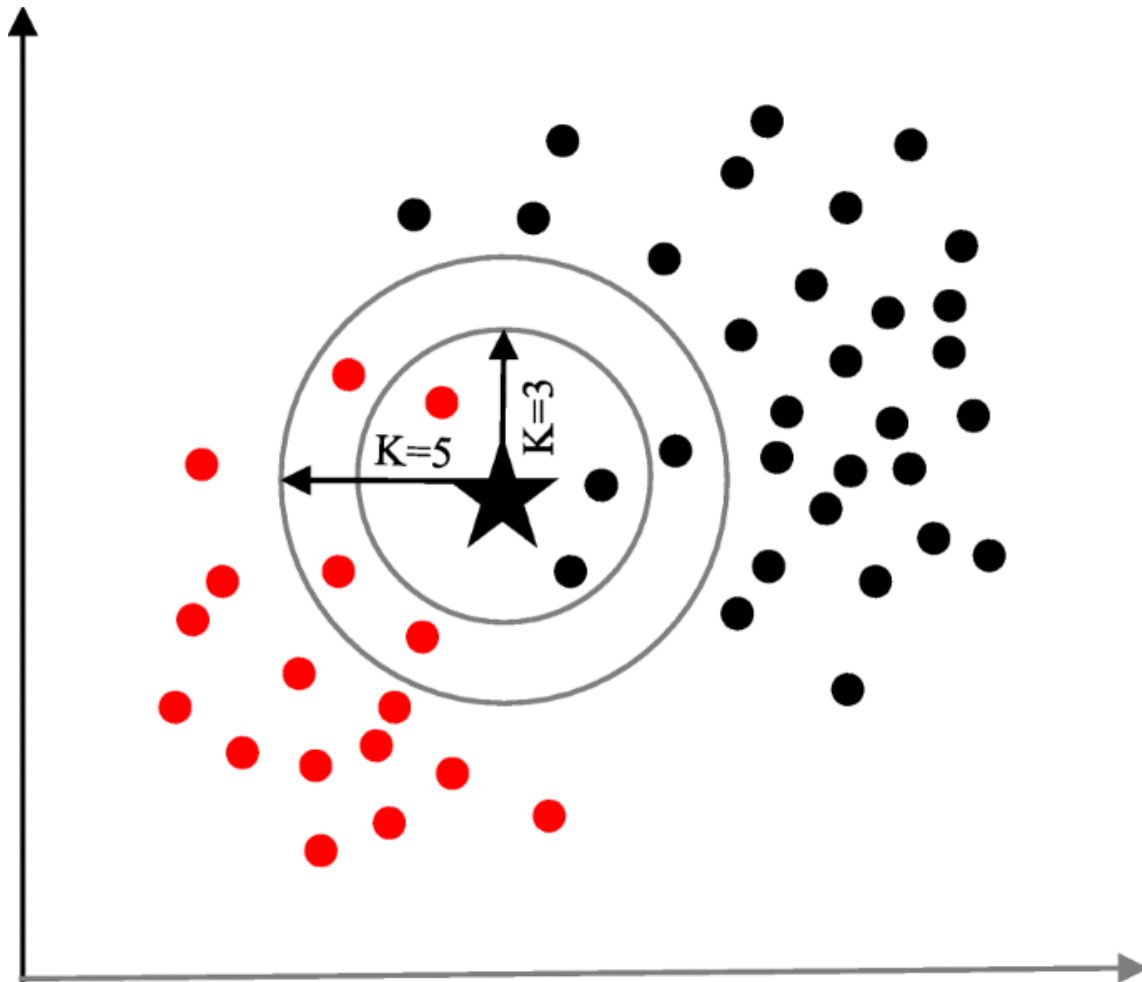


Figure 1.26: A basic depiction of the K-nearest neighbor method. With  $K=3$ , the data point (represented by a 'star') is identified as 'black' due to receiving a majority of 'votes' from the 'black' category. Conversely, when  $K=5$ , it's labeled as 'red' because it garners more 'votes' from the 'red' category. Adapted from “Comparing different supervised machine learning algorithms for disease prediction” by Uddin et al, 2019, BMC Medical Informatics and Decision Making ,19:281. <https://doi.org/10.1186/s12911-019-1004-8>

Artificial Neural Networks (ANNs) are machine learning models inspired by the neural networks of the human brain. First introduced by McCulloch and Pitts, their prominence grew due to the work of Rumelhart et al. in the 1980s. In the human brain, neurons create a web of connections through axon junctions. This intricate web can be reorganized, as seen with neuroplasticity, allowing for adaptation and the processing and storage of information. Similarly, ANNs are composed of interconnected nodes. The output from one node feeds into another based on the connections established. These nodes are organized into layers, often categorized by their functions. Beyond the primary input and output layers, ANNs can include several hidden layers. Each node and its connections carry specific weights, which can adjust the strength of signals, either intensifying or attenuating them through continuous training. As these weights are refined during training, the ANN becomes more adept at making accurate predictions on test data (Figure 1.27) (Abiodun et al. 2019; Uddin et al. 2019; Kriegeskorte 2015).

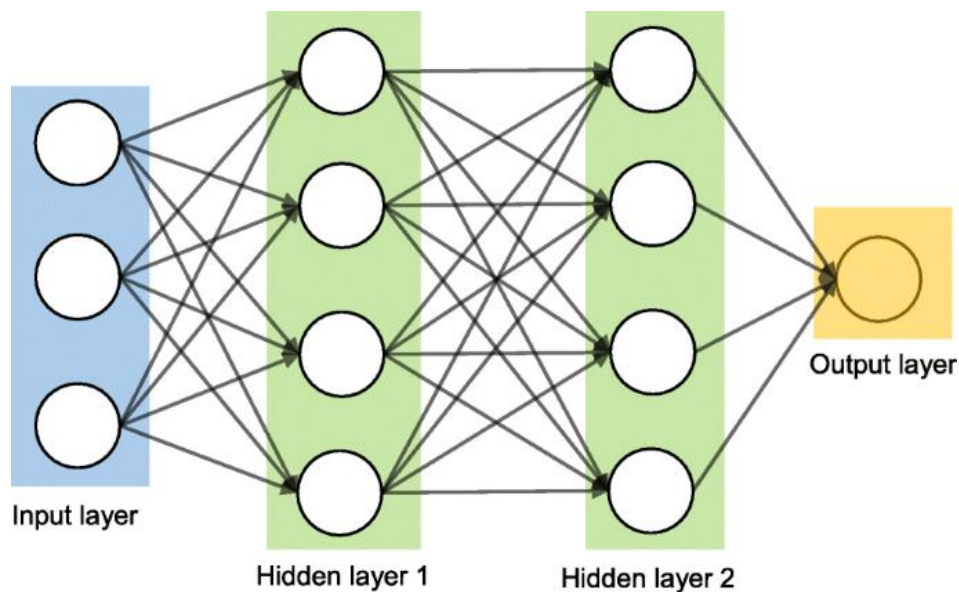


Figure 1.27: A Visual Representation Of An Artificial Neural Network With Two Hidden Layers. The arrows indicate the flow from the output nodes of one layer to the input nodes of the subsequent layer. Adapted from “Comparing different supervised machine learning algorithms for disease prediction” by Uddin et al, 2019, BMC Medical Informatics and Decision Making ,19:281. <https://doi.org/10.1186/s12911-019-1004-8>



Recently, the concept of knowledge transfer has gained increased attention in machine learning research. This is attributed to its potential in mirroring human proficiency in applying learned models to unfamiliar scenarios. Particularly in contexts where training data is sparse, knowledge transfer can enhance the speed of learning and its ability to generalize to analogous tasks. The "learning using privileged information" (LUPI) paradigm has introduced an innovative dimension to this domain. Within LUPI, knowledge transfer is visualized as an active interplay between a teaching entity and a learner. The teacher exploits exclusive information, known as privileged information (PI), during the training period. The inclusion of PI augments the complexity of the training samples and directs the student model towards a comprehensive understanding of the inherent data trends. However, during the evaluation phase, the student functions autonomously without the guidance of the teacher. This methodology is beneficial in medical domains where integrating diverse data sources can enhance the predictive accuracy of machine learning models; yet, some of these data may be challenging to acquire or unavailable during the evaluation phase. It's imperative to note that the efficacy of this approach heavily relies on the caliber of data offered by the teaching entity. To ensure the integrity of the learning process, the data should be pertinent and devoid of redundant features, thereby mitigating noise and optimizing the dimensionality of the resultant (Sabeti et al. 2021; Zhang, Bianchi, et al. 2021; Tang et al. 2019; Vapnik and Vashist 2009).

### ***1.9.2 Development, Evaluation and Explainability of ML models***

The process of developing machine learning models commences with a clearly articulated research question. This query forms the groundwork for subsequent tasks, including data collection and preparation, choosing a suitable machine learning approach, evaluating results, and deciphering outcomes (Arbet et al. 2020).

Acquiring a robust, accurate, and reliable dataset that is both comprehensive and sizable has a significant impact on the development and utilization of machine learning in clinical decision-making, even when advanced technologies are present. Three distinct datasets are utilized for constructing a machine learning model: one for training, another for validation, and a third for testing. The training dataset is used to create the machine learning model, followed by tuning model parameters using the validation dataset. The final stage involves assessing model performance on new and unseen data, i.e., the test dataset. In machine learning, raw data is often unsuitable for learning purposes; therefore, features or variables must be derived from the raw data via data mining. Additionally, raw data needs to be cleaned and prepared for data mining, as noise and errors within the raw data can hinder the detection of patterns and lead to inaccurate outcomes. The objectives of data cleaning and enhancement include data normalization, eliminating redundant features, standardizing data, removing duplicates, resolving inconsistent data, managing missing data, and harmonizing data across multiple sources. As an example of data preparation, the normalization of images is necessary before applying statistical or machine learning algorithms. Aligning images to a common statistical distribution based on size and pixel values (spatial normalization) facilitates accurate detection of differences between individuals or within the same individual across various time points. Moreover, when creating a model for disease classification or image synthesis (e.g., segmentation and transformation), normalization of image intensity is crucial to prevent bias and ensure model accuracy. Studies have shown that standardizing intensity features across training input images significantly impacts the accuracy of image synthesis models (Bianchi, Paniagua, et al. 2020; Ioshida et al. 2019; Reinhold et al. 2019; Tallón-Ballesteros and Riquelme 2014).

Data mining involves analyzing extensive datasets to uncover previously unknown patterns and comprehensible insights. Various functionalities or tasks, such as regression, clustering, and classification, can reveal knowledge within data mining. These findings can provide summaries of input data or be employed in supplementary analyses, such as machine learning and predictive analytics. While algorithms are pivotal in both data mining and machine learning, the outputs from data mining are particularly valuable for optimizing decisions. Detecting pertinent clinical information, for instance, aids practitioners in making informed decisions and enhancing the quality of care. However, training a machine with the acquired knowledge empowers the prediction of diagnoses or prognoses for new patients (Asiri et al. 2020; Al-Jabery et al. 2019; Liu 2010).

Dimensionality reduction is an important preprocessing step in machine learning, as it serves to reduce irrelevant and redundant input. Consequently, it enhances the accuracy of the learning process and improves the clarity of the model's output. The primary methods employed in dimensionality reduction include feature selection and feature extraction. The process of feature selection involves the identification and preservation of data that contains the most relevant information for effectively resolving a particular problem. This results in the creation of a reduced subset of the original data, which is then utilized for training machine learning models. In contrast, feature extraction involves the conversion of the initial features into a reduced and more meaningful set of characteristics, exemplified as the extraction of radiomics from CBCT images (Rahman et al. 2020; Zebari et al. 2020).

After the completion of data preparation, the utilization of artificial intelligence in clinical applications necessitates the careful selection of an appropriate machine-learning approach. The effi-

cacy of machine learning algorithms is contingent upon a comprehensive understanding of their capabilities, constraints, and their potential integration and alignment with clinical care. Therefore, effective communication among data analysts, data scientists, and clinicians' is crucial across all stages of the creation of machine learning models (Bastian, Baker, and Limon 2022; Allareddy et al. 2019b).

After careful consideration of appropriate methodologies, the model-building step can be initiated. After successfully constructing a model using the training dataset, it is necessary to evaluate its performance on the testing dataset. It is imperative to provide the evaluation metrics for all dataset and integrate them into the analytic findings (Arbet et al. 2020).

Performance indicators of machine learning models, such as accuracy, precision, recall, and F1 score, are extensively utilized in the field of disease diagnosis. Accuracy (Acc) refers to the overall number of accurately identified occurrences out of all the instances. Precision is quantified by calculating the ratio of accurately predicted positive observations to the total number of expected positive observations. Recall, in the context of information retrieval, pertains to the fraction of relevant results that are accurately identified by the algorithm. The concept of sensitivity refers to a measure that exclusively considers true positive cases in relation to the overall number of instances. The concept of specificity refers to the degree of detail or precision in a given context or situation. The metric determines the accurate identification of real negatives (Figure 1.28). The F-score is calculated as the harmonic mean of accuracy and recall. The maximum F score attainable is 1, which signifies an ideal balance between precision and memory scores (Ahsan, Luna, and Siddique 2022a; Hicks et al. 2021; 2022).

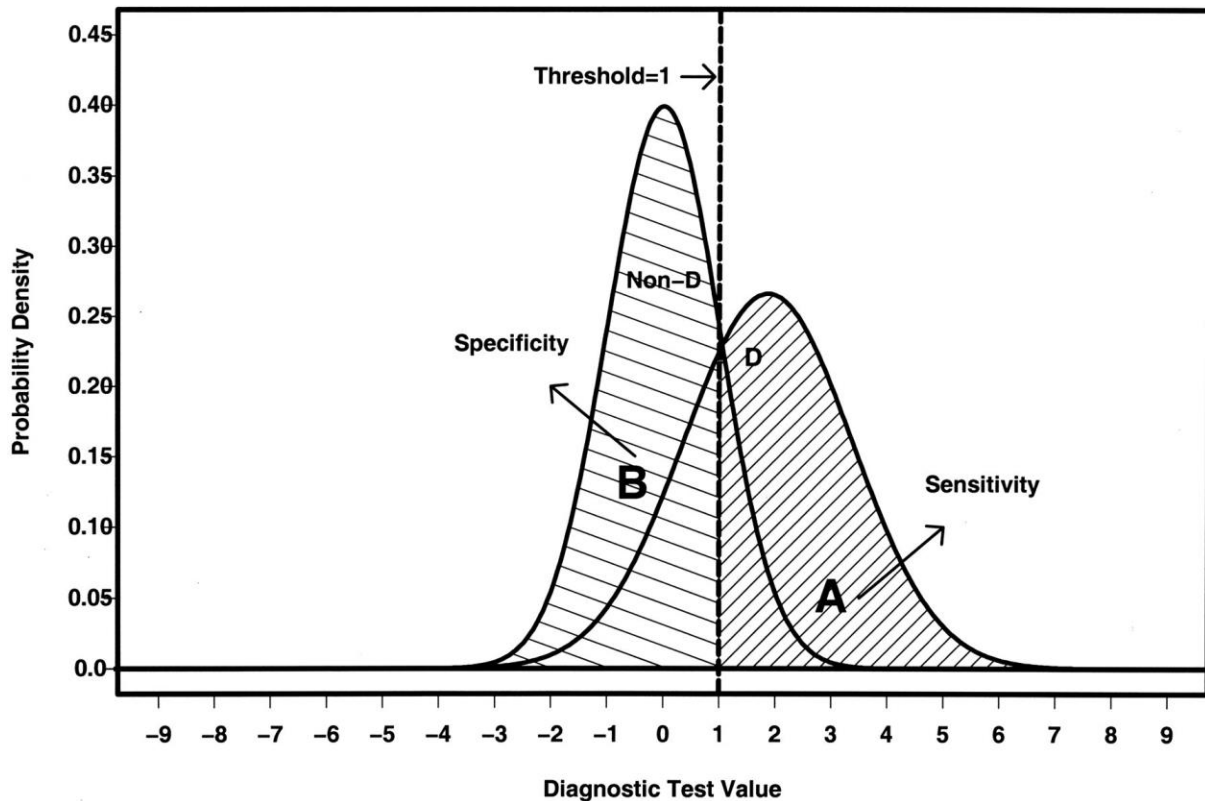


Figure 1.28: The Probability Density Curves of a Hypothetical Diagnostic Test. The density of the diagnostic test is graphed for two populations: the nondiseased population (Non-D) and the sick population (D). These populations are assumed to conform to the binormal model, with a mixture of  $N(0,1)$  and  $N(1.87,1.52)$  distributions, respectively. The representation of the diagnostic test's specificity is denoted by the shaded region beneath the distribution of individuals without the disease (A), when considering the arbitrary threshold of  $t=1$ . The measure of sensitivity is quantified by the region of shading that is beneath the distribution of the diseased population (B) when subjected to a common threshold value of 1. As an illustration, when the threshold value  $t$  is set to 1, the corresponding values for sensitivity and specificity are 0.72 and 0.84, respectively. When the test is dichotomized by considering a positive result if the test value exceeds a certain threshold, both the sensitivity and specificity exhibit changes in response. As the threshold increases, the sensitivity decreases while the specificity increases. Adapted from <https://www.ahajournals.org/doi/10.1161/circulationaha.105.594929>

The Receiver Operating Characteristic (ROC) curve is another tool for evaluation of diagnostic tests. It is constructed by graphing the true positive rate (i.e., sensitivity or recall) versus the false positive rate ( $1 - \text{specificity}$ ) at different threshold levels. The area under the ROC curve (AUC) is a prevalent method for assessing the predictive performance of a classifier. A classifier is considered superior when it has a higher AUC value, and conversely, it is considered inferior

when it has a lower AUC value. Figure 1.29 depicts the graphical representation of three ROC curves, which are derived from a hypothetical dataset. The region bounded by the blue ROC curve is equivalent to half of the size of the shaded rectangle. Therefore, its AUC value is considered 0.5. The AUC value for the red ROC curve is higher than that of the black ROC curve due to its coverage of a larger area. Therefore, the classifier that generated the red ROC curve demonstrates superior prediction accuracy in comparison to the other two classifiers that produced the blue and red ROC curves (Uddin et al. 2022; Kamarudin, Cox, and Kolamunnage-Dona 2017; Hajian-Tilaki 2013).

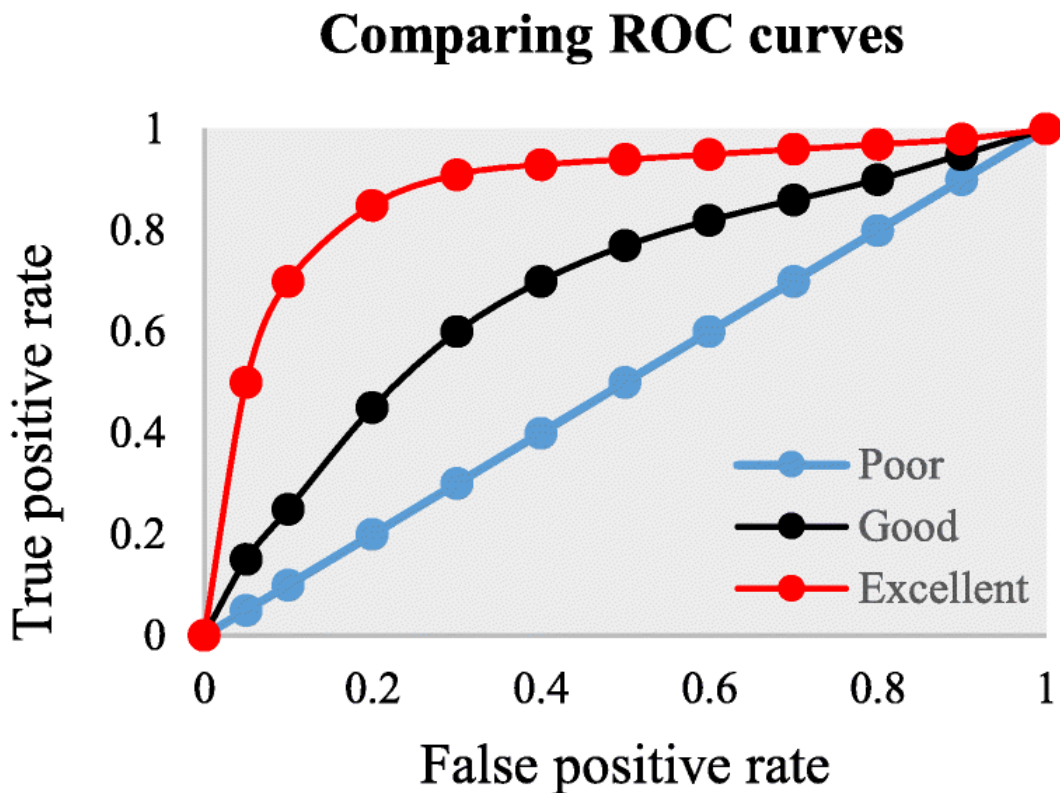


Figure 1.29: An illustration of the ROC curve . Adapted from “Comparing different supervised machine learning algorithms for disease prediction” by Uddin et al, 2019, BMC Med Inform Decis Mak 19, 281. <https://doi.org/10.1186/s12911-019-1004-8>.

While ML algorithms approved by regulatory agencies such as the Food and Drug Administration and Health Canada have seen proliferation in various medical applications like brain, lung, breast, and cardiology, a number of cutting-edge ML models, including deep learning and ensemble models, still maintain their "black box" nature. This particular aspect poses a significant obstacle to the widespread adoption of ML in medical settings, as the inability to assess the connection between variables and predictions not only hinders the potential to uncover biases and inaccuracies but also undermines the confidence and reliability of these models for informed medical choices. For instance, the lack of transparency and rationale behind predictions made by ML models for clinical deterioration could conceivably result in delayed treatments or unnecessary expenditure of clinician time, primarily due to false positives (Petch, Di, and Nelson 2022; Stiglic et al. 2020; Vellido 2020; Umscheid et al. 2015).

In response to the significant challenges presented by black-box models, the field of explainable ML has witnessed a surge in research over recent years. Much of this research focuses on addressing the need for intelligible explanations regarding how these models operate and the rationale behind specific individual predictions. These explanations can identify the variables that drive model predictions as well as translate the model's mechanisms into a transparent design that aligns more closely with evidence-based clinical reasoning. Both of these approaches have demonstrated their significance in boosting clinician confidence in utilizing ML models (Petch, Di, and Nelson 2022; Coussement and Benoit 2021).

One category of techniques, known as variable importance methods (referred to as "feature importance" in the ML domain), aims to generate explanations by quantifying the statistical contribution of each variable to a model's performance. During the model development phase, these methods are routinely employed to assess the model's learning accuracy and the clinical plausi-

bility of the variables that influence predictions. Examples of techniques for variable importance methods include permutation Importance, mean decrease in impurity and conditional variable importance (Hapfelmeier, Hornung, and Haller 2023; Petch, Di, and Nelson 2022; Li, Wang, et al. 2019).

An additional approach to explainability techniques revolves around surrogate methods. These methods elucidate the functioning of black-box models by constructing new interpretable models based on the predictions of the black-box model itself. Surrogate methods encompass both global and local perspectives. On a global scale, techniques like decision trees and logistic-linear regression are used to provide an overarching explanation of the black-box model's behavior. Conversely, local surrogate methods are customized to explain specific predictions made by the black-box model. Commonly utilized techniques in this category include local interpretable model-agnostic explanations (LIME) and shapley additive explanations (SHAP) (Hassija et al. 2023; Petch, Di, and Nelson 2022).

LIME was originally introduced in 2006 and has since emerged as one of the most widely used techniques for interpreting black-box models. The core concept involves generating simulated data points around a given instance and its corresponding prediction. These simulated instances are created in the vicinity of the input instance that led to the prediction. Subsequently, these simulated instances are used with the original model to obtain new predictions, which are then weighted based on their proximity to the original input. In the final step, a simple and easy-to-understand model, such as a decision tree, is trained using this new dataset of perturbed instances. This locally trained model provides an interpretation for the initial complex black-box model. While LIME is effective and conceptually clear, it does have limitations. For instance, poor parameter choices could cause LIME to overlook crucial features. On the other hand, SHAP has



gained recognition for providing a solution that satisfies the criteria of strong representativeness, fidelity, and considerable expressive capability. Moreover, this approach has undergone empirical validation and has been employed across diverse domains such as medicine, cheminformatics, and ecology (Bifarin 2023; Linardatos, Papastefanopoulos, and Kotsiantis 2021; Barredo Arrieta et al. 2020; Ribeiro, Singh, and Guestrin 2016).

The SHAP framework facilitates the interpretation of individual predictions by quantifying the significance of each feature's score for a given sample prediction. Moreover, SHAP has the capability to generate a precise and comprehensive global interpretation of the model, hence exhibiting its notable level of representativeness. The SHAP framework is essentially grounded in the utilization of Shapley values, which are derived from cooperative game theory principles. The way of attributing prizes from a cooperative game, known as the Shapley value, was developed by Lloyd Shapley. This system is both fair and axiomatically unique. In the context where a game is represented as a machine learning model, the individuals participating in the game can be seen as the values of each feature, and the projected class membership of a given sample can be considered as the outcome of the game. The Shapley value, in this scenario, provides a distinct and equitable solution for attributing the contributions made by each player to the overall outcome of the game (Bifarin 2023; Ning et al. 2022; Bloch, Friedrich, and for the Alzheimer's Disease Neuroimaging Initiative 2021).

The uniqueness of the Shapley value arises from its adherence to the axioms of symmetry (also known as consistency), dummy (or null effect), and additivity (or local accuracy). The concept of symmetry suggests that when the marginal contributions of two feature values,  $x_z$  and  $x_k$ , are equal, the corresponding Shapley values assigned to each feature value will likewise be equal. The term "dummy" is used to indicate that when a feature value, denoted as  $x_z$ , has no effect on a

model, the corresponding Shapley value will be zero. The concept of local accuracy refers to the condition where the total of the Shapley values assigned to each individual feature value within a model is equal to the output of the model. Therefore, the cumulative sum of all feature values will be equivalent to the overall effect of all feature values on the model's output, except the effect when no feature value is present (Bifarin 2023).

Figure 1.30 illustrates an example of the SHAP summary plot, commonly known as the beeswarm summary plot. This plot offers a thorough visual representation of the contribution of various features to the decision-making process of a machine learning model.

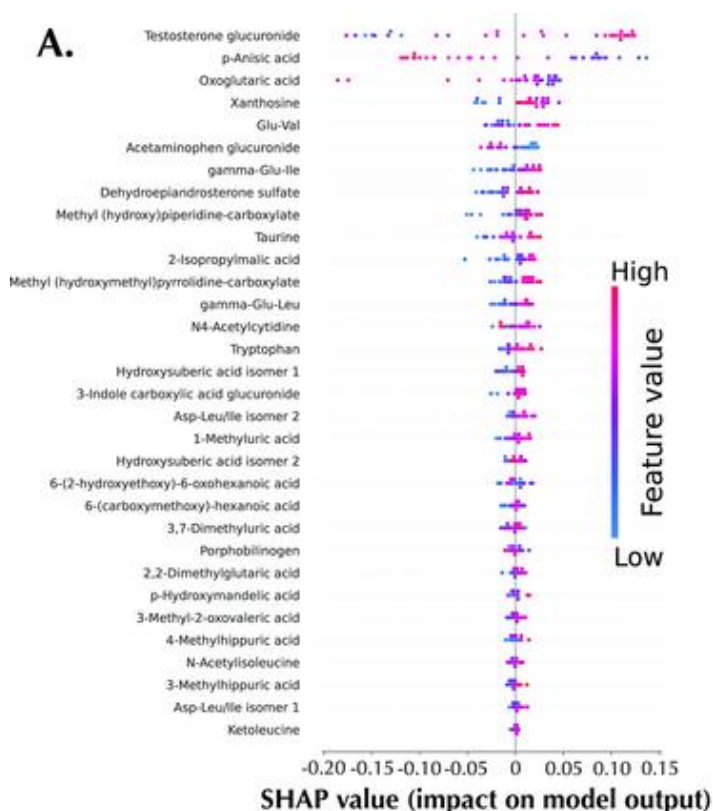
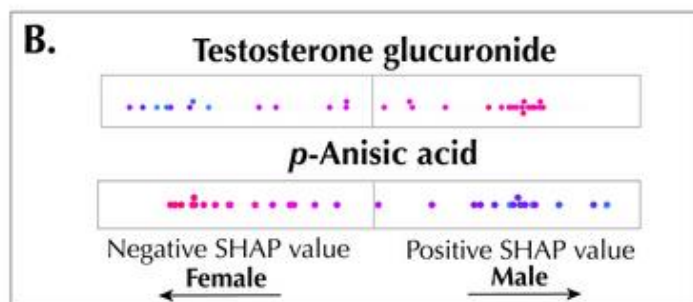


Figure 1.30: SHAP Summary Plot. The metabolic features are organized in a decreasing order according to their relative significance within the plot. Each data point in the summary plot represents a sample that has been plotted according to its influence on the model's output. The relative quantity of metabolites is visually represented by the hue of each sample, with lower abundance shown by blue and higher abundance indicated by red (A). Figure 4B exhibits the predominant metabolite inside the panel, namely testosterone glucuronide. Metabolites with high feature values generally exhibit positive SHAP values, leading the model to make predictions favoring males. Conversely, metabolites with low feature values, such as testosterone glucuronide, tend to have negative SHAP values, influencing the model to forecast the female sex. P-anisic acid displays a contrasting trend (B). Adapted from “Interpretable machine learning with tree-based shapley additive explanations: Application to metabolomics datasets for binary classification” by Bifarin et al, 2023, Application to metabolomics datasets for binary classification. PLOS ONE 18(5): e0284315.



### *1.9.3 Machine Learning in Osteoarthritis: Insights and Considerations*

The applications and advantages of machine learning techniques are evident across various domains, especially in scenarios involving limited observations and a multitude of predictors. It also effectively addresses the complexities of interactions, a challenge often faced by traditional statistical methods, which tend to focus on interactions between primary determinants and individual confounding factors. Furthermore, machine learning demonstrates the ability to assess a diverse range of data types, including imaging data, demographic information, and laboratory results. By effectively integrating diverse data types, machine learning enhances the ability to predict disease risks, enable accurate diagnoses, offer valuable prognostic insights, and propose effective treatment approaches. As a result, this enhancement has the potential to improve decision-making at the individual patient level, thereby promoting the adoption of precision medicine particularly with the availability of longitudinal data platforms related to individuals' health conditions (Kline et al. 2022; Johnson et al. 2021; Xu et al. 2021; Ahmed et al. 2020; Ghassemi et al. 2020; Hassaine et al. 2020).

The application of machine learning models in the field of knee osteoarthritis is clearly evident in the existing literature. A variety of machine learning models have been developed with the objective of automating various tasks, including radiological diagnosis and the evaluation of knee osteoarthritis severity. Furthermore, ML models have been utilized to predict the need for surgical interventions, improvement subsequent to surgical procedures, and the probability of postoperative complications for individuals with knee osteoarthritis. Additional research demonstrated the capabilities of utilizing machine learning to address hurdles in the realm of osteoarthritis. These challenges encompass the early-stage diagnosis of OA, predicting OA emergence within populations, and distinguishing between patients with gradual and rapid disease progression. Furthermore, studies have integrated strategies for interpretability into their ML models,

allowing them to identify the contributions of different features to the model's predictions (Xuan et al. 2023; Binvignat et al. 2022; Kokkotis et al. 2022; Harris et al. 2021; Heisinger et al. 2020; Leung et al. 2020; Harris et al. 2019; Huber, Kurz, and Leidl 2019; Norman et al. 2019; Richardson 2020; Tiulpin et al. 2018).

In contrast to knee osteoarthritis, which has received considerable attention in the context of machine learning models for disease diagnosis and progression prediction, TMJ OA remains an underexplored area. This disparity is alarming given the rising prevalence of TMJ OA, inability of existing treatments in mitigating degenerative bone and cartilage changes, the adverse impact on patients' quality of life, and the limited efficiency of the current clinical and imaging criteria in detecting early stages of the disease and predicting patients' response to conservative treatments. To bridge this knowledge deficit and address the multifactorial intricate nature of the disease, our pilot study showed the potential of advanced statistical and machine learning techniques in diagnosing TMJ OA. However, several critical factors need to be addressed. One of these is the necessity for a larger sample size to capture the varied phenotypic presentations of TMJ OA, ensuring the diagnostic tool's reliability, validity, and robustness. Alongside this, the persistent challenge of amassing diverse clinical datasets underscores the importance of exploring privileged information learning strategies for diagnosing TMJ OA. Beyond the diagnosis, it is crucial to pinpoint the complex factors driving the disease and to predict its progression accurately. Furthermore, understanding machine learning model predictions and demystifying their 'black-box' nature is essential for their successful implementation and future integration into routine clinical practice (Derwich et al. 2023; Murakami 2022; Yang, Ye, and Xia 2022; Yuan et al. 2022; Hawker and Lohmander 2021).

## **Chapter 2 Clinical Decision Support Systems in Orthodontics: A Narrative Review of Data Science Approaches**

Al Turkestani N, Bianchi J, ... Cevidanes LHS. *Orthod Craniofac Res.* 2021 Dec;24 Suppl 2(Suppl 2):26-36. doi: 10.1111/ocr.12492. Epub 2021 May 24. PMID: 33973362; PMCID: PMC8988880.

### **Abstract**

Advancements in technology and data collection generated immense amounts of information from various sources such as health records, clinical examination, imaging, medical devices, as well as experimental and biological data. Proper management and analysis of these data via high-end computing solutions, artificial intelligence and machine learning approaches can assist in extracting meaningful information that enhances population health and well-being. Furthermore, the extracted knowledge can provide new avenues for modern healthcare delivery via clinical decision support systems. This manuscript presents a narrative review of data science approaches for clinical decision support systems in orthodontics. We describe the fundamental components of data science approaches including (a) Data collection, storage and management; (b) Data processing; (c) In-depth data analysis; and (d) Data communication. Then, we introduce a web-based data management platform, the Data Storage for Computation and Integration, for temporomandibular joint and dental clinical decision support systems.

**Keywords:** artificial intelligence, decision support systems, machine learning, orthodontics

## 2.1 Introduction

Over the past decades, the digital revolution has transformed every facet of our world, including dental practice. Adopting modern technology in orthodontics has not only provided us with advanced diagnostic and treatment tools, but also given us the chance to shift clinical practice from a ‘disease-centered’ to a ‘patient-centered’ model (Mascitti and Campisi 2020). Establishing optimum and personalized orthodontic care requires (a) analysis of large and complex data sets derived from different sources, such as clinical examination, diagnostic images, biological and genetic data, and (b) identification of patterns/associations that turn the individual’s big data into knowledge for precise decisions and outcomes prediction (Finkelstein et al. 2020; Frank, Drikakis, and Charissis 2020; Dash et al. 2019). Big data analysis is associated with numerous challenges that necessitate the use of high-end computing solutions, advanced analytical methods (e.g. artificial intelligence and machine-learning algorithms) and data science approaches before communicating the acquired knowledge to healthcare providers via decision support systems (Frank, Drikakis, and Charissis 2020; Panahiazar et al. 2014).

Clinical Decision Support Systems (CDSSs) are computer programs developed to provide expert support for healthcare providers in making decisions regarding prevention, diagnosis and treatment of health diseases (Vikram and Karjodkar 2009). Lusted and Ledley were pioneers in explaining how the reasoning behind the foundation of diagnosis and treatment in medicine can be investigated and solved accurately using mathematical tools. Since then, researchers have been using different methods to supply clinical applications with knowledge. In orthodontics, CDSSs are being developed to reduce subjectivity, decrease errors, save time and increase the efficiency of diagnosis and treatment planning among clinicians (Bichu et al. 2021). Examples of CDSSs

include systems that aid in detecting cephalometric landmarks, determining the need for extractions, identifying the maturation stage of cervical vertebrae and predicting facial soft tissue changes following treatment (Khanagar et al. 2021). Over the last 5 years, our clinical research team, the Dental and Craniofacial Bionetwork for Image Analysis (DCBIA), has addressed knowledge gaps in dentistry that require CDSSs (Figure 2.1). In this manuscript, we present a narrative review of the data science approaches that are required to develop clinical decision support systems in orthodontics. We also describe a web-based data management platform for the temporomandibular joint and the dental clinical decision support systems.

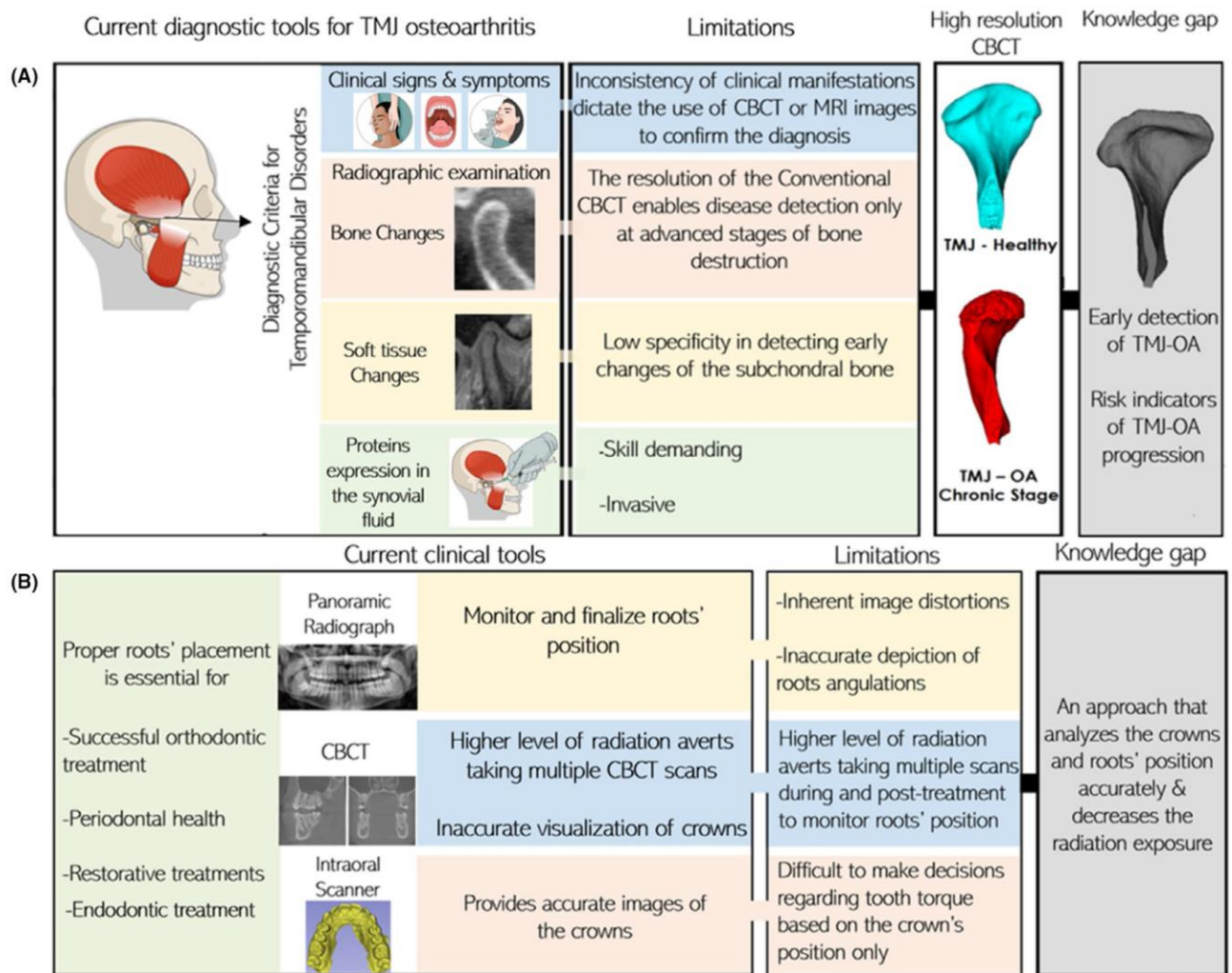


**Figure 2.1: Gaps of knowledge in (A) TMJ and (B) Dental diagnosis and prognosis assessment tools**

## **2.2 Development of Clinical Decision Support Systems (CDSSs)**

### ***2.2.1 Types of CDSSs***

Clinical decision support systems have been categorized according to (a) function of the support: provision of alerts (active) or reaction to patients' information/providers' inputs (passive); (b) time of support delivery: before, during or following decision-making and (c) method of development: knowledge or non-knowledge-based.

Knowledge-based CDSSs contain compiled data entered directly by users or extracted from patients' electronic records, phone apps and data about medications or clinical protocols and guidelines based on the intent of using a clinical decision system (Dash et al. 2019; Helmons et al. 2015). Such systems will deliver support to users, usually following the IF-THEN rule. For instance, in a system for detection of medication interactions, the rule will be IF drug X and IF drug Y are used, THEN alert the clinician. Non-knowledge-based CDSSs also require a data source; however, decisions are made with statistical pattern recognition or machine-learning (ML) approaches. Consequently, computers learn from previous experiences, discover patterns within the data and eliminate the need for expert inputs or rules. Artificial neural networks and genetic algorithms compose the main types of non-knowledge-based CDSSs (Zikos and DeLellis 2018; Helmons et al. 2015).



## 2.2.2 Data Science Approaches for the Development of CDSSs

Clinical decision support systems development is a highly challenging and multidisciplinary task that integrates clinical knowledge with decision science to adapt clinical practice and workflow with the decision system (Joda et al. 2019). Here, we provide a simplified overview of steps involved in creating a clinical decision support system (Figure 2.2A).

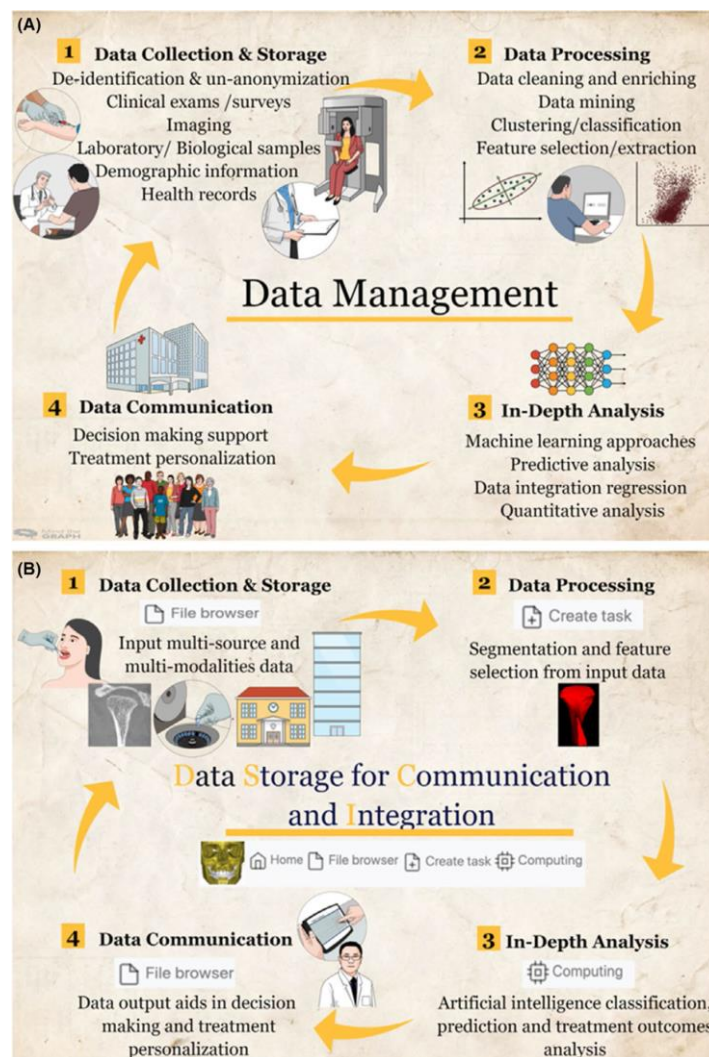


**Figure 2.2: Overview of steps involved in developing clinical decision support systems (CDSSs).** A, General spectrum of data science approaches in the CDSSs. B, Implementation of robust data management, Dental Storage for Computation and Integration, in the CDSSs.

### *Data collection, storage and management*

The advancement of information technology promoted exponential growth of health data and generation of big data; that is, large-volume data that are produced at high speed and integrates different types of data, such as: (a) clinical data (e.g. orthodontic diagnosis and treatment progress notes, imaging, health records), (b) omics data (e.g. genomics, proteomics, metabolomics), (c) patient-generated data (e.g. wearable devices and scanners, social media) and (d) normative data sets (e.g. data collected in clinical trials or nationwide surveys) (Joda et al. 2019; Nanayakkara, Zhou, and Spallek 2019; Raghupathi and Raghupathi 2014). Current evolution of data capturing, storage and analytical methods will allow us to transform the wealth of knowledge in big data into actionable plans to overcome challenges in clinical decision, deliver personalized care and improve the population's health (Lu et al. 2020; Joda et al. 2018).

Collection of patient diagnosis and treatment progress data is considered valuable when it is done in a systematic way following interlinkable and coherent data standards that produce high-quality information (Lu et al. 2020; Nanayakkara, Zhou, and Spallek 2019; Joda et al. 2018). Clinical data constitutes an essential resource for medical and health research—electronic health records (EHR) are one of the major types of clinical data. The use of EHR is highly encouraged to improve clinicians' compliance with documentation and enable data sharing among different members of the healthcare team (Raghupathi and Raghupathi 2014). In 2009, the Health Information Technology for Economic and Clinical Health (HITECH) Act was created to support the adoption and meaningful use of health information technology, including a provision of financial incentives for using EHR systems. By 2015, the adoption of certified EHR programs by hospitals and office-based physicians reached 96% and

78%, respectively (D'Amore et al. 2020). Nevertheless, the quality of data within EHR was affected by duplication, missing information, fragmentation and inconsistent organization. The accuracy and reliability of data can influence the development and use of CDSSs, even in the presence of sophisticated advanced technologies. Thus, there is a need to standardize the terminology within the dental and orthodontic fields using well-structured forms and templates to assist in ensuring consistency of the collected data. There have been several governmental efforts to standardize the data within different EHR systems; however, at this time no federal or professional association program has been able to produce universally accepted high-quality data. Indeed, data governance requires policies for care providers and auxiliary staff, hands-on training, a culture of responsibility and the right tools to improve and monitor data quality (Wynants et al. 2019; Raghupathi and Raghupathi 2014).

Multicentre data collection is commonly performed to construct clinical prediction models. Although such data structures create additional challenges for data analysis, they cover a broader population and can improve the generalizability of the artificial intelligence models (Perazzo et al. 2019). Digital data repositories provide web-based platforms that enable researchers from multiple institutions to access and manage their data securely. Data repositories are designed to store large amounts of data, ranging from thousands of data set repositories, supported by funding and government agencies, to small data sets, supported by a research team for a certain study (Favaretto et al. 2020).

'BigMouth' is an example of an oral health data repository that contains EHR from 11 dental schools across the United States. It provides access to the demographic, dental and medical data of over 3 million patients to facilitate the advancement of research and patient care outcomes (Tucker et al. 2016). Defining and establishing a code of conduct is important for big

data collaborations to guide the ethical and meaningful use of shared data. When preparing data for sharing, it is essential to strike a balance between privacy protection (e.g. de-identification & anonymization of patients' data, security measures, controlled data sharing) and maintenance of data utility (de Dumast et al. 2018; Raghupathi and Raghupathi 2014).

### *Data processing*

After defining the proper source for data collection, it is essential to verify the quality of data and prepare a final data set for analysis or machine training (Brosset et al. 2021).

In 1955, a mathematician named John McCarthy coined the term artificial intelligence (AI) to describe the ability of machines to conduct tasks that lie within the range of intelligent activities. Afterwards, Richard Bellman defined AI as the ability to automate activities with human thinking capabilities; for example, problem-solving, learning and decision-making (Schwendicke, Samek, and Krois 2020). Machine learning (ML) is a subfield of AI, whereby algorithms are utilized to find structures and patterns within data. Consequently, machines will learn to predict similar patterns on unseen data, and their actions will improve each time new data are introduced without human inputs (Asiri et al. 2020; Gudivada, Apon, and Ding 2017).

High-quality data sets are essential for developing effective machine learning models. To build an ML model, three non-overlapping data sets are utilized for training, validation and testing. The training data set is used to develop the ML model. Then, model parameters are adjusted with the validation data set. The last step involves testing the model performance on unseen data, that is, test data set (Tallón-Ballesteros and Riquelme 2014). In ML, raw data is not usually suitable for learning; features/variables should be identified and extracted from

the raw data via data mining. However, raw data should be cleaned and prepared for data mining; noise and errors within raw data might confuse the data mining process and thus result in faulty detection of patterns.<sup>36</sup> The aims of cleaning and enriching data are primarily data normalization, elimination of redundant features, data standardization, removal of duplicates, resolution of inconsistent data, management of missing data and data matching across multiple sources (Tallón-Ballesteros and Riquelme 2014). Images normalization is an example of a data preparation procedure required before applying statistical or ML algorithms. Putting several images in a common statistical distribution based on the size and pixel values (spatial normalization) will enable reliable detection of changes between several individuals or within the same individual at different time points (Ioshida et al. 2019; Ashburner and Friston 1999). Additionally, normalization of images' intensity should be performed when planning to develop a model that classifies a disease, to avoid biasing the results, or building a model for image synthesis, for example, segmentation and transformation. Evidence demonstrated the accuracy of the image synthesis model is greatly affected by standardizing the intensity features across the training's input image ("Data Mining" 2023; Bianchi, Paniagua, et al. 2020).

Data mining involves analysing large data sets to extract unknown patterns and comprehensible information from large data sets. Several functionalities or tasks can specify the knowledge found in data mining, such as regression, clustering and classification (Al-Jabery et al. 2019). These findings can summarize the input data or be utilized in additional analyses such as machine learning and predictive analytics. Although algorithms are used in data mining and ML, outputs from data mining help optimize decisions, for example, detecting valuable clinical information will help the practitioner make better decisions and increase the qual-

ity of care. However, training a machine with the extracted knowledge will enable predicting the diagnosis or prognosis of a new patient (Asiri et al. 2020).

Dimensionality reduction is performed before machine training to eliminate irrelevant and redundant data, improve learning accuracy, and enhance output comprehensibility. The main types of dimensionality reduction are feature selection and feature extraction. Feature selection involves selecting data that contains the most relevant information for solving a particular problem; a subset of the original data is maintained and used for machine training (Bianchi et al. 2020). For instance, Bianchi et al, conducted a study aiming to detect temporomandibular joint osteoarthritis (TMJ OA). Only the most robust features were selected for machine training out of the collected 52 clinical, biological and radiomic markers and 1326 interactions. Similarly, in AI systems for two-dimensional cephalometric analyses, the rates of success of landmark detection and classification of skeletal and dental problems depend on the proper selection of the diagnostic variables. On the other hand, feature extraction transforms the original features into a new, smaller set of more significant features (Hwang et al. 2021). In the study of Bianchi et al, twenty three-dimensional imaging features of bone texture and bone morphometry, that quantify the initial morphological changes in the condylar trabecular bone, were extracted and used for machine training instead of analyzing the whole Cone-Beam Computed Tomography (CBCT) scan grey level voxels.

After implementing and tailoring the previous steps according to the aim of the ML model, the data are considered ready for advanced analysis and machine learning.

### ***In-Depth Data Analysis***

Following data preparation, each clinical application of artificial intelligence in orthodontics requires the selection of the proper machine-learning methodology, training the ML model and evaluation of the developed model's performance.

The success of the ML algorithms depends on the thorough comprehension of what algorithms can provide, the limitations of algorithms, and how that will support and fit into clinical care. Hence, communication between data analysts, data scientists and clinicians is important during all phases of CDSSs development (Allareddy et al. 2019b). Within dentistry, different ML algorithms have been utilized based on the size of the data, variables/features to analyze, and the objective of the model. ML can involve unsupervised or supervised learning (Alloghani et al. 2020).

In unsupervised learning, algorithms detect hidden patterns within an unlabeled data set. That means all variables within the training data set are utilized as inputs, and the machine will automatically discover structures/patterns within that data set without receiving instructions about the desired outcomes. Based on the problem at hand, unsupervised learning algorithms will split the data set into groups (clustering) or find rules representing the relationship between variables within a data set (association) (Alloghani et al. 2020; Auconi et al. 2015). For example, in a study conducted by Auconi et al combinations of variables (inputs) were provided to the fuzzy cluster, which detected the best phenotypic factors to group a sample of Class-III patients into subjects with increased mandibular dimensions, subjects with increased maxillomandibular divergence, and subjects with intermediate characteristics between the two groups.

Supervised learning algorithms, on the other hand, analyze training data sets with predetermined inputs and outputs. Consequently, the inferred ML model can predict the outputs of new data. Common tasks of supervised learning algorithms include classification and regression (Auconi et al. 2015). The classification task aims to detect a function (discrete value) that aids in splitting the data set into classes based on various parameters (Jung and Kim 2016). For example, using a classification algorithm and a training data set consisting of patients' intra-oral and cephalometric findings, the supervised ML model can determine (i.e. classify) the cases that need or do not need a tooth extraction for orthodontic reason. In the regression task, the correlation between dependent and independent variables is detected during the machine training, and the developed model can predict continuous variables (Farhadian et al. 2019). For instance, an ML model trained with a regression algorithm can predict dental age (continuous variable) from the pulp-to-tooth ratio of the canines (Sidey-Gibbons and Sidey-Gibbons 2019). When training with supervised ML algorithms, it is possible to generate an overfit model that performs well only on the training data set. Thus, it is essential to evaluate the developed model's generalizability and tune the model parameters through validation methods, for example, cross-validation (Jiang, Gradus, and Rosellini 2020). Last, the performance of the model should be evaluated using the test data set. For that, various methods exist and should be selected based on the task of the ML algorithms (classification or regression) and the type of outcomes (Park et al. 2019).

Interestingly, a review conducted by Asiri et al. revealed that most of the ML applications in orthodontics have utilized supervised machine learning algorithms to automate clinical procedures that execute or assist in diagnosis and treatment planning. Radiographs were commonly targeted in developing those ML models as they are considered essential tools for or-



thodontic diagnosis, treatment planning and evaluation of treatment outcomes. Discrepancies in landmarks identification have been recognized as a critical source of error in cephalometric analyses. Since the analysis' diagnostic value relies on the reproducibility and precision of landmarks identification, interests to develop an automated approach have increased to reduce the laboriousness of the task and subjectivity of the analysts (Asiri et al. 2020). Park et al. reported that training the machine with the YOLOv3 algorithm for automatic labelling of 80 landmarks resulted in small error plots and 5% improvements in the accuracy compared to top benchmarks reported in the literature. Additionally, the mean computational time consumed per image was only 0.05 seconds (Park et al. 2019). Similarly, Kunz et al<sup>57</sup> reported promising results obtained with an AI algorithm that can analyze new cephalometric X-rays with precision comparable to the gold standard, that is, experienced human examiners. Furthermore, Lee et al. presented an automated framework for cephalometric landmarks detection with the implementation of confidence regions (95%) around the estimated positions of the landmarks. This will allow clinicians to gauge the accuracy of the size and location of the calculated landmarks (Lee, Yu, et al. 2020).

Besides using the two-dimensional radiographs for the cephalometric analysis, accurate measurements can be attained with CBCT imaging modality; CBCT provides an accurate three-dimensional spatial representation of the oral and craniofacial structures. However, the accuracy of manual landmarks plotting on the CBCT requires substantial effort, experience, and time. Gupta et al reported an automatic knowledge-based landmark detection algorithm able to produce accurate cephalometric measurements comparable to those computed from manual identification (Gupta et al. 2016). Automation of the radio-graphic analysis has also involved attempts to estimate the skeletal maturation that provides the best estimate of the

individual's biological age and aid treatment planning. Kashif et al used a classifier algorithm and developed a tool that can help predict the bone age from hand radiographs with a mean error of 0.6 years compared to the average reading of two experienced radiologists (Kashif et al. 2016). Kok et al, on the other hand, reported different algorithms that predict the skeletal maturation from the cervical vertebrae on lateral cephalograms (Kök, Acilar, and İzgi 2019). ML algorithms have also been utilized to develop an automated imaging system that provides objective morphological facial assessment during the orthodontic diagnosis process (Bayirli, Kim-Berman, and Puntillo 2020). Furthermore, various methods for automatic volumetric segmentation of CBCT images were developed using ML algorithms. This will allow objective generation of three-dimensional models for advanced diagnosis and treatment planning whilst saving the time and efforts required for manual segmentation (Varma et al. 2019).

Growth and development of orofacial complex are influenced by the interaction of the genetic and environmental factors. Orthodontists are mainly using phenotype-driven diagnostic tools like cephalometric analyses to predict the growth in individuals with Class-II or class-III skeletal malocclusions. However, future studies of genetics, epigenetics and metabolic pathways that utilize advanced machine learning tools will transform the process of orthodontic diagnosis and treatment planning (Wiens et al. 2019; Allareddy et al. 2019).

### ***Data Communication***

The next step after developing the ML-based model is to communicate the ML findings with the clinicians. Production of predictive models in a real-world healthcare setting is more challenging than developing models in an experimental environment. Therefore, it is important for clinical experts who were not involved in tools development to test and validate

the system's performance. Following the deployment of the ML model, it should be monitored for reliability and correction of errors since clinical protocols and populations are changing over time (Li, Kong, et al. 2019).

The CDSSs, reviewed in this manuscript, will improve Orthodontic care only if clinicians utilize ML and AI tools to analyze the inter-relationships among the dentition, craniofacial skeleton and soft tissues. Then, translate the acquired knowledge towards the advancement of orthodontic diagnosis, treatment planning, evaluation of growth and development, assessment of treatment progression, outcomes and stability.

### ***Data Storage for Computation and Integration***

Our clinical research team, the DBCIA, has developed a web-based system called Data Storage Computation and Integration (DSCI) for the management of data science approaches in TMJ and dental CDSSs. The DSCI allows clinicians and researchers to store and share de-identified data between multiple clinical centers. In addition, it allows data processing, in-depth data analysis with several machine learning algorithms and outcomes communication with the users (Figure 2.2B) (Heinrichs and Lim 2003)The security and privacy of the access to the DSCI are handled using Jason Web Tokens, with encryption of each user who requests to log in. The DSCI uses Amazon Web Services which enable distributed computing across multi-site clinical centres. Furthermore, the web data management server architecture facilitates scalability and inclusion of plugins or processing pipelines to exploit data sets stored in the web system resources.

### ***TMJ clinical decision support system***

***Rationale*** Osteoarthritis of the TMJ (TMJ OA) is a chronic debilitating disease that affects millions of people and poses a burden on public health globally (Bianchi et al. 2020) It is a multifactorial disease that results from biological and mechanical events that destabilize normal coupling of synthesis and degradation of the subchondral bone and the articular cartilage (Su et al. 2016). Diagnosis of the TMJ OA is currently based on pre-existent clinical signs and symptoms/imaging markers following the recommendations of the Diagnostic Criteria for Temporomandibular Disorders (DC/TMD) (Schiffman, Ohrbach, et al. 2014). However, several studies showed that clinical diagnosis is poorly correlated with the bony changes in CBCT images. Therefore, new assessment tools are needed for the precision of the diagnoses (Su et al. 2016).

### ***TMJ decision optimization***

The CDSS for the TMJ, deployed in the DSCI, enables reliable detection of the TMJ OA and visualization of surface changes of the affected condyles (Figure 2.3). The TMJ CDSS has components for data storage of biological, clinical and imaging data (e.g. magnetic resonance images, panoramic images, CT and CBCT scans). Furthermore, it possesses a tool for data processing (TMJseg) that allows automatic segmentation of the condyles from the CBCT scans (Brosset et al. 2020). Regarding the in-depth analytics component of the CDSS, the DSCI's statistical analysis, cross-validation and machine learning (Light GBM and XGBoost) tools permit users to integrate patient-specific multi-source data and to obtain a diagnosis of the TMJ condition, that is, healthy or diseased. A recent study by Bianchi et al. showed that the use of the DSCI tools facilitated the diagnosis of TMJ OA in its initial stages

with an accuracy of 0.823. Moreover, they demonstrated that the interaction of the biomolecular features has a large contribution to the prediction of the TMJ OA status (Bianchi et al. 2020). Furthermore, the DSCI has a machine-learning model that detects changes of the condyles' surfaces (Shape Variation Analyzer) which aids in classifying the TMJ OA disease into different categories based on the degree of the condylar degeneration (Ribera et al. 2019).

### ***Dental Clinical Decision Support System***

***Rationale*** Currently, the commercial companies that fabricate clear aligners are utilizing data from digital dental models and applying AI algorithms to predict and plan teeth movement, as well as to undertake teeth segmentation. However, such AI algorithms have not been validated and require caution by clinicians in terms of utilizing the provided predictions as well as monitoring treatments' results (Faber, Faber, and Faber 2019). Moreover, these technological advancements also require the integration of multi-source data capture, including clinical information and three-dimensional imaging exams such as CBCT, digital dental models (DDMs), photographs, lateral cephalogram and panoramic X-rays (Li et al. 2019).

Dental decision optimization The CDSS for dental applications deployed in the DSCI integrates dental crowns' and root canals' relevant clinical information from the DDMs and CBCT scans, respectively (Figure 2.4). In addition, it provides tools for automatic segmentation of root canals (RootCanalSeg), teeth and gums (DentalModelSeg) (Dumont et al. 2020). Overcoming the registration challenges created by merging the information from different imaging modalities and DDM, a work in progress, will enable reliable quantitative assessments of teeth movement (Figure 2.4).

# TMJ Decision Support System

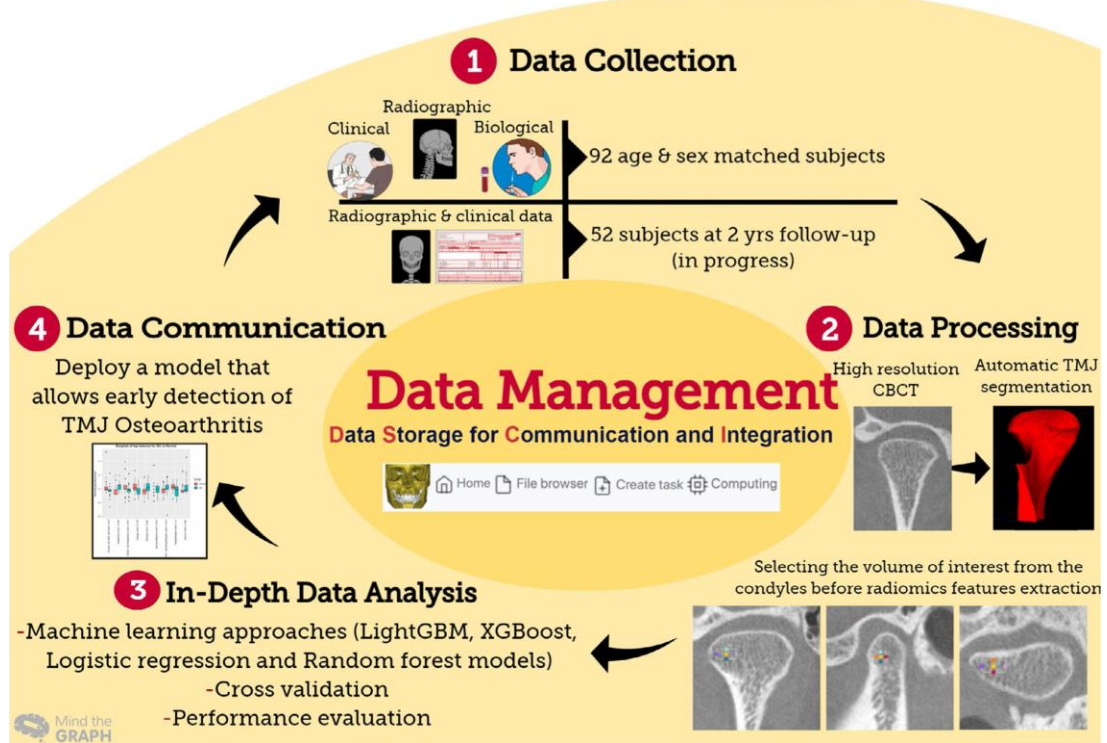
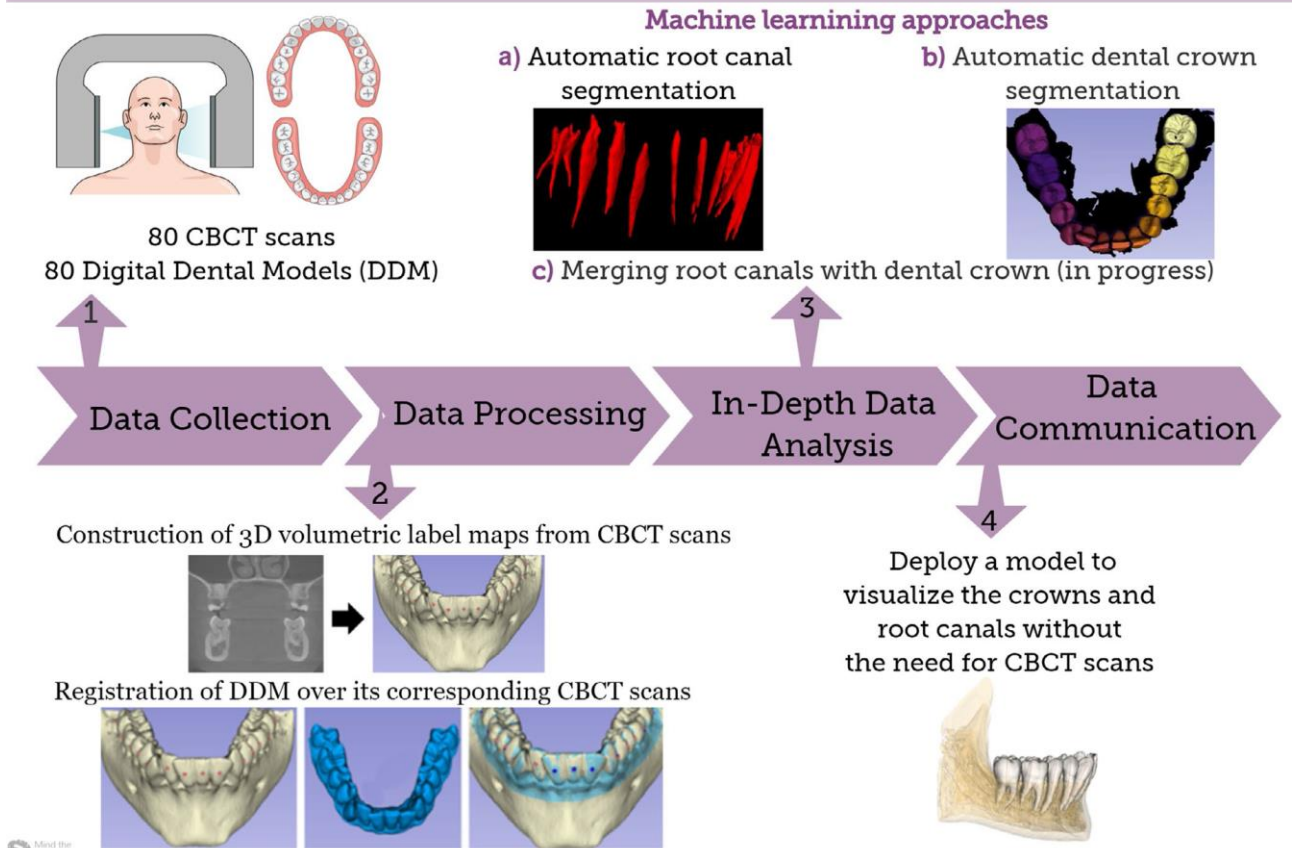


Figure 2.3: Data Science Approaches in the TMJ Clinical Decision Support System.

# Dental Decision Support System



**Figure 2.4: Sequence of Data Science Approaches in the Dental Decision Support System**

## 2.3 Conclusion

Clinical Decision Support Systems incorporate knowledge with patient-specific data to serve clinicians with tools that enhance their clinical decision-making process. Thorough understanding of the steps involved in developing DSS and communication between clinicians, data scientists and analysts are keys to creating successful tools that fit into the clinical workflow.

## **Chapter 3 A Comprehensive Patient-Specific Prediction Model for Temporomandibular Joint Osteoarthritis Progression**

### **Abstract**

Temporomandibular joint osteoarthritis (TMJ OA) is a multifactorial degenerative disease that affects 8-16 % of the global population. It leads to chronic pain, jaw dysfunction and in advanced stages may require joint replacement. To date, no prognostic tool or single biomarker can accurately predict the course of this intricate disease. Identification of patients at risk for severe prognosis is crucial for timely intervention and reducing the need for surgical management. Hence, we prospectively acquired clinical, imaging and biological data from 106 subjects, with 74 followed over 2-3 years. We proposed an open-source predictive modeling framework, called Ensemble via Hierarchical Predictions through Nested cross-validation tool, which combines 18 feature selection, statistical and machine learning methods, allowing prediction of disease progression with accuracy of 0.87, area under ROC curve of 0.72, and F1 score of 0.82. Importantly, using the interpretable SHAP analysis method, we identified the strongest predictors for TMJ OA progression. Lower values of headache, lower back pain, restless sleep, condyle high grey level-GL- run emphasis, articular fossa GL non uniformity and long run low GL emphasis, saliva levels of Osteoprotegerin and Angiogenin, and higher values of the superior joint space, mouth opening, saliva Vascular-endothelium-growth-factor and Matrix-metalloproteinase-7, serum Epithelial-neutrophil-activating-peptide and age indicate increased the probability of recovery for a



specific subject. Our multidimensional and multisource analytics tool can enhance clinicians' decision-making and pinpoint risk predictors for TMJ OA progression. The EHPN integrates biological and clinical sciences to solve TMJ OA prognosis in a translational infrastructure that will transform temporomandibular disorders practice.

### **Significance Statement**

This study identified a comprehensive set of clinical, quantitative imaging and biological biomarkers for precise prediction of TMJ OA disease progression. We developed an open-source tool based on a robust method called Ensemble via Hierarchical Predictions through Nested cross-validation (EHPN), which surpassed the performance of the 48 models tested. Importantly, the model demonstrated F1 score of 0.82, suggesting its high level of generalizability. The use of the EHPN model may revolutionize the standards of care, providing clinicians with an accurate tool for anticipating the future status of TMJ OA patients, thereby enhancing their decision-making process.

### **3.1 Introduction**

Temporomandibular Joint Osteoarthritis (TMJ OA) is a progressive degenerative joint disease that affects 8-16 percent of the population worldwide, impacting the quality of life, and imposing a large economic burden on society. It is characterized by synovitis, destruction of the articular tissues, and abnormal remodeling of the subchondral bone (Wang et al. 2023; Lee et al. 2019). This can lead to chronic joint pain, noises, jaw dysfunction, and in advanced stages may necessitate joint replacement (Wang et al. 2023; Yoda et al. 2020). Although TMJ OA is considered an age-related disease, it peaks between the age of 20-40 years, and the associated degenerative changes can appear in adolescents (Song et al. 2020; Lee, Hong, and Chun 2019),

Current understanding of the TMJ OA pathogenesis has shifted from a simple mechanical wear-tear model to a complex and multifactorial condition; biological, behavioral, psychosocial factors as well as comorbidities can contribute to disease onset (Wang et al. 2023; Jha, Lee, and Kim 2022; Lee et al. 2019). Despite the availability of different treatment options for TMJ OA, to date no clinically approved treatment is available to reverse the damage within the TMJ structure (Zhao et al. 2022). Thus, early identification of patients at risk for disease progression is crucial for timely intervention, enhancing the prognosis and reducing the need for surgical management.

Since 2014, the Diagnostic Criteria for Temporomandibular Disorders (DC/TMD) have become the international standard for TMJ OA diagnosis. These criteria improved the reliable detection of the clinical and radiographic features of TMJ OA (Jha, Lee, and Kim 2022; Schiffman, Ohrbach, et al. 2014). However, identifying individuals at risk for disease progression has remained challenging, as the severity of patients' reported symptoms is often not well correlated with the TMJ degenerative bone changes (Song et al. 2020). Therefore, there has been a growing need to identify other prognostic biomarkers.

The subchondral trabecular bone is characterized by a dynamic structure that uniquely adapts to the mechanical loads applied to the joint, altering bone density, shape and/or the spatial orientation and scale parameters of the trabeculae (Li et al. 2013). Mounting evidence indicated that the subchondral bone, in animal models, had an essential role in the initiation and progression of OA. Specifically, OA associated microstructural bone changes reduced the ability to absorb and dissipate energy and increased the transmission of forces through the joint and subsequent deformation of the articular surfaces (Neogi 2012). Recent advances in imaging techniques, e.g. high-resolution cone beam computed tomography (hr-CBCT) scans, enabled three-dimensional (3D) quantification of humans' trabecular bone microstructure with less radiation, reduced cost and improved accuracy, comparable to micro-CT (Liang, Zhang, et al. 2017).\_Importantly, improvement of the processing/analysis methods allowed extracting quantitative features (radiomics) of the images' textures, which reduced the subjectivity in radiographic interpretation Along with condylar bone changes, TMJ OA is characterized by joint space (JS) narrowing (Massilla Mani and Sivasubramanian 2016). Disturbance of normal JS might affect the condyle/articular disc movements, increase the friction among articulating bones and result in pain and functional degradation (Alqhtani et al. 2022). To the best of our knowledge, radiomics biomarkers and JS narrowing have contributed in predicting knee OA disease progression; however, their value in predicting TMJ OA progression remains unexplored (Halilaj et al. 2018; MacKay et al. 2018).

Biological markers have also demonstrated a pivotal role in reflecting changes within joint tissues. Over 100 protein mediators have been identified in integrated processes that contribute to arthritis initiation and progression (Shrivastava, Battaglino, and Ye 2021; Cevitanes et al. 2014). Interestingly, the work of Slade et al. (2011) and Shirvastava et al (2021) suggested that synovial

fluid proteins, which play a role in the cross-talk among different joint tissues and contribute to osteoarthritic degenerative changes, can be reflected in serum biomarkers. To date, no single biological marker has been well-established for the prognosis of OA. As multiple tissues are affected in TMJ OA, a set of biomarkers would provide comprehensive insight into this intricate disease and may improve the prediction of disease progression at an individual level (Rousseau, Chapurlat, and Garnero 2021; Cevidane et al. 2014).

Osteoarthritis has traditionally been considered a slowly progressing disease, however, recent research suggests that the disease progression varies widely among affected individuals (Halilaj et al. 2018). Hence, combining different biomarker modalities seems essential for comprehensive forecasting of OA progression (Ntakolia et al. 2021). With the advent of powerful multivariate data analysis and machine learning (ML) approaches, analysis of complex datasets derived from various sources became feasible (Jha, Lee, and Kim 2022). Nevertheless, before machine training, it is crucial to apply feature selection methods to select the most relevant data for a specific task. This process eliminates irrelevant data, resulting in improved learning accuracy and output comprehensibility (Al Turkestani et al. 2021). A prospective comparison of ML methods in predicting TMJ OA progression is currently lacking, and the few existing longitudinal studies have primarily focused on reporting the clinical and the qualitative imaging features of the disease observed in CT scans (Song et al. 2020). Therefore, the objectives of the present study were: 1) to develop a reliable prediction tool for TMJ OA progression, and 2) to identify the contributing factors in OA progression during a 2–3-year follow-up period. We hypothesized that the combination of specific clinical symptoms, protein markers and quantitative imaging features at baseline would result in a robust ML model for predicting the risk of TMJ OA disease progression over a period of 2-3 years.

To test the hypothesis, we acquired clinical, imaging (trabecular bone texture and morphometry) and biological (serum and saliva proteins) data features at baseline from a prospective cohort of TMJ OA and control participants. We characterized TMJ OA progression at 2-3 years of follow-up using clinical and imaging. We evaluated the contribution of baseline features and compared ML techniques to identify the most robust predictive model. We then developed the Ensemble via Hierarchical Predictions through the Nested cross validation (EHPN) learning tool, which efficiently managed the heterogeneity of the method and effectively integrated the heterogeneous features in this study. The rank of the contributing features in terms of their impact on the final ML output was tested using shapely and additive explanations. Our work provides an open-source tool for comprehensive patient specific prediction of TMJ OA progression.

## 3.2 Materials & Methods

### Study Design, Setting and Participants

The data collection for this prospective longitudinal study baseline sample was conducted from February 2016 to December 2018 and the follow-up was conducted from February 2019 to June 2021, as approved by the Institutional Review Board at the University of Michigan (HUM00113199). All data collection was performed after obtaining written informed consents from participants and in accordance with STROBE guidelines.

At baseline, we recruited 106 participants, 53 TMJ OA and 53 age and sex-matched control subjects, based on rigorous inclusion criteria: participants had no systemic diseases, no congenital bone/ cartilage disease, no history of cancer/trauma/surgery in the TMJ, no previous treatments for the TMJ OA, and their age ranged between 21–70 years. A single temporomandibular disorders specialist diagnosed subjects with TMJ OA following the Diagnostic Criteria for Temporomandibular Disorders (DC/TMD) (Schiffman, Ohrbach, et al. 2014). The TMJ OA diagnosis was confirmed with the radiographic signs of the disease, described in the DC/TMD, and the side with initial osseous alterations was included in the study. The control subjects were all asymptomatic, and the side without radiographic determinants for TMJ OA was included in the study. The retention rate for the follow-up data collection was 70%, which consisted of 74 recalled participants, 34 TMJ OA and 40 control subjects.

### Multi-Source Data Strategies and Processing

Our study acquired 3 main sources of data at baseline (T1): clinical features, imaging features (composed of trabecular bone texture and morphometry) and biological features (composed of serum and saliva proteins). At follow-up (T2), we acquired clinical and imaging data to evaluate

disease progression (Figure 3.5). Data processing was performed by a single examiner (N.A), unless stated otherwise.

### Clinical Data

The DC/TMD clinical exam and survey variables selected for statistical analyses were age, gender, last month distressed by headaches, muscle soreness or lower back pain, vertical range of unassisted mouth opening without pain (mm), and pain characteristics (current pain intensity, worst pain, average pain and pain interference with daily activities in the past 6 months). Participants rated their headaches, muscle soreness, and lower back pain on a scale ranging from 0-4: 0=not at all and 4= extremely. The TMJ OA participants rated their pain using a numeric rating scale that ranged from 0-10: 0= no pain and 10= the worst possible pain. All control subjects presented no orofacial pain at T1 and T2.

### Imaging Data

Acquisition Protocol: High resolution cone-beam computed tomography (hr-CBCT) scans were acquired for all participants using the 3D Accuitomo 170 machine. All patients were positioned with the Camper's horizontal plane parallel to the ground and were instructed to keep their jaws in the maximum intercuspal position. The acquisition protocol included 40 × 40 mm field of view; 90 kVp, 5 mAs, 30.8 sec scanning time and a voxel size of 0.08 mm. All images were coded and de-identified to prevent investigator bias in subsequent analyses.

Imaging Criteria for the TMJ OA Diagnosis: An American Board of Oral and Maxillofacial Radiology certified radiologist and an oral and maxillofacial radiologist evaluated the hr-CBCT scans of the recalled participants blindly. The radiological changes of the mandibular condylar head were scored based on the DC/TMD. Cases with different scores were discussed and con-

sensus data was used to assess progression or improvement of the radiographic changes at follow-up.

**Image Pre-Processing:** To allow reliable detection and comparison of changes between several individuals or within the same individual at different time points (Figure 3.2A), before extracting the quantitative bone texture/morphometry features, all hr-CBCT scans were pre-processed using validated protocols.

**Extraction of Trabecular Bone Texture-based and Morphometry Imaging Features:** Using the “crop-volume” tool in 3D Slicer, a rectangular shaped volume of interest (VOI) was cropped from the trabecular bone in the mandibular condyles and the articular fossa. Then, using the average minimum and maximum intensity values of all VOIs, we standardized the grey level intensities of the VOIs to eliminate inaccuracies of textural features calculation and possible dependency on the global characteristics of the images. Lastly, imaging markers were extracted from the standardized VOIs using “BoneTexture” module in 3D-slicer.

**Measurement of the 3D Articular Joint Space:** To assess the progression/improvement of osteoarthritic changes in the affected individuals, we measured the 3D superior joint space. We pre-labelled two landmarks in the sagittal view of the oriented CBCT scans: on the most superior point of the condyle and on the opposing surface of the articular fossa. To avoid biasing the landmarks’ placements, pre-labelling was performed simultaneously on T1 and T2 scans, using two independent windows in ITK-SNAP. After the volumetric reconstruction of the identified landmarks, linear measurements were obtained in millimeters using the Q3DC tool in 3D Slicer.

**Three-dimensional Shape Analyses and Quantification of Remodeling in the Condyles:** SPHARM-PDM software was used to compute the correspondence across 4002 surface points among all condyles. The output point-based models displayed color-coded maps that enabled



visual evaluation of consistent parametrization of all condyles. An average condyle shape for the TMJ OA and control groups was calculated through propagation of original surface point correspondences across all stages of deformations and averaging the condyle surface meshes. For visualization of the 3D qualitative changes of the average models within the same group at different time points or among different groups, semi-transparent overlays were created using 3D Slicer software. The vector differences were presented on the condyle surfaces, scaled according to the magnitude of difference, and pointing towards the direction of bone change. For quantification of remodeling in the condyles, calculation of signed distances across condyles surface meshes reflected the quantitative bone changes in the TMJ OA and control samples (Figure 3.3). To quantify regional bone changes across the lateral and anterior surfaces of the condyles, we used the Pick 'n Paint tool in 3D Slicer to propagate regional surface points to the corresponding regions of shapes across all subjects and time points (Figure 3.4A) (Cevidaneş et al. 2014).

#### Statistical Analysis and Machine Learning Approaches

We used SPSS version 27.0 (IBM Corp., Armonk, NY) for descriptive analyses, non-parametric tests and computing kappa statistics. To test the differences of the variables between control and TMJ OA subjects, we utilized Chi-square test, Independent Sample T test, and Mann–Whitney U test. To test the differences of variables between T1 and T2 in one group, we utilized Wilcoxon Signed Rank Test. Differences were considered significant when  $p < 0.05$ . Kappa statistics were employed to assess the agreement among two radiologists in grading the morphological changes of the condyles. Pearson's correlation and p-values based on the two-sided t-test between each pair of the imaging, biological and clinical features were calculated. P-values were adjusted based on false discovery rate (FDR) correction for multiple testing.

The health status of all participants at follow-up was scored by two clinicians' experts based on changes in levels of pain-related symptoms, the two radiologists' consensus on the radiographic signs of the disease (subchondral cyst, erosion, osteophyte), and the 3D morphological changes of the condyles compared to the baseline findings. The consensus resulted in four categories: 0=asymptomatic, 1=improved, 2=same, or 3=worsened. This resulted in a small and unbalanced sample size (eight asymptomatic, nine improved, thirteen remained the same, four worsened) that was inadequate for cross-validation and modeling. Thus, we binarized the follow-up evaluation scores and combined healthy and improved categories into one group (recovery) and same and worsened groups into another (no recovery). To build a robust prediction model for TMJ OA prognosis, we followed the steps below,

Nested 10-fold CV: To avoid overfitting, we employed the nested 10-fold CV method to build and evaluate the performance of various predictive models. Our method consisted of two nested CV loops, each implementing a 10-fold CV. The outer loop aimed to provide an unbiased evaluation of model performance, while the inner loop determined the hyperparameters for the final model. Specifically, all subjects were split into 10 folds:  $A_1, A_2, \dots, A_{10}$ . One fold  $A_i$  was kept as an independent test set, and the remaining folds  $\{A_j | j \neq i\}$  were further split into 10 subfolds:  $A_{i,1}, A_{i,2}, \dots, A_{i,10}$ ; the subfold  $A_{i,j}$  was considered an validation set and the remaining subfolds  $\{A_{i,k} | k \neq j\}$  made up the training set. We trained various statistical and machine learning models using the training dataset. The validation dataset was utilized to adjust the hyperparameters and determine the number of top features. In the inner loop of the nested CV, the validation dataset  $A_{i,j}$  looped over  $\{A_{i,1}, A_{i,2}, \dots, A_{i,10}\}$ , and the model trained on the training data  $\{A_{i,k} | k \neq j\}$  was applied to predict the outcome of the validation set  $A_{i,j}$ . In the outer loop of the nested CV,  $A_i$  looped over  $A_1, A_2, \dots, A_{10}$ , with  $A_j, j \neq i$  being the training and validation datasets, respectively,

and each subject was predicted once as an independent test subject. The 34 OA patients underwent the nested 10-fold CV process, while the 40 normal controls were added as additional training resources to the training data during each loop of the cross-validation.

**Feature Selection and Machine Learning (ML) Approaches:** We tested six feature selection (FS) methods including: FS1) selection frequency of LASSO (Glmnet), FS2) permutation importance for Random Forest (RF), FS3) gain for XGboost (XGboost), FS4) combinations of the absolute values of weights for neural network (NNET), FS5) absolute value of coefficients in Glmboost (Glmboost), FS6) AUC between each feature and the response (AUC). We evaluated eight predictive modeling (PM) methods including: PM1) elastic net (Glmnet), PM2) Glmboost, PM3) High-Dimensional Discriminant Analysis (HDDA), PM4) single-hidden-layer neural networks (NNET), PM5) RF, PM6) XGBoost, PM7) Kernel-based Support Vector Machine (SVM), and PM8) Linear Discriminant Analysis (LDA). In total there are  $6 \text{ FS} * 8 \text{ PM} = 48$  machine learning methods.

For each model, we employed three major steps on the training dataset: 1) calculation of feature importance scores based on FS1-FS6 methods, respectively, in the inner loop, 2) ranking of feature importance scores and selection of top features to train the ML models, 3) using the selected number of top features to train the model with the training and validation datasets together. Then, we evaluated the trained models' performances on the test set (outer loop of the nested CV). All feature selection, machine learning predictive modeling based on nested CV were carried out using the package "caret" of R/4.1.0 software, and the six feature importance scores were calculated by the intrinsic metrics of the corresponding ML methods in the package "caret", respectively.

We proposed a method called Ensemble via Hierarchical Predictions through the Nested CV (EHPN) to improve predictive performance. This method combines 18 models with optimal predictive performance based on the validation dataset, six FS models with PM2, six FS models with PM3, and six FS models with PM8, as PM2, PM3 and PM8 were the top three performing ML methods. We carried out the model ensemble on the validation dataset; specifically, a Glmboost model was trained to assign different weights to the 18 models during the validation step. We evaluated the performance of the combined model using the test dataset. Since the test set loops over the 10 folds, the Glmboost model was trained with different and fold-specific set each time.

Interpretability of the ML Models' Prediction: We used the SHapley Additive exPlanations (SHAP) method, we interpreted our EHPN prognosis predictions on the independent test set. Shapley values reflect the magnitude and direction (sign) of the methods'/features' contribution to the model outcome. We calculated the Shapley values to A) identify the top contributing FS and ML methods in the EHPN model and B) determine features' contribution to the model predictions in the top six methods. The Shapley values were calculated following Strumbelj et al. based on Monte-Carlo sampling. A higher Shapley value indicates a higher predicted probability for a patient to improve, compared to removing the method or feature.

### 3.3 Results

#### ***3.3.1 Improvement of the Clinical Symptoms in Participants with TMJ OA***

Seventy-four individuals participated at recall visits (63 females and 11 males, with a mean age of  $41.3 \pm 12.7$  years at baseline (Figure 3.1A). The mean follow-up period was  $2.4 \pm 0.9$  years. The majority of the TMJ OA group sustained the habits of teeth grinding at night (82%) and jaw clenching while awake (~65%). The TMJ OA participants received non-invasive, conservative treatments, such as occlusal splints, physical therapy, jaw exercises and NonSteroidal Anti-Inflammatory Drugs. As a result, they presented significant reduction in their pain intensity, average pain, worst pain levels and pain interferences with their daily activities in the past 6 months compared to baseline levels ( $p \leq 0.0001$ , Figure 3.1B). In comparison to the control group, the TMJ OA group continued demonstrating significantly reduced vertical range of unassisted mouth opening without pain (mouth opening) and higher levels of headaches, lower back pain, muscle soreness, and restless sleep at follow-up ( $p \leq 0.0004$ , Figure 3.1C-D).

#### ***3.3.2 Evidence of Persistence of Radiographic Signs of TMJ OA***

Degenerative bone changes observed in the condyles of the TMJ OA group are illustrated in Figure 3.1E, with their corresponding frequencies of occurrence presented in Figure 3.1F. The most frequent bone changes observed at baseline were flattening (97%) and sclerosis (82%), followed by erosions/osteophytes (79%), and subchondral cysts (76%). While the distribution of flattening, sclerosis and osteophytes did not change among the majority of the TMJ OA participants (82-88%), five surface erosions (~15%) and six subchondral cysts (~18%) were newly detected at follow-up visits. Interestingly, the study subjects presented several osteoarthritic changes concurrently, e.g., osteophytes, erosions and subchondral cysts occurred simultaneously in 19 indi-

viduals. Together, these findings illustrate that participants did not recover from the osteoarthritic changes of the condyles in a mean follow-up duration of  $876.58 \pm 273.75$  days.

The Kappa value of the two oral and maxillofacial radiologists' experts for scoring the condyles' degenerative bone changes was 0.61, indicating a substantial inter-observer agreement, and the overall similarity value agreement was 81%.

### ***3.3.3 Quantitative Imaging Features Vary Among Control and TMJ OA Participants***

Using a previously validated protocol (Figure 3.2A), we extracted imaging features from the trabecular bone at the lateral surface of the condyles and the anterolateral (AL) surface of the articular fossae, sites where greater OA bone remodeling develops.(Cevitanes et al. 2014) Definitions and values of the imaging features are provided in Supplementary Tables 3.1-3.2. Ten condylar imaging features were significantly different between the control and the TMJ OA groups at baseline ( $p < 0.05$ ). Surprisingly, the differences in these markers were not statistically significant following treatment, suggesting that they are sensitive indicators of improvements in patients' conditions (Figure 3.2B). The TMJ OA group had higher levels of entropy, short run emphasis (SRE), low grey level run emphasis (LGLRE), and short run low grey level run emphasis (SRLGLRE) than the control. These findings specified the characteristics of the condyles' trabecular bone texture in the hr-CBCT images at pixels' levels, i.e., the extracted images' volumes presented an increase in the randomness of the grey level intensities distribution, a decrease in texture roughness, and a texture dominated by many short runs of low grey levels. The TMJ OA participants also presented a significant decrease in the trabecular thickness as well as bone surface/bone volume ratio. Intriguingly, five condylar and seven articular fossa imaging features varied significantly between the baseline and the follow-up visits of the control group (Supple-

mentary Tables 3.2-3.3). Together, this suggests that radiomics have the potential to reflect pathological as well as physiological changes within the trabecular bone structure.

Along with the computation of the trabecular bones' radiomics and the structural parameters, we measured the three-dimensional joint spaces extending from the most superior point on the condyles to the opposing point on the articular fossae (Figure 3.2C); our preliminary findings demonstrated, at baseline, insignificant differences of other joint distances between the groups (Mackie et al. 2022). The TMJ OA group continued to display narrowing in their joint spaces at follow up visits, which was significantly different from the control group ( $P \leq 0.0001$ ); the average joint spaces were  $2.8 \pm 0.8$  and  $2.3 \pm 0.8$  mm in the control and the TMJ OA participants, successively. Alterations of the joint spaces' median values, interquartile ranges, minimum, and maximum values are illustrated in Figure 3.2D.

#### ***3.3.4 Osteoarthritis Alters the Morphology of the Mandibular Condyles***

To visualize changes of the mandibular condyles' morphology across both groups and between different time points of the same group, we constructed 3D surface models from the 2D CBCT images and created an average mesh model for each group (Figure 3.3A-B). The semi-transparent overlays between the baseline and follow-up visits demonstrated minor changes at the superior and lateral surfaces of the controls' composite condyle and greater alterations at the superior, medial and lateral surfaces of the TMJ OA average group condyle. In general, the TMJ OA group presented smaller condyles compared to the control's. The semi-transparent overlays, signed distances color-coded magnitude maps and the vector maps of the superimposed models showed that flattening of the articular surface, resorption of the lateral pole and apposition of the anterior surface were characteristics for the TMJ OA group's condyles; a similar pattern was evident at follow-up but to a lesser extent.

Along with the qualitative assessments, we measured regional bone changes in the lateral and anterior surfaces of the groups' composite condyles (Figure 3.4A). Although the control group showed a similar amount of bone changes across the examined regions ( $\sim 0.3$  mm, Figure 3.4B), the frequency of apposition and resorption were higher in the anterior and lateral surfaces of the condyles, successively (Figure 3.4C). Consistent with this finding, we observed a similar pattern of bone changes in the TMJ OA group, yet they exhibited almost double the amount of bone remodeling detected in that of the control group ( $\sim 0.6$  mm.). Collectively, these observations indicate that osteoarthritis affected condyles' shape, as well as the amount of bone formation and resorption.

### ***3.3.5 Individual Features Contribute Differently to the Prediction of TMJ OA Prognosis***

To determine the value of each clinical, imaging, and biological feature in differentiating the follow-up health status of the TMJ OA cases (0: asymptomatic/improved, 1: remained the same/worsened) from the whole sample ( $n=74$ ), we computed the Area Under the roc Curve (AUC). Supplementary Figure 3.1 shows a circle plot that consists of: the AUC values between each feature and the follow-up health status of the TMJ OA group, the negative logarithm of the p-values to base 10 for each feature between the two clinical groups using the two-sided two-sample t-test, and the negative logarithm of adjusted p-values to base 10 after the correction of all features. The clinical features had the highest AUC values followed by the structural parameters of the articular fossa, and the condyle's radiomics. Headache, lower back pain, and restless sleep features demonstrated significant correlations (Significance level:  $-\text{Log}_{10}(0.05)=1.3$ ) with the clinical diagnosis, while the remaining features did not. This implies that simple linear models may be inadequate in accurately predicting the participants' health status. Consequently,



more sophisticated statistical and machine learning techniques were suggested and subsequently examined.

### ***3.3.6 The EHPN Method Achieves the Highest Accuracy in Predicting TMJ OA Prognosis***

We developed our prediction mode using the baseline dataset which included: 6 clinical features, 40 trabecular bone texture-based and morphometry features, the 3D superior joint space, and 23 biological markers (Figure 3.5, Supplementary Table 3.4). To determine the participants' TMJ OA health status overtime, we utilized clinical and imaging features, as well as the 3D morphological assessments of the condyles at follow-up visits. The TMJ OA cases were labeled as asymptomatic/improved or stayed the same/worsened, as detailed in the methodology section and illustrated in Supplementary Figure 3.2.

To minimize overfitting, we performed nested 10-fold cross-validation (CV) and evaluated the prediction performance of 48 advanced statistical, feature selection, and machine-learning methods. The accuracy (ACC), Area Under the receiver operating characteristic Curve (AUC), and F1 score of all methods are provided in Supplementary Tables 3.5-3.6. The combination of Linear Discriminant Analysis (LDA) model with the absolute values of weights for the neural network (denoted by NNET), or the selection frequency of least absolute shrinkage and selection operator (denoted by Glmnet), or the eXtreme Gradient Boosting (denoted by XGBoost) feature selection methods yielded the highest ACC, AUC and F1 scores on the validation dataset, by average. However, these methods presented a decrease in their F1 scores on the test dataset (Figure 3.6A), suggesting that the top performing methods on the validation data may suffer from overfitting on the test set.

Consequently, we proposed the Ensemble via Hierarchical Predictions through Nested CV (EHPN) method, which combined the top 3 performing models on the validation dataset with the six feature selection methods (Figure 3.6B). The combined model showed improved performance on the test set, with accuracy= 0.87, AUC= 0.95, and F1=0.87 scores, outperforming those of the individual models by 8-12%, 3-14%, and 9-14%, respectively. Notably, the EHPN model's F1 score on the test dataset differed from that on the validation set by only 5%, compared to 9-13% of F1 scores' fluctuations in the top performing models. These findings indicate that the combined model achieved more accurate prediction results and potentially addressed the issue of overfitting in the individual models (Figure 3.6C).

### ***3.3.7 Features' Integration Enhances the EHPN Model's Prediction of TMJ OA Prognosis***

Since TMJ OA is a multifactorial disease and there is a need to identify quantitative features that enable the prediction of the disease prognosis, we carried out the above experiments using clinical, imaging and biological features. We next investigated if a particular subset of these features could predict the TMJ OA prognosis while attaining a comparable performance to using all features.

Figure 3.6C shows the prediction performances of the EHPN model utilizing distinct feature integration strategies. Using clinical, imaging, and biological features individually lead to a prediction accuracy of 62%, 59% and 44%, respectively, on the test set. The addition of the imaging features to the clinical dataset enhanced the models' accuracy and F1 score by 12% leading to the best model currently clinically feasible. In contrast, the combination of biological and clinical features alone did not improve the model's performance, suggesting that imaging features may play a more important role. Nevertheless, the inclusion of all features' sets further improved the model's performance (ACC = 0.87  $\pm$ .06, AUC = 0.72  $\pm$ .10 and F1 score = 0.82  $\pm$ .05). Col-

lectively, these findings indicate that the combination of all feature categories is essential for an accurate prediction of the TMJ OA prognosis.

### ***3.3.8 The SHAP Method Determines the Top Contributing Features for TMJ OA Prognosis***

Although the best learning strategy for our ensemble model was to incorporate all feature sets, this does not indicate that they all had the same impact on the model's predictions. Thus, we utilized the SHapley Additive exPlanations (SHAP) method to identify the top contributing features in the EHPN model's predictions using the independent test set.

We first computed the Shapley values to identify the top contributing methods in the EHPN model. Supplementary Figure 3.3 shows that the top six methods had a 76% global impact on the combined model predictions, with the NNET feature selection method and the LDA machine learning approach being the top contributors. We next calculated the Shapley values to determine the features with highest contribution to the model predictions, in the top six methods. Figure 3.7A shows that the top 21 features had a 90.79% impact on the model's predictions, along with a detailed description of each feature's predictive contribution. Among the top features, clinical features accounted for 32.35%, imaging for 36.39%, and biological features for 20.87%, with age contributing for 1.18%. Interestingly, these features demonstrated weak Pearson's correlation between them, which did not meet the threshold for false discovery rate (FDR) correction at a significance level of 0.05 due to limitations in the sample size (Figure 3.7B, Supplementary Table 3.7). This suggests that both imaging and biological features made independent contributions to predicting the disease prognosis. At the same time, part of the imaging's indirect effect on the TMJ OA status may be explained by the biological features.

The boxplots in Supplementary Figure 3.4 illustrate that the feature distinctions between the asymptomatic/improved and remained the same/worsened groups, for the top 21 features, respec-

tively. For instance, individuals in the OA worsened group manifest significantly elevated levels of headaches, lower back pains, and restless sleep.

### **3.4 Discussion**

This study demonstrates the significance of combining clinical, quantitative imaging, and biological features in addressing the complex, multifactorial nature of TMJ OA and forecasting its state over 2-3 years. By utilizing advanced statistical and machine learning approaches, we were able to disentangle the complex relationship between these features and integrate them towards a single outcome (predicting disease prognosis). Analysis of the experimental results yielded important insights into the relationship between the top 21 identified risk factors, that contribute to 90.79% of the model prediction, and disease progression (Figure 3.7A): headaches, lower back pain, restless sleep, limited mouth opening, condylar (high grey level-GL- run emphasis, short run high GL emphasis, bone /total volume) and articular fossa imaging features (bone surface/volume, GL non uniformity, long run low GL emphasis, correlation, bone/total volume, short run emphasis), superior joint space, age, saliva concentration of OPG, VEGF, MMP7, Angiogenin, and serum concentration levels of BDNF and ENA78. Our results add quantitative imaging to the DC/TMD clinical and subjective imaging criteria in the best clinically feasible model up to date. Our study demonstrated that incorporating specific biological markers enhanced the accuracy of the EHPN model in predicting TMJ OA prognosis, thereby highlighting its potential to indicate future changes in clinical care standards. Utilizing the EHPN model may serve as a valuable solution for clinicians to anticipate the future status of TMJ OA patients, enhancing their informed decision-making, promote personalized care, and ultimately improve patient outcomes.

The age and gender distribution of symptomatic TMJ OA patients in this study was consistent with previous research, facilitating the generalization of our results (Song et al. 2020; Alexiou, Stamatakis, and Tsiklakis 2009). Our clinical data analyses added to existing literature with respect to the efficiency of conservative treatments and the prevalence of comorbidities in painful TMJ OA cases. Recent evidence demonstrated that non-invasive treatments relieve TMJ OA associated symptoms, reduce muscles' contracture, decrease forces applied on the TMJ and balance stress distribution across the entire masticatory system (Wu et al. 2022; Al-Ani 2021). Despite the significant reduction of TMJ pain-related symptoms, only 24% of our TMJ OA participants presented no pain at the follow-up visit, supporting the notion that TMJ pain is not only elicited by local factors, e.g., joint inflammation, but might also involve central sensitization (Sperry et al. 2019). We also found that mouth opening increased in 41% of the TMJ OA group; the heterogeneity of structures involved in restricting mouth opening (arthrogenous with/without myogenous structures) might have contributed to differences in treatment responses (Nicolakis et al. 2001). Furthermore, our study confirmed the existence of frequently reported TMD comorbidities (headaches, lower back pain, and sleeping disturbances) in the majority of our TMJ OA participants, which may be implicated in the development of TMJ OA and worsening of joint/muscular pain (Shrivastava, Battaglino, and Ye 2021; Slade et al. 2016).

Radiographic image changes over time support the observation of other cross-sectional studies that identified flattening and sclerosis as the most common changes in TMJ OA patients (Jung, Lee, and Suh 2022; Koç 2020). Erosions, osteophytes and subchondral bone cysts co-occurred in over half of our TMJ OA group, indicating that OA affected several regions of the condyles at different times, with some areas displaying degenerative and others adaptive changes. Erosions represent an initial stage of TMJ degenerative changes, while osteophytes develop when the

body adjusts to repair the joint, broadening the surface and reducing stress overload. Subchondral cysts were postulated to form when the impact between opposing bone surfaces causes microfractures and necrosis, and the synovial fluid intrudes into these areas as the body repairs them and resorbs the necrotic bones (Dumbuya et al. 2020). Interestingly, the frequency of OA imaging characteristics in the current study differed from the literature (Dumbuya et al. 2020; Alexiou, Stamatakis, and Tsiklakis 2009). Furthermore, in the follow-up visits, erosions and subchondral cysts did not disappear nor transform into sclerosis, flattening or osteophytes. Previous retrospective studies reported that following a year of conservative treatments, the number of degenerative bone changes in CT and CBCT sections decreased, and the osteoarthritic joints healed through regaining of cortical lining and transformation of erosions and/or bone cysts into sclerosis or flattening (Kim et al., n.d.; Song et al. 2020). Our results corroborate prior findings that subjects' characteristics, diagnostic criteria for OA, and CBCT machine settings influence the accuracy of the detection of degenerative bone change (Cömert Kiliç, Kiliç, and Sümbüllü 2015). Specifically, recruiting our TMJ OA patients at their initial visit to the TMJ clinics might result in earlier diagnosis of TMJ OA and, hence, require longer time for healing/remodeling of bone change (Lee et al. 2012). Additionally, we utilized high resolution CBCT images (40 × 40 mm FOV, 0.08 mm voxel size), as CBCT is superior to CT in visualizing TMJ bone changes and detecting subtle alterations in the condyles' trabecular pattern, and high scan resolution can detect bone defects regardless of their size (Lee et al. 2012). Thus, standardizing imaging protocols and adapting them to specific equipment, as well as providing detailed guidelines for TMJ OA bone imaging characteristics, appear crucial for combining diverse findings, undertaking cross-domain analyses and improving our understanding of the disease (Basu et al. 2019).

The EHPN model's prediction was interpreted using Shapley analysis, identifying 21 risk factors that greatly contributed to the prognosis of TMJ OA disease. A specific subject's probability of recovery increases with lower values of headache, back pain, restless sleep, condyle HGLRE, articular fossa GLN and LRHGLRE, saliva levels of OPG and Angiogenin, and higher values of superior joint space, mouth opening, saliva concentrations of VEGF and MMP7, serum level of ENA78 and age. The imaging markers made the highest contribution to the model's predictions followed by clinical comorbidities. At follow-up, the health status of the participants was assessed using clinical and imaging features since it was not possible, prior to this longitudinal study, to determine the effect of biological features on TMJ OA disease progression. The biological data was collected only at baseline to test its contribution to the disease prognosis and minimize costs. Interestingly, even though follow-up levels of biological markers were not acquired, the baseline levels contributed to 20.87% of the EHPN predictive model.

Our findings indicate that clinical comorbidities contributed to 32.35% of the EHPN predictive model, which adds to the growing body of evidence linking temporomandibular disorders and clinical comorbidities (Conceição et al. 2022). Aside from the fact that comorbidities were highly prevalent in the TMJ OA group, having greater baseline levels of headache, sleeping disturbance, and lower back pain (LBP) negatively influenced their responsiveness to conservative treatments, (i.e., headache may increase the intensity and frequency of joint and muscle pain(39); individuals with painful TMD have poor sleeping quality; sleeping disorders can contribute to headache persistence(40); and LBP can complicate recruitment of neck muscles to assist with jaw-related tasks, placing greater stresses on the masticatory system and jaw muscle (Lee, Wu, et al. 2020).

Ten quantitative imaging markers had the strongest contribution to disease progression, including superior articular space, 3 condylar and 6 articular fossa markers. Although erosions and osteophytes are more frequently observed in the condyles, where the bone is from endochondral origin, interestingly, the intermembranous bone in the articular fossa, that does not present such marked surface changes, showed that its bone texture and morphometry were predictors of TMJ OA progression. Our findings showed that condylar HGLRE had the highest Shapley value among the ten quantitative imaging markers with significant contribution to TMJ OA progression prediction. Notably, patients with lower HGLRE baseline values presented a favorable prognosis. The distribution of high grey level intensity voxels was shown to increase in resorptive as well as sclerotic regions compared to normal bone, suggesting the marker's sensitivity to osteoarthritic bone alterations. Furthermore, when quantified using other applications, such as Ibex and BoneJ, the HGLRE value is highly consistent, indicating its high reliability (Bianchi et al. 2019). Although joint space narrowing was reported to occur in TMJ OA patients (Massilla Mani and Sivasubramanian 2016), in our study we found that the decrease in the superior joint space can serve as risk predictor of severe prognosis.

Considering the biological markers, OPG in saliva had the highest contribution to the EHPN model. Osteoprotegerin normally prevents excessive bone resorption through impeding osteoclasts' differentiation/activation, and inducing their apoptosis (Wang et al. 2015). Intriguingly, we detected a greater risk of disease worsening in TMJ OA patients with increased OPG protein levels (Figure 3.7A). This may pertain to the concurrent increase in RANKL levels, resulting in a decreased OPG/RANKL ratio, and an increased osteoclasts' activity that promote greater subchondral bone resorption (Cafferata et al. 2021). Moreover, we noted that TMJ OA patients with



higher MMP7 baseline protein levels in saliva presented favorable prognosis (Figure 3.7A). MMP7 was found to be involved in the breakdown of various components of the extracellular matrix in knee OA cases (Tao et al. 2015). Our results, on the other hand, suggest the involvement of MMP7 in bone tissues' repair, corroborating previous observation of a statistical association between MMP7 protein level in TMJ OA patients and bone apposition on the anterior surface of their condyles (Cevidane et al. 2014).

Furthermore, we found that VEGF and angiogenin in saliva, and ENA78 and BDNF proteins in serum were strong predictors of TMJ OA progression. Patients with TMJ OA frequently complain of joint pain related to synovitis and neuronal sensitization. In this context, VEGF, ENA78 and BDNF, can cause pain by stimulating inflammation, nociceptors and perivascular neuronal growth/survival (Cafferata et al. 2021; Lu et al. 2021). Notably, TMJ OA patients with increased VEGF and ENA78 protein levels demonstrated greater probability for disease improvement, which contradicts a number of findings contending the destructive role of these markers in OA (Dygas, Szarmach, and Radej 2022; Scanzello 2017). It has been reported, however, that VEGF stimulates angiogenesis, influences the activity of osteoblasts promoting bone formation, and maintains normal bone remodeling through the regulation of osteoclasts' differentiation and maturation (Hu and Olsen 2016). Also, ENA78 involvement in bone remodeling was recognized through the induction of osteoblasts proliferation and the upregulation of collagen type I expression (Lisignoli et al. 2006). In line with these observations, our results suggest that the identified biological markers have differential effects (degenerative as well as reparative) in the course of TMJ OA disease.

Several future directions could further improve the EHPN model's predictive performance and generalizability. First, increasing the sample size, while adhering to data collection and pro-

cessing quality requirements, will improve score features' weighting, enhance the marginal effect estimates, and the predictive values. It will also allow additional subdividing of the diseased group's treatment response, promoting greater accuracy in patient-specific treatment planning. Second, the majority of our sample was white and Caucasian. Increasing the sample's diversity is essential as OA-related pain differs between races/ethnicities. Lastly, it remains a question if integrating genetic data can result in a more transferable model for diverse populations.

While most previous studies modeled the progression of TMJ OA using clinical symptoms and qualitative imaging markers, here we incorporated biological and quantitative imaging variables to prospectively assess disease progression. We also used the 10-fold nested cross-validation method to make our EHPN prediction model generalizable. Additionally, we have made our open-source tool accessible on GitHub to enable the improvement of this model as additional sensitive biomarkers for TMJ OA become available. Ultimately, early prediction of TMJ OA progression trajectories may support efforts for the discovery of new therapies, e.g., including participants who are likely to undergo disease progression during the trial period is conducive to proper assessment of drugs' efficacy. Furthermore, exploration of the underlying mechanisms behind the identified top contributing factors and TMJ OA progression may facilitate future development of preventive and treatment strategies that stop or lessen disease advancement.

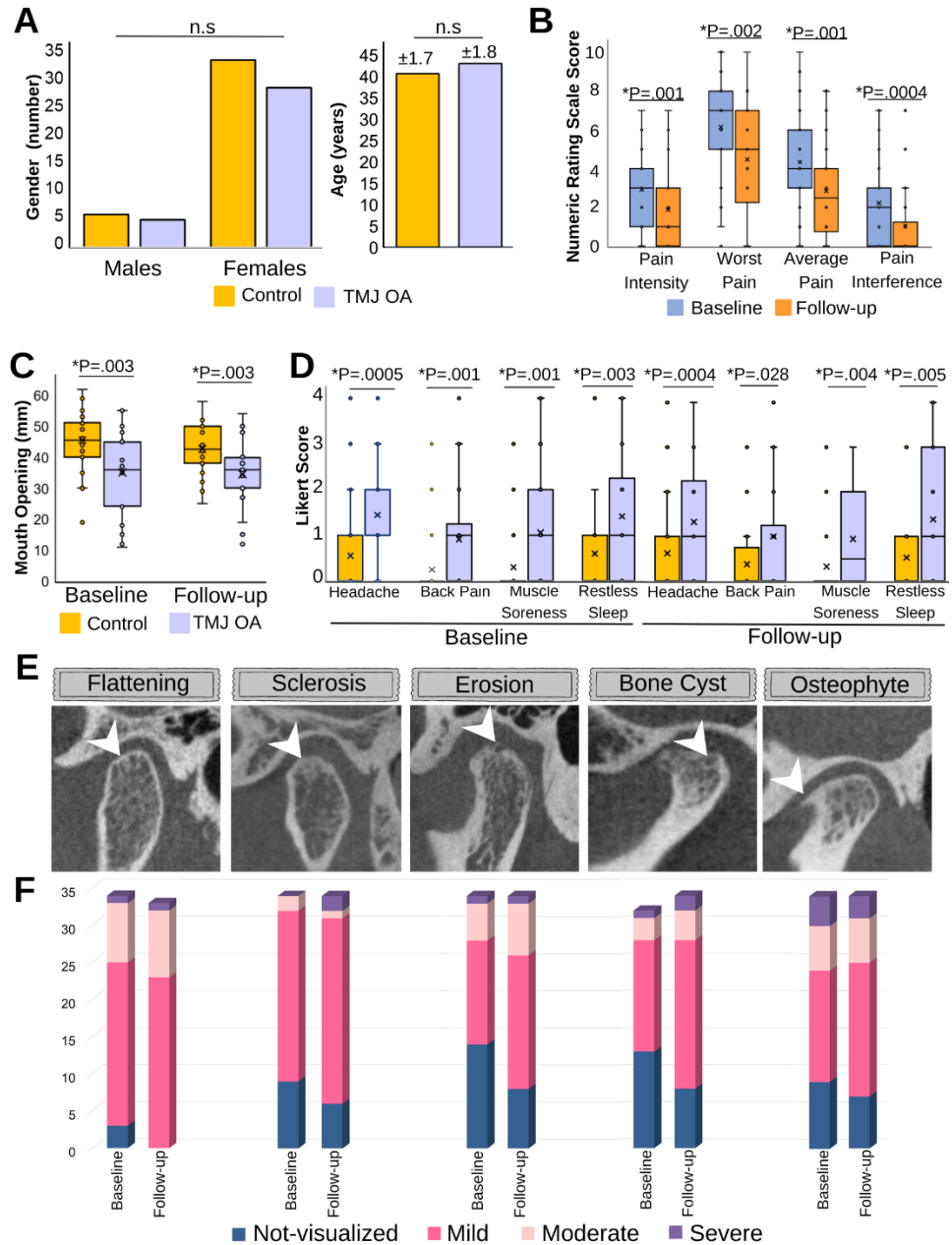
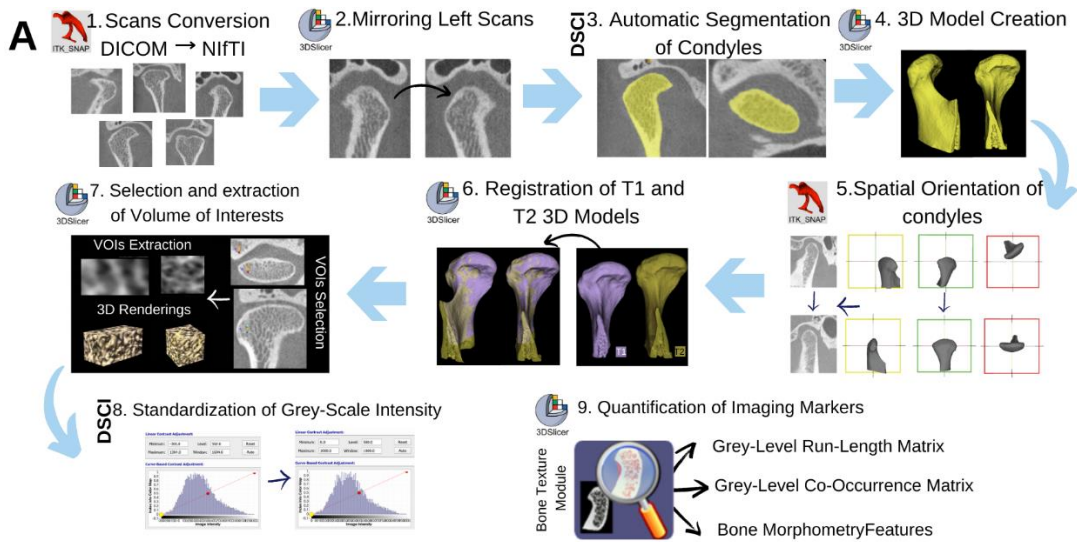


**Figure 3.1: Descriptive Values of the Participants' Clinical Characteristics and the Radiographic Determinants of Temporomandibular Joint Osteoarthritis.** A) The box plots depict gender distribution and mean age ( $\pm$ SD) of the participants at follow-up visit. B) The mean ( $\bar{x}$ ), median, interquartile range, and the range of TMJ pain related characteristics (0-10 scale:0= no pain and 10= the worst possible pain) are shown in the TMJ OA group. The control subjects did not present TMJ pain at baseline (an inclusion criteria) and follow-up visits. C,D) Values of the clinical co-morbidities rated using Likert scale that ranged from 0-4: 0=not at all and 4= extremely. As clinical variables were not statistically significant within each group, only group comparisons were reported. P-values were computed using <sup>A</sup>Chi-square test, <sup>A</sup>Independent samples t test, <sup>C</sup>Wilcoxon signed rank test, and <sup>D</sup>Mann-Whitney U tests, values<0.05 were considered statistically significant. E) Examples of the degenerative bone changes observed in the mandibular condyles of the study participants are indicated by arrowheads pointing towards the affected areas of the bone. B) The frequency of osteoarthritic condylar bone changes identified in the high resolution-CBCT scans of the TMJ OA subjects at baseline and follow-up visits.



**B**

Site	Imaging Features	Baseline			Follow-up		
		Control	TMJ OA	P-value	Control	TMJ OA	P-value
Lateral Surface of the Condyle	Energy	42.6	31.5	0.02*	40.28	34.24	0.22
	Entropy	32.5	43.38	0.03*	34.2	41.38	0.15
	Correlation	42.63	31.47	0.02*	40.88	33.53	0.14
	Short Run Emphasis	32.88	42.94	0.04*	35.45	39.91	0.37
	Long Run Emphasis	42.1	32.09	0.04*	40.65	33.79	0.17
	Low Grey Level Run Emphasis	31.53	44.53	0.01*	34.2	41.38	0.15
	High Grey Level Run Emphasis	40.75	33.68	0.002*	40.23	34.29	0.11
	Short Run Low Grey Level Emphasis	30.53	45.71	0.01*	33.85	41.79	0.25
	Short Run High Grey Level Emphasis	42.98	31.06	0.03*	40.15	34.38	0.45
	Long Run Low Grey Level Emphasis	32.73	43.12	0.03*	35.78	39.53	0.45
	Trabecular Thickness	42.28	31.88	0.02*	39.23	35.47	0.22
	Bone Surface/Bone Volume Ratio	42.6	31.5	0.03*	40.28	34.24	0.15

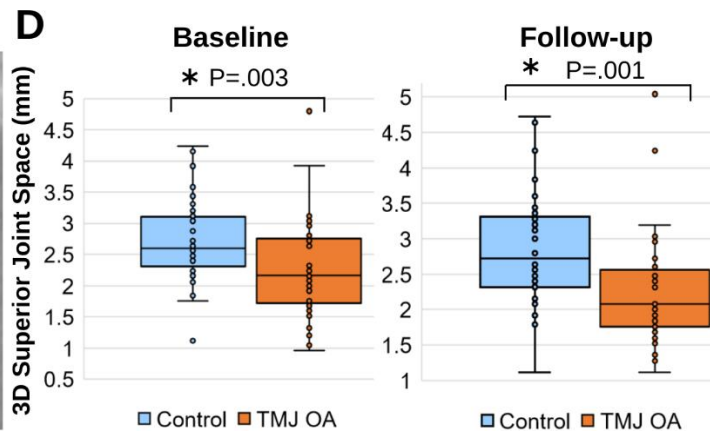
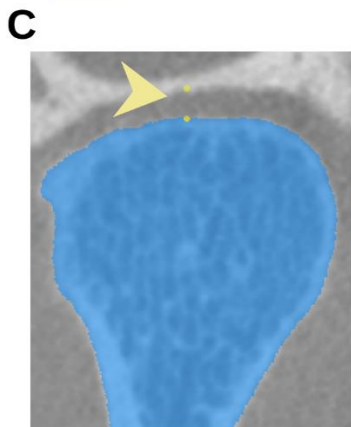


**Figure 3.2: Measurement of Trabecular Bone Textural and Structural Parameters, and the Three-dimensional Superior TMJ Space.** A) A workflow for the pre-processing steps of the hr-CBCT scans prior to quantification of the imaging markers in mandibular condyles and articular fossae. B) The median values for the radiomics and bone morphometry features that significantly varied between control and TMJ OA subjects at baseline visits. C) Left panel shows the placement of two landmarks in the sagittal view of the oriented CBCT scans in ITK-SNAP. After the volumetric reconstruction of the identified landmarks, linear measurements of the superior joint space were obtained in millimeters (mm), using the Quantification of 3D Components tool in 3D Slicer. The box plots demonstrate the median, interquartile, and the range of the SJS in the control and the TMJ OA participants at baseline and follow-up visits.  $P < 0.05$  were considered statistically significant.

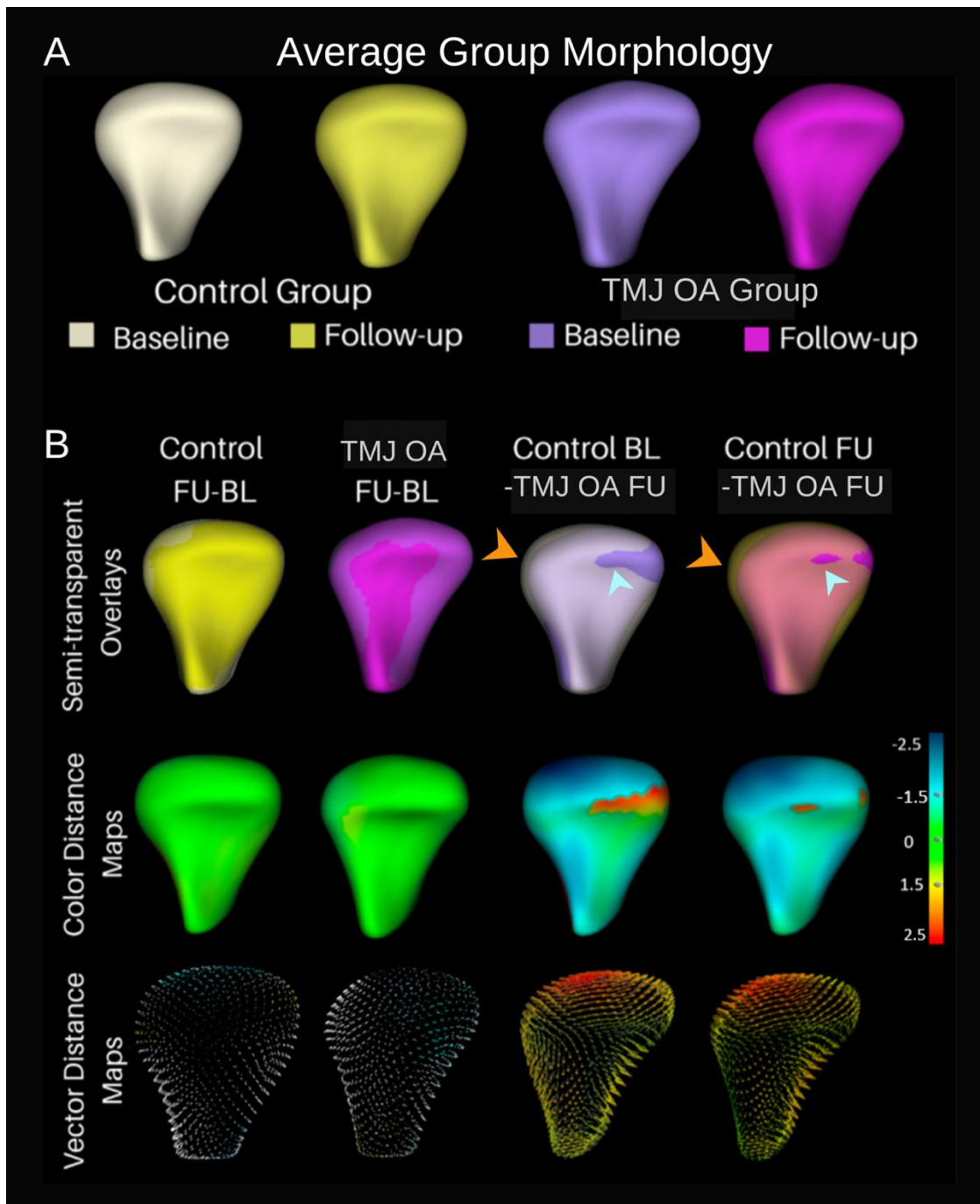


**Figure 3.3: The Three-Dimensional Analyses of Condyles' Morphology.** A) The average group morphology of condyles at baseline (BL) and follow-up (FU) visits. B) The semi-transparent overlays, in the top panel, are depicting morphological differences of the composite condyles within/between the control and TMJ OA groups- the orange and blue arrow heads are pointing, successively, at the resorptive and appositional changes along the condyles' surfaces. The color distance maps are showing the quantitative bone changes across the condyles' surface meshes- negative values denote areas of bone resorption (blue) and positive values indicate sites of bone proliferation (red). The vectors, in the lower panel, are representing the magnitude and direction of bone changes across the condyles- vectors are pointing inward and outward, successively, indicative of bone resorption and proliferation.

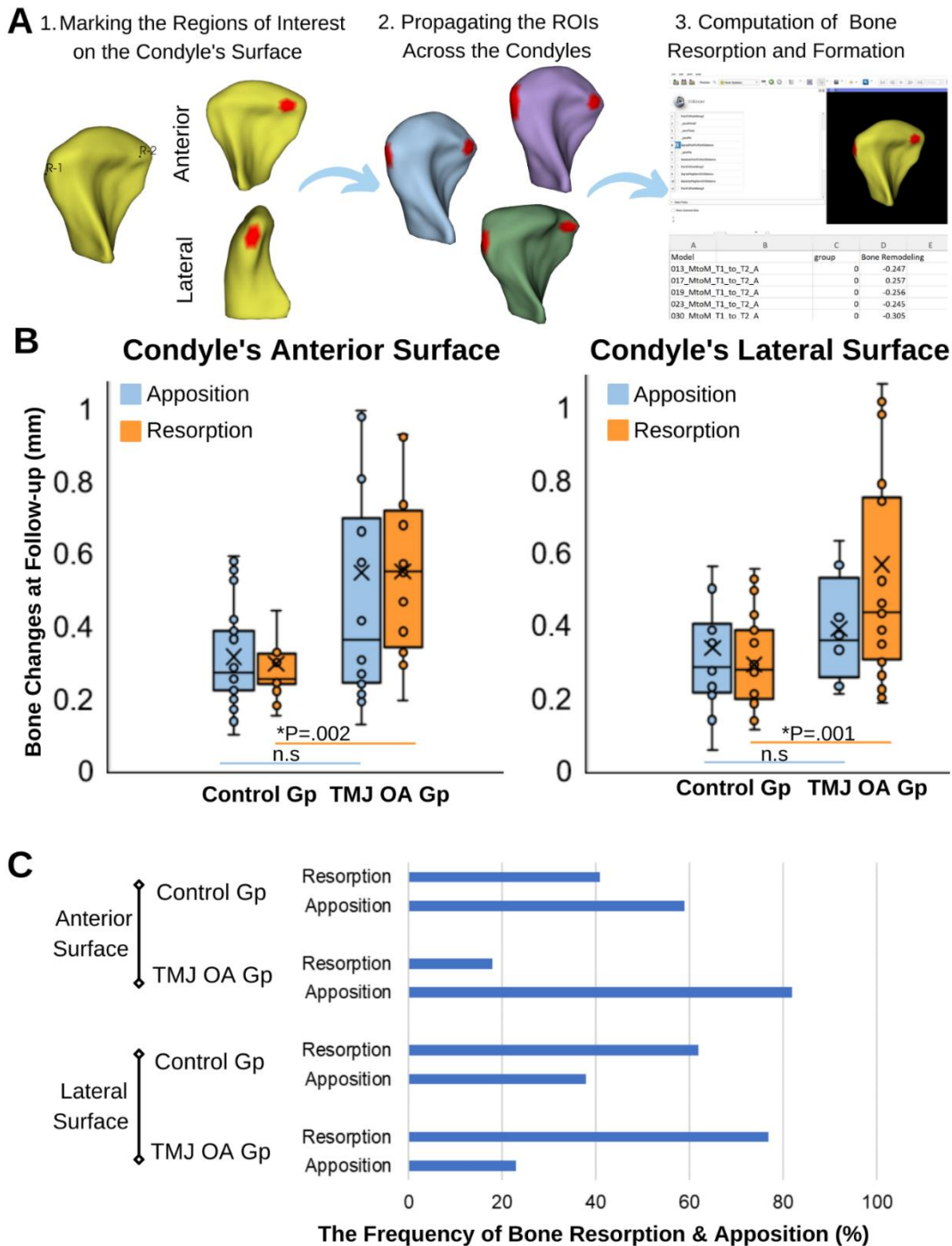


**Figure 3.4: Quantitative Assessment of Bone Remodeling in the Composite Condyles of the Control and the TMJ OA Groups.** A) The workflow for the steps of measuring regional bone changes in the average group condyles. B) The mean (x), median, interquartile, and range of appositional and resorptive bone changes observed in the anterior and lateral surfaces of the condyles, compared to baseline levels.  $P < 0.05$  were considered statistically significant. n.s., non-significant. C) The frequency of bone resorption and formation among the study participants.



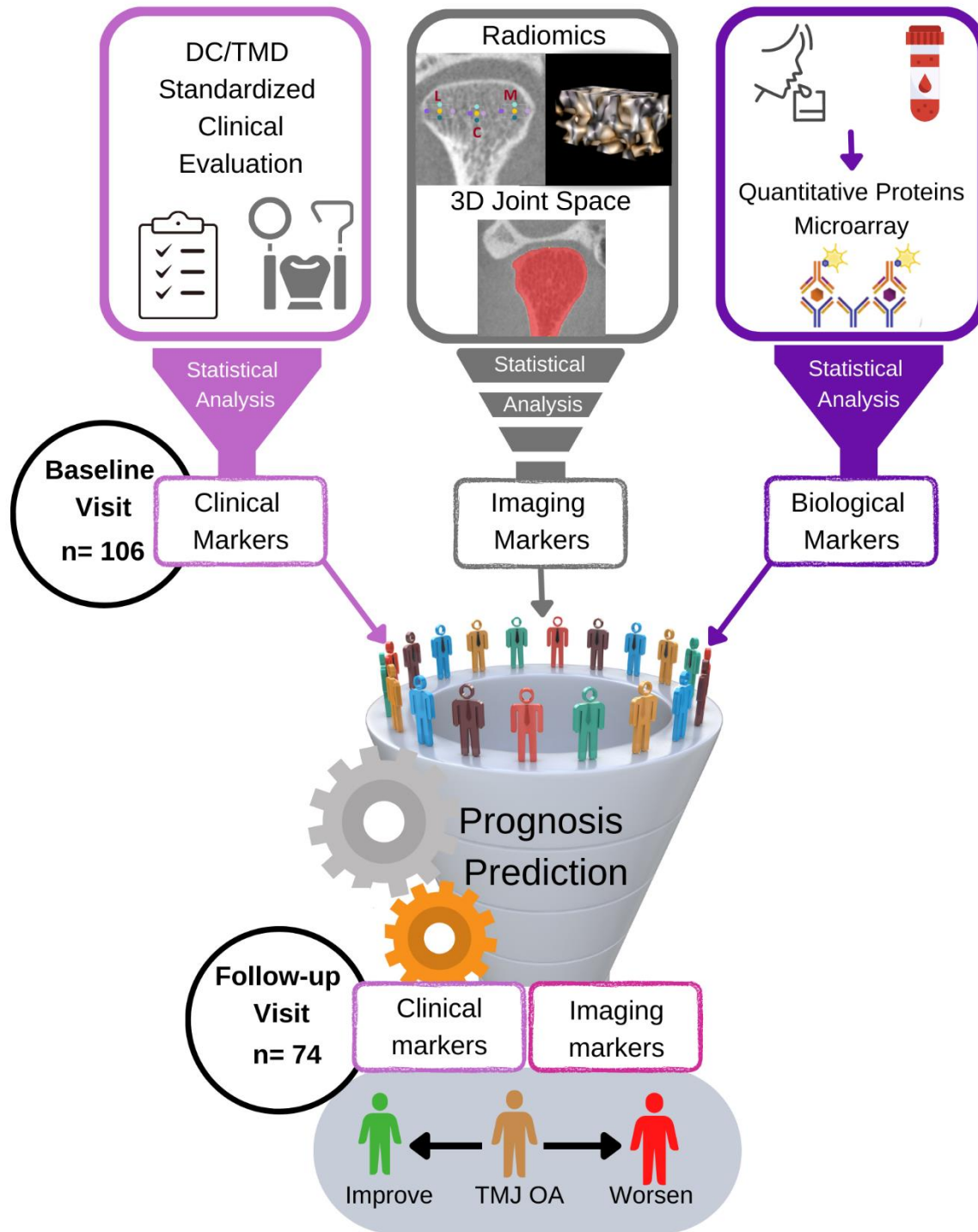
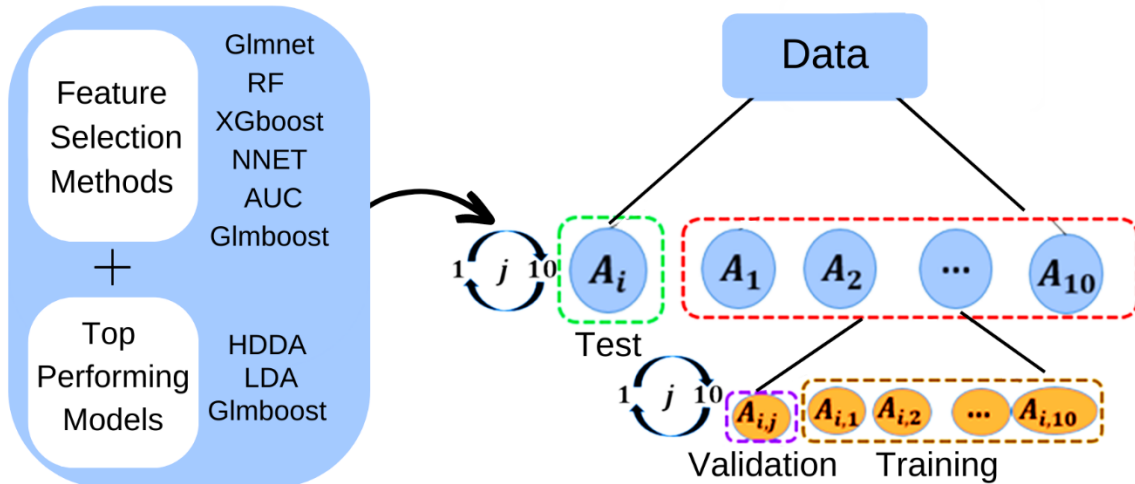


**Figure 3.5: Schematic Representation for the Steps of the TMJ OA Prognosis Prediction Model's Development.** A) Clinical, imaging and biological data were collected from the study subjects, at baseline, and utilized to create the OA Prognosis Prediction model. B) Clinical and imaging data were collected, at follow-up visits, to label the training dataset with the changes of the participants' health status following a 2-3 years of conservative management.

**A**

	Evaluation Metrics		ACC	AUC	F1 Score
	Methods				
Validation Dataset	NNET	+ LDA	0.787±0.073	0.928±0.044	0.780±0.058
	Glmnet	+ LDA	0.752±0.077	0.807±0.080	0.741±0.063
	XGBoost	+ LDA	0.748±0.078	0.813±0.080	0.733±0.068
Test Dataset	NNET	+ LDA	0.676±0.080	0.744±0.088	0.652±0.070
	Glmnet	+ LDA	0.676±0.080	0.625±0.103	0.652±0.071
	XGBoost	+ LDA	0.618±0.083	0.619±0.103	0.601±0.067

**B**  
Ensemble via Hierarchical Predictions through the Nested CV Method



**C**

Features' Set	Dataset	Evaluation Metrics				Precision Control	Precision TMJ OA	Recall Control	Recall TMJ OA
		ACC	AUC	F1					
Clinical + Imaging + Biological	Validation	.949±.04	.948±.04	.868±.04	.815±.09	.953±.04	.961±.04	.777±.10	
	Test	.869±.06	.723±.10	.818±.05	.739±.09	.999±.0003	.999±.0002	.647±.12	
Clinical	Validation	.791±.07	.873±.06	.787±.06	.731±.10	.900±.07	.922±.05	.660±.12	
	Test	.617±.08	.709±.09	.614±.06	.599±.11	.642±.13	.705±.11	.529±.12	
Imaging	Validation	.770±.08	.873±.07	.764±.06	.707±.10	.895±.09	.927±.06	.613±.12	
	Test	.588±.08	.501±.11	.564±.07	.559±.10	.666±.16	.823±.09	.352±.12	
Biological	Validation	.837±.06	.906±.05	.834±.05	.799±.09	.907±.06	.922±.06	.750±.10	
	Test	.441±.09	.606±.10	.399±.08	.462±.10	.375±.17	.706±.11	.177±.09	
Clinical + Imaging	Validation	.834±.07	.902±.05	.831±.05	.766±.10	.951±.04	.961±.03	.707±.12	
	Test	.735±.08	.698±.10	.729±.06	.681±.10	.833±.11	.882±.08	.588±.12	
Clinical + Biological	Validation	.830±.07	.941±.04	.827±.05	.762±.10	.948±.04	.960±.03	.700±.12	
	Test	.617±.08	.605±.10	.609±.06	.590±.10	.666±.14	.764±.10	.470±.12	

\*Acc, Accuracy; AUC, Area Under the receiver operating characteristics Curve

**Figure 3.6: Comparison of the Models' Performances in Predicting the TMJ OA Prognosis.** A) The performance of the top feature selection and machine learning approaches on the validation and test datasets. B) Schematic representation of the EHPN method that combines 18 models with optimal predictive performance on the validation dataset. Our data was split into 10 folds: a test set and the remaining were subdivided into training and test sets, ten-fold cross validation was applied in both loops. We carried out the model ensemble on the validation dataset and evaluated its performance using the test dataset. C) The performance of the EHPN method on the validation and test datasets using different feature sets.



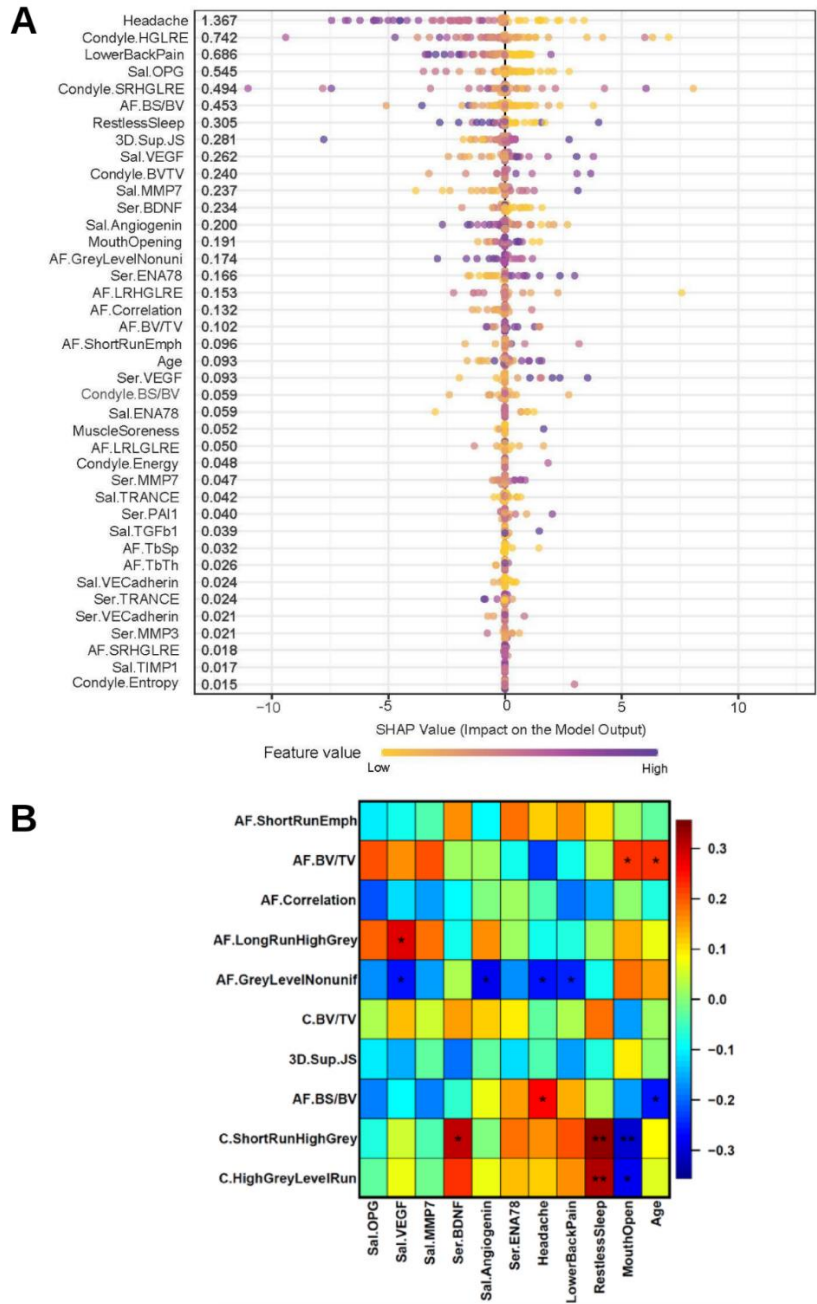


**Figure 3.7: The Top Contributing Features in Predicting TMJ OA Prognosis.** A) SHAP values for the features' impact on the EHPN model's prediction. The ranking numbers in the first column are the SHAP importance by averaging the absolute Shapley values per feature across the data. Each feature contribution is calculated by the SHAP importance of each feature/the sum of all SHAP importance. The SHAP value for each dot indicates the change of log-odds (increased probability) of no recovery for a specific subject if you exclude the specific feature. The location of the purple and yellow dots indicates the SHAP value for each subject. For example, if the purple dot for headache was on the left, it means higher occurrence of headache may negatively contribute to recovery from TMJ OA. B) Correlation matrix between the top contributing clinical, imaging and biological features in TMJ OA prognosis. The color-coding scale denotes the degree of positive and negative Pearson correlation between the features. \*Raw  $p < 0.05$ , \*\* raw  $p < 0.01$ , and \*\*\* raw  $p < 0.001$ .

**Supplementary Table 3.1: Description for the Trabecular Bone Texture-Based and Morphometry Features.**

Features	Variables	Definitions
Grey-Level Co-occurrence Matrix (GLCM)	Energy Entropy Correlation Inverse difference moment Inertia Cluster shade Cluster prominence Haralick correlation	Uniformity of the grey-level textural organization. Randomization of the grey-level distribution. Grey-level linear dependence among the pixels. Local homogeneity of the grey-level distribution. Contrast between a pixel and its neighbor. Skewness and uniformity of the grey-level distribution. Skewness and asymmetry of the grey-level distribution. Linear dependence between the pixels.
Grey-Level Run Length Matrix (GLRLM)	Short run emphasis (SRE) Long run emphasis (LRE) Grey level non-uniformity (GLN) Run length non-uniformity (RLN) Low grey level run emphasis (LGLRE) High grey level run emphasis (HGLRE) Short run low grey level run emphasis (SRLGLRE)  Short run high grey level run emphasis (SRHGLRE)  Long run low grey level run emphasis (LRLGLRE)  Long run high grey level run emphasis (LRHGLRE)	Distribution of short run lengths. Distribution of long run lengths. Variability of the grey-level intensity. Similarity of run lengths in the image. Distribution of the lower grey-level values. Distribution of the higher grey-level values. Joint distribution of shorter run lengths with lower grey-level values. Joint distribution of shorter run lengths with higher grey-level values. Joint distribution of long run lengths with lower grey-level values. Joint distribution of long run lengths with higher grey-level values.
Bone Morphometry	BV/TV Tb.Th Tb.Sp Tb.N BS/BV	Ratio between bone volume and total volume. Trabecular thickness. Trabecular separation. Trabecular number. Ratio between bone surface and bone volume.

**Supplementary Table 3.2: Descriptive Values for the Imaging Features in the Condyle and the Articular Fossa of the control group (n=40) at Baseline and Follow-up Visits.**

Site	Variables	Baseline (T1)			Follow-up (T2)			P-Value
		Median	IQ		Median	IQ		
			25	75		25	75	
Lateral Surface of the Condyle	Energy	0.26	0.22	0.28	0.23	0.21	0.28	0.03*
	Entropy	2.48	2.32	2.68	2.57	2.33	2.73	0.08
	Correlation	1.46	1.25	1.68	1.33	1.21	1.68	0.09
	Inverse Difference Moment	0.89	0.88	0.9	0.88	0.87	0.9	0.03*
	Inertia	0.23	0.2	0.25	0.23	0.21	0.26	0.03*
	Short Run Emphasis	0.35	0.32	0.37	0.36	0.34	0.38	0.10
	Long Run Emphasis	14.78	13.53	16.31	14.42	13.21	15.98	0.04*
	Grey Level Non-Uniformity	2754.92	2612.3	2917.3	2851.06	2665.33	2940.01	0.15
	Run Length Non-Uniformity	1579.13	1338.86	1814.89	1629.38	1377.82	1918.58	0.02*
	Low Grey Level Run Emphasis	0.07	0.06	0.08	0.07	0.06	0.08	0.13
	High Grey Level Run Emphasis	16.99	14.88	19.5	16.59	14.74	18.7	0.30
	Short Run Low Grey Level Emphasis	0.02	0.02	0.03	0.03	0.02	0.03	0.03*
	Short Run High Grey Level Emphasis	5.99	5.29	7.17	5.95	5.07	7.33	0.63
	Long Run Low Grey Level Emphasis	1.06	0.85	1.22	1.06	0.86	1.23	0.98
	Long Run High Grey Level Emphasis	242.27	206.29	293.1	235.29	194.54	264.56	0.21
	Bone Volume/Total Volume (%)	0.51	0.32	0.67	0.47	0.33	0.59	0.16
	Trabecular Thickness (mm)	0.32	0.25	0.42	0.32	0.25	0.38	0.45
	Trabecular Separation (mm)	0.32	0.22	0.5	0.37	0.26	0.51	0.08
Trabecular Number (mm <sup>-1</sup> )	1.47	1.26	1.58	1.41	1.25	1.52	0.13	
Bone Surface/Bone Volume Ratio (mm <sup>-1</sup> )	6.22	4.71	8.01	6.33	5.28	8.11	0.39	
Antero-Lateral (AL) Surface of the Articular Fossa	Energy	0.18	0.14	0.23	0.18	0.14	0.23	0.26
	Entropy	2.94	2.66	3.25	2.99	2.66	3.25	0.42
	Correlation	0.85	0.57	1.14	0.86	0.57	1.14	0.95
	Inverse Difference Moment	0.88	0.87	0.89	0.88	0.87	0.89	0.03*
	Inertia	0.23	0.22	0.26	0.24	0.22	0.26	0.03*
	Short Run Emphasis	0.36	-0.64	3.45	0.37	0.35	0.39	0.01*
	Long Run Emphasis	14.81	24.19	82.36	14.39	13.08	15.37	0.04
	Grey Level Non-Uniformity	1796.14	805.57	1738.27	1869.56	1681.81	2067.67	0.04
	Run Length Non-Uniformity	1421.83	0.35	0.39	1452.78	1331.43	1657.37	0.006*
	Low Grey Level Run Emphasis	0.03	13.08	15.37	0.04	0.03	0.04	0.05
	High Grey Level Run Emphasis	35.03	1681.81	2067.67	34.27	28.04	38.84	0.04*
	Short Run Low Grey Level Emphasis	0.01	1331.43	1657.37	.01	0.01	0.02	0.04*
	Short Run High Grey Level Emphasis	13.14	0.03	0.04	12.93	10.75	15.31	0.40
	Long Run Low Grey Level Emphasis	0.50	28.04	38.84	0.53	0.41	0.68	0.28
	Long Run High Grey Level Emphasis	496.49	0.01	0.02	450.26	358.55	553.83	0.01*
	Bone Volume/Total Volume (%)	0.74	10.75	15.31	0.71	0.48	0.87	0.11
	Trabecular Thickness (mm)	0.54	0.41	0.68	0.53	0.39	0.69	0.15
	Trabecular Separation (mm)	0.18	358.55	553.83	0.19	0.1	0.37	0.06
Trabecular Number (mm <sup>-1</sup> )	1.28	0.48	0.87	1.18	0.98	1.36	0.60	
Bone Surface/Bone Volume Ratio (mm <sup>-1</sup> )	3.69	0.39	0.69	3.78	2.9	5.16	0.11	

\* Wilcoxon signed rank test was used to compute P-value for the imaging variables within the same group at different time points, P< 0.05 were considered statistically significant.

**Supplementary Table 3.3: Descriptive Values for the Imaging Features in the Condyle and the Articular Fossa of the TMJ OA group (n=34) at Baseline and Follow-up Visits.**

Site	Variables	Baseline (T1)			Follow-up (T2)			P-Value
		Median	IQ		Median	IQ		
			25	75		25	75	
Lateral Surface of the Condyle	Energy	0.22	0.16	0.28	0.23	0.19	0.29	0.36
	Entropy	2.66	2.3	3.15	2.64	2.3	2.9	0.45
	Correlation	1.27	0.83	1.68	1.28	1.01	1.68	0.52
	Inverse Difference Moment	0.88	0.86	0.9	0.88	0.86	0.9	0.61
	Inertia	0.25	0.2	0.29	0.24	0.21	0.28	0.66
	Short Run Emphasis	0.37	0.33	0.42	0.39	0.33	0.4	0.62
	Long Run Emphasis	13.70	11.69	16.43	16.82	12.21	16.07	0.46
	Grey Level Non-Uniformity	2709.53	2503.04	2836.8	2663.71	2452.64	2855.49	0.96
	Run Length Non-Uniformity	1785.16	1322.05	2243.09	1853.33	1391.14	2118.1	0.78
	Low Grey Level Run Emphasis	0.06	0.05	0.07	0.06	0.06	0.08	0.14
	High Grey Level Run Emphasis	19.30	16.94	24.21	20.70	15.07	21.8	0.16
	Short Run Low Grey Level Emphasis	0.02	0.02	0.03	0.02	0.02	0.03	0.33
	Short Run High Grey Level Emphasis	7.54	5.72	9.24	8.16	5.14	8.95	0.27
	Long Run Low Grey Level Emphasis	0.85	0.68	1.11	0.91	0.75	1.28	0.11
	Long Run High Grey Level Emphasis	266.78	222.5	299.3	268.47	217.65	272.75	0.23
	Bone Volume/Total Volume (%)	0.60	0.43	0.75	0.59	0.34	0.66	0.14
	Trabecular Thickness (mm)	0.39	0.32	0.53	0.43	0.24	0.46	0.18
	Trabecular Separation (mm)	0.28	0.17	0.4	0.35	0.23	0.5	0.24
Trabecular Number (mm <sup>-1</sup> )	1.42	1.32	1.47	1.37	1.17	1.56	0.85	
Bone Surface/Bone Volume Ratio (mm <sup>-1</sup> )	5.09	3.81	6.22	5.46	4.32	8.29	0.22	
Antero-Lateral (AL) Surface of the Articular Fossa	Energy	0.19	0.16	0.24	0.22	0.16	0.23	0.44
	Entropy	2.91	2.66	3.09	2.81	2.66	3.11	0.44
	Correlation	0.78	0.65	1.03	0.87	0.67	1.01	0.75
	Inverse Difference Moment	0.89	0.88	0.9	0.89	0.88	0.9	0.30
	Inertia	0.22	0.2	0.24	0.23	0.2	0.25	0.56
	Short Run Emphasis	0.36	0.33	0.37	0.36	0.33	0.38	0.60
	Long Run Emphasis	15.29	14.09	16.66	15.45	13.78	16.6	0.18
	Grey Level Non-Uniformity	1741.66	1570.53	1883.24	1717.30	1581.22	1918.1	0.95
	Run Length Non-Uniformity	1280.12	1138.13	1506.12	1307.12	1140.36	1545.72	0.18
	Low Grey Level Run Emphasis	0.03	0.03	0.04	0.05	0.03	0.05	0.27
	High Grey Level Run Emphasis	34.96	29.95	42.85	35.28	27.34	41.31	0.21
	Short Run Low Grey Level Emphasis	0.01	0.01	0.01	0.02	0.01	0.02	0.24
	Short Run High Grey Level Emphasis	12.96	10.8	15.23	12.74	10.64	15.02	0.66
	Long Run Low Grey Level Emphasis	0.51	0.41	0.7	0.67	0.41	0.69	0.73
	Long Run High Grey Level Emphasis	506.31	382.8	661.42	533.00	378.78	600.31	0.08
	Bone Volume/Total Volume (%)	0.73	0.44	0.91	0.66	0.42	0.87	0.35
	Trabecular Thickness (mm)	0.61	0.36	0.91	0.60	0.37	0.77	0.14
	Trabecular Separation (mm)	0.20	0.08	0.49	2.70	0.11	0.5	0.72
Trabecular Number (mm <sup>-1</sup> )	1.17	0.95	1.38	1.12	0.95	1.36	0.61	
Bone Surface/Bone Volume Ratio (mm <sup>-1</sup> )	3.29	2.19	5.51	4.78	2.58	5.34	0.27	

\* Wilcoxon signed rank test was used to compute P-value for the imaging variables within the same group at different time points, P< 0.05 were considered statistically significant.

**Supplementary Table 3.4: Descriptive Values for the Biological Features Evaluated at Baseline.**

Variables (pg/ml)	Control Group			TMJ OA Group		
	Median	IQ Range		Median	IQ Range	
		25	75		25	75
Angiogenin Serum	1494.7	1303.01	1648.1	1459.05	1254.91	1625.09
BDNF Serum	251.5	100.99	550.39	350.76	141.78	1767.69
CXCL16 Serum	3585.1	3194.03	4217.57	3835.92	3418.28	4473.33
ENA-78 Serum	215.56	115.95	845.82	432.06	141.41	1222.28
MMP3 Serum	2513.6	1625.41	3038.46	2144.63	1489.03	2587.58
MMP7 Serum	532.16	350.98	732.69	453.77	338.15	725.9
OPG Serum	2539.16	1769.43	3264.09	2428.1	1800.75	3391.33
PAI-1 Serum	6735.86	4599.14	10756.23	6409.6	3962.96	9810.5
TGF-B1 Serum	77.55	26.69	174.19	99.13	37.16	204.99
TIMP-1 Serum	7447.5	6480.76	7947.06	7182.32	6687.84	7703.51
TRANCE Serum	2097.48	1336.39	2891.12	2496.35	1561.06	3543.89
VE-Cadherin Serum	6576.79	3242.09	9484.99	5105.12	2985.4	8912.61
VEGF Serum	80.86	24.75	163.02	85.75	41.64	160.37
Angiogenin Saliva	752.37	557.57	885.15	754.31	602.78	850.87
CXCL16 Saliva	4.41	1.35	13.52	3.15	0.17	10.28
ENA-78 Saliva	112.86	7.2	328.49	207.43	16.43	429.65
MMP7 Saliva	2387.77	1274.03	3008.14	2489.59	1426.22	3085.95
OPG Saliva	3710.54	2146.87	4859.81	3784.27	1926.76	5029.19
TGF-B1 Saliva	602.68	153.02	1265.04	693.66	276.69	1365.21
TIMP-1 Saliva	22.24	0.33	85.33	40.27	2.91	119.46
TRANCE Saliva	16.95	0	67.76	47.43	12.96	81.73
VE-Cadherin Saliva	4073.46	3184.25	4793.18	3959.61	3519.16	4285.56
VEGF Serum Saliva	627.6	0	1547.15	723.08	19.17	1278.86

\*BDNF, brain derived neurotrophic factor; CXCL16, chemokine ligand 16; ENA78, epithelial neutrophil-activating peptide; MMP, matrix metalloproteinases; OPG, osteoprotegerin, PAI-1, plasminogen activator inhibitor-1; TGF-B1, transforming growth factor-beta, TRANCE, TNF-related activation-induced cytokine; VE-Cadherin, vascular endothelial (VE)-cadherin; VEGF, vascular endothelium growth factor.

**Supplementary Table 3.5: Performance of the Feature Selection Methods and Machine Learning Approaches on the Validation Dataset.**

Methods	Accuracy	AUC	F1score
NNET_LDA	0.787±0.07	0.928±0.04	0.780±0.06
Glmnet_LDA	0.752±0.08	0.807±0.08	0.741±0.06
XGBoost_LDA	0.748±0.08	0.813±0.08	0.733±0.07
Glmboost_LDA	0.739±0.08	0.834±0.07	0.728±0.06
Glmboost_HDDA	0.735±0.08	0.813±0.08	0.725±0.06
NNET_SVM	0.748±0.07	0.893±0.05	0.725±0.06
NNET_HDDA	0.732±0.08	0.852±0.07	0.719±0.07
AUC_LDA	0.728±0.08	0.771±0.09	0.716±0.07
Glmboost_Glmboost	0.736±0.08	0.777±0.08	0.715±0.07
Glmboost_NNET	0.726±0.08	0.790±0.08	0.715±0.06
RF_LDA	0.729±0.08	0.763±0.09	0.714±0.07
RF_HDDA	0.719±0.08	0.797±0.08	0.712±0.06
RF_Glmboost	0.726±0.08	0.767±0.09	0.705±0.07
NNET_Glmboost	0.726±0.08	0.801±0.08	0.705±0.07
Glmnet_Glmboost	0.726±0.08	0.796±0.08	0.704±0.07
NNET_NNET	0.716±0.08	0.768±0.09	0.703±0.06
AUC_HDDA	0.706±0.08	0.765±0.09	0.696±0.06
XGBoost_HDDA	0.710±0.08	0.771±0.09	0.695±0.07
AUC_Glmboost	0.716±0.08	0.784±0.08	0.692±0.07
XGBoost_Glmboost	0.716±0.08	0.788±0.09	0.691±0.07
Glmnet_Glmnet	0.713±0.08	0.786±0.08	0.690±0.07
Glmnet_NNET	0.706±0.08	0.792±0.08	0.689±0.07
Glmnet_HDDA	0.696±0.08	0.753±0.09	0.688±0.06
AUC_NNET	0.702±0.08	0.760±0.09	0.688±0.07
Glmboost_Glmnet	0.710±0.08	0.802±0.08	0.684±0.07
NNET_Glmnet	0.706±0.08	0.791±0.08	0.682±0.07
XGBoost_NNET	0.691±0.08	0.777±0.08	0.676±0.07
XGBoost_Glmnet	0.696±0.08	0.784±0.08	0.665±0.07
RF_Glmnet	0.683±0.08	0.760±0.09	0.651±0.08
RF_NNET	0.660±0.09	0.740±0.09	0.641±0.07
Glmboost_SVM	0.673±0.08	0.813±0.08	0.634±0.08
Glmboost_XGBoost	0.664±0.08	0.739±0.09	0.629±0.08
Glmnet_SVM	0.667±0.08	0.801±0.08	0.626±0.08
AUC_Glmnet	0.670±0.08	0.765±0.09	0.625±0.08
Glmnet_XGBoost	0.654±0.09	0.721±0.09	0.618±0.08
XGBoost_XGBoost	0.648±0.08	0.788±0.08	0.614±0.08
AUC_XGBoost	0.647±0.09	0.689±0.10	0.613±0.07
AUC_RF	0.640±0.09	0.725±0.09	0.599±0.08
NNET_XGBoost	0.641±0.09	0.768±0.09	0.597±0.08
Glmboost_RF	0.628±0.09	0.779±0.08	0.573±0.08
Glmnet_RF	0.614±0.09	0.778±0.08	0.567±0.08
XGBoost_RF	0.624±0.09	0.785±0.08	0.564±0.08
RF_RF	0.615±0.09	0.791±0.08	0.562±0.08
XGBoost_SVM	0.624±0.09	0.786±0.08	0.559±0.08
RF_XGBoost	0.598±0.09	0.696±0.10	0.554±0.08
AUC_SVM	0.608±0.09	0.762±0.09	0.533±0.08
NNET_RF	0.592±0.09	0.751±0.09	0.527±0.09
RF_SVM	0.588±0.09	0.749±0.09	0.504±0.08

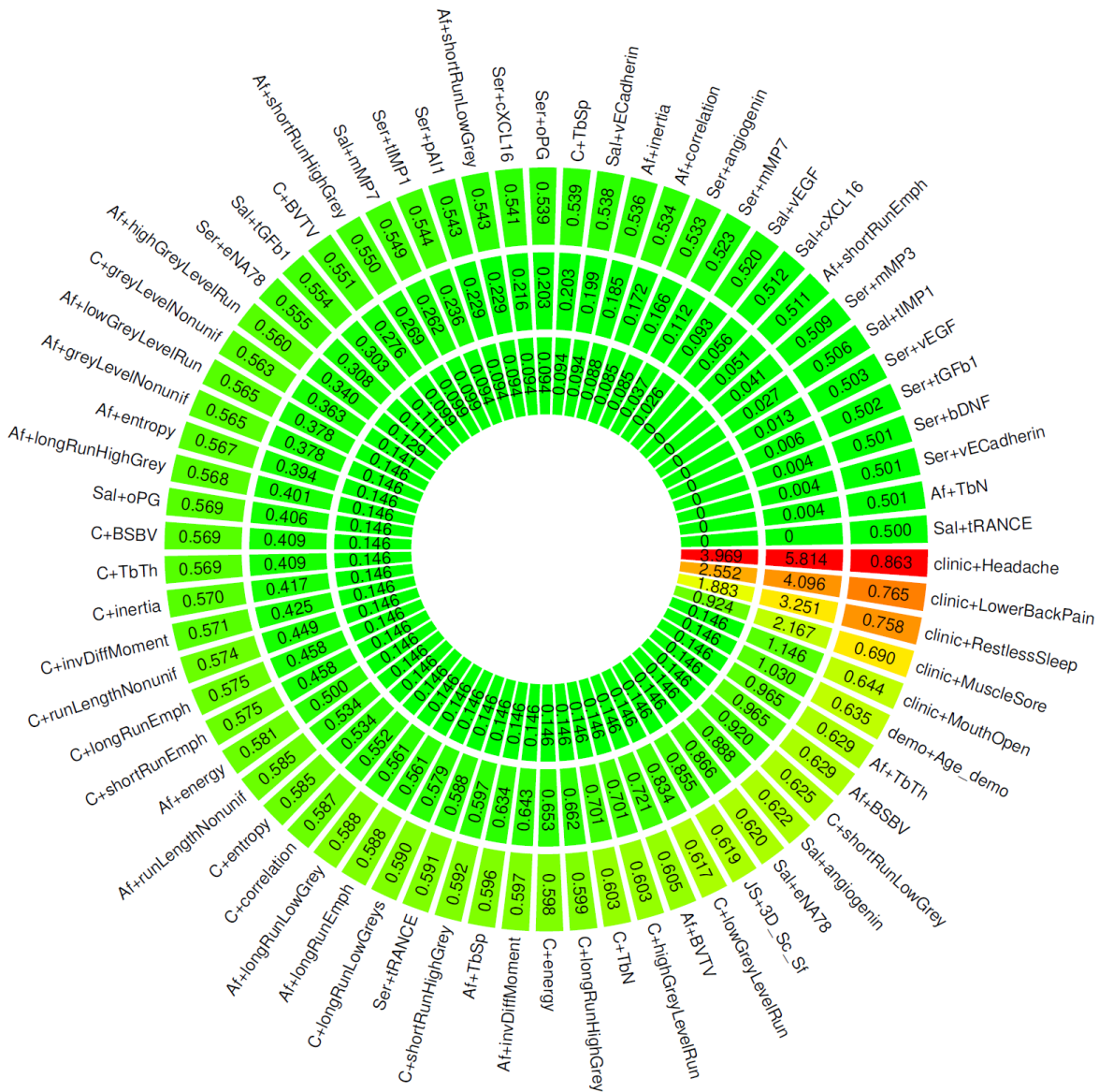
**Supplementary Table 3.6: Performance of the Feature Selection Methods and Machine Learning Approaches on the Test Dataset.**

Methods	Accuracy	AUC	F1score
XGBoost_Glmboost	0.706±0.08	0.737±0.09	0.689±0.06
Glmboost_Glmboost	0.706±0.08	0.668±0.10	0.678±0.07
Glmnet_Glmboost	0.706±0.08	0.716±0.09	0.678±0.07
NNET_NNET	0.676±0.08	0.644±0.10	0.662±0.06
Glmnet_Glmnet	0.676±0.08	0.616±0.10	0.652±0.07
Glmnet_LDA	0.676±0.08	0.625±0.10	0.652±0.07
AUC_Glmnet	0.676±0.08	0.683±0.10	0.652±0.07
NNET_Glmboost	0.676±0.08	0.661±0.10	0.652±0.07
NNET_LDA	0.676±0.08	0.744±0.09	0.652±0.07
RF_LDA	0.676±0.08	0.689±0.09	0.652±0.07
XGBoost_HDDA	0.676±0.08	0.716±0.09	0.652±0.07
RF_Glmboost	0.676±0.08	0.682±0.09	0.639±0.07
Glmboost_HDDA	0.647±0.08	0.656±0.09	0.626±0.07
Glmnet_HDDA	0.647±0.08	0.439±0.11	0.626±0.07
AUC_Glmboost	0.647±0.08	0.689±0.09	0.626±0.07
AUC_LDA	0.647±0.08	0.649±0.10	0.626±0.07
AUC_NNET	0.647±0.08	0.637±0.10	0.626±0.07
NNET_HDDA	0.647±0.08	0.692±0.09	0.614±0.07
XGBoost_Glmnet	0.647±0.08	0.666±0.10	0.614±0.07
RF_HDDA	0.618±0.08	0.588±0.10	0.601±0.07
XGBoost_LDA	0.618±0.08	0.619±0.10	0.601±0.07
Glmboost_Glmnet	0.618±0.08	0.647±0.10	0.589±0.07
NNET_Glmnet	0.618±0.08	0.706±0.09	0.589±0.07
XGBoost_NNET	0.618±0.08	0.671±0.09	0.589±0.07
AUC_RF	0.618±0.08	0.676±0.09	0.573±0.07
NNET_SVM	0.618±0.08	0.599±0.10	0.573±0.07
RF_Glmnet	0.618±0.08	0.602±0.10	0.573±0.08
Glmboost_SVM	0.588±0.08	0.580±0.10	0.549±0.07
Glmboost_XGBoost	0.588±0.08	0.642±0.10	0.549±0.07
AUC_SVM	0.588±0.08	0.633±0.10	0.549±0.07
Glmboost_LDA	0.559±0.09	0.408±0.10	0.539±0.07
Glmnet_RF	0.588±0.08	0.599±0.10	0.530±0.07
RF_NNET	0.588±0.08	0.640±0.10	0.530±0.07
RF_RF	0.588±0.08	0.600±0.10	0.530±0.07
AUC_HDDA	0.529±0.09	0.573±0.10	0.523±0.07
Glmboost_NNET	0.529±0.09	0.606±0.10	0.514±0.07
Glmnet_NNET	0.529±0.09	0.581±0.10	0.514±0.08
AUC_XGBoost	0.559±0.09	0.519±0.10	0.507±0.07
XGBoost_RF	0.559±0.09	0.675±0.10	0.507±0.07
XGBoost_XGBoost	0.559±0.09	0.491±0.10	0.507±0.08
Glmnet_SVM	0.559±0.09	0.471±0.10	0.483±0.07
NNET_RF	0.559±0.09	0.704±0.09	0.483±0.07
Glmboost_RF	0.529±0.09	0.668±0.10	0.462±0.08
RF_XGBoost	0.529±0.09	0.531±0.11	0.462±0.08
RF_SVM	0.559±0.09	0.621±0.10	0.452±0.08
XGBoost_SVM	0.559±0.09	0.671±0.10	0.452±0.08
Glmnet_XGBoost	0.500±0.09	0.540±0.10	0.442±0.07
NNET_XGBoost	0.500±0.09	0.567±0.10	0.442±0.07

**Supplementary Table 3.7: FDR Corrected P Values Between the Top Identified Clinical, Imaging, and Biological Features.**

Features	Sal. OPG	Sal. VEGF	Sal. MMP7	Ser. BDNF	Sal. Angiogenin	Ser. ENA78	Headache	Lower Back Pain	Restless Sleep	Mouth Opening	Age
C.HGLRE	0.95	0.78	0.95	0.50	0.79	0.63	0.60	0.44	0.14	0.19	0.77
C.SRHGLRE	0.78	0.89	0.95	0.34	0.97	0.50	0.44	0.37	0.14	0.14	0.74
AF.BS/BV	0.50	0.75	0.50	0.87	0.79	0.54	0.19	0.49	0.94	0.44	0.19
3D-Sup-JS	0.75	0.51	0.95	0.50	0.95	0.70	0.93	0.44	0.74	0.73	0.97
C.BV/TV	0.95	0.67	0.88	0.51	0.70	0.75	0.94	0.94	0.42	0.44	0.94
AF.GLN	0.50	0.37	0.50	0.95	0.34	0.50	0.19	0.21	0.74	0.42	0.48
AF.LRHGLRE	0.50	0.34	0.50	0.75	0.50	0.95	0.74	0.74	0.96	0.49	0.74
AF.Correlation	0.50	0.67	0.50	0.75	0.97	0.95	0.93	0.41	0.48	0.97	0.74
AF.BV/TV	0.50	0.50	0.50	0.95	0.95	0.75	0.23	0.74	0.94	0.23	0.23
AF.SRE	0.75	0.75	0.91	0.50	0.75	0.50	0.60	0.44	0.71	0.94	0.94





**Supplementary Figure 3.1: Logistic Regression Analysis for the Association between the Individual Features and the Presence of TMJ OA.** The AUC values, the  $-\log_{10}$  [P-values], and  $-\log_{10}$  [FDR adjusted p-values] are shown, successively, in the outer, middle and inner circles. Af, Articular fossa; C, Condyle; Sal, Saliva; JS, Joint Space; Ser, Serum.

**A** 1- Clinical TMJ Pain Related Features

Pain Intensity		Worst Pain		Average Pain		Pain Interference	
T1	T2	T1	T2	T1	T2	T1	T2
5	5	10	7	10	7	7	3

Pain levels  $\geq 5$

2- Clinical Comorbidities

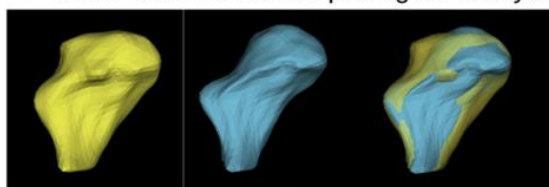
Headache		Lower Back Pain		Muscle Soreness		Restless sleep		Mouth opening	
T1	T2	T1	T2	T1	T2	T1	T2	T1	T2
2	3	3	3	2	2	3	3	24	30

Mouth opening  $< 40$

3- Radiographic Signs of the Disease

Osteophyte		Erosion		Bone cyst	
T1	T2	T1	T2	T1	T2
3	2	2	1	2	3

4- Three-dimensional Morphological Analysis



■ Baseline (T1) ■ Follow-up (T2)

**B** 1- Clinical TMJ Pain Related Features

Pain Intensity		Worst Pain		Average pain		Pain Interference	
T1	T2	T1	T2	T1	T2	T1	T2
3	1	5	5	5	2	1	0

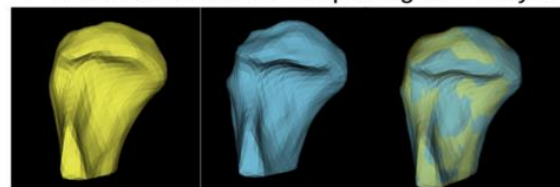
2- Clinical Comorbidities

Headache		Lower Back Pain		Muscle Soreness		Restless sleep		Mouth opening	
T1	T2	T1	T2	T1	T2	T1	T2	T1	T2
1	0	0	1	0	2	3	3	35	36

3- Radiographic Signs of the Disease

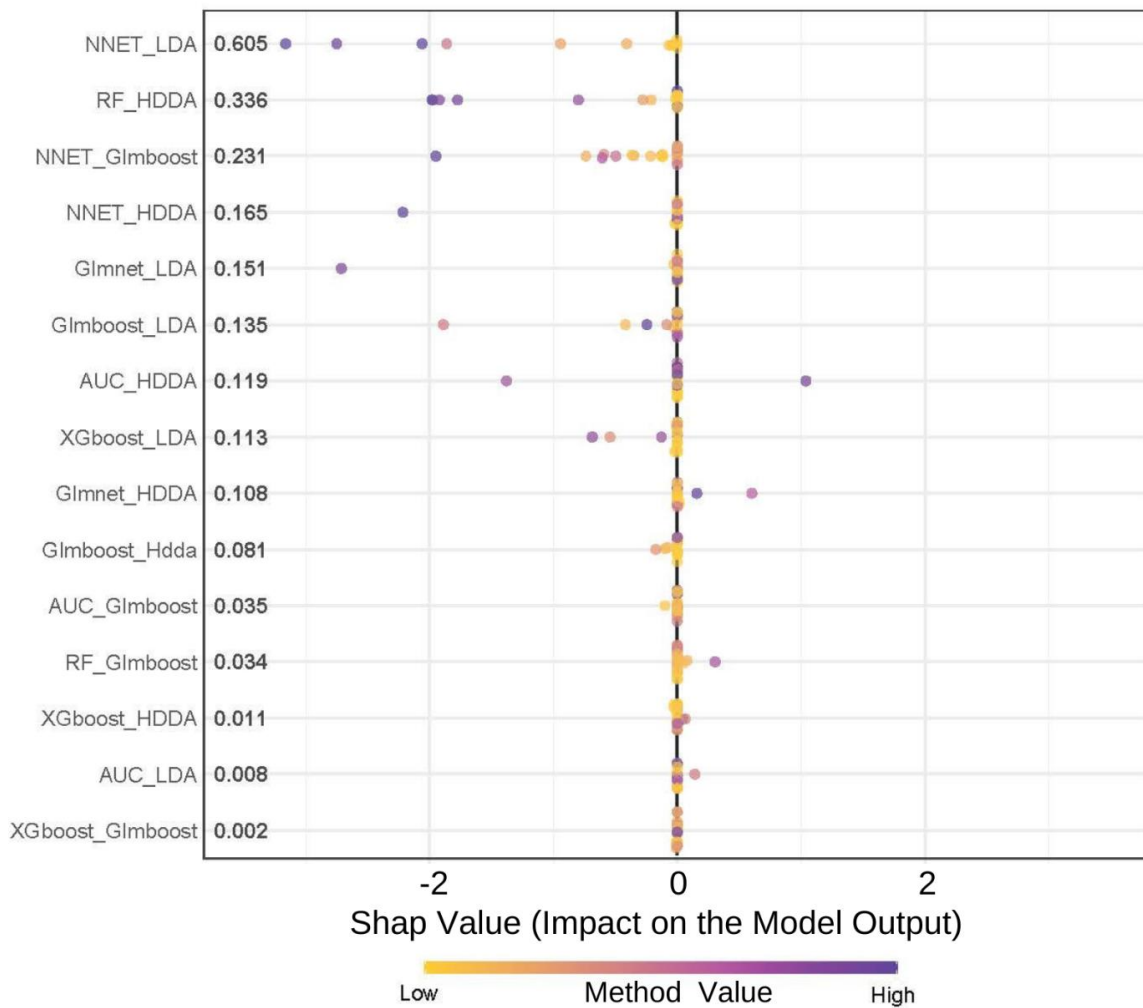
Osteophyte		Erosion		Bone cyst	
T1	T2	T1	T2	T1	T2
2	2	3	3	3	3

4- Three-dimensional Morphological Analysis

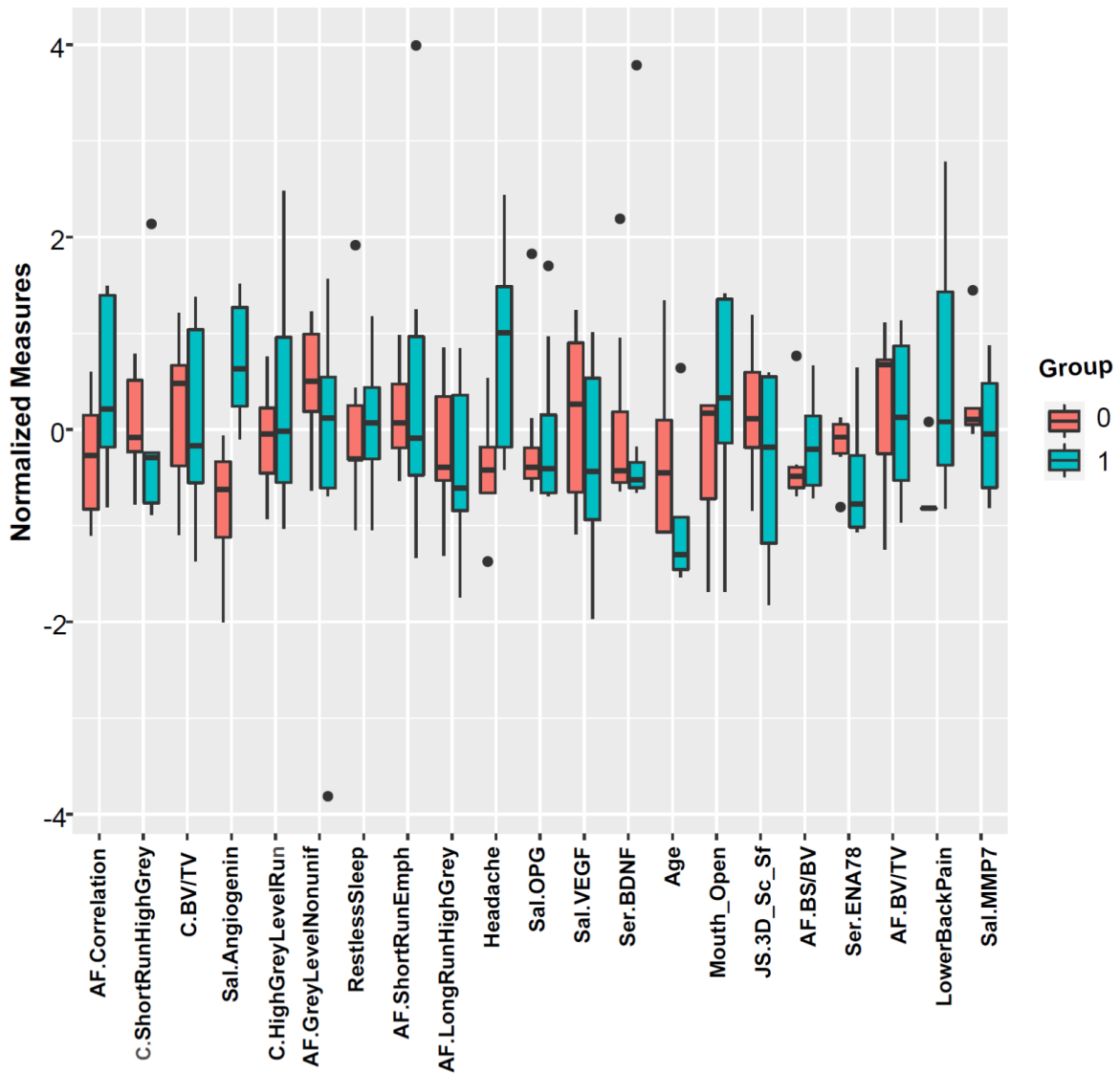


■ Baseline (T1) ■ Follow-up (T2)

**Supplemental Figure 3.2: Assessment of the Participants' Health Status at Follow-up.** (A) An example of a case that was labeled as worsened based on the overall changes of the clinical signs and symptoms, as well as the three-dimensional semi-transparent overlays that displayed significant bone degenerative changes at follow-up visit. (B) An example of a case that was labeled as stayed the same. Note that cases had to demonstrate pain levels less than 5 and a mouth opening equals to 40 to be considered as improved.



**Supplementary Figure 3.3: The Top Performing Methods in Predicting TMJ OA Prognosis.** A summary plot of the SHAP values for the methods' global impact on the EHPN model's prediction.



**Supplementary Figure 3.4: Graphical Display of the Top Contributing Features in TMJ OA Prognosis.** The box plots display the median, interquartile, and range of the top contributing features' values in the model prediction for the asymptomatic/improved (0) and remained the same/worsened (1) TMJ OA groups.

**Supplementary Text. The Pseudo code for the Ensemble via Hierarchical Predictions through Nested cross-validation (EHPN) learning tool.**

Step 1. Initialize  $p$  machine learning methods. Split the dataset  $D = \{(X_1, y_1), (X_2, y_2), \dots, (X_N, y_N)\}$  into 10 folds:  $D_1, D_2, \dots, D_{10}$  randomly.

Step 2. For  $i$  in  $\{1, 2, \dots, 10\}$ :

a. Initialize an empty list for storing  $Y_{k(i)}$  predictions for each method  $k$ .

b. For  $j$  in  $\{1, 2, \dots, 10\} \setminus \{i\}$ :

i. Set the training set =  $D \setminus \{D_i, D_j\}$  and the validation set =  $D_j$ .

ii. For each method  $k$  in  $\{1, 2, \dots, p\}$ :

Train method  $k$  on the training set with optimized tuning parameters obtained by an internal 10-fold cross-validation of the training set  $D \setminus \{D_i, D_j\}$ .

2) Predict  $y$  in  $D_j$  using the corresponding  $X_s$  and the trained method  $k$ .

3) Store the predicted  $y_s$  in the list  $Y_{k(i)}$ .

c. Create the new feature set  $X_{*(i)} = (Y_{1(i)}, Y_{2(i)}, \dots, Y_{p(i)})$  and the true response vector  $Y_{(i)}$  for subjects in  $D \setminus D_i$ .

d. Train the hierarchical predictive model  $M$  (e.g., Glmboost) using  $X_{*(i)}$  to predict  $Y_{(i)}$ .

e. Predict the true response vector  $Y_{(i)}$  for subjects in  $D_i$  using the model  $M$  and store the predicted values as  $pY_{(i)}$ .

Step 3. Compute the test set performance of the hierarchical predictive model  $M$  by comparing the predicted  $pY = \text{Union}(pY_{(1)}, pY_{(2)}, \dots, pY_{(10)})$  with the true  $Y = \text{Union}(Y_{(1)}, Y_{(2)}, \dots, Y_{(10)})$  using Accuracy, AUC, and F1-scores.

## **Chapter 4 Unleashing the Power of Machine Learning: Advancing TMJ Osteoarthritis Diagnosis**

### **Abstract**

Osteoarthritis (OA) is the most common degenerative disease affecting the temporomandibular joint (TMJ). It results in chronic pain, joint dysfunction, and adversely affects the quality of life. Unlike age-related osteoarthritis in weight-bearing joints, TMJ OA predominantly affects individuals aged 20-40 years and can also affect adolescents and young adults. The current diagnostic standards for TMJ OA are based on clinical and imaging criteria. However, the effectiveness of these criteria in detecting early-stage TMJ OA is limited, hindering timely intervention and mitigation of bone damage. Therefore, we prospectively obtained clinical, CBCT imaging, and biological data from 162 subjects: 81 with TMJ OA and 81 age and sex-matched controls. We evaluated 77 feature selection and machine learning methods and employed nested 10-fold cross-validation to develop a TMJ OA diagnostic tool. Among the methods tested, random forest demonstrated the best diagnostic performance, achieving AUC= 0.90, accuracy= 0.79, precision= 0.80, and F1=0.80. Integrating clinical, imaging, and biological markers enhanced TMJ OA diagnosis. The top contributing features were clinical variables (headache, restless sleep, mouth opening, muscle soreness), objective quantitative imaging markers (condyle Cluster Prominence, High Grey Level Run Emphasis (HGLRE), ShortRunHGLRE, Trabecular Thickness), and biological markers in saliva (TGFB-1, TRANCE, TIMP-1, PAI-1, VECadherin, CXCL-16) and serum (Angiogenin, PAI-1, VEGF, TRANCE, TIMP-1, BDNF, VECadherin). Our diagnostic tool synergizes diverse data dimensions, establishing new benchmarks in diag-

nostic precision with potential implications for timely interventions and a transformative impact on TMJ OA healthcare delivery.

**Keywords:** Degenerative joint disease, Temporomandibular joint osteoarthritis, Machine learning, Diagnosis, Interpretability.

## 4.1 Introduction

Osteoarthritis (OA) is the most common degenerative disease affecting the temporomandibular joint (TMJ). It is characterized by synovitis, articular tissue deterioration, cartilage destruction, and alterations in subchondral bone remodeling. These changes lead to pain, joint dysfunction, and negatively impact the quality of life (Mélou et al. 2023; X. D. Wang et al. 2015). Unlike age-related osteoarthritis in weight-bearing joints, TMJ OA primarily affects individuals aged 20-40 years and can impact adolescents and young adults (Mélou et al. 2023; Song et al. 2020). Furthermore, 18.01% to 84.74% of temporomandibular disorder (TMD) patients have TMJ OA (Pantoja et al. 2019).

Current TMJ OA diagnostic standards rely on clinical and imaging criteria, given the suboptimal sensitivity/specificity of clinical features alone (Hilgenberg-Sydney et al. 2018). Imaging criteria can provide insights into various disease stages, e.g., erosion indicates acute changes and sclerosis suggests advanced stages (Zhao et al. 2011). However, these criteria often overlook early-stage TMJ OA, hampering timely intervention and bone damage mitigation (Almășan et al. 2023). Therefore, integrating objective criteria might be instrumental in enhancing the rigor of diagnostic methodologies, facilitating early disease identification and advancing preventive strategies (Derwich et al. 2023; Hawker and Lohmander 2021). Nonetheless, retaining clinical criteria is crucial, as pain and limited mouth opening drive medical consultations and gauge treatment efficacy (Derwich et al. 2023; Suenaga et al. 2016).

In vitro studies have demonstrated the occurrence of aberrant subchondral bone remodeling in the mandibular condyles of various animal models during early stages of TMJ OA, preceding cartilage degeneration (Chen et al. 2018). Changes in the subchondral bone microstructure also positively correlate with OA severity histologically (Zhang et al. 2023). Consequently, its role in



osteoarthritis onset and the methods to detect these changes are of considerable interest (Hirvasniemi et al. 2021; Chen et al. 2018).

With technological advances in the horizon, the emerging field of radiomics provides a promising avenue. This discipline entails retrieving quantitative imaging features from radiological images, that are undetectable to humans' eyes, to analyze tissue pathology and improve data available to clinicians (Avery et al. 2022). Quantitative textural analysis of the subchondral bone in knee radiographs has shown radiomics' potential to differentiate not only between normal knee x-ray images and those with mild osteoarthritis but also among various grades of knee OA, including those challenging for clinicians to discern (Hirvasniemi et al. 2021; Avanzo et al. 2020). However, radiomics' potential in TMJ OA remains largely unexplored (Orhan et al. 2021; Bianchi et al. 2020). While radiomics offers promise in detecting subtle tissue changes, osteoarthritis' intricate pathology requires an integrative approach that combines imaging with clinical and other sensitive markers (Teoh et al. 2022).

Beyond radiomics, metabolic abnormalities in joint tissues are early indicators of osteoarthritis (Liem et al. 2022). Despite progress in studying osteoarthritis biomarkers, they aren't yet clinically established (Zwiri et al. 2020). Given the heterogeneous nature of osteoarthritis, assessing multiple biological markers in different biofluids may elucidate their complex interrelationships, harnessing their full potential (Bernotiene et al. 2020; Deveza and Loeser 2018).

Artificial intelligence and machine learning (ML) are emerging transformative elements of clinical practices (Soenksen et al. 2022). Their ability to rigorously analyze diverse datasets and address their interactions surpasses the limitations of traditional statistical methods, ultimately supporting precision medicine by tailoring decision-making to individual patient profiles (Johnson et al. 2021).

Despite its advances in diagnosing knee osteoarthritis, ML approaches for TMJ OA remains limited. Our previous studies showcased ML's potential for TMJ OA diagnosis. However, a larger sample size is essential for capturing diverse disease phenotypes and validating the tool's reliability (Xuan et al. 2023; Bianchi et al. 2020). A holistic approach to feature selection is also needed to heighten the results' accuracy (Liu et al. 2023). The inherent complexities of ML models, especially their 'black-box' nature, pose challenges Integrating explainability methods that clarify features' influence on model predictions can bolster clinicians' trust, paving the way for wider adoption (Petch, Di, and Nelson 2022). Therefore, the present work aimed to 1) Develop a comprehensive prediction tool tailored for TMJ OA diagnosis and 2) Employ explainable methods to identify key factors driving TMJ OA diagnosis.

## 4.2 Materials & Methods

### Study Design and Participants' Characteristics

This observational study was conducted with the University of Michigan Institutional Review Board permission (HUM00113199), adhering to STROBE standards. We included 162 participants, 81 with TMJ OA and 81 age and sex-matched controls. Inclusion criteria required participants to be aged 21-70 years, free from systemic diseases, congenital bone or cartilage disorders, cancer history, TMJ-related trauma or surgery, and prior treatments for TMJ OA. TMJ OA diagnoses were confirmed by a TMD specialist and radiographic osseous change evidence. Only the side of the TMJ displaying initial osseous changes was considered for the study. Control subjects were selected based on the absence of symptoms and the radiographic signs of TMJ OA on the included side. Figure 4.1 illustrates the overall study design.

### Integrated Data Approaches and Processing Methods

The data was collected from three primary sources: clinical, imaging, and biological markers.

### Clinical Data

In our statistical analyses, we considered multiple variables from the diagnostic criteria for temporomandibular disorders (DC/TMD) clinical exam and survey, including age, gender, and distress level in the past month due to headaches, muscle soreness, or lower back pain, vertical mouth opening range, and pain characteristics (current pain intensity, worst experienced pain, average pain, and pain interference with daily activities). Controls reported no orofacial pain.

### Imaging Data

#### Acquisition Protocol and TMJ OA Imaging Diagnosis

High-resolution cone-beam computed tomography (hr-CBCT) scans of all participants were obtained using a 3D Accuitomo 170 machine. The scanning protocol involved a  $40 \times 40$  mm field of view, 90 kVp, 5 mAs, 30.8-second scanning time, and a 0.08 mm voxel size. All images were

coded and de-identified prior to analysis to reduce potential investigator bias. Two oral and maxillofacial radiologists independently and blindly assessed radiological changes in the mandibular condyle based on the DC/TMD. Evaluations were guided by consensus data.

### Image Pre-Processing and Quantification of Imaging Markers

To ensure accurate detection and comparison of radiographic changes, hr-CBCT scans were pre-processed before measuring quantitative bone features. Using the "crop-volume" tool in 3D Slicer, a volume of interest (VOI) was extracted from the trabecular bone in the mandibular condyles and articular fossa. The VOIs' grey level intensities were standardized using the average minimum and maximum intensity values. Imaging markers were extracted from the standardized VOIs using the "BoneTexture" module in 3D Slicer, including 8 GLCM features, 10 GLRLM, and 5 bone morphometry features (Supplementary Table 4.1). Clustershade, Clusterprominence, and Haralickcorrelation measurements exhibited significant variability among participants and were excluded from further analysis.

For the 3D superior joint space measurement, two landmarks were pre-labelled in the sagittal view of the CBCT scans: the condyle's most superior point and the opposing surface of the articular fossa. Volumetric reconstruction of these landmarks was performed, and linear measurements were obtained using the Q3DC tool in 3D Slicer.

### Biological Data

We assessed 13 arthritis-related proteins in participants' serum and saliva samples including Angiogenin, BDNF, CXCL-16, ENA-78, MMP-3, MMP-7, OPG, PAI-1, TGF- $\beta$ 1, TIMP-1, TRANCE, VE-Cadherin, and VEGF. To assess protein expression, we utilized RayBiotech's custom human quantibody microarrays, employing duplicates for each measurement. Saliva BDNF and MMP3 were below the detection level and were therefore excluded from subsequent analysis.

### Statistical and Machine Learning (ML) Approaches

We utilized SPSS version 27.0 (IBM Corp., Armonk, NY) for statistical analysis. Differences between control and TMJ OA subjects were examined using independent samples t-test. Statistical significance was determined at  $p < 0.05$ . The agreement between the two radiologists was assessed using Kappa statistics. Due to the non-normal distribution of biological marker levels

within the groups, we applied a natural logarithm transformation to these variables prior to statistical analyses.

To develop the prediction model for TMJ OA diagnosis, we followed the steps outlined below.

### Nested 10-fold Cross Validation

To mitigate overfitting and ensure robustness, we employed the nested 10-fold cross-validation (CV) method to build and evaluate predictive models. Initially, all subjects were divided into 10 folds denoted as  $A_1, A_2, \dots, A_{10}$ . Within each iteration, one fold,  $A_i$ , was kept as an independent test set, while the remaining folds  $\{A_j | j \neq i\}$  were further subdivided into 10 subfolds:  $A_{i,1}, A_{i,2}, \dots, A_{i,10}$ . Each subfold,  $A_{i,j}$ , served as a validation set, and the remaining subfolds,  $\{A_j | j \neq i\}$ , formed the training set.

We trained various statistical and ML models on the training dataset, adjusted the parameters with the validation dataset, and employed the "caret" package in the R/4.1.0 software. In the inner loop of the nested CV, the validation dataset,  $A_{i,j}$ , iterated over  $\{A_{i,1}, A_{i,2}, \dots, A_{i,10}\}$ , and the model trained on the training data  $\{A_{i,k} | k \neq j\}$  was utilized to predict the outcome of the validation set,  $A_{i,j}$ . In the outer loop of the nested CV,  $A_i$  iterated over  $A_1, A_2, \dots, A_{10}$ , with  $A_j, j \neq i$  representing the training and validation datasets, respectively. Each subject was predicted once as an independent test subject, ensuring an unbiased assessment of model performance.

### Feature Selection and ML Approaches

We evaluated seven feature selection methods, including 1-selection frequency of LASSO (Glmnet), 2-permutation importance for Random Forest (RF), 3-gain for XGboost (XGBTree), 4-combinations of the absolute values of weights for neural network (NNET), 5-absolute value of coefficients in Glmboost (Glmboost), 6-A Area Under the receiver operating characteristic Curve (AUC) between each feature and the response, and 7-gain importance or Light Gradient-Boosting Machine (LightGBM). We also assessed 11 predictive modeling methods, namely 1-elastic net (Glmnet), 2-Glmboost, 3-High-Dimensional Discriminant Analysis (HDDA), 4-single-hidden-layer neural networks (NNET), 5-RF, 6-XGBTree, 7-Linear Support Vector Machine (SVM), 8-Linear Discriminant Analysis (LDA), 9-Naïve Bayes, 10-Bayesian Generalized

Linear Models (BayesGLM), and 11-LightGBM. Overall, we considered 77 machine learning methods. The reported model's performance relied on the test dataset across all repetitions.

#### Interpretability of LUPI Model's Prediction

Due to the "black box" nature of ML models hindering their adoption in medical settings, we employed the SHapley Additive exPlanations (SHAP) method. SHAP values interpret model predictions, highlighting the significance and direction of feature contributions to its decisions (Petch, Di, and Nelson 2022).

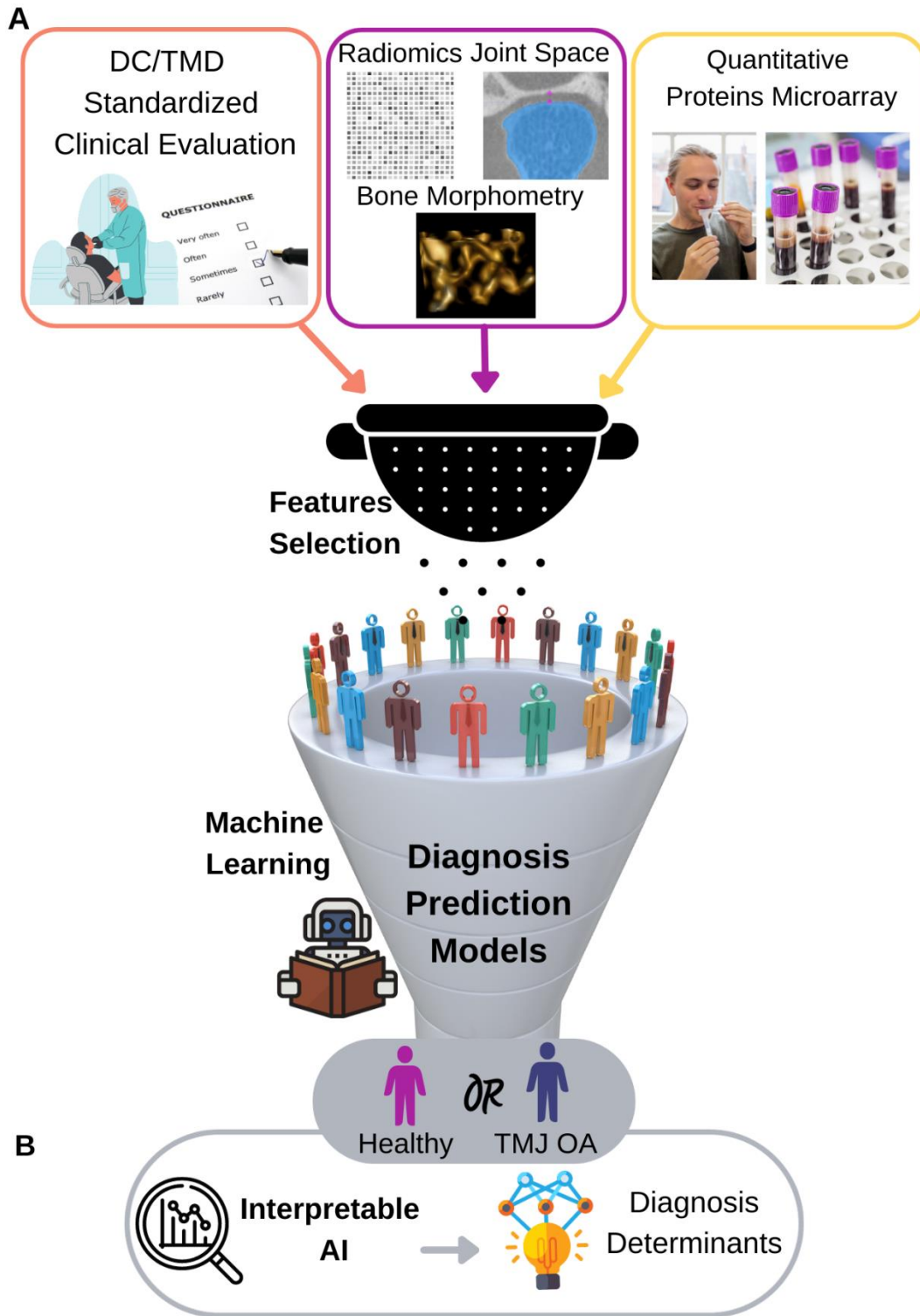


**Figure 4.1: Framework for the Development of TMJ OA Diagnosis Prediction Models.** A) Data Synthesis and Machine Learning Testing: Comprehensive integration of clinical, imaging, and biological data from study participants, followed by features' selection and exploration of the efficiency of ensemble learning and privileged information in model crafting. B) Insightful Interpretation: Application of shapley additive explanations (SHAP) analysis to discern the key features contributing to the models' predictions for TMJ OA cases. DC/TMD, diagnostic criteria for temporomandibular disorders; AI, artificial intelligence.

## 4.3 Results

### **4.3.1 Clinical Characteristics of the Study Population**

A total of 162 individuals participated in the study, 142 females and 20 males, with an average age of  $39.9 \pm 14.8$  years. Participants diagnosed with TMJ OA exhibited significantly higher levels of pain intensity, average pain, worst pain, and pain interference with daily activities over the past 6 months, compared to the controls ( $p < 0.0001$ , Figure 4.2A). Moreover, the TMJ OA group demonstrated a reduction in the vertical range of unassisted mouth opening without pain (mouth opening), as well as higher levels of headaches, lower back pain, muscle soreness, and restless sleep, when compared to controls ( $p < 0.001$ , Figure 4.2B-C). Approximately 78% of the TMJ OA group reported teeth grinding at night, while 59% reported jaw clenching during the day.

### **4.3.2 Destructive Bone Changes Detected in TMJ OA Participants**

Figure 4.2D-F demonstrates radiographic signs of OA evident in the condyles of the TMJ OA group. Around 75% demonstrated mild osseous changes. Grade 2&3 osseous alterations occurred in patients of different ages and pain levels, highlighting the need for additional quantitative disease indicators. Flattening emerged as the most prevalent change, affecting ~84% of cases, followed by sclerosis (69%), osteophyte (59%), erosion (51%), and cysts (~42%). Remarkably, over 60% of patients showed three or more concurrent signs, including osteophytes, cysts, and erosions, indicating dynamic changes in various TMJ regions. The weighted Kappa value for radiologists' scoring was 0.72, indicating substantial inter-observer agreement, with ~84% overall agreement rate.

### **5.3.3 Quantitative Bone Imaging Features Distinctively Characterize TMJ OA from Controls**

Subchondral bone remodeling alterations are hallmark of osteoarthritis (Chen et al. 2018). We examined the trabecular bone characteristics on the lateral surface of the condyles and the anterolateral surface of articular fossae (Figure 4.3A, Supplementary Table 4.2), sites recognized for enhanced remodeling (Cevidane et al. 2014). Our analysis demonstrated that ten condylar imaging features were significantly different between the groups ( $p < 0.05$ ) (Figure 4.3B, Supplemen-



tary Table 4.2). The TMJ OA group exhibited elevated levels of entropy, inertia, short run emphasis (SRE), high grey level run emphasis (HGLRE), and SRHGLRE compared to the controls. These observations highlight the nuances of the condylar trabecular bone texture in hr-CBCT images at pixels' level. Specifically, the extracted image volumes in OA cases displayed heightened randomness and heterogeneity, pronounced contrast between adjacent pixels, and numerous short runs of elevated grey level intensities.

In addition to variations in the trabecular bone texture features, the TMJ OA group showed a significant increase in trabecular thickness (TB.Th) and decrease in joint spaces compared to controls ( $P \leq 0.0001$ ). The average joint spaces measured  $2.3 \pm 0.7$  mm and  $2.5 \pm 0.7$  mm in TMJ OA participants and controls, respectively (Figure 4.3C).

#### **4.3.4 Comparable Expression Levels of Serum and Saliva Protein Biomarkers in Control and TMJ OA Participants**

Supplementary Table 4.3 and supplementary Figure 4.1 summarize the findings from the microarray analysis. Most biological markers were detected with high confidence ( $\geq 83\%$ ) and exhibited consistent standard curves for detection. Interestingly, noticeable variability in expression levels was observed among individuals, even within the same group. Nevertheless, no statistically significant differences between the groups were identified, Supplementary Table 4.4. These observations suggest that a panel of multiple biomarkers could offer enhanced diagnostic accuracy compared to a single biomarker.

#### **4.3.5 Features' Integration Amplifies the Robustness of TMJ OA Diagnosis**

Figure 4.4A provides an overview of the development process for the TMJ OA diagnostic tool. Supplementary Tables 4.5-4.12 present the evaluation metrics for the 77 tested methods. Notably, SVM excelled in analyses based solely on clinical data, as well as in those integrating clinical and imaging data. Conversely, RF demonstrated superior performance when biological data was combined with clinical data or when integrated with both clinical and imaging data (Figure 4.4B). This highlights the importance of tailoring machine learning models selection to the inherent characteristics of the data.

Coupling biological and clinical features produced an AUC of 88%, while combining imaging with clinical features resulted in an AUC of 80%. Remarkably, integrating clinical, quantitative imaging, and biological features yielded the highest predictive performance, with an AUC of 90%. These results emphasize the necessity of incorporating all feature categories for accurate diagnosis.

While incorporating all feature sets proved to be essential for the disease diagnosis, it is essential to emphasize that not all features wielded equal influence over the model's predictive performance. Applying SHAP analysis on the independent test set demonstrated the foremost contributing features. As depicted in Figure 4.4C, the top 24 features collectively commanded approximately 90% of the model's prediction. We further provide an in-depth exposition delineating the precise contribution of each feature to the predictive outcomes. Notably, among these top features, clinical attributes accounted for 17.41%, imaging markers for 7.71%, and biological attributes for the predominant 64.47% of the predictive influence.

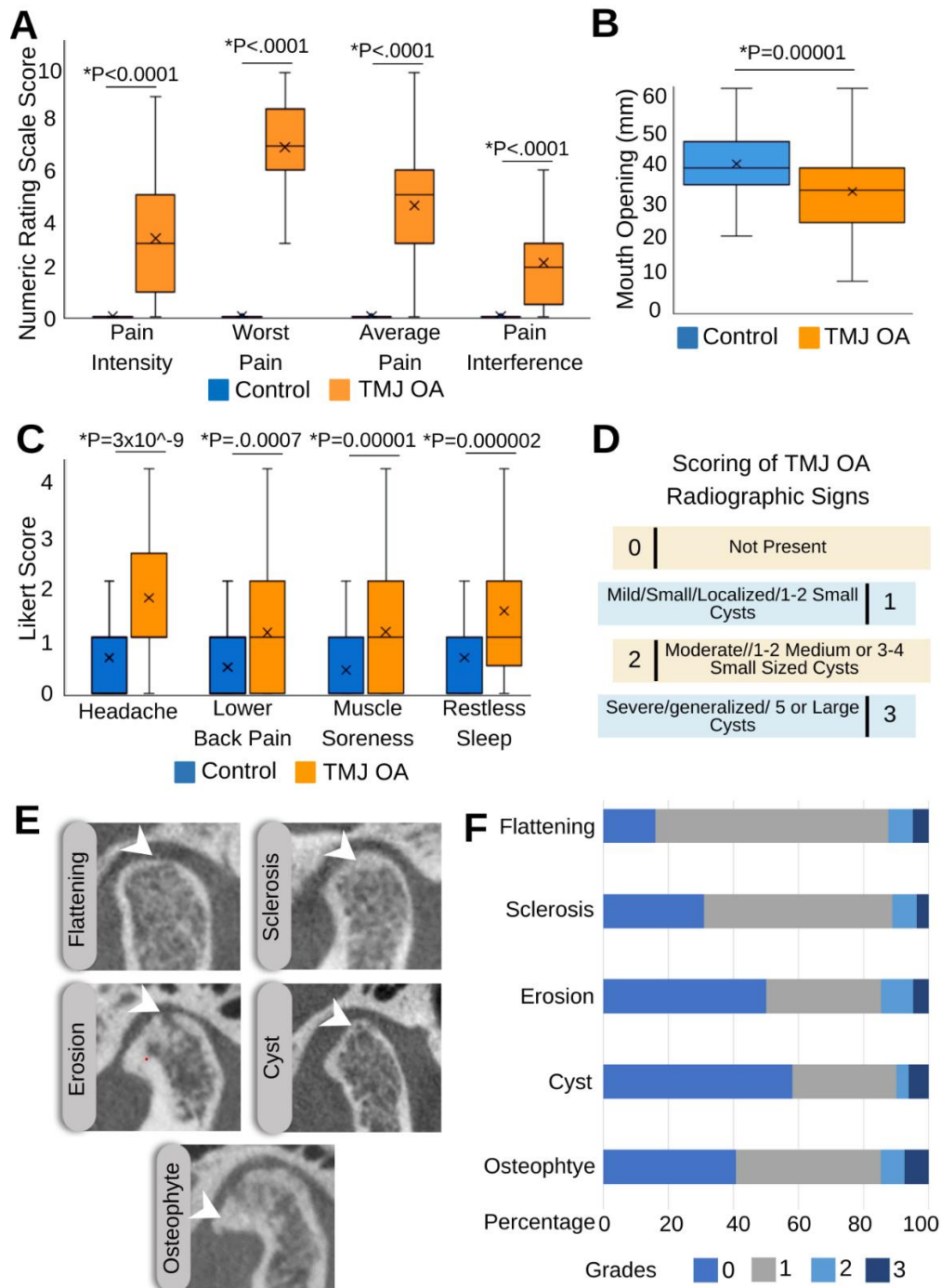
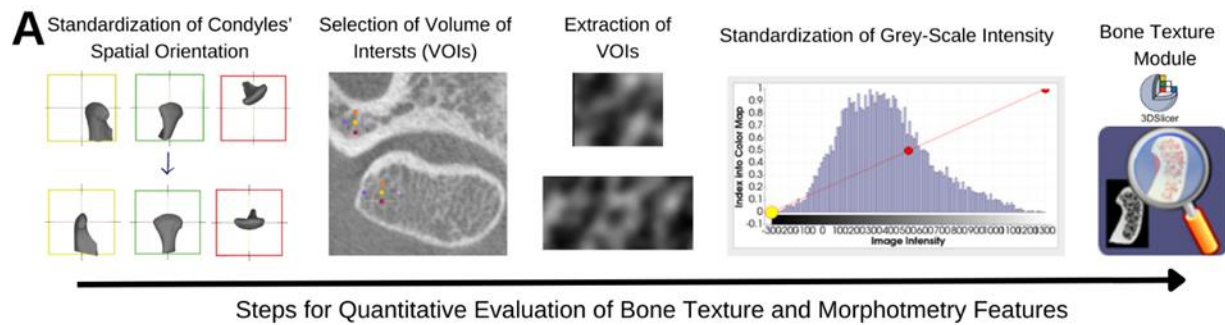


**Figure 4.2: Participants' Clinical Characteristics and Radiographic Determinants of Temporomandibular Joint Osteoarthritis.** A) Box plots illustrate the mean (x), median, and interquartile range for TMJ pain-related characteristics on a 0-10 scale, where 0 signifies no pain and 10 corresponds to the highest level of pain; control subjects reported no TMJ pain. B, C) Measurements of unassisted vertical mouth opening (mm) and the rates of clinical co-morbidities, evaluated using a Likert scale ranging from 0-4; 0 implies "not at all," and 4 signifies "extremely." A p-value below 0.05 was deemed statistically significant. D) Grading of radiographic signs of TMJ OA following the diagnostic criteria for temporomandibular disorder (DC/TMD). E) Examples of degenerative bone changes in the mandibular condyles of the TMJ OA participants, with arrowheads pointing to the affected areas. F) Percentage of osteoarthritic alterations in the condylar bone, identified in the high-resolution CBCT scans of the TMJ OA participants.



**B**

Variables	Control group		TMJ OA group		P-value
	Mean	SD	Mean	SD	
Energy	0.25	0.06	0.22	0.06	0.013*
Entropy	2.54	0.33	2.71	0.43	0.006*
Correlation	1.44	0.42	1.26	0.45	0.007*
Inverse Difference Moment	0.89	0.02	0.88	0.02	0.074*
Inertia	0.23	0.04	0.24	0.04	0.059*
Short Run Emphasis	0.36	0.04	0.37	0.04	0.030*
Grey Level Non-Uniformity	2726.79	249.41	2642.94	259.63	0.038*
High Grey Level Run Emphasis	18.08	3.85	20.52	6.25	0.003*
Short Run High Grey Level Emphasis	6.76	1.98	8.06	3.13	0.002*
Trabecular Thickness (mm)	0.36	0.15	0.43	0.20	0.008*

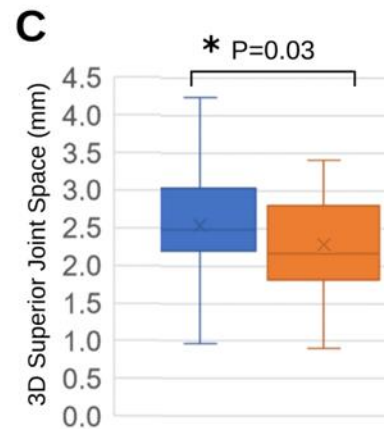


**Figure 4.3: Evaluation of Trabecular Bone Texture, Structural Parameters, and Three-Dimensional Superior TMJ Space.** A) Workflow outlining the pre-processing of high-resolution Cone Beam Computed Tomography (hr-CBCT) scans for the subsequent quantification of imaging markers in the mandibular condyles and articular fossae. B) Analysis highlighting significant differences in mean radiomics and bone morphotmetry features between control subjects and individuals with TMJ OA. C) Box plots presenting the mean, interquartile range, and variability of the superior TMJ space across control and TMJ OA participants. A threshold of  $P < 0.05$  was set for statistical significance.

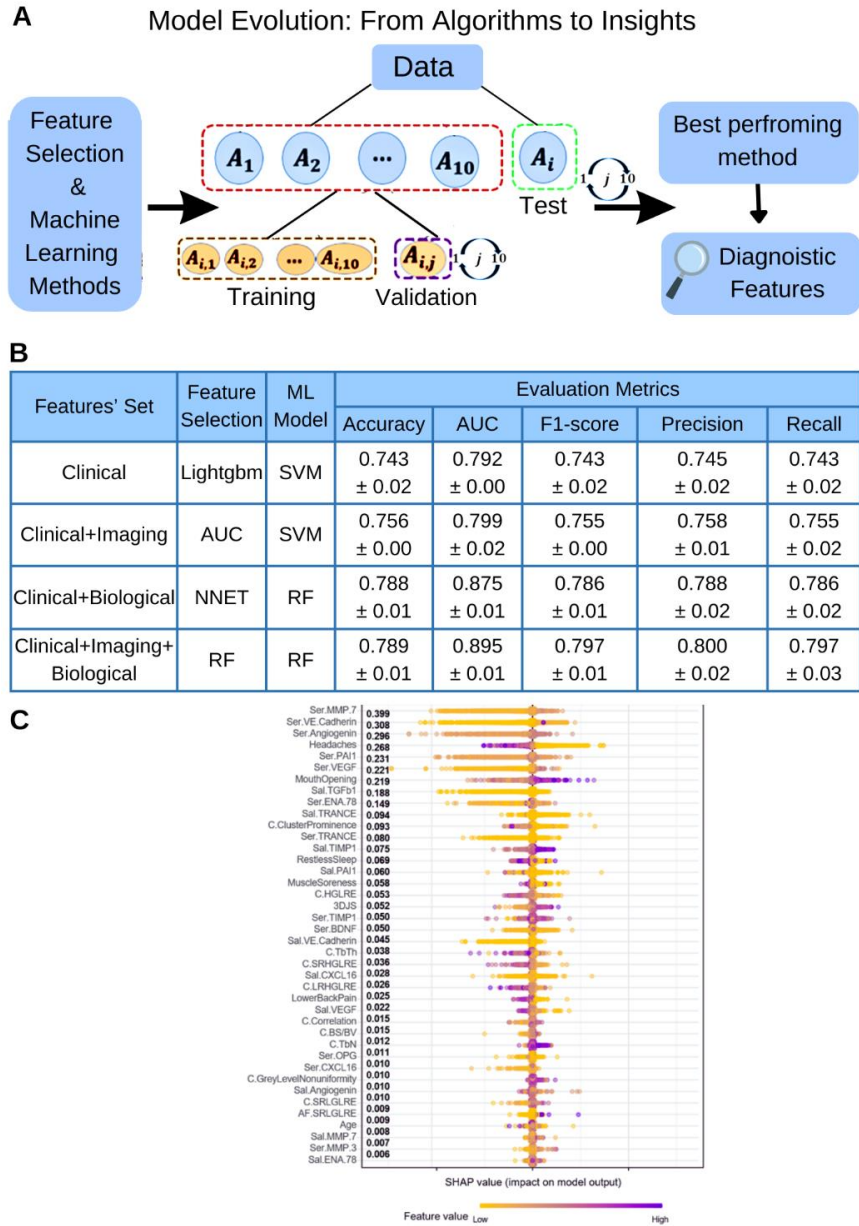


**Figure 4.4: Comparison of Models' Performances in Predicting the TMJ OA Diagnosis.** A) Schematic representation of the steps for developing the TMJOA model. Our dataset was divided into 10 folds, with one serving as a test set, while the rest were subdivided into training and validation sets. We applied ten-fold cross-validation in both loops and assessed model performance by averaging results across the 10-fold cross-validation on the test dataset. Additionally, we utilized Shapley values to identify contributing factors to the model's predictions. B) Performance evaluations of top feature selection and machine learning methods across various feature sets emphasize the key role of feature integration in optimizing TMJ OA diagnostic prediction models. Lightgbm, Light gradient boosting machine; SVM, Support vector machine; ; AUC, Area under the curve; NNET, Neural network. C) SHAP values interpret machine learning predictions for TMJ OA cases. On the y-axis, features are ranked based on their global importance, which is determined by averaging all SHAP values for a specific feature. Each dot on the plot represents the SHAP value of an individual prediction, corresponding to a specific subject from the testing dataset. The color of the dot reflects the value of the respective feature, while its position along the x-axis indicates its influence on the model's prediction. For instance, if a purple dot representing 'headache' is positioned to the left, it suggests that a higher occurrence of headaches decreases the probability of the individual not having TMJ OA.

#### 4.4 Discussion & Conclusion

In the realm of TMJ OA diagnostics, there is an evident need for tools that encapsulate the multifaceted nature of the disorder. In our present research, we ventured beyond conventional methodologies to craft a machine learning-powered diagnostic instrument that uniquely integrates clinical, quantitative imaging, and biological features. This integrative technique surpassed our expectations by not only heightening diagnostic precision but also enabling a granular understanding of the pivotal features that drive diagnostic outcomes. The SHAP analysis, in particular, illuminated key features that could pave the way for proactive detection and interventions, thereby potentially revolutionizing the current landscape of TMJ OA diagnostics.

Our clinical data analysis showed that the TMJ OA participants' demographics align with existing literature, confirming our findings' relevance (Song et al. 2020). While pain was the predominant reason for clinical consultations, many participants concurrently experienced headaches, lower back pain, and sleep disturbances. Such findings not only echo previous research but also accentuate that painful TMD doesn't exist in isolation and should be addressed using a multidisciplinary treatment approach. The interconnectedness could stem from genetic, anatomical, and neurological factors related to TMD, as well as its implications on posture and pain sensitivity (Shrivastava, Battaglino, and Ye 2021; Bond et al. 2020; Braido et al. 2020; Byun et al. 2020).

In evaluating the imaging characteristics inherent to TMJ OA, we observed distribution divergent from other studies. Such disparities maybe attributed to differences in sample size, study design, or retrospective analysis of data sourced from varied protocols (Arayasantiparb et al. 2020). Interestingly, TMJ OA patients often exhibited multiple degenerative bone changes, indicating heterogeneity of subchondral bone remodeling events in the joint. This variability could arise from differences in load-bearing conditions, disease stages, biomechanics, and the surrounding biological milieu (Lijun Wang et al. 2022; Zhu et al. 2021; Adebayo et al. 2017).

The SHAP analysis of our diagnostic tool revealed that the primary determinants for TMJ OA included: clinical (headache, restless sleep, vertical range of mouth opening, muscle soreness), objective quantitative imaging (condyle ClusterProminence, HGLRE, SRHGLRE, TrabecularThickness, joint space) and bio-logical markers in saliva (TGFB1, TRANCE, TIMP-1, PAI-1,

VECadherin, CXCL-16) and serum (Angiogen-in, PAI-1, VEGF, TRANCE, TIMP-1, BDNF, VECadherin).

Consistent with our results, headaches are notably common in TMJ OA patients, suggesting they might elevate TMJ OA risk (Yakkaphan et al. 2022). Sleep disturbances are related to TMD pain as well as its onset; those with primary sleep disorders are 44% more likely to develop TMD (Kim et al. 2021). Thus, clinicians should be attentive to these potential early indicators of TMJ OA.

The identified biological markers in our study are predominantly related to inflammation, angiogenesis, and the regulation of extracellular matrix degradation and bone remodeling, all of which are fundamental in OA pathogenesis (Ibáñez et al. 2022; van der Kraan 2022; Wilkinson 2021; Kitaura et al. 2020; Liu, Tan, and Liu 2020; Haraden et al. 2019; Pérez-García et al. 2019; Wang et al. 2015). Significantly, serum levels of MMP-7 and PAI-1 emerged as top contributors. Consistent with our findings, these markers had differential serum levels in patients with incident knee and/or hand osteoarthritis compared to controls, prior to the appearance of ra-diographic signs, suggesting they might be potential indicators of early OA pathogenesis (Ling et al. 2009). Similarly, angiogenin levels were significantly higher in early-stage cartilage destruction compared to more advanced knee-OA stages (Chae et al. 2021).

Changes in biological markers' levels may also have contributed to the observed changes in the subchondral bone's texture and morphometry. For instance, overexpression of TIMP-1 in osteoblasts enhances trabecular bone volume and reduces trabecular separation (Geoffroy et al. 2004). Elevated TIMP-1 levels in serum correlate with the rate of joint space narrowing in hip osteoarthritis and might have contributed to the reduced joint space observed in our TMJOA participants (Chevalier et al. 2001). Lack of PAI-1 significantly elevates RANKL (AKA TRANCE) expression and the RANKL/OPG mRNA ratio in mouse osteoblasts. This could increase osteoclastogenic activity, resulting in subchondral bone resorption (Moritake et al. 2017). TMJ OA participants had heightened BDNF levels corroborating with the observation of knee OA patients having significantly higher BDNF serum levels compared to the healthy group (Gowler et al. 2020). BDNF produced due to peripheral nerve damage was found to contribute to sclerotic changes in

the surrounding alveolar bone (Ida-Yonemochi et al. 2017). BDNF levels have also been linked to the joint pain mechanism during the early inflammatory phase of knee OA (Gowler et al. 2020). Concerning TGF $\beta$ -1, a study reported notable changes in the TMJ's sub-chondral bone in the TMD rat models, including a marked increase in trabecular-separation, compared to controls. Importantly, inhibiting the TGF- $\beta$ -receptor I mitigated the progression of TMJ OA in the TMD models, implying that the activation of TGF- $\beta$  signaling might be instrumental in TMJ OA development (Zheng et al. 2018).

In the past three decades, osteoarthritis has increasingly been recognized not as a singular disease but as a complex constellation of disorders. This complexity, compounded by the pronounced phenotypic heterogeneity among patients, has posed challenges in harnessing OA-related molecules as reliable biomarkers for clinical diagnosis (Sandhu et al. 2023; Bernotiene et al. 2020; Deveza and Loeser 2018; Arden et al. 2015; Henrotin, Pésesse, and Lambert 2014; Blagojevic et al. 2010; Felson 1993; Bjelle 1983) Here, we developed a diagnostic tool integrating various data sources and identified a set of markers that may aid in developing effective preventive therapies and optimizing patient care. Assessing these markers, in tandem with comprehensive multicenter studies, is imperative for firmly establishment of their role in clinical settings.



**Supplementary Table 4.1: Definitions of Trabecular Bone Texture and Morphometry Features Computed in the Study**

Features	Variables	Definitions
GLCM	Energy Entropy Correlation Inverse difference moment Inertia Cluster shade Cluster prominence Haralick correlation	Uniformity of the grey-level textural organization. Randomization of the grey-level distribution. Grey-level linear dependence among the pixels. Local homogeneity of the grey-level distribution. Contrast between a pixel and its neighbor. Skewness and uniformity of the grey-level distribution. Skewness and asymmetry of the grey-level distribution. Linear dependence between the pixels.
GLRLM	Short run emphasis (SRE) Long run emphasis (LRE) Grey level non-uniformity (GLN) Run length non-uniformity (RLN) Low grey level run emphasis (LGLRE) High grey level run emphasis (HGLRE) Short run low grey level run emphasis (SRLGLRE)  Short run high grey level run emphasis (SRHGLRE)  Long run low grey level run emphasis (LRLGLRE)  Long run high grey level run emphasis (LRHGLRE)	Distribution of short run lengths. Distribution of long run lengths. Variability of the grey-level intensity. Similarity of run lengths in the image. Distribution of the lower grey-level values. Distribution of the higher grey-level values. Joint distribution of shorter run lengths with lower grey-level values. Joint distribution of shorter run lengths with higher grey-level values. Joint distribution of long run lengths with lower grey-level values. Joint distribution of long run lengths with higher grey-level values.
Bone Morphometry	BV/TV Tb.Th Tb.Sp Tb.N BS/BV	Ratio between bone volume and total volume. Trabecular thickness. Trabecular separation. Trabecular number. Ratio between bone surface and bone volume.

\* GLCM, Grey level co-occurrence matrix; GLRLM, Grey level run length matrix.

**Supplementary Table 4.2: Quantitative Textural Imaging Features of the Condyle and Articular Fossa in Control and TMJ OA Groups.**

Site	Variables	Control group		TMJ OA group		P-value
		Mean	SD	Mean	SD	
Lateral Surface of the Condyle	Energy	0.25	0.06	0.22	0.06	0.013*
	Entropy	2.54	0.33	2.71	0.43	0.006*
	Correlation	1.44	0.42	1.26	0.45	0.007*
	Inverse Difference Moment	0.89	0.02	0.88	0.02	0.074*
	Inertia	0.23	0.04	0.24	0.04	0.059*
	Short Run Emphasis	0.36	0.04	0.37	0.04	0.030*
	Long Run Emphasis	14.72	2.32	14.16	2.21	0.120
	Grey Level Non-Uniformity	2726.79	249.41	2642.94	259.63	0.038*
	Run Length Non-Uniformity	1641.89	397.74	1772.40	471.91	0.059
	Low Grey Level Run Emphasis	0.07	0.02	0.07	0.02	0.106
	High Grey Level Run Emphasis	18.08	3.85	20.52	6.25	0.003*
	Short Run Low Grey Level Emphasis	0.02	0.01	0.02	0.01	0.294
	Short Run High Grey Level Emphasis	6.76	1.98	8.06	3.13	0.002*
	Long Run Low Grey Level Emphasis	1.05	0.32	0.96	0.38	0.105
	Long Run High Grey Level Emphasis	250.40	56.11	268.74	68.84	0.065
	Bone Volume/Total Volume (%)	0.51	0.21	0.57	0.24	0.084
	Trabecular Thickness (mm)	0.36	0.15	0.43	0.20	0.008*
	Trabecular Separation (mm)	0.40	0.35	0.38	0.39	0.723
	Trabecular Number (mm <sup>-1</sup> )	1.40	0.27	1.31	0.27	0.058
	Bone Surface/Bone Volume Ratio (mm <sup>-1</sup> )	6.39	2.36	5.63	2.61	0.054
Antero-Lateral (AL) Surface of the Articular Fossa	Energy	0.20	0.07	0.21	0.09	0.591
	Entropy	2.88	0.42	2.86	0.44	0.716
	Correlation	0.97	0.43	0.92	0.38	0.443
	Inverse Difference Moment	0.89	0.02	0.89	0.02	0.586
	Inertia	0.23	0.04	0.23	0.04	0.978
	Short Run Emphasis	0.36	0.04	0.36	0.04	0.795
	Long Run Emphasis	15.01	2.16	15.16	1.78	0.649
	Grey Level Non-Uniformity	1817.16	285.30	1800.83	287.33	0.718
	Run Length Non-Uniformity	1387.21	336.63	1363.03	313.48	0.638
	Low Grey Level Run Emphasis	0.04	0.02	0.04	0.05	0.626
	High Grey Level Run Emphasis	35.47	10.16	35.96	9.05	0.743
	Short Run Low Grey Level Emphasis	0.01	0.01	0.02	0.04	0.524
	Short Run High Grey Level Emphasis	13.00	3.51	13.09	3.09	0.868
	Long Run Low Grey Level Emphasis	0.59	0.37	0.61	0.50	0.837
	Long Run High Grey Level Emphasis	522.15	203.65	534.66	173.91	0.676
	Bone Volume/Total Volume (%)	0.69	0.25	0.71	0.25	0.500
	Trabecular Thickness (mm)	0.60	0.28	0.62	0.27	0.579
	Trabecular Separation (mm)	0.31	0.42	1.28	8.81	0.325
	Trabecular Number (mm <sup>-1</sup> )	1.18	0.27	1.17	0.28	0.828
	Bone Surface/Bone Volume Ratio (mm <sup>-1</sup> )	4.24	2.27	4.22	3.13	0.961

\* An independent samples t-test was used to compute the p-value for the imaging variables between the groups, P< 0.05 was considered statistically significant.

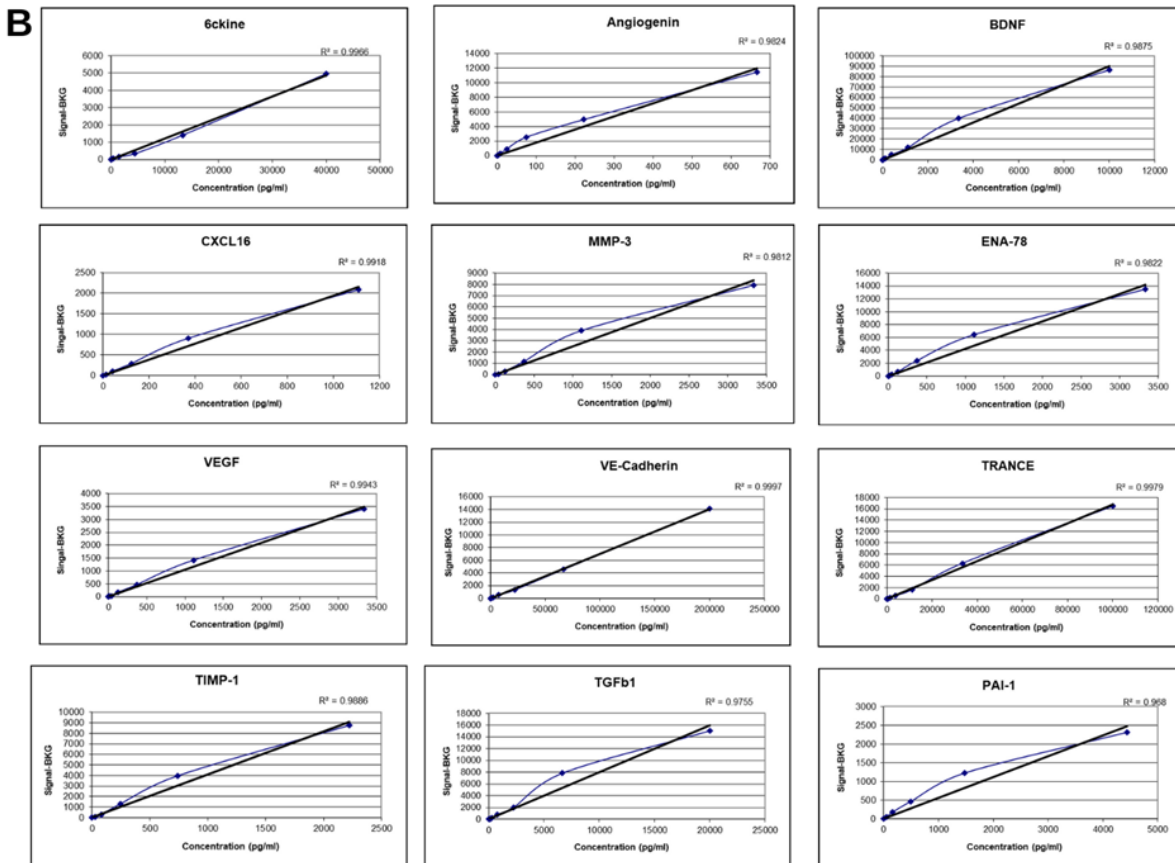
**Supplementary Table 4.3: Descriptive Values of Biological Features in Control and TMJ OA Groups.**

Variables	Control group		TMJ OA group	
	Mean	SD	Mean	SD
Angiogenin Serum	1456.86	215.63	1489.67	289.04
BDNF Serum	1017.65	1182.48	1214.25	1594.31
CXCL16 Serum	3258.74	1423.01	3683.30	2083.87
ENA-78 Serum	666.34	571.43	605.83	525.22
MMP3 Serum	4109.40	4319.59	3612.02	2699.62
MMP7 Serum	671.65	353.17	672.29	413.75
OPG Serum	5485.61	9106.16	6765.43	11596.90
PAI-1 Serum	8283.14	4019.92	7834.17	3574.73
shaTGF-B1 Serum	51576.77	127099.17	58606.49	133705.55
TIMP-1 Serum	4772.12	2971.32	4849.75	3010.91
TRANCE Serum	2002.93	1721.86	2176.02	1457.09
VE-Cadherin Serum	7006.40	8828.89	5739.20	5493.81
VEGF Serum	167.11	163.58	157.69	170.26
Angiogenin Saliva	914.70	409.73	995.89	447.96
CXCL16 Saliva	273.01	376.89	287.92	421.23
ENA-78 Saliva	1729.35	994.31	1872.39	1088.52
MMP7 Saliva	3253.07	2044.64	3189.01	1830.85
OPG Saliva	1327.39	2383.25	1315.95	1842.69
TGF-B1 Saliva	742.38	1593.07	765.47	2120.83
PAI-1 Saliva	12658.84	44860.31	16302.80	103331.65
TIMP-1 Saliva	3001.69	1392.01	2970.33	1216.38
TRANCE Saliva	1008.79	1743.27	837.63	1321.05
VE-Cadherin Saliva	3538.19	13269.55	2381.34	6445.33
VEGF Saliva	2085.77	1375.63	2266.99	1333.05

\*BDNF, brain derived neurotrophic factor; CXCL16, chemokine ligand 16; ENA78, epithelial neutrophil-activating peptide; MMP, matrix metalloproteinases; OPG, osteoprotegerin, PAI-1, plasminogen activator inhibitor-1; TGF-B1, transforming growth factor-beta, TRANCE, TNF-related activation-induced cytokine; VE-Cadherin, vascular endothelial (VE)-cadherin; VEGF, vascular endothelium growth factor.

**A**

Target	LOD (pg/ml)	Best Confident Range	Maximum Value	Highest Reported Value	Lowest Reported Value	% Below LOD	% Above LOD but <3xLOD	% in Best Confidence	% Above Maximum
Angiogenin	1.1	3.2 - 667	2,000	4,181.0	42.0	0.0	0.0	95.8	4.2
BDNF	0.3	0.8 - 667	2,000	4,776.5	0.0	14.6	6.8	69.8	8.9
CXCL16	20.0	60.0 - 1,852	5,556	22,657.9	0.0	2.1	7.8	83.9	6.3
ENA-78	0.6	1.8 - 617	1,852	2,536.8	11.1	0.0	0.0	93.2	6.8
MMP-3	8.4	25.3 - 5,556	16,667	45,836.2	0.0	9.6	1.8	84.9	3.6
MMP-7	1.9	5.6 - 1,235	3,704	7,725.7	55.4	0.0	0.0	90.9	9.1
OPG	14.5	43.5 - 6,667	20,000	100,635.3	0.0	0.5	1.0	90.4	8.1
PAI-1	16.9	50.6 - 7,407	22,222	36,193.6	100.2	0.0	0.0	99.2	0.8
TGFb1	200.0	600.0 - 33,333	100,000	1,836,016.1	0.0	15.6	2.6	61.5	20.3
TIMP-1	1.8	5.5 - 1,235	3,704	2,842.4	100.4	0.0	0.0	100.0	0.0
TRANCE	9.6	28.9 - 33,333	100,000	37,320.4	0.0	3.6	1.6	94.8	0.0
VE-Cadherin	52.8	158.4 - 66,667	200,000	244,581.2	0.0	3.6	3.9	91.9	0.5
VEGF	1.1	3.3 - 3,333	10,000	7,625.2	0.0	0.5	0.0	99.5	0.0
blank	#DIV/0!	#DIV/0!	0	#DIV/0!	#DIV/0!	#DIV/0!	#DIV/0!	#DIV/0!	#DIV/0!



**Supplementary Figure 4.1: Analysis of Biological Features in Control and TMJ OA Groups.** A) Summary report displaying protein levels in serum and saliva. B) Standard curves from microarray analysis for individual proteins. LOD, Limit of detection.

**Supplementary Table 4.4: Descriptive Statistics of Log-transformed Biological Features in Control and TMJ OA Groups.** Data presented as Mean  $\pm$  SD and p-values from independent t-test.

Variables	Control group		TMJ OA group		P value
	Mean	SD	Mean	SD	
Angiogenin Serum	7.27	0.15	7.29	0.19	0.58
BDNF Serum	6.25	1.30	6.36	1.33	0.19
CXCL16 Serum	8.01	0.41	8.10	0.47	0.58
ENA-78 Serum	6.08	1.08	5.99	1.03	0.52
MMP3 Serum	8.05	0.69	7.98	0.63	0.92
MMP7 Serum	6.32	0.78	6.33	0.73	0.29
OPG Serum	7.97	0.99	8.14	1.04	0.44
PAI-1 Serum	8.90	0.54	8.83	0.61	0.35
shaTGF-B1 Serum	6.99	3.26	7.50	3.44	0.85
TIMP-1 Serum	8.19	0.81	8.22	0.80	0.16
TRANCE Serum	7.10	1.18	7.34	0.98	0.99
VE-Cadherin Serum	8.14	1.37	8.14	1.18	0.52
VEGF Serum	4.66	1.14	4.76	0.82	0.17
Angiogenin Saliva	6.71	0.49	6.81	0.43	0.75
CXCL16 Saliva	4.82	1.43	4.90	1.60	0.42
ENA-78 Saliva	7.23	0.77	7.32	0.74	0.84
MMP7 Saliva	7.87	0.73	7.89	0.67	0.49
OPG Saliva	6.36	1.28	6.51	1.34	0.49
TGF-B1 Saliva	5.18	2.12	5.41	1.90	0.49
PAI-1 Saliva	6.19	2.70	5.88	2.59	0.78
TIMP-1 Saliva	7.88	0.53	7.90	0.46	0.59
TRANCE Saliva	5.99	1.54	6.12	1.44	0.67
VE-Cadherin Saliva	6.84	1.36	6.73	1.48	0.12
VEGF Saliva	7.40	0.74	7.57	0.57	0.59

\*BDNF, brain derived neurotrophic factor; CXCL16, chemokine ligand 16; ENA78, epithelial neutrophil-activating peptide; MMP, matrix metalloproteinases; OPG, osteoprotegerin, PAI-1, plasminogen activator inhibitor-1; TGF-B1, transforming growth factor-beta, TRANCE, TNF-related activation-induced cytokine; VE-Cadherin, vascular endothelial (VE)-cadherin; VEGF, vascular endothelium growth factor.

**Supplementary Table 4.5: Performance of the Feature Selection Methods and Machine Learning Approaches on the Validation Dataset Utilizing Clinical, Imaging, and Biological Features.**

Model	Evaluation Metrics	Accuracy	Precision_ TMJ OA	Precision_ Control	Recall_ TMJ OA	Recall_ Control	F1score	AUC
Lightgbm_RF		0.828 ± 0.01	0.841 ± 0.01	0.818 ± 0.01	0.811 ± 0.01	0.843 ± 0.02	0.827 ± 0.01	0.915 ± 0.00
XgbTree_RF		0.826 ± 0.01	0.836 ± 0.01	0.817 ± 0.00	0.811 ± 0.00	0.838 ± 0.01	0.825 ± 0.01	0.910 ± 0.00
Glmnet_RF		0.822 ± 0.01	0.839 ± 0.01	0.808 ± 0.01	0.799 ± 0.01	0.843 ± 0.01	0.821 ± 0.01	0.893 ± 0.01
Lightgbm_XgbTree		0.818 ± 0.01	0.822 ± 0.00	0.816 ± 0.01	0.814 ± 0.01	0.822 ± 0.00	0.818 ± 0.01	0.900 ± 0.00
RF_RF		0.815 ± 0.01	0.828 ± 0.01	0.804 ± 0.00	0.796 ± 0.00	0.831 ± 0.01	0.814 ± 0.01	0.908 ± 0.00
Lightgbm_Lightgbm		0.811 ± 0.01	0.813 ± 0.01	0.810 ± 0.01	0.809 ± 0.01	0.813 ± 0.01	0.811 ± 0.01	0.895 ± 0.00
XgbTree_XgbTree		0.810 ± 0.01	0.816 ± 0.02	0.806 ± 0.01	0.803 ± 0.01	0.818 ± 0.02	0.810 ± 0.01	0.895 ± 0.00
RF_XgbTree		0.809 ± 0.01	0.816 ± 0.01	0.804 ± 0.01	0.800 ± 0.01	0.818 ± 0.02	0.809 ± 0.01	0.893 ± 0.00
AUC_RF		0.809 ± 0.01	0.816 ± 0.02	0.803 ± 0.01	0.798 ± 0.01	0.817 ± 0.02	0.808 ± 0.01	0.892 ± 0.01
Glmboost_RF		0.807 ± 0.01	0.811 ± 0.01	0.805 ± 0.00	0.803 ± 0.01	0.810 ± 0.01	0.807 ± 0.01	0.879 ± 0.00
Glmboost_XgbTree		0.806 ± 0.01	0.811 ± 0.01	0.802 ± 0.01	0.799 ± 0.01	0.813 ± 0.01	0.806 ± 0.01	0.880 ± 0.01
AUC_XgbTree		0.806 ± 0.01	0.812 ± 0.01	0.801 ± 0.01	0.797 ± 0.01	0.815 ± 0.01	0.806 ± 0.01	0.881 ± 0.01
Glmnet_XgbTree		0.805 ± 0.01	0.812 ± 0.01	0.799 ± 0.01	0.794 ± 0.01	0.815 ± 0.01	0.804 ± 0.01	0.878 ± 0.01
NNET_RF		0.798 ± 0.01	0.800 ± 0.01	0.796 ± 0.01	0.795 ± 0.01	0.799 ± 0.01	0.797 ± 0.01	0.880 ± 0.00
RF_Lightgbm		0.793 ± 0.01	0.793 ± 0.01	0.793 ± 0.00	0.793 ± 0.00	0.792 ± 0.01	0.792 ± 0.01	0.876 ± 0.00
XgbTree_Lightgbm		0.792 ± 0.01	0.792 ± 0.01	0.794 ± 0.01	0.794 ± 0.02	0.791 ± 0.01	0.792 ± 0.01	0.877 ± 0.00
Glmnet_Lightgbm		0.788 ± 0.01	0.789 ± 0.01	0.787 ± 0.01	0.787 ± 0.01	0.789 ± 0.01	0.788 ± 0.01	0.865 ± 0.01
Glmboost_Lightgbm		0.784 ± 0.01	0.788 ± 0.01	0.782 ± 0.01	0.780 ± 0.01	0.789 ± 0.01	0.784 ± 0.01	0.858 ± 0.00
NNET_XgbTree		0.778 ± 0.01	0.779 ± 0.01	0.779 ± 0.01	0.778 ± 0.01	0.778 ± 0.01	0.778 ± 0.01	0.861 ± 0.01
AUC_Lightgbm		0.777 ± 0.01	0.782 ± 0.01	0.773 ± 0.01	0.770 ± 0.01	0.785 ± 0.01	0.777 ± 0.01	0.858 ± 0.01
NNET_Lightgbm		0.772 ± 0.01	0.770 ± 0.01	0.776 ± 0.01	0.778 ± 0.01	0.767 ± 0.02	0.772 ± 0.01	0.853 ± 0.01
Glmnet_Baysglm		0.772 ± 0.00	0.781 ± 0.01	0.765 ± 0.00	0.758 ± 0.00	0.787 ± 0.01	0.772 ± 0.00	0.860 ± 0.00
Glmboost_Baysglm		0.772 ± 0.00	0.781 ± 0.00	0.764 ± 0.01	0.756 ± 0.01	0.788 ± 0.01	0.772 ± 0.00	0.862 ± 0.00
Lightgbm_SVMlinear		0.771 ± 0.01	0.783 ± 0.01	0.762 ± 0.01	0.753 ± 0.01	0.790 ± 0.01	0.771 ± 0.01	0.837 ± 0.00
Glmboost_SVMlinear		0.771 ± 0.01	0.788 ± 0.01	0.757 ± 0.01	0.742 ± 0.01	0.800 ± 0.01	0.771 ± 0.01	0.853 ± 0.00
Glmnet_SVMlinear		0.770 ± 0.01	0.785 ± 0.01	0.757 ± 0.01	0.744 ± 0.01	0.795 ± 0.01	0.769 ± 0.01	0.852 ± 0.01
Glmboost_LDA		0.767 ± 0.01	0.793 ± 0.01	0.747 ± 0.01	0.724 ± 0.01	0.810 ± 0.01	0.767 ± 0.01	0.855 ± 0.00
Glmnet_LDA		0.767 ± 0.01	0.796 ± 0.01	0.744 ± 0.01	0.719 ± 0.01	0.815 ± 0.01	0.766 ± 0.01	0.854 ± 0.00
RF_SVMlinear		0.766 ± 0.00	0.775 ± 0.01	0.758 ± 0.01	0.750 ± 0.01	0.781 ± 0.01	0.765 ± 0.00	0.824 ± 0.01
Lightgbm_Baysglm		0.764 ± 0.00	0.772 ± 0.01	0.758 ± 0.01	0.751 ± 0.01	0.777 ± 0.01	0.764 ± 0.00	0.840 ± 0.00
Glmnet_Glmnet		0.763 ± 0.01	0.777 ± 0.01	0.752 ± 0.01	0.740 ± 0.01	0.787 ± 0.01	0.763 ± 0.01	0.850 ± 0.00
Glmboost_Glmboost		0.764 ± 0.01	0.788 ± 0.01	0.743 ± 0.01	0.722 ± 0.01	0.806 ± 0.01	0.763 ± 0.01	0.846 ± 0.00
RF_Baysglm		0.761 ± 0.01	0.765 ± 0.01	0.758 ± 0.01	0.754 ± 0.01	0.768 ± 0.01	0.761 ± 0.01	0.828 ± 0.01
Glmboost_Glmnet		0.761 ± 0.01	0.777 ± 0.00	0.748 ± 0.01	0.733 ± 0.01	0.790 ± 0.01	0.761 ± 0.01	0.849 ± 0.01
Glmnet_Glmboost		0.760 ± 0.01	0.786 ± 0.01	0.739 ± 0.01	0.716 ± 0.01	0.805 ± 0.01	0.760 ± 0.01	0.846 ± 0.00
NNET_SVMlinear		0.760 ± 0.00	0.775 ± 0.01	0.748 ± 0.01	0.734 ± 0.01	0.786 ± 0.01	0.760 ± 0.00	0.827 ± 0.00
XgbTree_SVMlinear		0.760 ± 0.01	0.774 ± 0.02	0.748 ± 0.01	0.736 ± 0.01	0.783 ± 0.02	0.760 ± 0.01	0.824 ± 0.01
NNET_Baysglm		0.758 ± 0.00	0.762 ± 0.01	0.756 ± 0.00	0.752 ± 0.00	0.764 ± 0.01	0.758 ± 0.00	0.834 ± 0.01
Glmnet_HDDA		0.759 ± 0.00	0.783 ± 0.00	0.740 ± 0.01	0.718 ± 0.01	0.799 ± 0.01	0.758 ± 0.00	0.841 ± 0.01
Lightgbm_Glmboost		0.758 ± 0.01	0.781 ± 0.01	0.740 ± 0.01	0.719 ± 0.01	0.798 ± 0.01	0.758 ± 0.01	0.838 ± 0.00
Lightgbm_Glmnet		0.757 ± 0.01	0.771 ± 0.01	0.746 ± 0.01	0.732 ± 0.01	0.782 ± 0.01	0.757 ± 0.01	0.835 ± 0.01
Glmboost>NNET		0.757 ± 0.01	0.755 ± 0.01	0.759 ± 0.00	0.759 ± 0.01	0.754 ± 0.01	0.756 ± 0.00	0.828 ± 0.00
Glmboost_HDDA		0.756 ± 0.01	0.783 ± 0.01	0.735 ± 0.01	0.710 ± 0.01	0.802 ± 0.01	0.755 ± 0.01	0.839 ± 0.01
RF_Glmboost		0.756 ± 0.01	0.775 ± 0.01	0.740 ± 0.01	0.722 ± 0.01	0.789 ± 0.01	0.755 ± 0.01	0.828 ± 0.01
Glmboost_Naivebayes		0.754 ± 0.01	0.783 ± 0.01	0.734 ± 0.00	0.706 ± 0.01	0.803 ± 0.01	0.753 ± 0.01	0.831 ± 0.01
Glmnet_Naivebayes		0.755 ± 0.00	0.798 ± 0.01	0.724 ± 0.00	0.683 ± 0.01	0.826 ± 0.02	0.753 ± 0.00	0.830 ± 0.01
Lightgbm>NNET		0.752 ± 0.01	0.751 ± 0.01	0.754 ± 0.01	0.756 ± 0.01	0.749 ± 0.01	0.752 ± 0.01	0.806 ± 0.00
XgbTree_Baysglm		0.751 ± 0.01	0.758 ± 0.01	0.745 ± 0.01	0.738 ± 0.00	0.764 ± 0.01	0.751 ± 0.01	0.831 ± 0.00

**Supplementary Table 4.5: Performance of the Feature Selection Methods and Machine Learning Approaches on the Validation Dataset Utilizing Clinical, Imaging, and Biological Features. (Cont.)**

Evaluation Metrics Model	Accuracy	Precision_ TMJ OA	Precision_ Control	Recall_ TMJ OA	Recall_ Control	F1score	AUC
Glmnet_NNET	0.751 ± 0.01	0.758 ± 0.01	0.746 ± 0.01	0.738 ± 0.02	0.764 ± 0.01	0.751 ± 0.01	0.822 ± 0.01
AUC_Glmboost	0.750 ± 0.01	0.770 ± 0.01	0.734 ± 0.01	0.715 ± 0.01	0.786 ± 0.02	0.750 ± 0.01	0.827 ± 0.01
AUC_Glmnet	0.750 ± 0.01	0.764 ± 0.01	0.738 ± 0.01	0.723 ± 0.01	0.776 ± 0.02	0.749 ± 0.01	0.826 ± 0.01
AUC_Baysglm	0.749 ± 0.01	0.754 ± 0.01	0.745 ± 0.01	0.741 ± 0.01	0.758 ± 0.01	0.749 ± 0.01	0.829 ± 0.01
Lightgbm_Naivebayes	0.749 ± 0.01	0.752 ± 0.01	0.750 ± 0.01	0.747 ± 0.01	0.750 ± 0.02	0.748 ± 0.01	0.812 ± 0.01
RF_Glmnet	0.748 ± 0.01	0.762 ± 0.01	0.737 ± 0.01	0.722 ± 0.01	0.774 ± 0.01	0.748 ± 0.01	0.825 ± 0.00
NNET_Glmnet	0.748 ± 0.00	0.760 ± 0.00	0.739 ± 0.01	0.726 ± 0.01	0.770 ± 0.01	0.748 ± 0.00	0.823 ± 0.00
AUC_SVMlinear	0.747 ± 0.01	0.760 ± 0.01	0.737 ± 0.01	0.724 ± 0.01	0.770 ± 0.02	0.747 ± 0.01	0.822 ± 0.01
AUC_NNET	0.746 ± 0.01	0.743 ± 0.01	0.750 ± 0.01	0.753 ± 0.01	0.739 ± 0.02	0.746 ± 0.01	0.791 ± 0.01
NNET_Glmboost	0.746 ± 0.01	0.775 ± 0.01	0.724 ± 0.01	0.695 ± 0.01	0.797 ± 0.01	0.745 ± 0.01	0.822 ± 0.01
XgbTree_Glmnet	0.745 ± 0.01	0.760 ± 0.01	0.732 ± 0.01	0.716 ± 0.01	0.773 ± 0.01	0.744 ± 0.01	0.821 ± 0.01
AUC_LDA	0.745 ± 0.01	0.767 ± 0.01	0.727 ± 0.01	0.705 ± 0.01	0.785 ± 0.02	0.744 ± 0.01	0.818 ± 0.01
XgbTree_Glmboost	0.745 ± 0.01	0.766 ± 0.01	0.727 ± 0.01	0.705 ± 0.02	0.784 ± 0.01	0.744 ± 0.01	0.827 ± 0.00
Lightgbm_LDA	0.744 ± 0.01	0.766 ± 0.01	0.727 ± 0.01	0.705 ± 0.01	0.784 ± 0.01	0.744 ± 0.01	0.827 ± 0.00
NNET_LDA	0.742 ± 0.01	0.766 ± 0.00	0.724 ± 0.01	0.699 ± 0.01	0.785 ± 0.00	0.742 ± 0.01	0.819 ± 0.01
RF_LDA	0.741 ± 0.01	0.759 ± 0.01	0.727 ± 0.01	0.708 ± 0.01	0.775 ± 0.01	0.741 ± 0.01	0.814 ± 0.01
XgbTree_LDA	0.741 ± 0.01	0.765 ± 0.01	0.722 ± 0.01	0.697 ± 0.01	0.785 ± 0.01	0.741 ± 0.01	0.822 ± 0.01
XgbTree_NNET	0.739 ± 0.01	0.737 ± 0.01	0.742 ± 0.01	0.743 ± 0.01	0.735 ± 0.02	0.739 ± 0.01	0.798 ± 0.01
NNET_Naivebayes	0.739 ± 0.01	0.752 ± 0.01	0.732 ± 0.01	0.719 ± 0.02	0.760 ± 0.02	0.738 ± 0.01	0.798 ± 0.01
NNET_NNET	0.736 ± 0.01	0.743 ± 0.01	0.733 ± 0.02	0.723 ± 0.02	0.748 ± 0.01	0.735 ± 0.02	0.777 ± 0.02
NNET_HDDA	0.735 ± 0.01	0.756 ± 0.01	0.719 ± 0.01	0.696 ± 0.01	0.774 ± 0.01	0.734 ± 0.01	0.808 ± 0.01
XgbTree_Naivebayes	0.729 ± 0.01	0.718 ± 0.01	0.747 ± 0.02	0.764 ± 0.03	0.694 ± 0.02	0.728 ± 0.01	0.795 ± 0.01
AUC_HDDA	0.729 ± 0.01	0.733 ± 0.01	0.730 ± 0.01	0.727 ± 0.01	0.730 ± 0.02	0.727 ± 0.01	0.790 ± 0.01
AUC_Naivebayes	0.728 ± 0.01	0.748 ± 0.01	0.715 ± 0.01	0.694 ± 0.01	0.762 ± 0.01	0.727 ± 0.01	0.787 ± 0.01
XgbTree_HDDA	0.723 ± 0.01	0.729 ± 0.02	0.729 ± 0.00	0.725 ± 0.01	0.720 ± 0.03	0.720 ± 0.01	0.796 ± 0.01
Lightgbm_HDDA	0.720 ± 0.02	0.723 ± 0.02	0.724 ± 0.02	0.721 ± 0.03	0.720 ± 0.02	0.719 ± 0.02	0.795 ± 0.01
RF_NNET	0.719 ± 0.01	0.716 ± 0.01	0.725 ± 0.01	0.731 ± 0.01	0.707 ± 0.02	0.719 ± 0.01	0.772 ± 0.01
RF_HDDA	0.712 ± 0.01	0.700 ± 0.01	0.739 ± 0.02	0.759 ± 0.02	0.665 ± 0.03	0.709 ± 0.01	0.786 ± 0.01
RF_Naivebayes	0.706 ± 0.02	0.689 ± 0.02	0.737 ± 0.02	0.770 ± 0.02	0.643 ± 0.02	0.703 ± 0.02	0.783 ± 0.01

\*RF, Random forest; XGBoost, Extreme gradient boosting; Lightgbm, Light gradient boosting machine; Glmnet, Generalized linear model with lasso and elastic net regularization; AUC, Area under the curve; Glmboost, Generalized linear model boosting; NNET, Neural network; Baysglm, Bayesian generalized linear model; SVM, Support vector machine; LDA, Linear discriminant analysis; HDDA, High-dimensional discriminant analysis.

**Supplementary Table 4.6: Performance of the Feature Selection Methods and Machine Learning Approaches on the Test Dataset Utilizing Clinical, Imaging, and Biological Features.**

Evaluation Model Metrics	Accuracy	Precision_ TMJ OA	Precision_ Control	Recall_ TMJ OA	Recall_ Control	F1score	AUC
RF_RF	0.798 ± 0.01	0.820 ± 0.02	0.779 ± 0.02	0.763 ± 0.03	0.830 ± 0.02	0.797 ± 0.01	0.895 ± 0.01
Glmnet_RF	0.798 ± 0.02	0.799 ± 0.02	0.796 ± 0.02	0.795 ± 0.02	0.795 ± 0.03	0.796 ± 0.02	0.864 ± 0.02
Lightgbm_RF	0.794 ± 0.02	0.806 ± 0.03	0.784 ± 0.03	0.775 ± 0.03	0.812 ± 0.03	0.794 ± 0.02	0.878 ± 0.01
XgbTree_RF	0.791 ± 0.01	0.813 ± 0.02	0.773 ± 0.01	0.758 ± 0.02	0.820 ± 0.03	0.790 ± 0.02	0.874 ± 0.01
AUC_RF	0.783 ± 0.02	0.789 ± 0.03	0.777 ± 0.01	0.773 ± 0.01	0.793 ± 0.03	0.783 ± 0.02	0.869 ± 0.02
Glmboost_RF	0.783 ± 0.02	0.788 ± 0.02	0.777 ± 0.02	0.773 ± 0.03	0.790 ± 0.02	0.782 ± 0.02	0.857 ± 0.02
Lightgbm_XgbTree	0.780 ± 0.03	0.792 ± 0.05	0.771 ± 0.03	0.763 ± 0.03	0.798 ± 0.06	0.780 ± 0.03	0.859 ± 0.02
Glmboost_XgbTree	0.779 ± 0.02	0.785 ± 0.02	0.776 ± 0.03	0.770 ± 0.05	0.788 ± 0.03	0.779 ± 0.02	0.856 ± 0.01
NNET_RF	0.779 ± 0.03	0.781 ± 0.02	0.778 ± 0.04	0.775 ± 0.05	0.780 ± 0.02	0.778 ± 0.03	0.852 ± 0.02
Lightgbm_Lightgbm	0.777 ± 0.03	0.772 ± 0.02	0.782 ± 0.03	0.785 ± 0.04	0.768 ± 0.02	0.776 ± 0.03	0.857 ± 0.02
RF_XgbTree	0.769 ± 0.02	0.773 ± 0.02	0.766 ± 0.02	0.763 ± 0.02	0.775 ± 0.02	0.769 ± 0.02	0.860 ± 0.02
XgbTree_XgbTree	0.769 ± 0.03	0.766 ± 0.03	0.773 ± 0.03	0.775 ± 0.04	0.763 ± 0.04	0.769 ± 0.03	0.861 ± 0.02
RF_Lightgbm	0.769 ± 0.01	0.777 ± 0.02	0.763 ± 0.02	0.756 ± 0.03	0.783 ± 0.03	0.769 ± 0.01	0.853 ± 0.01
AUC_XgbTree	0.765 ± 0.02	0.773 ± 0.03	0.760 ± 0.03	0.753 ± 0.04	0.778 ± 0.04	0.765 ± 0.02	0.846 ± 0.01
Glmnet_XgbTree	0.764 ± 0.01	0.772 ± 0.02	0.758 ± 0.02	0.751 ± 0.04	0.778 ± 0.03	0.764 ± 0.01	0.843 ± 0.01
Glmboost_Lightgbm	0.760 ± 0.01	0.768 ± 0.03	0.754 ± 0.01	0.748 ± 0.01	0.773 ± 0.04	0.760 ± 0.01	0.834 ± 0.02
Glmnet_Lightgbm	0.759 ± 0.03	0.760 ± 0.04	0.760 ± 0.02	0.760 ± 0.02	0.758 ± 0.05	0.759 ± 0.03	0.838 ± 0.02
XgbTree_Lightgbm	0.758 ± 0.02	0.766 ± 0.02	0.751 ± 0.02	0.743 ± 0.03	0.773 ± 0.02	0.758 ± 0.02	0.845 ± 0.01
RF_SVMlinear	0.757 ± 0.03	0.769 ± 0.03	0.747 ± 0.03	0.736 ± 0.04	0.778 ± 0.04	0.757 ± 0.03	0.815 ± 0.02
AUC_Lightgbm	0.756 ± 0.01	0.767 ± 0.03	0.747 ± 0.01	0.738 ± 0.03	0.773 ± 0.05	0.755 ± 0.01	0.835 ± 0.01
NNET_XgbTree	0.754 ± 0.03	0.755 ± 0.02	0.756 ± 0.04	0.753 ± 0.06	0.756 ± 0.03	0.754 ± 0.03	0.837 ± 0.03
NNET_Lightgbm	0.742 ± 0.01	0.742 ± 0.02	0.743 ± 0.01	0.743 ± 0.02	0.741 ± 0.03	0.742 ± 0.01	0.828 ± 0.01
AUC>NNET	0.741 ± 0.02	0.732 ± 0.02	0.751 ± 0.03	0.760 ± 0.03	0.721 ± 0.03	0.741 ± 0.02	0.783 ± 0.01
Lightgbm_SVMlinear	0.741 ± 0.01	0.751 ± 0.01	0.732 ± 0.02	0.721 ± 0.04	0.760 ± 0.02	0.741 ± 0.01	0.810 ± 0.01
Lightgbm_Glmboost	0.741 ± 0.02	0.763 ± 0.02	0.722 ± 0.01	0.699 ± 0.02	0.783 ± 0.03	0.740 ± 0.02	0.818 ± 0.00
AUC_SVMlinear	0.736 ± 0.03	0.745 ± 0.03	0.727 ± 0.03	0.716 ± 0.03	0.756 ± 0.03	0.736 ± 0.03	0.798 ± 0.01
Lightgbm>NNET	0.735 ± 0.01	0.731 ± 0.02	0.739 ± 0.02	0.743 ± 0.03	0.726 ± 0.04	0.734 ± 0.01	0.783 ± 0.01
RF_Glmboost	0.735 ± 0.01	0.750 ± 0.01	0.721 ± 0.02	0.704 ± 0.02	0.765 ± 0.02	0.734 ± 0.01	0.801 ± 0.01
Lightgbm_Baysglm	0.733 ± 0.01	0.739 ± 0.01	0.728 ± 0.02	0.721 ± 0.03	0.746 ± 0.02	0.733 ± 0.01	0.812 ± 0.01
XgbTree_Glmnet	0.733 ± 0.02	0.748 ± 0.02	0.720 ± 0.02	0.704 ± 0.02	0.763 ± 0.02	0.733 ± 0.02	0.797 ± 0.01
Glmboost_Glmboost	0.735 ± 0.03	0.753 ± 0.02	0.720 ± 0.03	0.699 ± 0.04	0.765 ± 0.02	0.733 ± 0.02	0.797 ± 0.02
XgbTree_Glmboost	0.732 ± 0.03	0.753 ± 0.03	0.715 ± 0.02	0.691 ± 0.02	0.773 ± 0.04	0.732 ± 0.03	0.806 ± 0.02
Lightgbm_Glmnet	0.731 ± 0.01	0.744 ± 0.01	0.719 ± 0.01	0.704 ± 0.01	0.758 ± 0.02	0.731 ± 0.01	0.811 ± 0.01
AUC_LDA	0.731 ± 0.02	0.748 ± 0.02	0.716 ± 0.01	0.696 ± 0.02	0.765 ± 0.02	0.731 ± 0.02	0.796 ± 0.01
Glmnet>NNET	0.728 ± 0.02	0.734 ± 0.02	0.723 ± 0.02	0.716 ± 0.03	0.741 ± 0.02	0.728 ± 0.02	0.794 ± 0.01
XgbTree_SVMlinear	0.728 ± 0.02	0.736 ± 0.02	0.723 ± 0.03	0.714 ± 0.04	0.743 ± 0.03	0.728 ± 0.02	0.794 ± 0.02
AUC_Glmboost	0.728 ± 0.02	0.754 ± 0.02	0.708 ± 0.01	0.679 ± 0.01	0.778 ± 0.03	0.728 ± 0.02	0.803 ± 0.01
NNET>NNET	0.727 ± 0.02	0.729 ± 0.02	0.726 ± 0.03	0.723 ± 0.04	0.731 ± 0.03	0.727 ± 0.02	0.769 ± 0.03
NNET_SVMlinear	0.725 ± 0.02	0.733 ± 0.02	0.717 ± 0.02	0.706 ± 0.02	0.743 ± 0.02	0.725 ± 0.02	0.789 ± 0.02
AUC_Glmnet	0.725 ± 0.02	0.733 ± 0.02	0.717 ± 0.02	0.706 ± 0.03	0.743 ± 0.02	0.725 ± 0.02	0.805 ± 0.01
Glmnet_Glmboost	0.725 ± 0.02	0.740 ± 0.02	0.712 ± 0.02	0.694 ± 0.03	0.756 ± 0.02	0.724 ± 0.02	0.804 ± 0.01
Lightgbm_HDDA	0.725 ± 0.03	0.725 ± 0.04	0.727 ± 0.01	0.731 ± 0.02	0.719 ± 0.07	0.724 ± 0.03	0.776 ± 0.02
NNET_LDA	0.725 ± 0.02	0.744 ± 0.03	0.709 ± 0.02	0.686 ± 0.03	0.763 ± 0.03	0.724 ± 0.02	0.781 ± 0.03
RF_Baysglm	0.723 ± 0.01	0.726 ± 0.01	0.721 ± 0.02	0.719 ± 0.02	0.728 ± 0.02	0.723 ± 0.01	0.807 ± 0.00
NNET_Glmnet	0.723 ± 0.02	0.734 ± 0.02	0.714 ± 0.02	0.701 ± 0.02	0.746 ± 0.02	0.723 ± 0.02	0.797 ± 0.01
NNET_Glmboost	0.723 ± 0.01	0.745 ± 0.01	0.706 ± 0.02	0.679 ± 0.03	0.768 ± 0.02	0.723 ± 0.01	0.799 ± 0.02
Glmboost_Naivebayes	0.723 ± 0.01	0.752 ± 0.02	0.702 ± 0.02	0.669 ± 0.03	0.778 ± 0.03	0.722 ± 0.01	0.774 ± 0.02
NNET_Baysglm	0.721 ± 0.02	0.723 ± 0.03	0.720 ± 0.02	0.719 ± 0.02	0.721 ± 0.04	0.720 ± 0.02	0.793 ± 0.02



**Supplementary Table 4.6: Performance of the Feature Selection Methods and Machine Learning Approaches on the Test Dataset Utilizing Clinical, Imaging, and Biological Features. (Cont.)**

Model	Accuracy	Precision_ TMJ OA	Precision_ Control	Recall_ TMJ OA	Recall_ Control	F1score	AUC
Glmboost_NNET	0.720 ± 0.01	0.719 ± 0.01	0.721 ± 0.02	0.721 ± 0.04	0.719 ± 0.02	0.720 ± 0.01	0.780 ± 0.03
Lightgbm_Naivebayes	0.720 ± 0.02	0.714 ± 0.03	0.728 ± 0.02	0.736 ± 0.03	0.704 ± 0.04	0.719 ± 0.02	0.773 ± 0.01
Glmnet_LDA	0.720 ± 0.02	0.741 ± 0.02	0.702 ± 0.02	0.677 ± 0.02	0.760 ± 0.02	0.719 ± 0.02	0.771 ± 0.02
Glmboost_Glmnet	0.719 ± 0.01	0.729 ± 0.01	0.710 ± 0.02	0.696 ± 0.03	0.741 ± 0.02	0.718 ± 0.01	0.788 ± 0.01
AUC_Baysglm	0.717 ± 0.02	0.721 ± 0.02	0.714 ± 0.02	0.709 ± 0.02	0.726 ± 0.02	0.717 ± 0.02	0.800 ± 0.02
RF_Glmnet	0.717 ± 0.02	0.723 ± 0.02	0.712 ± 0.02	0.704 ± 0.03	0.731 ± 0.02	0.717 ± 0.02	0.794 ± 0.02
XgbTree_NNET	0.717 ± 0.02	0.712 ± 0.04	0.726 ± 0.01	0.736 ± 0.02	0.699 ± 0.06	0.717 ± 0.02	0.782 ± 0.02
XgbTree_LDA	0.716 ± 0.03	0.741 ± 0.04	0.696 ± 0.03	0.667 ± 0.03	0.765 ± 0.05	0.715 ± 0.03	0.792 ± 0.02
Glmnet_Glmnet	0.712 ± 0.02	0.719 ± 0.02	0.706 ± 0.02	0.696 ± 0.03	0.728 ± 0.02	0.712 ± 0.02	0.787 ± 0.01
Glmnet_Naivebayes	0.715 ± 0.03	0.764 ± 0.04	0.682 ± 0.03	0.622 ± 0.05	0.807 ± 0.03	0.712 ± 0.03	0.787 ± 0.03
NNET_Naivebayes	0.712 ± 0.02	0.723 ± 0.03	0.705 ± 0.03	0.691 ± 0.05	0.733 ± 0.05	0.712 ± 0.02	0.782 ± 0.02
Lightgbm_LDA	0.712 ± 0.03	0.741 ± 0.04	0.690 ± 0.02	0.654 ± 0.02	0.770 ± 0.05	0.711 ± 0.03	0.791 ± 0.02
XgbTree_Baysglm	0.710 ± 0.03	0.713 ± 0.03	0.707 ± 0.03	0.704 ± 0.03	0.716 ± 0.04	0.710 ± 0.03	0.793 ± 0.02
RF_LDA	0.709 ± 0.01	0.722 ± 0.01	0.698 ± 0.02	0.679 ± 0.03	0.738 ± 0.02	0.708 ± 0.01	0.776 ± 0.02
Glmnet_Baysglm	0.709 ± 0.02	0.711 ± 0.02	0.707 ± 0.01	0.704 ± 0.02	0.711 ± 0.02	0.708 ± 0.02	0.786 ± 0.02
NNET_HDDA	0.707 ± 0.02	0.717 ± 0.02	0.699 ± 0.02	0.686 ± 0.03	0.728 ± 0.02	0.707 ± 0.02	0.769 ± 0.03
Glmnet_SVMlinear	0.707 ± 0.01	0.720 ± 0.01	0.696 ± 0.01	0.679 ± 0.02	0.736 ± 0.02	0.707 ± 0.01	0.771 ± 0.01
Glmboost_LDA	0.707 ± 0.02	0.731 ± 0.02	0.688 ± 0.01	0.657 ± 0.02	0.756 ± 0.02	0.706 ± 0.02	0.773 ± 0.03
Glmnet_HDDA	0.704 ± 0.00	0.723 ± 0.01	0.688 ± 0.01	0.662 ± 0.01	0.743 ± 0.02	0.703 ± 0.00	0.764 ± 0.02
Glmboost_SVMlinear	0.701 ± 0.03	0.711 ± 0.04	0.693 ± 0.03	0.681 ± 0.03	0.721 ± 0.05	0.701 ± 0.03	0.771 ± 0.03
RF_NNET	0.696 ± 0.04	0.699 ± 0.04	0.694 ± 0.05	0.689 ± 0.05	0.704 ± 0.04	0.696 ± 0.04	0.744 ± 0.02
Glmboost_HDDA	0.695 ± 0.03	0.711 ± 0.04	0.682 ± 0.03	0.659 ± 0.02	0.731 ± 0.04	0.695 ± 0.03	0.761 ± 0.03
Glmboost_Baysglm	0.694 ± 0.02	0.696 ± 0.03	0.692 ± 0.02	0.689 ± 0.03	0.699 ± 0.04	0.694 ± 0.02	0.775 ± 0.02
AUC_Naivebayes	0.694 ± 0.03	0.706 ± 0.03	0.684 ± 0.02	0.667 ± 0.02	0.721 ± 0.04	0.694 ± 0.03	0.736 ± 0.02
XgbTree_Naivebayes	0.693 ± 0.02	0.684 ± 0.01	0.704 ± 0.03	0.716 ± 0.05	0.669 ± 0.02	0.692 ± 0.02	0.750 ± 0.02
XgbTree_HDDA	0.686 ± 0.02	0.687 ± 0.02	0.687 ± 0.02	0.686 ± 0.03	0.686 ± 0.02	0.686 ± 0.02	0.756 ± 0.02
AUC_HDDA	0.686 ± 0.01	0.687 ± 0.01	0.687 ± 0.01	0.686 ± 0.03	0.686 ± 0.03	0.686 ± 0.01	0.760 ± 0.02
RF_HDDA	0.669 ± 0.02	0.652 ± 0.02	0.691 ± 0.03	0.723 ± 0.04	0.615 ± 0.02	0.668 ± 0.02	0.736 ± 0.02
RF_Naivebayes	0.664 ± 0.02	0.640 ± 0.02	0.699 ± 0.02	0.751 ± 0.02	0.578 ± 0.03	0.662 ± 0.02	0.734 ± 0.02

\*RF, Random forest; XGBoost, Extreme gradient boosting; Lightgbm, Light gradient boosting machine; Glmnet, Generalized linear model with lasso and elastic net regularization; AUC, Area under the curve; Glmboost, Generalized linear model boosting; NNET, Neural network; Baysglm, Bayesian generalized linear model; SVM, Support vector machine; LDA, Linear discriminant analysis; HDDA, High-dimensional discriminant analysis.

**Supplementary Table 4.7: Performance of the Feature Selection Methods and Machine Learning Approaches on the Validation Dataset Utilizing Clinical and Imaging Features.**

Model	Evaluation Metrics	Accuracy	Precision_TMJ OA	Precision_Control	Recall_TMJ OA	Recall_Control	F1score	AUC
Lightgbm_SVMlinear		0.750 ± 0.00	0.782 ± 0.00	0.725 ± 0.00	0.693 ± 0.01	0.807 ± 0.00	0.749 ± 0.00	0.813 ± 0.00
Glmboost_Bayesglm		0.749 ± 0.00	0.771 ± 0.00	0.731 ± 0.01	0.710 ± 0.01	0.789 ± 0.01	0.749 ± 0.00	0.818 ± 0.01
Glmnet_SVMlinear		0.749 ± 0.01	0.776 ± 0.01	0.727 ± 0.01	0.701 ± 0.01	0.797 ± 0.01	0.748 ± 0.01	0.812 ± 0.01
Glmboost_SVMlinear		0.749 ± 0.00	0.778 ± 0.00	0.727 ± 0.00	0.698 ± 0.01	0.800 ± 0.00	0.748 ± 0.00	0.815 ± 0.01
Glmnet_Glmboost		0.749 ± 0.00	0.788 ± 0.01	0.720 ± 0.00	0.683 ± 0.01	0.816 ± 0.01	0.748 ± 0.00	0.811 ± 0.00
AUC_SVMlinear		0.748 ± 0.01	0.777 ± 0.02	0.726 ± 0.00	0.698 ± 0.00	0.799 ± 0.02	0.747 ± 0.01	0.807 ± 0.01
RF_Bayesglm		0.748 ± 0.01	0.774 ± 0.01	0.727 ± 0.01	0.700 ± 0.01	0.795 ± 0.01	0.747 ± 0.01	0.809 ± 0.00
Glmboost_Glmboost		0.748 ± 0.00	0.785 ± 0.01	0.720 ± 0.01	0.684 ± 0.01	0.812 ± 0.01	0.747 ± 0.01	0.807 ± 0.01
Glmnet_Bayesglm		0.747 ± 0.01	0.769 ± 0.01	0.729 ± 0.01	0.707 ± 0.01	0.787 ± 0.01	0.747 ± 0.01	0.817 ± 0.00
Lightgbm_LDA		0.748 ± 0.01	0.791 ± 0.00	0.716 ± 0.01	0.673 ± 0.01	0.822 ± 0.00	0.746 ± 0.01	0.814 ± 0.00
Lightgbm_Bayesglm		0.747 ± 0.01	0.775 ± 0.01	0.724 ± 0.01	0.695 ± 0.01	0.798 ± 0.01	0.746 ± 0.01	0.816 ± 0.01
AUC_Bayesglm		0.746 ± 0.01	0.765 ± 0.01	0.730 ± 0.01	0.711 ± 0.01	0.781 ± 0.01	0.746 ± 0.01	0.807 ± 0.01
Lightgbm_Glmnet		0.747 ± 0.01	0.777 ± 0.01	0.722 ± 0.01	0.692 ± 0.01	0.801 ± 0.01	0.746 ± 0.01	0.813 ± 0.01
Glmboost_LDA		0.747 ± 0.01	0.784 ± 0.01	0.719 ± 0.01	0.682 ± 0.01	0.812 ± 0.01	0.746 ± 0.01	0.814 ± 0.01
Glmnet_LDA		0.747 ± 0.00	0.785 ± 0.01	0.718 ± 0.00	0.681 ± 0.01	0.812 ± 0.01	0.745 ± 0.00	0.813 ± 0.00
RF_SVMlinear		0.746 ± 0.00	0.779 ± 0.00	0.720 ± 0.00	0.687 ± 0.01	0.805 ± 0.01	0.745 ± 0.00	0.805 ± 0.00
Glmnet_Glmnet		0.745 ± 0.00	0.771 ± 0.01	0.724 ± 0.01	0.698 ± 0.01	0.792 ± 0.01	0.745 ± 0.00	0.812 ± 0.00
RF_Glmboost		0.745 ± 0.01	0.789 ± 0.01	0.714 ± 0.01	0.671 ± 0.01	0.820 ± 0.01	0.744 ± 0.01	0.804 ± 0.00
RF_Glmnet		0.744 ± 0.00	0.775 ± 0.01	0.720 ± 0.01	0.689 ± 0.01	0.800 ± 0.01	0.744 ± 0.00	0.807 ± 0.01
Lightgbm_Glmboost		0.745 ± 0.00	0.790 ± 0.00	0.712 ± 0.01	0.668 ± 0.01	0.822 ± 0.00	0.743 ± 0.00	0.812 ± 0.00
AUC_Glmnet		0.744 ± 0.01	0.771 ± 0.01	0.722 ± 0.01	0.694 ± 0.01	0.794 ± 0.01	0.743 ± 0.01	0.800 ± 0.00
Glmboost_Glmnet		0.744 ± 0.01	0.771 ± 0.02	0.722 ± 0.01	0.695 ± 0.01	0.793 ± 0.02	0.743 ± 0.01	0.808 ± 0.01
AUC_Glmboost		0.743 ± 0.01	0.780 ± 0.01	0.715 ± 0.01	0.678 ± 0.01	0.808 ± 0.01	0.742 ± 0.01	0.799 ± 0.01
RF_LDA		0.742 ± 0.01	0.784 ± 0.01	0.711 ± 0.00	0.667 ± 0.01	0.816 ± 0.01	0.740 ± 0.01	0.806 ± 0.00
XgbTree_Glmnet		0.740 ± 0.00	0.777 ± 0.00	0.713 ± 0.00	0.675 ± 0.00	0.806 ± 0.00	0.739 ± 0.00	0.794 ± 0.01
Glmboost_NNET		0.739 ± 0.01	0.764 ± 0.01	0.720 ± 0.00	0.694 ± 0.01	0.784 ± 0.02	0.738 ± 0.01	0.791 ± 0.00
XgbTree_Glmboost		0.738 ± 0.00	0.783 ± 0.00	0.706 ± 0.00	0.659 ± 0.01	0.817 ± 0.01	0.736 ± 0.00	0.797 ± 0.01
XgbTree_SVMlinear		0.737 ± 0.01	0.773 ± 0.00	0.710 ± 0.01	0.672 ± 0.01	0.802 ± 0.00	0.736 ± 0.01	0.794 ± 0.01
Glmnet_NNET		0.736 ± 0.01	0.760 ± 0.01	0.717 ± 0.01	0.691 ± 0.02	0.781 ± 0.01	0.735 ± 0.01	0.778 ± 0.01
AUC_LDA		0.736 ± 0.01	0.773 ± 0.01	0.708 ± 0.01	0.669 ± 0.01	0.803 ± 0.01	0.735 ± 0.01	0.799 ± 0.01
Lightgbm_NNET		0.734 ± 0.01	0.754 ± 0.01	0.719 ± 0.00	0.698 ± 0.00	0.771 ± 0.01	0.734 ± 0.01	0.790 ± 0.01
XgbTree_Bayesglm		0.735 ± 0.01	0.761 ± 0.01	0.714 ± 0.00	0.685 ± 0.00	0.784 ± 0.01	0.734 ± 0.01	0.798 ± 0.01
XgbTree_LDA		0.735 ± 0.00	0.776 ± 0.00	0.704 ± 0.00	0.660 ± 0.00	0.810 ± 0.00	0.733 ± 0.00	0.797 ± 0.00
Lightgbm_Lightgbm		0.733 ± 0.01	0.747 ± 0.01	0.721 ± 0.01	0.705 ± 0.01	0.761 ± 0.01	0.733 ± 0.01	0.811 ± 0.01
Lightgbm_Naivebayes		0.734 ± 0.01	0.787 ± 0.01	0.698 ± 0.01	0.640 ± 0.03	0.827 ± 0.01	0.731 ± 0.01	0.816 ± 0.01
Glmnet_Naivebayes		0.733 ± 0.01	0.800 ± 0.01	0.692 ± 0.01	0.623 ± 0.02	0.844 ± 0.01	0.730 ± 0.01	0.800 ± 0.00
RF_NNET		0.730 ± 0.00	0.744 ± 0.01	0.719 ± 0.01	0.703 ± 0.01	0.757 ± 0.01	0.729 ± 0.00	0.777 ± 0.01
AUC_HDDA		0.731 ± 0.01	0.767 ± 0.01	0.704 ± 0.01	0.665 ± 0.01	0.797 ± 0.01	0.729 ± 0.01	0.776 ± 0.01
Glmboost_HDDA		0.728 ± 0.01	0.770 ± 0.02	0.699 ± 0.01	0.653 ± 0.01	0.803 ± 0.02	0.726 ± 0.01	0.799 ± 0.02
Lightgbm_XgbTree		0.725 ± 0.01	0.734 ± 0.01	0.718 ± 0.01	0.708 ± 0.01	0.743 ± 0.01	0.725 ± 0.01	0.799 ± 0.01
NNET_Bayesglm		0.725 ± 0.01	0.748 ± 0.01	0.706 ± 0.01	0.677 ± 0.02	0.772 ± 0.01	0.724 ± 0.01	0.786 ± 0.01
Glmboost_Naivebayes		0.727 ± 0.01	0.787 ± 0.01	0.690 ± 0.01	0.624 ± 0.02	0.830 ± 0.01	0.724 ± 0.01	0.798 ± 0.01
Glmnet_HDDA		0.726 ± 0.01	0.772 ± 0.01	0.695 ± 0.01	0.643 ± 0.01	0.809 ± 0.01	0.724 ± 0.01	0.800 ± 0.01
RF_Naivebayes		0.726 ± 0.01	0.775 ± 0.01	0.693 ± 0.01	0.637 ± 0.02	0.815 ± 0.00	0.723 ± 0.01	0.803 ± 0.00
NNET_Glmboost		0.725 ± 0.02	0.769 ± 0.02	0.693 ± 0.02	0.638 ± 0.03	0.810 ± 0.01	0.722 ± 0.02	0.781 ± 0.02
AUC_NNET		0.722 ± 0.00	0.735 ± 0.01	0.712 ± 0.00	0.695 ± 0.01	0.748 ± 0.01	0.721 ± 0.00	0.748 ± 0.00
Glmnet_Lightgbm		0.720 ± 0.01	0.733 ± 0.01	0.710 ± 0.01	0.695 ± 0.01	0.745 ± 0.01	0.720 ± 0.01	0.793 ± 0.01
XgbTree_Naivebayes		0.722 ± 0.02	0.767 ± 0.02	0.691 ± 0.01	0.639 ± 0.02	0.805 ± 0.02	0.720 ± 0.02	0.792 ± 0.01

**Supplementary Table 4.7: Performance of the Feature Selection Methods and Machine Learning Approaches on the Validation Dataset Utilizing Clinical and Imaging Features. (Cont.)**

Model	Accuracy	Precision_ TMJ OA	Precision_ Control	Recall_ TMJ OA	Recall_ Control	F1score	AUC
Glmboost_Lightgbm	0.719 ± 0.01	0.732 ± 0.01	0.709 ± 0.01	0.693 ± 0.01	0.744 ± 0.01	0.718 ± 0.00	0.789 ± 0.01
RF_Lightgbm	0.718 ± 0.01	0.726 ± 0.01	0.713 ± 0.01	0.704 ± 0.01	0.732 ± 0.02	0.718 ± 0.01	0.794 ± 0.01
XgbTree_XgbTree	0.717 ± 0.01	0.725 ± 0.01	0.711 ± 0.01	0.702 ± 0.01	0.733 ± 0.01	0.717 ± 0.01	0.784 ± 0.01
Glmboost_XgbTree	0.717 ± 0.01	0.727 ± 0.01	0.709 ± 0.01	0.697 ± 0.01	0.737 ± 0.01	0.717 ± 0.01	0.779 ± 0.01
NNET_LDA	0.718 ± 0.01	0.751 ± 0.01	0.694 ± 0.01	0.655 ± 0.01	0.782 ± 0.01	0.717 ± 0.01	0.777 ± 0.01
XgbTree>NNET	0.717 ± 0.00	0.731 ± 0.01	0.706 ± 0.00	0.689 ± 0.01	0.745 ± 0.01	0.716 ± 0.00	0.763 ± 0.01
NNET_Glmnet	0.718 ± 0.00	0.750 ± 0.00	0.694 ± 0.00	0.649 ± 0.01	0.787 ± 0.01	0.716 ± 0.00	0.765 ± 0.01
AUC_Lightgbm	0.716 ± 0.01	0.726 ± 0.01	0.708 ± 0.01	0.695 ± 0.02	0.737 ± 0.01	0.716 ± 0.01	0.783 ± 0.01
XgbTree_HDDA	0.718 ± 0.01	0.768 ± 0.01	0.685 ± 0.01	0.626 ± 0.01	0.809 ± 0.01	0.715 ± 0.01	0.777 ± 0.01
RF_XgbTree	0.714 ± 0.01	0.722 ± 0.01	0.708 ± 0.01	0.698 ± 0.02	0.731 ± 0.02	0.714 ± 0.01	0.780 ± 0.01
NNET_SVMlinear	0.715 ± 0.02	0.743 ± 0.02	0.694 ± 0.02	0.654 ± 0.03	0.776 ± 0.01	0.713 ± 0.02	0.766 ± 0.03
XgbTree_Lightgbm	0.713 ± 0.01	0.721 ± 0.01	0.706 ± 0.01	0.696 ± 0.01	0.729 ± 0.01	0.713 ± 0.01	0.783 ± 0.01
AUC_XgbTree	0.708 ± 0.01	0.715 ± 0.01	0.701 ± 0.01	0.692 ± 0.01	0.723 ± 0.01	0.707 ± 0.01	0.768 ± 0.01
AUC_Naivebayes	0.712 ± 0.00	0.776 ± 0.00	0.673 ± 0.01	0.595 ± 0.01	0.829 ± 0.00	0.707 ± 0.00	0.789 ± 0.00
RF_RF	0.707 ± 0.01	0.706 ± 0.02	0.708 ± 0.01	0.710 ± 0.01	0.701 ± 0.02	0.706 ± 0.01	0.782 ± 0.01
Glmnet_XgbTree	0.705 ± 0.01	0.715 ± 0.01	0.696 ± 0.01	0.682 ± 0.01	0.728 ± 0.01	0.705 ± 0.01	0.776 ± 0.01
RF_HDDA	0.708 ± 0.01	0.768 ± 0.01	0.672 ± 0.01	0.598 ± 0.01	0.819 ± 0.01	0.704 ± 0.01	0.786 ± 0.01
NNET_Lightgbm	0.704 ± 0.02	0.710 ± 0.02	0.702 ± 0.01	0.695 ± 0.02	0.714 ± 0.03	0.704 ± 0.02	0.775 ± 0.01
Glmboost_RF	0.704 ± 0.00	0.704 ± 0.01	0.704 ± 0.00	0.704 ± 0.01	0.700 ± 0.01	0.703 ± 0.00	0.780 ± 0.01
Lightgbm_HDDA	0.708 ± 0.01	0.787 ± 0.01	0.665 ± 0.01	0.571 ± 0.02	0.845 ± 0.01	0.702 ± 0.01	0.802 ± 0.01
Lightgbm_RF	0.702 ± 0.01	0.702 ± 0.01	0.703 ± 0.01	0.704 ± 0.01	0.698 ± 0.02	0.701 ± 0.01	0.783 ± 0.01
Glmnet_RF	0.702 ± 0.01	0.703 ± 0.01	0.702 ± 0.00	0.701 ± 0.01	0.700 ± 0.01	0.701 ± 0.01	0.775 ± 0.01
XgbTree_RF	0.701 ± 0.00	0.705 ± 0.01	0.699 ± 0.00	0.694 ± 0.01	0.707 ± 0.01	0.701 ± 0.01	0.773 ± 0.01
NNET_HDDA	0.704 ± 0.01	0.748 ± 0.02	0.676 ± 0.01	0.616 ± 0.02	0.792 ± 0.02	0.700 ± 0.01	0.748 ± 0.01
AUC_RF	0.697 ± 0.01	0.698 ± 0.01	0.697 ± 0.01	0.695 ± 0.01	0.696 ± 0.02	0.696 ± 0.01	0.765 ± 0.00
NNET_XgbTree	0.675 ± 0.02	0.682 ± 0.02	0.670 ± 0.02	0.657 ± 0.02	0.694 ± 0.02	0.675 ± 0.02	0.732 ± 0.02
NNET_RF	0.675 ± 0.02	0.678 ± 0.02	0.673 ± 0.02	0.664 ± 0.03	0.681 ± 0.02	0.673 ± 0.02	0.731 ± 0.02
NNET_Naivebayes	0.672 ± 0.03	0.735 ± 0.03	0.637 ± 0.02	0.534 ± 0.04	0.810 ± 0.02	0.665 ± 0.03	0.718 ± 0.03
NNET>NNET	0.669 ± 0.03	0.691 ± 0.02	0.657 ± 0.04	0.601 ± 0.07	0.736 ± 0.01	0.664 ± 0.03	0.694 ± 0.04

\*RF, Random forest; XGBoost, Extreme gradient boosting; Lightgbm, Light gradient boosting machine; Glmnet, Generalized linear model with lasso and elastic net regularization; AUC, Area under the curve; Glmboost, Generalized linear model boosting; NNET, Neural network; Baysglm, Bayesian generalized linear model; SVM, Support vector machine; LDA, Linear discriminant analysis; HDDA, High-dimensional discriminant analysis.

**Supplementary Table 4.8: Performance of the Feature Selection Methods and Machine Learning Approaches on the Test Dataset Utilizing Clinical and Imaging Features.**

Models	Accuracy	Precision_ TMJ OA	Precision_ Control	Recall_ TMJ OA	Recall_ Control	F1score	AUC
AUC_SVMlinear	0.756 ± 0.00	0.779 ± 0.01	0.736 ± 0.01	0.714 ± 0.02	0.798 ± 0.02	0.755 ± 0.00	0.799 ± 0.02
AUC_Glmnet	0.749 ± 0.02	0.779 ± 0.02	0.725 ± 0.02	0.696 ± 0.02	0.802 ± 0.02	0.749 ± 0.02	0.792 ± 0.01
AUC_Bayesglm	0.748 ± 0.01	0.767 ± 0.02	0.732 ± 0.01	0.714 ± 0.01	0.783 ± 0.02	0.748 ± 0.01	0.795 ± 0.01
RF_Glmboost	0.742 ± 0.01	0.785 ± 0.01	0.710 ± 0.01	0.667 ± 0.02	0.817 ± 0.02	0.740 ± 0.01	0.790 ± 0.01
RF_Glmnet	0.740 ± 0.02	0.773 ± 0.03	0.714 ± 0.02	0.679 ± 0.02	0.800 ± 0.03	0.739 ± 0.02	0.779 ± 0.01
AUC_Glmboost	0.740 ± 0.01	0.776 ± 0.00	0.712 ± 0.01	0.674 ± 0.01	0.805 ± 0.01	0.738 ± 0.01	0.786 ± 0.02
Lightgbm_SVMlinear	0.738 ± 0.01	0.763 ± 0.01	0.718 ± 0.01	0.691 ± 0.02	0.785 ± 0.02	0.738 ± 0.01	0.799 ± 0.01
Lightgbm_Glmboost	0.738 ± 0.01	0.784 ± 0.02	0.706 ± 0.00	0.659 ± 0.01	0.817 ± 0.02	0.737 ± 0.01	0.796 ± 0.02
Lightgbm_Bayesglm	0.736 ± 0.01	0.762 ± 0.02	0.715 ± 0.02	0.686 ± 0.02	0.785 ± 0.02	0.735 ± 0.01	0.797 ± 0.01
Lightgbm_NNET	0.733 ± 0.02	0.753 ± 0.02	0.717 ± 0.01	0.696 ± 0.02	0.770 ± 0.03	0.733 ± 0.02	0.769 ± 0.02
Lightgbm_Glmnet	0.733 ± 0.01	0.762 ± 0.02	0.710 ± 0.01	0.679 ± 0.01	0.788 ± 0.02	0.733 ± 0.01	0.802 ± 0.02
AUC_LDA	0.733 ± 0.02	0.767 ± 0.03	0.708 ± 0.02	0.672 ± 0.02	0.795 ± 0.03	0.732 ± 0.02	0.787 ± 0.01
RF_Bayesglm	0.732 ± 0.01	0.757 ± 0.01	0.712 ± 0.01	0.684 ± 0.01	0.780 ± 0.02	0.731 ± 0.01	0.788 ± 0.02
XgbTree_Glmboost	0.731 ± 0.01	0.766 ± 0.03	0.705 ± 0.01	0.667 ± 0.02	0.795 ± 0.03	0.730 ± 0.01	0.779 ± 0.01
Glmnet_Glmnet	0.730 ± 0.01	0.758 ± 0.01	0.707 ± 0.02	0.674 ± 0.03	0.785 ± 0.01	0.729 ± 0.01	0.778 ± 0.02
Lightgbm_LDA	0.728 ± 0.01	0.773 ± 0.01	0.697 ± 0.01	0.647 ± 0.02	0.810 ± 0.01	0.727 ± 0.01	0.797 ± 0.01
AUC_Lightgbm	0.726 ± 0.02	0.738 ± 0.04	0.716 ± 0.01	0.704 ± 0.01	0.746 ± 0.05	0.725 ± 0.02	0.788 ± 0.02
RF_SVMlinear	0.723 ± 0.01	0.753 ± 0.02	0.701 ± 0.01	0.667 ± 0.01	0.780 ± 0.03	0.723 ± 0.01	0.785 ± 0.01
XgbTree_Glmnet	0.721 ± 0.01	0.751 ± 0.01	0.698 ± 0.01	0.662 ± 0.01	0.780 ± 0.02	0.720 ± 0.01	0.783 ± 0.01
Glmboost_Glmboost	0.721 ± 0.01	0.757 ± 0.01	0.694 ± 0.01	0.652 ± 0.01	0.790 ± 0.02	0.720 ± 0.01	0.768 ± 0.02
Glmnet_Glmboost	0.721 ± 0.02	0.758 ± 0.02	0.694 ± 0.02	0.649 ± 0.03	0.793 ± 0.02	0.719 ± 0.02	0.778 ± 0.01
RF_LDA	0.721 ± 0.01	0.761 ± 0.02	0.692 ± 0.01	0.644 ± 0.02	0.798 ± 0.02	0.719 ± 0.01	0.784 ± 0.01
Lightgbm_Naivebayes	0.721 ± 0.03	0.761 ± 0.02	0.692 ± 0.03	0.644 ± 0.04	0.798 ± 0.02	0.719 ± 0.03	0.787 ± 0.02
NNET_Glmboost	0.721 ± 0.03	0.763 ± 0.03	0.691 ± 0.04	0.640 ± 0.06	0.802 ± 0.02	0.719 ± 0.04	0.773 ± 0.03
XgbTree_SVMlinear	0.720 ± 0.02	0.755 ± 0.03	0.694 ± 0.02	0.652 ± 0.03	0.788 ± 0.03	0.718 ± 0.02	0.761 ± 0.02
Glmnet_NNET	0.719 ± 0.02	0.736 ± 0.02	0.704 ± 0.02	0.681 ± 0.02	0.756 ± 0.02	0.718 ± 0.02	0.754 ± 0.01
Glmboost_Glmnet	0.719 ± 0.02	0.744 ± 0.02	0.698 ± 0.02	0.667 ± 0.02	0.770 ± 0.03	0.718 ± 0.02	0.762 ± 0.01
XgbTree_LDA	0.719 ± 0.01	0.756 ± 0.03	0.691 ± 0.00	0.647 ± 0.01	0.790 ± 0.03	0.717 ± 0.01	0.766 ± 0.01
Glmnet_Bayesglm	0.717 ± 0.02	0.738 ± 0.02	0.700 ± 0.02	0.674 ± 0.03	0.760 ± 0.02	0.717 ± 0.02	0.774 ± 0.02
AUC_HDDA	0.717 ± 0.02	0.752 ± 0.02	0.691 ± 0.02	0.649 ± 0.03	0.785 ± 0.02	0.716 ± 0.02	0.746 ± 0.01
RF_NNET	0.716 ± 0.01	0.729 ± 0.01	0.705 ± 0.02	0.689 ± 0.03	0.743 ± 0.02	0.716 ± 0.01	0.761 ± 0.01
Glmnet_SVMlinear	0.716 ± 0.02	0.737 ± 0.02	0.699 ± 0.02	0.672 ± 0.03	0.760 ± 0.01	0.715 ± 0.02	0.763 ± 0.01
Glmboost_LDA	0.716 ± 0.01	0.746 ± 0.02	0.693 ± 0.01	0.657 ± 0.02	0.775 ± 0.03	0.715 ± 0.01	0.762 ± 0.01
Glmnet_Lightgbm	0.715 ± 0.03	0.727 ± 0.03	0.704 ± 0.03	0.689 ± 0.03	0.741 ± 0.04	0.715 ± 0.03	0.789 ± 0.01
NNET_Bayesglm	0.715 ± 0.03	0.732 ± 0.03	0.701 ± 0.04	0.677 ± 0.05	0.753 ± 0.03	0.714 ± 0.03	0.767 ± 0.03
XgbTree_Bayesglm	0.715 ± 0.02	0.742 ± 0.04	0.694 ± 0.02	0.662 ± 0.03	0.768 ± 0.05	0.714 ± 0.02	0.764 ± 0.01
AUC_NNET	0.714 ± 0.01	0.733 ± 0.02	0.697 ± 0.01	0.672 ± 0.01	0.756 ± 0.02	0.713 ± 0.01	0.741 ± 0.01
Glmnet_Naivebayes	0.716 ± 0.02	0.779 ± 0.03	0.677 ± 0.01	0.605 ± 0.01	0.827 ± 0.03	0.713 ± 0.02	0.773 ± 0.01
RF_Lightgbm	0.712 ± 0.02	0.725 ± 0.03	0.702 ± 0.02	0.686 ± 0.01	0.738 ± 0.04	0.712 ± 0.02	0.781 ± 0.02
NNET_Lightgbm	0.711 ± 0.03	0.707 ± 0.03	0.715 ± 0.03	0.721 ± 0.03	0.701 ± 0.03	0.711 ± 0.03	0.772 ± 0.02
XgbTree_Lightgbm	0.711 ± 0.02	0.723 ± 0.02	0.701 ± 0.01	0.686 ± 0.01	0.736 ± 0.03	0.711 ± 0.02	0.775 ± 0.02
Lightgbm_Lightgbm	0.711 ± 0.03	0.724 ± 0.04	0.701 ± 0.02	0.686 ± 0.02	0.736 ± 0.05	0.711 ± 0.03	0.796 ± 0.03
NNET_Glmnet	0.711 ± 0.02	0.741 ± 0.02	0.688 ± 0.02	0.649 ± 0.04	0.773 ± 0.02	0.710 ± 0.02	0.751 ± 0.03
XgbTree_NNET	0.707 ± 0.01	0.722 ± 0.02	0.695 ± 0.01	0.677 ± 0.02	0.738 ± 0.03	0.707 ± 0.01	0.752 ± 0.03
RF_HDDA	0.711 ± 0.01	0.778 ± 0.03	0.671 ± 0.01	0.593 ± 0.02	0.830 ± 0.03	0.707 ± 0.01	0.748 ± 0.02
Glmnet_LDA	0.707 ± 0.02	0.739 ± 0.03	0.683 ± 0.02	0.642 ± 0.02	0.773 ± 0.03	0.706 ± 0.02	0.767 ± 0.01
AUC_XgbTree	0.706 ± 0.01	0.714 ± 0.02	0.700 ± 0.01	0.691 ± 0.02	0.721 ± 0.04	0.706 ± 0.01	0.772 ± 0.01
XgbTree_HDDA	0.707 ± 0.02	0.742 ± 0.02	0.682 ± 0.02	0.635 ± 0.04	0.780 ± 0.01	0.706 ± 0.02	0.738 ± 0.02

**Supplementary Table 4.8: Performance of the Feature Selection Methods and Machine Learning Approaches on the Test Dataset Utilizing Clinical and Imaging Features. (Cont.)**

Model	Evaluation Metrics	Accuracy	Precision_TMJ OA	Precision_Control	Recall_TMJ OA	Recall_Control	F1score	AUC
Glmboost_Bayesglm		0.706 ± 0.02	0.725 ± 0.02	0.691 ± 0.02	0.664 ± 0.03	0.748 ± 0.02	0.706 ± 0.02	0.765 ± 0.01
Glmboost_Lightgbm		0.705 ± 0.02	0.715 ± 0.03	0.697 ± 0.02	0.684 ± 0.02	0.726 ± 0.04	0.705 ± 0.02	0.777 ± 0.02
Lightgbm_XgbTree		0.704 ± 0.01	0.717 ± 0.01	0.692 ± 0.01	0.674 ± 0.01	0.733 ± 0.01	0.703 ± 0.01	0.761 ± 0.02
Glmboost_NNET		0.702 ± 0.01	0.722 ± 0.01	0.687 ± 0.02	0.659 ± 0.03	0.746 ± 0.01	0.702 ± 0.01	0.751 ± 0.03
AUC_Naivebayes		0.706 ± 0.02	0.772 ± 0.02	0.666 ± 0.01	0.585 ± 0.02	0.827 ± 0.02	0.702 ± 0.02	0.765 ± 0.02
Glmnet_HDDA		0.705 ± 0.02	0.758 ± 0.03	0.671 ± 0.02	0.605 ± 0.03	0.805 ± 0.04	0.702 ± 0.02	0.754 ± 0.02
Glmboost_SVMlinear		0.700 ± 0.03	0.722 ± 0.02	0.682 ± 0.03	0.649 ± 0.04	0.751 ± 0.02	0.699 ± 0.03	0.749 ± 0.02
Glmboost_Naivebayes		0.696 ± 0.02	0.752 ± 0.04	0.661 ± 0.02	0.588 ± 0.03	0.805 ± 0.04	0.692 ± 0.02	0.761 ± 0.02
NNET_LDA		0.694 ± 0.02	0.725 ± 0.02	0.671 ± 0.02	0.625 ± 0.03	0.763 ± 0.01	0.692 ± 0.02	0.745 ± 0.02
RF_Naivebayes		0.693 ± 0.01	0.737 ± 0.03	0.663 ± 0.01	0.600 ± 0.03	0.785 ± 0.03	0.690 ± 0.01	0.736 ± 0.02
AUC_RF		0.689 ± 0.02	0.688 ± 0.02	0.690 ± 0.02	0.691 ± 0.02	0.684 ± 0.03	0.688 ± 0.02	0.748 ± 0.01
Glmnet_XgbTree		0.688 ± 0.02	0.701 ± 0.02	0.677 ± 0.03	0.654 ± 0.04	0.721 ± 0.02	0.687 ± 0.03	0.760 ± 0.01
XgbTree_Naivebayes		0.686 ± 0.02	0.724 ± 0.02	0.660 ± 0.02	0.602 ± 0.04	0.770 ± 0.02	0.684 ± 0.02	0.744 ± 0.02
Lightgbm_HDDA		0.690 ± 0.02	0.773 ± 0.03	0.646 ± 0.02	0.538 ± 0.03	0.842 ± 0.02	0.683 ± 0.02	0.773 ± 0.02
Glmboost_RF		0.684 ± 0.02	0.688 ± 0.02	0.681 ± 0.02	0.674 ± 0.03	0.689 ± 0.03	0.683 ± 0.02	0.747 ± 0.02
Glmboost_XgbTree		0.683 ± 0.01	0.693 ± 0.02	0.674 ± 0.02	0.657 ± 0.03	0.709 ± 0.03	0.682 ± 0.01	0.760 ± 0.02
NNET_SVMlinear		0.684 ± 0.04	0.713 ± 0.04	0.662 ± 0.04	0.615 ± 0.05	0.751 ± 0.03	0.682 ± 0.04	0.733 ± 0.03
Glmboost_HDDA		0.684 ± 0.02	0.723 ± 0.02	0.657 ± 0.01	0.598 ± 0.03	0.770 ± 0.03	0.681 ± 0.02	0.730 ± 0.02
Lightgbm_RF		0.683 ± 0.03	0.681 ± 0.03	0.685 ± 0.03	0.689 ± 0.04	0.672 ± 0.04	0.681 ± 0.03	0.754 ± 0.02
XgbTree_RF		0.680 ± 0.02	0.688 ± 0.02	0.673 ± 0.02	0.659 ± 0.02	0.701 ± 0.03	0.680 ± 0.02	0.734 ± 0.03
NNET_HDDA		0.680 ± 0.04	0.720 ± 0.04	0.653 ± 0.04	0.588 ± 0.07	0.773 ± 0.03	0.677 ± 0.04	0.717 ± 0.04
RF_XgbTree		0.677 ± 0.02	0.686 ± 0.02	0.668 ± 0.01	0.652 ± 0.02	0.701 ± 0.02	0.676 ± 0.02	0.741 ± 0.02
Glmnet_RF		0.675 ± 0.01	0.671 ± 0.01	0.680 ± 0.02	0.686 ± 0.04	0.657 ± 0.01	0.673 ± 0.01	0.739 ± 0.01
XgbTree_XgbTree		0.667 ± 0.02	0.668 ± 0.02	0.666 ± 0.02	0.664 ± 0.03	0.669 ± 0.03	0.666 ± 0.02	0.734 ± 0.03
RF_RF		0.663 ± 0.02	0.667 ± 0.02	0.660 ± 0.02	0.652 ± 0.03	0.672 ± 0.02	0.662 ± 0.02	0.726 ± 0.02
NNET_XgbTree		0.653 ± 0.04	0.652 ± 0.04	0.654 ± 0.04	0.657 ± 0.04	0.649 ± 0.05	0.653 ± 0.04	0.712 ± 0.05
NNET_RF		0.647 ± 0.03	0.649 ± 0.03	0.645 ± 0.03	0.640 ± 0.03	0.652 ± 0.03	0.646 ± 0.03	0.717 ± 0.04
NNET_Naivebayes		0.649 ± 0.02	0.695 ± 0.03	0.621 ± 0.02	0.533 ± 0.02	0.765 ± 0.03	0.645 ± 0.02	0.706 ± 0.04
NNET_NNET		0.646 ± 0.02	0.679 ± 0.02	0.624 ± 0.03	0.553 ± 0.07	0.738 ± 0.03	0.642 ± 0.03	0.710 ± 0.02

\*RF, Random forest; XGBoost, Extreme gradient boosting; Lightgbm, Light gradient boosting machine; Glmnet, Generalized linear model with lasso and elastic net regularization; AUC, Area under the curve; Glmboost, Generalized linear model boosting; NNET, Neural network; Baysglm, Bayesian generalized linear model; SVM, Support vector machine; LDA, Linear discriminant analysis; HDDA, High-dimensional discriminant analysis.

**Supplementary Table 4.9: Performance of the Feature Selection Methods and Machine Learning Approaches on the Validation Dataset Utilizing Clinical and Biological Features.**

Model	Accuracy	Precision_ TMJ OA	Precision_ Control	Recall_ TMJ OA	Recall_ Control	F1score	AUC
XgbTree_XgbTree	0.813 ± 0.00	0.818 ± 0.01	0.810 ± 0.00	0.807 ± 0.00	0.819 ± 0.01	0.813 ± 0.00	0.898 ± 0.01
Lightgbm_XgbTree	0.812 ± 0.01	0.817 ± 0.01	0.809 ± 0.01	0.806 ± 0.01	0.818 ± 0.02	0.812 ± 0.01	0.900 ± 0.01
XgbTree_RF	0.805 ± 0.00	0.821 ± 0.01	0.791 ± 0.01	0.780 ± 0.01	0.827 ± 0.01	0.804 ± 0.00	0.899 ± 0.00
Lightgbm_RF	0.802 ± 0.01	0.814 ± 0.01	0.793 ± 0.01	0.785 ± 0.01	0.818 ± 0.01	0.802 ± 0.01	0.901 ± 0.00
RF_RF	0.802 ± 0.00	0.815 ± 0.00	0.791 ± 0.00	0.782 ± 0.00	0.818 ± 0.01	0.801 ± 0.00	0.900 ± 0.01
Glmboost_XgbTree	0.798 ± 0.01	0.807 ± 0.01	0.791 ± 0.01	0.785 ± 0.01	0.811 ± 0.01	0.798 ± 0.01	0.879 ± 0.01
AUC_XgbTree	0.797 ± 0.01	0.804 ± 0.01	0.792 ± 0.01	0.788 ± 0.01	0.807 ± 0.01	0.797 ± 0.01	0.881 ± 0.00
Glmnet_XgbTree	0.797 ± 0.01	0.806 ± 0.01	0.790 ± 0.01	0.785 ± 0.01	0.810 ± 0.01	0.797 ± 0.01	0.878 ± 0.01
AUC_RF	0.798 ± 0.01	0.810 ± 0.01	0.787 ± 0.01	0.778 ± 0.01	0.814 ± 0.01	0.797 ± 0.01	0.890 ± 0.00
Glmnet_RF	0.796 ± 0.01	0.814 ± 0.00	0.781 ± 0.01	0.768 ± 0.01	0.822 ± 0.00	0.795 ± 0.01	0.882 ± 0.00
Lightgbm_Lightgbm	0.795 ± 0.00	0.794 ± 0.01	0.796 ± 0.00	0.796 ± 0.01	0.793 ± 0.01	0.794 ± 0.00	0.883 ± 0.00
RF_XgbTree	0.792 ± 0.01	0.799 ± 0.02	0.787 ± 0.01	0.782 ± 0.01	0.802 ± 0.02	0.792 ± 0.01	0.882 ± 0.00
Glmboost_RF	0.788 ± 0.01	0.804 ± 0.01	0.775 ± 0.00	0.763 ± 0.01	0.811 ± 0.01	0.787 ± 0.01	0.877 ± 0.00
XgbTree_Lightgbm	0.785 ± 0.01	0.787 ± 0.02	0.785 ± 0.01	0.784 ± 0.02	0.787 ± 0.02	0.785 ± 0.01	0.873 ± 0.01
NNET_XgbTree	0.783 ± 0.01	0.789 ± 0.01	0.777 ± 0.01	0.772 ± 0.01	0.793 ± 0.01	0.782 ± 0.01	0.863 ± 0.01
NNET_RF	0.781 ± 0.01	0.790 ± 0.00	0.773 ± 0.01	0.765 ± 0.01	0.793 ± 0.01	0.780 ± 0.01	0.873 ± 0.00
Glmboost_Lightgbm	0.775 ± 0.00	0.778 ± 0.01	0.772 ± 0.01	0.769 ± 0.01	0.780 ± 0.01	0.775 ± 0.00	0.858 ± 0.01
RF_Lightgbm	0.774 ± 0.01	0.773 ± 0.01	0.776 ± 0.01	0.778 ± 0.01	0.770 ± 0.02	0.774 ± 0.01	0.863 ± 0.01
AUC_Lightgbm	0.773 ± 0.01	0.776 ± 0.01	0.770 ± 0.01	0.768 ± 0.01	0.778 ± 0.01	0.773 ± 0.01	0.859 ± 0.01
Glmnet_Lightgbm	0.771 ± 0.01	0.773 ± 0.01	0.771 ± 0.01	0.769 ± 0.01	0.774 ± 0.02	0.771 ± 0.01	0.856 ± 0.01
Glmnet_SVMlinear	0.764 ± 0.00	0.765 ± 0.01	0.764 ± 0.01	0.763 ± 0.01	0.765 ± 0.01	0.763 ± 0.00	0.836 ± 0.00
NNET_Lightgbm	0.763 ± 0.01	0.766 ± 0.01	0.762 ± 0.02	0.759 ± 0.02	0.767 ± 0.02	0.763 ± 0.01	0.845 ± 0.01
Glmboost_SVMlinear	0.762 ± 0.01	0.765 ± 0.01	0.760 ± 0.01	0.756 ± 0.01	0.767 ± 0.01	0.762 ± 0.01	0.835 ± 0.00
Glmboost_Bayesglm	0.757 ± 0.01	0.762 ± 0.01	0.753 ± 0.01	0.748 ± 0.01	0.767 ± 0.01	0.757 ± 0.01	0.838 ± 0.00
Glmnet_Bayesglm	0.756 ± 0.01	0.757 ± 0.01	0.755 ± 0.01	0.755 ± 0.01	0.757 ± 0.01	0.756 ± 0.01	0.840 ± 0.00
Glmnet_LDA	0.753 ± 0.00	0.764 ± 0.00	0.744 ± 0.01	0.734 ± 0.01	0.773 ± 0.01	0.753 ± 0.00	0.833 ± 0.01
NNET_SVMlinear	0.752 ± 0.01	0.759 ± 0.00	0.747 ± 0.01	0.740 ± 0.02	0.765 ± 0.01	0.752 ± 0.01	0.820 ± 0.01
Glmboost_LDA	0.752 ± 0.00	0.768 ± 0.00	0.739 ± 0.01	0.723 ± 0.01	0.781 ± 0.01	0.752 ± 0.00	0.831 ± 0.00
Glmnet_Naivebayes	0.752 ± 0.01	0.771 ± 0.01	0.738 ± 0.01	0.719 ± 0.02	0.785 ± 0.01	0.751 ± 0.01	0.815 ± 0.01
Glmboost_Naivebayes	0.751 ± 0.01	0.762 ± 0.01	0.745 ± 0.01	0.735 ± 0.02	0.767 ± 0.02	0.750 ± 0.01	0.814 ± 0.01
NNET_Bayesglm	0.750 ± 0.01	0.752 ± 0.01	0.749 ± 0.01	0.747 ± 0.01	0.753 ± 0.01	0.750 ± 0.01	0.823 ± 0.01
Glmboost_Glmnet	0.746 ± 0.00	0.752 ± 0.00	0.740 ± 0.00	0.733 ± 0.01	0.759 ± 0.01	0.746 ± 0.00	0.825 ± 0.00
Glmnet_Glmnet	0.745 ± 0.01	0.751 ± 0.01	0.740 ± 0.01	0.734 ± 0.01	0.756 ± 0.01	0.745 ± 0.01	0.829 ± 0.00
Glmboost_NNET	0.745 ± 0.01	0.741 ± 0.01	0.751 ± 0.01	0.754 ± 0.01	0.735 ± 0.02	0.744 ± 0.01	0.805 ± 0.01
AUC_LDA	0.745 ± 0.01	0.764 ± 0.01	0.728 ± 0.01	0.709 ± 0.01	0.781 ± 0.01	0.744 ± 0.01	0.813 ± 0.01
Glmnet_Glmboost	0.744 ± 0.01	0.755 ± 0.01	0.736 ± 0.01	0.725 ± 0.01	0.764 ± 0.01	0.744 ± 0.01	0.820 ± 0.00
AUC_SVMlinear	0.744 ± 0.01	0.755 ± 0.01	0.735 ± 0.01	0.724 ± 0.01	0.765 ± 0.01	0.744 ± 0.01	0.817 ± 0.01
NNET_LDA	0.744 ± 0.00	0.756 ± 0.01	0.734 ± 0.01	0.723 ± 0.01	0.765 ± 0.01	0.744 ± 0.00	0.816 ± 0.01
Lightgbm_Naivebayes	0.744 ± 0.02	0.734 ± 0.02	0.761 ± 0.01	0.776 ± 0.01	0.713 ± 0.03	0.743 ± 0.02	0.820 ± 0.01
AUC_Bayesglm	0.742 ± 0.01	0.745 ± 0.01	0.740 ± 0.01	0.737 ± 0.01	0.747 ± 0.01	0.742 ± 0.01	0.812 ± 0.01
Glmboost_Glmboost	0.743 ± 0.00	0.753 ± 0.01	0.734 ± 0.01	0.722 ± 0.01	0.763 ± 0.01	0.742 ± 0.00	0.821 ± 0.00
AUC_Glmboost	0.741 ± 0.01	0.752 ± 0.01	0.731 ± 0.01	0.719 ± 0.01	0.763 ± 0.02	0.741 ± 0.01	0.812 ± 0.01
Lightgbm_SVMlinear	0.741 ± 0.01	0.753 ± 0.01	0.731 ± 0.01	0.718 ± 0.01	0.764 ± 0.01	0.741 ± 0.01	0.806 ± 0.01
XgbTree_NNET	0.740 ± 0.01	0.736 ± 0.01	0.747 ± 0.01	0.752 ± 0.01	0.729 ± 0.01	0.740 ± 0.01	0.797 ± 0.01
Lightgbm_NNET	0.740 ± 0.01	0.736 ± 0.01	0.745 ± 0.01	0.749 ± 0.01	0.731 ± 0.01	0.740 ± 0.01	0.795 ± 0.01
Glmnet_HDDA	0.740 ± 0.00	0.746 ± 0.01	0.736 ± 0.01	0.729 ± 0.02	0.750 ± 0.02	0.739 ± 0.00	0.814 ± 0.01
Glmnet_NNET	0.739 ± 0.00	0.738 ± 0.01	0.742 ± 0.01	0.744 ± 0.01	0.735 ± 0.01	0.739 ± 0.00	0.794 ± 0.00
NNET_NNET	0.740 ± 0.01	0.735 ± 0.01	0.747 ± 0.02	0.755 ± 0.02	0.725 ± 0.02	0.739 ± 0.01	0.772 ± 0.01

**Supplementary Table 4.9: Performance of the Feature Selection Methods and Machine Learning Approaches on the Validation Dataset Utilizing Clinical and Biological Features. (Cont.)**

Model	Accuracy	Precision_ TMJ OA	Precision_ Control	Recall_ TMJ OA	Recall_ Control	F1score	AUC
NNET_Glmnet	0.739 ± 0.00	0.748 ± 0.01	0.731 ± 0.01	0.721 ± 0.01	0.756 ± 0.01	0.738 ± 0.00	0.810 ± 0.01
RF_Bayesglm	0.739 ± 0.01	0.744 ± 0.01	0.734 ± 0.01	0.728 ± 0.01	0.749 ± 0.01	0.738 ± 0.01	0.805 ± 0.01
AUC_Glmnet	0.739 ± 0.01	0.748 ± 0.01	0.730 ± 0.01	0.720 ± 0.01	0.757 ± 0.01	0.738 ± 0.01	0.807 ± 0.00
AUC_NNET	0.738 ± 0.01	0.734 ± 0.01	0.744 ± 0.01	0.748 ± 0.01	0.728 ± 0.02	0.738 ± 0.01	0.788 ± 0.01
Lightgbm_Bayesglm	0.737 ± 0.01	0.743 ± 0.01	0.733 ± 0.01	0.726 ± 0.01	0.747 ± 0.01	0.737 ± 0.01	0.812 ± 0.00
XgbTree_Bayesglm	0.736 ± 0.01	0.744 ± 0.01	0.730 ± 0.01	0.720 ± 0.01	0.752 ± 0.01	0.736 ± 0.01	0.813 ± 0.00
RF_SVMlinear	0.736 ± 0.01	0.747 ± 0.01	0.726 ± 0.01	0.714 ± 0.01	0.757 ± 0.01	0.735 ± 0.01	0.793 ± 0.01
NNET_Glmboost	0.734 ± 0.01	0.748 ± 0.01	0.722 ± 0.01	0.706 ± 0.01	0.762 ± 0.01	0.733 ± 0.01	0.808 ± 0.01
Lightgbm_Glmboost	0.733 ± 0.00	0.743 ± 0.01	0.726 ± 0.00	0.715 ± 0.01	0.752 ± 0.01	0.733 ± 0.00	0.809 ± 0.00
AUC_Naivebayes	0.734 ± 0.01	0.761 ± 0.02	0.716 ± 0.00	0.689 ± 0.01	0.779 ± 0.02	0.733 ± 0.01	0.796 ± 0.00
Lightgbm_Glmnet	0.733 ± 0.00	0.744 ± 0.01	0.725 ± 0.01	0.713 ± 0.01	0.753 ± 0.01	0.733 ± 0.00	0.806 ± 0.00
XgbTree_SVMlinear	0.733 ± 0.00	0.746 ± 0.01	0.724 ± 0.01	0.710 ± 0.01	0.756 ± 0.01	0.733 ± 0.00	0.801 ± 0.00
RF_Glmboost	0.732 ± 0.01	0.741 ± 0.01	0.723 ± 0.01	0.712 ± 0.01	0.751 ± 0.01	0.731 ± 0.01	0.807 ± 0.00
XgbTree_LDA	0.731 ± 0.00	0.752 ± 0.00	0.714 ± 0.00	0.690 ± 0.01	0.772 ± 0.01	0.730 ± 0.00	0.809 ± 0.00
Lightgbm_LDA	0.731 ± 0.01	0.752 ± 0.01	0.714 ± 0.01	0.691 ± 0.01	0.771 ± 0.01	0.730 ± 0.01	0.806 ± 0.00
Glmboost_HDDA	0.730 ± 0.01	0.739 ± 0.01	0.724 ± 0.00	0.714 ± 0.01	0.747 ± 0.01	0.730 ± 0.01	0.799 ± 0.01
XgbTree_Glmboost	0.729 ± 0.01	0.742 ± 0.01	0.718 ± 0.01	0.703 ± 0.01	0.754 ± 0.01	0.728 ± 0.01	0.810 ± 0.00
RF_LDA	0.729 ± 0.01	0.745 ± 0.01	0.715 ± 0.01	0.697 ± 0.01	0.761 ± 0.00	0.728 ± 0.01	0.796 ± 0.01
XgbTree_Glmnet	0.727 ± 0.01	0.738 ± 0.01	0.717 ± 0.01	0.704 ± 0.01	0.750 ± 0.01	0.727 ± 0.01	0.803 ± 0.00
RF_Glmnet	0.725 ± 0.01	0.736 ± 0.01	0.716 ± 0.01	0.702 ± 0.01	0.748 ± 0.01	0.725 ± 0.01	0.799 ± 0.01
NNET_HDDA	0.726 ± 0.00	0.734 ± 0.01	0.726 ± 0.01	0.718 ± 0.01	0.734 ± 0.01	0.725 ± 0.00	0.792 ± 0.01
XgbTree_Naivebayes	0.722 ± 0.01	0.707 ± 0.01	0.745 ± 0.01	0.768 ± 0.01	0.676 ± 0.01	0.721 ± 0.01	0.796 ± 0.01
AUC_HDDA	0.715 ± 0.01	0.710 ± 0.02	0.725 ± 0.00	0.734 ± 0.01	0.696 ± 0.03	0.714 ± 0.01	0.772 ± 0.01
NNET_Naivebayes	0.714 ± 0.02	0.706 ± 0.03	0.734 ± 0.01	0.756 ± 0.03	0.672 ± 0.06	0.710 ± 0.02	0.784 ± 0.01
RF_NNET	0.709 ± 0.00	0.707 ± 0.01	0.713 ± 0.01	0.717 ± 0.01	0.702 ± 0.02	0.709 ± 0.00	0.769 ± 0.00
Lightgbm_HDDA	0.703 ± 0.01	0.691 ± 0.01	0.733 ± 0.01	0.755 ± 0.02	0.652 ± 0.03	0.700 ± 0.01	0.780 ± 0.00
RF_HDDA	0.699 ± 0.01	0.688 ± 0.00	0.722 ± 0.02	0.744 ± 0.03	0.655 ± 0.02	0.697 ± 0.01	0.766 ± 0.01
XgbTree_HDDA	0.698 ± 0.01	0.682 ± 0.02	0.733 ± 0.00	0.759 ± 0.02	0.638 ± 0.04	0.695 ± 0.01	0.773 ± 0.00
RF_Naivebayes	0.686 ± 0.01	0.664 ± 0.00	0.726 ± 0.01	0.777 ± 0.01	0.595 ± 0.01	0.681 ± 0.01	0.769 ± 0.01

\*RF, Random forest; XGBoost, Extreme gradient boosting; Lightgbm, Light gradient boosting machine; Glmnet, Generalized linear model with lasso and elastic net regularization; AUC, Area under the curve; Glmboost, Generalized linear model boosting; NNET, Neural network; Baysglm, Bayesian generalized linear model; SVM, Support vector machine; LDA, Linear discriminant analysis; HDDA, High-dimensional discriminant analysis.

**Supplementary Table 4.10: Performance of the Feature Selection Methods and Machine Learning Approaches on the Test Dataset Utilizing Clinical and Biological Features.**

Model	Accuracy	Precision_ TMJ OA	Precision_ Control	Recall_ TMJ OA	Recall_ Control	F1score	AUC
NNET_RF	0.788 ± 0.01	0.795 ± 0.02	0.781 ± 0.01	0.775 ± 0.02	0.795 ± 0.02	0.786 ± 0.01	0.875 ± 0.01
XgbTree_RF	0.786 ± 0.02	0.795 ± 0.02	0.779 ± 0.02	0.773 ± 0.02	0.798 ± 0.02	0.786 ± 0.02	0.881 ± 0.01
AUC_RF	0.784 ± 0.02	0.800 ± 0.03	0.770 ± 0.02	0.758 ± 0.02	0.810 ± 0.03	0.784 ± 0.02	0.889 ± 0.01
RF_RF	0.784 ± 0.01	0.792 ± 0.01	0.777 ± 0.02	0.770 ± 0.03	0.795 ± 0.01	0.783 ± 0.01	0.883 ± 0.01
Lightgbm_Lightgbm	0.783 ± 0.02	0.779 ± 0.02	0.788 ± 0.02	0.790 ± 0.03	0.775 ± 0.02	0.783 ± 0.02	0.850 ± 0.01
AUC_XgbTree	0.783 ± 0.02	0.793 ± 0.04	0.775 ± 0.02	0.768 ± 0.02	0.798 ± 0.05	0.783 ± 0.02	0.862 ± 0.02
XgbTree_XgbTree	0.781 ± 0.03	0.795 ± 0.04	0.771 ± 0.03	0.760 ± 0.04	0.802 ± 0.04	0.781 ± 0.03	0.866 ± 0.01
RF_XgbTree	0.779 ± 0.01	0.784 ± 0.02	0.775 ± 0.03	0.770 ± 0.04	0.788 ± 0.03	0.779 ± 0.01	0.869 ± 0.02
Lightgbm_RF	0.777 ± 0.01	0.787 ± 0.01	0.767 ± 0.01	0.758 ± 0.02	0.795 ± 0.01	0.776 ± 0.01	0.872 ± 0.01
Lightgbm_XgbTree	0.777 ± 0.03	0.780 ± 0.04	0.774 ± 0.02	0.773 ± 0.02	0.780 ± 0.05	0.776 ± 0.03	0.866 ± 0.02
Glmboost_XgbTree	0.773 ± 0.03	0.789 ± 0.04	0.760 ± 0.01	0.748 ± 0.01	0.798 ± 0.05	0.773 ± 0.03	0.856 ± 0.02
Glmnet_RF	0.772 ± 0.01	0.788 ± 0.01	0.757 ± 0.01	0.743 ± 0.02	0.793 ± 0.01	0.770 ± 0.01	0.860 ± 0.01
Glmnet_XgbTree	0.767 ± 0.03	0.767 ± 0.03	0.767 ± 0.02	0.768 ± 0.02	0.763 ± 0.05	0.766 ± 0.03	0.847 ± 0.01
AUC_Lightgbm	0.765 ± 0.03	0.767 ± 0.03	0.764 ± 0.03	0.763 ± 0.03	0.768 ± 0.03	0.765 ± 0.03	0.856 ± 0.02
Glmboost_RF	0.765 ± 0.00	0.779 ± 0.02	0.755 ± 0.01	0.743 ± 0.02	0.785 ± 0.03	0.765 ± 0.00	0.855 ± 0.01
RF_Lightgbm	0.759 ± 0.01	0.756 ± 0.02	0.764 ± 0.02	0.768 ± 0.03	0.751 ± 0.03	0.759 ± 0.01	0.844 ± 0.01
XgbTree_Lightgbm	0.753 ± 0.03	0.765 ± 0.04	0.743 ± 0.03	0.733 ± 0.03	0.773 ± 0.05	0.753 ± 0.03	0.851 ± 0.01
NNET_XgbTree	0.746 ± 0.02	0.759 ± 0.03	0.735 ± 0.03	0.721 ± 0.04	0.770 ± 0.04	0.745 ± 0.02	0.846 ± 0.03
Glmboost_Lightgbm	0.742 ± 0.03	0.756 ± 0.04	0.730 ± 0.03	0.716 ± 0.03	0.768 ± 0.04	0.742 ± 0.03	0.830 ± 0.02
AUC_SVMlinear	0.741 ± 0.02	0.756 ± 0.03	0.727 ± 0.02	0.711 ± 0.03	0.770 ± 0.03	0.740 ± 0.02	0.811 ± 0.01
AUC_LDA	0.740 ± 0.01	0.761 ± 0.02	0.721 ± 0.01	0.699 ± 0.01	0.780 ± 0.02	0.739 ± 0.01	0.806 ± 0.01
Glmnet_Lightgbm	0.737 ± 0.03	0.734 ± 0.03	0.741 ± 0.04	0.743 ± 0.05	0.731 ± 0.03	0.737 ± 0.03	0.832 ± 0.01
AUC_Glmboost	0.737 ± 0.02	0.745 ± 0.01	0.731 ± 0.03	0.721 ± 0.04	0.753 ± 0.01	0.737 ± 0.02	0.808 ± 0.01
AUC_Glmnet	0.736 ± 0.02	0.746 ± 0.02	0.726 ± 0.03	0.714 ± 0.04	0.758 ± 0.01	0.736 ± 0.02	0.798 ± 0.01
XgbTree_Glmboost	0.733 ± 0.01	0.738 ± 0.01	0.729 ± 0.01	0.723 ± 0.02	0.743 ± 0.02	0.733 ± 0.01	0.800 ± 0.00
AUC_Bayesglm	0.733 ± 0.01	0.736 ± 0.01	0.731 ± 0.01	0.728 ± 0.02	0.738 ± 0.02	0.733 ± 0.01	0.802 ± 0.01
RF_Bayesglm	0.728 ± 0.01	0.729 ± 0.01	0.728 ± 0.01	0.728 ± 0.02	0.728 ± 0.02	0.728 ± 0.01	0.787 ± 0.01
RF_SVMlinear	0.728 ± 0.03	0.731 ± 0.03	0.727 ± 0.03	0.723 ± 0.04	0.733 ± 0.04	0.728 ± 0.03	0.776 ± 0.01
NNET_Bayesglm	0.728 ± 0.02	0.740 ± 0.01	0.718 ± 0.03	0.704 ± 0.04	0.753 ± 0.01	0.728 ± 0.02	0.786 ± 0.02
NNET_Lightgbm	0.727 ± 0.01	0.732 ± 0.02	0.723 ± 0.01	0.719 ± 0.02	0.736 ± 0.03	0.727 ± 0.01	0.823 ± 0.02
RF_Glmboost	0.725 ± 0.01	0.731 ± 0.02	0.719 ± 0.02	0.711 ± 0.03	0.738 ± 0.02	0.725 ± 0.01	0.789 ± 0.01
NNET_Glmnet	0.725 ± 0.02	0.733 ± 0.02	0.717 ± 0.03	0.706 ± 0.03	0.743 ± 0.02	0.725 ± 0.02	0.790 ± 0.02
AUC>NNET	0.725 ± 0.02	0.719 ± 0.03	0.731 ± 0.02	0.738 ± 0.02	0.711 ± 0.04	0.724 ± 0.02	0.786 ± 0.01
Glmnet_Bayesglm	0.723 ± 0.03	0.724 ± 0.03	0.723 ± 0.04	0.721 ± 0.04	0.726 ± 0.02	0.723 ± 0.03	0.784 ± 0.01
Lightgbm>NNET	0.723 ± 0.02	0.720 ± 0.02	0.727 ± 0.02	0.731 ± 0.02	0.716 ± 0.02	0.723 ± 0.02	0.774 ± 0.03
NNET>NNET	0.723 ± 0.02	0.713 ± 0.02	0.736 ± 0.03	0.748 ± 0.03	0.699 ± 0.03	0.723 ± 0.02	0.753 ± 0.02
Lightgbm_Bayesglm	0.721 ± 0.02	0.726 ± 0.03	0.717 ± 0.02	0.711 ± 0.02	0.731 ± 0.03	0.721 ± 0.02	0.792 ± 0.01
RF_Glmnet	0.721 ± 0.01	0.730 ± 0.01	0.713 ± 0.01	0.701 ± 0.01	0.741 ± 0.01	0.721 ± 0.01	0.791 ± 0.00
XgbTree_LDA	0.721 ± 0.02	0.740 ± 0.03	0.705 ± 0.02	0.681 ± 0.02	0.758 ± 0.03	0.720 ± 0.02	0.782 ± 0.01
Lightgbm_Glmboost	0.720 ± 0.03	0.728 ± 0.03	0.712 ± 0.03	0.701 ± 0.03	0.738 ± 0.03	0.720 ± 0.03	0.793 ± 0.01
Glmnet_Glmboost	0.720 ± 0.03	0.727 ± 0.03	0.714 ± 0.03	0.704 ± 0.04	0.736 ± 0.02	0.720 ± 0.03	0.792 ± 0.01
RF_LDA	0.719 ± 0.02	0.718 ± 0.02	0.719 ± 0.02	0.721 ± 0.01	0.716 ± 0.03	0.718 ± 0.02	0.772 ± 0.02
Lightgbm_Glmnet	0.719 ± 0.02	0.717 ± 0.01	0.720 ± 0.03	0.721 ± 0.04	0.716 ± 0.01	0.718 ± 0.02	0.790 ± 0.01
NNET_LDA	0.719 ± 0.03	0.736 ± 0.03	0.704 ± 0.04	0.681 ± 0.05	0.756 ± 0.03	0.718 ± 0.03	0.787 ± 0.02
XgbTree_Bayesglm	0.717 ± 0.02	0.720 ± 0.02	0.715 ± 0.02	0.711 ± 0.02	0.723 ± 0.03	0.717 ± 0.02	0.789 ± 0.01
Glmnet_Glmnet	0.716 ± 0.03	0.726 ± 0.03	0.707 ± 0.03	0.694 ± 0.03	0.738 ± 0.03	0.716 ± 0.03	0.785 ± 0.01
XgbTree_Glmnet	0.715 ± 0.01	0.721 ± 0.01	0.709 ± 0.00	0.701 ± 0.01	0.728 ± 0.02	0.715 ± 0.01	0.795 ± 0.00
Lightgbm_SVMlinear	0.714 ± 0.03	0.718 ± 0.03	0.709 ± 0.02	0.704 ± 0.03	0.723 ± 0.04	0.713 ± 0.03	0.785 ± 0.02



**Supplementary Table 4.10: Performance of the Feature Selection Methods and Machine Learning Approaches on the Test Dataset Utilizing Clinical and Biological Features. (Cont.)**

Model	Evaluation Metrics	Accuracy	Precision_TMJ OA	Precision_Control	Recall_TMJ OA	Recall_Control	F1score	AUC
XgbTree_NNET		0.714 ± 0.02	0.709 ± 0.02	0.719 ± 0.02	0.726 ± 0.02	0.701 ± 0.03	0.713 ± 0.02	0.771 ± 0.02
NNET_HDDA		0.714 ± 0.03	0.704 ± 0.03	0.725 ± 0.03	0.738 ± 0.03	0.689 ± 0.03	0.713 ± 0.03	0.767 ± 0.03
Glmnet_Naivebayes		0.714 ± 0.01	0.725 ± 0.02	0.704 ± 0.02	0.689 ± 0.03	0.738 ± 0.03	0.713 ± 0.01	0.772 ± 0.02
NNET_SVMlinear		0.714 ± 0.02	0.727 ± 0.03	0.702 ± 0.02	0.686 ± 0.02	0.741 ± 0.04	0.713 ± 0.02	0.783 ± 0.02
Glmnet_NNET		0.712 ± 0.02	0.712 ± 0.02	0.713 ± 0.02	0.714 ± 0.03	0.711 ± 0.02	0.712 ± 0.02	0.776 ± 0.01
Glmboost_Glmboost		0.712 ± 0.02	0.721 ± 0.02	0.705 ± 0.02	0.694 ± 0.02	0.731 ± 0.02	0.712 ± 0.02	0.793 ± 0.02
AUC_Naivebayes		0.712 ± 0.02	0.728 ± 0.03	0.699 ± 0.02	0.679 ± 0.02	0.746 ± 0.03	0.712 ± 0.02	0.776 ± 0.02
Glmboost_NNET		0.711 ± 0.02	0.706 ± 0.02	0.717 ± 0.03	0.723 ± 0.04	0.699 ± 0.02	0.711 ± 0.02	0.752 ± 0.02
Lightgbm_LDA		0.711 ± 0.03	0.731 ± 0.04	0.695 ± 0.02	0.669 ± 0.03	0.753 ± 0.04	0.710 ± 0.03	0.781 ± 0.03
Lightgbm_Naivebayes		0.710 ± 0.02	0.700 ± 0.02	0.722 ± 0.03	0.736 ± 0.04	0.684 ± 0.03	0.710 ± 0.02	0.768 ± 0.02
Glmboost_Naivebayes		0.709 ± 0.01	0.723 ± 0.01	0.697 ± 0.02	0.677 ± 0.03	0.741 ± 0.02	0.708 ± 0.01	0.762 ± 0.02
XgbTree_SVMlinear		0.707 ± 0.01	0.715 ± 0.01	0.700 ± 0.02	0.689 ± 0.02	0.726 ± 0.02	0.707 ± 0.01	0.776 ± 0.02
NNET_Glmboost		0.706 ± 0.01	0.723 ± 0.01	0.692 ± 0.02	0.669 ± 0.03	0.743 ± 0.02	0.706 ± 0.01	0.788 ± 0.02
Glmboost_Glmnet		0.705 ± 0.02	0.710 ± 0.02	0.701 ± 0.02	0.694 ± 0.03	0.716 ± 0.02	0.705 ± 0.02	0.781 ± 0.01
Glmboost_Bayesglm		0.705 ± 0.02	0.707 ± 0.02	0.704 ± 0.03	0.701 ± 0.04	0.709 ± 0.03	0.705 ± 0.02	0.781 ± 0.01
Glmnet_SVMlinear		0.700 ± 0.03	0.708 ± 0.03	0.692 ± 0.03	0.679 ± 0.04	0.721 ± 0.02	0.700 ± 0.03	0.772 ± 0.02
Glmboost_LDA		0.700 ± 0.02	0.710 ± 0.02	0.693 ± 0.02	0.679 ± 0.04	0.721 ± 0.04	0.700 ± 0.02	0.772 ± 0.02
Glmboost_SVMlinear		0.699 ± 0.03	0.701 ± 0.03	0.697 ± 0.03	0.694 ± 0.04	0.704 ± 0.03	0.699 ± 0.03	0.771 ± 0.02
Glmnet_LDA		0.699 ± 0.03	0.710 ± 0.03	0.689 ± 0.04	0.672 ± 0.05	0.726 ± 0.02	0.698 ± 0.03	0.771 ± 0.02
Glmboost_HDDA		0.696 ± 0.01	0.699 ± 0.01	0.695 ± 0.02	0.691 ± 0.03	0.701 ± 0.02	0.696 ± 0.01	0.753 ± 0.02
NNET_Naivebayes		0.698 ± 0.03	0.693 ± 0.06	0.712 ± 0.02	0.728 ± 0.06	0.667 ± 0.10	0.696 ± 0.03	0.766 ± 0.02
Glmnet_HDDA		0.693 ± 0.02	0.695 ± 0.03	0.692 ± 0.03	0.689 ± 0.05	0.696 ± 0.05	0.692 ± 0.02	0.743 ± 0.02
XgbTree_Naivebayes		0.693 ± 0.03	0.675 ± 0.03	0.715 ± 0.03	0.743 ± 0.04	0.642 ± 0.04	0.692 ± 0.03	0.752 ± 0.02
AUC_HDDA		0.681 ± 0.02	0.675 ± 0.02	0.689 ± 0.01	0.701 ± 0.01	0.662 ± 0.03	0.681 ± 0.02	0.732 ± 0.02
RF_HDDA		0.681 ± 0.04	0.672 ± 0.06	0.699 ± 0.03	0.726 ± 0.05	0.637 ± 0.10	0.679 ± 0.04	0.733 ± 0.03
XgbTree_HDDA		0.678 ± 0.02	0.654 ± 0.02	0.712 ± 0.02	0.758 ± 0.03	0.598 ± 0.04	0.675 ± 0.02	0.741 ± 0.04
Lightgbm_HDDA		0.669 ± 0.02	0.651 ± 0.03	0.696 ± 0.03	0.733 ± 0.05	0.605 ± 0.07	0.667 ± 0.03	0.734 ± 0.04
RF_NNET		0.658 ± 0.02	0.656 ± 0.01	0.662 ± 0.03	0.664 ± 0.06	0.652 ± 0.03	0.658 ± 0.02	0.723 ± 0.02
RF_Naivebayes		0.643 ± 0.02	0.621 ± 0.02	0.675 ± 0.03	0.733 ± 0.03	0.553 ± 0.03	0.640 ± 0.02	0.707 ± 0.01

\*RF, Random forest; XGBoost, Extreme gradient boosting; Lightgbm, Light gradient boosting machine; Glmnet, Generalized linear model with lasso and elastic net regularization; AUC, Area under the curve; Glmboost, Generalized linear model boosting; NNET, Neural network; Bayesglm, Bayesian generalized linear model; SVM, Support vector machine; LDA, Linear discriminant analysis; HDDA, High-dimensional discriminant analysis.

**Supplementary Table 4.11: Performance of the Feature Selection Methods and Machine Learning Approaches on the Validation Dataset Utilizing Clinical Features.**

Model	Evaluation Metrics	Accuracy	Precision_TMJ OA	Precision_Control	Recall_TMJ OA	Recall_Control	F1score	AUC
Lightgbm_SVMlinear		0.743 ± 0.00	0.769 ± 0.01	0.722 ± 0.00	0.696 ± 0.01	0.790 ± 0.01	0.743 ± 0.00	0.796 ± 0.00
Lightgbm_HDDA		0.740 ± 0.01	0.773 ± 0.02	0.715 ± 0.01	0.680 ± 0.01	0.800 ± 0.02	0.739 ± 0.01	0.784 ± 0.01
Lightgbm_LDA		0.740 ± 0.01	0.773 ± 0.01	0.714 ± 0.00	0.679 ± 0.01	0.801 ± 0.01	0.739 ± 0.01	0.793 ± 0.00
Lightgbm_Glmnet		0.736 ± 0.01	0.759 ± 0.01	0.717 ± 0.01	0.692 ± 0.01	0.780 ± 0.01	0.735 ± 0.01	0.792 ± 0.00
Lightgbm_Glmboost		0.736 ± 0.01	0.764 ± 0.01	0.713 ± 0.00	0.682 ± 0.01	0.789 ± 0.01	0.735 ± 0.01	0.792 ± 0.00
Lightgbm_Bayesglm		0.734 ± 0.00	0.755 ± 0.01	0.717 ± 0.00	0.694 ± 0.01	0.774 ± 0.01	0.734 ± 0.00	0.793 ± 0.00
Glmboost_Glmnet		0.733 ± 0.01	0.758 ± 0.01	0.713 ± 0.01	0.684 ± 0.01	0.782 ± 0.01	0.732 ± 0.01	0.783 ± 0.01
AUC_Glmnet		0.733 ± 0.01	0.758 ± 0.01	0.713 ± 0.01	0.684 ± 0.01	0.782 ± 0.01	0.732 ± 0.01	0.783 ± 0.01
NNET_Glmnet		0.733 ± 0.01	0.758 ± 0.01	0.713 ± 0.00	0.686 ± 0.00	0.780 ± 0.01	0.732 ± 0.01	0.783 ± 0.01
RF_Glmnet		0.733 ± 0.01	0.758 ± 0.01	0.712 ± 0.00	0.684 ± 0.01	0.782 ± 0.01	0.732 ± 0.01	0.783 ± 0.01
XgbTree_Glmnet		0.732 ± 0.01	0.758 ± 0.01	0.712 ± 0.00	0.684 ± 0.00	0.781 ± 0.01	0.732 ± 0.01	0.783 ± 0.01
RF_SVMlinear		0.732 ± 0.01	0.760 ± 0.01	0.709 ± 0.01	0.677 ± 0.01	0.786 ± 0.01	0.731 ± 0.01	0.779 ± 0.01
Glmnet_Glmnet		0.732 ± 0.01	0.757 ± 0.01	0.712 ± 0.00	0.684 ± 0.00	0.779 ± 0.01	0.731 ± 0.01	0.783 ± 0.01
Glmnet_SVMlinear		0.731 ± 0.00	0.758 ± 0.00	0.710 ± 0.00	0.680 ± 0.01	0.782 ± 0.01	0.730 ± 0.00	0.779 ± 0.01
NNET_SVMlinear		0.731 ± 0.00	0.760 ± 0.01	0.708 ± 0.00	0.676 ± 0.01	0.786 ± 0.01	0.730 ± 0.00	0.778 ± 0.01
Glmboost_SVMlinear		0.730 ± 0.01	0.759 ± 0.01	0.708 ± 0.00	0.676 ± 0.01	0.785 ± 0.01	0.730 ± 0.01	0.780 ± 0.01
AUC_SVMlinear		0.730 ± 0.01	0.759 ± 0.01	0.708 ± 0.00	0.676 ± 0.01	0.785 ± 0.01	0.730 ± 0.01	0.780 ± 0.01
XgbTree_SVMlinear		0.730 ± 0.00	0.757 ± 0.01	0.708 ± 0.00	0.677 ± 0.00	0.783 ± 0.01	0.729 ± 0.00	0.779 ± 0.01
RF_Glmboost		0.729 ± 0.01	0.758 ± 0.01	0.706 ± 0.00	0.674 ± 0.01	0.785 ± 0.01	0.728 ± 0.01	0.781 ± 0.01
XgbTree_Glmboost		0.729 ± 0.01	0.758 ± 0.01	0.706 ± 0.00	0.674 ± 0.00	0.785 ± 0.01	0.728 ± 0.01	0.781 ± 0.01
Glmboost_Naivebayes		0.731 ± 0.02	0.785 ± 0.02	0.694 ± 0.01	0.636 ± 0.02	0.825 ± 0.01	0.728 ± 0.02	0.769 ± 0.01
AUC_Naivebayes		0.731 ± 0.02	0.785 ± 0.02	0.694 ± 0.01	0.636 ± 0.02	0.825 ± 0.01	0.728 ± 0.02	0.769 ± 0.01
RF_Naivebayes		0.730 ± 0.02	0.785 ± 0.02	0.693 ± 0.01	0.634 ± 0.02	0.826 ± 0.01	0.728 ± 0.02	0.768 ± 0.01
Glmboost_Glmboost		0.729 ± 0.01	0.758 ± 0.01	0.706 ± 0.00	0.673 ± 0.00	0.784 ± 0.01	0.728 ± 0.01	0.781 ± 0.01
AUC_Glmboost		0.729 ± 0.01	0.758 ± 0.01	0.706 ± 0.00	0.673 ± 0.00	0.784 ± 0.01	0.728 ± 0.01	0.781 ± 0.01
Glmnet_Naivebayes		0.730 ± 0.02	0.783 ± 0.02	0.694 ± 0.01	0.637 ± 0.02	0.823 ± 0.01	0.727 ± 0.02	0.768 ± 0.01
XgbTree_Naivebayes		0.730 ± 0.01	0.786 ± 0.01	0.693 ± 0.01	0.633 ± 0.02	0.827 ± 0.01	0.727 ± 0.01	0.769 ± 0.01
Glmnet_Glmboost		0.728 ± 0.01	0.759 ± 0.01	0.704 ± 0.00	0.670 ± 0.00	0.787 ± 0.01	0.727 ± 0.01	0.780 ± 0.01
NNET_Glmboost		0.728 ± 0.01	0.758 ± 0.01	0.705 ± 0.00	0.671 ± 0.00	0.785 ± 0.01	0.727 ± 0.01	0.780 ± 0.01
NNET_Naivebayes		0.730 ± 0.01	0.785 ± 0.01	0.693 ± 0.01	0.633 ± 0.02	0.826 ± 0.01	0.727 ± 0.01	0.769 ± 0.01
Lightgbm>NNET		0.726 ± 0.00	0.737 ± 0.01	0.718 ± 0.01	0.705 ± 0.01	0.747 ± 0.01	0.726 ± 0.00	0.753 ± 0.01
Glmboost_Bayesglm		0.724 ± 0.01	0.746 ± 0.01	0.706 ± 0.00	0.679 ± 0.00	0.769 ± 0.01	0.723 ± 0.01	0.775 ± 0.01
Glmnet_Bayesglm		0.724 ± 0.01	0.746 ± 0.01	0.706 ± 0.00	0.679 ± 0.00	0.769 ± 0.01	0.723 ± 0.01	0.775 ± 0.01
AUC_Bayesglm		0.724 ± 0.01	0.746 ± 0.01	0.706 ± 0.00	0.679 ± 0.00	0.769 ± 0.01	0.723 ± 0.01	0.775 ± 0.01
NNET_Bayesglm		0.724 ± 0.01	0.746 ± 0.01	0.706 ± 0.00	0.679 ± 0.00	0.769 ± 0.01	0.723 ± 0.01	0.775 ± 0.01
RF_Bayesglm		0.724 ± 0.01	0.746 ± 0.01	0.706 ± 0.00	0.679 ± 0.00	0.769 ± 0.01	0.723 ± 0.01	0.775 ± 0.01
XgbTree_Bayesglm		0.724 ± 0.01	0.746 ± 0.01	0.706 ± 0.00	0.679 ± 0.00	0.769 ± 0.01	0.723 ± 0.01	0.775 ± 0.01
Glmboost_LDA		0.724 ± 0.01	0.755 ± 0.01	0.699 ± 0.01	0.663 ± 0.01	0.784 ± 0.01	0.722 ± 0.01	0.772 ± 0.01
Glmnet_LDA		0.724 ± 0.01	0.755 ± 0.01	0.699 ± 0.01	0.663 ± 0.01	0.784 ± 0.01	0.722 ± 0.01	0.772 ± 0.01
AUC_LDA		0.724 ± 0.01	0.755 ± 0.01	0.699 ± 0.01	0.663 ± 0.01	0.784 ± 0.01	0.722 ± 0.01	0.772 ± 0.01
NNET_LDA		0.724 ± 0.01	0.755 ± 0.01	0.699 ± 0.01	0.663 ± 0.01	0.784 ± 0.01	0.722 ± 0.01	0.772 ± 0.01
RF_LDA		0.724 ± 0.01	0.755 ± 0.01	0.699 ± 0.01	0.663 ± 0.01	0.784 ± 0.01	0.722 ± 0.01	0.772 ± 0.01
XgbTree_LDA		0.724 ± 0.01	0.755 ± 0.01	0.699 ± 0.01	0.663 ± 0.01	0.784 ± 0.01	0.722 ± 0.01	0.772 ± 0.01
Glmboost_HDDA		0.722 ± 0.01	0.753 ± 0.01	0.698 ± 0.01	0.662 ± 0.01	0.782 ± 0.01	0.721 ± 0.01	0.770 ± 0.01
AUC_HDDA		0.722 ± 0.01	0.753 ± 0.01	0.698 ± 0.01	0.662 ± 0.01	0.782 ± 0.01	0.721 ± 0.01	0.770 ± 0.01
RF_HDDA		0.722 ± 0.01	0.753 ± 0.01	0.698 ± 0.01	0.661 ± 0.01	0.782 ± 0.01	0.721 ± 0.01	0.770 ± 0.01
XgbTree_HDDA		0.722 ± 0.01	0.752 ± 0.01	0.698 ± 0.01	0.662 ± 0.01	0.782 ± 0.01	0.721 ± 0.01	0.770 ± 0.01
NNET_HDDA		0.721 ± 0.01	0.751 ± 0.01	0.698 ± 0.01	0.663 ± 0.01	0.780 ± 0.01	0.720 ± 0.01	0.768 ± 0.01

**Supplementary Table 4.11: Performance of the Feature Selection Methods and Machine Learning Approaches on the Validation Dataset Utilizing Clinical Features. (Cont.)**

Model	Evaluation Metrics	Accuracy	Precision_TMJ OA	Precision_Control	Recall_TMJ OA	Recall_Control	F1score	AUC
Glmnet_HDDA		0.721 ± 0.01	0.752 ± 0.01	0.697 ± 0.01	0.661 ± 0.01	0.781 ± 0.01	0.720 ± 0.01	0.770 ± 0.01
Lightgbm_Naivebayes		0.722 ± 0.01	0.779 ± 0.01	0.685 ± 0.00	0.620 ± 0.01	0.823 ± 0.01	0.719 ± 0.01	0.789 ± 0.00
Lightgbm_Lightgbm		0.714 ± 0.01	0.723 ± 0.01	0.708 ± 0.01	0.697 ± 0.02	0.731 ± 0.01	0.714 ± 0.01	0.770 ± 0.01
Glmnet_Lightgbm		0.710 ± 0.01	0.715 ± 0.01	0.709 ± 0.01	0.703 ± 0.02	0.718 ± 0.02	0.710 ± 0.01	0.763 ± 0.01
AUC_Lightgbm		0.710 ± 0.01	0.713 ± 0.01	0.710 ± 0.02	0.706 ± 0.02	0.713 ± 0.02	0.709 ± 0.01	0.763 ± 0.01
NNET_Lightgbm		0.709 ± 0.01	0.712 ± 0.01	0.709 ± 0.01	0.705 ± 0.02	0.713 ± 0.02	0.708 ± 0.01	0.763 ± 0.00
RF_Lightgbm		0.709 ± 0.01	0.713 ± 0.01	0.707 ± 0.01	0.702 ± 0.02	0.715 ± 0.01	0.708 ± 0.01	0.763 ± 0.01
AUC_NNET		0.708 ± 0.01	0.712 ± 0.01	0.705 ± 0.01	0.698 ± 0.02	0.717 ± 0.01	0.707 ± 0.01	0.728 ± 0.01
Glmboost_Lightgbm		0.708 ± 0.01	0.712 ± 0.01	0.706 ± 0.02	0.700 ± 0.02	0.715 ± 0.01	0.707 ± 0.01	0.761 ± 0.01
XgbTree_Lightgbm		0.707 ± 0.01	0.710 ± 0.01	0.706 ± 0.02	0.701 ± 0.02	0.712 ± 0.02	0.706 ± 0.01	0.763 ± 0.01
Glmboost_NNET		0.706 ± 0.01	0.708 ± 0.01	0.705 ± 0.01	0.701 ± 0.02	0.710 ± 0.01	0.705 ± 0.01	0.726 ± 0.01
RF_NNET		0.705 ± 0.01	0.709 ± 0.01	0.704 ± 0.01	0.698 ± 0.02	0.713 ± 0.01	0.705 ± 0.01	0.723 ± 0.01
NNET_NNET		0.704 ± 0.01	0.708 ± 0.01	0.702 ± 0.01	0.697 ± 0.02	0.711 ± 0.02	0.704 ± 0.01	0.729 ± 0.01
XgbTree_NNET		0.704 ± 0.01	0.708 ± 0.00	0.701 ± 0.01	0.695 ± 0.01	0.712 ± 0.01	0.703 ± 0.01	0.725 ± 0.01
Glmnet_NNET		0.702 ± 0.01	0.710 ± 0.01	0.697 ± 0.01	0.685 ± 0.02	0.720 ± 0.01	0.702 ± 0.01	0.721 ± 0.01
Lightgbm_XgbTree		0.698 ± 0.01	0.704 ± 0.01	0.693 ± 0.01	0.685 ± 0.02	0.711 ± 0.01	0.698 ± 0.01	0.754 ± 0.00
Lightgbm_RF		0.688 ± 0.01	0.695 ± 0.01	0.681 ± 0.01	0.669 ± 0.02	0.705 ± 0.01	0.687 ± 0.01	0.745 ± 0.01
RF_RF		0.684 ± 0.01	0.688 ± 0.01	0.682 ± 0.01	0.677 ± 0.02	0.691 ± 0.01	0.684 ± 0.01	0.741 ± 0.01
NNET_XgbTree		0.684 ± 0.01	0.693 ± 0.01	0.676 ± 0.01	0.661 ± 0.01	0.707 ± 0.01	0.684 ± 0.01	0.734 ± 0.01
Glmnet_RF		0.683 ± 0.01	0.685 ± 0.01	0.681 ± 0.01	0.678 ± 0.02	0.686 ± 0.01	0.682 ± 0.01	0.741 ± 0.01
Glmnet_XgbTree		0.682 ± 0.02	0.692 ± 0.02	0.673 ± 0.02	0.656 ± 0.02	0.708 ± 0.01	0.682 ± 0.02	0.736 ± 0.02
NNET_RF		0.682 ± 0.01	0.684 ± 0.01	0.680 ± 0.01	0.677 ± 0.02	0.685 ± 0.02	0.681 ± 0.01	0.741 ± 0.01
Glmboost_RF		0.682 ± 0.01	0.684 ± 0.01	0.680 ± 0.01	0.677 ± 0.02	0.685 ± 0.01	0.681 ± 0.01	0.741 ± 0.01
AUC_XgbTree		0.681 ± 0.01	0.689 ± 0.01	0.673 ± 0.01	0.658 ± 0.02	0.703 ± 0.01	0.680 ± 0.01	0.731 ± 0.01
XgbTree_RF		0.681 ± 0.01	0.683 ± 0.00	0.680 ± 0.01	0.677 ± 0.02	0.683 ± 0.01	0.680 ± 0.01	0.741 ± 0.01
AUC_RF		0.681 ± 0.01	0.684 ± 0.01	0.679 ± 0.01	0.674 ± 0.02	0.684 ± 0.02	0.680 ± 0.01	0.740 ± 0.01
RF_XgbTree		0.678 ± 0.01	0.687 ± 0.01	0.669 ± 0.01	0.652 ± 0.02	0.703 ± 0.01	0.677 ± 0.01	0.731 ± 0.01
Glmboost_XgbTree		0.677 ± 0.01	0.684 ± 0.01	0.670 ± 0.01	0.655 ± 0.02	0.698 ± 0.01	0.676 ± 0.01	0.732 ± 0.01
XgbTree_XgbTree		0.675 ± 0.02	0.686 ± 0.02	0.667 ± 0.02	0.647 ± 0.02	0.703 ± 0.01	0.675 ± 0.02	0.727 ± 0.02

\*RF, Random forest; XGBoost, Extreme gradient boosting; Lightgbm, Light gradient boosting machine; Glmnet, Generalized linear model with lasso and elastic net regularization; AUC, Area under the curve; Glmboost, Generalized linear model boosting; NNET, Neural network; Baysglm, Bayesian generalized linear model; SVM, Support vector machine; LDA, Linear discriminant analysis; HDDA, High-dimensional discriminant analysis.

**Supplementary Table 4.12: Performance of the Feature Selection Methods and Machine Learning Approaches on the Test Dataset Utilizing Clinical Features.**

Model	Evaluation Metrics	Accuracy	Precision_TMJ OA	Precision_Control	Recall_TMJ OA	Recall_Control	F1score	AUC
Lightgbm_SVMlinear		0.743 ± 0.02	0.766 ± 0.02	0.724 ± 0.01	0.701 ± 0.02	0.785 ± 0.02	0.743 ± 0.02	0.792 ± 0.00
Glmboost_Naivebayes		0.742 ± 0.01	0.797 ± 0.01	0.704 ± 0.01	0.649 ± 0.01	0.835 ± 0.01	0.740 ± 0.01	0.771 ± 0.01
Glmnet_Naivebayes		0.742 ± 0.01	0.797 ± 0.01	0.704 ± 0.01	0.649 ± 0.01	0.835 ± 0.01	0.740 ± 0.01	0.771 ± 0.01
AUC_Naivebayes		0.742 ± 0.01	0.797 ± 0.01	0.704 ± 0.01	0.649 ± 0.01	0.835 ± 0.01	0.740 ± 0.01	0.771 ± 0.01
RF_Naivebayes		0.742 ± 0.01	0.797 ± 0.01	0.704 ± 0.01	0.649 ± 0.01	0.835 ± 0.01	0.740 ± 0.01	0.772 ± 0.01
Lightgbm_HDDA		0.740 ± 0.02	0.774 ± 0.02	0.713 ± 0.01	0.677 ± 0.02	0.802 ± 0.03	0.738 ± 0.02	0.787 ± 0.01
XgbTree_Naivebayes		0.740 ± 0.01	0.796 ± 0.01	0.701 ± 0.01	0.644 ± 0.01	0.835 ± 0.01	0.737 ± 0.01	0.772 ± 0.01
NNET_Glmnet		0.736 ± 0.01	0.762 ± 0.01	0.715 ± 0.01	0.686 ± 0.01	0.785 ± 0.02	0.735 ± 0.01	0.787 ± 0.01
NNET_Glmboost		0.736 ± 0.01	0.765 ± 0.01	0.713 ± 0.01	0.681 ± 0.01	0.790 ± 0.02	0.735 ± 0.01	0.785 ± 0.01
XgbTree_Glmboost		0.736 ± 0.01	0.765 ± 0.01	0.713 ± 0.01	0.681 ± 0.01	0.790 ± 0.01	0.735 ± 0.01	0.783 ± 0.01
Lightgbm_LDA		0.736 ± 0.01	0.765 ± 0.02	0.713 ± 0.00	0.681 ± 0.01	0.790 ± 0.02	0.735 ± 0.01	0.791 ± 0.01
Lightgbm_Glmnet		0.735 ± 0.01	0.757 ± 0.01	0.716 ± 0.01	0.691 ± 0.01	0.778 ± 0.01	0.734 ± 0.01	0.792 ± 0.01
Glmnet_Glmnet		0.735 ± 0.01	0.758 ± 0.01	0.715 ± 0.01	0.689 ± 0.01	0.780 ± 0.02	0.734 ± 0.01	0.788 ± 0.01
Glmboost_Glmnet		0.735 ± 0.01	0.760 ± 0.01	0.714 ± 0.01	0.686 ± 0.01	0.783 ± 0.01	0.734 ± 0.01	0.787 ± 0.01
AUC_Glmnet		0.735 ± 0.01	0.760 ± 0.01	0.714 ± 0.01	0.686 ± 0.01	0.783 ± 0.01	0.734 ± 0.01	0.787 ± 0.01
Glmnet_Glmboost		0.735 ± 0.00	0.763 ± 0.01	0.712 ± 0.00	0.681 ± 0.01	0.788 ± 0.01	0.734 ± 0.00	0.781 ± 0.01
XgbTree_SVMlinear		0.733 ± 0.01	0.759 ± 0.01	0.712 ± 0.01	0.684 ± 0.01	0.783 ± 0.01	0.733 ± 0.01	0.780 ± 0.01
Glmnet_SVMlinear		0.733 ± 0.00	0.759 ± 0.01	0.712 ± 0.00	0.684 ± 0.01	0.783 ± 0.01	0.733 ± 0.00	0.781 ± 0.01
RF_Glmboost		0.733 ± 0.01	0.760 ± 0.01	0.711 ± 0.00	0.681 ± 0.01	0.785 ± 0.01	0.733 ± 0.01	0.784 ± 0.01
Lightgbm_Glmboost		0.733 ± 0.01	0.761 ± 0.01	0.711 ± 0.01	0.681 ± 0.01	0.785 ± 0.02	0.733 ± 0.01	0.791 ± 0.00
Glmboost_SVMlinear		0.733 ± 0.01	0.761 ± 0.01	0.712 ± 0.01	0.681 ± 0.02	0.785 ± 0.02	0.733 ± 0.01	0.778 ± 0.01
AUC_SVMlinear		0.733 ± 0.01	0.761 ± 0.01	0.712 ± 0.01	0.681 ± 0.02	0.785 ± 0.02	0.733 ± 0.01	0.778 ± 0.01
Glmboost_Glmboost		0.733 ± 0.01	0.762 ± 0.01	0.710 ± 0.00	0.679 ± 0.00	0.788 ± 0.01	0.733 ± 0.01	0.782 ± 0.01
AUC_Glmboost		0.733 ± 0.01	0.762 ± 0.01	0.710 ± 0.00	0.679 ± 0.00	0.788 ± 0.01	0.733 ± 0.01	0.782 ± 0.01
RF_SVMlinear		0.733 ± 0.01	0.762 ± 0.01	0.711 ± 0.01	0.679 ± 0.02	0.788 ± 0.01	0.733 ± 0.01	0.778 ± 0.01
XgbTree_Glmnet		0.733 ± 0.01	0.758 ± 0.01	0.713 ± 0.01	0.686 ± 0.01	0.778 ± 0.02	0.732 ± 0.01	0.786 ± 0.01
RF_Glmnet		0.732 ± 0.01	0.756 ± 0.01	0.713 ± 0.01	0.686 ± 0.01	0.775 ± 0.02	0.731 ± 0.01	0.789 ± 0.01
NNET_Naivebayes		0.733 ± 0.02	0.792 ± 0.01	0.694 ± 0.02	0.632 ± 0.03	0.835 ± 0.01	0.730 ± 0.02	0.771 ± 0.01
NNET_SVMlinear		0.731 ± 0.01	0.756 ± 0.01	0.710 ± 0.01	0.681 ± 0.01	0.780 ± 0.01	0.730 ± 0.01	0.783 ± 0.01
Lightgbm_Lightgbm		0.730 ± 0.01	0.735 ± 0.01	0.725 ± 0.01	0.719 ± 0.01	0.741 ± 0.02	0.730 ± 0.01	0.772 ± 0.01
Lightgbm_Bayesglm		0.730 ± 0.01	0.749 ± 0.01	0.713 ± 0.01	0.691 ± 0.01	0.768 ± 0.01	0.729 ± 0.01	0.792 ± 0.01
XgbTree_Lightgbm		0.727 ± 0.02	0.725 ± 0.03	0.730 ± 0.02	0.733 ± 0.03	0.721 ± 0.04	0.727 ± 0.02	0.771 ± 0.00
Glmboost_Bayesglm		0.726 ± 0.00	0.747 ± 0.00	0.708 ± 0.00	0.684 ± 0.01	0.768 ± 0.01	0.725 ± 0.00	0.778 ± 0.01
Glmnet_Bayesglm		0.726 ± 0.00	0.747 ± 0.00	0.708 ± 0.00	0.684 ± 0.01	0.768 ± 0.01	0.725 ± 0.00	0.778 ± 0.01
AUC_Bayesglm		0.726 ± 0.00	0.747 ± 0.00	0.708 ± 0.00	0.684 ± 0.01	0.768 ± 0.01	0.725 ± 0.00	0.778 ± 0.01
NNET_Bayesglm		0.726 ± 0.00	0.747 ± 0.00	0.708 ± 0.00	0.684 ± 0.01	0.768 ± 0.01	0.725 ± 0.00	0.778 ± 0.01
RF_Bayesglm		0.726 ± 0.00	0.747 ± 0.00	0.708 ± 0.00	0.684 ± 0.01	0.768 ± 0.01	0.725 ± 0.00	0.778 ± 0.01
XgbTree_Bayesglm		0.726 ± 0.00	0.747 ± 0.00	0.708 ± 0.00	0.684 ± 0.01	0.768 ± 0.01	0.725 ± 0.00	0.778 ± 0.01
NNET_HDDA		0.725 ± 0.01	0.749 ± 0.01	0.705 ± 0.01	0.677 ± 0.01	0.773 ± 0.01	0.724 ± 0.01	0.776 ± 0.01
RF_HDDA		0.725 ± 0.01	0.752 ± 0.01	0.703 ± 0.01	0.672 ± 0.01	0.775 ± 0.01	0.723 ± 0.01	0.777 ± 0.02
Glmboost_LDA		0.723 ± 0.01	0.748 ± 0.01	0.703 ± 0.00	0.674 ± 0.01	0.773 ± 0.01	0.723 ± 0.01	0.776 ± 0.01
Glmnet_LDA		0.723 ± 0.01	0.748 ± 0.01	0.703 ± 0.00	0.674 ± 0.01	0.773 ± 0.01	0.723 ± 0.01	0.776 ± 0.01
AUC_LDA		0.723 ± 0.01	0.748 ± 0.01	0.703 ± 0.00	0.674 ± 0.01	0.773 ± 0.01	0.723 ± 0.01	0.776 ± 0.01
NNET_LDA		0.723 ± 0.01	0.748 ± 0.01	0.703 ± 0.00	0.674 ± 0.01	0.773 ± 0.01	0.723 ± 0.01	0.776 ± 0.01
RF_LDA		0.723 ± 0.01	0.748 ± 0.01	0.703 ± 0.00	0.674 ± 0.01	0.773 ± 0.01	0.723 ± 0.01	0.776 ± 0.01
XgbTree_HDDA		0.723 ± 0.01	0.748 ± 0.01	0.703 ± 0.00	0.674 ± 0.01	0.773 ± 0.01	0.723 ± 0.01	0.775 ± 0.02
XgbTree_LDA		0.723 ± 0.01	0.748 ± 0.01	0.703 ± 0.00	0.674 ± 0.01	0.773 ± 0.01	0.723 ± 0.01	0.776 ± 0.01
Glmnet_Lightgbm		0.722 ± 0.02	0.723 ± 0.03	0.723 ± 0.01	0.723 ± 0.02	0.721 ± 0.04	0.722 ± 0.02	0.772 ± 0.00

**Supplementary Table 4.12: Performance of the Feature Selection Methods and Machine Learning Approaches on the Test Dataset Utilizing Clinical Features. (Cont.)**

Model	Accuracy	Precision_TMJ OA	Precision_Control	Recall_TMJ OA	Recall_Control	F1score	AUC
RF_Lightgbm	0.722 ± 0.02	0.721 ± 0.02	0.724 ± 0.02	0.726 ± 0.04	0.719 ± 0.04	0.722 ± 0.02	0.770 ± 0.01
Glmnet_HDDA	0.722 ± 0.01	0.747 ± 0.01	0.702 ± 0.01	0.672 ± 0.01	0.770 ± 0.01	0.721 ± 0.01	0.775 ± 0.01
Glmboost_Lightgbm	0.721 ± 0.02	0.727 ± 0.03	0.717 ± 0.01	0.711 ± 0.02	0.731 ± 0.05	0.721 ± 0.02	0.776 ± 0.01
Glmboost_HDDA	0.720 ± 0.01	0.745 ± 0.01	0.700 ± 0.01	0.669 ± 0.01	0.770 ± 0.01	0.719 ± 0.01	0.775 ± 0.01
AUC_HDDA	0.720 ± 0.01	0.745 ± 0.01	0.700 ± 0.01	0.669 ± 0.01	0.770 ± 0.01	0.719 ± 0.01	0.775 ± 0.01
NNET_Lightgbm	0.719 ± 0.02	0.721 ± 0.02	0.717 ± 0.02	0.714 ± 0.03	0.723 ± 0.03	0.718 ± 0.02	0.770 ± 0.01
Lightgbm_Naivebayes	0.721 ± 0.01	0.777 ± 0.01	0.684 ± 0.02	0.620 ± 0.03	0.822 ± 0.01	0.718 ± 0.01	0.790 ± 0.01
AUC_Lightgbm	0.717 ± 0.02	0.720 ± 0.03	0.716 ± 0.02	0.714 ± 0.03	0.721 ± 0.04	0.717 ± 0.02	0.774 ± 0.01
XgbTree_NNET	0.716 ± 0.01	0.719 ± 0.01	0.713 ± 0.01	0.709 ± 0.02	0.723 ± 0.02	0.716 ± 0.01	0.736 ± 0.01
RF_NNET	0.712 ± 0.01	0.711 ± 0.01	0.714 ± 0.02	0.716 ± 0.03	0.709 ± 0.02	0.712 ± 0.01	0.734 ± 0.01
Lightgbm_NNET	0.710 ± 0.00	0.725 ± 0.01	0.697 ± 0.00	0.677 ± 0.01	0.743 ± 0.02	0.710 ± 0.00	0.745 ± 0.01
Lightgbm_XgbTree	0.709 ± 0.03	0.719 ± 0.03	0.699 ± 0.03	0.684 ± 0.04	0.733 ± 0.03	0.708 ± 0.03	0.756 ± 0.02
Glmboost_NNET	0.707 ± 0.01	0.714 ± 0.02	0.703 ± 0.02	0.694 ± 0.04	0.721 ± 0.03	0.707 ± 0.02	0.731 ± 0.02
Glmnet_NNET	0.705 ± 0.02	0.707 ± 0.01	0.703 ± 0.03	0.699 ± 0.04	0.711 ± 0.01	0.705 ± 0.02	0.723 ± 0.02
AUC_NNET	0.705 ± 0.01	0.710 ± 0.02	0.701 ± 0.02	0.694 ± 0.03	0.716 ± 0.03	0.705 ± 0.01	0.735 ± 0.02
NNET_NNET	0.698 ± 0.01	0.695 ± 0.02	0.702 ± 0.02	0.706 ± 0.04	0.689 ± 0.04	0.697 ± 0.01	0.727 ± 0.02
XgbTree_XgbTree	0.694 ± 0.02	0.705 ± 0.02	0.684 ± 0.02	0.667 ± 0.03	0.721 ± 0.01	0.694 ± 0.02	0.744 ± 0.02
Glmnet_RF	0.686 ± 0.01	0.687 ± 0.01	0.686 ± 0.02	0.684 ± 0.02	0.686 ± 0.01	0.686 ± 0.01	0.747 ± 0.01
Lightgbm_RF	0.684 ± 0.02	0.695 ± 0.03	0.674 ± 0.02	0.657 ± 0.02	0.711 ± 0.03	0.684 ± 0.02	0.746 ± 0.02
AUC_XgbTree	0.684 ± 0.01	0.698 ± 0.01	0.672 ± 0.01	0.649 ± 0.02	0.719 ± 0.02	0.684 ± 0.01	0.745 ± 0.01
Glmboost_RF	0.684 ± 0.01	0.685 ± 0.02	0.683 ± 0.01	0.681 ± 0.02	0.684 ± 0.03	0.683 ± 0.01	0.744 ± 0.01
AUC_RF	0.683 ± 0.01	0.682 ± 0.00	0.683 ± 0.01	0.684 ± 0.02	0.681 ± 0.01	0.683 ± 0.01	0.744 ± 0.01
XgbTree_RF	0.681 ± 0.01	0.681 ± 0.01	0.682 ± 0.01	0.684 ± 0.01	0.677 ± 0.03	0.681 ± 0.01	0.746 ± 0.01
NNET_RF	0.683 ± 0.01	0.683 ± 0.01	0.683 ± 0.01	0.681 ± 0.02	0.677 ± 0.02	0.681 ± 0.01	0.746 ± 0.01
Glmboost_XgbTree	0.675 ± 0.02	0.688 ± 0.02	0.665 ± 0.02	0.642 ± 0.04	0.709 ± 0.02	0.675 ± 0.02	0.739 ± 0.01
RF_RF	0.674 ± 0.02	0.673 ± 0.02	0.676 ± 0.01	0.679 ± 0.02	0.667 ± 0.02	0.673 ± 0.02	0.739 ± 0.01
RF_XgbTree	0.672 ± 0.02	0.682 ± 0.01	0.663 ± 0.02	0.642 ± 0.03	0.701 ± 0.02	0.671 ± 0.02	0.739 ± 0.03
Glmnet_XgbTree	0.668 ± 0.01	0.678 ± 0.01	0.660 ± 0.01	0.642 ± 0.03	0.694 ± 0.03	0.667 ± 0.01	0.738 ± 0.01
NNET_XgbTree	0.665 ± 0.02	0.676 ± 0.02	0.657 ± 0.02	0.637 ± 0.02	0.694 ± 0.03	0.665 ± 0.02	0.733 ± 0.02

\*RF, Random forest; XGBoost, Extreme gradient boosting; Lightgbm, Light gradient boosting machine; Glmnet, Generalized linear model with lasso and elastic net regularization; AUC, Area under the curve; Glmboost, Generalized linear model boosting; NNET, Neural network; Baysglm, Bayesian generalized linear model; SVM, Support vector machine; LDA, Linear discriminant analysis; HDDA, High-dimensional discriminant analysis.

## **Chapter 5 Osteoarthritis Diagnosis Integrating Whole Joint Radiomics and Clinical Features for Ro-bust Learning Models using Biological Privileged Information**

Najla Al Turkestani\*, Lingrui Cai\*, ... Reza Soroushmehr

\*These authors contributed equally to this work.

### **Abstract**

This paper proposes a machine learning model using privileged information (LUPI) and normalized mutual information feature selection method (NMIFS) to build a robust and accurate framework to diagnose patients with Temporomandibular Joint Osteoarthritis (TMJ OA). To build such a model, we employ clinical, quantitative imaging and additional biological markers as privileged information. We show that clinical features play a leading role in the TMJ OA diagnosis and quantitative imaging features, extracted from cone-beam computerized tomography (CBCT) scans, improve the model performance. As the proposed LUPI model employs biological data in the training phase (which boosted the model performance), this data is unnecessary for the testing stage, indicating the model can be widely used even when only clinical and imaging data are collected. The model was validated using 5-fold stratified cross-validation with hyperparameter tuning to avoid the bias of data splitting. Our method achieved an AUC, specificity and precision of 0.81, 0.79 and 0.77, respectively.

**Keywords:** Temporomandibular joint, Osteoarthritis, Machine learning, Feature selection, Learning using privileged information

## 5.1 Introduction

Osteoarthritis (OA) of the temporomandibular joint (TMJ) is a chronic, degenerative disease that affects articular cartilage, synovial tissue and osseous structures of the condyle, articular eminence and articular fossa (Abrahamsson et al. 2017). It causes chronic pain, jaw dysfunction, deterioration of the quality of life and, in advanced stages, necessitates joint replacement (Tanaka, Detamore, and Mercuri 2008). Current diagnosis of TMJ OA occurs primarily at moderate-severe stage of the disease, following the protocols of the diagnostic criteria for temporomandibular disorders (DC/TMD). Although various therapeutic measures can relieve disease symptoms at these stages, to date, no treatment modality can cure or reverse degenerative changes within the joint tissues (Shi et al. 2017). Hence, identification of diagnostic biomarkers that reflect early pathological changes of the joint is crucial for prevention of the irreversible sequelae of the disease.

Animal studies indicated that microstructural change of the subchondral bone was essential for the initiation and progression of OA (Hu, Chen, Wang, et al. 2021). However, no robust tools were available to assess these changes, in humans, at early stages of the disease. More recently, advancement of image processing/analysis and high-performance computing techniques allowed extracting quantitative imaging features, i.e., radiomics, which reflect subtle changes within the examined tissues (Marias 2021). Along with radiomics, the level of biochemical markers in saliva or blood samples could reflect incipient pathological changes and improve diagnosis, severity assessment and risk of progression of osteoarthritis (Munjal et al. 2019). The potential of radiomics and biochemical markers has been elucidated in early detection of various diseases, including knee OA; nevertheless, their value in TMJ OA diagnosis has been scarcely investigated (Hu, Chen, Wang, et al. 2021). Our preliminary studies (Cevidanees et al. 2010), showed a signif-

icant difference in radiomics at the condyles' subchondral bone in TMJ OA and control subjects. We also found a correlation between the resorptive/anabolic changes of the condyles and the level of several biological markers in TMJ OA subjects (Cevidaneş et al. 2014). As it is unlikely that a single biomarker would drive or identify a complex disease such as osteoarthritis (Al Turkestani et al. 2021), we hypothesize that clinical symptoms, subchondral bone radiomics and biological markers are optimal integrative indicators of TMJ health status.

Analysis of large and complex datasets derived from different sources yields better understanding of the disease. However, detection of unknown patterns in big data requires the use of high-end computing solutions and advanced analytical approaches such as machine-learning algorithms. Although prediction models can analyze a large amount of data, incorporating less variables into the model reduces computing resources' consumption and prevents model overfitting (Aas, Jullum, and Løland 2021). Therefore, using a dimensionality reduction technique to identify the optimal subset of the original features is crucial for accurate construction of prediction models. Another challenge for developing a predictive model for TMJ OA diagnosis is inclusion of the biochemical markers. This is due to the restricted specimens' collection, cost and limitations of protein expression measurement systems (Shoukri et al. 2019).

In this study, we address the need for comprehensive quantitative phenotyping of OA in the whole jaw joint. We employ a machine learning paradigm called learning using privileged information (LUPI) and train it with clinical, quantitative imaging and additional biological features as privileged information to classify TMJ OA patients. We also adopt feature selection method to remove redundant and irrelevant features from the feature space. Furthermore, we utilize features occurrence and Shapely additive explanations method to interpret the model predictions.



## 5.2 Materials & Methods

Our dataset consisted of 46 early-stage TMJ OA patients and 46 age and gender-matched healthy controls recruited at the University of Michigan School of Dentistry. All the diagnoses were confirmed by a TMD and orofacial pain specialist based on the DC/TMD. The clinical, biological and radiographic data described below were collected from TMJ OA and control subjects with informed consent and following the guidelines of the Institutional Review Board HUM00113199.

### Clinical Data

Clinical dataset entailed three features obtained from diagnostic tests assessed by the same investigator: 1) headaches in the last month, 2) muscle soreness in the last month, 3) vertical range of unassisted jaw opening without pain (mouth opening).

### Biological Data

Association of proteins expression with arthritis initiation and progression was investigated in a previous study [12]. In this project, using customized protein microarrays (RayBiotech, Inc. Norcross, GA), the expression level of 13 proteins was measured in the participants' saliva and serum samples. The analyzed proteins included: Angiogenin, BDNF, CXCL16, ENA-78, MMP-3, MMP-7, OPG, PAI-1, TGFb1, TIMP-1, TRANCE, VE-Cadherin and VEGF. As the protein expression of MMP3 was not detected in the saliva, it was excluded from subsequent analysis.

### Radiological Data

Using the 3D Accuitomo machine (J. Morita MFG. CORP Tokyo, Japan), cone-beam computed tomography (CBCT) scans were performed for each subject. Radiomics analysis was centered on the lateral region of the articular fossa, articular eminence and condyle, a site where greater OA bone degeneration occurs. Radiomic features were extracted using BoneTexture module in 3D-

slicer software v.4.11(www.3Dslicer.org). We measured 23 texture features: 5 bone morphometry features, 8 Gray Level Co-occurrence Matrix(GLCM) and 10 Grey-Level Run Length Matrix (GLRLM) features. ClusterShade and HaralickCorrelation measurements were highly variable among all participants, therefore, they were not included in the following analysis.

Joint space measurement was evaluated using 3D condylar-to-fossa distances at the anterior, anterolateral, medial, superior and posterior regions.

### Statistical and Machine Learning Approaches

In this section, we describe methods utilized for building a robust TMJOA diagnosis model (Figure 5.1). These methods include: 1) cross-validation and grid search, 2) feature selection and 3) learning using privileged information.

#### Cross-Validation and Grid Search

Cross-validation is an effective approach to model hyperparameter optimization and model selection that attempts to overcome the overfitting issue. The dataset was split into 80% for training and 20% holdout for testing. The 5fold cross-validation with the same portion of data split was nested inside the 80% train dataset, and grid search was performed in each fold of data for hyperparameters tuning. The best combination of hyperparameters was picked based on the mean and standard deviation of F1 scores over the 5-fold cross-validation. The overall procedure was repeated 10 times with 10 random seeds to avoid sampling bias from data partitioning. The final evaluation scores reported in this study are the mean±standard deviation of the holdout test set performance across all 10 repetitions.

#### Feature Selection

Feature selection is a common dimensional reduction technique for building a machine learning model. Increasing the number of features often results in decreasing the prediction error. Howev-

er, it increases the risk of model overfitting particularly with small datasets. Here, we customized a feature selection method that takes the advantages of privileged variables and mutual information to improve the performance of the classifier.

Normalized mutual information feature selection (NMIFS) method and its modified version called NMIFS+ was used to measure the relevance and redundancy of features with the primary objective of high accuracy with the least possible time complexity. NMIFS+ extends the NMIFS algorithm with the LUPI framework, which could take full account of the privilege features along with standard features and make feature selection from those two sets separately. The NMIFS+ was applied to all the LUPI models in this study and, correspondingly, the NMIFS on non-LUPI models.

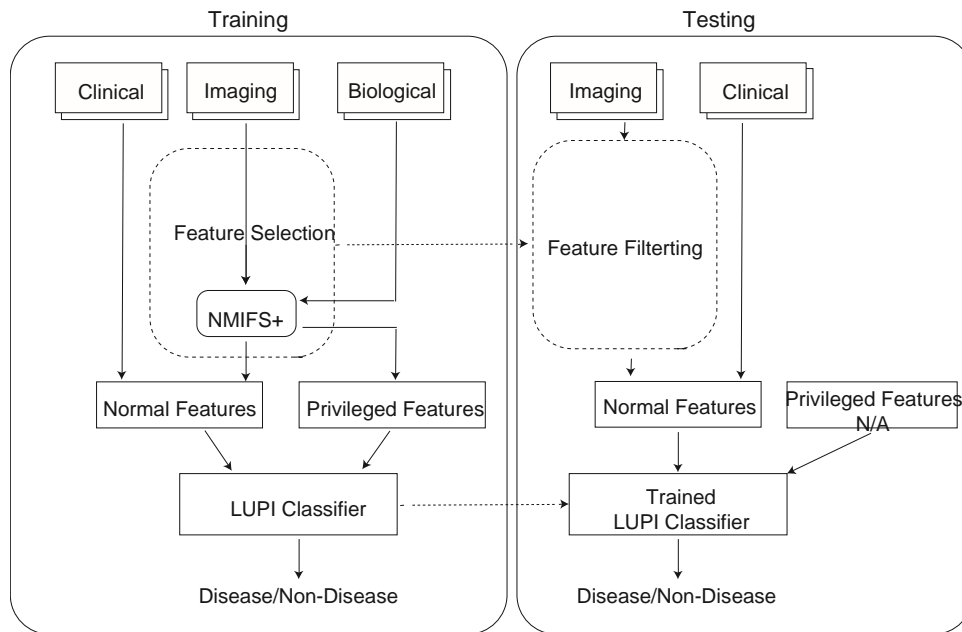


Figure 5.1: Diagram of Training and Testing Process

### LUPI Framework

The idea of learning using privileged information (LUPI) was first proposed as capturing the essence of teacher-student-based learning by Vapnik and Vashist. In contrast to the existing ma-

chine learning paradigm, where the model learns and makes predictions with fixed information, the LUPI paradigm considers several specific forms of privileged information, just like a teacher who provides additional information, which can include comments, explanations, and logic to students and thus increases the learning efficiency.

In the classical binary classification model, we were given training pairs  $(x_1, y_1), \dots, (x_l, y_l)$ , where  $x_i \in X$ ,  $y_i \in \{-1, 1\}$ ,  $i = 1, \dots, l$ , and each pair is independently generated by some underlying distribution  $P_{XY}$ , which is unknown. The model is trained to find among a given set of functions  $f(x, \alpha)$ ,  $\alpha \in \Lambda$ , the function  $y = f(x, \alpha)$  that minimizes the probability of incorrect classifications over the unknown distribution  $P_{XY}$ .

In the LUPI framework, we were given training triplets  $(x_1, x_{*1}, y_1), \dots, (x_l, x_{*l}, y_l)$ ,  $x_i \in X$ ,  $x_{*i} \in X^*$ ,  $y_i \in \{-1, 1\}$ ,  $i = 1, \dots, l$ , which is slightly different from the classical one. Each triplet is independently generated by some underlying distribution  $P_{XX^*Y}$ , which is still unknown. The additional privileged information is available only for the training examples, not for the test phase. In this scenario, we can utilize  $X^*$  to improve learning performance.

There are a few implementations of LUPI models. One of them is based on random vector functional link network (RVFL) that is a randomized version of the functional link neural network. A kernel-based RVFL, called KRVFL+, has been proposed based on the LUPI paradigm. It incorporates efficient ways to use kernel tricks for highly complicated nonlinear feature training and train RVFL networks with privileged information (Figure 5.2). The parameters, including weights and biases, from the input layer to the hidden layers are generated randomly from a fixed domain, and only the output weights need to be computed.

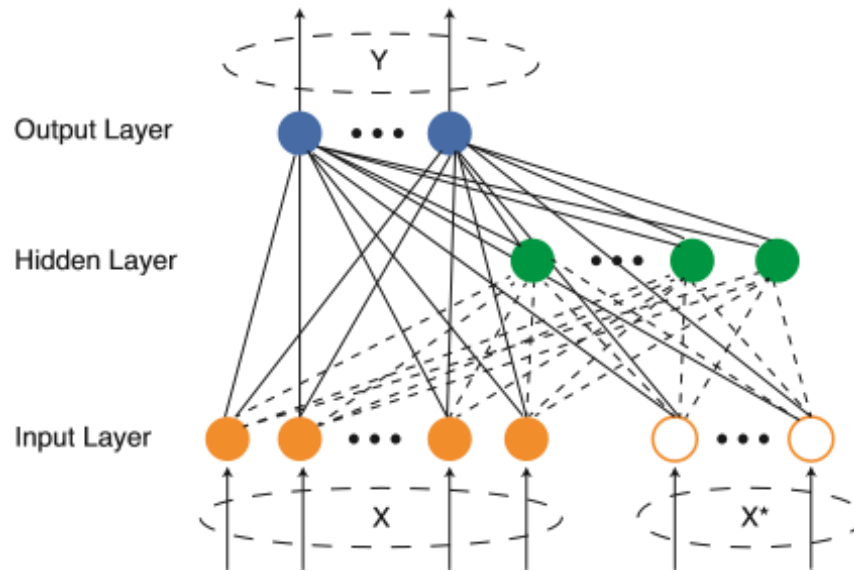


**Figure 5.2: The Architecture of KRVFL+ Network.** Solid lines are output weights and dash lines stand for random weights and biases.

### 5.3 Results

#### 5.3.1 LUPI and non-LUPI models

Figure 5.3 shows the comparison of the classification performance between LUPI and non-LUPI models. We evaluated the diagnostic potential of imaging features extracted from the articular eminence, articular fossa, condyle, and joint space measurement, as well as clinical features. Only the clinical feature sets provided discriminative models (AUC=0.723) for TMJ OA diagnosis. By introducing LUPI-based models with additional biological features, LUPI paradigm significantly enhanced the model performance on clinical (AUC=0.794), joint space measurement (AUC=0.625), and condyle (AUC=0.641) datasets.

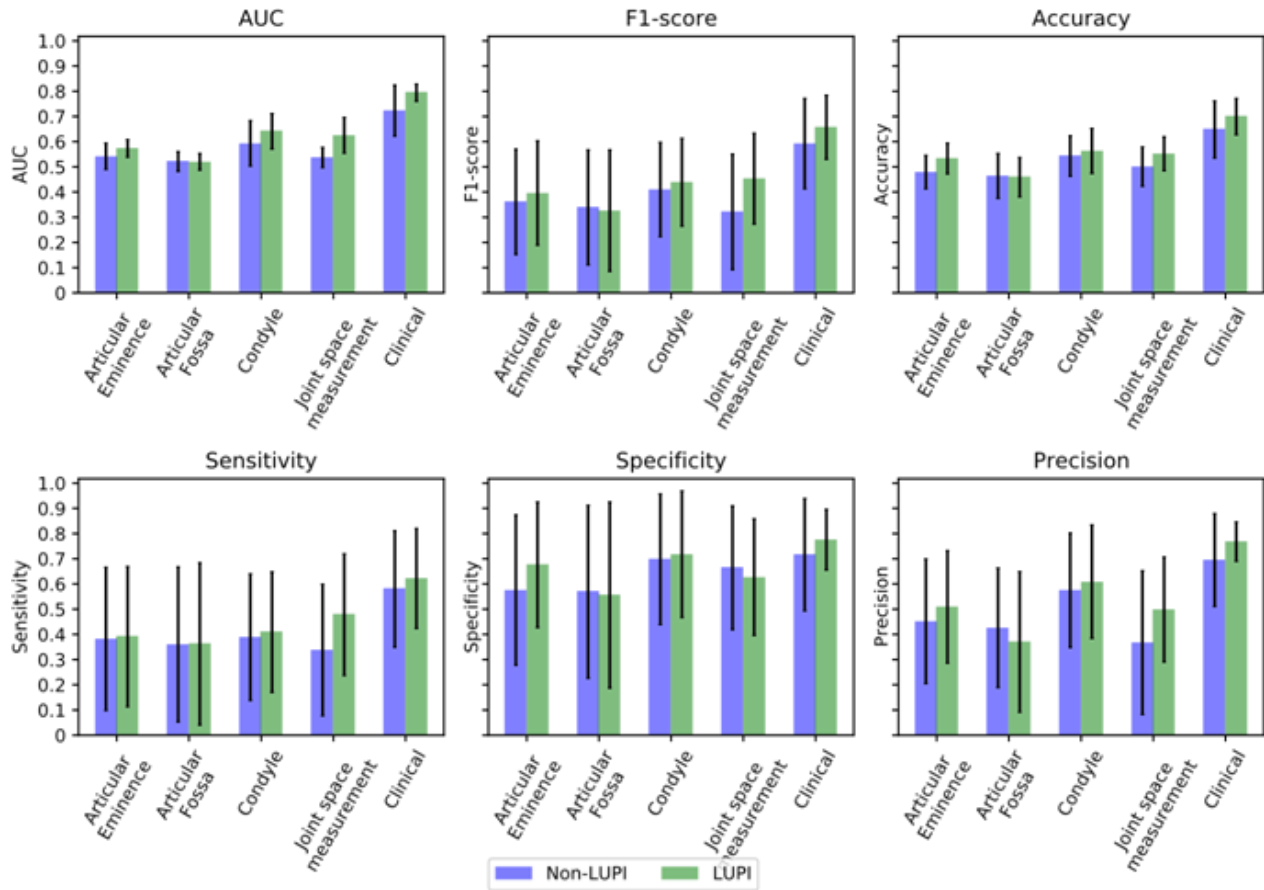


**Figure 5.3: Comparison of LUPI and non-LUPI Models.** The non-LUPI models only trained with normal features and RVFL model. The LUPI model trained with KRVFL+ and biological data as privilege information.

### 5.3.2 Feature Integration Comparison

Table 5.1 shows the classification performances with different feature integration strategies. Given that clinical features had strong discriminative power for TMJ OA diagnosis, two groups of experiments were conducted to investigate the effect of an enlarged candidate pool for feature selection. Adding more features into the clinical dataset and selecting from combined set improved the model performance markedly, i.e., the models had higher AUC scores. With an AUC=0.794, the clinical feature model achieved fairly well performance. Selecting features from a pool of condyle radiomic features together with the clinical features increased the AUC score to 0.804. The performance was even higher when feature selection was conducted on all condyle,

3D measurements and clinical datasets, AUC=0.807. Keeping all clinical criteria and applying feature selection on the remaining dataset resulted in slightly higher AUC values. The AUC scores became 0.808 and 0.809 for the condyle and condyle with additional 3D measurement features models, respectively.

**Table 5.1: Comparison of Different Feature Integration Methods (in Percentage %)**

Feature Set	AUC	F1 score	Accuracy	Sensitivity	Specificity	Precision
Cl	79.4±3.4	65.7±12.7	69.9±7.2	62.2.0±19.8	77.6±12.0	76.8±7.8
(Cl+Cd)*	80.4±3.8	67.5±9.4	70.4±5.6	64.4±18.6	76.4±16.0	76.1±9.2
Cl+Cd*	80.8±4.1	64.8±11.6	69.4±6.4	60.2±19.4	78.7±13.5	76.0±9.3
(Cl+Cd JS)*	80.7±3.8	64.2±15.0	69.8±6.9	61.3±22.9	78.2±15.3	75.1±12.2
Cl+Cd JS*	80.9±3.6	66.1±12.2	70.9±6.0	62.7±19.7	79.1±13.6	77.4±9.8

Cl: Clinical; Cd: Condyle; Cd JS: Condyle and 3D Joint Space measurements.\* indicates feature selection by NMIFS+ method. The feature sets in parentheses have been pooled together for feature selection, otherwise it proceeded on feature set with \* separately. All the models have been trained with KRVFL+ with biological data as privilege information.

### 5.3.3 Feature Occurrence and Importance

To interpret the prediction of our proposed model, we utilized feature occurrence and Shapley values. The NMIFS+ method is a measure of redundancy among features. The calculation of mutual information and redundancy highly depends on the training samples which varied from split to split. Feature occurrence means how many times a feature was selected by NMIFS+ method among the total 50 models. The more times a feature occurs, the more reliable its importance is (Figure 5.4A). Shapley values were used to interpret the contribution of individual features into the prediction of the trained model. Contributing features are shown in Figure 5.4B according to the order of the mean absolute of Shapley values across all the data, which indicate the average impact of feature on model output magnitude. Figure 5.4C provides further indication of Shapley values and shows the complexity of feature contribution in models. Each circle represents a fea-

ture value of one patient/control, either increases or decreases the prediction(positive value and negative value). Figure 5.4D combines feature importance with feature effects. Here we picked one model for visualization instead of pulling all 50 models together. Each point in the summary plot is a Shapley value for a feature and a patient/control. The order of the features on the y-axis is based on their importance. The color represents the Shapley value of the features from low to high. We divided the instances into TMJ OA diseased group and Control group, displayed in different markers. Higher values of headache, LongRunHighGreyLevelRunEmphasis and muscle soreness increased the probability of assigning TMJ OA diagnosis.

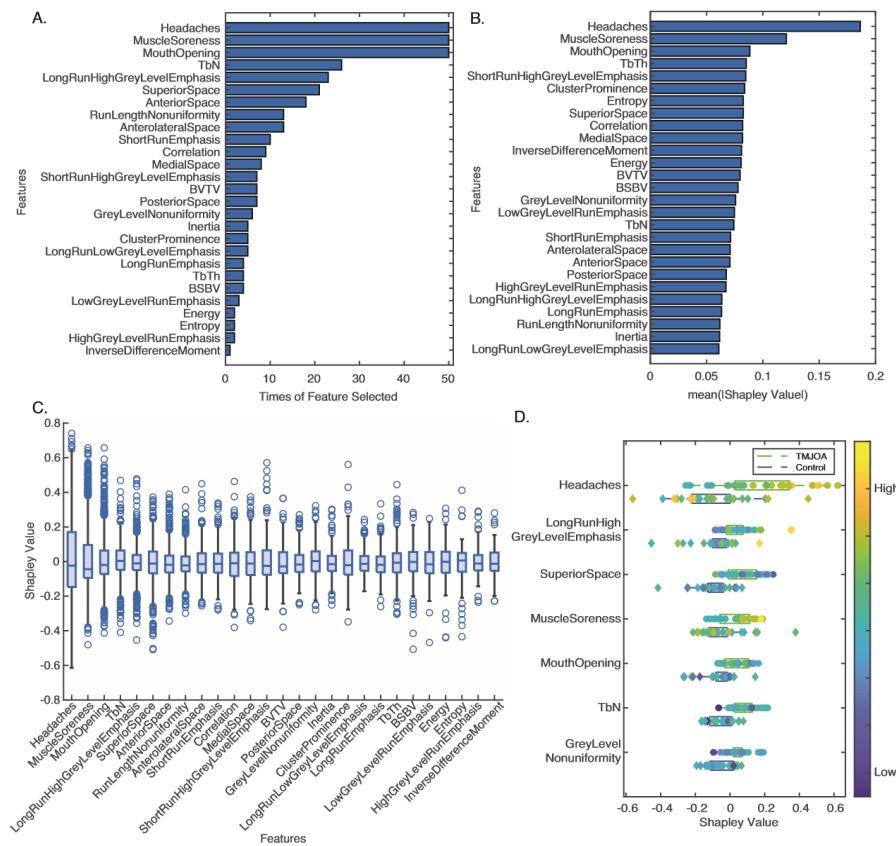


**Figure 5.4:** A. Feature occurrence in 50 trained models using NMIFS method. B. Feature importance measured as the mean absolute Shapley values in 50 models. C. Distribution of Shapley values in each query point in the 50 models. The order of the features shown in the x-axis is based on the feature occurrence. D. Shapley summary plot for one model. The boxplots represent the distribution of TMJOA and control groups (each TMJOA patient is shown as a circle and control as a diamond). The Heatmap color bar shows the value of the feature itself from high to low (yellow to blue). Low number of Shapley value of features reduce the predicted TMJOA diseased probability, a large number of Shapley value increase the probability.



## 5.5 Discussion

This study developed an enhanced model for TMJ OA diagnosis, utilizing state-of-the-art machine learning technology and considering clinical, quantitative imaging markers, and additional biological features used only for training. This is the first study to utilize quantitative imaging markers of the whole joint: condyle, articular space, articular fossa and articular eminence. We employed feature selection to minimize feature sets and improve the model robustness. Furthermore, feature occurrence and Shapley value were assessed to reduce the black-box nature of the machine learning model, as well as improve the domain experts' confidence in the model's prediction. This study findings demonstrate excellent performance of the feature integration methods and LUPI paradigm in predicting TMJ OA status.

The Diagnostic Criteria for Temporomandibular Disorders (DC/TMD) have been the most utilized protocol for TMJ OA diagnosis. However, these criteria are dependent on subjective clinical signs/symptoms and subjective radiological interpretation of imaging features associated with irreversible bone changes (Hu, Chen, Wang, et al. 2021; Marias 2021). Early treatment and modification of the disease course requires precise diagnosis of TMJ OA at initial stages. In this study, we utilized multi-source data collected from subjects at early stages of TMJ OA. We employed the LUPI paradigm and used biological features of inflammation, neuroception, bone resorption and angiogenesis as privileged information. The LUPI algorithm allowed benefiting from diagnostic information within the existing biological data and eliminated future need for biological samples' collection and analysis. Inclusion of biological data with the LUPI framework boosted our model performance, confirming the need for biological data only for model training. We developed a robust model for TMJ OA diagnosis and validated its performance using extensive evaluation metrics (Figure 5.1). Our model demonstrated sensitivity and specificity

of 63% and 79%, respectively. These values exceeded the sensitivity and specificity, 58% and 72%, of TMJ OA diagnosis following DC/TMD protocol without imaging. Honda and colleagues reported that the CBCT scan's use improved the sensitivity and specificity for detecting condylar osseous defects to 80% and 90%, sequentially (Zhang and Yang 2019). Nevertheless, CBCT sensitivity is dependent on the defects' size, it is challenging to detect early alterations that are <2mm. Hence, we extracted objective, quantitative imaging features from the subchondral bones of the condyle, articular fossa and articular eminence. Using the LUPI-based model, we found that only condyle's radiomics could differentiate between healthy and diseased subjects (Table 4.1). In line with this observation, it was reported that patients with early TMJ OA had osteoarthritic bone alterations in their condyles (69.93%) more than articular fossa (10%) and articular eminence (6.6%) (Massilla Mani and Sivasubramanian 2016). Interestingly, we noted that the superior 3D joint space distinguished TMJ OA subjects using LUPI-based models (AUC=.63), denoting the importance of this feature in detecting osteoarthritic changes. Along with radiomics and joint space measurements, we supplemented the model with clinical signs that were measurable in both groups.

Machine learning models are leveraged for clinical predictive modeling, where clinical values are used to predict clinical diagnosis. However, these models do not explain the basis for their prediction. This raise concerns in medical domains and challenge researchers to identify reasons behind the model outcomes (Petch, Di, and Nelson 2022). Here, we facilitated the interpretability of our model by reducing the number of candidate features. In general, for a fixed sample size, the error of designed classifier decreases and then increases as the number of features grows. Finding an optimal number of features is crucial in terms of reducing the time to build the learning model and increasing the accuracy in the learning process. For uncorrelated features, the op-

timal feature size is  $N-1$ , where the  $N$  is the sample size. As the feature correlation increases, the optimal feature size becomes proportional to  $N$  for highly correlated features. Furthermore, texture features turned out to be highly correlated in Cho's work. Those further proof of the necessity of feature selection.

Using the NMIFS method, we calculated feature occurrence to identify the discriminative features of TMJ OA. Moreover, we calculated Shapley values to demonstrate how each clinical and imaging feature is contributing to the outcome/disease diagnosis in individual patients. Headache, muscle soreness and limited range of vertical mouth opening without pain were among the top features that contributed to the model prediction for TMJ OA. TrabecularNumber, superior 3D joint space and LongRunHighGreyLevelRunEmphasis were the top imaging features selected in the majority of the trained models. Importantly, the amalgamation of different data-sources in this study is essential for comprehensive assessment of individuals' health. In line with our results, Liang and colleagues found significant differences of the TrabecularNumber in subjects with TMJ OA compared to healthy individuals (Liang, Liu, et al. 2017). Our findings corroborate those that indicate radiomics provide an objective assessment of the pathological changes and may overcome the subjectivity of patients-reported symptoms (Patel et al. 2013). Zhang et al. validated the importance of detecting TMJ morphological changes using 3D measurements, showing that 2D and 3D TMJ space measurements varied significantly in CBCT scans of healthy individuals (Zhang, Xu, and Liu 2017). The present study is the first to test whole joint (condylar, articular eminence and articular fossa) radiomics and incorporate 3D joint space measurements into a comprehensive diagnostic tool for TMJ OA.

### ***5.5 Conclusion***

Normalized mutual information feature selection method and LUPI paradigm established a robust model for TMJ OA diagnosis. The identified clinical and quantitative imaging markers can be considered a foundation for reliable detection of TMJ OA pathological alterations and are potential markers for prediction of disease progression in future longitudinal studies.

## Bibliography

- Aas, Kjersti, Martin Jullum, and Anders Løland. 2021. "Explaining Individual Predictions When Features Are Dependent: More Accurate Approximations to Shapley Values." *Artificial Intelligence* 298 (September): 103502. <https://doi.org/10.1016/j.artint.2021.103502>.
- Abiodun, Oludare Isaac, Aman Jantan, Abiodun Esther Omolara, Kemi Victoria Dada, Abubakar Malah Umar, Okafor Uchenwa Linus, Humaira Arshad, Abdullahi Aminu Kazaure, Usman Gana, and Muhammad Ubale Kiru. 2019. "Comprehensive Review of Artificial Neural Network Applications to Pattern Recognition." *IEEE Access* 7: 158820–46. <https://doi.org/10.1109/ACCESS.2019.2945545>.
- Abouelhuda, Amira Mokhtar, Hyun-Seok Kim, Sang-Yun Kim, and Young-Kyun Kim. 2017. "Association between Headache and Temporomandibular Disorder." *Journal of the Korean Association of Oral and Maxillofacial Surgeons* 43 (6): 363–67. <https://doi.org/10.5125/jkaoms.2017.43.6.363>.
- Abrahamsson, AK., M. Kristensen, L. Z. Arvidsson, T. K. Kvien, T. A. Larheim, and I. K. Haugen. 2017. "Frequency of Temporomandibular Joint Osteoarthritis and Related Symptoms in a Hand Osteoarthritis Cohort." *Osteoarthritis and Cartilage* 25 (5): 654–57. <https://doi.org/10.1016/j.joca.2016.12.028>.
- Abu Alfeilat, Haneen Arafat, Ahmad B. A. Hassanat, Omar Lasassmeh, Ahmad S. Tarawneh, Mahmoud Bashir Alhasanat, Hamzeh S. Eyal Salman, and V. B. Surya Prasath. 2019. "Effects of Distance Measure Choice on K-Nearest Neighbor Classifier Performance: A Review." *Big Data* 7 (4): 221–48. <https://doi.org/10.1089/big.2018.0175>.
- Agha-Hosseini, Farzaneh, Iraj Mirzaii-Dizgah, Shiva Shirazian, and Maryam Javaheri-Mahd. 2023. "Treating Parafunctional Habits for Alleviating Temporomandibular Disorder and Lower Back Pain: A Phase II Clinical Trial." *Frontiers in Dentistry* 20 (May): 11. <https://doi.org/10.18502/fid.v20i11.12657>.
- Ahmad, El Mabrouk, Sylvester, and Zafarullah. 2009. "Human Osteoarthritic Chondrocytes Are Impaired in Matrix Metalloproteinase-13 Inhibition by IFN-Gamma Due to Reduced IFN-Gamma Receptor Levels." *Osteoarthritis and Cartilage* 17 (8): 1049–55. <https://doi.org/10.1016/j.joca.2009.02.008>.
- Ahmad, Mansur, Lars, Odont, Quentin Anderson, Krishnan Kartha, Richard K. Ohrbach, Edmond L. Truelove, Mike T. John, and Eric L. Schiffman. 2009. "Research Diagnostic Criteria for Temporomandibular Disorders (RDC/TMD): Development of Image Analysis Criteria and Examiner Reliability for Image Analysis." *Oral Surgery, Oral Medicine, Oral Pathology, Oral Radiology, and Endodontics* 107 (6): 844–60. <https://doi.org/10.1016/j.tripleo.2009.02.023>.
- Ahmad, Mansur, and Eric L. Schiffman. 2016. "Temporomandibular Joint Disorders and Orofacial Pain." *Dental Clinics of North America* 60 (1): 105–24. <https://doi.org/10.1016/j.cden.2015.08.004>.

- Ahmed, Zeeshan, Khalid Mohamed, Saman Zeeshan, and Xinqi Dong. 2020. "Artificial Intelligence with Multi-Functional Machine Learning Platform Development for Better Healthcare and Precision Medicine." *Database: The Journal of Biological Databases and Curation* 2020 (March): baaa010. <https://doi.org/10.1093/database/baaa010>.
- Ahsan, Md Manjurul, Shahana Akter Luna, and Zahed Siddique. 2022a. "Machine-Learning-Based Disease Diagnosis: A Comprehensive Review." *Healthcare* 10 (3). <https://doi.org/10.3390/healthcare10030541>.
- . 2022b. "Machine-Learning-Based Disease Diagnosis: A Comprehensive Review." *Healthcare* 10 (3): 541. <https://doi.org/10.3390/healthcare10030541>.
- Aiken, Alison, and Rama Khokha. 2010. "Unraveling Metalloproteinase Function in Skeletal Biology and Disease Using Genetically Altered Mice." *Biochimica et Biophysica Acta (BBA) - Molecular Cell Research, Matrix Metalloproteinases*, 1803 (1): 121–32. <https://doi.org/10.1016/j.bbamcr.2009.07.002>.
- Ajekigbe, B., K. Cheung, Y. Xu, A.J. Skelton, A. Panagiotopoulos, J. Soul, T.E. Hardingham, D.J. Deehan, M.J. Barter, and D.A. Young. 2019. "Identification of Long Non-Coding RNAs Expressed in Knee and Hip Osteoarthritic Cartilage." *Osteoarthritis and Cartilage* 27 (4): 694–702. <https://doi.org/10.1016/j.joca.2018.12.015>.
- Akeson, Graham, and Charles J. Malemud. 2017. "A Role for Soluble IL-6 Receptor in Osteoarthritis." *Journal of Functional Morphology and Kinesiology* 2 (3): 27. <https://doi.org/10.3390/jfmk2030027>.
- Al Turkestani, Najla, Jonas Bianchi, Romain Deleat-Besson, Celia Le, Li Tengfei, Juan Carlos Prieto, Marcela Gurgel, et al. 2021. "Clinical Decision Support Systems in Orthodontics: A Narrative Review of Data Science Approaches." *Orthodontics & Craniofacial Research* 24 (Suppl 2): 26–36. <https://doi.org/10.1111/ocr.12492>.
- Al-Ani, Ziad. 2021. "Temporomandibular Joint Osteoarthrosis: A Review of Clinical Aspects and Management." *Primary Dental Journal* 10 (1): 132–40. <https://doi.org/10.1177/2050168420980977>.
- Alderson, Philip O, and Ronald M Summers. 2020. "The Evolving Status of Radiomics." *JNCI Journal of the National Cancer Institute* 112 (9): 869–70. <https://doi.org/10.1093/jnci/djaa018>.
- Alexiou, Ke, Hc Stamatakis, and K. Tsiklakis. 2009. "Evaluation of the Severity of Temporomandibular Joint Osteoarthritic Changes Related to Age Using Cone Beam Computed Tomography." *Dento Maxillo Facial Radiology* 38 (3): 141–47. <https://doi.org/10.1259/dmfr/59263880>.
- Ali, and Ahmed. 2022. "Employment of Instrumented Vehicles to Identify Real-Time Snowy Weather Conditions on Freeways Using Supervised Machine Learning Techniques – A Naturalistic Driving Study." *IATSS Research* 46 (4): 525–36. <https://doi.org/10.1016/j.iatssr.2022.09.001>.
- Ali, Aleksandra Turkiewicz, Velocity Hughes, Elin Folkesson, Jon Tjörnstand, Paul Neuman, Patrik Önnérkjord, and Martin Englund. 2022. "Proteomics Profiling of Human Synovial Fluid Suggests Increased Protein Interplay in Early-Osteoarthritis (OA) That Is Lost in Late-Stage OA." *Molecular & Cellular Proteomics: MCP* 21 (3): 100200. <https://doi.org/10.1016/j.mcpro.2022.100200>.
- Alimoradi, Nahid, Mohammad Tahami, Negar Firouzabadi, Elham Haem, and Amin Ramezani. 2023. "Metformin Attenuates Symptoms of Osteoarthritis: Role of Genetic Diversity of

- Bcl2 and CXCL16 in OA.” *Arthritis Research & Therapy* 25 (1): 35.  
<https://doi.org/10.1186/s13075-023-03025-7>.
- Al-Jabery, Khalid, Tayo Obafemi-Ajayi, Gayla Olbricht, and Donald Wunsch. 2019. *Computational Learning Approaches to Data Analytics in Biomedical Applications*. Academic Press.
- Alkinani, Husam H., Abo Taleb T. Al-Hameedi, and Shari Dunn-Norman. 2020. “Artificial Neural Network Models to Predict Lost Circulation in Natural and Induced Fractures.” *SN Applied Sciences* 2 (12): 1980. <https://doi.org/10.1007/s42452-020-03827-3>.
- Allareddy, Shankar Rengasamy Venugopalan, Romesh P. Nalliah, Jennifer L. Caplin, Min Kyeong Lee, and Veeratrishul Allareddy. 2019a. “Orthodontics in the Era of Big Data Analytics.” *Orthodontics & Craniofacial Research* 22 Suppl 1 (May): 8–13.  
<https://doi.org/10.1111/ocr.12279>.
- Allareddy, Veerasathpurush, Shankar Rengasamy Venugopalan, Romesh P. Nalliah, Jennifer L. Caplin, Min Kyeong Lee, and Veeratrishul Allareddy. 2019b. “Orthodontics in the Era of Big Data Analytics.” *Orthodontics & Craniofacial Research* 22 (May): 8–13.  
<https://doi.org/10.1111/ocr.12279>.
- Alloghani, Mohamed, Dhiya Al-Jumeily, Jamila Mustafina, Abir Hussain, and Ahmed J. Aljaaf. 2020. “A Systematic Review on Supervised and Unsupervised Machine Learning Algorithms for Data Science.” In *Supervised and Unsupervised Learning for Data Science*, edited by Michael W. Berry, Azlinah Mohamed, and Bee Wah Yap, 3–21. Unsupervised and Semi-Supervised Learning. Cham: Springer International Publishing.  
[https://doi.org/10.1007/978-3-030-22475-2\\_1](https://doi.org/10.1007/978-3-030-22475-2_1).
- Almarza, Alejandro J., Bryan N. Brown, Boaz Arzi, David Faustino Ângelo, William Chung, Stephen F. Badylak, and Michael Detamore. 2018. “Preclinical Animal Models for Temporomandibular Joint Tissue Engineering.” *Tissue Engineering Part B: Reviews* 24 (3): 171–78. <https://doi.org/10.1089/ten.teb.2017.0341>.
- Almășan, Oana, Daniel-Corneliu Leucuța, Mihaela Hedeșiu, Sorana Mureșanu, and Ștefan Lucian Popa. 2023. “Temporomandibular Joint Osteoarthritis Diagnosis Employing Artificial Intelligence: Systematic Review and Meta-Analysis.” *Journal of Clinical Medicine* 12 (3): 942. <https://doi.org/10.3390/jcm12030942>.
- Almhdie-Imjabbar, Ahmad, Khac-Lan Nguyen, Hechmi Toumi, Rachid Jennane, and Eric Lespessailles. 2022. “Prediction of Knee Osteoarthritis Progression Using Radiological Descriptors Obtained from Bone Texture Analysis and Siamese Neural Networks: Data from OAI and MOST Cohorts.” *Arthritis Research & Therapy* 24 (1): 66.  
<https://doi.org/10.1186/s13075-022-02743-8>.
- Alqhtani, Nasser Raqe, Malak Sultan Alkhaldi, Alhanoof Falah Alanazi, Abdullatif Saad Alabdulsalam, Adel Alenazi, Mahmud Uz Zaman, Adel Alzahrani, Ahmad Alshadwi, Ali Al Rafedah, and Mohammed AlOtaibi. 2022. “Temporomandibular Joint Space Dimensions among Saudi Patients with Temporomandibular Disorders: MRI-Based Retrospective Study.” *International Journal of Clinical Practice* 2022 (August): 5846255.  
<https://doi.org/10.1155/2022/5846255>.
- Anderson, Gary C., Yoly M. Gonzalez, Richard Ohrbach, Edmond L. Truelove, Earl Sommers, John O. Look, and Eric L. Schiffman. 2010. “Research Diagnostic Criteria for Temporomandibular Disorders: Future Directions.” *Journal of Orofacial Pain* 24 (1): 79–88.

- Aoun, Yasmina, Rita Ejbeh, Abboud Youssef, and Joseph Hobeiche. 2023. “Salivary Biomarkers as Potential Diagnostic Tool for Temporomandibular Disorders: A Comprehensive Review.” *CRANIO®*, July, 1–10. <https://doi.org/10.1080/08869634.2023.2229607>.
- Aragon-Sanabria, Virginia, Steven E. Pohler, Vikram J. Eswar, Matthew Bierowski, Esther W. Gomez, and Cheng Dong. 2017. “VE-Cadherin Disassembly and Cell Contractility in the Endothelium Are Necessary for Barrier Disruption Induced by Tumor Cells.” *Scientific Reports* 7 (1): 45835. <https://doi.org/10.1038/srep45835>.
- Arayasantiparb, Raweewan, Somsak Mitrirattanakul, Panupol Kunasarapun, Harakun Chutima-taewin, Pawares Netneparat, and Worapol Sae-Heng. 2020. “Association of Radiographic and Clinical Findings in Patients with Temporomandibular Joints Osseous Alteration.” *Clinical Oral Investigations* 24 (1): 221–27. <https://doi.org/10.1007/s00784-019-02945-6>.
- Arbet, Jaron, Cole Brokamp, Jareen Meinzen-Derr, Katy E. Trinkley, and Heidi M. Spratt. 2020. “Lessons and Tips for Designing a Machine Learning Study Using EHR Data.” *Journal of Clinical and Translational Science* 5 (1): e21. <https://doi.org/10.1017/cts.2020.513>.
- Arden, Nigel, Pascal Richette, Cyrus Cooper, Olivier Bruyère, Eric Abadie, Jaime Branco, Maria Luisa Brandi, et al. 2015. “Can We Identify Patients with High Risk of Osteoarthritis Progression Who Will Respond to Treatment? A Focus on Biomarkers and Frailty.” *Drugs & Aging* 32 (7): 525–35. <https://doi.org/10.1007/s40266-015-0276-7>.
- Asami, Toshio, Takuya Ito, Hidefumi Fukumitsu, Hiroshi Nomoto, Yoshiko Furukawa, and Shoei Furukawa. 2006. “Autocrine Activation of Cultured Macrophages by Brain-Derived Neurotrophic Factor.” *Biochemical and Biophysical Research Communications* 344 (3): 941–47. <https://doi.org/10.1016/j.bbrc.2006.03.228>.
- Ashburner, J., and K. J. Friston. 1999. “Nonlinear Spatial Normalization Using Basis Functions.” *Human Brain Mapping* 7 (4): 254–66. [https://doi.org/10.1002/\(SICI\)1097-0193\(1999\)7:4<#x0003c;254::AID-HBM4>#x0003e;3.0.CO;2-G](https://doi.org/10.1002/(SICI)1097-0193(1999)7:4<#x0003c;254::AID-HBM4>#x0003e;3.0.CO;2-G).
- Asiri, Saeed N., Larry P. Tadlock, Emet Schneiderman, and Peter H. Buschang. 2020. “Applications of Artificial Intelligence and Machine Learning in Orthodontics.” *APOS Trends in Orthodontics* 10 (March): 17–24. [https://doi.org/10.25259/APOS\\_117\\_2019](https://doi.org/10.25259/APOS_117_2019).
- Atzeni, F., and P. Sarzi-Puttini. 2013. “Tumor Necrosis Factor.” In *Brenner’s Encyclopedia of Genetics (Second Edition)*, edited by Stanley Maloy and Kelly Hughes, 229–31. San Diego: Academic Press. <https://doi.org/10.1016/B978-0-12-374984-0.01594-1>.
- Auconi, Pietro, Marco Scazzocchio, Paola Cozza, James A. McNamara, and Lorenzo Franchi. 2015. “Prediction of Class III Treatment Outcomes through Orthodontic Data Mining.” *European Journal of Orthodontics* 37 (3): 257–67. <https://doi.org/10.1093/ejo/cju038>.
- Avanzo, Michele, Lise Wei, Joseph Stancanello, Martin Vallières, Arvind Rao, Olivier Morin, Sarah A. Mattonen, and Issam El Naqa. 2020. “Machine and Deep Learning Methods for Radiomics.” *Medical Physics* 47 (5): e185–202. <https://doi.org/10.1002/mp.13678>.
- Avery, Emily, Pina C. Sanelli, Mariam Aboian, and Seyedmehdi Payabvash. 2022. “Radiomics: A Primer on Processing Workflow and Analysis.” *Seminars in Ultrasound, CT, and MR* 43 (2): 142–46. <https://doi.org/10.1053/j.sult.2022.02.003>.
- Awad, Mariette, and Rahul Khanna. 2015a. “Machine Learning.” In *Efficient Learning Machines: Theories, Concepts, and Applications for Engineers and System Designers*, edited by Mariette Awad and Rahul Khanna, 1–18. Berkeley, CA: Apress. [https://doi.org/10.1007/978-1-4302-5990-9\\_1](https://doi.org/10.1007/978-1-4302-5990-9_1).
- . 2015b. “Support Vector Machines for Classification.” In *Efficient Learning Machines: Theories, Concepts, and Applications for Engineers and System Designers*, edited by



- Mariette Awad and Rahul Khanna, 39–66. Berkeley, CA: Apress.  
[https://doi.org/10.1007/978-1-4302-5990-9\\_3](https://doi.org/10.1007/978-1-4302-5990-9_3).
- Bae, SunMee, Moon-Soo Park, Jin-Woo Han, and Young-Jun Kim. 2017. “Correlation between Pain and Degenerative Bony Changes on Cone-Beam Computed Tomography Images of Temporomandibular Joints.” *Maxillofacial Plastic and Reconstructive Surgery* 39 (1): 19. <https://doi.org/10.1186/s40902-017-0117-1>.
- Bair, Eric, Sheila Gaynor, Gary D. Slade, Richard Ohrbach, Roger B. Fillingim, Joel D. Greenspan, Ronald Dubner, Shad B. Smith, Luda Diatchenko, and William Maixner. 2016. “Identification of Clusters of Individuals Relevant to Temporomandibular Disorders and Other Chronic Pain Conditions: The OPPERA Study.” *Pain* 157 (6): 1266–78. <https://doi.org/10.1097/j.pain.0000000000000518>.
- Bakke, Merete, Arne Petersson, Mie Wiesel, Palle Svanholt, and Liselotte Sonnesen. 2014. “Bony Deviations Revealed by Cone Beam Computed Tomography of the Temporomandibular Joint in Subjects without Ongoing Pain.” *Journal of Oral & Facial Pain and Headache* 28 (4): 331–37. <https://doi.org/10.11607/ofph.1255>.
- Bancroft, Laura W, Jeffrey J Peterson, and Mark J Kransdorf. 2004. “Cysts, Geodes, and Erosions.” *Radiologic Clinics of North America, Arthritis Imaging*, 42 (1): 73–87. [https://doi.org/10.1016/S0033-8389\(03\)00165-9](https://doi.org/10.1016/S0033-8389(03)00165-9).
- Banerjee, Mousumi, Evan Reynolds, Hedvig B Andersson, and Brahmajee Nallamothu. 2019. “Tree-Based Analysis: A Practical Approach to Create Clinical Decision Making Tools.” *Circulation. Cardiovascular Quality and Outcomes* 12 (5): e004879. <https://doi.org/10.1161/CIRCOUTCOMES.118.004879>.
- Baran, Paul, Selina Hansen, Georg H. Waetzig, Mohammad Akbarzadeh, Larissa Lamertz, Heinrich J. Huber, M. Reza Ahmadian, Jens M. Moll, and Jürgen Scheller. 2018. “The Balance of Interleukin (IL)-6, IL-6-soluble IL-6 Receptor (sIL-6R), and IL-6·sIL-6R·sgp130 Complexes Allows Simultaneous Classic and Trans-Signaling.” *The Journal of Biological Chemistry* 293 (18): 6762–75. <https://doi.org/10.1074/jbc.RA117.001163>.
- Barghan, S, S Tetradis, and Sm Mallya. 2012. “Application of Cone Beam Computed Tomography for Assessment of the Temporomandibular Joints.” *Australian Dental Journal* 57 (s1): 109–18. <https://doi.org/10.1111/j.1834-7819.2011.01663.x>.
- Barredo Arrieta, Alejandro, Natalia Díaz-Rodríguez, Javier Del Ser, Adrien Bénéttot, Siham Tabik, Alberto Barbado, Salvador Garcia, et al. 2020. “Explainable Artificial Intelligence (XAI): Concepts, Taxonomies, Opportunities and Challenges toward Responsible AI.” *Information Fusion* 58 (June): 82–115. <https://doi.org/10.1016/j.inffus.2019.12.012>.
- Barry, Adrienne K., Ning Wang, and Deborah E. Leckband. 2015. “Local VE-Cadherin Mechanotransduction Triggers Long-Ranged Remodeling of Endothelial Monolayers.” *Journal of Cell Science* 128 (7): 1341–51. <https://doi.org/10.1242/jcs.159954>.
- Bastian, Grace, George Hamilton Baker, and Alfonso Limon. 2022. “Bridging the Divide between Data Scientists and Clinicians.” *Intelligence-Based Medicine* 6 (January): 100066. <https://doi.org/10.1016/j.ibmed.2022.100066>.
- Basu, Amrita, Denise Warzel, Aras Eftekhari, Justin S. Kirby, John Freymann, Janice Knable, Ashish Sharma, and Paula Jacobs. 2019. “Call for Data Standardization: Lessons Learned and Recommendations in an Imaging Study.” *JCO Clinical Cancer Informatics* 3 (December): CCI.19.00056. <https://doi.org/10.1200/CCI.19.00056>.

- Bathina, Siresha, and Undurti N. Das. 2015. "Brain-Derived Neurotrophic Factor and Its Clinical Implications." *Archives of Medical Science : AMS* 11 (6): 1164–78. <https://doi.org/10.5114/aoms.2015.56342>.
- Bayirli, B., Hera Kim-Berman, and A. Puntillo. 2020. "Embracing Novel Technologies in Dentistry and Orthodontics." In . <https://www.semanticscholar.org/paper/Embracing-Novel-Technologies-in-Dentistry-and-Bayirli-Kim-Berman/f0fc3f0c8a5f068dedcdbad2a6b8164e1170255f>.
- Bechtold, Till E., Cheri Saunders, Rebekah S. Decker, Hyo-Bin Um, Naiga Cottingham, Imad Salhab, Naito Kurio, et al. 2016. "Osteophyte Formation and Matrix Mineralization in a TMJ Osteoarthritis Mouse Model Are Associated with Ectopic Hedgehog Signaling." *Matrix Biology : Journal of the International Society for Matrix Biology* 52–54: 339–54. <https://doi.org/10.1016/j.matbio.2016.03.001>.
- Beekhuizen, M., L. M. Gierman, W. E. van Spil, G. J. V. M. Van Osch, T. W. J. Huizinga, D. B. F. Saris, L. B. Creemers, and A. -M. Zuurmond. 2013. "An Explorative Study Comparing Levels of Soluble Mediators in Control and Osteoarthritic Synovial Fluid." *Osteoarthritis and Cartilage* 21 (7): 918–22. <https://doi.org/10.1016/j.joca.2013.04.002>.
- Bera, Kaustav, Vamsidhar Velcheti, and Anant Madabhushi. 2018. "Novel Quantitative Imaging for Predicting Response to Therapy: Techniques and Clinical Applications." *American Society of Clinical Oncology Educational Book. American Society of Clinical Oncology. Annual Meeting*, no. 38 (May): 1008–18. [https://doi.org/10.1200/EDBK\\_199747](https://doi.org/10.1200/EDBK_199747).
- Bernotiene, Eiva, Edvardas Bagdonas, Gailute Kirdaite, Paulius Bernotas, Ursule Kalvaityte, Ilona Uzieliene, Christian S. Thudium, et al. 2020. "Emerging Technologies and Platforms for the Immunodetection of Multiple Biochemical Markers in Osteoarthritis Research and Therapy." *Frontiers in Medicine* 7: 622. <https://doi.org/10.3389/fmed.2020.572977>.
- Bessa, Felipe, Jonathan Rasio, Alexander Newhouse, Benedict U. Nwachukwu, and Shane Nho. 2020. "Surgical Treatment of Subchondral Bone Cysts of the Acetabulum With Calcium Phosphate Bone Substitute Material in Patients Without Advanced Arthritic Hips." *Arthroscopy Techniques* 9 (9): e1375–79. <https://doi.org/10.1016/j.eats.2020.05.018>.
- Bianchi, J. R. Gonçalves, A. C. de Oliveira Ruellas, L. M. Ashman, J.-B. Vimort, M. Yatabe, B. Paniagua, et al. 2021. "Quantitative Bone Imaging Biomarkers to Diagnose Temporomandibular Joint Osteoarthritis." *International Journal of Oral and Maxillofacial Surgery* 50 (2): 227–35. <https://doi.org/10.1016/j.ijom.2020.04.018>.
- Bianchi, João Roberto Gonçalves, Antonio Carlos de Oliveira Ruellas, Jean-Baptiste Vimort, Marília Yatabe, Beatriz Paniagua, Pablo Hernandez, Erika Benavides, Fabiana Naomi Soki, and Lucia Helena Soares Cevidanes. 2019. "Software Comparison to Analyze Bone Radiomics from High Resolution CBCT Scans of Mandibular Condyles." *Dentomaxillofacial Radiology* 48 (6): 20190049. <https://doi.org/10.1259/dmfr.20190049>.
- Bianchi, Antônio Carlos de Oliveira Ruellas, João Roberto Gonçalves, Beatriz Paniagua, Juan Carlos Prieto, Martin Styner, Tengfei Li, et al. 2020. "Osteoarthritis of the Temporomandibular Joint Can Be Diagnosed Earlier Using Biomarkers and Machine Learning." *Scientific Reports* 10 (1): 8012. <https://doi.org/10.1038/s41598-020-64942-0>.
- Bianchi, Beatriz Paniagua, Antonio Carlos De Oliveira Ruellas, Jean-Christophe Fillion-Robin, Juan C. Prieto, João Roberto Gonçalves, James Hoctor, et al. 2020. "3D Slicer Cranio-maxillofacial Modules Support Patient-Specific Decision-Making for Personalized Healthcare in Dental Research." *Multimodal Learning for Clinical Decision Support and*

- Clinical Image-Based Procedures: 10th International Workshop, ML-CDS 2020, and 9th International Workshop, CLIP 2020, Held in Conjunction with MICCAI 2020, Lima, Peru, October 4-8, ...* 12445 (October): 44–53. [https://doi.org/10.1007/978-3-030-60946-7\\_5](https://doi.org/10.1007/978-3-030-60946-7_5).
- Bianco, Daniel, Atanas Todorov, Tomislav Čengić, Geert Pagenstert, Stefan Schären, Cordula Netzer, Thomas Hügle, and Jeroen Geurts. 2018. “Alterations of Subchondral Bone Progenitor Cells in Human Knee and Hip Osteoarthritis Lead to a Bone Sclerosis Phenotype.” *International Journal of Molecular Sciences* 19 (2): 475. <https://doi.org/10.3390/ijms19020475>.
- Bichu, Yashodhan M., Ismael Hansa, Aditi Y. Bichu, Pratik Premjani, Carlos Flores-Mir, and Nikhilesh R. Vaid. 2021. “Applications of Artificial Intelligence and Machine Learning in Orthodontics: A Scoping Review.” *Progress in Orthodontics* 22 (1): 18. <https://doi.org/10.1186/s40510-021-00361-9>.
- Bifarin, Olatomiwa O. 2023. “Interpretable Machine Learning with Tree-Based Shapley Additive Explanations: Application to Metabolomics Datasets for Binary Classification.” *PLOS ONE* 18 (5): e0284315. <https://doi.org/10.1371/journal.pone.0284315>.
- Binvinat, Marie, Valentina Padoia, Atul J Butte, Karine Louati, David Klatzmann, Francis Berenbaum, Encarnita Mariotti-Ferrandiz, and Jérémie Sellam. 2022. “Use of Machine Learning in Osteoarthritis Research: A Systematic Literature Review.” *RMD Open* 8 (1): e001998. <https://doi.org/10.1136/rmdopen-2021-001998>.
- Bjelle, A. 1983. “On the Heterogeneity of Osteoarthritis.” *Clinical Rheumatology* 2 (2): 111–13. <https://doi.org/10.1007/BF02032165>.
- Blagojevic, M., C. Jinks, A. Jeffery, and K. P. Jordan. 2010. “Risk Factors for Onset of Osteoarthritis of the Knee in Older Adults: A Systematic Review and Meta-Analysis.” *Osteoarthritis and Cartilage* 18 (1): 24–33. <https://doi.org/10.1016/j.joca.2009.08.010>.
- Blaschke, Sabine, Michael Koziol, Andreas Schwarz, Peter Benöhr, Peter Middel, Gerhard Schwarz, Klaus-M. Hummel, and Gerhard A. Müller. 2003. “Proinflammatory Role of Fractalkine (CX3CL1) in Rheumatoid Arthritis.” *The Journal of Rheumatology* 30 (9): 1918–27.
- Bloch, Louise, Christoph M. Friedrich, and for the Alzheimer’s Disease Neuroimaging Initiative. 2021. “Data Analysis with Shapley Values for Automatic Subject Selection in Alzheimer’s Disease Data Sets Using Interpretable Machine Learning.” *Alzheimer’s Research & Therapy* 13 (1): 155. <https://doi.org/10.1186/s13195-021-00879-4>.
- Boer, E. W. J. de, P. U. Dijkstra, B. Stegenga, L. G. M. de Bont, and F. K. L. Spijkervet. 2014. “Value of Cone-Beam Computed Tomography in the Process of Diagnosis and Management of Disorders of the Temporomandibular Joint.” *British Journal of Oral and Maxillofacial Surgery* 52 (3): 241–46. <https://doi.org/10.1016/j.bjoms.2013.12.007>.
- Bratus-Neuenschwander, Anna, Francesc Castro-Giner, Mojca Frank-Bertoncelj, Sirisha Aluri, Sandro F. Fucntese, Ralph Schlapbach, and Haiko Sprott. 2018. “Pain-Associated Transcriptome Changes in Synovium of Knee Osteoarthritis Patients.” *Genes* 9 (7): 338. <https://doi.org/10.3390/genes9070338>.
- Brew, Keith, and Hideaki Nagase. 2010. “The Tissue Inhibitors of Metalloproteinases (TIMPs): An Ancient Family with Structural and Functional Diversity.” *Biochimica et Biophysica Acta* 1803 (1): 55–71. <https://doi.org/10.1016/j.bbamcr.2010.01.003>.
- Brosset, Serge, Maxime Dumont, Jonas Bianchi, Antonio Ruellas, Lucia Cevitanes, Marilia Yatabe, Joao Goncalves, et al. 2020. “3D Auto-Segmentation of Mandibular Condyles.”

- Annual International Conference of the IEEE Engineering in Medicine and Biology Society. IEEE Engineering in Medicine and Biology Society. Annual International Conference 2020* (July): 1270–73. <https://doi.org/10.1109/EMBC44109.2020.9175692>.
- Brosset, Serge, Maxime Dumont, Lucia Cevidanes, Reza Soroushmehr, Jonas Bianchi, Marcela Gurgel, Romain Deleat-Besson, et al. 2021. “Web Infrastructure for Data Management, Storage and Computation.” *Proceedings of SPIE--the International Society for Optical Engineering* 11600 (February): 116001N. <https://doi.org/10.1117/12.2582283>.
- Brylka, Laura J., and Thorsten Schinke. 2019. “Chemokines in Physiological and Pathological Bone Remodeling.” *Frontiers in Immunology* 10: 2182. <https://doi.org/10.3389/fimmu.2019.02182>.
- Burland, Julie P., Emily R. Hunt, and Christian Lattermann. 2023. “Serum Biomarkers in Healthy, Injured, and Osteoarthritic Knees: A Critical Review.” *Journal of Cartilage & Joint Preservation* 3 (2): 100091. <https://doi.org/10.1016/j.jcjp.2022.100091>.
- Byun, Soo-Hwan, Chanyang Min, Dae-Myoung Yoo, Byoung-Eun Yang, and Hyo-Geun Choi. 2020. “Increased Risk of Migraine in Patients with Temporomandibular Disorder: A Longitudinal Follow-Up Study Using a National Health Screening Cohort.” *Diagnostics* 10 (9): 724. <https://doi.org/10.3390/diagnostics10090724>.
- Cabral-Pacheco, Griselda A, Idalia Garza-Veloz, Claudia Castruita-De la Rosa, Jesús M Ramirez-Acuña, Braulio A Perez-Romero, Jesús F Guerrero-Rodriguez, Nadia Martinez-Avila, and Margarita L Martinez-Fierro. 2020. “The Roles of Matrix Metalloproteinases and Their Inhibitors in Human Diseases.” *International Journal of Molecular Sciences* 21 (24): 9739. <https://doi.org/10.3390/ijms21249739>.
- Cafferata, Emilio A., Gustavo Monasterio, Francisca Castillo, Paola Carvajal, Guillermo Flores, Walter Díaz, Aler D. Fuentes, and Rolando Vernal. 2021. “Overexpression of MMPs, Cytokines, and RANKL/OPG in Temporomandibular Joint Osteoarthritis and Their Association with Joint Pain, Mouth Opening, and Bone Degeneration: A Preliminary Report.” *Oral Diseases* 27 (4): 970–80. <https://doi.org/10.1111/odi.13623>.
- Cairns, B. E. 2010. “Pathophysiology of TMD Pain – Basic Mechanisms and Their Implications for Pharmacotherapy.” *Journal of Oral Rehabilitation* 37 (6): 391–410. <https://doi.org/10.1111/j.1365-2842.2010.02074.x>.
- Califf, Robert M. 2018. “Biomarker Definitions and Their Applications.” *Experimental Biology and Medicine* 243 (3): 213–21. <https://doi.org/10.1177/1535370217750088>.
- Cardoneanu, Anca, Luana Andreea Macovei, Alexandra Maria Burlui, Ioana Ruxandra Mihai, Ioana Bratoiu, Ioana Irina Rezus, Patricia Richter, Bogdan-Ionel Tamba, and Elena Rezus. 2022. “Temporomandibular Joint Osteoarthritis: Pathogenic Mechanisms Involving the Cartilage and Subchondral Bone, and Potential Therapeutic Strategies for Joint Regeneration.” *International Journal of Molecular Sciences* 24 (1): 171. <https://doi.org/10.3390/ijms24010171>.
- Castellano, G., L. Bonilha, L.M. Li, and F. Cendes. 2004. “Texture Analysis of Medical Images.” *Clinical Radiology* 59 (12): 1061–69. <https://doi.org/10.1016/j.crad.2004.07.008>.
- Cevidanes, A-K Hajati, B Paniagua, PF Lim, DG Walker, G Palconet, AG Nackley, et al. 2010. “Quantification of Condylar Resorption in TMJ Osteoarthritis.” *Oral Surgery, Oral Medicine, Oral Pathology, Oral Radiology, and Endodontics* 110 (1): 110–17. <https://doi.org/10.1016/j.tripleo.2010.01.008>.
- Cevidanes, David Walker, Juan Schilling, James Sugai, William Giannobile, Beatriz Paniagua, Erika Benavides, et al. 2014. “3D Osteoarthritic Changes in TMJ Condylar Morphology

- Correlates with Specific Systemic and Local Biomarkers of Disease.” *Osteoarthritis and Cartilage / OARS, Osteoarthritis Research Society* 22 (10): 1657–67.  
<https://doi.org/10.1016/j.joca.2014.06.014>.
- Chae, Dong-Sik, Mi Eun Kim, Kyung-Yil Kang, Nae Yoon Lee, Woo-Suk Lee, and Jun Sik Lee. 2021. “Quantitative Proteomic Analysis Comparing Grades ICRS1 and ICRS3 in Patients with Osteoarthritis.” *Experimental and Therapeutic Medicine* 22 (6): 1–10.  
<https://doi.org/10.3892/etm.2021.10905>.
- Chen, Huang, Du, and Tong. 2014. “Expression and Significance of MMP3 in Synovium of Knee Joint at Different Stage in Osteoarthritis Patients.” *Asian Pacific Journal of Tropical Medicine* 7 (4): 297–300. [https://doi.org/10.1016/S1995-7645\(14\)60042-0](https://doi.org/10.1016/S1995-7645(14)60042-0).
- Chen, Wendy Walwyn, Helena S. Ennes, Hyeyoung Kim, James A. McRoberts, and Juan Carlos G. Marvizón. 2014. “BDNF Released during Neuropathic Pain Potentiates NMDA Receptors in Primary Afferent Terminals.” *The European Journal of Neuroscience* 39 (9): 1439–54. <https://doi.org/10.1111/ejn.12516>.
- Chen, Yan, Yizhong Hu, Y Eric Yu, Xingjian Zhang, Tezita Watts, Bin Zhou, Ji Wang, et al. 2018. “Subchondral Trabecular Rod Loss and Plate Thickening in the Development of Osteoarthritis.” *Journal of Bone and Mineral Research* 33 (2): 316–27.  
<https://doi.org/10.1002/jbmr.3313>.
- Cheng, Yuan, Xue-lei Ma, Yu-quan Wei, and Xia-Wei Wei. 2019. “Potential Roles and Targeted Therapy of the CXCLs/CXCR2 Axis in Cancer and Inflammatory Diseases.” *Biochimica et Biophysica Acta (BBA) - Reviews on Cancer* 1871 (2): 289–312.  
<https://doi.org/10.1016/j.bbcan.2019.01.005>.
- Chevalier, T. Conrozier, M. Gehrman, P. Claudepierre, P. Mathieu, S. Unger, and E. Vignon. 2001. “Tissue Inhibitor of Metalloprotease-1 (TIMP-1) Serum Level May Predict Progression of Hip Osteoarthritis.” *Osteoarthritis and Cartilage* 9 (4): 300–307.  
<https://doi.org/10.1053/joca.2000.0389>.
- Chevalier, and Eymard. 2019. “Anti-IL-1 for the Treatment of OA: Dead or Alive?” *Nature Reviews Rheumatology* 15 (4): 191–92. <https://doi.org/10.1038/s41584-019-0185-y>.
- Chevalier, Eymard, and Richette. 2013. “Biologic Agents in Osteoarthritis: Hopes and Disappointments.” *Nature Reviews. Rheumatology* 9 (7): 400–410.  
<https://doi.org/10.1038/nrrheum.2013.44>.
- Chiba, Ko, Andrew J. Burghardt, Makoto Osaki, and Sharmila Majumdar. 2014. “Three-Dimensional Analysis of Subchondral Cysts in Hip Osteoarthritis: An Ex Vivo HR-PQCT Study.” *Bone* 66 (September): 140–45.  
<https://doi.org/10.1016/j.bone.2014.06.001>.
- Chow, Yoke Yue, and Kok-Yong Chin. 2020. “The Role of Inflammation in the Pathogenesis of Osteoarthritis.” *Mediators of Inflammation* 2020 (March): e8293921.  
<https://doi.org/10.1155/2020/8293921>.
- Christidis, Nikolaos, Marika Doepel, EwaCarin Ekberg, Malin Ernberg, Yrsa Le Bell, and Maria Nilner. 2014. “Effectiveness of a Prefabricated Occlusal Appliance in Patients with Temporomandibular Joint Pain: A Randomized Controlled Multicenter Study.” *Journal of Oral & Facial Pain and Headache* 28 (2): 128–37. <https://doi.org/10.11607/ofph.1216>.
- Chung, Geun-Seok Choi, Ki-Young Shin, and Joon-Soo Park. 2016. “Gait Changes after Using a Temporomandibular Joint Exerciser in Patients Who Underwent Lower Limb Joint Surgery.” *Journal of Physical Therapy Science* 28 (5): 1584–87.  
<https://doi.org/10.1589/jpts.28.1584>.

- Chung, Sheng Wang, Ishraq Alshantiti, Jiabin Hu, and Jin Y. Ro. 2023. "The Degeneration-Pain Relationship in the Temporomandibular Joint: Current Understandings and Rodent Models." *Frontiers in Pain Research* 4. <https://www.frontiersin.org/articles/10.3389/fpain.2023.1038808>.
- Claesson-Welsh, Lena, Elisabetta Dejana, and Donald M. McDonald. 2021. "Permeability of the Endothelial Barrier: Identifying and Reconciling Controversies." *Trends in Molecular Medicine* 27 (4): 314–31. <https://doi.org/10.1016/j.molmed.2020.11.006>.
- Collins, Jamie E, Tuhina Neogi, and Elena Losina. 2021. "Trajectories of Structural Disease Progression in Knee Osteoarthritis." *Arthritis Care & Research* 73 (9): 1354–62. <https://doi.org/10.1002/acr.24340>.
- Cömert Kiliç, S., N. Kiliç, and M.A. Sümbüllü. 2015. "Temporomandibular Joint Osteoarthritis: Cone Beam Computed Tomography Findings, Clinical Features, and Correlations." *International Journal of Oral and Maxillofacial Surgery* 44 (10): 1268–74. <https://doi.org/10.1016/j.ijom.2015.06.023>.
- Conceição, Heida Natali dos Santos, Tharcilla Calíope Azevêdo, Alcylene Carla de Jesus dos Santos, and Maria Rita Sancho Rios Xavier. 2022. "Comorbidities Associated with Temporomandibular Joint Disorders and the Role of Central Sensitization: Literature Review." *Brazilian Journal Of Pain* 5 (1). <https://doi.org/10.5935/2595-0118.20220003>.
- Coussement, Kristof, and Dries F. Benoit. 2021. "Interpretable Data Science for Decision Making." *Decision Support Systems, Interpretable Data Science For Decision Making*, 150 (November): 113664. <https://doi.org/10.1016/j.dss.2021.113664>.
- Crema, M.D., F.W. Roemer, M.D. Marra, J. Niu, J.A. Lynch, D.T. Felson, and A. Guermazi. 2010. "CONTRAST-ENHANCED MRI OF SUBCHONDRAL CYSTS IN PATIENTS WITH OR AT RISK FOR KNEE OSTEOARTHRITIS: THE MOST STUDY." *European Journal of Radiology* 75 (1): e92–96. <https://doi.org/10.1016/j.ejrad.2009.08.009>.
- Cruz, Diogo, Francisca Monteiro, Maria Paço, Manuel Vaz-Silva, Carolina Lemos, Miguel Alves-Ferreira, and Teresa Pinho. 2022. "Genetic Overlap between Temporomandibular Disorders and Primary Headaches: A Systematic Review." *The Japanese Dental Science Review* 58 (November): 69–88. <https://doi.org/10.1016/j.jdsr.2022.02.002>.
- Cuadra, Meritxell Bach, Julien Favre, and Patrick Omoumi. 2020. "Quantification in Musculoskeletal Imaging Using Computational Analysis and Machine Learning: Segmentation and Radiomics." *Seminars in Musculoskeletal Radiology* 24 (01): 50–64. <https://doi.org/10.1055/s-0039-3400268>.
- Cui, Ning, Min Hu, and Raouf A. Khalil. 2017. "Biochemical and Biological Attributes of Matrix Metalloproteinases." *Progress in Molecular Biology and Translational Science* 147: 1–73. <https://doi.org/10.1016/bs.pmbts.2017.02.005>.
- Czekay, Ralf-Peter, Cynthia E. Wilkins-Port, Stephen P. Higgins, Jennifer Freytag, Jessica M. Overstreet, R. Matthew Klein, Craig E. Higgins, Rohan Samarakoon, and Paul J. Higgins. 2011. "PAI-1: An Integrator of Cell Signaling and Migration." *International Journal of Cell Biology* 2011: 562481. <https://doi.org/10.1155/2011/562481>.
- D'Amore, John, MS, President, Informatics, Diameter Health, Sandra Mitchell, RPH, MSIS, FASHP, and J. P. Systems; HIMSS Members. 2020. "Electronic Health Record Data Governance and Data Quality in the Real World | HIMSS." July 28, 2020. <https://www.himss.org/resources/electronic-health-record-data-governance-and-data-quality-real-world>.

- Dash, Sabyasachi, Sushil Kumar Shakyawar, Mohit Sharma, and Sandeep Kaushik. 2019. “Big Data in Healthcare: Management, Analysis and Future Prospects.” *Journal of Big Data* 6 (1): 54. <https://doi.org/10.1186/s40537-019-0217-0>.
- “Data Mining.” 2023. In *Wikipedia*. [https://en.wikipedia.org/w/index.php?title=Data\\_mining&oldid=1173461237](https://en.wikipedia.org/w/index.php?title=Data_mining&oldid=1173461237).
- Dawes, C., and D.T.W. Wong. 2019. “Role of Saliva and Salivary Diagnostics in the Advancement of Oral Health.” *Journal of Dental Research* 98 (2): 133–41. <https://doi.org/10.1177/0022034518816961>.
- Delpachitra, S. N., and G. Dimitroulis. 2022. “Osteoarthritis of the Temporomandibular Joint: A Review of Aetiology and Pathogenesis.” *British Journal of Oral and Maxillofacial Surgery* 60 (4): 387–96. <https://doi.org/10.1016/j.bjoms.2021.06.017>.
- Derwich, Marcin, Bartłomiej Górski, Elie Amm, and Elżbieta Pawłowska. 2023. “Oral Glucosamine in the Treatment of Temporomandibular Joint Osteoarthritis: A Systematic Review.” *International Journal of Molecular Sciences* 24 (5): 4925. <https://doi.org/10.3390/ijms24054925>.
- Derwich, Marcin, Maria Mitus-Kenig, and Elżbieta Pawłowska. 2020. “Interdisciplinary Approach to the Temporomandibular Joint Osteoarthritis—Review of the Literature.” *Medicina* 56 (5): 225. <https://doi.org/10.3390/medicina56050225>.
- . 2021. “Mechanisms of Action and Efficacy of Hyaluronic Acid, Corticosteroids and Platelet-Rich Plasma in the Treatment of Temporomandibular Joint Osteoarthritis—A Systematic Review.” *International Journal of Molecular Sciences* 22 (14): 7405. <https://doi.org/10.3390/ijms22147405>.
- Deveza, Leticia A, and Richard F Loeser. 2018. “Is Osteoarthritis One Disease or a Collection of Many?” *Rheumatology (Oxford, England)* 57 (Suppl 4): iv34–42. <https://doi.org/10.1093/rheumatology/kex417>.
- Di Paolo, Carlo, Anna D’Urso, Piero Papi, Francesco Di Sabato, Daniele Rosella, Giorgio Pompa, and Antonella Polimeni. 2017. “Temporomandibular Disorders and Headache: A Retrospective Analysis of 1198 Patients.” *Pain Research & Management* 2017: 3203027. <https://doi.org/10.1155/2017/3203027>.
- Doshi, Tina L., Donald R. Nixdorf, Claudia M. Campbell, and Srinivasa N. Raja. 2020. “Biomarkers in Temporomandibular Disorder and Trigeminal Neuralgia: A Conceptual Framework for Understanding Chronic Pain.” *Canadian Journal of Pain* 4 (1): 1–18. <https://doi.org/10.1080/24740527.2019.1709163>.
- Doube, Michael, Michał M Kłosowski, Ignacio Arganda-Carreras, Fabrice P Cordelières, Robert P Dougherty, Jonathan S Jackson, Benjamin Schmid, John R Hutchinson, and Sandra J Shefelbine. 2010. “BoneJ: Free and Extensible Bone Image Analysis in ImageJ.” *Bone* 47 (6): 1076–79. <https://doi.org/10.1016/j.bone.2010.08.023>.
- Dumast, Priscille de, Clément Mirabel, Lucia Cevitanes, Antonio Ruellas, Marilia Yatabe, Marcos Ioshida, Nina Tubau Ribera, et al. 2018. “A Web-Based System for Neural Network Based Classification in Temporomandibular Joint Osteoarthritis.” *Computerized Medical Imaging and Graphics: The Official Journal of the Computerized Medical Imaging Society* 67 (July): 45–54. <https://doi.org/10.1016/j.compmedimag.2018.04.009>.
- Dumbuya, Aminata, Amanda Farias Gomes, Leonardo Marchini, Erliang Zeng, Carissa L. Comnick, and Saulo L. Sousa Melo. 2020. “Bone Changes in the Temporomandibular Joints of Older Adults: A Cone-Beam Computed Tomography Study.” *Special Care in Dentistry: Official Publication of the American Association of Hospital Dentists, the Academy*

- of Dentistry for the Handicapped, and the American Society for Geriatric Dentistry* 40 (1): 84–89. <https://doi.org/10.1111/scd.12441>.
- Dumont, Maxime, Juan Carlos Prieto, Serge Brosset, Lucia Cevidanes, Jonas Bianchi, Antonio Ruellas, Marcela Gurgel, et al. 2020. “Patient Specific Classification of Dental Root Canal and Crown Shape.” *Shape in Medical Imaging: International Workshop, ShapeMI 2020, Held in Conjunction with MICCAI 2020, Lima, Peru, October 4, 2020, Proceedings* 12474 (October): 145–53. [https://doi.org/10.1007/978-3-030-61056-2\\_12](https://doi.org/10.1007/978-3-030-61056-2_12).
- Dworkin, S. F., and L. LeResche. 1992. “Research Diagnostic Criteria for Temporomandibular Disorders: Review, Criteria, Examinations and Specifications, Critique.” *Journal of Craniomandibular Disorders: Facial & Oral Pain* 6 (4): 301–55.
- Dygas, Sebastian, Izabela Szarmach, and Ilona Radej. 2022. “Assessment of the Morphology and Degenerative Changes in the Temporomandibular Joint Using CBCT According to the Orthodontic Approach: A Scoping Review.” *BioMed Research International* 2022 (February): e6863014. <https://doi.org/10.1155/2022/6863014>.
- Ebrahim, F. H., A. C. O. Ruellas, B. Paniagua, E. Benavides, K. Jepsen, L. Wolford, J. R. Gonçalves, and L. H. S. Cevidanes. 2017. “ACCURACY OF BIOMARKERS OBTAINED FROM CONE BEAM COMPUTED TOMOGRAPHY IN ASSESSING THE INTERNAL TRABECULAR STRUCTURE OF THE MANDIBULAR CONDYLE.” *Oral Surgery, Oral Medicine, Oral Pathology and Oral Radiology* 124 (6): 588. <https://doi.org/10.1016/j.oooo.2017.08.013>.
- Elmahdy, Mahmoud, and Ronnie Sebro. 2023. “Radiomics Analysis in Medical Imaging Research.” *Journal of Medical Radiation Sciences* 70 (1): 3–7. <https://doi.org/10.1002/jmrs.662>.
- Embree, M., M. Ono, T. Kilts, D. Walker, J. Langguth, J. Mao, Y. Bi, J.L. Barth, and M. Young. 2011. “Role of Subchondral Bone during Early-Stage Experimental TMJ Osteoarthritis.” *Journal of Dental Research* 90 (11): 1331–38. <https://doi.org/10.1177/0022034511421930>.
- Emshoff, I. Brandlmaier, R. Bösch, S. Gerhard, A. Rudisch, and S. Bertram. 2002. “Validation of the Clinical Diagnostic Criteria for Temporomandibular Disorders for the Diagnostic Subgroup - Disc Derangement with Reduction.” *Journal of Oral Rehabilitation* 29 (12): 1139–45. <https://doi.org/10.1046/j.1365-2842.2002.00980.x>.
- Emshoff, Rüdiger, Annika Bertram, Linus Hupp, and Ansgar Rudisch. 2021. “A Logistic Analysis Prediction Model of TMJ Condylar Erosion in Patients with TMJ Arthralgia.” *BMC Oral Health* 21 (1): 374. <https://doi.org/10.1186/s12903-021-01687-w>.
- Emshoff, Rüdiger, Felix Bertram, Dagmar Schnabl, Robert Stigler, Otto Steinmaßl, and Ansgar Rudisch. 2016. “Condylar Erosion in Patients With Chronic Temporomandibular Joint Arthralgia: A Cone-Beam Computed Tomography Study.” *Journal of Oral and Maxillofacial Surgery* 74 (7): 1343.e1-1343.e8. <https://doi.org/10.1016/j.joms.2016.01.029>.
- Esteva, Andre, Brett Kuprel, Roberto A. Novoa, Justin Ko, Susan M. Swetter, Helen M. Blau, and Sebastian Thrun. 2017. “Dermatologist-Level Classification of Skin Cancer with Deep Neural Networks.” *Nature* 542 (7639): 115–18. <https://doi.org/10.1038/nature21056>.
- Faber, Jorge, Carolina Faber, and Pedro Faber. 2019. “Artificial Intelligence in Orthodontics.” *APOS Trends in Orthodontics* 9 (4): 201–5. [https://doi.org/10.25259/APOS\\_123\\_2019](https://doi.org/10.25259/APOS_123_2019).



- Farhadian, Maryam, Fatemeh Salemi, Samira Saati, and Nika Nafisi. 2019. "Dental Age Estimation Using the Pulp-to-Tooth Ratio in Canines by Neural Networks." *Imaging Science in Dentistry* 49 (1): 19–26. <https://doi.org/10.5624/isd.2019.49.1.19>.
- Favaretto, Maddalena, David Shaw, Eva De Clercq, Tim Joda, and Bernice Simone Elger. 2020. "Big Data and Digitalization in Dentistry: A Systematic Review of the Ethical Issues." *International Journal of Environmental Research and Public Health* 17 (7): 2495. <https://doi.org/10.3390/ijerph17072495>.
- Favero, Marta, Elisa Belluzzi, Giovanni Trisolino, Mary B Goldring, Steven R Goldring, Augusto Cigolotti, Assunta Pozzuoli, et al. 2019. "Inflammatory Molecules Produced by Meniscus and Synovium in Early and End-Stage Osteoarthritis: A Coculture Study." *Journal of Cellular Physiology* 234 (7): 11176–87. <https://doi.org/10.1002/jcp.27766>.
- Fedorov, Andriy, Reinhard Beichel, Jayashree Kalpathy-Cramer, Julien Finet, Jean-Christophe Fillion-Robin, Sonia Pujol, Christian Bauer, et al. 2012. "3D Slicer as an Image Computing Platform for the Quantitative Imaging Network." *Magnetic Resonance Imaging* 30 (9): 1323–41. <https://doi.org/10.1016/j.mri.2012.05.001>.
- Felson, D. T. 1993. "The Course of Osteoarthritis and Factors That Affect It." *Rheumatic Diseases Clinics of North America* 19 (3): 607–15.
- Ferrazzo, K. L., L. B. Osório, and V. A. Ferrazzo. 2013. "CT Images of a Severe TMJ Osteoarthritis and Differential Diagnosis with Other Joint Disorders." *Case Reports in Dentistry* 2013: 242685. <https://doi.org/10.1155/2013/242685>.
- Ferrillo, Martina, Amerigo Giudice, Nicola Marotta, Francesco Fortunato, Daniela Di Venere, Antonio Ammendolia, Pietro Fiore, and Alessandro de Sire. 2022. "Pain Management and Rehabilitation for Central Sensitization in Temporomandibular Disorders: A Comprehensive Review." *International Journal of Molecular Sciences* 23 (20): 12164. <https://doi.org/10.3390/ijms232012164>.
- Fields, James K., Sebastian Günther, and Eric J. Sundberg. 2019. "Structural Basis of IL-1 Family Cytokine Signaling." *Frontiers in Immunology* 10. <https://www.frontiersin.org/articles/10.3389/fimmu.2019.01412>.
- Finkelstein, Joseph, Frederick Zhang, Seth A. Levitin, and David Cappelli. 2020. "Using Big Data to Promote Precision Oral Health in the Context of a Learning Healthcare System." *Journal of Public Health Dentistry* 80 (Suppl 1): S43–58. <https://doi.org/10.1111/jphd.12354>.
- Finnilä, Mikko A. J., Jérôme Thevenot, Olli-Matti Aho, Virpi Tiitu, Jari Rautiainen, Sami Kauppinen, Miika T. Nieminen, et al. 2017. "Association between Subchondral Bone Structure and Osteoarthritis Histopathological Grade." *Journal of Orthopaedic Research* 35 (4): 785–92. <https://doi.org/10.1002/jor.23312>.
- Fischl, Bruce. 2012. "FreeSurfer." *NeuroImage* 62 (2): 774–81. <https://doi.org/10.1016/j.neuroimage.2012.01.021>.
- Forsgren, Sture. 2009. "New Data Favouring That Neurotrophins Are of Importance in Arthritis." *Arthritis Research & Therapy* 11 (4): 122. <https://doi.org/10.1186/ar2754>.
- Frank, Michael, Dimitris Drikakis, and Vassilis Charissis. 2020. "Machine-Learning Methods for Computational Science and Engineering." *Computation* 8 (1): 15. <https://doi.org/10.3390/computation8010015>.
- Fransès, R.E., D.F. McWilliams, P.I. Mapp, and D.A. Walsh. 2010. "Osteochondral Angiogenesis and Increased Protease Inhibitor Expression in OA." *Osteoarthritis and Cartilage* 18 (4): 563–71. <https://doi.org/10.1016/j.joca.2009.11.015>.

- Gaballah, Abdellatif, Naglaa A. Hussein, Moustafa Risk, Noha Elsayy, and Somaya Elabasiry. 2016. "Correlation between Synovial Vascular Endothelial Growth Factor, Clinical, Functional and Radiological Manifestations in Knee Osteoarthritis." *The Egyptian Rheumatologist* 38 (1): 29–34. <https://doi.org/10.1016/j.ejr.2015.01.002>.
- Garstka, Adam Andrzej, Monika Brzózka, Aleksandra Bitenc-Jasiejko, Roman Ardan, Helena Gronwald, Piotr Skomro, and Danuta Lietz-Kijak. 2022. "Cause-Effect Relationships between Painful TMD and Postural and Functional Changes in the Musculoskeletal System: A Preliminary Report." *Pain Research and Management* 2022 (February): e1429932. <https://doi.org/10.1155/2022/1429932>.
- Geoffroy, Valérie, Caroline Marty-Morieux, Nathalie Le Goupil, Phillippe Clement-Lacroix, Catherine Terraz, Monique Frain, Sophie Roux, Jérôme Rossert, and Marie Christine de Vernejoul. 2004. "In Vivo Inhibition of Osteoblastic Metalloproteinases Leads to Increased Trabecular Bone Mass." *Journal of Bone and Mineral Research* 19 (5): 811–22. <https://doi.org/10.1359/jbmr.040119>.
- Georgiev, Tsvetoslav, Mariana Ivanova, Aleksandar Kopchev, Tsvetelina Velikova, Asen Miloshov, Ekaterina Kurteva, Kalina Yuzeir, et al. 2018. "Cartilage Oligomeric Protein, Matrix Metalloproteinase-3, and Coll2-1 as Serum Biomarkers in Knee Osteoarthritis: A Cross-Sectional Study." *Rheumatology International* 38 (5): 821–30. <https://doi.org/10.1007/s00296-017-3887-y>.
- Ghaffar Nia, Nafiseh, Erkan Kaplanoglu, and Ahad Nasab. 2023. "Evaluation of Artificial Intelligence Techniques in Disease Diagnosis and Prediction." *Discover Artificial Intelligence* 3 (1): 5. <https://doi.org/10.1007/s44163-023-00049-5>.
- Ghassemi, Marzyeh, Tristan Naumann, Peter Schulam, Andrew L. Beam, Irene Y. Chen, and Rajesh Ranganath. 2020. "A Review of Challenges and Opportunities in Machine Learning for Health." *AMIA Summits on Translational Science Proceedings 2020* (May): 191–200.
- Gholami, Raouf, and Nikoo Fakhari. 2017. "Chapter 27 - Support Vector Machine: Principles, Parameters, and Applications." In *Handbook of Neural Computation*, edited by Pijush Samui, Sanjiban Sekhar, and Valentina E. Balas, 515–35. Academic Press. <https://doi.org/10.1016/B978-0-12-811318-9.00027-2>.
- Giatromanolaki, Alexandra, Efthimios Sivridis, Efstratios Maltezos, Nick Athanassou, Dimitrios Papazoglou, Kevin C Gatter, Adrian L Harris, and Michael I Koukourakis. 2003. "Up-regulated Hypoxia Inducible Factor-1 $\alpha$  and -2 $\alpha$  Pathway in Rheumatoid Arthritis and Osteoarthritis." *Arthritis Research & Therapy* 5 (4): R193–201. <https://doi.org/10.1186/ar756>.
- Girish, V., and A. Vijayalakshmi. 2004. "Affordable Image Analysis Using NIH Image/ImageJ." *Indian Journal of Cancer* 41 (1): 47.
- Glyn-Jones, S., A. J. R. Palmer, R. Agricola, A. J. Price, T. L. Vincent, H. Weinans, and A. J. Carr. 2015. "Osteoarthritis." *Lancet (London, England)* 386 (9991): 376–87. [https://doi.org/10.1016/S0140-6736\(14\)60802-3](https://doi.org/10.1016/S0140-6736(14)60802-3).
- Gogas, Periklis, and Theophilos Papadimitriou. 2021. "Machine Learning in Economics and Finance." *Computational Economics* 57 (1): 1–4. <https://doi.org/10.1007/s10614-021-10094-w>.
- Gohari, Kimiya, Anoshirvan Kazemnejad, Marjan Mohammadi, Farzad Eskandari, Samaneh Saberi, Maryam Esmaili, and Ali Sheidaei. 2023. "A Bayesian Latent Class Extension of Naive Bayesian Classifier and Its Application to the Classification of Gastric Cancer Pa-

- tients.” *BMC Medical Research Methodology* 23 (1): 190.  
<https://doi.org/10.1186/s12874-023-02013-4>.
- Gordon, Kelly J., and Gerard C. Blobe. 2008. “Role of Transforming Growth Factor-Beta Superfamily Signaling Pathways in Human Disease.” *Biochimica Et Biophysica Acta* 1782 (4): 197–228. <https://doi.org/10.1016/j.bbadis.2008.01.006>.
- Grimsley-Myers, Cynthia M., Robin H. Isaacson, Chantel M. Cadwell, Jazmin Campos, Marina S. Hernandez, Kenneth R. Myers, Tadahiko Seo, William Giang, Kathy K. Griendling, and Andrew P. Kowalczyk. 2020. “VE-Cadherin Endocytosis Controls Vascular Integrity and Patterning during Development.” *The Journal of Cell Biology* 219 (5): e201909081. <https://doi.org/10.1083/jcb.201909081>.
- Gudivada, V., A. Apon, and Junhua Ding. 2017. “Data Quality Considerations for Big Data and Machine Learning: Going Beyond Data Cleaning and Transformations.” In . <https://www.semanticscholar.org/paper/Data-Quality-Considerations-for-Big-Data-and-Going-Gudivada-Apon/625a9e9822603b79f754c4ce044760f7363b5eb6>.
- Guo, Wen, Pengcheng Xu, Tianbo Jin, Jihong Wang, Dongsheng Fan, Zengtao Hao, Yuntao Ji, et al. 2017. “MMP-3 Gene Polymorphisms Are Associated with Increased Risk of Osteoarthritis in Chinese Men.” *Oncotarget* 8 (45): 79491–97. <https://doi.org/10.18632/oncotarget.18493>.
- Gupta, Om Prakash Kharbanda, Viren Sardana, Rajiv Balachandran, and Harish Kumar Sardana. 2016. “Accuracy of 3D Cephalometric Measurements Based on an Automatic Knowledge-Based Landmark Detection Algorithm.” *International Journal of Computer Assisted Radiology and Surgery* 11 (7): 1297–1309. <https://doi.org/10.1007/s11548-015-1334-7>.
- Gupta, Saurabh, Kenneth E. McCarson, K.m.a. Welch, and Nancy E.J. Berman. 2011. “Mechanisms of Pain Modulation by Sex Hormones in Migraine.” *Headache: The Journal of Head and Face Pain* 51 (6): 905–22. <https://doi.org/10.1111/j.1526-4610.2011.01908.x>.
- Haeusler, G., I. Walter, M. Helmreich, and M. Egerbacher. 2005. “Localization of Matrix Metalloproteinases, (MMPs) Their Tissue Inhibitors, and Vascular Endothelial Growth Factor (VEGF) in Growth Plates of Children and Adolescents Indicates a Role for MMPs in Human Postnatal Growth and Skeletal Maturation.” *Calcified Tissue International* 76 (5): 326–35. <https://doi.org/10.1007/s00223-004-0161-6>.
- Haghnegahdar, A.A., S. Kolahi, L. Khojastepour, and F. Tajeripour. 2018. “Diagnosis of Temporomandibular Disorders Using Local Binary Patterns.” *Journal of Biomedical Physics & Engineering* 8 (1): 87–96.
- Hajian-Tilaki, Karimollah. 2013. “Receiver Operating Characteristic (ROC) Curve Analysis for Medical Diagnostic Test Evaluation.” *Caspian Journal of Internal Medicine* 4 (2): 627–35.
- Halilaj, E., Y. Le, J. L. Hicks, T. J. Hastie, and S. L. Delp. 2018. “Modeling and Predicting Osteoarthritis Progression: Data from the Osteoarthritis Initiative.” *Osteoarthritis and Cartilage* 26 (12): 1643–50. <https://doi.org/10.1016/j.joca.2018.08.003>.
- Hamilton, John L., Masashi Nagao, Brett R. Levine, Di Chen, Bjorn R. Olsen, and Hee-Jeong Im. 2016. “Targeting VEGF and Its Receptors for the Treatment of Osteoarthritis and Associated Pain.” *Journal of Bone and Mineral Research : The Official Journal of the American Society for Bone and Mineral Research* 31 (5): 911–24. <https://doi.org/10.1002/jbmr.2828>.

- Hapfelmeier, Alexander, Roman Hornung, and Bernhard Haller. 2023. "Efficient Permutation Testing of Variable Importance Measures by the Example of Random Forests." *Computational Statistics & Data Analysis* 181 (May): 107689. <https://doi.org/10.1016/j.csda.2022.107689>.
- Haraden, Collin A., Janet L. Huebner, Ming-Feng Hsueh, Yi-Ju Li, and Virginia Byers Kraus. 2019. "Synovial Fluid Biomarkers Associated with Osteoarthritis Severity Reflect Macrophage and Neutrophil Related Inflammation." *Arthritis Research & Therapy* 21: 146. <https://doi.org/10.1186/s13075-019-1923-x>.
- Haralick, Robert M., K. Shanmugam, and Its' Hak Dinstein. 1973. "Textural Features for Image Classification." *IEEE Transactions on Systems, Man, and Cybernetics SMC-3* (6): 610–21. <https://doi.org/10.1109/TSMC.1973.4309314>.
- Haringman, J. J., J. Ludikhuizen, and P. P. Tak. 2004. "Chemokines in Joint Disease: The Key to Inflammation?" *Annals of the Rheumatic Diseases* 63 (10): 1186–94. <https://doi.org/10.1136/ard.2004.020529>.
- Harrar, Khaled, Khadidja Messaoudene, and Mohammed Ammar. 2018. "Combining GLCM with LBP Features for Knee Osteoarthritis Prediction: Data from the Osteoarthritis Initiative." *ICST Transactions on Scalable Information Systems*, July, 171550. <https://doi.org/10.4108/eai.20-10-2021.171550>.
- Harris, Alex H. S., Alfred C. Kuo, Thomas R. Bowe, Luisa Manfredi, Narlina F. Lalani, and Nicholas J. Giori. 2021. "Can Machine Learning Methods Produce Accurate and Easy-to-Use Preoperative Prediction Models of One-Year Improvements in Pain and Functioning After Knee Arthroplasty?" *The Journal of Arthroplasty* 36 (1): 112–117.e6. <https://doi.org/10.1016/j.arth.2020.07.026>.
- Harris, Alex H. S., Alfred C. Kuo, Yingjie Weng, Amber W. Trickey, Thomas Bowe, and Nicholas J. Giori. 2019. "Can Machine Learning Methods Produce Accurate and Easy-to-Use Prediction Models of 30-Day Complications and Mortality After Knee or Hip Arthroplasty?" *Clinical Orthopaedics and Related Research* 477 (2): 452–60. <https://doi.org/10.1097/CORR.0000000000000601>.
- Harris, and Nelson. 2010. "VE-Cadherin: At the Front, Center, and Sides of Endothelial Cell Organization and Function." *Current Opinion in Cell Biology* 22 (5): 651–58. <https://doi.org/10.1016/j.ceb.2010.07.006>.
- Hassaine, Abdelaali, Gholamreza Salimi-Khorshidi, Dexter Canoy, and Kazem Rahimi. 2020. "Untangling the Complexity of Multimorbidity with Machine Learning." *Mechanisms of Ageing and Development* 190 (September): 111325. <https://doi.org/10.1016/j.mad.2020.111325>.
- Hassija, Vikas, Vinay Chamola, Atmesh Mahapatra, Abhinandan Singal, Divyansh Goel, Kaizhu Huang, Simone Scardapane, Indro Spinelli, Mufti Mahmud, and Amir Hussain. 2023. "Interpreting Black-Box Models: A Review on Explainable Artificial Intelligence." *Cognitive Computation*, August. <https://doi.org/10.1007/s12559-023-10179-8>.
- Hawker, G. A., and L. S. Lohmander. 2021. "What an Earlier Recognition of Osteoarthritis Can Do for OA Prevention." *Osteoarthritis and Cartilage* 29 (12): 1632–34. <https://doi.org/10.1016/j.joca.2021.08.007>.
- Haynes, Mark K., Eric L. Hume, and J. Bruce Smith. 2002. "Phenotypic Characterization of Inflammatory Cells from Osteoarthritic Synovium and Synovial Fluids." *Clinical Immunology* 105 (3): 315–25. <https://doi.org/10.1006/clim.2002.5283>.

- He, Jianwei, Weiwei Cao, Inayat Azeem, Qiang Zhao, and Zengwu Shao. 2017. “Transforming Growth Factor Beta1 Being Considered a Novel Biomarker in Knee Osteoarthritis.” *Clinica Chimica Acta* 472 (September): 96–101. <https://doi.org/10.1016/j.cca.2017.07.021>.
- Heinrichs, John H., and Jeen-Su Lim. 2003. “Integrating Web-Based Data Mining Tools with Business Models for Knowledge Management.” *Decision Support Systems* 35 (1): 103–12. [https://doi.org/10.1016/S0167-9236\(02\)00098-2](https://doi.org/10.1016/S0167-9236(02)00098-2).
- Heisinger, Stephan, Wolfgang Hitzl, Gerhard M. Hobusch, Reinhard Windhager, and Sebastian Cotofana. 2020. “Predicting Total Knee Replacement from Symptomology and Radiographic Structural Change Using Artificial Neural Networks-Data from the Osteoarthritis Initiative (OAI).” *Journal of Clinical Medicine* 9 (5): 1298. <https://doi.org/10.3390/jcm9051298>.
- Helgeland, Espen, Siddharth Shanbhag, Torbjørn Ostvik Pedersen, Kamal Mustafa, and Annika Rosén. 2018. “Scaffold-Based Temporomandibular Joint Tissue Regeneration in Experimental Animal Models: A Systematic Review An Abstract of This Article Was Presented as a Poster, at The Bergen Stem Cell Consortium (BSCC), Annual Meeting, Bergen, Norway, September 3–4, 2017.” *Tissue Engineering Part B: Reviews* 24 (4): 300–316. <https://doi.org/10.1089/ten.teb.2017.0429>.
- Helmons, Pieter J., Bas O. Suijkerbuijk, Prashant V. Nannan Panday, and Jos G. W. Kosterink. 2015. “Drug-Drug Interaction Checking Assisted by Clinical Decision Support: A Return on Investment Analysis.” *Journal of the American Medical Informatics Association: JAMIA* 22 (4): 764–72. <https://doi.org/10.1093/jamia/ocu010>.
- Henrotin, Laurence Pesesse, and Cecile Lambert. 2014. “Targeting the Synovial Angiogenesis as a Novel Treatment Approach to Osteoarthritis.” *Therapeutic Advances in Musculoskeletal Disease* 6 (1): 20–34. <https://doi.org/10.1177/1759720X13514669>.
- Henrotin, Y. 2022. “Osteoarthritis in Year 2021: Biochemical Markers.” *Osteoarthritis and Cartilage* 30 (2): 237–48. <https://doi.org/10.1016/j.joca.2021.11.001>.
- Hicks, Steven A., Inga Strümke, Vajira Thambawita, Malek Hammou, Michael A. Riegler, Pål Halvorsen, and Sravanthi Parasa. 2021. “On Evaluation Metrics for Medical Applications of Artificial Intelligence.” medRxiv. <https://doi.org/10.1101/2021.04.07.21254975>.
- . 2022. “On Evaluation Metrics for Medical Applications of Artificial Intelligence.” *Scientific Reports* 12 (April): 5979. <https://doi.org/10.1038/s41598-022-09954-8>.
- Hilgenberg-Sydney, Priscila Brenner, Danielle Veiga Bonotto, José Stechman-Neto, Liete Figueiredo Zwir, Camila Pachêco-Pereira, Graziela De Luca Canto, and André Luís Porporatti. 2018. “Diagnostic Validity of CT to Assess Degenerative Temporomandibular Joint Disease: A Systematic Review.” *Dentomaxillofacial Radiology* 47 (5): 20170389. <https://doi.org/10.1259/dmfr.20170389>.
- Hirvasniemi, Jukka, Stefan Klein, Sita Bierma-Zeinstra, Meike W. Vernooij, Dieuwke Schiphof, and Edwin H. G. Oei. 2021. “A Machine Learning Approach to Distinguish between Knees without and with Osteoarthritis Using MRI-Based Radiomic Features from Tibial Bone.” *European Radiology* 31 (11): 8513–21. <https://doi.org/10.1007/s00330-021-07951-5>.
- Hu, Xiao Chen, Sicheng Wang, Yingying Jing, and Jiacaan Su. 2021. “Subchondral Bone Microenvironment in Osteoarthritis and Pain.” *Bone Research* 9 (1): 1–13. <https://doi.org/10.1038/s41413-021-00147-z>.

- Hu, Yueqi Chen, Ce Dou, and Shiwu Dong. 2021. "Microenvironment in Subchondral Bone: Predominant Regulator for the Treatment of Osteoarthritis." *Annals of the Rheumatic Diseases* 80 (4): 413–22. <https://doi.org/10.1136/annrheumdis-2020-218089>.
- Hu, Kai, and Bjorn R. Olsen. 2016. "Osteoblast-Derived VEGF Regulates Osteoblast Differentiation and Bone Formation during Bone Repair." *The Journal of Clinical Investigation* 126 (2): 509–26. <https://doi.org/10.1172/JCI82585>.
- Huber, Manuel, Christoph Kurz, and Reiner Leidl. 2019. "Predicting Patient-Reported Outcomes Following Hip and Knee Replacement Surgery Using Supervised Machine Learning." *BMC Medical Informatics and Decision Making* 19 (1): 3. <https://doi.org/10.1186/s12911-018-0731-6>.
- Huddleston Slater, Lobbezoo, and Naeije. 2002. "Mandibular Movement Characteristics of an Anterior Disc Displacement with Reduction." *Journal of Orofacial Pain* 16 (2): 135–42.
- Hügle, Thomas, and Jeroen Geurts. 2017. "What Drives Osteoarthritis?-Synovial versus Subchondral Bone Pathology." *Rheumatology (Oxford, England)* 56 (9): 1461–71. <https://doi.org/10.1093/rheumatology/kew389>.
- Hussain, A. M., G. Packota, P. W. Major, and C. Flores-Mir. 2008. "Role of Different Imaging Modalities in Assessment of Temporomandibular Joint Erosions and Osteophytes: A Systematic Review." *Dento Maxillo Facial Radiology* 37 (2): 63–71. <https://doi.org/10.1259/dmfr/16932758>.
- Hwang, Hye-Won, Jun-Ho Moon, Min-Gyu Kim, Richard E. Donatelli, and Shin-Jae Lee. 2021. "Evaluation of Automated Cephalometric Analysis Based on the Latest Deep Learning Method." *The Angle Orthodontist* 91 (3): 329–35. <https://doi.org/10.2319/021220-100.1>.
- Ibáñez, Lidia, Paloma Guillem-Llobat, Marta Marín, and María Isabel Guillén. 2022. "Connection between Mesenchymal Stem Cells Therapy and Osteoclasts in Osteoarthritis." *International Journal of Molecular Sciences* 23 (9): 4693. <https://doi.org/10.3390/ijms23094693>.
- Ibi, Miho, Sawa Horie, Seiko Kyakumoto, Naoyuki Chosa, Mariko Yoshida, Masaharu Kamo, Masato Ohtsuka, and Akira Ishisaki. 2018. "Cell-Cell Interactions between Monocytes/Macrophages and Synoviocyte-like Cells Promote Inflammatory Cell Infiltration Mediated by Augmentation of MCP-1 Production in Temporomandibular Joint." *Bioscience Reports* 38 (2): BSR20171217. <https://doi.org/10.1042/BSR20171217>.
- Ida-Yonemochi, Hiroko, Yurie Yamada, Hiroyuki Yoshikawa, and Kenji Seo. 2017. "Locally Produced BDNF Promotes Sclerotic Change in Alveolar Bone after Nerve Injury." *PLOS ONE* 12 (1): e0169201. <https://doi.org/10.1371/journal.pone.0169201>.
- Ioshida, Marcos, Brian Andres Muñoz, Hector Rios, Lucia Cevitanes, Juan Fernando Aristizabal, Diego Rey, Hera Kim-Berman, et al. 2019. "Accuracy and Reliability of Mandibular Digital Model Registration with Use of the Mucogingival Junction as the Reference." *Oral Surgery, Oral Medicine, Oral Pathology and Oral Radiology* 127 (4): 351–60. <https://doi.org/10.1016/j.oooo.2018.10.003>.
- Ishibashi, Kyota, Eiji Sasaki, Seiya Ota, Daisuke Chiba, Yuji Yamamoto, Eiichi Tsuda, Sugimura Yoshikuni, Kazushige Ihara, and Yasuyuki Ishibashi. 2020. "Detection of Synovitis in Early Knee Osteoarthritis by MRI and Serum Biomarkers in Japanese General Population." *Scientific Reports* 10 (1): 12310. <https://doi.org/10.1038/s41598-020-69328-w>.
- Ishii, H., H. Tanaka, K. Katoh, H. Nakamura, M. Nagashima, and S. Yoshino. 2002. "Characterization of Infiltrating T Cells and Th1/Th2-Type Cytokines in the Synovium of Patients

- with Osteoarthritis.” *Osteoarthritis and Cartilage* 10 (4): 277–81.  
<https://doi.org/10.1053/joca.2001.0509>.
- Ita, Meagan E., Prabesh Ghimire, Eric J. Granquist, and Beth A. Winkelstein. 2022. “MMPs in Tissues Retrieved during Surgery from Patients with TMJ Disorders Relate to Pain More than to Radiological Damage Score.” *Journal of Orthopaedic Research* 40 (2): 338–47.  
<https://doi.org/10.1002/jor.25048>.
- Iwasaki, L.R., Y.M. Gonzalez, Y. Liu, H. Liu, M. Markova, L.M. Gallo, and J.C. Nickel. 2017. “TMJ Energy Densities in Healthy Men and Women.” *Osteoarthritis and Cartilage* 25 (6): 846–49. <https://doi.org/10.1016/j.joca.2016.12.027>.
- Jalloul, Reem, H. K. Chethan, and Ramez Alkhatib. 2023. “A Review of Machine Learning Techniques for the Classification and Detection of Breast Cancer from Medical Images.” *Diagnostics* 13 (14): 2460. <https://doi.org/10.3390/diagnostics13142460>.
- Jang, Dan-in, A-Hyeon Lee, Hye-Yoon Shin, Hyo-Ryeong Song, Jong-Hwi Park, Tae-Bong Kang, Sang-Ryong Lee, and Seung-Hoon Yang. 2021. “The Role of Tumor Necrosis Factor Alpha (TNF- $\alpha$ ) in Autoimmune Disease and Current TNF- $\alpha$  Inhibitors in Therapeutics.” *International Journal of Molecular Sciences* 22 (5): 2719.  
<https://doi.org/10.3390/ijms22052719>.
- Janvier, T., R. Jennane, A. Valery, K. Harrar, M. Delplanque, C. Lelong, D. Loeuille, H. Toumi, and E. Lespessailles. 2017. “Subchondral Tibial Bone Texture Analysis Predicts Knee Osteoarthritis Progression: Data from the Osteoarthritis Initiative: Tibial Bone Texture & Knee OA Progression.” *Osteoarthritis and Cartilage* 25 (2): 259–66.  
<https://doi.org/10.1016/j.joca.2016.10.005>.
- Jarecki, Jaromir, Teresa Małeczka-Masalska, Ewa Kosior-Jarecka, Wojciech Widuchowski, Piotr Krasowski, Martina Gutbier, Maciej Dobrzyński, and Tomasz Blicharski. 2022. “Concentration of Selected Metalloproteinases and Osteocalcin in the Serum and Synovial Fluid of Obese Women with Advanced Knee Osteoarthritis.” *International Journal of Environmental Research and Public Health* 19 (6): 3530.  
<https://doi.org/10.3390/ijerph19063530>.
- Jasim, Hajer, Anders Carlsson, Britt Hedenberg-Magnusson, Bijar Ghafouri, and Malin Ernberg. 2018. “Saliva as a Medium to Detect and Measure Biomarkers Related to Pain.” *Scientific Reports* 8 (February). <https://doi.org/10.1038/s41598-018-21131-4>.
- Jasim, Hajer, Bijar Ghafouri, Björn Gerdle, Britt Hedenberg-Magnusson, and Malin Ernberg. 2020. “Altered Levels of Salivary and Plasma Pain Related Markers in Temporomandibular Disorders.” *The Journal of Headache and Pain* 21 (1): 105.  
<https://doi.org/10.1186/s10194-020-01160-z>.
- Jehan, Frédéric, Mylène Zarka, Guillaume de la Houssaye, Joëlle Veziers, Agnès Ostertag, Martine Cohen-Solal, and Valérie Geoffroy. 2022. “New Insights into the Role of Matrix Metalloproteinase 3 (MMP3) in Bone.” *FASEB BioAdvances* 4 (8): 524–38.  
<https://doi.org/10.1096/fba.2021-00092>.
- Jenei-Lanzl, Zsuzsa, Andrea Meurer, and Frank Zaucke. 2019. “Interleukin-1 $\beta$  Signaling in Osteoarthritis - Chondrocytes in Focus.” *Cellular Signalling* 53 (January): 212–23.  
<https://doi.org/10.1016/j.cellsig.2018.10.005>.
- Jeon, Hye-Mi, Yong-Woo Ahn, Soo-Min Ok, Hye-Min Ju, Kyung-Hwa Jung, Eun-Young Kwon, and Sung-Hee Jeong. 2022. “A Large Subchondral Cyst in an Osteoarthritic Temporomandibular Joint: A Case Report.” *Journal of Oral Medicine and Pain* 47 (1): 67–71.  
<https://doi.org/10.14476/jomp.2022.47.1.67>.

- Jha, Nayansi, Kwang-sig Lee, and Yoon-Ji Kim. 2022. "Diagnosis of Temporomandibular Disorders Using Artificial Intelligence Technologies: A Systematic Review and Meta-Analysis." *PLOS ONE* 17 (8): e0272715. <https://doi.org/10.1371/journal.pone.0272715>.
- Jiang, Tammy, Jaimie L. Gradus, and Anthony J. Rosellini. 2020. "Supervised Machine Learning: A Brief Primer." *Behavior Therapy* 51 (5): 675–87. <https://doi.org/10.1016/j.beth.2020.05.002>.
- Jiao, Kai, Li-Na Niu, Mei-Qing Wang, Juan Dai, Shi-Bin Yu, Xiao-Dong Liu, and Jun Wang. 2011. "Subchondral Bone Loss Following Orthodontically Induced Cartilage Degradation in the Mandibular Condyles of Rats." *Bone* 48 (2): 362–71. <https://doi.org/10.1016/j.bone.2010.09.010>.
- Jiao, M. Zhang, L. Niu, S. Yu, G. Zhen, L. Xian, B. Yu, et al. 2014. "Overexpressed TGF- $\beta$  in Subchondral Bone Leads to Mandibular Condyle Degradation." *Journal of Dental Research* 93 (2): 140–47. <https://doi.org/10.1177/0022034513513034>.
- Joda, Tim, Tuomas Waltimo, Christiane Pauli-Magnus, Nicole Probst-Hensch, and Nicola U. Zitzmann. 2018. "Population-Based Linkage of Big Data in Dental Research." *International Journal of Environmental Research and Public Health* 15 (11): 2357. <https://doi.org/10.3390/ijerph15112357>.
- Joda, Tim, Tuomas Waltimo, Nicole Probst-Hensch, Christiane Pauli-Magnus, and Nicola U. Zitzmann. 2019. "Health Data in Dentistry: An Attempt to Master the Digital Challenge." *Public Health Genomics* 22 (1–2): 1–7. <https://doi.org/10.1159/000501643>.
- Johnson, Kevin B., Wei-Qi Wei, Dilhan Weeraratne, Mark E. Frisse, Karl Misulis, Kyu Rhee, Juan Zhao, and Jane L. Snowdon. 2021. "Precision Medicine, AI, and the Future of Personalized Health Care." *Clinical and Translational Science* 14 (1): 86–93. <https://doi.org/10.1111/cts.12884>.
- Jung, and Tae-Woo Kim. 2016. "New Approach for the Diagnosis of Extractions with Neural Network Machine Learning." *American Journal of Orthodontics and Dentofacial Orthopedics: Official Publication of the American Association of Orthodontists, Its Constituent Societies, and the American Board of Orthodontics* 149 (1): 127–33. <https://doi.org/10.1016/j.ajodo.2015.07.030>.
- Jung, Won, Kyung-Eun Lee, and Bong-Jik Suh. 2022. "Comparison of Clinical and Radiological Characteristics of Temporomandibular Joint Osteoarthritis in Older and Young People." *The Open Dentistry Journal* 16 (1). <https://doi.org/10.2174/18742106-v16-e2112290>.
- Kaggie, Joshua D, Rob Tovey, James MacKay, Fiona J Gilbert, Ferdia Gallagher, Andrew McCaskie, and Martin J Graves. 2018. "Automated Textural Classification of Osteoarthritis Magnetic Resonance Images."
- Kaimal, Shanti, Mansur Ahmad, Wenjun Kang, Donald Nixdorf, and Eric L. Schiffman. 2018. "Diagnostic Accuracy of Panoramic Radiography and MRI for Detecting Signs of TMJ Degenerative Joint Disease." *General Dentistry* 66 (4): 34–40.
- Kaji, Hiroshi. 2016. "Adipose Tissue-Derived Plasminogen Activator Inhibitor-1 Function and Regulation." In *Comprehensive Physiology*, 1873–96. John Wiley & Sons, Ltd. <https://doi.org/10.1002/cphy.c160004>.
- Kalogera, Stefania, Mylène P. Jansen, Anne-Christine Bay-Jensen, Peder Frederiksen, Morten A. Karsdal, Christian S. Thudium, and Simon C. Mastbergen. 2023. "Relevance of Biomarkers in Serum vs. Synovial Fluid in Patients with Knee Osteoarthritis." *International Journal of Molecular Sciences* 24 (11): 9483. <https://doi.org/10.3390/ijms24119483>.



- Kamarudin, Adina Najwa, Trevor Cox, and Ruwanthi Kolamunnage-Dona. 2017. "Time-Dependent ROC Curve Analysis in Medical Research: Current Methods and Applications." *BMC Medical Research Methodology* 17 (1): 53. <https://doi.org/10.1186/s12874-017-0332-6>.
- Kang, Jeong-Hyun. 2020. "Associations Among Temporomandibular Joint Osteoarthritis, Airway Dimensions, and Head and Neck Posture." *Journal of Oral and Maxillofacial Surgery* 78 (12): 2183.e1-2183.e12. <https://doi.org/10.1016/j.joms.2020.08.006>.
- Kapos, Flavia Penteado, Fernando Gustavo Exposto, Juan Fernando Oyarzo, and Justin Durham. 2020. "Temporomandibular Disorders: A Review of Current Concepts in Aetiology, Diagnosis and Management." *Oral Surgery* 13 (4): 321–34. <https://doi.org/10.1111/ors.12473>.
- Kashif, Muhammad, Thomas M. Deserno, Daniel Haak, and Stephan Jonas. 2016. "Feature Description with SIFT, SURF, BRIEF, BRISK, or FREAK? A General Question Answered for Bone Age Assessment." *Computers in Biology and Medicine* 68 (January): 67–75. <https://doi.org/10.1016/j.combiomed.2015.11.006>.
- Kaspiris, Angelos, Argyris C. Hadjimichael, Ioanna Lianou, Ilias D. Iliopoulos, Dimitrios Ntourantonis, Dimitra Melissaridou, Olga D. Savvidou, Evangelia Papadimitriou, and Efsthios Chronopoulos. 2023. "Subchondral Bone Cyst Development in Osteoarthritis: From Pathophysiology to Bone Microarchitecture Changes and Clinical Implementations." *Journal of Clinical Medicine* 12 (3): 815. <https://doi.org/10.3390/jcm12030815>.
- Kaspiris, L. Khaldi, T. B. Grivas, E. Vasiliadis, I. Kouvaras, S. Dagkas, E. Chronopoulos, and E. Papadimitriou. 2013. "Subchondral Cyst Development and MMP-1 Expression during Progression of Osteoarthritis: An Immunohistochemical Study." *Orthopaedics & Traumatology: Surgery & Research* 99 (5): 523–29. <https://doi.org/10.1016/j.otsr.2013.03.019>.
- Keemu, Hannes, Felix Vaura, Anu Maksimow, Mikael Maksimow, Aleksi Jokela, Maija Hollmén, and Keijo Mäkelä. 2021. "Novel Biomarkers for Diagnosing Periprosthetic Joint Infection from Synovial Fluid and Serum." *JBJS Open Access* 6 (2): e20.00067. <https://doi.org/10.2106/JBJS.OA.20.00067>.
- Kellesarian, Sergio Varela, Abdulaziz A. Al-Kheraif, Fahim Vohra, Alexis Ghanem, Hans Malmstrom, Georgios E. Romanos, and Fawad Javed. 2016. "Cytokine Profile in the Synovial Fluid of Patients with Temporomandibular Joint Disorders: A Systematic Review." *Cytokine* 77 (January): 98–106. <https://doi.org/10.1016/j.cyto.2015.11.005>.
- Khanagar, Sanjeev B., Ali Al-Ehaideb, Satish Vishwanathaiah, Prabhadevi C. Maganur, Shankargouda Patil, Sachin Naik, Hosam A. Baeshen, and Sachin S. Sarode. 2021. "Scope and Performance of Artificial Intelligence Technology in Orthodontic Diagnosis, Treatment Planning, and Clinical Decision-Making - A Systematic Review." *Journal of Dental Sciences* 16 (1): 482–92. <https://doi.org/10.1016/j.jds.2020.05.022>.
- Kim, Jin-Hwa, Soo-Min Ok, Jun-Young Heo, Kyung-Hee Kim, Sung-Hee Jeong, Yong-Woo Ahn, and Myung-Yun Ko. n.d. "The Clinical and Radiographic Features of Patients with Temporomandibular Joint Osteoarthritis" 39 (1): 2–9.
- Kim, Seong-Gyu Ko, Eun-Kyoung Lee, and Boyoung Jung. 2019. "The Relationship between Spinal Pain and Temporomandibular Joint Disorders in Korea: A Nationwide Propensity Score-Matched Study." *BMC Musculoskeletal Disorders* 20 (1): 631. <https://doi.org/10.1186/s12891-019-3003-4>.

- Kim, Sang Min Park, Hyun-Jae Cho, and Ji Woon Park. 2021. "The Relationship Between Primary Sleep Disorders and Temporomandibular Disorders: An 8-Year Nationwide Cohort Study in South Korea." *International Journal of General Medicine* 14 (October): 7121–31. <https://doi.org/10.2147/IJGM.S331387>.
- Kim, Aleksandra Wojczyńska, and Jeong-Yun Lee. 2016. "The Incidence of Osteoarthritic Change on Computed Tomography of Korean Temporomandibular Disorder Patients Diagnosed by RDC/TMD; a Retrospective Study." *Acta Odontologica Scandinavica* 74 (5): 337–42. <https://doi.org/10.3109/00016357.2015.1136678>.
- Kim, Gwanghyun Yang, Jumi Park, Jene Choi, Eunju Kang, and Bu-Kyu Lee. 2019. "Therapeutic Effect of Mesenchymal Stem Cells Derived from Human Umbilical Cord in Rabbit Temporomandibular Joint Model of Osteoarthritis." *Scientific Reports* 9 (1): 13854. <https://doi.org/10.1038/s41598-019-50435-2>.
- Kirk, William S., and Benjamin S. Kirk. 2006. "A Biomechanical Basis for Primary Arthroplasty of the Temporomandibular Joint." *Oral and Maxillofacial Surgery Clinics of North America, Modern Surgical Management of the Temporomandibular Joint*, 18 (3): 345–68. <https://doi.org/10.1016/j.coms.2006.03.006>.
- Kishimoto, Koji, Shumei Liu, Takanori Tsuji, Karen A. Olson, and Guo-Fu Hu. 2005. "Endogenous Angiogenin in Endothelial Cells Is a General Requirement for Cell Proliferation and Angiogenesis." *Oncogene* 24 (3): 445–56. <https://doi.org/10.1038/sj.onc.1208223>.
- Kitaura, Hideki, Aseel Marahleh, Fumitoshi Otori, Takahiro Noguchi, Wei-Ren Shen, Jiawei Qi, Yasuhiko Nara, Adya Pramusita, Ria Kinjo, and Itaru Mizoguchi. 2020. "Osteocyte-Related Cytokines Regulate Osteoclast Formation and Bone Resorption." *International Journal of Molecular Sciences* 21 (14): 5169. <https://doi.org/10.3390/ijms21145169>.
- Kline, Adrienne, Hanyin Wang, Yikuan Li, Saya Dennis, Meghan Hutch, Zhenxing Xu, Fei Wang, Feixiong Cheng, and Yuan Luo. 2022. "Multimodal Machine Learning in Precision Health: A Scoping Review." *Npj Digital Medicine* 5 (1): 1–14. <https://doi.org/10.1038/s41746-022-00712-8>.
- Koç, Nagihan. 2020. "Evaluation of Osteoarthritic Changes in the Temporomandibular Joint and Their Correlations with Age: A Retrospective CBCT Study." *Dental and Medical Problems* 57 (1): 67–72. <https://doi.org/10.17219/dmp/112392>.
- Koch, A. E., M. V. Volin, J. M. Woods, S. L. Kunkel, M. A. Connors, L. A. Harlow, D. C. Woodruff, M. D. Burdick, and R. M. Strieter. 2001. "Regulation of Angiogenesis by the C-X-C Chemokines Interleukin-8 and Epithelial Neutrophil Activating Peptide 78 in the Rheumatoid Joint." *Arthritis and Rheumatism* 44 (1): 31–40. [https://doi.org/10.1002/1529-0131\(200101\)44:1<31::AID-ANR5>3.0.CO;2-4](https://doi.org/10.1002/1529-0131(200101)44:1<31::AID-ANR5>3.0.CO;2-4).
- Kocher, Martin, Maximilian I. Ruge, Norbert Galldiks, and Philipp Lohmann. 2020. "Applications of Radiomics and Machine Learning for Radiotherapy of Malignant Brain Tumors." *Strahlentherapie Und Onkologie* 196 (10): 856–67. <https://doi.org/10.1007/s00066-020-01626-8>.
- Kohli, Sarvraj Singh, and Virinder Singh Kohli. 2011. "Role of RANKL–RANK/Osteoprotegerin Molecular Complex in Bone Remodeling and Its Immunopathologic Implications." *Indian Journal of Endocrinology and Metabolism* 15 (3): 175–81. <https://doi.org/10.4103/2230-8210.83401>.
- Kök, Hatice, Ayse Merve Acilar, and Mehmet Said İzgi. 2019. "Usage and Comparison of Artificial Intelligence Algorithms for Determination of Growth and Development by Cervical

- Vertebrae Stages in Orthodontics.” *Progress in Orthodontics* 20 (November): 41. <https://doi.org/10.1186/s40510-019-0295-8>.
- Kokkotis, Christos, Charis Ntakolia, Serafeim Moustakidis, Giannis Giakas, and Dimitrios Tsaopoulos. 2022. “Explainable Machine Learning for Knee Osteoarthritis Diagnosis Based on a Novel Fuzzy Feature Selection Methodology.” *Physical and Engineering Sciences in Medicine* 45 (1): 219–29. <https://doi.org/10.1007/s13246-022-01106-6>.
- Kokol, Peter, Marko Kokol, and Sašo Zagoranski. 2022. “Machine Learning on Small Size Samples: A Synthetic Knowledge Synthesis.” *Science Progress* 105 (1): 00368504211029777. <https://doi.org/10.1177/00368504211029777>.
- Kothari, Simple Futarmal, Lene Baad-Hansen, Lars Bolvig Hansen, Niels Bang, Leif Hovgaard Sørensen, Helle Wulf Eskildsen, and Peter Svensson. 2016. “Pain Profiling of Patients with Temporomandibular Joint Arthralgia and Osteoarthritis Diagnosed with Different Imaging Techniques.” *The Journal of Headache and Pain* 17 (1): 61. <https://doi.org/10.1186/s10194-016-0653-6>.
- Kraan, Peter M. van der. 2022. “Inhibition of Transforming Growth Factor- $\beta$  in Osteoarthritis. Discrepancy with Reduced TGF $\beta$  Signaling in Normal Joints.” *Osteoarthritis and Cartilage Open* 4 (1): 100238. <https://doi.org/10.1016/j.ocarto.2022.100238>.
- Kraan, Peter M. van der, and Wim B. van den Berg. 2007. “Osteophytes: Relevance and Biology.” *Osteoarthritis and Cartilage* 15 (3): 237–44. <https://doi.org/10.1016/j.joca.2006.11.006>.
- Krause, Adam J., Aric A. Prather, Tor D. Wager, Martin A. Lindquist, and Matthew P. Walker. 2019. “The Pain of Sleep Loss: A Brain Characterization in Humans.” *Journal of Neuroscience* 39 (12): 2291–2300. <https://doi.org/10.1523/JNEUROSCI.2408-18.2018>.
- Kriegeskorte, Nikolaus. 2015. “Deep Neural Networks: A New Framework for Modeling Biological Vision and Brain Information Processing.” *Annual Review of Vision Science* 1 (1): 417–46. <https://doi.org/10.1146/annurev-vision-082114-035447>.
- Krishnamoorthy, Bhuvana, NS Mamatha, and Vinod AR Kumar. 2013. “TMJ Imaging by CBCT: Current Scenario.” *Annals of Maxillofacial Surgery* 3 (1): 80–83. <https://doi.org/10.4103/2231-0746.110069>.
- Kristensen, K. D., P. Alstergren, P. Stoustrup, A. Küseler, T. Herlin, and T. K. Pedersen. 2014. “Cytokines in Healthy Temporomandibular Joint Synovial Fluid.” *Journal of Oral Rehabilitation* 41 (4): 250–56. <https://doi.org/10.1111/joor.12146>.
- La Touche, Roy, Alba Paris-Aleman, Amanda Hidalgo-Pérez, Ibai López-de-Uralde-Villanueva, Santiago Angulo-Díaz-Parreño, and Daniel Muñoz-García. 2018. “Evidence for Central Sensitization in Patients with Temporomandibular Disorders: A Systematic Review and Meta-Analysis of Observational Studies.” *Pain Practice* 18 (3): 388–409. <https://doi.org/10.1111/papr.12604>.
- Lai, Jung-Pin, Ying-Lei Lin, Ho-Chuan Lin, Chih-Yuan Shih, Yu-Po Wang, and Ping-Feng Pai. 2023. “Tree-Based Machine Learning Models with Optuna in Predicting Impedance Values for Circuit Analysis.” *Micromachines* 14 (2): 265. <https://doi.org/10.3390/mi14020265>.
- Lamot, Urška, Primož Strojjan, and Katarina Šurlan Popovič. 2013. “Magnetic Resonance Imaging of Temporomandibular Joint Dysfunction-Correlation with Clinical Symptoms, Age, and Gender.” *Oral Surgery, Oral Medicine, Oral Pathology and Oral Radiology* 116 (2): 258–63. <https://doi.org/10.1016/j.oooo.2013.04.019>.

- Lan, Kai-Wen, Jia-Min Chen, Liu-Lin Jiang, Yi-Fan Feng, and Ying Yan. 2022. "Treatment of Condylar Osteophyte in Temporomandibular Joint Osteoarthritis with Muscle Balance Occlusal Splint and Long-Term Follow-up: A Case Report." *World Journal of Clinical Cases* 10 (13): 4264–72. <https://doi.org/10.12998/wjcc.v10.i13.4264>.
- Lange-Brokaar, B. J. E. de, A. Ioan-Facsinay, G. J. V. M. van Osch, A.-M. Zuurmond, J. Schoones, R. E. M. Toes, T. W. J. Huizinga, and M. Kloppenburg. 2012. "Synovial Inflammation, Immune Cells and Their Cytokines in Osteoarthritis: A Review." *Osteoarthritis and Cartilage* 20 (12): 1484–99. <https://doi.org/10.1016/j.joca.2012.08.027>.
- Larheim, A-K Abrahamsson, M Kristensen, and L Z Arvidsson. 2015. "Temporomandibular Joint Diagnostics Using CBCT." *Dentomaxillofacial Radiology* 44 (1): 20140235. <https://doi.org/10.1259/dmfr.20140235>.
- Larheim, Tore A. 2005. "Role of Magnetic Resonance Imaging in the Clinical Diagnosis of the Temporomandibular Joint." *Cells, Tissues, Organs* 180 (1): 6–21. <https://doi.org/10.1159/000086194>.
- Larroza, Andrés, Vicente Bodí, David Moratal, Andrés Larroza, Vicente Bodí, and David Moratal. 2016. "Texture Analysis in Magnetic Resonance Imaging: Review and Considerations for Future Applications." In *Assessment of Cellular and Organ Function and Dysfunction Using Direct and Derived MRI Methodologies*. IntechOpen. <https://doi.org/10.5772/64641>.
- Latourte, Augustin, Chahrazad Cherifi, Jérémy Maillet, Hang-Korng Ea, Wafa Bouaziz, Thomas Funck-Brentano, Martine Cohen-Solal, Eric Hay, and Pascal Richette. 2017. "Systemic Inhibition of IL-6/Stat3 Signalling Protects against Experimental Osteoarthritis." *Annals of the Rheumatic Diseases* 76 (4): 748–55. <https://doi.org/10.1136/annrheumdis-2016-209757>.
- Lavigne, G.J., and B.J Sessle. 2016. "The Neurobiology of Orofacial Pain and Sleep and Their Interactions." *Journal of Dental Research* 95 (10): 1109–16. <https://doi.org/10.1177/0022034516648264>.
- Lee, and Q.-Schick Auh. 2022. "Comparison of Sleep Quality Deterioration by Subgroup of Painful Temporomandibular Disorder Based on Diagnostic Criteria for Temporomandibular Disorders." *Scientific Reports* 12 (1): 9026. <https://doi.org/10.1038/s41598-022-12976-x>.
- Lee, Il Ki Hong, and Yang-Hyun Chun. 2019. "Prediction of Painful Temporomandibular Joint Osteoarthritis in Juvenile Patients Using Bone Scintigraphy." *Clinical and Experimental Dental Research* 5 (3): 225–35. <https://doi.org/10.1002/cre2.175>.
- Lee, Dae-Jung Kim, Sang-Goo Lee, and Jin-Woo Chung. 2012. "A Longitudinal Study on the Osteoarthritic Change of the Temporomandibular Joint Based on 1-Year Follow-up Computed Tomography." *Journal of Cranio-Maxillo-Facial Surgery: Official Publication of the European Association for Cranio-Maxillo-Facial Surgery* 40 (8): e223-228. <https://doi.org/10.1016/j.jcms.2011.10.023>.
- Lee, Cheolkyu Park, Hyung Joon Kim, Yong Deok Lee, Zang Hee Lee, Yeong Wook Song, and Hong-Hee Kim. 2017. "Stimulation of Osteoclast Migration and Bone Resorption by C-C Chemokine Ligands 19 and 21." *Experimental & Molecular Medicine* 49 (7): e358. <https://doi.org/10.1038/emm.2017.100>.
- Lee, Hee-Kyung Park, Q.-Schick Auh, Haram Nah, Jae Seo Lee, Ho-Jin Moon, Dong Nyoung Heo, In San Kim, and Il Keun Kwon. 2020. "Emerging Potential of Exosomes in Regen-

- erative Medicine for Temporomandibular Joint Osteoarthritis.” *International Journal of Molecular Sciences* 21 (4): 1541. <https://doi.org/10.3390/ijms21041541>.
- Lee, Alexander R. Stanton, Austin E. Schumacher, Edmond Truelove, and Lars G. Hollender. 2019. “Osteoarthritis of the Temporomandibular Joint and Increase of the Horizontal Condylar Angle: A Longitudinal Study.” *Oral Surgery, Oral Medicine, Oral Pathology and Oral Radiology* 127 (4): 339–50. <https://doi.org/10.1016/j.oooo.2018.12.014>.
- Lee, Yung-Tsan Wu, Wu-Chien Chien, Chi-Hsiang Chung, Liang-Cheng Chen, and Yi-Shing Shieh. 2020. “The Prevalence of First-Onset Temporomandibular Disorder in Low Back Pain and Associated Risk Factors.” *Medicine* 99 (3): e18686. <https://doi.org/10.1097/MD.00000000000018686>.
- Lee, Yu, Min-ji Kim, Kim, and Choi. 2020. “Automated Cephalometric Landmark Detection with Confidence Regions Using Bayesian Convolutional Neural Networks.” *BMC Oral Health* 20 (1): 270. <https://doi.org/10.1186/s12903-020-01256-7>.
- Lenard, Anna, Elin Ellertsdottir, Lukas Herwig, Alice Krudewig, Loïc Sauter, Heinz-Georg Belting, and Markus Affolter. 2013. “In Vivo Analysis Reveals a Highly Stereotypic Morphogenetic Pathway of Vascular Anastomosis.” *Developmental Cell* 25 (5): 492–506. <https://doi.org/10.1016/j.devcel.2013.05.010>.
- Leung, Kevin, Bofei Zhang, Jimin Tan, Yiqiu Shen, Krzysztof J. Geras, James S. Babb, Kyunghyun Cho, Gregory Chang, and Cem M. Deniz. 2020. “Prediction of Total Knee Replacement and Diagnosis of Osteoarthritis by Using Deep Learning on Knee Radiographs: Data from the Osteoarthritis Initiative.” *Radiology* 296 (3): 584–93. <https://doi.org/10.1148/radiol.2020192091>.
- Li, Chang-hong, Lin-lin Xu, Jin-xia Zhao, Lin Sun, Zhong-qiang Yao, Xiao-li Deng, Rui Liu, Lin Yang, Rui Xing, and Xiang-yuan Liu. 2016. “CXCL16 Upregulates RANKL Expression in Rheumatoid Arthritis Synovial Fibroblasts through the JAK2/STAT3 and P38/MAPK Signaling Pathway.” *Inflammation Research: Official Journal of the European Histamine Research Society ... [et Al.]* 65 (3): 193–202. <https://doi.org/10.1007/s00011-015-0905-y>.
- Li, Guangzhao Guan, Li Mei, Kai Jiao, and Huang Li. 2021. “Pathological Mechanism of Chondrocytes and the Surrounding Environment during Osteoarthritis of Temporomandibular Joint.” *Journal of Cellular and Molecular Medicine* 25 (11): 4902–11. <https://doi.org/10.1111/jcmm.16514>.
- Li, Deyu Kong, Tian Tang, Di Su, Pu Yang, Huixia Wang, Zhihe Zhao, and Yang Liu. 2019. “Orthodontic Treatment Planning Based on Artificial Neural Networks.” *Scientific Reports* 9 (1): 2037. <https://doi.org/10.1038/s41598-018-38439-w>.
- Li, and Leung. 2021. “Temporomandibular Disorders: Current Concepts and Controversies in Diagnosis and Management.” *Diagnostics* 11 (3): 459. <https://doi.org/10.3390/diagnostics11030459>.
- Li, Zhenxing Li, Yuyan Li, Xi Hu, Yu Zhang, and Pei Fan. 2020. “Profiling of Inflammatory Mediators in the Synovial Fluid Related to Pain in Knee Osteoarthritis.” *BMC Musculoskeletal Disorders* 21 (1): 99. <https://doi.org/10.1186/s12891-020-3120-0>.
- Li, Wei Luo, Shou-An Zhu, and Guang-Hua Lei. 2017. “T Cells in Osteoarthritis: Alterations and Beyond.” *Frontiers in Immunology* 8: 356. <https://doi.org/10.3389/fimmu.2017.00356>.
- Li, Yiying Mai, Peihua Cao, Xin Wen, Tianxiang Fan, Xiaoshuai Wang, Guangfeng Ruan, Su’an Tang, Changhai Ding, and Zhaohua Zhu. 2022. “Relative Efficacy and Safety of Anti-

- Inflammatory Biologic Agents for Osteoarthritis: A Conventional and Network Meta-Analysis.” *Journal of Clinical Medicine* 11 (14). <https://doi.org/10.3390/jcm11143958>.
- Li, Jie Pan, Hongqi Chen, Yongliang Fang, and Yang Sun. 2022. “CXCR6-Based Immunotherapy in Autoimmune, Cancer and Inflammatory Inflammation.” *Acta Pharmaceutica Sinica. B* 12 (8): 3255–62. <https://doi.org/10.1016/j.apsb.2022.03.012>.
- Li, Yu Wang, Sumanta Basu, Karl Kumbier, and Bin Yu. 2019. “A Debiased MDI Feature Importance Measure for Random Forests.” arXiv. <http://arxiv.org/abs/1906.10845>.
- Li, Jimin Yin, Junjie Gao, Tak S. Cheng, Nathan J. Pavlos, Changqing Zhang, and Ming H. Zheng. 2013. “Subchondral Bone in Osteoarthritis: Insight into Risk Factors and Microstructural Changes.” *Arthritis Research & Therapy* 15 (6): 223. <https://doi.org/10.1186/ar4405>.
- Liang, Xin, Shuming Liu, Xingmin Qu, Zhihui Wang, Jianbo Zheng, Xiaoyan Xie, Guowu Ma, Zuyan Zhang, and Xuchen Ma. 2017. “Evaluation of Trabecular Structure Changes in Osteoarthritis of the Temporomandibular Joint with Cone Beam Computed Tomography Imaging.” *Oral Surgery, Oral Medicine, Oral Pathology and Oral Radiology* 124 (3): 315–22. <https://doi.org/10.1016/j.oooo.2017.05.514>.
- Liang, Xin, Zuyan Zhang, Jianping Gu, Zhihui Wang, Bart Vandenberghe, Reinhilde Jacobs, Jie Yang, Guowu Ma, Haibin Ling, and Xuchen Ma. 2017. “Comparison of Micro-CT and Cone Beam CT on the Feasibility of Assessing Trabecular Structures in Mandibular Condyle.” *Dento Maxillo Facial Radiology* 46 (5): 20160435. <https://doi.org/10.1259/dmfr.20160435>.
- Liang, Joshua Xu, Meilang Xue, and Christopher J. Jackson. 2016. “Matrix Metalloproteinases in Bone Development and Pathology: Current Knowledge and Potential Clinical Utility.” *Metalloproteinases In Medicine* 3 (December): 93–102. <https://doi.org/10.2147/MNM.S92187>.
- Liem, Yulia, Andrew Judge, Yunfei Li, and Mohammed Sharif. 2022. “Biochemical, Clinical, Demographic and Imaging Biomarkers for Disease Progression in Knee Osteoarthritis.” *Biomarkers in Medicine* 16 (8): 633–45. <https://doi.org/10.2217/bmm-2021-0579>.
- Limchaichana, N., H. Nilsson, E. C. Ekberg, M. Nilner, and A. Petersson. 2007. “Clinical Diagnoses and MRI Findings in Patients with TMD Pain.” *Journal of Oral Rehabilitation* 34 (4): 237–45. <https://doi.org/10.1111/j.1365-2842.2006.01719.x>.
- Lin, Fan-ching, and Howard A. Young. 2014. “Interferons: Success in Anti-Viral Immunotherapy.” *Cytokine & Growth Factor Reviews* 25 (4): 369–76. <https://doi.org/10.1016/j.cytogfr.2014.07.015>.
- Linardatos, Pantelis, Vasilis Papastefanopoulos, and Sotiris Kotsiantis. 2021. “Explainable AI: A Review of Machine Learning Interpretability Methods.” *Entropy* 23 (1): 18. <https://doi.org/10.3390/e23010018>.
- Ling, S. M., D. D. Patel, P. Garner, M. Zhan, M. Vaduganathan, D. Muller, D. Taub, et al. 2009. “Serum Protein Signatures Detect Early Radiographic Osteoarthritis.” *Osteoarthritis and Cartilage* 17 (1): 43–48. <https://doi.org/10.1016/j.joca.2008.05.004>.
- Lisignoli, Gina, Stefania Toneguzzi, Anna Piacentini, Sandra Cristino, Francesco Grassi, Carola Cavallo, and Andrea Facchini. 2006. “CXCL12 (SDF-1) and CXCL13 (BCA-1) Chemokines Significantly Induce Proliferation and Collagen Type I Expression in Osteoblasts from Osteoarthritis Patients.” *Journal of Cellular Physiology* 206 (1): 78–85. <https://doi.org/10.1002/jcp.20435>.

- Liu. 2010. "Feature Selection." In *Encyclopedia of Machine Learning*, edited by Claude Sammut and Geoffrey I. Webb, 402–6. Boston, MA: Springer US. [https://doi.org/10.1007/978-0-387-30164-8\\_306](https://doi.org/10.1007/978-0-387-30164-8_306).
- Liu, Yu Chai, Guanqiao Liu, Weiping Su, Qiaoyue Guo, Xiao Lv, Peisong Gao, et al. 2021. "Osteoclasts Protect Bone Blood Vessels against Senescence through the Angiogenin/Plexin-B2 Axis." *Nature Communications* 12 (1): 1832. <https://doi.org/10.1038/s41467-021-22131-1>.
- Liu, Shuo Chen, Dawei Geng, Jie Lei, Jiankang Zhang, Liangliang Li, Yucheng Lin, et al. 2022. "Local Drug-Induced Modulation of Gp130 Receptor Signaling Delays Disease Progression in a Pig Model of Temporomandibular Joint Osteoarthritis." *Frontiers in Dental Medicine* 3. <https://www.frontiersin.org/articles/10.3389/fdmed.2022.937819>.
- Liu, Liangliang, Jing Chang, Pei Zhang, Qingzhi Ma, Hui Zhang, Tong Sun, and Hongbo Qiao. 2023. "A Joint Multi-Modal Learning Method for Early-Stage Knee Osteoarthritis Disease Classification." *Heliyon* 9 (4): e15461. <https://doi.org/10.1016/j.heliyon.2023.e15461>.
- Liu, Roderick J. Tan, and Youhua Liu. 2020. "The Many Faces of Matrix Metalloproteinase-7 in Kidney Diseases." *Biomolecules* 10 (6): 960. <https://doi.org/10.3390/biom10060960>.
- Lohmann, Philipp, Martin Kocher, Maximilian I. Ruge, Veerle Visser-Vandewalle, N. Jon Shah, Gereon R. Fink, Karl-Josef Langen, and Norbert Galldiks. 2020. "PET/MRI Radiomics in Patients With Brain Metastases." *Frontiers in Neurology* 11. <https://www.frontiersin.org/articles/10.3389/fneur.2020.00001>.
- Look, John O., Eric L. Schiffman, Edmond L. Truelove, and Mansur Ahmad. 2010. "Reliability and Validity of Axis I of the Research Diagnostic Criteria for Temporomandibular Disorders (RDC/TMD) with Proposed Revisions." *Journal of Oral Rehabilitation* 37 (10): 744–59. <https://doi.org/10.1111/j.1365-2842.2010.02121.x>.
- Lu, Ke, Feng Ma, Dan Yi, Huan Yu, Liping Tong, and Di Chen. 2021. "Molecular Signaling in Temporomandibular Joint Osteoarthritis." *Journal of Orthopaedic Translation* 32 (September): 21–27. <https://doi.org/10.1016/j.jot.2021.07.001>.
- Lu, Anjin Liu, Yiliao Song, and Guangquan Zhang. 2020. "Data-Driven Decision Support under Concept Drift in Streamed Big Data." *Complex & Intelligent Systems* 6 (1): 157–63. <https://doi.org/10.1007/s40747-019-00124-4>.
- Ludin, A., J. J. Sela, A. Schroeder, Y. Samuni, D. W. Nitzan, and G. Amir. 2013. "Injection of Vascular Endothelial Growth Factor into Knee Joints Induces Osteoarthritis in Mice." *Osteoarthritis and Cartilage* 21 (3): 491–97. <https://doi.org/10.1016/j.joca.2012.12.003>.
- Ma, Yuanjun, Xiaohua Chen, Feng He, Shi Li, Rui He, Qian Liu, Qingshan Dong, et al. 2022. "Low Frequency Pulsed Electromagnetic Fields Exposure Alleviate the Abnormal Subchondral Bone Remodeling at the Early Stage of Temporomandibular Joint Osteoarthritis." *BMC Musculoskeletal Disorders* 23 (1): 987. <https://doi.org/10.1186/s12891-022-05916-3>.
- MacKay, James W., Geeta Kapoor, Jeffrey B. Driban, Grace H. Lo, Timothy E. McAlindon, Andoni P. Toms, Andrew W. McCaskie, and Fiona J. Gilbert. 2018. "Association of Subchondral Bone Texture on Magnetic Resonance Imaging with Radiographic Knee Osteoarthritis Progression: Data from the Osteoarthritis Initiative Bone Ancillary Study." *European Radiology* 28 (11): 4687–95. <https://doi.org/10.1007/s00330-018-5444-9>.
- Mackie, Tamara, Najla Al Turkestani, Jonas Bianchi, Tengfei Li, Antonio Ruellas, Marcela Gurgel, Erika Benavides, Fabiana Soki, and Lucia Cevidanes. 2022. "Quantitative Bone

- Imaging Biomarkers and Joint Space Analysis of the Articular Fossa in Temporomandibular Joint Osteoarthritis Using Artificial Intelligence Models.” *Frontiers in Dental Medicine* 3. <https://www.frontiersin.org/articles/10.3389/fdmed.2022.1007011>.
- Madrid, Juan, Silvia Ruiz-España, Tania Piñeiro-Vidal, José Manuel Santabarbara, Alicia M. Maceira, and David Moratal. 2022. “Texture Analysis in MRI of the Knee for an Early Diagnosis of Osteoarthritis.” In *2022 44th Annual International Conference of the IEEE Engineering in Medicine & Biology Society (EMBC)*, 493–96. <https://doi.org/10.1109/EMBC48229.2022.9871296>.
- Manfredini, Daniele, Luca Guarda-Nardini, Ephraim Winocur, Fabio Piccotti, Jari Ahlberg, and Frank Lobbezoo. 2011. “Research Diagnostic Criteria for Temporomandibular Disorders: A Systematic Review of Axis I Epidemiologic Findings.” *Oral Surgery, Oral Medicine, Oral Pathology, Oral Radiology, and Endodontology* 112 (4): 453–62. <https://doi.org/10.1016/j.tripleo.2011.04.021>.
- Manfredini, Daniele, Marzia Segù, Niki Arveda, Luca Lombardo, Giuseppe Siciliani, Alessandro Rossi, and Luca Guarda-Nardini. 2016. “Temporomandibular Joint Disorders in Patients With Different Facial Morphology. A Systematic Review of the Literature.” *Journal of Oral and Maxillofacial Surgery* 74 (1): 29–46. <https://doi.org/10.1016/j.joms.2015.07.006>.
- Marias, Kostas. 2021. “The Constantly Evolving Role of Medical Image Processing in Oncology: From Traditional Medical Image Processing to Imaging Biomarkers and Radiomics.” *Journal of Imaging* 7 (8): 124. <https://doi.org/10.3390/jimaging7080124>.
- Massilla Mani, and S. Satha Sivasubramanian. 2016. “A Study of Temporomandibular Joint Osteoarthritis Using Computed Tomographic Imaging.” *Biomedical Journal* 39 (3): 201–6. <https://doi.org/10.1016/j.bj.2016.06.003>.
- Matheus, H. R., Ş D. Özdemir, and F. P. S. Guastaldi. 2022. “Stem Cell-Based Therapies for Temporomandibular Joint Osteoarthritis and Regeneration of Cartilage/Osteochondral Defects: A Systematic Review of Preclinical Experiments.” *Osteoarthritis and Cartilage* 30 (9): 1174–85. <https://doi.org/10.1016/j.joca.2022.05.006>.
- Matsuzaki, Koichi. 2013. “Smad Phospho-Isoforms Direct Context-Dependent TGF- $\beta$  Signaling.” *Cytokine & Growth Factor Reviews* 24 (4): 385–99. <https://doi.org/10.1016/j.cytogfr.2013.06.002>.
- Mayerhoefer, Marius E., Andrzej Materka, Georg Langs, Ida Häggström, Piotr Szczypiński, Peter Gibbs, and Gary Cook. 2020. “Introduction to Radiomics.” *Journal of Nuclear Medicine* 61 (4): 488–95. <https://doi.org/10.2967/jnumed.118.222893>.
- Mehana, El-Sayed E., Asmaa F. Khafaga, and Samar S. El-Blehi. 2019. “The Role of Matrix Metalloproteinases in Osteoarthritis Pathogenesis: An Updated Review.” *Life Sciences* 234 (October): 116786. <https://doi.org/10.1016/j.lfs.2019.116786>.
- Mehndiratta, Anurag, Jyoti Kumar, Alpana Manchanda, Ishwar Singh, Sujata Mohanty, Novee Seth, and Richa Gautam. 2019. “Painful Clicking Jaw: A Pictorial Review of Internal Derangement of the Temporomandibular Joint.” *Polish Journal of Radiology* 84 (December): e598–615. <https://doi.org/10.5114/pjr.2019.92287>.
- Mello, Christiane-Espinola-Bandeira, José-Luiz-Góes Oliveira, Alan-Chester-Feitosa Jesus, Mila-Leite-de Moraes Maia, Jonielly-Costa-Vasconcelos de Santana, Loren-Suyane-Oliveira Andrade, Jullyana-de Souza Siqueira Quintans, Lucindo-José Quintans-Junior, Paulo-César-Rodrigues Conti, and Leonardo-Rigoldi Bonjardim. 2012. “Temporoman-



- dibular Disorders in Headache Patients.” *Medicina Oral, Patología Oral y Cirugía Bucal* 17 (6): e1042–46. <https://doi.org/10.4317/medoral.18007>.
- Mélou, Caroline, Pascal Pellen-Mussi, Sylvie Jeanne, Agnès Novella, Sylvie Tricot-Doleux, and Dominique Chauvel-Lebret. 2023. “Osteoarthritis of the Temporomandibular Joint: A Narrative Overview.” *Medicina* 59 (1): 8. <https://doi.org/10.3390/medicina59010008>.
- Menz, Hylton B., Alyssa B. Dufour, Jody L. Riskowski, Howard J. Hillstrom, and Marian T. Hannan. 2013. “Foot Posture, Foot Function and Low Back Pain: The Framingham Foot Study.” *Rheumatology (Oxford, England)* 52 (12): 2275–82. <https://doi.org/10.1093/rheumatology/ket298>.
- Messaoudene, Khadidja, and Khaled Harrar. 2022. “A Hybrid LBP-HOG Model and Naive Bayes Classifier for Knee Osteoarthritis Detection: Data from the Osteoarthritis Initiative.” In *Artificial Intelligence and Its Applications*, edited by Brahim Lejdel, Eliseo Clementini, and Louai Alarabi, 458–67. Lecture Notes in Networks and Systems. Cham: Springer International Publishing. [https://doi.org/10.1007/978-3-030-96311-8\\_42](https://doi.org/10.1007/978-3-030-96311-8_42).
- Miller, R. E., P. B. Tran, S. Ishihara, J. Larkin, and A. M. Malfait. 2016. “Therapeutic Effects of an Anti-ADAMTS-5 Antibody on Joint Damage and Mechanical Allodynia in a Murine Model of Osteoarthritis.” *Osteoarthritis and Cartilage* 24 (2): 299–306. <https://doi.org/10.1016/j.joca.2015.09.005>.
- Minervini, Giuseppe, Rocco Franco, Maria Maddalena Marrapodi, Salvatore Crimi, Almir Badnjević, Gabriele Cervino, Alberto Bianchi, and Marco Cicciù. 2023. “Correlation between Temporomandibular Disorders (TMD) and Posture Evaluated Through the Diagnostic Criteria for Temporomandibular Disorders (DC/TMD): A Systematic Review with Meta-Analysis.” *Journal of Clinical Medicine* 12 (7): 2652. <https://doi.org/10.3390/jcm12072652>.
- Miranda, Magdalena, Juan Facundo Morici, María Belén Zanoni, and Pedro Bekinschtein. 2019. “Brain-Derived Neurotrophic Factor: A Key Molecule for Memory in the Healthy and the Pathological Brain.” *Frontiers in Cellular Neuroscience* 13 (August): 363. <https://doi.org/10.3389/fncel.2019.00363>.
- Mishra, Sairam, Ranjan Kumar Mallick, Debadatta Amaresh Gadanayak, and Pravati Nayak. 2021. “A Novel Hybrid Downsampling and Optimized Random Forest Approach for Islanding Detection and Non-Islanding Power Quality Events Classification in Distributed Generation Integrated System.” *IET Renewable Power Generation* 15 (8): 1662–77. <https://doi.org/10.1049/rpg2.12137>.
- Mishra, Shailendra. 2022. “An Optimized Gradient Boost Decision Tree Using Enhanced African Buffalo Optimization Method for Cyber Security Intrusion Detection.” *Applied Sciences* 12 (24): 12591. <https://doi.org/10.3390/app122412591>.
- Miyatake, Kazumasa, Kenjiro Iwasa, Sean M. McNary, Gordon Peng, and A. Hari Reddi. 2016. “Modulation of Superficial Zone Protein/Lubricin/PRG4 by Kartogenin and Transforming Growth Factor-B1 in Surface Zone Chondrocytes in Bovine Articular Cartilage.” *Cartilage* 7 (4): 388–97. <https://doi.org/10.1177/1947603516630789>.
- Mogi, M., A. Kondo, K. Kinpara, and A. Togari. 2000. “Anti-Apoptotic Action of Nerve Growth Factor in Mouse Osteoblastic Cell Line.” *Life Sciences* 67 (10): 1197–1206. [https://doi.org/10.1016/s0024-3205\(00\)00705-0](https://doi.org/10.1016/s0024-3205(00)00705-0).
- Molnar, Vilim, Vid Matišić, Ivan Kodvanj, Roko Bjelica, Željko Jeleč, Damir Hudetz, Eduard Rod, et al. 2021. “Cytokines and Chemokines Involved in Osteoarthritis Pathogenesis.”

- International Journal of Molecular Sciences* 22 (17): 9208.  
<https://doi.org/10.3390/ijms22179208>.
- Monaco, Annalisa, Ruggero Cattaneo, Maria Chiara Marci, Davide Pietropaoli, and Eleonora Ortu. 2017. "Central Sensitization-Based Classification for Temporomandibular Disorders: A Pathogenetic Hypothesis." *Pain Research and Management* 2017 (August): e5957076. <https://doi.org/10.1155/2017/5957076>.
- Moritake, Akihiro, Naoyuki Kawao, Kiyotaka Okada, Kohei Tatsumi, Masayoshi Ishida, Katsumi Okumoto, Osamu Matsuo, Masao Akagi, and Hiroshi Kaji. 2017. "Plasminogen Activator Inhibitor-1 Deficiency Enhances Subchondral Osteopenia after Induction of Osteoarthritis in Mice." *BMC Musculoskeletal Disorders* 18 (1): 392. <https://doi.org/10.1186/s12891-017-1752-5>.
- Munjal, Akul, Santul Bapat, Daniel Hubbard, Monte Hunter, Ravindra Kolhe, and Sadanand Fulzele. 2019. "Advances in Molecular Biomarker for Early Diagnosis of Osteoarthritis." *Biomolecular Concepts* 10 (1): 111–19. <https://doi.org/10.1515/bmc-2019-0014>.
- Murakami, Ken-ichiro. 2022. "Current Role of Arthrocentesis, Arthroscopy and Open Surgery for Temporomandibular Joint Internal Derangement with Inflammatory/Degenerative Disease; -Pitfalls and Pearls-." *Journal of Oral and Maxillofacial Surgery, Medicine, and Pathology* 34 (1): 1–11. <https://doi.org/10.1016/j.ajoms.2021.06.009>.
- Muratovic, D., D.M. Findlay, R.D. Quarrington, X. Cao, L.B. Solomon, G.J. Atkins, and J.S. Kuliwaba. 2022. "Elevated Levels of Active Transforming Growth Factor B1 in the Subchondral Bone Relate Spatially to Cartilage Loss and Impaired Bone Quality in Human Knee Osteoarthritis." *Osteoarthritis and Cartilage* 30 (6): 896–907. <https://doi.org/10.1016/j.joca.2022.03.004>.
- Nakase, Hiroshi, Minoru Matsuura, Sakae Mikami, Norimitsu Uza, and Tsutomu Chiba. 2012. "Role of the CXCL12-CXCR4 Axis and CXCL16 in Inflammatory Bowel Disease." *Intestinal Research* 10 (2): 125–33.
- Nanayakkara, Shanika, Xiaoyan Zhou, and Heiko Spallek. 2019. "Impact of Big Data on Oral Health Outcomes." *Oral Diseases* 25 (5): 1245–52. <https://doi.org/10.1111/odi.13007>.
- Neisius, Ulf, Hossam El-Rewaidy, Shiro Nakamori, Jennifer Rodriguez, Warren J. Manning, and Reza Nezafat. 2019. "Radiomic Analysis of Myocardial Native T1 Imaging Discriminates between Hypertensive Heart Disease and Hypertrophic Cardiomyopathy." *JACC. Cardiovascular Imaging* 12 (10): 1946–54. <https://doi.org/10.1016/j.jcmg.2018.11.024>.
- Neogi, Tuhina. 2012. "Clinical Significance of Bone Changes in Osteoarthritis." *Therapeutic Advances in Musculoskeletal Disease* 4 (4): 259–67. <https://doi.org/10.1177/1759720X12437354>.
- Neri, Emanuele, Marzia Del Re, Fabiola Paiar, Paola Erba, Paola Cocuzza, Daniele Regge, and Romano Danesi. 2018. "Radiomics and Liquid Biopsy in Oncology: The Holons of Systems Medicine." *Insights into Imaging* 9 (6): 915–24. <https://doi.org/10.1007/s13244-018-0657-7>.
- Neve, Anna, Francesco Paolo Cantatore, Addolorata Corrado, Annamaria Gaudio, Simona Ruggeri, and Domenico Ribatti. 2013. "In Vitro and in Vivo Angiogenic Activity of Osteoarthritic and Osteoporotic Osteoblasts Is Modulated by VEGF and Vitamin D3 Treatment." *Regulatory Peptides* 184 (June): 81–84. <https://doi.org/10.1016/j.regpep.2013.03.014>.
- Nicolakis, Peter, Erdogmus Celal Burak, Josef Kollmitzer, Andreas Kopf, Eva Piehslinger, Günther Franz Wiesinger, and Veronika Fialka-Moser. 2001. "An Investigation of the Effec-

- tiveness of Exercise and Manual Therapy in Treating Symptoms of TMJ Osteoarthritis.” *CRANIO*® 19 (1): 26–32. <https://doi.org/10.1080/08869634.2001.11746148>.
- Niessen, Carien M., Deborah Leckband, and Alpha S. Yap. 2011. “Tissue Organization by Cadherin Adhesion Molecules: Dynamic Molecular and Cellular Mechanisms of Morphogenetic Regulation.” *Physiological Reviews* 91 (2): 691–731. <https://doi.org/10.1152/physrev.00004.2010>.
- Ning, Yilin, Marcus Eng Hock Ong, Bibhas Chakraborty, Benjamin Alan Goldstein, Daniel Shu Wei Ting, Roger Vaughan, and Nan Liu. 2022. “Shapley Variable Importance Cloud for Interpretable Machine Learning.” *Patterns* 3 (4): 100452. <https://doi.org/10.1016/j.patter.2022.100452>.
- Nisbett, William H., Amar Kavuri, and Mini Das. 2020. “On the Correlation between Second Order Texture Features and Human Observer Detection Performance in Digital Images.” *Scientific Reports* 10 (1): 13510. <https://doi.org/10.1038/s41598-020-69816-z>.
- Nixdorf, Donald R., Ana M. Velly, and Aurelio A. Alonso. 2008. “Neurovascular Pains: Implications of Migraine for the Oral & Maxillofacial Surgeon.” *Oral and Maxillofacial Surgery Clinics of North America* 20 (2): 221–vii. <https://doi.org/10.1016/j.coms.2007.12.008>.
- Norman, Berk, Valentina Pedoia, Adam Noworolski, Thomas M. Link, and Sharmila Majumdar. 2019. “Applying Densely Connected Convolutional Neural Networks for Staging Osteoarthritis Severity from Plain Radiographs.” *Journal of Digital Imaging* 32 (3): 471–77. <https://doi.org/10.1007/s10278-018-0098-3>.
- Ntakolia, Charis, Christos Kokkotis, Serafeim Moustakidis, and Dimitrios Tsaopoulos. 2021. “Prediction of Joint Space Narrowing Progression in Knee Osteoarthritis Patients.” *Diagnostics (Basel, Switzerland)* 11 (2): 285. <https://doi.org/10.3390/diagnostics11020285>.
- Ogura, N., K. Satoh, M. Akutsu, M. Tobe, K. Kuyama, N. Kuboyama, H. Sakamaki, H. Kuji-raoka, and T. Kondoh. 2010. “MCP-1 Production in Temporomandibular Joint Inflammation.” *Journal of Dental Research* 89 (10): 1117–22. <https://doi.org/10.1177/0022034510376041>.
- Ohlmann, Brigitte, Peter Rammelsberg, Volkmar Henschel, Bodo Kress, Olaf Gabbert, and Mark Schmitter. 2006. “Prediction of TMJ Arthralgia According to Clinical Diagnosis and MRI Findings.” *The International Journal of Prosthodontics* 19 (4): 333–38.
- Orhan, Kaan, Lukas Driesen, Sohaib Shujaat, Reinhilde Jacobs, and Xiangfei Chai. 2021. “Development and Validation of a Magnetic Resonance Imaging-Based Machine Learning Model for TMJ Pathologies.” *BioMed Research International* 2021 (July): 6656773. <https://doi.org/10.1155/2021/6656773>.
- Orhurhu, Vwaire, Robert Chu, Sebele Ogunsoola, Loretta Akpala, Mariam Salisu Orhurhu, Ivan Urits, Anh L. Ngo, Omar Viswanath, and Alan D. Kaye. 2020. “The Role of Peripheral Brain-Derived Neurotrophic Factor in Chronic Osteoarthritic Joint Pain.” *Annals of Palliative Medicine* 9 (4): 1361365–1361365. <https://doi.org/10.21037/apm-20-888>.
- Ota, Kuniaki, Patrick Quint, Megan M. Weivoda, Ming Ruan, Larry Pederson, Jennifer J. Westendorf, Sundeep Khosla, and Merry Jo Oursler. 2013. “Transforming Growth Factor Beta 1 Induces CXCL16 and Leukemia Inhibitory Factor Expression in Osteoclasts to Modulate Migration of Osteoblast Progenitors.” *Bone* 57 (1): 10.1016/j.bone.2013.07.023. <https://doi.org/10.1016/j.bone.2013.07.023>.
- Ottersen, Margareth Kristensen, Anna-Karin Abrahamsson, Tore Arne Larheim, and Linda Zamoline Arvidsson. 2019. “CBCT Characteristics and Interpretation Challenges of Tem-

- poromandibular Joint Osteoarthritis in a Hand Osteoarthritis Cohort.” *Dentomaxillofacial Radiology* 48 (4): 20180245. <https://doi.org/10.1259/dmfr.20180245>.
- Ozsari, Sifa, Mehmet Serdar Güzel, Dilek Yılmaz, and Kıvanç Kamburoğlu. 2023. “A Comprehensive Review of Artificial Intelligence Based Algorithms Regarding Temporomandibular Joint Related Diseases.” *Diagnostics* 13 (16): 2700. <https://doi.org/10.3390/diagnostics13162700>.
- Panahiazar, Maryam, Vahid Taslimitehrani, Ashutosh Jadhav, and Jyotishman Pathak. 2014. “Empowering Personalized Medicine with Big Data and Semantic Web Technology: Promises, Challenges, and Use Cases.” *Proceedings : ... IEEE International Conference on Big Data. IEEE International Conference on Big Data 2014* (October): 790–95. <https://doi.org/10.1109/BigData.2014.7004307>.
- Pantoja, Leticia Lopes Quirino, Isabela Porto de Toledo, Yasmine Mendes Pupo, André Luís Porporatti, Graziela De Luca Canto, Liete Figueiredo Zwir, and Eliete Neves Silva Guerra. 2019. “Prevalence of Degenerative Joint Disease of the Temporomandibular Joint: A Systematic Review.” *Clinical Oral Investigations* 23 (5): 2475–88. <https://doi.org/10.1007/s00784-018-2664-y>.
- Parekh, Vishwa, and Michael A. Jacobs. 2016. “Radiomics: A New Application from Established Techniques.” *Expert Review of Precision Medicine and Drug Development* 1 (2): 207–26. <https://doi.org/10.1080/23808993.2016.1164013>.
- Park, Dongmin Choi, Joonho Lee, Sung Soo Ahn, Seung-Koo Lee, Sang-Hyuk Lee, and Minji Bang. 2020. “Differentiating Patients with Schizophrenia from Healthy Controls by Hippocampal Subfields Using Radiomics.” *Schizophrenia Research* 223 (September): 337–44. <https://doi.org/10.1016/j.schres.2020.09.009>.
- Park, and Jin Woo Chung. 2016. “Inflammatory Cytokines and Sleep Disturbance in Patients with Temporomandibular Disorders.” *Journal of Oral & Facial Pain and Headache* 30 (1): 27–33. <https://doi.org/10.11607/ofph.1367>.
- Park, Ji-Hoon, Hye-Won Hwang, Jun-Ho Moon, Youngsung Yu, Hansuk Kim, Soo-Bok Her, Girish Srinivasan, Mohammed Noori A. Aljanabi, Richard E. Donatelli, and Shin-Jae Lee. 2019. “Automated Identification of Cephalometric Landmarks: Part 1—Comparisons between the Latest Deep-Learning Methods YOLOV3 and SSD.” *The Angle Orthodontist* 89 (6): 903–9. <https://doi.org/10.2319/022019-127.1>.
- Park, Donghyun Kim, Ho Sung Kim, Seo Young Park, Jung Youn Kim, Se Jin Cho, Jae Ho Shin, and Jeong Hoon Kim. 2020. “Quality of Science and Reporting of Radiomics in Oncologic Studies: Room for Improvement According to Radiomics Quality Score and TRIPOD Statement.” *European Radiology* 30 (1): 523–36. <https://doi.org/10.1007/s00330-019-06360-z>.
- Park, Park, and Lee. 2020. “Radiomics and Deep Learning: Hepatic Applications.” *Korean Journal of Radiology* 21 (4): 387–401. <https://doi.org/10.3348/kjr.2019.0752>.
- Patel, Alpesh, Boon Ching Tee, Henry Fields, Elizabeth Jones, Jahanzeb Chaudhry, and Zongyang Sun. 2014. “Evaluation of Cone-Beam Computed Tomography in the Diagnosis of Simulated Small Osseous Defects in the Mandibular Condyle.” *American Journal of Orthodontics and Dentofacial Orthopedics* 145 (2): 143–56. <https://doi.org/10.1016/j.ajodo.2013.10.014>.
- Patel, Sagar K. Naik, David P. Naidich, William D. Travis, Jeremy A. Weingarten, Richard Lazarro, David D. Gutterman, Catherine Wentowski, Horiana B. Grosu, and Suhail Raouf. 2013. “A Practical Algorithmic Approach to the Diagnosis and Management of Solitary

- Pulmonary Nodules: Part 2: Pretest Probability and Algorithm.” *Chest* 143 (3): 840–46. <https://doi.org/10.1378/chest.12-1487>.
- Pedregosa, Fabian, Gaël Varoquaux, Alexandre Gramfort, Vincent Michel, Bertrand Thirion, Olivier Grisel, Mathieu Blondel, et al. 2011. “Scikit-Learn: Machine Learning in Python.” *Journal of Machine Learning Research* 12 (85): 2825–30.
- Pedullà, E., G. A. Meli, A. Garufi, M. L. Mandalà, A. Blandino, and P. Cascone. 2009. “Neuropathic Pain in Temporomandibular Joint Disorders: Case-Control Analysis by MR Imaging.” *American Journal of Neuroradiology* 30 (7): 1414–18. <https://doi.org/10.3174/ajnr.A1575>.
- Perazzo, Joseph, Margaret Rodriguez, Jackson Currie, Robert Salata, and Allison R. Webel. 2019. “Creation of Data Repositories to Advance Nursing Science.” *Western Journal of Nursing Research* 41 (1): 78–95. <https://doi.org/10.1177/0193945917749481>.
- Pérez-García, Selene, Mar Carrión, Irene Gutiérrez-Cañas, Raúl Villanueva-Romero, David Castro, Carmen Martínez, Isidoro González-Álvaro, Francisco J. Blanco, Yasmina Juarranz, and Rosa P. Gomariz. 2019. “Profile of Matrix-Remodeling Proteinases in Osteoarthritis: Impact of Fibronectin.” *Cells* 9 (1): 40. <https://doi.org/10.3390/cells9010040>.
- Pessler, F., L. X. Chen, L. Dai, C. Gomez-Vaquero, C. Diaz-Torne, M. E. Paessler, C. Scanzello, N. Cakir, E. Einhorn, and H. R. Schumacher. 2008. “A Histomorphometric Analysis of Synovial Biopsies from Individuals with Gulf War Veterans’ Illness and Joint Pain Compared to Normal and Osteoarthritis Synovium.” *Clinical Rheumatology* 27 (9): 1127–34. <https://doi.org/10.1007/s10067-008-0878-0>.
- Petch, Jeremy, Shuang Di, and Walter Nelson. 2022. “Opening the Black Box: The Promise and Limitations of Explainable Machine Learning in Cardiology.” *The Canadian Journal of Cardiology* 38 (2): 204–13. <https://doi.org/10.1016/j.cjca.2021.09.004>.
- Pfander, D., D. Körtje, R. Zimmermann, G. Weseloh, T. Kirsch, M. Gesslein, T. Cramer, and B. Swoboda. 2001. “Vascular Endothelial Growth Factor in Articular Cartilage of Healthy and Osteoarthritic Human Knee Joints.” *Annals of the Rheumatic Diseases* 60 (11): 1070–73. <https://doi.org/10.1136/ard.60.11.1070>.
- Plesh, Octavia, Carolyn Noonan, Dedra S. Buchwald, Jack Goldberg, and Niloo Afari. 2012. “Temporomandibular Disorder-Type Pain and Migraine Headache in Women: A Preliminary Twin Study.” *Journal of Orofacial Pain* 26 (2): 91–98.
- Plsikova Matejova, Jana, Timea Spakova, Denisa Harvanova, Marek Lacko, Vladimir Filip, Rastislav Sepitka, Istvan Mitro, and Jan Rosocha. 2021. “A Preliminary Study of Combined Detection of COMP, TIMP-1, and MMP-3 in Synovial Fluid: Potential Indicators of Osteoarthritis Progression.” *CARTILAGE* 13 (2\_suppl): 1421S-1430S. <https://doi.org/10.1177/1947603520946385>.
- Pm, van der Kraan, Blaney Davidson En, Blom A, and van den Berg Wb. 2009. “TGF-Beta Signaling in Chondrocyte Terminal Differentiation and Osteoarthritis: Modulation and Integration of Signaling Pathways through Receptor-Smads.” *Osteoarthritis and Cartilage* 17 (12). <https://doi.org/10.1016/j.joca.2009.06.008>.
- Podgorelec, Vili, and Milan Zorman. 2014. “Decision Tree Learning.” In *Encyclopedia of Complexity and Systems Science*, edited by Robert A. Meyers, 1–28. Berlin, Heidelberg: Springer. [https://doi.org/10.1007/978-3-642-27737-5\\_117-2](https://doi.org/10.1007/978-3-642-27737-5_117-2).
- Ponchel, F., A. N. Burska, E. M. A. Hensor, R. Raja, M. Campbell, P. Emery, and P. G. Conaghan. 2015. “Changes in Peripheral Blood Immune Cell Composition in Osteoarthritis.”

- Osteoarthritis and Cartilage* 23 (11): 1870–78.  
<https://doi.org/10.1016/j.joca.2015.06.018>.
- PORPORATTI, André Luís, Yuri Martins COSTA, Paulo César Rodrigues CONTI, Leonardo Rigoldi BONJARDIM, and Patrícia dos Santos CALDERON. 2015. “Primary Headaches Interfere with the Efficacy of Temporomandibular Disorders Management.” *Journal of Applied Oral Science* 23 (2): 129–34. <https://doi.org/10.1590/1678-775720130557>.
- Pouders, Caroline, Michel De Maeseneer, Peter Van Roy, Jan Gielen, Annieta Goossens, and Maryam Shahabpour. 2008. “Prevalence and MRI-Anatomic Correlation of Bone Cysts in Osteoarthritic Knees.” *American Journal of Roentgenology* 190 (1): 17–21.  
<https://doi.org/10.2214/AJR.07.2098>.
- Prim, Julianna H, Sangtae Ahn, Maria I Davila, Morgan L Alexander, Karen L McCulloch, and Flavio Fröhlich. 2019. “Targeting the Autonomic Nervous System Balance in Patients with Chronic Low Back Pain Using Transcranial Alternating Current Stimulation: A Randomized, Crossover, Double-Blind, Placebo-Controlled Pilot Study.” *Journal of Pain Research* 12 (December): 3265–77. <https://doi.org/10.2147/JPR.S208030>.
- Puntmann, V. O. 2009. “How-to Guide on Biomarkers: Biomarker Definitions, Validation and Applications with Examples from Cardiovascular Disease.” *Postgraduate Medical Journal* 85 (1008): 538–45. <https://doi.org/10.1136/pgmj.2008.073759>.
- Qi, Changlin, Yuxing Shan, Jing Wang, Fupeng Ding, Ding Zhao, Teng Yang, and Yanfang Jiang. 2016. “Circulating T Helper 9 Cells and Increased Serum Interleukin-9 Levels in Patients with Knee Osteoarthritis.” *Clinical and Experimental Pharmacology & Physiology* 43 (5): 528–34. <https://doi.org/10.1111/1440-1681.12567>.
- Qiao, Yusen, Jun Li, Catherine Yuh, Frank Ko, Louis G. Mercuri, Jad Alkhudari, Robin Pourzal, and Chun-do Oh. 2023. “Chemokine Regulation in Temporomandibular Joint Disease: A Comprehensive Review.” *Genes* 14 (2): 408. <https://doi.org/10.3390/genes14020408>.
- Raghupathi, Wullianallur, and Viju Raghupathi. 2014. “Big Data Analytics in Healthcare: Promise and Potential.” *Health Information Science and Systems* 2 (February): 3.  
<https://doi.org/10.1186/2047-2501-2-3>.
- Raheem1, Noor Natik, Mohammed Faris2, Athraa Y. Al-Hijazi3, and Ali I. Alqurshi4. 2020. “Roles of Brain-Derived Neurotrophic Factor (BDNF) In Developing Jaw.” *Medico Legal Update* 20 (3): 1082–87. <https://doi.org/10.37506/mlu.v20i3.1546>.
- Rahman, Md. Mokhlesur, Opeyemi Lateef Usman, Ravie Chandren Muniyandi, Shahnorbanun Sahran, Suziyani Mohamed, and Rogayah A Razak. 2020. “A Review of Machine Learning Methods of Feature Selection and Classification for Autism Spectrum Disorder.” *Brain Sciences* 10 (12): 949. <https://doi.org/10.3390/brainsci10120949>.
- Raman, Dayanidhi, Tammy Sobolik-Delmaire, and Ann Richmond. 2011. “Chemokines in Health and Disease.” *Experimental Cell Research* 317 (5): 575–89.  
<https://doi.org/10.1016/j.yexcr.2011.01.005>.
- Ranganathan, Priya, C. S. Pramesh, and Rakesh Aggarwal. 2017. “Common Pitfalls in Statistical Analysis: Logistic Regression.” *Perspectives in Clinical Research* 8 (3): 148–51.  
[https://doi.org/10.4103/picr.PICR\\_87\\_17](https://doi.org/10.4103/picr.PICR_87_17).
- Ray, Bimal K., Arvind Shakya, and Alpana Ray. 2007. “Vascular Endothelial Growth Factor Expression in Arthritic Joint Is Regulated by SAF-1 Transcription Factor.” *Journal of Immunology (Baltimore, Md.: 1950)* 178 (3): 1774–82.  
<https://doi.org/10.4049/jimmunol.178.3.1774>.

- Redding, S., L. Junginger, P. Rzeczycki, C. Rasner, and T. Maerz. 2020. "CXCL16 Expression during Post-Traumatic Osteoarthritis Development: Implications for Mesenchymal Stem Cell Recruitment." *Osteoarthritis and Cartilage* 28 (April): S508–9. <https://doi.org/10.1016/j.joca.2020.02.799>.
- Reeh, Heike, Nadine Rudolph, Ulrike Billing, Henrike Christen, Stefan Streif, Eric Bullinger, Monica Schliemann-Bullinger, et al. 2019. "Response to IL-6 Trans- and IL-6 Classic Signalling Is Determined by the Ratio of the IL-6 Receptor  $\alpha$  to Gp130 Expression: Fusing Experimental Insights and Dynamic Modelling." *Cell Communication and Signaling : CCS* 17 (May): 46. <https://doi.org/10.1186/s12964-019-0356-0>.
- Reid, Matthew J., Abhishek Dave, Claudia M. Campbell, Jennifer Haythornthwaite, Patrick H. Finan, and Michael T. Smith. 2022. "Increased Pain Sensitivity Is Associated with Reduced REM Sleep in Females with Temporomandibular Joint Disorder (TMD)." *The Journal of Pain* 23 (5, Supplement): 58–59. <https://doi.org/10.1016/j.jpain.2022.03.220>.
- Reinhold, Jacob C., Blake E. Dewey, Aaron Carass, and Jerry L. Prince. 2019. "Evaluating the Impact of Intensity Normalization on MR Image Synthesis." *Proceedings of SPIE--the International Society for Optical Engineering* 10949 (March): 109493H. <https://doi.org/10.1117/12.2513089>.
- Renner-Sitar, Ksenija, Mike T. John, Snigdha S. Pusalavidyasagar, Dipankar Bandyopadhyay, and Eric L. Schiffman. 2016. "Sleep Quality in Temporomandibular Disorder Cases." *Sleep Medicine* 25 (September): 105–12. <https://doi.org/10.1016/j.sleep.2016.06.031>.
- Ribeiro, Marco Tulio, Sameer Singh, and Carlos Guestrin. 2016. "“Why Should I Trust You?": Explaining the Predictions of Any Classifier." In *Proceedings of the 22nd ACM SIGKDD International Conference on Knowledge Discovery and Data Mining*, 1135–44. KDD '16. New York, NY, USA: Association for Computing Machinery. <https://doi.org/10.1145/2939672.2939778>.
- Ribera, Nina Tubau, Priscille de Dumast, Marilia Yatabe, Antonio Ruellas, Marcos Ioshida, Beatriz Paniagua, Martin Styner, et al. 2019. "Shape Variation Analyzer: A Classifier for Temporomandibular Joint Damaged by Osteoarthritis." *Proceedings of SPIE--the International Society for Optical Engineering* 10950 (February): 1095021. <https://doi.org/10.1117/12.2506018>.
- Richardson, Michael L. 2020. "Deep Learning Improves Predictions of the Need for Total Knee Replacement." *Radiology* 296 (3): 594–95. <https://doi.org/10.1148/radiol.2020202332>.
- Robinson, Jennifer L., Pamela M. Johnson, Karolina Kister, Michael T. Yin, Jing Chen, and Sunil Wadhwa. 2020. "Estrogen Signaling Impacts Temporomandibular Joint and Periodontal Disease Pathology." *Odontology* 108 (2): 153–65. <https://doi.org/10.1007/s10266-019-00439-1>.
- Rodriguez-Fontenla, Cristina, Manuel Calaza, Evangelos Evangelou, Ana M. Valdes, Nigel Arden, Francisco J. Blanco, Andrew Carr, et al. 2014. "Assessment of Osteoarthritis Candidate Genes in a Meta-Analysis of Nine Genome-Wide Association Studies." *Arthritis & Rheumatology (Hoboken, N.J.)* 66 (4): 940–49. <https://doi.org/10.1002/art.38300>.
- Roithmann, Camila Caspary, Carlos Augusto Gomes da Silva, Marcos Pascoal Pattussi, and Márcio Lima Grossi. 2021. "Subjective Sleep Quality and Temporomandibular Disorders: Systematic Literature Review and Meta-Analysis." *Journal of Oral Rehabilitation* 48 (12): 1380–94. <https://doi.org/10.1111/joor.13265>.

- Rollín, R., F. Marco, J. A. Jover, J. A. García-Asenjo, L. Rodríguez, L. López-Durán, and B. Fernández-Gutiérrez. 2008. “Early Lymphocyte Activation in the Synovial Microenvironment in Patients with Osteoarthritis: Comparison with Rheumatoid Arthritis Patients and Healthy Controls.” *Rheumatology International* 28 (8): 757–64. <https://doi.org/10.1007/s00296-008-0518-7>.
- Rose-John, Stefan. 2018. “Interleukin-6 Family Cytokines.” *Cold Spring Harbor Perspectives in Biology* 10 (2): a028415. <https://doi.org/10.1101/cshperspect.a028415>.
- Rousseau, Jean-Charles, Roland Chapurlat, and Patrick Garnero. 2021. “Soluble Biological Markers in Osteoarthritis.” *Therapeutic Advances in Musculoskeletal Disease* 13 (September): 1759720X211040300. <https://doi.org/10.1177/1759720X211040300>.
- Ruth, Jeffrey H., Christian S. Haas, Christy C. Park, M. Asif Amin, Rita J. Martinez, G. Kenneth Haines, Shiva Shahrara, Phillip L. Campbell, and Alisa E. Koch. 2006. “CXCL16-Mediated Cell Recruitment to Rheumatoid Arthritis Synovial Tissue and Murine Lymph Nodes Is Dependent Upon the MAPK Pathway.” *Arthritis and Rheumatism* 54 (3): 765–78. <https://doi.org/10.1002/art.21662>.
- Sabeti, Elyas, Joshua Drews, Narathip Reamaroon, Elisa Warner, Michael W. Sjoding, Jonathan Gryak, and Kayvan Najarian. 2021. “Learning Using Partially Available Privileged Information and Label Uncertainty: Application in Detection of Acute Respiratory Distress Syndrome.” *IEEE Journal of Biomedical and Health Informatics* 25 (3): 784–96. <https://doi.org/10.1109/JBHI.2020.3008601>.
- Sadaksharam, Jayachandran, and Priyanka Khobre. 2016. “Osteophytes in Temporomandibular Joint, a Spectrum of Appearance in Cone-Beam Computed Tomography: Report of Four Cases.” *Journal of Indian Academy of Oral Medicine and Radiology* 28 (3): 289. <https://doi.org/10.4103/0972-1363.195672>.
- Sakkas, Lazaros I., and Chris D. Platsoucas. 2007. “The Role of T Cells in the Pathogenesis of Osteoarthritis.” *Arthritis and Rheumatism* 56 (2): 409–24. <https://doi.org/10.1002/art.22369>.
- Salemi, Fatemeh, Abbas Shokri, Fatemeh Hafez Maleki, Maryam Farhadian, Gholamreza Dashti, Farzane Ostovarrad, and Hadi Ranjzad. 2016. “Effect of Field of View on Detection of Condyle Bone Defects Using Cone Beam Computed Tomography.” *The Journal of Craniofacial Surgery* 27 (3): 644–48. <https://doi.org/10.1097/SCS.0000000000002592>.
- Sandhu, Amit, Jason S. Rockel, Starlee Lively, and Mohit Kapoor. 2023. “Emerging Molecular Biomarkers in Osteoarthritis Pathology.” *Therapeutic Advances in Musculoskeletal Disease* 15 (June): 1759720X231177116. <https://doi.org/10.1177/1759720X231177116>.
- Sannajust, Sébastien, Ian Imbert, Victoria Eaton, Terry Henderson, Lucy Liaw, Meghan May, Mary F. Barbe, and Tamara King. 2019. “Females Have Greater Susceptibility to Develop Ongoing Pain and Central Sensitization in a Rat Model of Temporomandibular Joint Pain.” *Pain* 160 (9): 2036–49. <https://doi.org/10.1097/j.pain.0000000000001598>.
- Santos, Glaucia Nize Martins, Helbert Eustáquio Cardoso da Silva, Filipe Eduard Leite Ossege, Paulo Tadeu de Souza Figueiredo, Nilce de Santos Melo, Cristine Miron Stefani, and André Ferreira Leite. 2023. “Radiomics in Bone Pathology of the Jaws.” *Dentomaxillofacial Radiology* 52 (1): 20220225. <https://doi.org/10.1259/dmfr.20220225>.
- Sarchielli, Paola, Maria Luisa Mancini, Alessandro Floridi, Francesca Coppola, Cristiana Rossi, Katuscia Nardi, Monica Acciarresi, Luigi Alberto Pini, and Paolo Calabresi. 2007. “Increased Levels of Neurotrophins Are Not Specific for Chronic Migraine: Evidence from



- Primary Fibromyalgia Syndrome.” *The Journal of Pain* 8 (9): 737–45. <https://doi.org/10.1016/j.jpain.2007.05.002>.
- Sarker, Iqbal H. 2021. “Machine Learning: Algorithms, Real-World Applications and Research Directions.” *Sn Computer Science* 2 (3): 160. <https://doi.org/10.1007/s42979-021-00592-x>.
- Sauteur, Loïc, Alice Krudewig, Lukas Herwig, Nikolaus Ehrenfeuchter, Anna Lenard, Markus Affolter, and Heinz-Georg Belting. 2014. “Cdh5/VE-Cadherin Promotes Endothelial Cell Interface Elongation via Cortical Actin Polymerization during Angiogenic Sprouting.” *Cell Reports* 9 (2): 504–13. <https://doi.org/10.1016/j.celrep.2014.09.024>.
- Scanzello, Carla R. 2017. “Chemokines and Inflammation in Osteoarthritis: Insights From Patients and Animal Models.” *Journal of Orthopaedic Research : Official Publication of the Orthopaedic Research Society* 35 (4): 735–39. <https://doi.org/10.1002/jor.23471>.
- Scapicchio, Camilla, Michela Gabelloni, Andrea Barucci, Dania Cioni, Luca Saba, and Emanuele Neri. 2021. “A Deep Look into Radiomics.” *La Radiologia Medica* 126 (10): 1296–1311. <https://doi.org/10.1007/s11547-021-01389-x>.
- Schaible, Hans-Georg. 2014. “Nociceptive Neurons Detect Cytokines in Arthritis.” *Arthritis Research & Therapy* 16 (5): 470. <https://doi.org/10.1186/s13075-014-0470-8>.
- Scheller, Jürgen, Athena Chalaris, Dirk Schmidt-Arras, and Stefan Rose-John. 2011. “The Pro- and Anti-Inflammatory Properties of the Cytokine Interleukin-6.” *Biochimica Et Biophysica Acta* 1813 (5): 878–88. <https://doi.org/10.1016/j.bbamcr.2011.01.034>.
- Schiffman, and Ohrbach. 2016. “Executive Summary of the Diagnostic Criteria for Temporomandibular Disorders for Clinical and Research Applications.” *The Journal of the American Dental Association* 147 (6): 438–45. <https://doi.org/10.1016/j.adaj.2016.01.007>.
- Schiffman, Richard Ohrbach, Edmond L. Truelove, Tai Feng, Gary C. Anderson, Wei Pan, Yoly M. Gonzalez, et al. 2010. “The Revised Research Diagnostic Criteria for Temporomandibular Disorders: Methods Used to Establish and Validate Revised Axis I Diagnostic Algorithms.” *Journal of Orofacial Pain* 24 (1): 63–78.
- Schiffman, Richard Ohrbach, Edmond Truelove, John Look, Gary Anderson, Jean-Paul Goulet, Thomas List, et al. 2014. “Diagnostic Criteria for Temporomandibular Disorders (DC/TMD) for Clinical and Research Applications: Recommendations of the International RDC/TMD Consortium Network and Orofacial Pain Special Interest Group.” *Journal of Oral & Facial Pain and Headache* 28 (1): 6–27.
- Schiffman, A. M. Velly, J. O. Look, J. S. Hodges, J. Q. Swift, K. L. Decker, Q. N. Anderson, et al. 2014. “Effects of Four Treatment Strategies for Temporomandibular Joint Closed Lock.” *International Journal of Oral and Maxillofacial Surgery* 43 (2): 217–26. <https://doi.org/10.1016/j.ijom.2013.07.744>.
- Schmitter, Marc, Bodo Kress, Michael Leckel, Volkmar Henschel, Brigitte Ohlmann, and Peter Rammelsberg. 2008. “Validity of Temporomandibular Disorder Examination Procedures for Assessment of Temporomandibular Joint Status.” *American Journal of Orthodontics and Dentofacial Orthopedics: Official Publication of the American Association of Orthodontists, Its Constituent Societies, and the American Board of Orthodontics* 133 (6): 796–803. <https://doi.org/10.1016/j.ajodo.2006.06.022>.
- Schroder, Kate, Paul J. Hertzog, Timothy Ravasi, and David A. Hume. 2004. “Interferon- $\gamma$ : An Overview of Signals, Mechanisms and Functions.” *Journal of Leukocyte Biology* 75 (2): 163–89. <https://doi.org/10.1189/jlb.0603252>.

- Schwendicke, F., W. Samek, and J. Krois. 2020. "Artificial Intelligence in Dentistry: Chances and Challenges." *Journal of Dental Research* 99 (7): 769–74. <https://doi.org/10.1177/0022034520915714>.
- Shaefer, J.R., D.L. Jackson, E.L. Schiffman, and Q.N. Anderson. 2001. "Pressure-Pain Thresholds and MRI Effusions in TMJ Arthralgia." *Journal of Dental Research* 80 (10): 1935–39. <https://doi.org/10.1177/00220345010800101401>.
- Shan, Yuxing, Changlin Qi, Yijun Liu, Hui Gao, Ding Zhao, and Yanfang Jiang. 2017. "Increased Frequency of Peripheral Blood Follicular Helper T Cells and Elevated Serum IL-21 Levels in Patients with Knee Osteoarthritis." *Molecular Medicine Reports* 15 (3): 1095–1102. <https://doi.org/10.3892/mmr.2017.6132>.
- Shen, ZiXian Jiao, Ji Si Zheng, Wei Feng Xu, Shang Yong Zhang, An Qin, and Chi Yang. 2015. "Injecting Vascular Endothelial Growth Factor into the Temporomandibular Joint Induces Osteoarthritis in Mice." *Scientific Reports* 5 (1): 16244. <https://doi.org/10.1038/srep16244>.
- Shen, Li, and Chen. 2014. "TGF- $\beta$  Signaling and the Development of Osteoarthritis." *Bone Research* 2 (1): 1–7. <https://doi.org/10.1038/boneres.2014.2>.
- Shen, C.-L. Wu, I.-M. Jou, C.-H. Lee, H.-Y. Juan, P.-J. Lee, S.-H. Chen, and J.-L. Hsieh. 2011. "T Helper Cells Promote Disease Progression of Osteoarthritis by Inducing Macrophage Inflammatory Protein-1 $\gamma$ ." *Osteoarthritis and Cartilage* 19 (6): 728–36. <https://doi.org/10.1016/j.joca.2011.02.014>.
- Sheng, Jinghao, and Zhengping Xu. 2016. "Three Decades of Research on Angiogenin: A Review and Perspective." *Acta Biochimica et Biophysica Sinica* 48 (5): 399–410. <https://doi.org/10.1093/abbs/gmv131>.
- Shi, J., S. Lee, H.C. Pan, A. Mohammad, A. Lin, W. Guo, E. Chen, et al. 2017. "Association of Condylar Bone Quality with TMJ Osteoarthritis." *Journal of Dental Research* 96 (8): 888–94. <https://doi.org/10.1177/0022034517707515>.
- Shim, Ji Suk, Chulhan Kim, Jae Jun Ryu, and Sung Jae Choi. 2020. "Correlation between TM Joint Disease and Rheumatic Diseases Detected on Bone Scintigraphy and Clinical Factors." *Scientific Reports* 10 (March): 4547. <https://doi.org/10.1038/s41598-020-60804-x>.
- Shoukri, B., J. C. Prieto, A. Ruellas, M. Yatabe, J. Sugai, M. Styner, H. Zhu, et al. 2019. "Minimally Invasive Approach for Diagnosing TMJ Osteoarthritis." *Journal of Dental Research* 98 (10): 1103–11. <https://doi.org/10.1177/0022034519865187>.
- Shrivastava, Mayank, Ricardo Battaglino, and Liang Ye. 2021. "A Comprehensive Review on Biomarkers Associated with Painful Temporomandibular Disorders." *International Journal of Oral Science* 13 (1): 1–13. <https://doi.org/10.1038/s41368-021-00129-1>.
- Sidey-Gibbons, Jenni A. M., and Chris J. Sidey-Gibbons. 2019. "Machine Learning in Medicine: A Practical Introduction." *BMC Medical Research Methodology* 19 (1): 64. <https://doi.org/10.1186/s12874-019-0681-4>.
- Simão, Adriano Prado, Vanessa Amaral Mendonça, Tássio Málber de Oliveira Almeida, Sérgio Antunes Santos, Wellington Fabiano Gomes, Candido Celso Coimbra, and Ana Cristina Rodrigues Lacerda. 2014. "Involvement of BDNF in Knee Osteoarthritis: The Relationship with Inflammation and Clinical Parameters." *Rheumatology International* 34 (8): 1153–57. <https://doi.org/10.1007/s00296-013-2943-5>.
- Skaper, Stephen D. 2008. "The Biology of Neurotrophins, Signalling Pathways, and Functional Peptide Mimetics of Neurotrophins and Their Receptors." *CNS & Neurological Disorders Drug Targets* 7 (1): 46–62. <https://doi.org/10.2174/187152708783885174>.

- Slade, Mathew S. Conrad, Luda Diatchenko, Naim U. Rashid, Sheng Zhong, Shad Smith, Jesse Rhodes, et al. 2011. "Cytokine Biomarkers and Chronic Pain: Association of Genes, Transcription, and Circulating Proteins with Temporomandibular Disorders and Widespread Palpation Tenderness." *PAIN* 152 (12): 2802–12. <https://doi.org/10.1016/j.pain.2011.09.005>.
- Slade, R. Ohrbach, J.D. Greenspan, R.B. Fillingim, E. Bair, A.E. Sanders, R. Dubner, et al. 2016. "Painful Temporomandibular Disorder." *Journal of Dental Research* 95 (10): 1084–92. <https://doi.org/10.1177/0022034516653743>.
- Smith, James O., Richard O. C. Oreffo, Nicholas M. P. Clarke, and Helmtrud I. Roach. 2003. "Changes in the Antiangiogenic Properties of Articular Cartilage in Osteoarthritis." *Journal of Orthopaedic Science: Official Journal of the Japanese Orthopaedic Association* 8 (6): 849–57. <https://doi.org/10.1007/s00776-003-0717-8>.
- Sobue, T., Y. Hakeda, Y. Kobayashi, H. Hayakawa, K. Yamashita, T. Aoki, M. Kumegawa, T. Noguchi, and T. Hayakawa. 2001. "Tissue Inhibitor of Metalloproteinases 1 and 2 Directly Stimulate the Bone-Resorbing Activity of Isolated Mature Osteoclasts." *Journal of Bone and Mineral Research: The Official Journal of the American Society for Bone and Mineral Research* 16 (12): 2205–14. <https://doi.org/10.1359/jbmr.2001.16.12.2205>.
- Soenksen, Luis R., Yu Ma, Cynthia Zeng, Leonard Boussieux, Kimberly Villalobos Carballo, Liangyuan Na, Holly M. Wiberg, Michael L. Li, Ignacio Fuentes, and Dimitris Bertsimas. 2022. "Integrated Multimodal Artificial Intelligence Framework for Healthcare Applications." *Npj Digital Medicine* 5 (1): 1–10. <https://doi.org/10.1038/s41746-022-00689-4>.
- Sohn, Dong Hyun, Jeremy Sokolove, Orr Sharpe, Jennifer C. Erhart, Piyanka E. Chandra, Lauren J. Lahey, Tamsin M. Lindstrom, et al. 2012. "Plasma Proteins Present in Osteoarthritic Synovial Fluid Can Stimulate Cytokine Production via Toll-like Receptor 4." *Arthritis Research & Therapy* 14 (1): R7. <https://doi.org/10.1186/ar3555>.
- Song, Hwanhee, Jeong Yun Lee, Kyung-Hoe Huh, and Ji Woon Park. 2020. "Long-Term Changes of Temporomandibular Joint Osteoarthritis on Computed Tomography." *Scientific Reports* 10 (April): 6731. <https://doi.org/10.1038/s41598-020-63493-8>.
- Souza, Gilberto Francisco Martha de, Adherbal Caminada Netto, Arthur Henrique de Andrade Melani, Miguel Angelo de Carvalho Michalski, and Renan Favarão da Silva. 2022. "Chapter 6 - Engineering Systems' Fault Diagnosis Methods." In *Reliability Analysis and Asset Management of Engineering Systems*, edited by Gilberto Francisco Martha de Souza, Adherbal Caminada Netto, Arthur Henrique de Andrade Melani, Miguel Angelo de Carvalho Michalski, and Renan Favarão da Silva, 165–87. Advances in Reliability Science. Elsevier. <https://doi.org/10.1016/B978-0-12-823521-8.00006-2>.
- Sperry, M. M., S. Kartha, B. A. Winkelstein, and E. J. Granquist. 2019. "Experimental Methods to Inform Diagnostic Approaches for Painful TMJ Osteoarthritis." *Journal of Dental Research* 98 (4): 388–97. <https://doi.org/10.1177/0022034519828731>.
- Spin-Neto, Rubens, Erik Gotfredsen, and Ann Wenzel. 2013. "Impact of Voxel Size Variation on CBCT-Based Diagnostic Outcome in Dentistry: A Systematic Review." *Journal of Digital Imaging* 26 (4): 813–20. <https://doi.org/10.1007/s10278-012-9562-7>.
- Stafford, I. S., M. Kellermann, E. Mossotto, R. M. Beattie, B. D. MacArthur, and S. Ennis. 2020. "A Systematic Review of the Applications of Artificial Intelligence and Machine Learning in Autoimmune Diseases." *Npj Digital Medicine* 3 (1): 1–11. <https://doi.org/10.1038/s41746-020-0229-3>.

- Stannus, O., G. Jones, F. Cicuttini, V. Parameswaran, S. Quinn, J. Burgess, and C. Ding. 2010. “Circulating Levels of IL-6 and TNF- $\alpha$  Are Associated with Knee Radiographic Osteoarthritis and Knee Cartilage Loss in Older Adults.” *Osteoarthritis and Cartilage* 18 (11): 1441–47. <https://doi.org/10.1016/j.joca.2010.08.016>.
- Stiglic, Gregor, Primož Kocbek, Nino Fijacko, Marinka Zitnik, Katrien Verbert, and Leona Cilar. 2020. “Interpretability of Machine Learning-Based Prediction Models in Healthcare.” *WIREs Data Mining and Knowledge Discovery* 10 (5): e1379. <https://doi.org/10.1002/widm.1379>.
- Su, Naichuan, Yan Liu, Xianrui Yang, Jiefei Shen, and Hang Wang. 2016. “Correlation between Oral Health-Related Quality of Life and Clinical Dysfunction Index in Patients with Temporomandibular Joint Osteoarthritis.” *Journal of Oral Science* 58 (4): 483–90. <https://doi.org/10.2334/josnusd.16-0224>.
- Su, Zhaoqian, Kalyani Dhusia, and Yinghao Wu. 2022. “Understanding the Functional Role of Membrane Confinements in TNF-Mediated Signaling by Multiscale Simulations.” *Communications Biology* 5 (1): 1–11. <https://doi.org/10.1038/s42003-022-03179-1>.
- Suenaga, Shigeaki, Kunihiro Nagayama, Taisuke Nagasawa, Hiroko Indo, and Hideyuki J. Majima. 2016. “The Usefulness of Diagnostic Imaging for the Assessment of Pain Symptoms in Temporomandibular Disorders.” *Japanese Dental Science Review* 52 (4): 93–106. <https://doi.org/10.1016/j.jdsr.2016.04.004>.
- Szekanecz, M. M. Halloran, M. V. Volin, J. M. Woods, R. M. Strieter, G. Kenneth Haines, S. L. Kunkel, M. D. Burdick, and A. E. Koch. 2000. “Temporal Expression of Inflammatory Cytokines and Chemokines in Rat Adjuvant-Induced Arthritis.” *Arthritis and Rheumatism* 43 (6): 1266–77. [https://doi.org/10.1002/1529-0131\(200006\)43:6<1266::AID-ANR9>3.0.CO;2-P](https://doi.org/10.1002/1529-0131(200006)43:6<1266::AID-ANR9>3.0.CO;2-P).
- Szekanecz, Aniko Vegvari, Zoltan Szabo, and Alisa E. Koch. 2010. “Chemokines and Chemokine Receptors in Arthritis.” *Frontiers in Bioscience (Scholar Edition)* 2 (January): 153–67.
- Takahara, Namiaki, Satoshi Nakagawa, Kanako Sumikura, Yuji Kabasawa, Ichiro Sakamoto, and Hiroyuki Harada. 2017. “Association of Temporomandibular Joint Pain According to Magnetic Resonance Imaging Findings in Temporomandibular Disorder Patients.” *Journal of Oral and Maxillofacial Surgery* 75 (9): 1848–55. <https://doi.org/10.1016/j.joms.2017.03.026>.
- Tallón-Ballesteros, Antonio J., and José Riquelme. 2014. *Deleting or Keeping Outliers for Classifier Training? 2014 6th World Congress on Nature and Biologically Inspired Computing, NaBIC 2014*. <https://doi.org/10.1109/NaBIC.2014.6921892>.
- TALMACEANU, DANIEL, LAVINIA MANUELA LENGHEL, NICOLAE BOLOG, MIHAELA HEDESIU, SMARANDA BUDURU, HORATIU ROTAR, MIHAELA BACIUT, and GRIGORE BACIUT. 2018. “Imaging Modalities for Temporomandibular Joint Disorders: An Update.” *Clujul Medical* 91 (3): 280–87. <https://doi.org/10.15386/cjmed-970>.
- Tanaka, E., M. S. Detamore, and L. G. Mercuri. 2008. “Degenerative Disorders of the Temporomandibular Joint: Etiology, Diagnosis, and Treatment.” *Journal of Dental Research* 87 (4): 296–307. <https://doi.org/10.1177/154405910808700406>.
- Tang, Fengyi, Cao Xiao, Fei Wang, Jiayu Zhou, and Li-wei H. Lehman. 2019. “Retaining Privileged Information for Multi-Task Learning.” *KDD : Proceedings. International Confer-*

- ence on Knowledge Discovery & Data Mining* 2019 (July): 1369–77.  
<https://doi.org/10.1145/3292500.3330907>.
- Tao, Yulei, Xianxing Qiu, Changbo Xu, Bo Sun, and Changxiu Shi. 2015. “Expression and Correlation of Matrix Metalloproteinase-7 and Interleukin-15 in Human Osteoarthritis.” *International Journal of Clinical and Experimental Pathology* 8 (8): 9112–18.
- Teoh, Yun Xin, Khin Wee Lai, Juliana Usman, Siew Li Goh, Hamidreza Mohafez, Khairunnisa Hasikin, Pengjiang Qian, Yizhang Jiang, Yuanpeng Zhang, and Samiappan Dhanalakshmi. 2022. “Discovering Knee Osteoarthritis Imaging Features for Diagnosis and Prognosis: Review of Manual Imaging Grading and Machine Learning Approaches.” *Journal of Healthcare Engineering* 2022 (February): 4138666.  
<https://doi.org/10.1155/2022/4138666>.
- Theeuwes, Wessel F., Martijn H. J. van den Bosch, Rogier M. Thurlings, Arjen B. Blom, and Peter L. E. M. van Lent. 2021. “The Role of Inflammation in Mesenchymal Stromal Cell Therapy in Osteoarthritis, Perspectives for Post-Traumatic Osteoarthritis: A Review.” *Rheumatology (Oxford, England)* 60 (3): 1042–53.  
<https://doi.org/10.1093/rheumatology/keaa910>.
- Thielen, Nathalie, Margot Neefjes, Renske Wiegertjes, Guus van den Akker, Elly Vitters, Henk van Beuningen, Esmeralda Blaney Davidson, et al. 2021. “Osteoarthritis-Related Inflammation Blocks TGF- $\beta$ 's Protective Effect on Chondrocyte Hypertrophy via (de)Phosphorylation of the SMAD2/3 Linker Region.” *International Journal of Molecular Sciences* 22 (15): 8124. <https://doi.org/10.3390/ijms22158124>.
- Thiolloy, Sophie, Jennifer Halpern, Ginger E. Holt, Herbert S. Schwartz, Gregory R. Mundy, Lynn M. Matrisian, and Conor C. Lynch. 2009. “Osteoclast Derived Matrix Metalloproteinase-7 but Not Matrix Metalloproteinase-9 Contributes to Tumor Induced Osteolysis.” *Cancer Research* 69 (16): 6747–55. <https://doi.org/10.1158/0008-5472.CAN-08-3949>.
- Thomas, M., Z. Fronk, A. Gross, D. Willmore, A. Arango, C. Higham, V. Nguyen, et al. 2019. “Losartan Attenuates Progression of Osteoarthritis in the Synovial Temporomandibular and Knee Joints of a Chondrodysplasia Mouse Model through Inhibition of TGF-B1 Signaling Pathway.” *Osteoarthritis and Cartilage* 27 (4): 676–86.  
<https://doi.org/10.1016/j.joca.2018.12.016>.
- Timmeren, Janita E. van, Davide Cester, Stephanie Tanadini-Lang, Hatem Alkadhi, and Bettina Baessler. 2020. “Radiomics in Medical Imaging—‘How-to’ Guide and Critical Reflection.” *Insights into Imaging* 11 (1): 91. <https://doi.org/10.1186/s13244-020-00887-2>.
- Tipton, David A., James Christian, and Adam Blumer. 2016. “Effects of Cranberry Components on IL-1 $\beta$ -Stimulated Production of IL-6, IL-8 and VEGF by Human TMJ Synovial Fibroblasts.” *Archives of Oral Biology* 68 (August): 88–96.  
<https://doi.org/10.1016/j.archoralbio.2016.04.005>.
- Tiulpin, Aleksei, Jérôme Thevenot, Esa Rahtu, Petri Lehenkari, and Simo Saarakkala. 2018. “Automatic Knee Osteoarthritis Diagnosis from Plain Radiographs: A Deep Learning-Based Approach.” *Scientific Reports* 8 (1): 1727. <https://doi.org/10.1038/s41598-018-20132-7>.
- Tokuhara, Cintia Kazuko, Mariana Rodrigues Santesso, Gabriela Silva Neubern de Oliveira, Talita Mendes da Silva Ventura, Julio Toshimi Doyama, Willian Fernando Zambuzzi, and Rodrigo Cardoso de Oliveira. 2019. “Updating the Role of Matrix Metalloproteinases in Mineralized Tissue and Related Diseases.” *Journal of Applied Oral Science: Revista FOB* 27 (September): e20180596. <https://doi.org/10.1590/1678-7757-2018-0596>.

- Toshima, Hiroo, and Ichiro Ogura. 2020. "Characteristics of Patients with Temporomandibular Joint Osteoarthritis on Magnetic Resonance Imaging." *Journal of Medical Imaging and Radiation Oncology* 64 (5): 615–19. <https://doi.org/10.1111/1754-9485.13054>.
- Truelove, Edmond L., Earl E. Sommers, Linda LeResche, Samuel F. Dworkin, and Michael Von Korff. 1992. "Clinical Diagnostic Criteria for TMD New Classification Permits Multiple Diagnoses." *The Journal of the American Dental Association* 123 (4): 47–54. <https://doi.org/10.14219/jada.archive.1992.0094>.
- Tucker, Katherine, Janice Branson, Maria Dilleen, Sally Hollis, Paul Loughlin, Mark J. Nixon, and Zoë Williams. 2016. "Protecting Patient Privacy When Sharing Patient-Level Data from Clinical Trials." *BMC Medical Research Methodology* 16 (1): 77. <https://doi.org/10.1186/s12874-016-0169-4>.
- Uddin, Shahadat, Ibtisham Haque, Haohui Lu, Mohammad Ali Moni, and Ergun Gide. 2022. "Comparative Performance Analysis of K-Nearest Neighbour (KNN) Algorithm and Its Different Variants for Disease Prediction." *Scientific Reports* 12 (1): 6256. <https://doi.org/10.1038/s41598-022-10358-x>.
- Uddin, Shahadat, Arif Khan, Md Ekramul Hossain, and Mohammad Ali Moni. 2019. "Comparing Different Supervised Machine Learning Algorithms for Disease Prediction." *BMC Medical Informatics and Decision Making* 19 (1): 281. <https://doi.org/10.1186/s12911-019-1004-8>.
- Umscheid, Craig A., Joel Betesh, Christine VanZandbergen, Asaf Hanish, Gordon Tait, Mark E. Mikkelsen, Benjamin French, and Barry D. Fuchs. 2015. "Development, Implementation, and Impact of an Automated Early Warning and Response System for Sepsis." *Journal of Hospital Medicine* 10 (1): 26–31. <https://doi.org/10.1002/jhm.2259>.
- Vapnik, Vladimir, and Akshay Vashist. 2009. "A New Learning Paradigm: Learning Using Privileged Information." *Neural Networks* 22 (5–6): 544–57. <https://doi.org/10.1016/j.neunet.2009.06.042>.
- Varghese, Bino A., Steven Y. Cen, Darryl H. Hwang, and Vinay A. Duddalwar. 2019. "Texture Analysis of Imaging: What Radiologists Need to Know." *American Journal of Roentgenology* 212 (3): 520–28. <https://doi.org/10.2214/AJR.18.20624>.
- Varma, G. R. Raveendra, B. Harsha, Santosh Palla, S. P. Amulya Sravan, J. Raju, and K. Rajavardhan. 2019. "Genetics in an Orthodontic Perspective." Edited by Tejavathi Nagaraj. *Journal of Advanced Clinical and Research Insights* 6 (3): 86–90. <https://doi.org/10.15713/ins.jcri.267>.
- Vellido, Alfredo. 2020. "The Importance of Interpretability and Visualization in Machine Learning for Applications in Medicine and Health Care." *Neural Computing and Applications* 32 (24): 18069–83. <https://doi.org/10.1007/s00521-019-04051-w>.
- Venkatesh, Elluru, and Snehal Venkatesh Elluru. 2017. "Cone Beam Computed Tomography: Basics and Applications in Dentistry." *Journal of Istanbul University Faculty of Dentistry* 51 (3 Suppl 1): S102–21. <https://doi.org/10.17096/jiufd.00289>.
- Vergunst, C. E., M. G. H. van de Sande, M. C. Lebre, and P. P. Tak. 2005. "The Role of Chemokines in Rheumatoid Arthritis and Osteoarthritis." *Scandinavian Journal of Rheumatology* 34 (6): 415–25. <https://doi.org/10.1080/03009740500439159>.
- Vikram, Khanna, and F. R. Karjodkar. 2009. "Decision Support Systems in Dental Decision Making: An Introduction." *The Journal of Evidence-Based Dental Practice* 9 (2): 73–76. <https://doi.org/10.1016/j.jebdp.2009.03.003>.

- Vimort, Jean-Baptiste, Antonio Ruellas, Jack Prothero, J. S. Marron, Matthew McCormick, Lucia Cevitanes, Erika Benavides, and Beatriz Paniagua. 2018. "Detection of Bone Loss via Subchondral Bone Analysis." *Proceedings of SPIE--the International Society for Optical Engineering* 10578 (February): 105780Q. <https://doi.org/10.1117/12.2293654>.
- Vrbanović, Ema, and Iva Z. Alajbeg. 2017. "A Young Patient with Temporomandibular Joint Osteoarthritis: Case Report." *Acta Stomatologica Croatica* 51 (3): 232–39. <https://doi.org/10.15644/asc51/3/7>.
- Walsh, David A., Dan F. McWilliams, Matthew J. Turley, Madeleine R. Dixon, Rebecca E. Fransès, Paul I. Mapp, and Deborah Wilson. 2010. "Angiogenesis and Nerve Growth Factor at the Osteochondral Junction in Rheumatoid Arthritis and Osteoarthritis." *Rheumatology (Oxford, England)* 49 (10): 1852–61. <https://doi.org/10.1093/rheumatology/keq188>.
- Wan, Jiangtao, Guowei Zhang, Xin Li, Xianshuai Qiu, Jun Ouyang, Jingxing Dai, and Shaoxiong Min. 2021. "Matrix Metalloproteinase 3: A Promoting and Destabilizing Factor in the Pathogenesis of Disease and Cell Differentiation." *Frontiers in Physiology* 12. <https://www.frontiersin.org/articles/10.3389/fphys.2021.663978>.
- Wang, Dongyun, Yajie Qi, Zhubing Wang, Anyun Guo, Yingxin Xu, and Yang Zhang. 2023. "Recent Advances in Animal Models, Diagnosis, and Treatment of Temporomandibular Joint Osteoarthritis." *Tissue Engineering Part B: Reviews* 29 (1): 62–77. <https://doi.org/10.1089/ten.teb.2022.0065>.
- Wang, Jiang, and Zhang. 2019. "Significantly Dysregulated Genes in Osteoarthritic Labrum Cells Identified through Gene Expression Profiling." *Molecular Medicine Reports* 20 (2): 1716–24. <https://doi.org/10.3892/mmr.2019.10389>.
- Wang, Xiang Qun Shi, Wenjia Wu, Maria Gueorguieva, Mu Yang, and Ji Zhang. 2018. "Sustained and Repeated Mouth Opening Leads to Development of Painful Temporomandibular Disorders Involving Macrophage/Microglia Activation in Mice." *PAIN* 159 (7): 1277. <https://doi.org/10.1097/j.pain.0000000000001206>.
- Wang, J.N. Zhang, Y.H. Gan, and Y.H. Zhou. 2015. "Current Understanding of Pathogenesis and Treatment of TMJ Osteoarthritis." *Journal of Dental Research* 94 (5): 666–73. <https://doi.org/10.1177/0022034515574770>.
- Wassan, Sobia, Beenish Suhail, Riaqa Mubeen, Bhavana Raj, Ujjwal Agarwal, Eti Khatri, Sujith Gopinathan, and Gaurav Dhiman. 2022. "Gradient Boosting for Health IoT Federated Learning." *Sustainability* 14 (24): 16842. <https://doi.org/10.3390/su142416842>.
- Watanabe, Haruhisa, Takashi Iori, Ji-Won Lee, Takashi S. Kajii, Aya Takakura, Ryoko Takao-Kawabata, Yoshimasa Kitagawa, Yutaka Maruoka, and Tadahiro Imura. 2023. "Association between an Increased Serum CCL5 Level and Pathophysiology of Degenerative Joint Disease in the Temporomandibular Joint in Females." *International Journal of Molecular Sciences* 24 (3): 2775. <https://doi.org/10.3390/ijms24032775>.
- Wichtmann, Barbara D., Felix N. Harder, Kilian Weiss, Stefan O. Schönberg, Ulrike I. Attenberger, Hatem Alkadhi, Daniel Pinto Dos Santos, and Bettina Baeßler. 2023. "Influence of Image Processing on Radiomic Features From Magnetic Resonance Imaging." *Investigative Radiology* 58 (3): 199–208. <https://doi.org/10.1097/RLI.0000000000000921>.
- Wieckiewicz, Mieszko, Yuh-Yuan Shiau, and Klaus Boening. 2018. "Pain of Temporomandibular Disorders: From Etiology to Management." *Pain Research & Management* 2018 (June): 4517042. <https://doi.org/10.1155/2018/4517042>.

- Wiegertjes, R., A. van Caam, H. van Beuningen, M. Koenders, P. van Lent, P. van der Kraan, F. van de Loo, and E. Blaney Davidson. 2019. "TGF- $\beta$  Dampens IL-6 Signaling in Articular Chondrocytes by Decreasing IL-6 Receptor Expression." *Osteoarthritis and Cartilage* 27 (8): 1197–1207. <https://doi.org/10.1016/j.joca.2019.04.014>.
- Wiens, Jenna, Suchi Saria, Mark Sendak, Marzyeh Ghassemi, Vincent X. Liu, Finale Doshi-Velez, Kenneth Jung, et al. 2019. "Do No Harm: A Roadmap for Responsible Machine Learning for Health Care." *Nature Medicine* 25 (9): 1337–40. <https://doi.org/10.1038/s41591-019-0548-6>.
- Wiesinger, Birgitta, Hans Malaker, Erling Englund, and Anders Wänman. 2007. "Back Pain in Relation to Musculoskeletal Disorders in the Jaw-Face: A Matched Case–Control Study." *PAIN* 131 (3): 311. <https://doi.org/10.1016/j.pain.2007.03.018>.
- Wilkinson, David J. 2021. "Serpins in Cartilage and Osteoarthritis: What Do We Know?" *Biochemical Society Transactions* 49 (2): 1013–26. <https://doi.org/10.1042/BST20201231>.
- Withrow, Joseph, Cameron Murphy, Yutao Liu, Monte Hunter, Sadanand Fulzele, and Mark W. Hamrick. 2016. "Extracellular Vesicles in the Pathogenesis of Rheumatoid Arthritis and Osteoarthritis." *Arthritis Research & Therapy* 18 (1): 286. <https://doi.org/10.1186/s13075-016-1178-8>.
- Wojdasiewicz, Piotr, Łukasz A. Poniatowski, and Dariusz Szukiewicz. 2014. "The Role of Inflammatory and Anti-Inflammatory Cytokines in the Pathogenesis of Osteoarthritis." *Mediators of Inflammation* 2014: 561459. <https://doi.org/10.1155/2014/561459>.
- Wu, Chuan Bin, Tie Ma, Lin Ma, and Qing Zhou. 2022. "Efficacy Analysis of Splint Combined with PRP Injection in the Treatment of Temporomandibular Joint Osteoarthritis." *Journal of Surgical Oncology* 2022 (1): 1–6. <https://doi.org/10.31487/j.JSO.2022.01.03>.
- Wynants, L., D. M. Kent, D. Timmerman, C. M. Lundquist, and B. Van Calster. 2019. "Untapped Potential of Multicenter Studies: A Review of Cardiovascular Risk Prediction Models Revealed Inappropriate Analyses and Wide Variation in Reporting." *Diagnostic and Prognostic Research* 3 (1): 6. <https://doi.org/10.1186/s41512-019-0046-9>.
- Xi, Yongming, Hui Huang, Zheng Zhao, Jinfeng Ma, and Yan Chen. 2020. "Tissue Inhibitor of Metalloproteinase 1 Suppresses Growth and Differentiation of Osteoblasts and Differentiation of Osteoclasts by Targeting the AKT Pathway." *Experimental Cell Research* 389 (2): 111930. <https://doi.org/10.1016/j.yexcr.2020.111930>.
- Xu, Yan Ke, Bin Wang, and Jian-hao Lin. 2015. "The Role of MCP-1-CCR2 Ligand-Receptor Axis in Chondrocyte Degradation and Disease Progress in Knee Osteoarthritis." *Biological Research* 48 (November): 64. <https://doi.org/10.1186/s40659-015-0057-0>.
- Xu, Yongjun, Xin Liu, Xin Cao, Changping Huang, Enke Liu, Sen Qian, Xingchen Liu, et al. 2021. "Artificial Intelligence: A Powerful Paradigm for Scientific Research." *The Innovation* 2 (4): 100179. <https://doi.org/10.1016/j.xinn.2021.100179>.
- Xuan, Anran, Haowei Chen, Tianyu Chen, Jia Li, Shilong Lu, Tianxiang Fan, Dong Zeng, et al. 2023. "The Application of Machine Learning in Early Diagnosis of Osteoarthritis: A Narrative Review." *Therapeutic Advances in Musculoskeletal Disease* 15 (March): 1759720X231158198. <https://doi.org/10.1177/1759720X231158198>.
- Xue, Zhihao, Liao Wang, Qi Sun, Jia Xu, Ying Liu, Songtao Ai, Lichi Zhang, and Chenglei Liu. 2022. "Radiomics Analysis Using MR Imaging of Subchondral Bone for Identification of Knee Osteoarthritis." *Journal of Orthopaedic Surgery and Research* 17 (1): 414. <https://doi.org/10.1186/s13018-022-03314-y>.



- Yakkaphan, Pankaew, Jared G Smith, Pav Chana, Tara Renton, and Giorgio Lambru. 2022. “Temporomandibular Disorder and Headache Prevalence: A Systematic Review and Meta-Analysis.” *Cephalalgia Reports* 5 (January): 25158163221097350. <https://doi.org/10.1177/25158163221097352>.
- Yang, Guang, Qinghao Ye, and Jun Xia. 2022. “Unbox the Black-Box for the Medical Explainable AI via Multi-Modal and Multi-Centre Data Fusion: A Mini-Review, Two Showcases and Beyond.” *An International Journal on Information Fusion* 77 (January): 29–52. <https://doi.org/10.1016/j.inffus.2021.07.016>.
- Yang, Yazhen Li, Ying Liu, Qiang Zhang, Qi Zhang, Junbo Chen, Xiao Yan, and Xiao Yuan. 2020. “Role of the SDF-1/CXCR4 Signaling Pathway in Cartilage and Subchondral Bone in Temporomandibular Joint Osteoarthritis Induced by Overloaded Functional Orthopedics in Rats.” *Journal of Orthopaedic Surgery and Research* 15 (1): 330. <https://doi.org/10.1186/s13018-020-01860-x>.
- Yang, J. Zhang, Y. Cao, M. Zhang, L. Jing, K. Jiao, S. Yu, W. Chang, D. Chen, and M. Wang. 2015. “Wnt5a/Ror2 Mediates Temporomandibular Joint Subchondral Bone Remodeling.” *Journal of Dental Research* 94 (6): 803–12. <https://doi.org/10.1177/0022034515576051>.
- Yeh, Chih-Chang, Hsin-I Chang, Jui-Kun Chiang, Wang-Ting Tsai, Li-Ming Chen, Chean-Ping Wu, Shu Chien, and Cheng-Nan Chen. 2009. “Regulation of Plasminogen Activator Inhibitor 1 Expression in Human Osteoarthritic Chondrocytes by Fluid Shear Stress: Role of Protein Kinase Ca.” *Arthritis & Rheumatism* 60 (8): 2350–61. <https://doi.org/10.1002/art.24680>.
- Yoda, Tetsuya, Nobumi Ogi, Hiroyuki Yoshitake, Tetsuji Kawakami, Ritsuo Takagi, Kenichiro Murakami, Hidemichi Yuasa, Toshiro Kondoh, Kanchu Tei, and Kenichi Kurita. 2020. “Clinical Guidelines for Total Temporomandibular Joint Replacement.” *The Japanese Dental Science Review* 56 (1): 77–83. <https://doi.org/10.1016/j.jdsr.2020.03.001>.
- Yoshida, Ken, Olexandr Korchynskyi, Paul P. Tak, Takeo Isozaki, Jeffrey H. Ruth, Phillip L. Campbell, Dominique L. Baeten, Danielle M. Gerlag, M. Asif Amin, and Alisa E. Koch. 2014. “Citruination of Epithelial Neutrophil-Activating Peptide 78/CXCL5 Results in Conversion From a Non-Monocyte-Recruiting Chemokine to a Monocyte-Recruiting Chemokine.” *Arthritis & Rheumatology* 66 (10): 2716–27. <https://doi.org/10.1002/art.38750>.
- Yost, Olivia, Cathy T. Liverman, Rebecca English, Sean Mackey, and Enriqueta C. Bond, eds. 2020. *Temporomandibular Disorders: Priorities for Research and Care*. The National Academies Collection: Reports Funded by National Institutes of Health. Washington (DC): National Academies Press (US). <http://www.ncbi.nlm.nih.gov/books/NBK555057/>.
- Yuan, Li Sun, Jian-Jun Li, and Chun-Hou An. 2014. “Elevated VEGF Levels Contribute to the Pathogenesis of Osteoarthritis.” *BMC Musculoskeletal Disorders* 15 (1): 437. <https://doi.org/10.1186/1471-2474-15-437>.
- Yuan, Yange Wu, Maotuan Huang, Xueman Zhou, Jiaqi Liu, Yating Yi, Jun Wang, and Jin Liu. 2022. “A New Frontier in Temporomandibular Joint Osteoarthritis Treatment: Exosome-Based Therapeutic Strategy.” *Frontiers in Bioengineering and Biotechnology* 10 (November): 1074536. <https://doi.org/10.3389/fbioe.2022.1074536>.
- Yushkevich, Paul A., null Yang Gao, and Guido Gerig. 2016. “ITK-SNAP: An Interactive Tool for Semi-Automatic Segmentation of Multi-Modality Biomedical Images.” *Annual International Conference of the IEEE Engineering in Medicine and Biology Society. IEEE*

- Engineering in Medicine and Biology Society. Annual International Conference* 2016 (August): 3342–45. <https://doi.org/10.1109/EMBC.2016.7591443>.
- Zebari, Rizgar, Adnan Abdulazeez, Diyar Zeebaree, Dilovan Zebari, and Jwan Saeed. 2020. “A Comprehensive Review of Dimensionality Reduction Techniques for Feature Selection and Feature Extraction.” *Journal of Applied Science and Technology Trends* 1 (2): 56–70. <https://doi.org/10.38094/jastt1224>.
- Zelová, Hana, and Jan Hošek. 2013. “TNF- $\alpha$  Signalling and Inflammation: Interactions between Old Acquaintances.” *Inflammation Research: Official Journal of the European Histamine Research Society ... [et Al.]* 62 (7): 641–51. <https://doi.org/10.1007/s00011-013-0633-0>.
- Zhang, Jonas Bianchi, Najla Al Turkestani, Celia Le, Romain Deleat-Besson, Antonio Ruellas, Lucia Cevidanes, et al. 2021. “Temporomandibular Joint Osteoarthritis Diagnosis Using Privileged Learning of Protein Markers.” *Annual International Conference of the IEEE Engineering in Medicine and Biology Society. IEEE Engineering in Medicine and Biology Society. Annual International Conference 2021* (November): 1810–13. <https://doi.org/10.1109/EMBC46164.2021.9629990>.
- Zhang, Monte S. Buchsbaum, King-Wai Chu, and Erin A. Hazlett. 2013. “A Manual, Semi-Automated and Automated ROI Study of fMRI Hemodynamic Response.” *Studies in Health Technology and Informatics* 192: 921.
- Zhang, David V. Fried, Xenia J. Fave, Luke A. Hunter, Jinzhong Yang, and Laurence E. Court. 2015. “Ibex: An Open Infrastructure Software Platform to Facilitate Collaborative Work in Radiomics.” *Medical Physics* 42 (3): 1341–53. <https://doi.org/10.1118/1.4908210>.
- Zhang, Di Liu, Djandan Tadum Arthur Vithran, Bosomtwe Richmond Kwabena, Wenfeng Xiao, and Yusheng Li. 2023. “CC Chemokines and Receptors in Osteoarthritis: New Insights and Potential Targets.” *Arthritis Research & Therapy* 25 (1): 113. <https://doi.org/10.1186/s13075-023-03096-6>.
- Zhang, Shihua, Tingting Li, Yao Feng, Keping Zhang, Jun Zou, Xiquan Weng, Yu Yuan, and Lan Zhang. 2023. “Exercise Improves Subchondral Bone Microenvironment through Regulating Bone-Cartilage Crosstalk.” *Frontiers in Endocrinology* 14. <https://www.frontiersin.org/articles/10.3389/fendo.2023.1159393>.
- Zhang, Yuyuan Xiong, Bangjun Wang, Yi Zhou, Zijian Wang, Jiaqi Shi, Chao Li, Xinyan Lu, and Gang Chen. 2022. “Potential Value of Serum Brain-Derived Neurotrophic Factor, Vascular Endothelial Growth Factor, and S100B for Identifying Major Depressive Disorder in Knee Osteoarthritis Patients.” *Frontiers in Psychiatry* 13. <https://www.frontiersin.org/articles/10.3389/fpsy.2022.1019367>.
- Zhang, Lili Xu, Dandong Wu, Chunhua Yu, Shuai Fan, and Bin Cai. 2021. “Effectiveness of Exercise Therapy versus Occlusal Splint Therapy for the Treatment of Painful Temporomandibular Disorders: A Systematic Review and Meta-Analysis.” *Annals of Palliative Medicine* 10 (6): 6122132–132. <https://doi.org/10.21037/apm-21-451>.
- Zhang, Xu, and Liu. 2017. “Comparison of Morphologic Parameters of Temporomandibular Joint for Asymptomatic Subjects Using the Two-Dimensional and Three-Dimensional Measuring Methods.” *Journal of Healthcare Engineering* 2017: 5680708. <https://doi.org/10.1155/2017/5680708>.
- Zhang, and Yang. 2019. “A New Learning Paradigm for Random Vector Functional-Link Network: RVFL+.” *Neural Networks* 122 (October). <https://doi.org/10.1016/j.neunet.2019.09.039>.

- Zhao. 2021. “Understanding Sources of Variation to Improve the Reproducibility of Radiomics.” *Frontiers in Oncology* 11. <https://www.frontiersin.org/articles/10.3389/fonc.2021.633176>.
- Zhao, Yanhui Ding, Ying Han, Yong Fan, Aaron F. Alexander-Bloch, Tong Han, Dan Jin, et al. 2020. “Independent and Reproducible Hippocampal Radiomic Biomarkers for Multisite Alzheimer’s Disease: Diagnosis, Longitudinal Progress and Biological Basis.” *Science Bulletin* 65 (13): 1103–13. <https://doi.org/10.1016/j.scib.2020.04.003>.
- Zhao, Shaopeng Liu, Chuan Ma, Shixing Ma, Guokun Chen, Lingyu Yuan, Lei Chen, and Huaqiang Zhao. 2019. “Estrogen-Related Receptor  $\gamma$  Induces Angiogenesis and Extracellular Matrix Degradation of Temporomandibular Joint Osteoarthritis in Rats.” *Frontiers in Pharmacology* 10 (November): 1290. <https://doi.org/10.3389/fphar.2019.01290>.
- Zhao, Yuqing, Yanxin An, Libo Zhou, Fan Wu, Gaoyi Wu, Jing Wang, and Lei Chen. 2022. “Animal Models of Temporomandibular Joint Osteoarthritis: Classification and Selection.” *Frontiers in Physiology* 13. <https://www.frontiersin.org/articles/10.3389/fphys.2022.859517>.
- Zhao, Zu-yan Zhang, Yun-tang Wu, Wan-Lin Zhang, and Xu-chen Ma. 2011. “Investigation of the Clinical and Radiographic Features of Osteoarthritis of the Temporomandibular Joints in Adolescents and Young Adults.” *Oral Surgery, Oral Medicine, Oral Pathology, Oral Radiology, and Endodontology* 111 (2): e27–34. <https://doi.org/10.1016/j.tripleo.2010.09.076>.
- Zhen, Gehua, Chunyi Wen, Xiaofeng Jia, Yu Li, Janet L. Crane, Simon C. Mears, Frederic B. Askin, et al. 2013. “Inhibition of TGF- $\beta$  Signaling in Subchondral Bone Mesenchymal Stem Cells Attenuates Osteoarthritis.” *Nature Medicine* 19 (6): 704–12. <https://doi.org/10.1038/nm.3143>.
- Zheng, Liwei, Caixia Pi, Jun Zhang, Yi Fan, Chen Cui, Yang Zhou, Jianxun Sun, et al. 2018. “Aberrant Activation of Latent Transforming Growth Factor- $\beta$  Initiates the Onset of Temporomandibular Joint Osteoarthritis.” *Bone Research* 6 (September): 26. <https://doi.org/10.1038/s41413-018-0027-6>.
- Zhu, Xiaobo, Yau Tsz Chan, Patrick S. H. Yung, Rocky S. Tuan, and Yangzi Jiang. 2021. “Subchondral Bone Remodeling: A Therapeutic Target for Osteoarthritis.” *Frontiers in Cell and Developmental Biology* 8. <https://www.frontiersin.org/articles/10.3389/fcell.2020.607764>.
- Zikos, Dimitrios, and Nailya DeLellis. 2018. “CDSS-RM: A Clinical Decision Support System Reference Model.” *BMC Medical Research Methodology* 18 (1): 137. <https://doi.org/10.1186/s12874-018-0587-6>.
- Zuo, Qiliang, Shifeier Lu, Zhibin Du, Thor Friis, Jiangwu Yao, Ross Crawford, Indira Prasadam, and Yin Xiao. 2016. “Characterization of Nano-Structural and Nano-Mechanical Properties of Osteoarthritic Subchondral Bone.” *BMC Musculoskeletal Disorders* 17 (1): 367. <https://doi.org/10.1186/s12891-016-1226-1>.
- Zwanenburg, Alex, Stefan Leger, Linda Agolli, Karoline Pilz, Esther G. C. Troost, Christian Richter, and Steffen Löck. 2019. “Assessing Robustness of Radiomic Features by Image Perturbation.” *Scientific Reports* 9 (1): 614. <https://doi.org/10.1038/s41598-018-36938-4>.
- Zwiri, Abdalwhab, Mohammad A. I. Al-Hatamleh, Wan Muhamad Amir W. Ahmad, Jawaad Ahmed Asif, Suan Phaik Khoo, Adam Husein, Zuryati Ab-Ghani, and Nur Karyatee Kasim. 2020. “Biomarkers for Temporomandibular Disorders: Current Status and Future Directions.” *Diagnostics* 10 (5). <https://doi.org/10.3390/diagnostics10050303>.